

## **Appendix B**

# **Development of Groundwater Flow, Geochemical, and Solute Transport Models**

---

*Note: For conservation reasons, the hardcopy version of this appendix does not include the Section 10 figures for this report; please see the version of Appendix B on the CD-ROM enclosed inside the BOD Report binder to review these figures.*

**Pacific Gas & Electric**

**Appendix B: Development of  
Groundwater Flow, Geochemical,  
and Solute Transport Models**

Pacific Gas & Electric  
Topock Compressor Station  
Needles, California

April 2013



<b>Acronyms and Abbreviations</b>	<b>xv</b>
<b>1. Introduction and Objectives</b>	<b>1</b>
1.1 Introduction	1
1.2 Study Objectives and Scope	1
<b>2. Conceptual Site Model</b>	<b>3</b>
2.1 Regional Geologic Framework	3
2.2 Site Hydrogeology and Groundwater Occurrence	4
2.3 Site Geochemistry	6
2.4 Geochemical Conceptual Model of the Selected Remedy	7
<b>3. In-Situ Pilot Scale Studies and Design Implications</b>	<b>10</b>
3.1 Floodplain Pilot Test Overview	10
3.2 Upland Pilot Test Overview	11
3.3 Basis for Recirculation Design	12
3.4 ISPT-Derived Solute Transport Model Parameters	13
3.4.1 Relationship between TOC Distribution and Cr(VI) Reduction	13
3.4.2 TOC Degradation Half-Life	15
3.4.3 Manganese and Arsenic Generation and Attenuation	15
3.4.4 Mobile Porosity	16
3.5 Effects of Groundwater Geochemistry on Cr(VI) Treatment	16
3.5.1 Competing Electron Acceptors	16
3.5.2 Total Dissolved Solids	17
<b>4. Groundwater Flow Model Development</b>	<b>18</b>
4.1 Groundwater Flow Submodel Code Selection and Description	18
4.2 Submodel Domain	19
4.3 Submodel Discretization	19
4.4 Boundary Conditions	20

4.5	Hydraulic Conductivity	20
<b>5.</b>	<b>Geochemical Model Development</b>	<b>21</b>
5.1	Geochemical and Reactive Transport Code Selection	21
5.2	Full-Redox Geochemical Model	21
5.3	Manganese Generation and Attenuation	23
5.3.1	Manganese Oxide Reductive Dissolution	24
5.3.2	Mn(II) Sorption	24
5.3.3	Mn(II) Oxidation and Precipitation	27
5.4	Arsenic Generation and Attenuation	28
5.4.1	Arsenic Generation in the IRZ	28
5.4.2	Arsenic Coprecipitation	29
5.4.3	Arsenate Sorption	29
<b>6.</b>	<b>Solute Transport Model Development</b>	<b>32</b>
6.1	Code Selection	32
6.2	Solute Transport Parameters	33
6.2.1	Porosity	33
6.2.2	Mass Transfer Coefficient	33
6.2.3	Chromium Adsorption	34
6.2.4	Chromium Reduction	34
6.2.5	Initial Hexavalent Chromium Distribution	34
6.2.6	Byproduct Generation	35
6.2.7	Byproduct Adsorption and Precipitation	36
6.2.8	Naturally Occurring Manganese	36
6.3	Parameter Assessment	37
6.4	Remediation Design	37
6.4.1	NTH IRZ	39
6.4.2	Riverbank Extraction	40

6.4.3	Uplands Injection	41
6.4.4	Transwestern Bench Extraction	41
6.4.5	East Ravine Extraction	42
6.4.6	Topock Compressor Station Injection	42
6.4.7	Freshwater Injection	43
6.5	Flow Conditions	43
<b>7.</b>	<b>Solute Transport Model Results</b>	<b>45</b>
7.1	Hexavalent Chromium	45
7.2	Manganese	45
7.3	Arsenic	46
7.4	Transient and IM-3 Transition Hexavalent Chromium Simulations	46
<b>8.</b>	<b>Manganese Hyporheic Zone Model Results</b>	<b>50</b>
8.1	Hyporheic Zone Model Domain, Parameters, and Execution	50
8.1.1	Flow and Transport Model Parameters	50
8.1.2	Geochemical Model Parameters	51
8.2	Results	52
<b>9.</b>	<b>Geochemical Reactive Transport Model Results and Sensitivity Analyses</b>	<b>54</b>
9.1	Solute Transport Model and Geochemical Reactive Transport Model Comparison	54
9.1.1	Model Comparison Domain and Geochemical Inputs	54
9.1.2	Transport Model Comparison Results	56
9.2	Geochemical Sensitivity Analysis	57
<b>10.</b>	<b>Solute Transport Model Sensitivity Analysis</b>	<b>59</b>
10.1	NTH IRZ Well Spacing	59
10.2	Injected TOC Concentrations	60
10.3	Riverbank Extraction Rates	62
10.4	Manganese Sorption, Generation, and Oxidation	63
10.5	Arsenic Precipitation, Generation, and Sorption	64

10.6	Chromium Sorption	65
10.7	Conditioned Remedy-Produced Water NTH IRZ Injection	66
10.8	IRL/Freshwater Oscillation	66
10.9	Off-Cycle NTH IRZ Extraction	67
10.10	TOC Half-Life Sensitivity	68
10.11	NTH IRZ Rate Sensitivity	69
10.12	Freshwater Injection Rate Sensitivity	70
10.13	Intermediate Recirculation Well Sensitivity	71
10.14	IRL TOC Injection Sensitivity	71
10.15	TOC/Hexavalent Chromium Trigger Sensitivity	72
<b>11.</b>	<b>Uncertainty</b>	<b>73</b>
<b>12.</b>	<b>Conclusions</b>	<b>74</b>
<b>13.</b>	<b>References</b>	<b>75</b>

## Tables

Table 6.2-1	Byproduct Generation Terms Used in Fate and Transport Model
Table 6.2-2	Byproduct Sorption Terms Used in Fate and Transport Model
Table 8.2-1	Mn(II) Oxidation in the Hyporheic Zone

## Figures

Figure 2.3-1	Correlation of ORP with Dissolved Iron and Organic Carbon in Riverbank Monitoring Wells
Figure 2.4-1	Redox Ladder
Figure 3.4-1	Floodplain ISPT Results for PT-1D, Injection Events 1 - 4
Figure 3.4-2	Arsenic Concentrations Observed in PT-1D and PT-2D, Injection Events 1 - 4
Figure 3.5-1	TDS and Sodium Concentrations in Floodplain and Upland ISPT Wells
Figure 4-1	Regional Model and Submodel Domain Extents
Figure 4.2-1	Submodel Domain and Finite Difference Grid
Figure 4.2-2	Thickness Model Layer 1
Figure 4.2-3	Thickness Model Layer 2

Figure 4.2-4	Thickness Model Layer 3
Figure 4.2-5	Thickness Model Layer 4
Figure 4.2-6	Thickness Model Layer 5
Figure 4.5-1	Hydraulic Conductivity Model Layer 1
Figure 4.5-2	Hydraulic Conductivity Model Layer 2
Figure 4.5-3	Hydraulic Conductivity Model Layer 3
Figure 4.5-4	Hydraulic Conductivity Model Layer 4
Figure 4.5-5	Hydraulic Conductivity Model Layer 5
Figure 5.3-1	Batch Manganese and Arsenic Generation Comparisons
Figure 5.3-2	Manganese Surface Complexation Model Results and Fitted Freundlich Isotherm
Figure 5.4-1	Arsenate Surface Complexation Model Results and Fitted Freundlich Isotherm
Figure 6.2-1	Initial Hexavalent Chromium Concentration Distribution Model Layer 1
Figure 6.2-2	Initial Hexavalent Chromium Concentration Distribution Model Layer 2
Figure 6.2-3	Initial Hexavalent Chromium Concentration Distribution Model Layer 3
Figure 6.2-4	Initial Hexavalent Chromium Concentration Distribution Model Layer 4
Figure 6.2-5	Delineation of Average Floodplain Manganese Concentrations in Groundwater (July 1997 – December 2011) in Model Layers 1 and 2
Figure 6.2-6	Delineation of Average Floodplain Manganese Concentrations in Groundwater (July 1997 – December 2011) in Model Layers 3 and 4
Figure 6.4-1	Remediation Design Well Locations
Figure 6.4-2	Conceptual Final Groundwater Remedy Cross-Section Locations
Figure 6.4-3	Conceptual Final Groundwater Remedy Cross-Section A-A'
Figure 6.4-4	Conceptual Final Groundwater Remedy Cross-Section B-B'
Figure 6.4-5	Conceptual Final Groundwater Remedy Cross-Section C-C'
Figure 6.4-6	Conceptual Final Groundwater Remedy Cross-Section D-D'
Figure 6.4-7	Conceptual Final Groundwater Remedy Cross-Section E-E'
Figure 6.4-8	Conceptual Final Groundwater Remedy Cross-Section F-F'
Figure 6.5-1	Simulated Groundwater Contours Under Ambient Flow Conditions in Model Layer 1

Figure 6.5-2	Simulated Groundwater Contours Under Ambient Flow Conditions in Model Layer 2
Figure 6.5-3	Simulated Groundwater Contours Under Ambient Flow Conditions in Model Layer 3
Figure 6.5-4	Simulated Groundwater Contours Under Ambient Flow Conditions in Model Layer 4
Figure 6.5-5	Simulated Groundwater Contours Under Active Remedy Flow Conditions in Model Layer 1
Figure 6.5-6	Simulated Groundwater Contours Under Active Remedy Flow Conditions in Model Layer 2
Figure 6.5-7	Simulated Groundwater Contours Under Active Remedy Flow Conditions in Model Layer 3
Figure 6.5-8	Simulated Groundwater Contours Under Active Remedy Flow Conditions in Model Layer 4
Figure 6.5-9	Simulated Groundwater Capture Under Active Remedy Flow Conditions in Model Layer 1
Figure 6.5-10	Simulated Groundwater Capture Under Active Remedy Flow Conditions in Model Layer 2
Figure 6.5-11	Simulated Groundwater Capture Under Active Remedy Flow Conditions in Model Layer 3
Figure 6.5-12	Simulated Groundwater Capture Under Active Remedy Flow Conditions in Model Layer 4
Figure 7.1-1	Simulated Hexavalent Chromium Transport Results in Model Layer 1
Figure 7.1-2	Simulated Hexavalent Chromium Transport Results in Model Layer 2
Figure 7.1-3	Simulated Hexavalent Chromium Transport Results in Model Layer 3
Figure 7.1-4	Simulated Hexavalent Chromium Transport Results in Model Layer 4
Figure 7.2-1	Simulated IRZ Generated Manganese Byproduct Transport Results in Model Layer 1
Figure 7.2-2	Simulated IRZ Generated Manganese Byproduct Transport Results in Model Layer 2
Figure 7.2-3	Simulated IRZ Generated Manganese Byproduct Transport Results in Model Layer 3
Figure 7.2-4	Simulated IRZ Generated Manganese Byproduct Transport Results in Model Layer 4
Figure 7.2-5	Simulated Maximum IRZ Generated Manganese Byproduct and Naturally Occuring Average Floodplain Manganese in Model Layer 1
Figure 7.2-6	Simulated Maximum IRZ Generated Manganese Byproduct and Naturally Occuring Average Floodplain Manganese in Model Layer 2
Figure 7.2-7	Simulated Maximum IRZ Generated Manganese Byproduct and Naturally Occuring Average Floodplain Manganese in Model Layer 3
Figure 7.2-8	Simulated Maximum IRZ Generated Manganese Byproduct and Naturally Occuring Average Floodplain Manganese in Model Layer 4
Figure 7.3-1	Simulated Arsenic Transport Results in Model Layer 1
Figure 7.3-2	Simulated Arsenic Transport Results in Model Layer 2

Figure 7.3-3	Simulated Arsenic Transport Results in Model Layer 3
Figure 7.3-4	Simulated Arsenic Transport Results in Model Layer 4
Figure 7.4-1	Simulated Transient Water Levels and Flow Vectors in Model Layer 1 Months 0 to 5
Figure 7.4-2	Simulated Transient Water Levels and Flow Vectors in Model Layer 1 Months 6 to 12
Figure 7.4-3	Transient and Steady State Simulated Chromium Transport Results After 3 Months Transition in Model Layer 2
Figure 7.4-4	Transient and Steady State Simulated Chromium Transport Results After 3 Months Transition in Model Layer 4
Figure 7.4-5	Transient and Steady State Simulated Chromium Transport Results After 6 Months Transition in Model Layer 2
Figure 7.4-6	Transient and Steady State Simulated Chromium Transport Results After 6 Months Transition in Model Layer 4
Figure 7.4-7	Transient and Steady State Simulated Chromium Transport Results After 9 Months Transition in Model Layer 2
Figure 7.4-8	Transient and Steady State Simulated Chromium Transport Results After 9 Months Transition in Model Layer 4
Figure 7.4-9	Simulated Hexavalent Chromium Transport in Model Layer 2 for 1 Year Start Up Scenarios
Figure 7.4-10	Simulated Hexavalent Chromium Transport in Model Layer 4 for 1 Year Start Up Scenarios
Figure 7.4-11	Simulated Hexavalent Chromium Transport in Model Layer 2 for 2 Year Start Up Scenarios
Figure 7.4-12	Simulated Hexavalent Chromium Transport in Model Layer 4 for 2 Year Start Up Scenarios
Figure 8.2-1	Mn(II) Oxidation in the Hyporheic Zone
Figure 9.1-1	Hypothetical IRZ Model Domain and Calibrated Hydraulic Head Profile
Figure 9.1-2	Geochemical Reactive Transport Model Results for the 1D IRZ System: TOC, Cr(VI), DO, and Nitrate
Figure 9.1-3	Geochemical Reactive Transport Model Results for the 1D IRZ System: Mn, As, pH, and Alkalinity
Figure 9.1-4	Comparison of PHT3D and MT3D Simulation Results for the 1D IRZ System
Figure 9.2-1	Variation in Manganese Sorption with Aqueous Geochemical Conditions
Figure 10.1-1	NTH IRZ Well Spacing Sensitivity: 150 ft and 75 ft Spacing with Simulated Hexavalent Chromium Transport Results for Year 10 in Model Layer 2

Figure 10.1-2	NTH IRZ Well Spacing Sensitivity: 150 ft and 75 ft Spacing with Simulated Hexavalent Chromium Transport Results for Year 10 in Model Layer 4
Figure 10.1-3	NTH IRZ Well Spacing Sensitivity: 150 ft and 75 ft Spacing with Simulated Hexavalent Chromium Transport Results for Year 30 in Model Layer 2
Figure 10.1-4	NTH IRZ Well Spacing Sensitivity: 150 ft and 75 ft Spacing with Simulated Hexavalent Chromium Transport Results for Year 30 in Model Layer 4
Figure 10.1-5	NTH IRZ Well Spacing Sensitivity: 150 ft and 75 ft Spacing with Simulated Manganese Transport Results for Year 10 in Model Layer 2
Figure 10.1-6	NTH IRZ Well Spacing Sensitivity: 150 ft and 75 ft Spacing with Simulated Manganese Transport Results for Year 10 in Model Layer 4
Figure 10.1-7	NTH IRZ Well Spacing Sensitivity: 150 ft and 75 ft Spacing with Simulated Manganese Transport Results for Year 30 in Model Layer 2
Figure 10.1-8	NTH IRZ Well Spacing Sensitivity: 150 ft and 75 ft Spacing with Simulated Manganese Transport Results for Year 30 in Model Layer 4
Figure 10.2-1	TOC Concentration Sensitivity: Simulated Hexavalent Chromium Transport Results for Year 10 in Model Layer 2
Figure 10.2-2	TOC Concentration Sensitivity: Simulated Hexavalent Chromium Transport Results for Year 10 in Model Layer 4
Figure 10.2-3	TOC Concentration Sensitivity: Simulated Hexavalent Chromium Transport Results for Year 30 in Model Layer 2
Figure 10.2-4	TOC Concentration Sensitivity: Simulated Hexavalent Chromium Transport Results for Year 30 in Model Layer 4
Figure 10.2-5	TOC Concentration Sensitivity: Simulated Manganese Transport Results for Year 10 in Model Layer 2
Figure 10.2-6	TOC Concentration Sensitivity: Simulated Manganese Transport Results for Year 10 in Model Layer 4
Figure 10.2-7	TOC Concentration Sensitivity: Simulated Manganese Transport Results for Year 30 in Model Layer 2
Figure 10.2-8	TOC Concentration Sensitivity: Simulated Manganese Transport Results for Year 30 in Model Layer 4
Figure 10.2-9	TOC Concentration Sensitivity: Simulated Arsenic Transport Results for Year 30 in Model Layer 2
Figure 10.2-10	TOC Concentration Sensitivity: Simulated Arsenic Transport Results for Year 30 in Model Layer 4
Figure 10.3-1	Riverbank Extraction Rate Sensitivity: Simulated Hexavalent Chromium Transport Results for Year 10 in Model Layer 2



Figure 10.3-2	Riverbank Extraction Rate Sensitivity: Simulated Hexavalent Chromium Transport Results for Year 10 in Model Layer 4
Figure 10.3-3	Riverbank Extraction Rate Sensitivity: Simulated Hexavalent Chromium Transport Results for Year 30 in Model Layer 2
Figure 10.3-4	Riverbank Extraction Rate Sensitivity: Simulated Hexavalent Chromium Transport Results for Year 30 in Model Layer 4
Figure 10.3-5	Riverbank Extraction Rate Sensitivity: Simulated Manganese Transport Results for Year 10 in Model Layer 2
Figure 10.3-6	Riverbank Extraction Rate Sensitivity: Simulated Manganese Transport Results for Year 10 in Model Layer 4
Figure 10.3-7	Riverbank Extraction Rate Sensitivity: Simulated Manganese Transport Results for Year 30 in Model Layer 2
Figure 10.3-8	Riverbank Extraction Rate Sensitivity: Simulated Manganese Transport Results for Year 30 in Model Layer 4
Figure 10.4-1	Manganese Sorption Sensitivity: Simulated Manganese Transport Results for Year 10 in Model Layer 2
Figure 10.4-2	Manganese Sorption Sensitivity: Simulated Manganese Transport Results for Year 10 in Model Layer 4
Figure 10.4-3	Manganese Sorption Sensitivity: Simulated Manganese Transport Results for Year 30 in Model Layer 2
Figure 10.4-4	Manganese Sorption Sensitivity: Simulated Manganese Transport Results for Year 30 in Model Layer 4
Figure 10.4-5	Manganese Generation Sensitivity: Simulated Manganese Transport Results for Year 10 in Model Layer 2
Figure 10.4-6	Manganese Generation Sensitivity: Simulated Manganese Transport Results for Year 10 in Model Layer 4
Figure 10.4-7	Manganese Generation Sensitivity: Simulated Manganese Transport Results for Year 30 in Model Layer 2
Figure 10.4-8	Manganese Generation Sensitivity: Simulated Manganese Transport Results for Year 30 in Model Layer 4
Figure 10.4-9	Manganese Oxidation Sensitivity: Simulated Manganese Transport Results for Year 10 in Model Layer 2
Figure 10.4-10	Manganese Oxidation Sensitivity: Simulated Manganese Transport Results for Year 10 in Model Layer 4
Figure 10.4-11	Manganese Oxidation Sensitivity: Simulated Manganese Transport Results for Year 30 in Model Layer 2

Figure 10.4-12	Manganese Oxidation Sensitivity: Simulated Manganese Transport Results for Year 30 in Model Layer 4
Figure 10.5-1	Arsenic Generation Sensitivity: Simulated Arsenic Transport Results for Year 30 in Model Layer 2
Figure 10.5-2	Arsenic Generation Sensitivity: Simulated Arsenic Transport Results for Year 30 in Model Layer 4
Figure 10.6-1	Hexavalent Chromium Sorption Sensitivity: Simulated Hexavalent Chromium Transport Results for Year 10 in Model Layer 2
Figure 10.6-2	Hexavalent Chromium Sorption Sensitivity: Simulated Hexavalent Chromium Transport Results for Year 10 in Model Layer 4
Figure 10.6-3	Hexavalent Chromium Sorption Sensitivity: Simulated Hexavalent Chromium Transport Results for Year 30 in Model Layer 2
Figure 10.6-4	Hexavalent Chromium Sorption Sensitivity: Simulated Hexavalent Chromium Transport Results for Year 30 in Model Layer 4
Figure 10.7-1	Addition of Conditioned Remedy-Produced Water to NTH IRZ Sensitivity: Simulated Hexavalent Chromium Transport Results for Year 10 in Model Layer 2
Figure 10.7-2	Addition of Conditioned Remedy-Produced Water to NTH IRZ Sensitivity: Simulated Hexavalent Chromium Transport Results for Year 10 in Model Layer 4
Figure 10.7-3	Addition of Conditioned Remedy-Produced Water to NTH IRZ Sensitivity: Simulated Hexavalent Chromium Transport Results for Year 30 in Model Layer 2
Figure 10.7-4	Addition of Conditioned Remedy-Produced Water to NTH IRZ Sensitivity: Simulated Hexavalent Chromium Transport Results for Year 30 in Model Layer 4
Figure 10.7-5	Addition of Conditioned Remedy-Produced Water to NTH IRZ Sensitivity: Simulated Manganese Transport Results for Year 10 in Model Layer 2
Figure 10.7-6	Addition of Conditioned Remedy-Produced Water to NTH IRZ Sensitivity: Simulated Manganese Transport Results for Year 10 in Model Layer 4
Figure 10.7-7	Addition of Conditioned Remedy-Produced Water to NTH IRZ Sensitivity: Simulated Manganese Transport Results for Year 30 in Model Layer 2
Figure 10.7-8	Addition of Conditioned Remedy-Produced Water to NTH IRZ Sensitivity: Simulated Manganese Transport Results for Year 30 in Model Layer 4
Figure 10.8-1	IRL/FW Oscillation Sensitivity: Simulated Hexavalent Chromium Transport Results for Year 20 in Model Layer 2
Figure 10.8-2	IRL/FW Oscillation Sensitivity: Simulated Hexavalent Chromium Transport Results for Year 20 in Model Layer 4
Figure 10.8-3	IRL/FW Oscillation Sensitivity: Simulated Hexavalent Chromium Transport Results for Year 30 in Model Layer 2

Figure 10.8-4	IRL/FW Oscillation Sensitivity: Simulated Hexavalent Chromium Transport Results for Year 30 in Model Layer 4
Figure 10.8-5	IRL/FW Oscillation Sensitivity: Simulated Manganese Transport Results for Year 20 in Model Layer 2
Figure 10.8-6	IRL/FW Oscillation Sensitivity: Simulated Manganese Transport Results for Year 20 in Model Layer 4
Figure 10.8-7	IRL/FW Oscillation Sensitivity: Simulated Manganese Transport Results for Year 30 in Model Layer 2
Figure 10.8-8	IRL/FW Oscillation Sensitivity: Simulated Manganese Transport Results for Year 30 in Model Layer 4
Figure 10.9-1	NTH IRZ Off-Cycle Extraction Sensitivity: Simulated Hexavalent Chromium Transport Results for Year 10 in Model Layer 2
Figure 10.9-2	NTH IRZ Off-Cycle Extraction Sensitivity: Simulated Hexavalent Chromium Transport Results for Year 10 in Model Layer 4
Figure 10.9-3	NTH IRZ Off-Cycle Extraction Sensitivity: Simulated Hexavalent Chromium Transport Results for Year 30 in Model Layer 2
Figure 10.9-4	NTH IRZ Off-Cycle Extraction Sensitivity: Simulated Hexavalent Chromium Transport Results for Year 30 in Model Layer 4
Figure 10.9-5	NTH IRZ Off-Cycle Extraction Sensitivity: Simulated Manganese Transport Results for Year 10 in Model Layer 2
Figure 10.9-6	NTH IRZ Off-Cycle Extraction Sensitivity: Simulated Manganese Transport Results for Year 10 in Model Layer 4
Figure 10.9-7	NTH IRZ Off-Cycle Extraction Sensitivity: Simulated Manganese Transport Results for Year 30 in Model Layer 2
Figure 10.9-8	NTH IRZ Off-Cycle Extraction Sensitivity: Simulated Manganese Transport Results for Year 30 in Model Layer 4
Figure 10.10-1	TOC Half-Life Sensitivity: Simulated Hexavalent Chromium Transport Results for Year 10 in Model Layer 2
Figure 10.10-2	TOC Half-Life Sensitivity: Simulated Hexavalent Chromium Transport Results for Year 10 in Model Layer 4
Figure 10.10-3	TOC Half-Life Sensitivity: Simulated Hexavalent Chromium Transport Results for Year 30 in Model Layer 2
Figure 10.10-4	TOC Half-Life Sensitivity: Simulated Hexavalent Chromium Transport Results for Year 30 in Model Layer 4
Figure 10.10-5	TOC Half-Life Sensitivity: Simulated Manganese Transport Results for Year 10 in Model Layer 2

Figure 10.10-6	TOC Half-Life Sensitivity: Simulated Manganese Transport Results for Year 10 in Model Layer 4
Figure 10.10-7	TOC Half-Life Sensitivity: Simulated Manganese Transport Results for Year 30 in Model Layer 2
Figure 10.10-8	TOC Half-Life Sensitivity: Simulated Manganese Transport Results for Year 30 in Model Layer 4
Figure 10.11-1	NTH IRZ Rate Sensitivity: Simulated Hexavalent Chromium Transport Results for Year 10 in Model Layer 2
Figure 10.11-2	NTH IRZ Rate Sensitivity: Simulated Hexavalent Chromium Transport Results for Year 10 in Model Layer 4
Figure 10.11-3	NTH IRZ Rate Sensitivity: Simulated Hexavalent Chromium Transport Results for Year 30 in Model Layer 2
Figure 10.11-4	NTH IRZ Rate Sensitivity: Simulated Hexavalent Chromium Transport Results for Year 30 in Model Layer 4
Figure 10.11-5	NTH IRZ Rate Sensitivity: Simulated Manganese Transport Results for Year 10 in Model Layer 2
Figure 10.11-6	NTH IRZ Rate Sensitivity: Simulated Manganese Transport Results for Year 10 in Model Layer 4
Figure 10.11-7	NTH IRZ Rate Sensitivity: Simulated Manganese Transport Results for Year 30 in Model Layer 2
Figure 10.11-8	NTH IRZ Rate Sensitivity: Simulated Manganese Transport Results for Year 30 in Model Layer 4
Figure 10.12-1	Freshwater Injection Rate Sensitivity: Simulated Hexavalent Chromium Transport Results for Year 10 in Model Layer 2
Figure 10.12-2	Freshwater Injection Rate Sensitivity: Simulated Hexavalent Chromium Transport Results for Year 10 in Model Layer 4
Figure 10.12-3	Freshwater Injection Rate Sensitivity: Simulated Hexavalent Chromium Transport Results for Year 30 in Model Layer 2
Figure 10.12-4	Freshwater Injection Rate Sensitivity: Simulated Hexavalent Chromium Transport Results for Year 30 in Model Layer 4
Figure 10.12-5	Freshwater Injection Rate Sensitivity: Simulated Manganese Transport Results for Year 10 in Model Layer 2
Figure 10.12-6	Freshwater Injection Rate Sensitivity: Simulated Manganese Transport Results for Year 10 in Model Layer 4
Figure 10.12-7	Freshwater Injection Rate Sensitivity: Simulated Manganese Transport Results for Year 30 in Model Layer 2

Figure 10.12-8	Freshwater Injection Rate Sensitivity: Simulated Manganese Transport Results for Year 30 in Model Layer 4
Figure 10.13-1	Intermediate Recirculation Loop Sensitivity: Simulated Hexavalent Chromium Transport Results for Year 30 in Model Layer 2
Figure 10.13-2	Intermediate Recirculation Loop Sensitivity: Simulated Hexavalent Chromium Transport Results for Year 30 in Model Layer 4
Figure 10.13-3	Intermediate Recirculation Loop Sensitivity: Simulated Manganese Transport Results for Year 30 in Model Layer 2
Figure 10.13-4	Intermediate Recirculation Loop Sensitivity: Simulated Manganese Transport Results for Year 30 in Model Layer 4
Figure 10.13-5	Intermediate Recirculation Loop Sensitivity: Simulated Arsenic Transport Results for Year 30 in Model Layer 2
Figure 10.13-6	Intermediate Recirculation Loop Sensitivity: Simulated Arsenic Transport Results for Year 30 in Model Layer 4
Figure 10.14-1	4.5 Year IRL TOC Injection Sensitivity: Simulated Hexavalent Chromium Transport Results for Year 5 in Model Layer 2
Figure 10.14-2	4.5 Year IRL TOC Injection Sensitivity: Simulated Hexavalent Chromium Transport Results for Year 5 in Model Layer 4
Figure 10.14-3	4.5 Year IRL TOC Injection Sensitivity: Simulated Hexavalent Chromium Transport Results for Year 10 in Model Layer 2
Figure 10.14-4	4.5 Year IRL TOC Injection Sensitivity: Simulated Hexavalent Chromium Transport Results for Year 10 in Model Layer 4
Figure 10.14-5	4.5 Year IRL TOC Injection Sensitivity: Simulated Manganese Transport Results for Year 5 in Model Layer 2
Figure 10.14-6	4.5 Year IRL TOC Injection Sensitivity: Simulated Manganese Transport Results for Year 5 in Model Layer 4
Figure 10.14-7	4.5 Year IRLTOC Injection Sensitivity: Simulated Manganese Transport Results for Year 10 in Model Layer 2
Figure 10.14-8	4.5 Year IRLTOC Injection Sensitivity: Simulated Manganese Transport Results for Year 10 in Model Layer 4
Figure 10.15-1	TOC/Hexavalent Chromium Trigger Sensitivity: Simulated Hexavalent Chromium Transport Results for Year 10 in Model Layer 2
Figure 10.15-2	TOC/Hexavalent Chromium Trigger Sensitivity: Simulated Hexavalent Chromium Transport Results for Year 10 in Model Layer 4
Figure 10.15-3	TOC/Hexavalent Chromium Trigger Sensitivity: Simulated Hexavalent Chromium Transport Results for Year 30 in Model Layer 2

Figure 10.15-4 TOC/Hexavalent Chromium Trigger Sensitivity: Simulated Hexavalent Chromium Transport Results for Year 30 in Model Layer 4

## Acronyms and Abbreviations

amsl	above mean sea level
Appendix B	Appendix B: Development of Groundwater Flow, Geochemical, and Solute Transport Models
bgs	below ground surface
CMS/FS	Corrective Measures Study/Feasibility Study
Cr(III)	trivalent chromium
Cr(VI)	hexavalent chromium
CSM	conceptual site model
ft <sup>2</sup>	square feet
ft <sup>3</sup>	cubic feet
ft/ft	foot per foot
Floodplain ISPT Final Completion Report	Floodplain Reductive Zone In-Situ Pilot Test Final Completion Report
gpm	gallons per minute
IM	interim measure
IRL	Inner Recirculation Loop
IRZ	in-site reactive zone
ISPT	in-situ pilot test
kg/day	kilograms per day
L/kg	liters per kilogram

m <sup>2</sup> /g	square meters per gram
mg	milligram
mg/kg	milligrams per kilogram
mg/L	milligrams per liter
MTC	mass transfer coefficient
mV	millivolt
ng/L	nanograms per liter
NTH	National Trails Highway
OPR	oxidation-reduction potential
PG&E	Pacific Gas and Electric Company
redox	oxidation-reduction
SCM	surface complexation model
TCS	Topock Compressor Station
TDS	total dissolved solid
TOC	total organic carbon
µg/L	micrograms per liter
USEPA	United States Environmental Protection Agency



## **1. Introduction and Objectives**

### **1.1 Introduction**

Pacific Gas and Electric Company (PG&E) is actively pursuing a strategy to remediate the hexavalent chromium [Cr(VI)] in groundwater resulting from historical operations at the Topock Compressor Station (TCS) and immediate surrounding area (herein referred to as the Site) located in eastern San Bernardino County approximately 12 miles southeast of the City of Needles, California. The TCS is approximately 1,500 feet west of the Colorado River and ½ mile west of Topock, Arizona. This Appendix B: Development of Groundwater Flow, Geochemical, and Solute Transport Models (Appendix B) documents the groundwater flow and solute transport model that was generated for the Site.

### **1.2 Study Objectives and Scope**

The objectives of this modeling study were to develop a groundwater flow and solute transport model for use as follows:

- evaluate subsurface flow conditions
- evaluate the fate and transport of Cr(VI)
- evaluate fate and transport of manganese and arsenic
- evaluate potential remedial system configurations

This appendix describes the results of six major components of the modeling study at the Site:

- updates to the groundwater flow model
- development of a groundwater flow submodel
- development of a geochemical model
- solute transport model development
- development of a hyporheic zone model for manganese
- remediation system analysis

The above components are presented in the following sections of this Appendix B:



## **Appendix B: Development of Groundwater Flow, Geochemical, and Solute Transport Models**

Topock Compressor Station  
Needles, California

- Section 2 – Conceptual Site Model (CSM)
- Section 3 – In-Situ Pilot Scale Studies and Design Implications
- Section 4 – Groundwater Flow Model Development
- Section 5 – Geochemical Model Development
- Section 6 – Solute Transport Model Development
- Section 7 – Solute Transport Model Results
- Section 8 – Manganese Hyporheic Zone Model Results
- Section 9 – Geochemical Reactive Transport Model Results and Sensitivity Analysis
- Section 10 – Solute Transport Model Sensitivity Analysis

## **2. Conceptual Site Model**

A CSM is a description of an understanding of a system. With regard to hydrogeology and associated geochemistry, such a conceptual model describes an understanding of the physical, biological, and chemical systems at a site by using a basic framework of Source-Pathway-Receptor. Thus, a CSM describes how contaminants enter an environmental system (source), migrate within it (pathway), and eventually reach their ultimate fate in terms of potential exposure to humans and other environmental receptors (receptor). For the Site, the conceptual model forms the single most important guide for the design and operation of the proposed remediation system, as it is the basis for the numeric modeling, comprised of groundwater flow and contaminant fate and transport that simulate the operation of the remediation system.

The conceptual model for the Site includes both the conceptual hydrogeologic/groundwater component and the contaminant fate and transport component. The conceptual model for groundwater flow herein is a narrative description of the principal components of the groundwater flow system developed from regional, local, and site-specific data. The primary components of the groundwater flow system include: (1) areal extent, configuration, and types of aquifers and aquitards; (2) hydraulic properties of aquifers and aquitards; (3) natural groundwater recharge and discharge zones; (4) anthropogenic influence on groundwater (sources and sinks); and (5) areal and vertical distribution of groundwater hydraulic head potential. These aquifer system components serve as the framework for the construction of the numerical groundwater flow model (described in Section 4). Sections 2.1 and 2.2, below, describe the regional and Site hydrogeology, respectively, and are taken from earlier investigation reports.

The conceptual model for contaminant fate and transport is provided in Sections 2.3 and 2.4, which provide updated information regarding the Site geochemistry and geochemical conceptual model of the selected remedy, respectively.

### **2.1 Regional Geologic Framework**

The Site is situated in a basin-and-range geologic environment in the Mohave Valley. The Colorado River is the main source of water to this groundwater basin, but at the southern end where the Site is located, groundwater is fed by a relatively modest amount of local recharge from mountain runoff. The most prominent geologic structural feature in the area of the Site is a Miocene-age, low-angle normal fault (referred to as a detachment fault) that forms the northern boundary of the Chemehuevi Mountains that are located to the southeast of the Site. The surface expression of the Chemehuevi detachment fault is evident as a pronounced northeast-southwest linear feature that can be traced along the northern boundary of the Chemehuevi Mountains, terminating at the abrupt bend in the Colorado River east of the TCS. The exposed Chemehuevi Mountains are Precambrian- and Mesozoic-age metamorphic and igneous rocks formed by tectonic uplift along the present-day trace of the Chemehuevi detachment fault.

Sedimentary deposits in the area are comprised of Pliocene lacustrine deposits, Tertiary- and Quaternary-age to recent alluvial fan deposits, and fluvial deposits of the Colorado River. The younger Colorado River fluvial deposits occur at the Site within the saturated zone underlying the floodplain, the present river channel, and the associated marsh area (Metzger and Loeltz 1973; Howard et al. 1997).

## **2.2 Site Hydrogeology and Groundwater Occurrence**

The Site is located at the southern (downstream) end of the Mohave Valley groundwater basin. On a regional scale, groundwater in the northern and central area of the valley is recharged primarily by the Colorado River, while under natural conditions net groundwater discharges occurs in the southern area, above where the alluvial aquifer thins near the entrance to Topock Gorge. The groundwater directly beneath the Site is derived mostly from the relatively small recharge from the nearby mountains. Under natural conditions, groundwater flows from west/southwest to east/northeast across the Site.

The Colorado River is 1,500 feet east of the TCS with a mean elevation of approximately 450 feet above mean sea level (amsl). The TCS is at an elevation of approximately 600 feet amsl on an extensive alluvial terrace that is locally incised by erosional channels formed by surface runoff. Thus, the surface slope is generally toward the river from areas west of the river. Bat Cave Wash, a large north-south erosional channel adjacent to the TCS, only has surface-water flow after large precipitation events. The stretch of the Colorado River east of the Site is 600 to 700 feet wide. Flow in the river fluctuates daily and seasonally due to upstream-regulated water releases by the Bureau of Reclamation at Davis Dam on Lake Mohave. Measured flows range from 4,000 to 25,000 cubic feet per second, and river levels fluctuate between 2 and 3 feet within a single day, depending on the time of year.

Groundwater occurs in the Tertiary-age and younger alluvial fan and fluvial deposits. These deposits are unconsolidated alluvial and fluvial deposits and are underlain by the Miocene-age conglomerate, which is consolidated, and pre-Tertiary-age metamorphic and igneous rocks. Both the conglomerate and igneous/metamorphic units are considered to be bedrock at the Site. The bedrock typically has lower permeability; therefore groundwater movement occurs primarily in the overlying unconsolidated deposits. There is no evidence to indicate any sizable potential for development of groundwater in the bedrock, although locally, small yields may be developed from fractures (Metzger and Loeltz 1973).

This conceptual framework for the bedrock system is supported by recent investigation work in the East Ravine and TCS areas. Of the 17 boreholes that have been drilled into appreciable depths within the bedrock in the East Ravine and TCS areas, only two boreholes, MW-57-185 and MW-70BR-225 (which are both located in close proximity to the approximate bedrock/alluvial aquifer contact at elevation 455 feet amsl), have yielded enough groundwater to sustain pumping for relatively low-volume hydraulic testing. During the test at MW-57-185 (pumped at approximately 3 gallons per minute [gpm] for 7 hours), approximately 78 feet of drawdown was observed within the pumping well, while drawdown of more than

0.05 foot was observed in only one of the seven observation wells (MW-58BR, 0.07 foot). Drawdown in the other six bedrock observation wells was less than 0.05 foot. During the test at MW-70BR-225 (pumped at approximately 9 gpm for 12 hours), approximately 34 feet of drawdown was observed in the pumping well, while drawdown of more than 0.05 foot was observed in only one of the 10 bedrock observation wells (MW-58BR, 0.18 foot).<sup>1</sup> Drawdown in the other nine bedrock observation wells was less than 0.05 foot. During both tests, the yield from the bedrock was insufficient to induce measurable drawdown in wells screened within the unconsolidated alluvial sediments. All other Site bedrock monitoring wells yield very small quantities of groundwater, with several that have become dewatered during routine sampling. These data are consistent with the regional hydrogeology.

The alluvial aquifer within the groundwater basin and beneath the Site consists of: (1) unconsolidated alluvial sands and gravels shed from local mountain ranges that ring the valley and (2) unconsolidated fluvial material deposited by the Colorado River. Groundwater occurs under unconfined to semi-confined conditions within the alluvial and fluvial sediments beneath most of the Site. The alluvial sediments consist primarily of silty sand and gravel deposits (with a relatively minor amount of clay) interfingered with more permeable sand and gravel deposits. The alluvial deposits exhibit an expected considerable variability in hydraulic conductivity between fine- and coarse-grained sequences. The fluvial sediments similarly consist of interbedded sand, sandy gravel, and silt/clay.

The water table in the alluvial aquifer is nearly flat and typically equilibrates to an elevation within 2 to 3 feet of the river level. Due to the variable topography, the depth to groundwater ranges from as shallow as 5 feet below ground surface (bgs) in the floodplain near the river to approximately 170 feet bgs in the upland alluvial terrace areas. The saturated thickness of the alluvial aquifer is approximately 100 feet in the floodplain and thins to the south, pinching out along locations where the Miocene Conglomerate and igneous/metamorphic rocks outcrop. In the western and northern portions of the Site, where the depth to bedrock increases, the saturated thickness of the alluvial aquifer is over 200 feet.

Several other important hydrogeologic features of the Site are summarized below:

- Under ambient conditions in the vicinity of the Site, the Colorado River recharges groundwater during the higher-flow stages in the spring and summer months, and discharges groundwater to the river during the months of lower river stages in fall and winter. Since 2004, the Interim Measure (IM) groundwater extraction and treatment system has maintained a consistent, year-round landward gradient in the area where the plume is present in the floodplain (i.e., maintains a situation where the river discharges to groundwater). The hydraulic gradient imposed by IM-3 pumping is measured in

---

<sup>1</sup> This excludes drawdown observed in the water-table well adjacent to pumping well (MW-70-105), which showed a dewatering trend during the test.

three pairs of monitoring wells. Over the period from August 2007 through December 2011, the average landward gradient in these three well pairs was approximately 0.005 foot per foot (ft/ft).

- Under natural conditions, groundwater flow is generally from the west-southwest to east-northeast across the Site. Localized areas of northward flow likely occur along the mountain front to the south of the TCS. Hydraulic gradients are very small due to the limited recharge, with a typical value of 0.0005 ft/ft in the alluvial area. Under average conditions, groundwater velocity in the alluvial aquifer ranges from approximately 25 to 46 feet per year, according to numerical model estimates. The vertical component of the hydraulic gradient is upward between bedrock and the overlying alluvial aquifer and typically, but not universally, upward within the alluvial aquifer.
- Groundwater level monitoring in the East Ravine area indicates that the groundwater in fractured bedrock is in hydraulic communication with the alluvial aquifer and equilibrates to an approximate elevation similar to the water table in the alluvial aquifer. Compared to the alluvial aquifer, the fractured rock permeabilities are very low, based on well tests in this area.

### **2.3 Site Geochemistry**

The unconsolidated aquifer consists of alluvial sands and gravels derived primarily from the metadiorite and gneissic rocks from the mountains that ring the groundwater basin, as well as fluvial material deposited by the Colorado River over time. These materials govern the observed groundwater geochemistry at the Site. A detailed description of the general groundwater quality and geochemistry at the Site can be found in the RCRA Facility Investigation/Remedial Investigation Report (CH2M HILL 2009a); a brief summary is provided herein.

The groundwater at the Site is a sodium chloride-dominated type with a highly variable total dissolved solid (TDS), varying from below 1,000 milligrams per liter (mg/L) in shallow zones and increasing to greater than 10,000 mg/L in some areas, generally increasing with depth. The groundwater is near neutral pH and slightly alkaline. Alkalinity and pH at the site are also somewhat variable at the Site, with pH generally ranging between 7 and 8.5 and alkalinity generally ranging between 30 and 300 mg/L as calcium carbonate (although values as high as 800 to 1,000 mg/L have been measured in some areas).

Although the alluvial fan and fluvial deposits are of different origin, groundwater flows from the alluvial fan sediments into the fluvial zone sediments; therefore, the groundwater geochemistry in the fluvial zone is strongly influenced by alluvial groundwater geochemistry. One important difference between alluvial and fluvial zones is the presence of a reducing environment in shallow and mid-depth fluvial zones located within the Colorado River floodplain, caused by organic material deposited with the sediment. This reducing zone is characterized by generally lower levels of oxidation-reduction potential (ORP). Alluvial fan zones at the Site tend to exhibit ORP levels in the 0 to 300 millivolt (mV) range, while groundwater in the floodplain “reducing rind” fluvial aquifer can exhibit values in the -220 to -90 mV range, sufficiently reducing for Cr(VI)

reduction. This reducing rind exists in the shallow portion of the fluvial aquifer, extending 200 to 500 feet away from the riverbank, generally getting thicker (i.e., penetrating deeper) with proximity to the river. The reducing rind correlates with decreases in nitrate concentrations, which vary considerably across the site from less than 1 mg/L to greater than 20 mg/L  $\text{NO}_3\text{-N}$  in the alluvial aquifer, to non-detect in most areas of the reducing rind. Higher dissolved concentrations of manganese, iron, and organic carbon in the floodplain are also consistent with the more strongly reducing environment resulting from organic deposition (greater than 5 mg/L manganese and greater than 10 mg/L iron in some monitoring wells). These higher concentrations of manganese and iron are due to the reductive dissolution of naturally occurring iron and manganese oxides present within the floodplain.

The boundary of this reducing rind is defined herein using multiple geochemical oxidation-reduction (redox) indicators, including dissolved iron, organic carbon, and ORP. Generally, ORP is not as reliable an indicator of reducing conditions as the direct measurement of the concentration of redox couples. The determination of ORP is based upon field electrode measurements, and these are more likely to be subject to measurement error than measurement of concentrations of redox indicators, such as iron and manganese. A cutoff of -90 mV is used herein as a flag to determine where conditions are likely not sufficient for sustained  $\text{Cr(VI)}$  reduction. Thus, this ORP value was used to delineate the reducing rind boundary in the fluvial aquifer. This criterion yields the reducing rind boundaries for model layers 1, 2, 3, and 4 in regions where these model layers pass through the fluvial aquifer, as described in Section 6.4 (Figure 6.4-2).

In contrast, ORP values below -90 mV were not assumed to be sufficient for delineating the reducing rind outside of the fluvial aquifer. Specifically, although ORP values below -90 mV were observed in alluvial wells lining the riverbank, the reducing rind was assumed to stop at the boundary between fluvial and alluvial aquifers (see Section 6.4, Figure 6.4-3). This is based on the observation that the alluvial aquifer does not exhibit the same levels of organic carbon and dissolved iron as the fluvial aquifer. Figure 2.3-1 shows correlation plots for total organic carbon (TOC) and dissolved iron with ORP for monitoring wells bordering the riverbank along the Site. To capture current conditions, dissolved iron and TOC values represent averages of data collected between 2009 and 2011 (TOC values represent averages extending before 2009 in some cases due to a limitation of data). The data demonstrate that ORP is highly variable in both alluvial and fluvial zones. Within the fluvial zones, iron and organic carbon concentrations are variable, as expected, due to natural variability in the distribution of deposited materials. However, iron and carbon concentrations within the alluvial zone are lower as a whole, supporting the fact that the fluvial aquifer is more actively reducing than the alluvial aquifer despite low ORP values.

## **2.4 Geochemical Conceptual Model of the Selected Remedy**

The in-situ reactive zone (IRZ) technology proposed as a component of the design remedy involves the biologically mediated reduction and precipitation of  $\text{Cr(VI)}$ . Specifically, this involves the stimulation of native microorganisms through the delivery of a degradable source of organic carbon, providing an electron donor

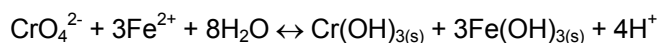
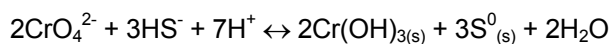


for microbial growth. The goal of this process is to provide a sufficient quantity of electron donors to overcome the aquifer's supply of aerobic electron acceptors (primarily oxygen and nitrate), such that Cr(VI) will be reduced by microbes (i.e., used as an electron acceptor). Whereas Cr(VI) is highly soluble (present in solution at neutral pH as the chromate anion,  $\text{CrO}_4^{2-}$ ), chromium reduced to its trivalent form [Cr(III)] is relatively insoluble and precipitates out of solution as Cr(III)-hydroxide and mixed metal-hydroxide phases.

The electron acceptors utilized via microbial respiration in a reductive IRZ will follow a sequence governed by equilibrium thermodynamics. This sequence is illustrated schematically on Figure 2.4-1. Oxygen is predicted to be the first electron acceptor consumed, because the reduction of  $\text{O}_2$  to  $\text{H}_2\text{O}$  is thermodynamically the more favorable reaction. As oxygen is consumed, other electron acceptors will, in turn, be utilized based on their thermodynamic favorability. In groundwater at the Site, nitrate is predicted to be consumed after oxygen, followed by chromate. Note that the reduction of chromate is thermodynamically more favorable than the reduction of Mn(III/IV), Fe(III), and  $\text{SO}_4^{2-}$  [S(VI)]; therefore, it is not theoretically necessary to achieve manganese-, iron-, or sulfate-reducing conditions in order to reduce Cr(VI).

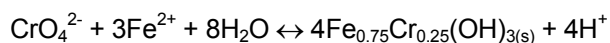
In practice, although thermodynamic favorability will tend to drive the order in which electron acceptors are utilized, kinetic factors and spatial heterogeneity within the aquifer also play a role, particularly for solid-phase electron acceptors. As such, many of these redox reactions can occur simultaneously. For example, although reduction of Mn(III/IV) to Mn(II) is thermodynamically more favorable than Fe(III) reduction, microbes may reduce Fe(III)-oxides before all of the Mn(III/IV)-oxides are depleted from a system because the reduction of Mn(III/IV)-oxides is kinetically limited and the oxides may be variably distributed within the aquifer down to the pore scale. Similarly, sulfate reduction can also occur before depletion of Fe(III)-oxides if the strength of the reducing environment is sufficient. The goal within the IRZ is to make the reducing environment strong enough that the desired reduction reactions are achieved, without making it so strong as to drive unnecessary or undesirable reduction reactions that may generate byproducts (discussed below).

Although they are not strictly necessary to achieve Cr(VI) reduction, some iron and sulfate reduction is beneficial to the Cr(VI) reduction process. The reduction of naturally occurring iron and sulfate creates ferrous iron [Fe(II)] and sulfide ( $\text{H}_2\text{S}$ ,  $\text{HS}^-$ ) that can react abiotically with Cr(VI), thereby enhancing Cr(VI) reduction by the following reactions:



Furthermore, Cr(VI) can also react with  $\text{Fe}^{2+}$  to form a mixed iron-chromium hydroxide that is considerably less soluble and more stable than pure chromium hydroxide (Sass and Rai 1987; Eary and Rai 1987), as follows:





These reactions are illustrated for aqueous ferrous iron and sulfide species, but they can also occur between aqueous Cr(VI) and solid-phase Fe(II) and sulfide phases. In the case of iron, this includes adsorbed Fe(II), mixed-valence iron oxides, such as magnetite and green rust, and iron sulfides/carbonates. These phases are beneficial because they help to provide immobile, stored reductive capacity between organic carbon injection events. After an injection event has been completed and the injected organic carbon has been consumed by microbes, Cr(VI) reduction will continue to occur over long periods via abiotic reactions (reduction by ferrous iron and sulfide phases) and biotic reactions (cell lysis and consumption of secondary organic matter). Thus, it is important to note that although iron and sulfate can be seen as “competing” electron acceptors with respect to Cr(VI), they in fact store reduction capacity that can eventually react biotically and abiotically with Cr(VI), dissolved oxygen, and nitrate. In practice, however, an attempt will be made to minimize sulfate reduction in order to prevent the release of barium (discussed below).

These reduction reactions can also temporarily mobilize certain naturally occurring metals within the treatment zone, including iron, manganese, arsenic, and potentially barium. These secondary byproducts are important to acknowledge, and can be successfully managed during system operation. Reduction of Mn(III/IV)-oxides generates Mn(II). Although more soluble in the reduced form, the concentration and mobility of Mn(II) in solution will be limited by adsorption to mineral surfaces and precipitation of  $\text{MnCO}_3$  (rhodochrosite). Abiotic and biotic reoxidation of Mn(II) will also occur in the presence of dissolved oxygen. Arsenic, which is predominantly present in soil sorbed to and coprecipitated with iron oxides, is released during the reductive dissolution of iron. As ferrous iron is transported downgradient and reoxidizes outside of the IRZ footprint, arsenic will again be taken up via sorption and coprecipitation. Barium, which may be largely present in the soil as barite ( $\text{BaSO}_4$ ), can be released during sulfate reduction. The release of barium during IRZ operations is, therefore, best controlled by limiting the strength of the reducing environment (i.e., limiting the amount of sulfate reduction that occurs). Additional details on the anticipated chemistry that will occur within the IRZ can be found in Appendix G of the Corrective Measures Study/Feasibility Study Report for Chromium in Groundwater (CMS/FS) (CH2M HILL 2009b).

The site-wide solute transport model described in Section 6 attempts to capture the most important processes involved in Cr(VI) removal in the presence of added TOC, byproduct generation, and byproduct attenuation. It was not possible to capture all of the different redox reactions described above within the solute transport model, but geochemical models (described in Section 5) were developed that do capture many of these processes to aid in parameter estimation and validation of the solute transport model. Empirical relationships were also developed using data collected during the in-situ pilot tests (ISPTs), as described in the Section 3. Together, these results demonstrate that the solute transport model adequately captures the processes governing Cr(VI) treatment and byproduct dynamics within and downgradient of the IRZ.

### **3. In-Situ Pilot Scale Studies and Design Implications**

#### **3.1 Floodplain Pilot Test Overview**

A reductive ISPT was conducted in the floodplain from January 2006 to July 2007. The objective of the floodplain ISPT was to test the effectiveness of organic carbon injection on the in-situ reductive precipitation of Cr(VI) in a field setting. The pilot test well array consisted of one injection well cluster screened in shallow, middle, and deep intervals (PTI-1S/M/D) and six three-level monitoring well nests (PT-1S/M/D through PT-6S/M/D), located radially outward within approximately 20 to 50 feet of the injection well. Six injections of organic carbon-amended solution (6,000 to 18,000 gallons per event) were performed between May 2006 and July 2007, primarily into the deep injection well where Cr(VI) concentrations were highest. The injection solutions were amended with lactate, yeast extract, and non-reactive tracers, with TOC concentrations between 250 and 2,000 mg/L carbon. IM-3 pumping activities resulted in the westward movement of the injectate towards wells TW-2D and TW-3D, such that the greatest impacts of the treatment were observed in wells PT-1 and PT-2, located approximately 25 and 50 feet east and downgradient of the injection well, respectively. Additional details on the setup, execution, and results of the floodplain ISPT can be found in the Floodplain Reductive Zone In-Situ Pilot Test Final Completion Report (Floodplain ISPT Final Completion Report) (ARCADIS 2008), which provides monitoring results for 4 months following the final injection. Post-pilot monitoring has continued to date and is reported annually.

The results of the floodplain ISPT indicated that Cr(VI) was successfully reduced from concentrations of greater than 3,000 micrograms per liter ( $\mu\text{g/L}$ ) to less than 0.2  $\mu\text{g/L}$  as a result of microbial stimulation by lactate. Cr(VI) reduction resulted in the formation and precipitation of Cr(III) to dissolved concentrations of less than 1  $\mu\text{g/L}$ . Other important observations from the floodplain ISPT are as follows:

- Reductions in Cr(VI) concentration to below 0.2  $\mu\text{g/L}$  were observed after sustained delivery of a sufficient amount of TOC.
- The reduction of Cr(VI) was sustained between injections in the absence of injected tracer and TOC. Continued monitoring through February 2012 indicated sustained Cr(VI) concentrations below 0.2  $\mu\text{g/L}$  in wells PT-1D and PT-2D 4 years after the last injection event.
- Lactate degradation rates were calculated based on a comparison of TOC and tracer concentrations at monitoring wells. First-order lactate degradation half-lives over the six injection events ranged between approximately 4 and 30 days, with the range likely reflecting differences in microbial activity as a function of time between injection events.
- Reduction of lactate in the ISPT resulted in the mobilization of the secondary byproducts iron, manganese, and arsenic. Manganese concentrations reached a maximum value of 10,600  $\mu\text{g/L}$ , observed in PT-1D following the fourth injection event, and iron reached a maximum concentration of

2,260  $\mu\text{g/L}$  in PT-2D following the sixth event. The lag in aqueous iron increase relative to manganese was believed to be due to greater sorption of Fe(II), formation of Fe(II) phases (e.g., magnetite and pyrite), and consumption of Fe(II) by residual oxidants [e.g., oxygen, Cr(VI)].

- Dissolved arsenic concentrations increased (maximum of 20.8  $\mu\text{g/L}$ ) due to the reductive dissolution of iron oxide minerals, releasing arsenic that had been sorbed and/or coprecipitated with these minerals. Comparison of PT-1D and PT-2D results during injection events 1 to 4 indicate rapid attenuation of arsenic downgradient of the reductive zone, and these results were used to determine the arsenic attenuation rate (described below).

### **3.2 Upland Pilot Test Overview**

A second ISPT was conducted in the upland between April 2007 (start of well installation) and December 2008. The objectives of this second ISPT were to test a recirculation well system for distribution of organic carbon and to test ethanol as a carbon substrate. Reagent recirculation ran continuously between March and December 2008, with injection activities in two recirculation wells (PTR-1 and PTR-2), placed approximately 140 feet apart, perpendicular to the groundwater flow direction. Each recirculation well was screened at two depth intervals, allowing for simultaneous injection and extraction at each well in a transverse dipole configuration. The system was operated at recirculation rates between 15 and 30 gpm at each well. Forty percent ethanol was added to each recirculation well at dose rates of 95 gallons per day and lower. Although the target TOC concentration was 400 mg/L, TOC concentrations as high as 12,900 mg/L were observed in monitoring well MW-24A (approximately 15 feet from PTR-2) resulting from vertical short-circuiting of ethanol between injection and extraction intervals in the same recirculation well. Important observations from the upland ISPT are as follows:

- Injection of ethanol as a carbon substrate was successful in reducing dissolved Cr(VI) concentrations. Monitoring wells located in zones where organic carbon distribution was the most successful (particularly PT-7M, PT-7D, PT-8S, and MW-24A) saw reductions in Cr(VI) concentrations from as high as 7,260  $\mu\text{g/L}$  to less than 0.2  $\mu\text{g/L}$ .
- Horizontal distribution of tracer was complicated by vertical “short-circuiting” of the recirculation wells (i.e., a significant portion of amended water traveled vertically from the injection well screen to the extraction well screen). This effect was more pronounced in PTR-1 than PTR-2. Attempts to optimize the recirculation hydraulics during operation were somewhat successful in reducing short-circuiting and enhancing reagent distribution between wells.
- As observed in the floodplain ISPT, the establishment of actively reducing conditions resulted in the release of the secondary byproducts iron, manganese, and arsenic. Given the much higher localized concentrations of organic carbon in the upland ISPT due to vertical short-circuiting, concentrations of these byproducts were correspondingly higher; as high as 97.4  $\mu\text{g/L}$  for arsenic, 21,400  $\mu\text{g/L}$  for

manganese, and 11,200 µg/L for iron. These results demonstrate that byproduct generation is directly related to the strength of the reducing environment created. The reducing environment can be adjusted to minimize byproduct liberation without negatively impacting Cr(VI) reduction by properly controlling organic carbon dosing and distribution.

- Increases in dissolved barium were observed in zones that received the highest concentrations of TOC, with barium concentrations as high as 2,800 µg/L observed in PT-7D the year following the ISPT (collection of barium data began in August 2009). Of the four wells that exhibited the highest barium increases (PT-7M, PT-7D, PT-8S, and MW-24A), the observed barium concentrations correlated with the level of sustained TOC concentration over the course of the pilot test. PT-7D (sustained TOC of 8,000 to 10,000 mg/L) exhibited the highest barium concentration of 2,800 µg/L. MW-24A had one measured TOC concentration of 12,000 mg/L, but all other values were below 6,000 mg/L; observed barium concentrations in this well exhibited a peak of 229 µg/L. These results suggest that barium concentrations can be limited if the strength of the reducing environment (as established by the TOC concentration) is controlled.

Additional details on the upland ISPT can be found in the Upland Reductive Zone In-Situ Pilot Test Final Completion Report (ARCADIS 2009).

### **3.3 Basis for Recirculation Design**

Several recirculation designs were presented in the CMS/FS (CH2M HILL 2009b) and considered for the National Trails Highway (NTH) IRZ, including the use of dual-screen wells (with injection and extraction intervals within a single well), alternating injection and extraction wells along the IRZ, and the configuration proposed herein (see Section 6.4.1), which includes injection wells along the IRZ line with minimal extraction wells. The third option was chosen here based on complexities that have been observed with the first two approaches.

Although dual-screened wells, such as those used in the uplands pilot test, can potentially enhance substrate distribution within the aquifer by inducing vertical and lateral gradients, in practice, it is difficult to operate such configurations without extracting organic carbon substrate or treated water and thus complicating system maintenance and potentially overloading carbon substrate into the subsurface. This effect was observed in the upland ISPT, where organic carbon was overloaded due to the use of dual-recirculation wells (see Section 3.2). As noted above, a portion of the organic carbon substrate injected into PTR-1 short-circuited vertically and was extracted by the extraction interval in the same location, thereby limiting the lateral distribution of substrate between recirculation wells and locally overloading carbon substrate.

The method of alternating injection and extraction wells, which has been implemented at the PG&E Hinkley Compressor Station site, has also proven difficult in practice. Experience in operating the Hinkley IRZ

system demonstrated that it was very difficult to distribute sufficient carbon to treat the space between injection and extraction wells without extracting substantial amounts of organic carbon and dissolved metals in treated groundwater in the extraction wells. The result was a discontinuous IRZ that produced fingers of treated water downgradient of the IRZ, interspersed with gaps where Cr(VI) was not treated. As a result, the Hinkley IRZ system was reconfigured to include injection wells along the IRZ line, with a minimal number of extraction wells placed along the line and at the ends of the line, similar to the design proposed for the Site. Although many of the IRZ wells at the Site will include multiple screen intervals, this will be to confirm a controlled injection of substrate at multiple depths, not to run the wells in simultaneous injection-extraction mode.

The currently proposed design includes continuous operation of injection wells along the IRZ, which will allow for significantly higher injection volumes and greater radii of influence than could be achieved with the point injection method that was applied during the floodplain ISPT. For comparison, an injection well in the proposed design that receives 20 gpm for a 6-month operational period will receive 5.2 million gallons of water, whereas PTI-1D received 60,000 gallons during the floodplain ISPT.

### **3.4 ISPT-Derived Solute Transport Model Parameters**

This section presents the basis for solute transport model parameters that were derived from the floodplain and upland ISPT results. Further details regarding development of the solute transport model and how the ISPT-derived parameters were applied to the model are provided in Section 6.

#### **3.4.1 Relationship between TOC Distribution and Cr(VI) Reduction**

The floodplain and upland ISPTs demonstrated that both lactate and ethanol are highly effective substrates for the stimulation of microbial growth, resulting in the development of a reducing environment suitable for the removal of Cr(VI) from solution. Based on past successes, level of experience, and cost effectiveness, ethanol was chosen as the carbon substrate for IRZ operation, although lactate and ethanol exhibited similar characteristics, including degradation rate (see below). In addition, other reagents will be considered during the IRZ operation depending on need and substrate costs.

Although the maximum concentrations of TOC utilized in the ISPTs were high, the test results indicate that effective Cr(VI) treatment can be achieved with relatively low TOC concentrations. For example, Cr(VI) concentrations decreased to below 5 µg/L in the floodplain ISPT (monitoring well PT-1D) within the first three of six injection events with observed TOC concentrations between 10 and 50 mg/L (Figure 3.4-1). These results also highlight the importance of a sustained TOC concentration to achieve Cr(VI) treatment, particularly within the first several weeks to months following startup. For the first TOC pulse, Cr(VI) concentrations dropped to approximately 1,000 µg/L, leveling off until the next injection event. Subsequent injections were sufficient to establish a sustained reducing environment due to the combination of an

established microbial community (including the active cycling of the solid-phase TOC pool) and stored reductive potential in the form of ferrous oxides and sulfides.

The solute transport model (described below; see Section 6) assumes Cr(VI) reduction in the presence of organic carbon above 0.1 mg/L. However, it is recognized that a higher concentration than this will initially be needed along the IRZ line in order to establish the microbial population and active reducing conditions. Specifically, a target injection TOC concentration must be chosen that is sufficient to achieve lateral distribution of organic carbon across the spaces in between injection wells, taking into account TOC degradation as it travels away from the injection wells. Based on the ISPT results summarized above, a sustained TOC concentration of between 10 and 50 mg/L will be sufficient to establish these conditions. The solute transport model outputs have been assessed at the weakest points of the IRZ located halfway between injection wells to confirm that this is the case (in practice, a slightly higher anticipated range of 15 to 50 mg/L will be used to confirm adequate TOC distribution and account for spatial heterogeneity across the screened interval of dose-response wells). Because the required concentration conditions will be achieved within the first active cycle of the remedy (within the first 6 to 9 months), it is not necessary to explicitly capture the kinetics of microbial community establishment within the solute transport model. Thus, in the model, the TOC concentration required to initiate Cr(VI) precipitation was increased to 10 mg/L (a 10-mg/L TOC trigger) for the initial cycle of TOC injection. After the initial 6 months of active TOC injection, the TOC trigger was reduced to 0.1 mg/L to represent the more established reducing environment that is generated by an extended period of active TOC injection. This TOC trigger development is analyzed in Section 7.4.

Although some monitoring well data collected during the floodplain and upland ISPTs appear to contradict these results, care must be taken to avoid confounding the results from monitoring wells located either on the periphery of the treatment zone (i.e., outside of the radius of influence) or in areas that did not achieve sufficient and sustained distribution of TOC. For example, TOC concentrations as high as 146 mg/L were observed in well PT-9S during the upland ISPT, nominally high enough to completely reduce Cr(VI), yet complete reduction of Cr(VI) was not observed. However, because this well is located on the downgradient and lateral edge of the treatment zone, it is likely that the high observed Cr(VI) concentrations resulted from the mixing of treated and untreated water within the well screen interval, as indicated by the low observed tracer concentration in comparison with the injected concentration. Likewise, due to the complexities of the TOC distribution encountered in the upland ISPT, sustained elevated TOC was not achieved in all monitoring wells located between the recirculation wells. For example, although TOC reached a maximum of 896 mg/L in PT-7S, the TOC and tracer results indicate that uniformly high concentrations were not sustained near this well for an extended period of time.

A similar argument may apply to the fact that a poor correlation was observed between ORP and TOC concentration in the pilot tests. Cases where high ORP was observed in the presence of TOC, particularly in the upland ISPT (e.g., PT-7S), were likely due to the mixing of treated and untreated water, as well as the time required for initial establishment of a reducing environment with an active microbial community. A poor



correlation was also observed in PTR-1; however, because PTR-1 was a recirculation well and not a monitoring well, this lack of correlation was due to mixing within the well and is not representative of aquifer conditions. In addition, ORP determination is based on field electrode measurements, which are subject to measurement error and are generally less reliable than direct measurement of redox couples. As such, redox couple concentrations should be used as a primary metric for redox conditions over ORP measurements.

#### 3.4.2 TOC Degradation Half-Life

Due to the very high TOC concentrations and the difficulties encountered in uniformly distributing organic carbon, it was not possible to calculate reliable degradation rates for ethanol from the upland ISPT results. Therefore, it is assumed that ethanol will have a degradation rate similar to that of lactate, which exhibited a half-life of between 4 and 30 days during the floodplain ISPT. This is a reasonable assumption based on data developed from the Hinkley site, where lactate and ethanol were used interchangeably under identical conditions and achieved comparable results. A half-life of 20 days was used in the solute transport modeling based on the test results for ethanol and lactate here and at the Hinkley site.

#### 3.4.3 Manganese and Arsenic Generation and Attenuation

The ISPT results demonstrated that the amount of byproducts (manganese, arsenic, iron, and barium) liberated within the IRZ are proportional to the strength of the reducing environment created by TOC injection, which, in turn, is proportional to the concentrations of TOC used. The correlation between byproduct concentration and organic carbon concentration was presented for multiple IRZ sites in Appendix G of the CMS/FS (CH2M HILL 2009b). The relationship between TOC and manganese concentration is shown in Figure G13 of Appendix G of the CMS/FS, while Figure G14 of the CMS/FS shows the relationship for TOC and arsenic.

In the solute transport model, these correlations are used as the basis for manganese and arsenic generation. Manganese and arsenic generation rates were calculated based on the average amount of byproduct observed in solution for TOC concentrations greater than 10 mg/L and less than 100 mg/L within the upland and floodplain ISPT datasets. This analysis yielded generation rates of 0.016 milligrams (mg) manganese per mg TOC and 0.000108 mg arsenic per mg TOC. These rates are implemented in the solute transport model by introducing byproduct as TOC is degraded; for example, for a given mass of TOC that is degraded within a given timestep, 0.016 times that mass of manganese is introduced into solution.

Attenuation of manganese occurs via sorption, reoxidation, and precipitation of  $\text{MnCO}_3$  (rhodochrosite). Precipitation of rhodochrosite can serve to limit the concentration of manganese generated within the reactive zone where alkalinity can be highest. Generally, rhodochrosite precipitation will be strongly controlled by precipitation kinetics and is difficult to model accurately. This reaction was ignored in the

geochemical and solute transport models because it would be captured in the manganese generation rate derived from field data.

Parameters for manganese sorption and reoxidation could not be accurately determined from the ISPT data available, due to the confounding effects of generation and attenuation between monitoring wells (i.e., attenuation parameters would be underestimated where generation is still occurring). Therefore, solute transport model parameters to account for these effects were derived from literature data, field parameters, and geochemical modeling. These results are described in Section 7.

Very strong arsenic attenuation was observed in the ISPTs, which was attributed to coprecipitation with ferrous iron that reoxidized more quickly than manganese outside of the TOC footprint. Given this observation, it was possible to derive an arsenic attenuation rate from the ISPT data for use in the solute transport model. Figure 3.4-2 shows arsenic concentration data in PT-1D and PT-2D through the first four injection events of the floodplain ISPT. The maximum concentration of arsenic observed in PT-1D was 11.2 µg/L. During this period (allowing for a 39-day travel time between PT-1D and PT-2D), arsenic concentrations observed in PT-2D remained below the detection limit of 5 µg/L. Tracer dilution between PT-1S and PT-2S was minimal (tracer was diluted in PT-2D to 85% of its PT-1D value). Based on these results, an arsenic attenuation half-life of between 20 and 40 days was calculated (base-case half-life assigned as 30 days), assuming a PT-2D arsenic concentration between 2.5 and 5 µg/L. This provides a minimum estimate of attenuation rate, because TOC is still degrading between PT-1D and PT-2D. For this reason, a similar procedure could not be used to obtain manganese sorption parameters.

#### 3.4.4 Mobile Porosity

Aquifer mobile porosity estimates were obtained from the floodplain ISPT during tracer injection. These results, which are described in detail and presented in Table 6 of the Floodplain ISPT Final Completion Report (ARCADIS 2008), indicate a mobile porosity of 12%.

### 3.5 Effects of Groundwater Geochemistry on Cr(VI) Treatment

#### 3.5.1 Competing Electron Acceptors

As discussed above, the injection of organic carbon to stimulate microbial reduction within the IRZ will result in electron transfer to multiple electron acceptors, including dissolved oxygen, nitrate, iron, manganese, and sulfate, in addition to Cr(VI). The electron acceptors utilized will depend on both thermodynamic favorability and the kinetics of reduction. Thermodynamic equilibrium arguments dictate that nitrate will be consumed before Cr(VI). However, depending on the strength of the reducing environment, iron and sulfate reduction can also occur and often do occur simultaneously with reduction of more favorable electron acceptors.



The ISPT results clearly illustrate that complete Cr(VI) reduction can be achieved in the presence of competing electron acceptors with relatively low concentrations of TOC. To illustrate this point, nitrate and sulfate concentrations observed in PT-1D during the first four floodplain ISPT injections are shown on Figure 3.4-1. TOC injections resulted in the near-complete reduction of nitrate within the first injection event, as anticipated. The reducing environment was sufficiently strong such that some sulfate reduction was also observed. Regardless, in the presence of 2.5 mg/L nitrate and nearly 1,000 mg/L sulfate, complete Cr(VI) reduction was observed by the fourth injection event. It is, therefore, apparent that the presence of competing electron acceptors did not inhibit the reduction of Cr(VI). The effect of competing electron acceptors was not explicitly considered in the solute transport model because TOC consumption by these electron acceptors is effectively included in the TOC degradation rate derived from field data in which the reduction of the various electron acceptors was occurring.

### 3.5.2 Total Dissolved Solids

The results of the upland and floodplain ISPTs suggest that successful Cr(VI) reduction can be achieved within a wide range of TDS contents relevant to the application of the remedy. The average TDS of the floodplain groundwater from 1997 to 2012 is approximately 7,200 mg/L. This average is similar to the TDS observed in monitoring well PT-1D during the floodplain ISPT, in which complete Cr(VI) reduction was observed (Figure 3.5-1). These results suggest that TDS levels representative of floodplain conditions will not adversely affect Cr(VI) reduction.

Complete reduction of Cr(VI) was also observed in upland ISPT wells over a range of TDS levels. Using sodium as a proxy, because TDS was not measured in the upland ISPT, Figure 3.5-1 shows that salt concentrations observed in wells PT-7D, PT-7M, and PT-8S spanned a range of -60% to +70% of the average concentration in PT-1D. This range in TDS did not have an apparent effect on Cr(VI) reduction. Similarly, it is not anticipated that any particular TDS component (e.g., sodium, chloride, calcium, sulfate) will have an adverse effect on Cr(VI) reduction. Accordingly, no dependence of organic carbon degradation or Cr(VI) reduction on TDS was included in the solute transport model.

#### **4. Groundwater Flow Model Development**

The groundwater flow model used in the CMS/FS (CH2M HILL 2009b) was calibrated in 2005. The details of the model design and calibration have been described in a previous report (CH2M HILL 2005b). The model was developed using MicroFEM (Hemker 2006), a finite element flow model code, and the domain extends several miles from the Site in all directions (Figure 4-1; CH2M HILL 2005b). The groundwater flow model was calibrated against: (a) long-term average groundwater levels, (b) average monthly floodplain water levels responding to fluctuating river levels, (c) short-term responses to pump testing events, and (d) plume development over time. The auto-calibration program PEST was employed to refine the calibration and to reduce effects of uncertainty in each calibration target. The PEST program addresses heterogeneity in the aquifer by establishing a variable hydraulic conductivity distribution across the groundwater flow model domain during the calibration process. Groundwater budget was developed from regional river gradient and estimates of precipitation recharge, subsurface inflow beneath major and minor washes, evapotranspiration, and subsurface outflow. The Colorado River acts as both a source and sink for groundwater flow, as does Topock Marsh. This water budget, as well as with aquifer parameters estimated from pumping tests and regional literature, form the basis of the hydrogeological understanding of the Site and its environs, and provide the framework for the solute transport model.

Some modifications were made to the 2005 model prior to the CMS to incorporate basic properties in the East Ravine area (CH2M HILL 2009b, Appendix E); and to support the design of the selected remedy, the regional flow model was further updated with lithologic and hydraulic data that had become available since the original calibration.

From the finite element flow model, a submodel was extracted and converted to MODFLOW to improve the resolution for solute transport modeling using MT3DMS. The submodel domain was selected to be able to model the full extent of the hexavalent chromium plume, as well as the proposed remedial elements. The relative model domains are depicted on Figure 4-1.

The groundwater flow model was then used to develop the solute transport submodel. The domain of the solute transport submodel was focused on the plume area to design the IRZ and to estimate concentrations of selected constituents over the duration of the remedy. The boundary conditions of the solute transport model were assigned using groundwater fluxes exported from the flow model. The hydraulic properties in the solute transport model are consistent with the flow model.

##### **4.1 Groundwater Flow Submodel Code Selection and Description**

The simulation program MODFLOW was selected for the construction of the numerical groundwater flow submodel at the Site. MODFLOW is a publicly available groundwater flow simulation program developed by the U.S. Geological Survey (McDonald and Harbaugh 1988). MODFLOW is thoroughly documented; widely

used by consultants, government agencies, and researchers; and is consistently accepted in regulatory and litigation proceedings.

MODFLOW simulates transient or steady-state, saturated groundwater flow in three dimensions. The program is designed to simplify the specification of boundary conditions by designing the data input to align with common field variables. The boundary conditions supported by MODFLOW include specified head, precipitation recharge, injection or extraction wells, evapotranspiration, horizontal flow barriers, drains, and rivers or streams. Aquifers simulated by MODFLOW can be confined or unconfined, or convertible between conditions. For the Site, which consists of a heterogeneous geologic system with variable unit thicknesses and boundary conditions, MODFLOW's three-dimensional capability and boundary condition versatility are essential for the proper simulation of groundwater flow conditions.

MODFLOW uses the method of finite differences to solve the equations of groundwater flow. Using a block-centered finite-difference approach, MODFLOW replaces the continuous system represented by the equations of flow, by a system of discrete blocks in space. The solution of the finite-difference equations produces time-varying values of head at each of the discrete points representing the real aquifer system.

#### **4.2 Submodel Domain**

The submodel was designed to represent groundwater conditions over approximately 1.3 square miles of the original groundwater flow model. The submodel domain is shown on Figure 4.2-1. The submodel extents were designed to incorporate the extent of the Cr(VI) distribution, the Colorado River adjacent to the Site, and the extent of the proposed remediation system.

#### **4.3 Submodel Discretization**

The model contains 232 rows, 256 columns, and five layers for a total of 296,960 active cells (Figure 4.2-1). A uniform cell size of 25 feet by 25 feet occurs throughout the entire submodel domain. The boundaries of the model grid are defined as constant flux cells that reflect the flux of the original groundwater flow model under the same flow conditions.

Consistent with the regional groundwater flow model, the extracted submodel layers have variable thickness. Figures 4.2-2 through 4.2-6 depict how the thicknesses of the model layers vary in the solute transport submodel. In general, the aquifer decreases in thickness from north to south as the southern bedrock outcrop is approached. South of the bedrock contact, the upper four layers in the groundwater flow model represent bedrock, whereas to the north of the bedrock contact, the upper four layers represent the alluvial aquifer. Therefore, the hydraulic conductivities vary within the layers to represent the different lithologies.

#### **4.4 Boundary Conditions**

In order to properly translate groundwater flow conditions from the regional model to the extracted submodel, constant flux boundaries were simulated around the edges of the extracted submodel. The perimeter constant flux boundaries reflect the actual flow conditions of the regional model; therefore, the relative distance of these perimeter boundaries to the interior submodel boundary conditions is not a constraint. The Colorado River and portion of the marshland located on the east side of the Colorado River is represented by river cells with stage and conductance values consistent with the original groundwater flow model. The third type of boundary condition simulated in the submodel domain is the constant flux well cells, which represent the proposed extraction and injection locations for the various remedial scenarios.

#### **4.5 Hydraulic Conductivity**

Model layers 1 through 4 represent the alluvial aquifer throughout the majority of the submodel, with the exception of the southern portion of the model where all layers represent the bedrock. Model layer 5 represents the bedrock throughout the full model domain. The hydraulic conductivity distribution of the upper four layers representing the alluvial aquifer were simulated as highly heterogeneous layers as depicted on Figures 4.5-1 to 4.5-5. All hydraulic conductivity values in the submodel were assigned on the basis of the original regional groundwater flow model properties.

## **5. Geochemical Model Development**

Geochemical modeling (batch and one-dimensional transport simulations) was performed to evaluate the anticipated behavior of reactive species during remedy implementation, including TOC, Cr(VI), and byproducts as a function of groundwater geochemistry and aquifer properties. The goals of these studies were to characterize known geochemical reactions that will occur and to aid in the estimation of parameters used in the site-wide solute transport model. Another important goal of the geochemical modeling was to test the validity of the site-wide solute transport model in describing Cr(VI) reduction and byproduct dynamics. In some cases, the site-wide solute transport model (described in Section 6) could not explicitly take into account the geochemistry and thermodynamics of the modeled reactions. In these cases, the geochemical model was used to confirm that these geochemical processes were being adequately captured by the simplified representations used in the solute transport model. This approach was strongly preferred over attempts to implement a full-scale, site-wide geochemical/reactive transport model, which would have been so computationally intensive as to be impractical to complete.

The geochemical model simulations included batch systems (i.e., well-mixed, no transport) and simplified one-dimensional transport simulations highly representative of aquifer conditions. One-dimensional simulations included an IRZ flowpath (750 feet long, passing through an IRZ well towards the river) for comparison with the site-wide solute transport model (Section 9.1) and a hyporheic zone flowpath (5 feet long, normal to the sediment-river water interface) to evaluate hyporheic zone dynamics and solute discharge to the river (Section 8).

### **5.1 Geochemical and Reactive Transport Code Selection**

Batch simulations were performed with the geochemical modeling software PHREEQC using the default PHREEQC thermodynamic database (Parkhurst and Appelo 1999). Additional geochemical parameters that were not listed in the default database were collected from literature sources, including Dzombak and Morel (1990), Morel and Hering (1993), and others as indicated below. One-dimensional reactive transport simulations were performed using PHT3D (Prommer et al. 2003), which links the solute transport modeling software MT3D (used here for site-wide solute transport modeling; see Section 6) with PHREEQC. Although PHREEQC alone can be used for one-dimensional transport modeling, the linkage with MT3D provides a more robust, stable, and efficient numerical code for transport calculations. The same modified PHREEQC thermodynamic database was used in the PHT3D simulations.

### **5.2 Full-Redox Geochemical Model**

Batch and one-dimensional geochemical models were constructed that explicitly include the biogeochemical reactions governing solute behavior in the aquifer. The following sets of reactions were included in the geochemical modeling:

- Aqueous species equilibria based on thermodynamic data for aqueous components, including  $H^+$  (pH), bicarbonate (alkalinity), calcium, magnesium, sodium, potassium, chloride, nitrogen, sulfur, manganese, arsenic, and chromium. In most cases, ion concentrations were based on measured values, except for chloride, which was adjusted in the model to achieve charge balance.
- Redox equilibria for redox active components, including Cr(III)/Cr(VI), O(-II)/O(0), N(0)/N(III)/N(V), Fe(II)/Fe(III), Mn(II)/Mn(IV), S(-II)/S(VI), As(III)/(V), and organic carbon; specifically, ethanol [C(-II)] going to carbonate [C(VI)].
- Kinetic oxidation of ethanol with a 20-day half-life. This was accomplished in the model by introducing ethanol as a non-redox-active species, then kinetically converting it to a redox-active species that instantaneously reacts with the other redox-active components listed above.
- Mineral solubility equilibria, including the Fe(II)/(III)-oxides Fe(III)(OH)<sub>3</sub> (ferrihydrite), Fe(II/III)<sub>3</sub>O<sub>4</sub> (magnetite), and Fe(II)OH<sub>2</sub> (green rust); ferrous sulfates and sulfides Fe(II)SO<sub>4</sub> (melanterite), Fe(II)S<sub>2</sub> (pyrite), and Fe(II)S (mackinawite); chromium(III) hydroxides Cr(OH)<sub>3</sub> and Fe<sub>3</sub>Cr(OH)<sub>12</sub> (Sass and Rai, 1987); and the manganese(IV) oxide MnO<sub>2</sub> (pyrolusite). Dissolution and precipitation were allowed to proceed to equilibrium for all phases except pyrolusite (see Section 5.3.3) and Fe<sub>3</sub>Cr(OH)<sub>12</sub>; the latter was given a kinetically limited oxidative dissolution rate based on the observation that this phase is highly stable to reoxidation in the presence of oxygen (e.g., Eary and Rai 1987; Hwang et al. 2002). Additionally, to limit the consumption of ferrihydrite by the formation of magnetite, some supersaturation of magnetite was assumed, as described below.
- Adsorption of manganese, arsenic, and ferrous iron to iron oxides via a surface complexation model (SCM) (see Sections 5.3.2 and 5.4.2).
- Release of arsenic via reductive dissolution of an arsenic-containing iron oxide (see Section 5.4.3).
- pH buffering by the solid phase via an ion exchange reaction. This is based on ISPT observations that the actual changes in groundwater pH were minimal in spite of redox reactions that might normally cause large changes in pH, such as organic carbon oxidation and iron reductive dissolution.

All geochemical speciation and redox calculations were based on published thermodynamic constants, with the exception of nitrate/nitrite reduction to nitrogen gas. It is well known that the thermodynamics and kinetics of denitrification ( $NO_3^-$  reduction to  $N_2$ ) are limited by the formation of intermediates, including nitrite ( $NO_2^-$ ) and gaseous forms of nitrogen ( $NO_2$  and  $N_2O$ ). To accurately capture this effect, the reduction potential for  $N_2$  was artificially lowered, while keeping the  $NO_3^-/NO_2^-$  reduction potential the same. In this way,  $N_2$  only formed when the redox potential dropped low enough to favor nitrite over nitrate.

Magnetite formation was based on the thermodynamic constant given in Morel and Hering (1993), with the reaction reformulated in terms of  $\text{Fe}^{2+}$  and  $\text{Fe}^{3+}$ , rather than as an explicit redox reaction. As  $\text{Fe}(\text{II})$  is produced, the magnetite precipitation reaction consumes aqueous  $\text{Fe}(\text{II})$  and  $\text{Fe}(\text{III})$ , causing the dissolution of  $\text{Fe}(\text{III})$  phases, such as ferrihydrite. Although this reaction is observed in natural systems, the concentrations of  $\text{Fe}(\text{II})$  observed in the pilot tests and in the Topock floodplain indicate that this reaction is kinetically limited and/or does not proceed to equilibrium, given the slow dissolution rates of  $\text{Fe}(\text{III})$ -oxide phases in practice. To account for this, a supersaturation of magnetite was assumed by adjusting the log K for the reaction to yield more realistic aqueous  $\text{Fe}(\text{II})$  concentration under reducing conditions.

Carbonate minerals ( $\text{CaCO}_3$ ,  $\text{MnCO}_3$ ) were not allowed to precipitate in the model. Geochemical data from the floodplain and upland ISPTs indicate that the groundwater can sustain supersaturation with respect to calcite ( $\text{CaCO}_3$ ) and rhodochrosite ( $\text{MnCO}_3$ ) for long periods. Furthermore, sufficient uncertainty in the  $\text{MnCO}_3$  solubility product exists in the literature that, including the precipitation reaction, would not have strengthened predictions of manganese behavior. It is assumed that rhodochrosite precipitation may be controlling net manganese generation and is, therefore, already partially accounted for in the generation term.

This geochemical model was used in the batch models described in the subsections below, as well as in the one-dimensional reactive transport models representing the NTH IRZ (Sections 6 and 7) and the Colorado River hyporheic zone (Section 8). The flow and transport domains will be described in more detail in those respective sections.

### **5.3 Manganese Generation and Attenuation**

The following sections describe the mechanisms for manganese generation and attenuation associated with the remedy. The introduction of dissolved organic carbon into the aquifer is expected to result in the reductive dissolution of naturally occurring  $\text{Mn}(\text{III/IV})$ -oxides (Section 5.3.1), as demonstrated by the floodplain and upland ISPT results (see Section 3.4.3). However, as this dissolved manganese migrates out of the IRZ under the influence of groundwater flow, it will undergo sorption (Section 5.3.2) and oxidation/precipitation (Section 5.3.3) reactions that will remove it from groundwater. Manganese has been shown to sorb to aquifer materials in a variety of environments (Fuller and Harvey 2000; Smedley and Kinniburgh 2002), and the floodplain and upland ISPTs demonstrated that manganese was not detected outside of the organic carbon footprint in downgradient monitoring wells. In addition, an evaluation of the concentrations of natural manganese at a transect of wells (MW-34, MW-36, MW-30, MW-39, and MW-20, moving from east to west) under IM-3 pumping conditions (pumping results in a gradient reversal on the floodplain) demonstrated that natural byproducts from the rind (reducing conditions) attenuated across the floodplain. The decline in concentration was due to adsorption of  $\text{Mn}(\text{II})$  to mineral surfaces, as well as  $\text{Mn}(\text{II})$  oxidation in the location of the aquifer where the oxidation-reduction potential transitioned from reducing conditions (negative redox potential) to less reducing conditions (positive redox potential). The long-term



persistence of manganese was generally associated with persistent reducing conditions, and, under less reducing conditions, manganese concentrations declined gradually with time. The field data provide a validation of the conceptual model used as the basis for attenuation in the byproduct fate and transport model.

#### 5.3.1 Manganese Oxide Reductive Dissolution

As observed in the ISPTs, microbial metabolism of the injected carbon substrate resulted in the reductive dissolution of Mn(III/IV)-oxides naturally present within the aquifer. The ISPT results demonstrated that the rate of manganese release into solution is proportional to the strength of the reducing environment, as governed by the concentration of TOC injected. The solute transport model, therefore, links the generation of manganese directly to the concentration of TOC through a proportionality constant, as described in Section 3.4.3.

In the geochemical model, this reaction can be represented more explicitly as a kinetically limited reductive dissolution of a manganese oxide phase. For comparison, a PHREEQC batch simulation was run that included the full geochemical thermodynamic model with a kinetic limitation on manganese reduction. The model results were then compared to a simpler, non-redox model in which manganese generation was linked to the organic carbon concentration as in the site-wide solute transport model. Comparison of the two model outputs demonstrates that when the kinetic reductive dissolution rate of manganese oxide is assumed to be first order with respect to carbon concentration (as observed in the ISPTs), the results are nearly identical to a model in which manganese generation is linked directly to organic carbon (Figure 5.3-1), after calibration of the rate constant for manganese reduction. This result demonstrates that the representation of manganese generation in the solute transport model is adequate.

#### 5.3.2 Mn(II) Sorption

The transport of aqueous manganese generated in the IRZ will primarily be limited by adsorption to mineral surfaces, particularly naturally occurring iron oxides and fresh iron oxides formed as Fe(II) generated within the IRZ reoxidizes and precipitates. Sorption of dissolved cations (including  $\text{Mn}^{2+}$ ) and anions by iron minerals is well documented in the technical literature, and SCMs have been developed to describe these reactions. The advantage of the SCM approach is that it accounts for the effects of solution chemistry (pH, alkalinity, ionic strength), as well as competition for sorption sites by other ions in solution. For example, cations tend to sorb more strongly to iron surfaces at a higher pH. This is because the net positive charge on the surface decreases as the solution pH is increased and surface hydroxyl groups deprotonate. The effects of these geochemical parameters on Mn(II) sorption in the floodplain are investigated in Section 9.2.

The SCM can easily be implemented in a geochemical model, but it cannot be implemented directly in the solute transport model. Therefore, an SCM is used here to calibrate a sorption isotherm specific to the



geochemical conditions of the floodplain that can be used in the solute transport model. The published SCM of Dzombak and Morel (1990) for ion sorption by amorphous iron was implemented in PHREEQC, supplemented with the bicarbonate sorption parameters of Appelo et al. (2002), and a Freundlich sorption isotherm was fitted to the SCM results. The following procedure was used to calibrate the SCM and sorption isotherm:

- a) The form and concentration of iron in the soil was determined through soil sampling and sequential selective extraction testing (Gleyzes et al. 2002). Soil was recovered from the alluvial aquifer in the upland during installation of the upland ISPT wells (ARCADIS 2009b) and from the floodplain during collection of cores for aerobic versus anaerobic solid-phase characterization studies (CH2M HILL 2005a).
- b) The concentrations of amorphous iron oxides in the samples were determined via hydroxylamine-hydrochloride extraction. The results for aerobic floodplain, anaerobic floodplain, and upland soils were averaged. Because relatively fine-grained material was collected in the upland, only upland samples with the coarsest (silty-sand) lithology were included in the average to avoid a sample bias by fine-grained material. This resulted in a site-average estimate of amorphous iron content of 840 mg iron per gram dry solid. This iron fraction was interpreted as ferrihydrite, with an assumed surface area of 300 square meters per gram ( $\text{m}^2/\text{g}$ ), which is on the low conservative end of the literature range (Dzombak and Morel 1990).
- c) The concentrations of crystalline iron oxides were determined via citrate-bicarbonate-dithionite extraction. Results for floodplain and upland samples were averaged as above, yielding a site-average crystalline iron oxide content of 2,500 mg iron per gram dry solid. This iron fraction was assumed to be representative of goethite, with a surface area of 30  $\text{m}^2/\text{g}$ . As with ferrihydrite, a surface area was chosen that was on the low end but still well within the observed literature range (Kosmulski et al. 2004).
- d) Surface site concentrations for the SCM were estimated based on the above iron contents. The Dzombak and Morel SCM was originally developed for ferrihydrite with a surface area of 600  $\text{m}^2/\text{g}$ . The material was found to have two surface site types, with site concentrations of 0.2 moles “weak” sites per mole of iron and 0.005 moles “strong” sites per mole iron (Dzombak and Morel 1990). These concentrations were scaled in half here to reflect the lower assumed ferrihydrite surface area (300  $\text{m}^2/\text{g}$ ). Based on literature support (Van Geen et al. 1994; Manceau 1995), the model was also assumed valid for goethite, with surface site concentrations scaled by surface area; this results in goethite contributing far fewer sorption sites than ferrihydrite on a mass basis.
- e) Surface site concentrations were summed for crystalline and amorphous iron contributions. These surface sites are assumed to be uniformly distributed between mobile and immobile porosity. Based on

a total aquifer porosity of 35% and bulk density of 1.73 kilograms per liter, the following site concentration estimates were obtained:

9.6 millimoles weak sites per liter of solution  
0.24 millimoles of strong sites per liter of solution

- f) The SCM was then run in PHREEQC using the above surface site concentrations and the floodplain-average groundwater chemistry, determined from the average of all available floodplain well data between 1997 and the present:

pH	7.56
Alkalinity	200 mg/L as CaCO <sub>3</sub>
Ca	318 mg/L
Mg	83 mg/L
K	29 mg/L
Na	2,220 mg/L
Cl	2,600 mg/L (before adjustment to achieve charge balance)
Sulfate	840 mg/L
Nitrate	2.6 mg/L

The geochemical model was run over a range of aqueous manganese concentrations between 0.02 and 20 mg/L to construct a sorption isotherm. This sorption isotherm was linearized on a log-log scale to allow fitting of a Freundlich isotherm (Essington 2004). The Freundlich equation is as follows:

$$q_e = K_F C_e^N$$

Where:

$q_e$  is the concentration of manganese sorbed to the soil (in milligrams per kilogram [mg/kg] soil)

$K_F$  is the Freundlich partition coefficient

$C_e$  is the concentration of manganese in the dissolved phase (in mg/L solution)

$N$  is an exponent used to fit the curve.

The exponent is also a measure of surface site heterogeneity; as  $N$  approaches 1, surface sites are more homogenous in their chemical identity. The Freundlich partition coefficient ( $K_F$ ) is similar to the linear solid-solution partition coefficient ( $K_D$ ), except that  $K_F$  accommodates non-linear sorption behavior, where sorption is greatest at lower concentrations of dissolved manganese and as concentrations increase, surface sorption sites become filled and the magnitude of partitioning to the solid phase decreases.

The geochemical modeling results using the site-calibrated SCM are shown on Figure 5.3-2, as well as with the least-squares-fitted Freundlich isotherm. The fit to the geochemical results yielded the following Freundlich parameters:

K<sub>F</sub>: 1.37  
N: 0.875

These parameters were used in the site-wide solute transport model as described in Section 6.2.7. The procedure outlined above to obtain Freundlich parameters for the solute transport model represents a refinement over the procedure used in the 30% Basis of Design Report, particularly in how the iron sequential selective extraction data were interpreted. The objective of the modified procedure was to provide a more scientifically defensible interpretation of field data and literature results. Ultimately, however, the updated Freundlich model was very similar to the isotherm used in the 30% design, and the new Freundlich parameters yielded a very small difference in the predicted behavior of byproduct manganese downgradient of the IRZ.

#### 5.3.3 Mn(II) Oxidation and Precipitation

Immediately downgradient of the IRZ and within the naturally reducing zone of the floodplain, oxidation of Mn(II) is expected to be limited. However, in less reducing environments where dissolved oxygen is present, Mn(II) oxidation is expected to play a stronger role in the attenuation of aqueous manganese. These areas include the upland, the alluvial aquifer beneath the floodplain, and the Colorado River sediment-surface-water interface or hyporheic zone (i.e., the shallow mixing zone within the sediments at the bottom of the river where groundwater and surface water meet).

Aqueous Mn(II) can be reoxidized biotically and abiotically in the presence of oxygen, resulting in precipitation. Abiotic oxidation of Mn(II) is slow, with a rate that is dependent on manganese concentration, dissolved oxygen concentration, and pH. For example, at pH 8 with a dissolved oxygen content of 2 mg/L (approximately 25% air-saturation), the half-life for Mn(II) oxidation is approximately 400 days (Morgan 2005). Although abiotic oxidation of Mn(II) is slow, microbially catalyzed oxidation of Mn(II) is much faster. Biotic oxidation of manganese has been studied extensively in the context of mining-derived pollution of streams, where Mn(II) oxidation has been observed in stream hyporheic zones (Gandy et al. 2006; Harvey and Fuller 1998; Kay et al. 2001). These results demonstrate that metal oxidation can be rapid, particularly at redox interfaces with active microbial consortia and an adequate nutrient supply. Harvey and Fuller (1998) studied the oxidation Mn(II) within the hyporheic zone of Pinal Creek, Arizona. Oxidation rates were observed to be first order with respect to manganese concentration, with Mn(II) half-lives between 0.7 and 8.3 hours. Laboratory work further confirmed these rates, while demonstrating the importance of the solid to solution ratio (highlighting the combined role of mineral surface and microbial catalysis) and nutrient availability. Further work (Marble et al. 1999) demonstrated that these rates were independent of dissolved

oxygen concentration above 30% saturation (approximately 2.5 mg/L) and first-order with respect to oxygen below 30%.

Oxidation of Mn(II) was incorporated in the Topock solute transport model assuming a half-life of 29 days. This value was obtained by starting with a first-order rate coefficient of  $0.083 \text{ h}^{-1}$ , representing the slowest rate observed by Harvey and Fuller (1998) at the Pinal Creek, Arizona site, and scaling it back by two orders of magnitude to conservatively account for potential differences in nutrient status and microbial population. This rate was used to simulate Mn(II) oxidation in the upland, where Mn(II) oxidation was assumed to be active outside of the TOC footprint (TOC less than 0.1 mg/L) of the remedy. At these interfaces, it is expected that biotic oxidation of manganese will occur due to the presence of organic carbon and naturally occurring microorganisms.

In addition, Mn(II) oxidation in the hyporheic zone was simulated within a one-dimensional coupled geochemical-reactive transport model using PHT3D. This model simulated Mn(II) oxidation in the presence of dissolved oxygen and precipitation as the Mn(IV) oxide pyrolusite. Pyrolusite is one of the main products known to form from Mn(II) oxidation in hyporheic zone environments (Kay et al. 2001). Although several other mixed Mn(III/IV) oxides, such as birnessite may also form, all of these phases have sufficiently low solubilities, such that manganese sequestration can be effectively simulated using just one representative phase. In the hyporheic zone model, a Mn(II) oxidation rate of  $0.083 \text{ h}^{-1}$  was chosen, representing the lowest hyporheic zone rate observed by Harvey and Fuller (1998). The hyporheic zone model and results are described further in Section 8.

The PHT3D hyporheic zone model more explicitly accounts for the geochemical reactions involved in Mn(II) oxidation and precipitation than the site-wide solute transport model, which only utilizes a half-life for manganese immobilization. However, the hyporheic zone simulations presented in Section 8 demonstrate that manganese oxidative precipitation yields a phase with very low solubility, such that aqueous manganese attenuation is governed completely by the kinetic oxidation step. Therefore, the hyporheic zone PHT3D results demonstrate that the immobilization reaction used in the site-wide solute transport model adequately accounts for the chemical reactions that take place.

## **5.4 Arsenic Generation and Attenuation**

### **5.4.1 Arsenic Generation in the IRZ**

As with manganese, the release of arsenic in the ISPTs correlated with the strength of the reducing environment, which was observed to be a function of organic carbon content. Based on this observation, a generation rate for arsenic was established based on TOC content, as described in Section 3.4.3.

The actual control on arsenic release in the aquifer is the reductive dissolution of iron oxides, which releases arsenic coprecipitated within the iron oxide minerals. To verify that the simpler depiction of arsenic generation in the solute transport model was adequate, the batch geochemical thermodynamic model (see Section 5.2) was modified to include reductive dissolution of an iron oxide phase containing arsenic. Because ferrihydrite reductive dissolution was already included in the model, this involved defining a new ferrihydrite phase containing iron and arsenic in a defined stoichiometric ratio.

The model results on Figure 5.3-1 show arsenic release simulated using the TOC-linked generation term of 0.000108 mg arsenic per mg TOC (Section 3.4.3), compared with the results of the full geochemical model in which arsenic release is controlled by iron oxide dissolution. The comparison illustrates that the results are nearly identical after calibration of the iron:arsenic stoichiometric ratio in the iron solid, suggesting that the representation of arsenic generation in the solute transport model is adequate. Small differences at early times are the result of the consumption of other electron acceptors before iron, including dissolved oxygen, nitrate, and chromium.

#### 5.4.2 Arsenic Coprecipitation

Arsenic released into solution within the IRZ will adsorb to iron oxide surfaces and will coprecipitate with mixed Fe(II)/(III) and Fe(III)-oxides that form as Fe(II) reoxidizes and precipitates in redox recovery zones. This coprecipitation reaction is expected to be the dominant mechanism by which arsenic is attenuated downgradient of the IRZ. However, although an attempt is made to capture iron redox dynamics in the geochemical model for electron accounting purposes, no attempt was made to explicitly simulate arsenic coprecipitation with iron in a geochemical model. This is because the reactions governing iron transformation and concurrent arsenic uptake are too numerous, complex, and poorly characterized to be able to construct and calibrate a model for this process that would be more robust than the current model. The current model assumes that the net result of these multiple, complex processes is the kinetic uptake of arsenic outside of the IRZ footprint with a rate proportional to the arsenic concentration. This is modeled directly in the solute transport model by assigning a half-life to arsenic below a threshold TOC level, as described in Section 3.4.3.

#### 5.4.3 Arsenate Sorption

In the absence of aqueous Fe(II), the mobility of aqueous arsenic in groundwater is limited by adsorption to mineral surfaces. Both arsenate – As(III), which tends to be dominant in suboxic environments – and arsenite – As(V), dominant under oxidizing conditions – are known to adsorb strongly to mineral surfaces, particularly iron oxides (e.g., Dixit and Hering 2003). As with Mn(II), the adsorption of As(III) and As(V) is dependent on solution chemistry (pH, alkalinity, ionic strength/composition), which controls surface charge and the extent of competition for sorption sites with other ions. Therefore, a similar SCM approach was used to calibrate a Freundlich isotherm for arsenic.

Determination of adsorption site concentrations for arsenic followed a similar procedure as that outlined for manganese (see Section 5.3.2). However, an additional model calibration step was applied for arsenic that included the arsenic total digestion data obtained in the upland sequential selective extraction tests. Inclusion of this calibration step helped to establish an upper limit on the reasonable arsenate adsorption strength within the system. Arsenic SCM development followed the procedure outlined below:

- a) An SCM was developed to specifically represent the conditions in the vicinity of upland well PTR-1, where a core was collected for sequential selective extraction tests. Sorption site concentrations were calculated based on the hydroxylamine-hydrochloride and citrate-bicarbonate-dithionite extraction results for iron, following the procedure described in Section 5.3.2, but using only the extraction results from the PTR-1 sample.
- b) The SCM of Dzombak and Morel (1990), supplemented with bicarbonate sorption parameters from Appelo et al. (2002), was run in PHREEQC using the sorption site concentrations calculated above. The model was run using PTR-1 water chemistry, including the measured aqueous arsenate concentration of 2.0  $\mu\text{g/L}$ . This yielded an estimate of the sorbed arsenate concentration for comparison with the actual arsenate content of the soil, measured via total digestion. The measured total soil arsenic content at PTR-1 was 3.7 mg/kg, but it was assumed that less than 10% of this would be present as adsorbed arsenate; the majority would be present as a coprecipitate in iron oxides. For the purposes here, a value of 0.25 mg/kg sorbed arsenate was assumed (approximately 7% of total).
- c) A calibration factor was obtained based on the measured and calculated estimates of sorbed arsenate at PTR-1. The SCM significantly overestimated arsenate sorption at PTR-1, and agreement was achieved when the surface site concentration was scaled down to 3.3% of the originally estimated value. This 0.033 scale factor was then applied to the adsorption site concentration calculated in Section 5.3.2 to obtain a calibrated adsorption site concentration for the arsenic SCM. This yielded a weak site concentration of 0.32 millimoles per liter of solution (the Dzombak and Morel model assumes no arsenate adsorption to strong sites). Note that this calibration factor was not applied to the manganese SCM; rather, it was assumed that precipitation of iron oxides downgradient of the IRZ would generate additional surface area for manganese sorption, which would compensate for a potential overestimation in site concentration.
- d) The geochemical model was run with the calibrated SCM over a range of aqueous arsenate concentrations between 2 and 18  $\mu\text{g/L}$  to construct a sorption isotherm, and a Freundlich isotherm was fit to the SCM results.

The geochemical model-derived adsorption isotherm and the fitted Freundlich isotherm are shown on Figure 5.4-1. The fit to the geochemical results yielded the following Freundlich parameters:



**Appendix B: Development of  
Groundwater Flow,  
Geochemical, and Solute  
Transport Models**

Topock Compressor Station  
Needles, California

$K_F$ : 2.77  
N: 0.465

These parameters were used in the site-wide solute transport model as described in Section 6.2.7.

## **6. Solute Transport Model Development**

Solute transport modeling was performed to evaluate the migration and fate of Cr(VI) detected in the groundwater, as well as the fate and transport of potential IRZ byproducts (i.e., manganese and arsenic). The solute transport model used the results from the calibrated groundwater flow model to simulate solute transport under average flow conditions. The solute transport model was used to evaluate the fate and transport of Cr(VI), as well as select byproducts (manganese and arsenic) to evaluate various potential remedial systems.

### **6.1 Code Selection**

The solute transport modeling was performed using the modular three-dimensional transport model referred to as MT3D. MT3D was originally developed by Zheng (1990) at S.S. Papadopoulos & Associates, Inc. for the Robert S. Kerr Environmental Research Laboratory of the U.S. Environmental Protection Agency (USEPA). The MT3D code uses the flows computed by MODFLOW in its transport calculations. MT3D also uses the same finite-difference grid structure and boundary conditions as MODFLOW, simplifying the effort to construct the solute transport model. MT3D is regularly updated (Zheng and Wang 1999), and the most recent version is referred to in the literature as MT3DMS, where MS denotes the Multi-Species structure for accommodating add-on reaction packages. MT3DMS has a comprehensive set of options and capabilities for simulating advection, dispersion/diffusion, and chemical reactions of contaminants in groundwater flow systems under a range of hydrogeologic conditions. Recent updates to MT3DMS have included the dual-domain formulation and the ability to incorporate site-specific processes.

The major inputs to MT3DMS for the modeling assessment are as follows:

- Mobile and Immobile Porosity: affecting the groundwater velocity and dissolved storage
- Mass Transfer Coefficient: affecting the exchange of mass between mobile and immobile portions of the aquifer
- Partition Coefficient: affecting the adsorption of Cr(VI) and byproducts to soil particles
- Carbon Degradation Rate: affecting the rate of Cr(VI) reduction/precipitation
- Byproduct Generation Rate: affecting the rate of generation of manganese and arsenic from the introduction of carbon to aquifer



## **6.2 Solute Transport Parameters**

### **6.2.1 Porosity**

The first phase of calibration was to accurately represent the groundwater velocity in the impacted portion of the aquifer. The groundwater velocity is computed within MT3DMS by dividing the groundwater flux term from MODFLOW by the mobile porosity. The mobile porosity is that fraction of the aquifer through which the majority of groundwater is moving. While often conceptualized as solely a pore-scale concept, it also represents aquifer-scale behavior driven by hydraulic conductivity contrasts in different portions of the aquifer matrix. The immobile porosity is the remaining portion of the void space, where groundwater flows much slower or not at all, and the void space is primarily a storage reservoir for dissolved mass. Mass is exchanged between mobile and immobile portions of the aquifer by diffusion. This conceptualization of solute transport is the dual-domain formulation, and is often referred to as advection-diffusion. There is extensive literature on the dual-domain model (Gillham et al. 1984; Molz et al. 2006; Flach et al. 2004; Harvey and Gorelick 2000; Feehley et al. 2000; Julian et al. 2001; Zheng and Bennet 2002) and it is generally considered the most accurate approach for simulating solute transport.

The total (combination of mobile and immobile) porosity of the aquifer is controlled by grain sizes and sorting. The mechanics of deposition and consolidation of unconsolidated materials result in aquifer soils at the Site exhibiting a total porosity of approximately 35%. Local variability will not have an impact on overall results, and 35% is a reliable estimate for the total porosity of modeled layers 1 through 4. This is the reference value that was used to divide the aquifer between mobile and immobile regions.

The simulated mobile porosity of the aquifer is 12% of the total volume, with the immobile porosity to be 28% of the total volume. The mobile porosity was determined through site ISPT tracer studies (see Section 3.4.4), including the breakthrough of IM-3 injection water. These values are typical of porosity values obtained at other sites (Payne et al. 2008).

### **6.2.2 Mass Transfer Coefficient**

An estimated mass transfer coefficient (MTC) value of  $1.0 \times 10^{-3}$  was utilized for all model layers in the solute transport model. This MTC was developed based on a range of literature values and models of similar dimensions and aquifer properties (Gillham et al. 1984; Molz et al. 2006; Flach et al. 2004; Harvey and Gorelick, 2000; Feehley et al. 2000; Julian et al. 2001). The solute transport model was then run with initialized current plumes to determine if the selected MTC produced reasonable results with the constituent distribution currently observed. It was recognized that variations in historic plume interpretations were not just a function of plume movement, but also improved delineation of the plume that developed over time as the monitoring well network density evolved. The current plume interpretation is based on a much more advanced monitoring well network, which improved the resolution of the plume delineation. The MTC value

for the solute transport model was systematically adjusted between  $1.0 \times 10^{-05}$  [1/day] and 1.0 [1/day], and small-scale and short-term plume movements were evaluated until the solute transport model produced reasonable plume movement.

#### 6.2.3 Chromium Adsorption

The retardation factor ( $R_f$ ) is used by the solute transport model to represent the amount of adsorption of a constituent from the dissolved or solute phase. The retardation factor used for Cr(VI) is based on the linear sorption isotherm and is calculated in MT3D using the bulk density ( $\rho_b$ ), the porosity ( $n$ ) of the aquifer material, and a distribution coefficient ( $K_d$ ), according to the following equation:

$$R_f = 1 + \frac{\rho_b K_d}{n} \quad (4-1)$$

The presence of background Cr(VI) concentrations associated with the naturally occurring mineralogy suggests nominal adsorption (low  $K_d$  value) is representative of the aquifer. This assessment is consistent with the literature, which identifies a wide range of  $K_d$  values (USEPA 1999) for naturally occurring Cr(VI) in aquifer soils with a normal pH range. The model includes a small amount of adsorption for Cr(VI), incorporating a distribution coefficient ( $K_d$ ) of 0.05 liter per kilogram (L/kg). A  $K_d$  value of 0.05 L/kg results in a retardation factor of approximately 1.25 for the Cr(VI) plume in the solute transport model. This indicates the plume will migrate about 25% slower than the ambient groundwater flow velocity. Given the limits of the current plume and the understanding of groundwater flow through the region, the  $K_d$  value of 0.05 L/kg is a reasonable estimate of natural chromium adsorption rates at the Site.

#### 6.2.4 Chromium Reduction

The reduction and precipitation of Cr(VI) in the aquifer was simulated by accounting for the reduction/precipitation of chromium in the presence of injected carbon (as part of an in-situ remediation approach). To account for this, the model utilized a Cr(VI) reduction/precipitation whenever the injected carbon exceeds a concentration of 0.1 mg/L (see Section 3.4.1). At the same time, a carbon half-life of 20 days (see Section 3.4.2) was assigned to account for the degradation of the injected carbon over time. By simulating both Cr(VI) and carbon simultaneously, the interactions between the plume and the active IRZ were accounted for in the solute transport model.

#### 6.2.5 Initial Hexavalent Chromium Distribution

The initial chromium plume concentration distribution was based on first quarter 2012 and historical data. In the upper four model layers, the plume delineation varied to reflect the differing Cr(VI) concentrations encountered with depth. The initialized Cr(VI) distributions are the same in both the mobile and immobile

portions of the aquifer. The distribution of the Cr(VI), based on observed data through February 2012, was initialized in the model for model layers 1 through 4 as shown on Figures 6.2-1 through 6.2-4.

#### 6.2.6 Byproduct Generation

As discussed previously, the introduction of dissolved organic carbon into the aquifer will facilitate treatment of Cr(VI) in groundwater through precipitation of stable, low-solubility Cr(III) minerals (see Section 2.4). This precipitation reaction results from the formation of geochemical conditions that are similar to those currently present in the fluvial aquifer that comprises the rind adjacent to the river. Naturally occurring minerals in the rind are currently dissolved due to the presence of natural organic carbon, at the same time that Cr(VI) is undergoing precipitation in this rind. The goals of the in-situ groundwater treatment are to promote these geochemical conditions in the deeper aquifer where the majority of the Cr(VI) is present in order to facilitate treatment. Once geochemical conditions form in the alluvial aquifer that are similar to the fluvial aquifer, there will be natural minerals that dissolve (specifically natural iron minerals), and naturally occurring manganese and arsenic associated with these natural minerals may become soluble. These byproducts of the introduction of organic carbon will be generated only in the presence of organic carbon, and their migration will be limited in distance outside of the reactive zone where Cr(VI) is treated. These secondary water quality effects are discussed in detail in Appendix G of the CMS/FS (CH2M HILL, 2009b). Byproducts will be generated due to dissolution of naturally occurring iron minerals in the aquifer, and the distance over which they travel will be controlled by attenuation mechanisms, principally sorption. The solute transport model was used to evaluate the generation of byproducts and their fate and transport.

Byproduct generation is simulated in the fate and transport model by linking the concentration of organic carbon to a corresponding concentration of dissolved manganese and arsenic. As described in Section 3.4.3, based on the floodplain and upland ISPT results (ARCADIS 2008, 2009), the generation rates for manganese and arsenic were determined to be 0.016 mg of manganese per mg of organic carbon and 0.000108 mg of arsenic per mg of organic carbon, respectively. A range of generation rates for manganese and arsenic were selected based upon this base case, as detailed in Table 6.2-1.

**Table 6.2-1  
Byproduct Generation Terms Used in Fate and Transport Model**

Byproduct	Generation Term (mg of Byproduct per mg Organic Carbon per Liter)		
	Low	Base Case	High
Manganese	0.005	0.016	0.05
Arsenic	0.00005	0.000108	0.00018

#### 6.2.7 Byproduct Adsorption and Precipitation

As discussed in Section 6.2.6, the dissolution of iron, manganese, and arsenic in the IRZs is temporary and these elements will then return to baseline concentrations. Iron, manganese, and arsenic that have dissolved and moved out of the reactive zone under the influence of groundwater flow will undergo reactions that will transition these dissolved, naturally occurring elements to sorbed or precipitated forms, thereby removing them from groundwater. Dissolved iron will react by sorbing to solid-phase iron minerals outside of the reactive zone, and it will also precipitate through reaction with dissolved oxygen in the aquifer. Manganese concentrations will attenuate via sorption, reoxidation, and precipitation reactions as discussed in Section 5.3; and arsenic concentrations will attenuate via coprecipitation and sorption reactions as discussed in Section 5.4.

Oxidation of Mn(II) was incorporated into the solute transport model by assuming a half-life of 29 days (see Section 5.3.3), and coprecipitation of arsenic was accounted for by assigning a half-life of 30 days (base case) derived from the ISPT data (see Sections 3.4.3 and 5.4.2).

A summary of the sorption parameters used in the model is provided in Table 6.2-2, below. Development of these parameters is discussed in Sections 5.3.2 (for manganese) and 5.4.3 (for arsenic).

**Table 6.2-2  
Byproduct Sorption Terms Used in Fate and Transport Model**

Byproduct	Freundlich Parameters		
	Low	Base Case	High
Manganese	$K_F=0.137$ , $N=0.875$	$K_F=1.37$ , $N=0.875$	$K_F=6.85$ , $N=0.875$
Arsenic	$K_F=0.277$ , $N=0.465$	$K_F=2.77$ , $N=0.465$	$K_F=13.85$ , $N=0.465$

#### 6.2.8 Naturally Occurring Manganese

In addition to the manganese and arsenic concentrations generated as byproducts as a result of the IRZ remediation strategy, there is naturally occurring manganese that is accounted for in the solute transport model. With respect to manganese, there is a naturally occurring reducing rind that surrounds the Colorado River. This naturally occurring manganese in groundwater is the result of the decay of organic debris located in the Colorado River floodplain. Observed reducing rind manganese concentrations range in concentration from less than 1 mg/L to as high as 9 mg/L. Anaerobic core study data indicate that, although the rind area surrounding the Colorado River is generally reducing, the reducing conditions are naturally distributed with pockets of weaker and stronger reducing activity. Furthermore, total manganese content of the fluvial matrix is variable such that observed manganese concentrations are relatively low even in some areas exhibiting reducing conditions that would support dissolved manganese [i.e., strongly negative ORP and absence of

Cr(VI)]. It is also possible that manganese concentrations are lower in parts of the shallow zone immediately adjacent to the river due to the presence of the hyporheic zone (groundwater/surface water mixing zone), which serves to deliver oxic river water that can dilute aqueous manganese concentrations and/or oxidatively precipitate manganese.

To account for the naturally occurring manganese in the floodplain, the average observed manganese concentrations in the floodplain were delineated based on well data correlated to model layer elevations. Figures 6.2-5 and 6.2-6 display the delineated naturally occurring average floodplain manganese in model layers 1 through 4. In order to more clearly visualize the simulated manganese associated with IRZ byproduct generation, the solute transport model was run separately from the naturally occurring average floodplain manganese delineation. This new treatment of naturally occurring manganese differs from the approach used in the 30% Basis of Design Report, where a uniform 2 mg/L baseline manganese concentration was assumed within the reducing rind. This change was made to more accurately reflect the actual natural manganese distribution.

### **6.3 Parameter Assessment**

A sensitivity analysis quantifies the impact that variations on model parameter values have on differences between Site observations and model predictions. This approach is extremely challenging for this study because of the various complexities of the area. However, various aspects of the Cr(VI) plume and behavior of manganese and arsenic were analyzed in detail with the solute transport model to determine an appropriate range of solute transport parameters to use for the predictive modeling.

By adjusting parameters, such as chromium partition coefficient, manganese Freundlich constants, arsenic precipitation rate, manganese liberation rate, and arsenic liberation rate, a reasonable qualitative and quantitative fit to the observed data and flow conditions was obtained.

In addition to varying the parameters for the constituents of concern, additional analyses were conducted to evaluate additional parameter impacts on the solute transport model. These parameters include the TOC injection concentration, the riverbank extraction well rate, and the NTH IRZ well spacing. The solute transport modeling sensitivity analysis is presented in Section 10.

### **6.4 Remediation Design**

There are seven different components of the proposed remediation design that are simulated concurrently with the solute transport model to effectively remediate the hexavalent chromium plume while reducing the impact of potential byproducts:

- NTH IRZ (NTH IRZ Injection and Extraction Wells)

- Riverbank extraction (Riverbank Extraction Wells)
- Uplands injection (Inner Recirculation Loop [IRL] Injection Wells)
- Bench extraction (Transwestern Bench Extraction Wells)
- East Ravine extraction (East Ravine Extraction Wells)
- TCS injection (TCS Injection Wells)
- Freshwater injection (Freshwater Injection Wells)

Each of these components is described in more detail in Sections 6.4.1 through 6.4.7, respectively. Figure 6.4-1 shows the locations of each of the proposed wells. Conceptual remedy cross-sections were developed based on the model structure, and the locations of these cross-sections are shown on Figure 6.4-2. Figures 6.4-3 through 6.4-8 show the individual cross-sections that depict the intercepted remedial wells in cross-section relative to the submodel structure. The cross-sections display the proposed well screens and interpolated Cr(VI) distributions, as well as with the model structure. Additionally, the plan view cross-section location figure (Figure 6.4-2) and the Cross-Section A-A' figure (Figure 6.4-3) through the floodplain on the western edge of the Colorado River depict the approximate extent of the reducing rind relative to the model layer structure. This approximate extent of the reducing rind is consistent with the fluvial/alluvial aquifer contact as described in Section 2.3.

Potential well locations were carefully selected by first avoiding culturally or otherwise sensitive areas to minimize impact – delineated areas were closely evaluated and sensitive areas were avoided to the extent possible during well placement. Numerous iterations of the remedial system layout and operational strategy were then considered and simulated in order to arrive at an optimized remedial approach and to account for uncertainties in the model predictions. Parameters that were adjusted between model runs included well locations, well extraction or injection rates, well cycling patterns (i.e., duration of active operation versus shutdown), carbon substrate amendment injection concentrations, and reinjection destinations. Optimization criteria included the following:

- reduce the anticipated remedial timeframe for effective capture and treatment of the Cr(VI) plume
- minimize the necessary remediation infrastructure (i.e., total number of well locations) or “footprint” of the remedial system
- minimize the impact of potential byproducts (i.e., arsenic and manganese)

#### 6.4.1 NTH IRZ

The NTH IRZ consists of a line of IRZ wells located along NTH running north-south for a distance of approximately 3,000 feet. These wells are designed to create a reducing zone along the downgradient axis of the Cr(VI) plume that is simulated in the upper 4 model layers. This system component is designed to be a recirculating system where all the water extracted along the NTH IRZ will be amended with carbon and injected into the NTH IRZ line, resulting in a net flow of 0 gpm along the NTH IRZ line. Numerous elements of the NTH IRZ were evaluated with the solute transport model to determine the optimum treatment pattern. These elements include:

- extraction/injection well locations
- well spacing
- well cycling pattern (active operation/full shutdown)
- carbon loading concentration
- extraction/injection well rates

The first system design that produced reasonable effects was an NTH IRZ layout that consisted of a 20 well location system and is shown on Figure 6.4-1. The total extraction and injection rate for this layout was 300 gpm. The 300 gpm was extracted from four of the IRZ well locations, three located at the northern end of the NTH IRZ operating at 40 gpm, 80 gpm, and 80 gpm each, and one located toward the middle of the NTH IRZ operating at 100 gpm. By extracting at these locations, the natural west to east flow gradient is generally preserved to encourage flow through the reduced groundwater. The spacing between each the northern NTH IRZ extraction well locations is approximately 300 feet. In this area, initialized Cr(VI) concentrations are at relatively low levels with respect to the rest of the Cr(VI) plume. In addition to the four NTH IRZ extraction well locations, 16 injection well locations were simulated in all four model layers. The injection rates were varied along the NTH IRZ based on the aquifer thickness. The aquifer thickness varies from over 300 feet thick at the northern end of the NTH IRZ to approximately 10 feet thick at the southern end of the NTH IRZ. The majority of the injection well locations were spaced 150 feet apart, except at two locations towards the northern end of the NTH IRZ where spacing was reduced to 75 feet to prevent breakthrough of the Cr(VI) plume. The simulated carbon concentration injected was 100 mg/L. Higher TOC concentrations result in a more comprehensive reducing zone; however, it also produces increased levels of byproducts. A carbon inject concentration of 100 mg/L in the 150-foot spacing layout limits the potential for gaps in treated groundwater while managing byproducts generated. A pattern of 6 months on, followed by 18 months off, allowed for completed coverage of the Cr(VI) passing through the reduced groundwater. Turning the system



off allows for the established anaerobic conditions to continue without adding additional carbon that would increase the potential of byproduct generation.

While this simulated layout was effective in the solute transport model simulations and minimizes the number of well locations necessary, additional well locations should be considered as a conservative approach to establish a comprehensive treatment zone across the NTH IRZ. A second layout that was considered consisted of a well location spacing of 75 feet along the NTH IRZ. Figure 6.4-4 shows the provisional wells with the 75-foot spacing NTH IRZ in cross-section. Despite increasing the number of injection wells in this scenario, the total extraction and injection rates were still maintained at 300 gpm.

The design goal is to minimize the total number of NTH IRZ wells necessary while maintaining effective remediation; therefore, the 20 NTH IRZ well location layout depicted on Figure 6.4-1, which provides the desired remedial impact with less infrastructure, has been selected for the remedy design. However, provisional well locations are included in the event that additional infrastructure is deemed necessary. While the model suggests that either of these NTH IRZ layouts (150-foot spacing or 75-foot spacing) are viable options, the design should still be flexible enough to adapt to observed field conditions and system performance.

#### 6.4.2 Riverbank Extraction

Along the west side of the Colorado River, a series of extraction wells were simulated with the goal of providing hydraulic capture of the Cr(VI) groundwater concentrations, accelerating cleanup of the floodplain, enhancing the flow of contaminated groundwater through the NTH IRZ line [Cr(VI) located upgradient (west) of the NTH IRZ is anticipated to be treated by the NTH IRZ], and control migration of IRZ-generated byproducts toward the Colorado River in the deeper part of the aquifer. The Riverbank Extraction Wells will be constructed with one screened interval to target the deeper portions of the aquifer (model layers 3 and 4), as well as a second shallow screen interval (model layers 1 and 2) for potential future use, which will be isolated from the deeper screen interval with a pneumatic packer. The proposed layout of the Riverbank Extraction Wells consists of five wells (RB-1 through RB-5) that are simulated in model layers 3 and 4 (beneath the naturally occurring rind in the fluvial sediments). The naturally occurring, shallow reducing rind provides ideal conditions for Cr(VI) precipitation in the event that there is breakthrough past the NTH IRZ in model layers 1 and 2. Additionally, the reducing rind typically contains elevated manganese and iron concentrations that could contribute to well fouling. Because the Riverbank Extraction Wells could potentially pull down the groundwater from the reducing rind, consideration was taken to keep the extraction rate at a reasonable level, and the simulated total extraction rate of 150 gpm was utilized for the solute transport model runs. Section 10.3 provides a detailed discussion of the sensitivity analysis that was performed to evaluate the relative impact of Riverbank Extraction Well pumping rates on the solute transport model results. The locations and rates of the Riverbank Extraction Wells are shown on Figure 6.4-1. Figure 6.4-3 shows the Riverbank Extraction Wells in cross-section.



#### 6.4.3 Uplands Injection

To accelerate the movement of the Cr(VI) plume through the NTH IRZ, four injection wells (the IRL Injection Wells; IRL-1 through IRL-4) were simulated in the upland area (upgradient of the plume extent) in all four model layers. The baseline analysis of the IRL wells do not include carbon dosing; however, if elevated Cr(VI) concentrations are observed in the groundwater extracted from the Riverbank Extraction wells, carbon dosing can be implemented. This evaluation of the carbon dosing of the extracted groundwater from the Riverbank Extraction wells is discussed in Section 10.14. Additional IRL well locations were considered as future provisional wells to potentially enhance the performance of the remedy. These future provisional wells include IRL-5 (located between IRL-3 and IRL-4), IRL-6 (located in the vicinity of MW-25), and IRL-7 (located in the vicinity of PT-9, north of the compressor station). The purpose of IRL-5 would be to provide an additional eastward hydraulic push along the western edge of the Cr(VI) plume. Future provisional wells IRL-6 and IRL-7 are located in the current central portion of the Cr(VI) plume and are designed as late time remedial wells that are intended to accelerate the remediation process once the Cr(VI) plume has progressed significantly in the eastward direction. Future provisional wells IRL-6 and IRL-7 were also considered as a carbon-amended recirculation well pair. The impact of future provisional wells IRL-6 and IRL-7 on the simulated Cr(VI) plume are presented in a sensitivity analysis in Section 10.13. The naturally occurring hydraulic gradient toward the Colorado River is relatively low, which leads to an extended remediation timeframe. The purpose of the injections along the upgradient portion of the plume is to accelerate the groundwater and solute transport velocities to shorten the period of performance of the active remedy.

Water injected via the IRL Injection Wells includes groundwater captured by the Riverbank Extraction Wells (and amended with carbon, as necessary) and freshwater (see Section 6.4.7). The current model layout has the two northern IRL Injection Wells (IRL-1 and IRL-2) receiving water from the Riverbank Extraction Wells (without carbon amendment) at 75 gpm each, while freshwater is injected at the two southern wells, IRL-3 and IRL-4, at rates of 100 gpm and 200 gpm, respectively. However, the design layout of the IRL will be flexible enough to accommodate either injection water source to be injected into any of the four IRL wells.

The IRL Injection Wells inject into model layers 1 through 4 for a total injection flow rate of 450 gpm. Special consideration was taken in the solute transport model to allow any potential byproduct concentrations extracted at the Riverbank Extraction Wells to be accounted for in the IRL Injection Wells. The IRL Injection Wells are depicted on Figure 6.4-1, and Figure 6.4-6 shows these wells in cross-section.

#### 6.4.4 Transwestern Bench Extraction

Two extraction wells were simulated (the Transwestern Bench Extraction Wells; TWB-1 and TWB-2) between the TCS and the NTH IRZ in the aquifer area referred to as the “Transwestern Bench.” Two provisional Transwestern Bench Extraction Wells are also being considered in the event that additional

hydrogeologic findings or remedy performance evaluations indicate additional wells would be necessary in this area. The purpose of these extraction wells is to accelerate the capture and treatment of the Cr(VI) plume immediately downgradient of the TCS. These wells are simulated in model layers 1 through 4 and operate at a total rate of 22 gpm. The rate at each of the individual wells is varied based on the thickness of the screened aquifer, with the highest rate in the thicker northwestern portion of the aquifer and the lowest rate in the thinner southeastern portion of the aquifer. This extracted water is assumed to be treated and injected into the two TCS Injection Wells (TCS-1 and TCS-2; see Section 6.4.6). The locations and rates of TWB-1 and TWB-2 are shown on Figure 6.4-1. Figure 6.4-5 shows the Transwestern Bench Extraction Wells in cross-section.

#### 6.4.5 East Ravine Extraction

Located in the southeastern portion of the plume that exists in the bedrock, four extraction wells (ER-1 through ER-4) were simulated and are referred to as the East Ravine Extraction Wells. The purpose of these wells is to extract the Cr(VI)-impacted groundwater located in the bedrock. These wells are screened in the upper four layers of the model. In this portion of the model, the upper four layers represent the shallow bedrock, and the hydraulic conductivities are considerably lower than the hydraulic conductivities of the alluvial aquifer. Because of the tighter material in this vicinity, sustainable extraction rates are limited. In the solute transport model, the East Ravine Extraction Wells extract at a total rate of only 2 gpm, with the rate divided evenly over all four wells. Additionally, a fifth bedrock extraction well (ER-6) is located at Site H and will utilize existing monitoring well MW-70BR-225. Elevated Cr(VI) groundwater concentrations were detected at the bottom of this well location and a relatively high groundwater extraction rate could be obtained. An extraction rate of 3 gpm was simulated at ER-6. The extracted bedrock groundwater from ER-1 through ER-4 and ER-6 is proposed to be injected, as well as with the groundwater from the Transwestern Bench Extraction Wells, into the two TCS Injection Wells. The location of the East Ravine Extraction Wells is shown on Figure 6.4-1. Figure 6.4-4 shows the East Ravine Extraction Wells in cross-section. The performance of these five bedrock extraction wells will be evaluated to determine the necessity of additional extraction wells in the East Ravine. One future provisional well location has been included in the 60% design to accommodate data collected in the vicinity of Site K (ER-5). Additional data collection in Sites K and the performance of the East Ravine Extraction Wells will be considered in determining the need for installing this future provisional well.

#### 6.4.6 Topock Compressor Station Injection

Water from the Transwestern Bench and the East Ravine Extraction Wells is amended with carbon substrate and injected into two wells located in the immediate vicinity of the TCS (the TCS Injection Wells; TCS-1 and TCS-2). These two wells are screened in model layers 1 through 4 and inject at rates of 13.5 gpm each. They are located within the footprint of the plume and serve to treat Cr(VI)-impacted water in the immediate vicinity and accelerate groundwater flow towards the Transwestern Bench Extraction Wells and

the NTH IRZ. Similar to the NTH IRZ, these injection wells are carbon amended. They are proposed to operate constantly, although carbon loading was varied over time to reduce the impact of byproducts. During the 6-month period where the NTH IRZ is active, TCS injection well carbon concentrations are 100 mg/L, and during the 18-month NTH IRZ off period, carbon concentrations are reduced to 5 mg/L. An additional element considered for the TCS Injection Wells is that because they are located within the footprint of the plume, stagnation points may develop upgradient of these wells. To compensate for these potential stagnation areas, it is recommended that the southern freshwater injection well located upgradient of the TCS should inject at a higher rate than the TCS Injection Wells. In these solute transport runs, the southern freshwater injection rate is maintained at 50 gpm to continue the eastward push of groundwater despite the 27 gpm injected at the TCS. The locations of the two TCS Injection Wells are shown on Figure 6.4-1. Figure 6.4-7 shows the TCS Injection Wells in cross-section.

#### 6.4.7 Freshwater Injection

Two Freshwater Injection Wells (FW-1 and FW-2) were simulated upgradient of the plume extent in all 4 upper model layers. The purpose of the Freshwater Injection Wells, similar to the function of the IRL Injection Wells, is to accelerate the groundwater and solute transport velocities to shorten the period of performance of the active remedy. The simulated total freshwater injection rate is 450 gpm (150 gpm into FW-1 and FW-2, and 300 gpm into IRL-3 and IRL-4; see Section 6.4.3); the source of this water is assumed to be HNWR-1 located on the eastern side of the Colorado River in Arizona. The layout and extraction rates for FW-1 and FW-2 (as well as IRL-3 and IRL-4) are shown on Figures 6.4-1 and 6.4-2. The northern Freshwater Injection Well, FW-1, operates at a rate of 100 gpm, and the injection rate at FW-2, located to the west of the TCS, operates at a rate of 50 gpm. Previous remedial design analyses suggested a freshwater injection located to the north of the NTH IRZ a few hundred feet west of the Colorado River. This well was originally positioned to help control flow under a higher flow remedial design. Under the current remedial design flow conditions and based on solute transport model results, this freshwater injection well provided little to no hydraulic benefit to the performance of the remedy. Therefore, the freshwater injection well north of the NTH IRZ and in the vicinity of the Colorado River was removed from the remedial design. It is assumed that the HNWR-1 freshwater source will be treated for naturally occurring arsenic concentrations; therefore, the simulated Freshwater Injection Wells did not contain arsenic. Figures 6.4-6 and 6.4-8 show the injection wells receiving freshwater in cross-section.

### 6.5 Flow Conditions

The simulated groundwater contours for the solute transport model under ambient conditions are shown on Figures 6.5-1 through 6.5-4 (model layers 1 through 4, respectively). The impact of the proposed remediation design on the submodel groundwater flow is shown on Figures 6.5-5 through 6.5-8 (model layers 1 through 4, respectively). Figures 6.5-6 through 6.5-8 depict the two potential groundwater conditions that exist with the proposed remedial design. One frame of each figure depicts the contours with the NTH

IRZ under operating conditions for a 6-month period, while the second image shows conditions with the NTH IRZ turned off for an 18-month period. In both the active remediation scenarios, flow direction of the groundwater within the footprint of the plume remains from west to east towards the Colorado River; however, gradients are steeper than the original ambient conditions, indicating an enhanced gradient and a more rapid period of performance.

Figures 6.5-9 through 6.5-12 show simulated groundwater capture zones under active remedy flow conditions in model layers 1 through 4, respectively. These groundwater capture figures were generated using MODALL (Potter et al. 2008). Specifically, MODALL was utilized to compute the percentage of water located in each of the finite difference grid cells that is captured by selected groundwater sinks (extraction wells) simulated in the groundwater flow model. Areas where the percentage of captured groundwater by extraction wells exceeded 50% were delineated by a single capture zone. These figures, therefore, display the relative extent of the capture zone for the simulated active groundwater extraction wells in each of the four model layers. This analysis demonstrates that the Riverbank Extraction Wells primarily pull water from the deep aquifer (model layers 3 and 4) below the river and reducing rind. Limited extracted water comes from the shallow aquifer (model layers 1 and 2), and the largest fraction of captured shallow groundwater comes from upgradient (west) of the Riverbank Extraction Wells. These capture zone figures also demonstrate that the capture zone associated with the two Transwestern Bench Extraction Wells is successful in capturing groundwater from the TCS area and there are no gaps between TWB-1 and TWB-2 or between the Transwestern Bench Extraction Wells and the bedrock. The simulated capture zone associated with the East Ravine Extraction Wells is due to the low-simulated hydraulic conductivity of the bedrock and does not account for the potential of hydraulic fractures in the bedrock. It is also of note that the remedy does not capture the entire plume footprint of all four model layers. This is because the remedial design does not call for capturing the entire plume, but rather a combination of capture and IRZ treatment. Therefore, the portions of the aquifer Cr(VI) plume that are not within the simulated capture zone will pass through the IRZ areas and be reduced. To effectively evaluate the performance of the remedial design, the solute transport model was utilized to understand the movement of the plume rather than relying on the simulated capture zones.

## **7. Solute Transport Model Results**

### **7.1 Hexavalent Chromium**

The solute transport model was run for a period of 50 years utilizing the transport parameters and flow conditions described in Section 6 for the simulated Cr(VI). The results are shown for years 0.5, 1.5, 10, 20, and 30 for each of the four model layers on Figures 7.1-1 through 7.1-4. These figures show the impact of the injected carbon concentrations and remediation design flow conditions have on the chromium distribution over time. Carbon is actively injected into the NTH IRZ during the first 6 months of the simulation, followed by an 18-month period where the NTH IRZ is turned off. This 6-month on/18-month off NTH IRZ cycle period is repeated for the full duration of the 30-year transport run. This solute transport run indicates the NTH IRZ successfully creates a remediation barrier along the majority of the NTH IRZ line in all four model layers. The sections of the plume that are initialized on the east side of the NTH IRZ and the low Cr(VI) concentrations in the vicinity of the NTH IRZ wells that are not treated by the NTH IRZ (e.g., the low concentration finger of the plume that migrates past the northern NTH IRZ in model layers 3 and 4; see Figures 7.1-3 and 7.1-4, during the 18-month rest cycle when active pumping is suspended) are hydraulically controlled by the Riverbank Extraction Wells.

A design option to reduce Cr(VI) migration past the northern portion of the NTH IRZ by conducting 18-month off-cycle NTH IRZ extraction is presented in sensitivity analysis Section 10.9. By year 30 of the simulated transport run, the majority of the alluvial Cr(VI) plume in all four model layers has been remediated. The alluvial aquifer Cr(VI) remaining at year 30 is a relatively small footprint located just upgradient of the central portion of the NTH IRZ. The actual time for all simulated alluvial aquifer Cr(VI) concentrations to reduce to below 32 µg/L is 38 years in model layers 1 and 2, 44 years in model layer 3, and 48 years in model layer 4. These timeframes are based upon the initial remedial layout and do not incorporate additional optimizations to address the simulated persistent Cr(VI) impacts in the aquifer that occur at later times in the remedy. Optimizations to these Cr(VI) transport simulations were evaluated in Section 10. The portion of the Cr(VI) that persists for the greatest duration is initialized in the bedrock in the vicinity of the East Ravine Extraction Wells. This is due to the tight hydraulic conductivity values simulated in the bedrock limit flow velocities and remediation timeframes. This is a limitation of the groundwater flow model and solute transport model because potential fractured bedrock or high conductivity channels that potentially exist in the bedrock cannot be accounted for in this analysis. The effectiveness of the East Ravine Extraction Wells located in the bedrock need to be closely monitored during the remediation design implementation.

### **7.2 Manganese**

The results for the simulated manganese are presented for the same 30-year period and 4 model layers as were the Cr(VI) results. Figures 7.2-1 through 7.2-4 show potential manganese generated as a byproduct from the injection of carbon-amended groundwater. The manganese runs shown on Figures 7.2-5 through

7.2-8 take into account both the naturally occurring manganese, as well as potential generated manganese byproduct. The delineated naturally occurring manganese distribution was based on observed concentrations and, due to the limited data density particularly to the east of the river, assumptions based on the operating conceptual model explains the presence of manganese in the floodplain (i.e., elevated dissolved manganese concentrations are typically observed under reducing conditions). The comparison of Figures 7.2-1 through 7.2-4 to 7.2-5 through 7.2-8 indicates that generated byproduct manganese concentrations are estimated to be generally lower than the heterogeneous naturally occurring manganese distribution. The manganese transport run indicates that portions of the naturally occurring manganese and generated manganese byproduct will be extracted by the Riverbank Extraction Wells and injected into IRL-1 and IRL-2, located in the upland area. This potential manganese impact in the uplands needs to be monitored over time to avoid elevated manganese concentrations. A potential method to mitigate this upland manganese impact would be to blend the riverbank extracted water with the freshwater injection.

### **7.3 Arsenic**

The results for the simulated arsenic transport (Figures 7.3-1 through 7.3-4) are presented for the same 30-year period and 4 model layers as were the Cr(VI) and manganese results. The arsenic runs take into account potential arsenic generated as a byproduct from carbon-amended injection wells. The solute transport run indicates that arsenic concentrations associated with carbon-amended injection never exceed 10 µg/L in the 30-year simulation period.

### **7.4 Transient and IM-3 Transition Hexavalent Chromium Simulations**

The submodel was also utilized to evaluate the impact that seasonal fluctuations in Colorado River stage elevations have on the groundwater flow and solute transport modeling. Based on observed Colorado River stage data from 2004 to 2012 average trends were apparent for typical yearlong cycles. The difference between the average high stage elevation and low stage elevation is 3.77 feet. The average duration to go from a low stage elevation is 4.5 months, while the duration to return from low stage to high stage is 7.5 months. The simulated yearlong transient period starts with the lowest average river stage, increases to the highest average stage, and ultimately returns to the lowest average river stage. The transient model was setup so the average change in Colorado River stage elevation between transient stress periods is 0.5 feet, in order to simulate the time variant impact of the river stage on groundwater flow in the submodel. The transient model was run with ambient conditions without active remedial activity. Monthly simulated potentiometric surfaces and groundwater flow vectors for this 1-year transient model are shown on Figures 7.4-1 and 7.4-2. Within each map on these figures is a graph indicating which stress period and relative river stage is represented by the simulated potentiometric surface and groundwater flow vector map. These figures indicate the primary flow direction along the western edge of the Colorado River for the majority of the transient stress periods is towards the Colorado River. Only three maps (months 4, 4.5, and 5) indicate a dominant landward flow from the western edge of the Colorado River, and transient month 3 indicates a



more neutral flow pattern along the western Colorado River boundary. This indicates that despite fluctuations in Colorado River stage during an average year, the dominant flow direction on the western edge of the Colorado River is towards the Colorado River.

Upon completion of the ambient transient flow analysis, a transient transport analysis was utilized to simulate the Cr(VI) transport during the transition from IM-3 shutdown to active remedial pumping. Once again, starting conditions were during the lowest average stage of the Colorado River to represent the maximum flow conditions towards the Colorado River on the western edge of the Colorado River. The initial pumping conditions simulated were NTH IRZ operation for a 6-month period (300 gpm injection and extraction) with active carbon injection, followed by a 3-month period where the NTH IRZ is shutoff and the Riverbank Extraction Wells are turned on at 150 gpm and the extracted water is injected into IRL-1 and IRL-2. To simulate the approximate time needed to develop an effective IRZ, the TOC concentration required to initiate Cr(VI) precipitation was increased to 10 mg/L (a 10 mg/L TOC trigger). After this initial 6 months of active TOC injection, the TOC trigger was reduced back down to 0.1 mg/L to represent the more established reducing environment that is generated by an extended period of active TOC injection. In conjunction with this transient transport model, a steady-state (average Colorado River stage elevation) transport model was conducted with the exact same pumping schedule and assumptions as the initial transient transport model. Figures 7.4-3 and 7.4-4 depict the Cr(VI) and TOC transport results for a 3-month period (NTH IRZ only) for both the transient and steady-state models for layers 2 and 4, respectively. During the first 3 months, the development of the NTH IRZ reducing zone occurs. The main observations that can be made from Figures 7.4-3 and 7.4-4 are that the transient and steady-state transport runs are very similar and that the floodplain Cr(VI) does not migrate a significant distance towards the Colorado River. Figures 7.4-5 and 7.4-6 depict the Cr(VI) and TOC transport results for a 6-month period (NTH IRZ only) for both the transient and steady-state models for layers 2 and 4, respectively. Similar to the 3-month results, by month 6, the transient and steady-state transport runs are very similar, and the floodplain Cr(VI) still has not migrated a significant distance towards the Colorado River. Figures 7.4-7 and 7.4-8 depict the Cr(VI) and TOC 9-month transport results where the NTH IRZ has been off for 3 months and the IRL has been active for 3 months for both the transient and steady-state models for layers 2 and 4, respectively. Despite the increased flow velocity induced by the IRL, the steady-state and transient results are still very similar. At this stage, the comprehensive reducing zone along the NTH IRZ has been established and the plume has not migrated a significant distance in the floodplain. The main conclusion drawn from this analysis is that the steady-state model and transient model produced very similar Cr(VI) transport results, which supports the use of the steady-state model for the solute transport modeling scenarios. Additionally, this analysis indicates that this transition schedule from IM-3 would be protective of the Colorado River.

To further evaluate the IM-3 transition to a full active remedy schedule, several additional solute transport modeling runs were conducted. Two 1-year and two 2-year startup schedules were evaluated with the solute transport model. The primary difference in these startup schedules, other than duration, is the order in which the different remedial pumping wells are turned on. The details of these four scenarios are described below:

- Scenario 1A (1 year)
  - Month 0 to 6: NTH IRZ ON
  - Month 6 to 9: NTH IRZ OFF and Freshwater Injection<sup>2</sup> ON
  - Month 9 to 12: NTH IRZ OFF and Freshwater Injection, TCS Recirculation Loop, and IRL ON
- Scenario 2A (1 year)
  - Month 0 to 6: NTH IRZ ON
  - Month 6 to 9: NTH IRZ OFF and IRL<sup>2</sup> ON
  - Month 9 to 12: NTH IRZ OFF and Freshwater Injection, TCS Recirculation Loop, and IRL ON
- Scenario 1B (2 years)
  - Month 0 to 12: NTH IRZ ON
  - Month 12 to 18: NTH IRZ OFF and Freshwater Injection<sup>2</sup> ON
  - Month 18 to 24: NTH IRZ OFF and Freshwater Injection, TCS Recirculation Loop, and IRL ON
- Scenario 2B (2 years)
  - Month 0 to 12: NTH IRZ ON
  - Month 12 to 18: NTH IRZ OFF and IRL<sup>2</sup> ON
  - Month 18 to 24: NTH IRZ OFF and Freshwater Injection, TCS Recirculation Loop, and IRL ON

Figures 7.4-9 and 7.4-10 depict the simulated hexavalent chromium transport results for the two 1-year IM-3 transition schedules (Scenarios 1A and 2A) for model layers 2 and 4, respectively. The primary difference that is apparent between these two 1-year scenarios is that, within the first year, the Cr(VI) plume migrates slightly farther to the east when the freshwater injection is turned on in month 6 (Scenario 1A) instead of month 9 (Scenario 2A). Despite this slight difference, the simulation results indicate that both of the proposed 1-year IM-3 transition pumping schedules are protective of the Colorado River [i.e., the Cr(VI) plume does not migrate a significant distance in the floodplain during startup and the portion of the plume located downgradient of the NTH IRZ does not migrate past the capture zone of the Riverbank Extraction Wells].

---

<sup>2</sup> The intermediate (60% design) nominal scenario assumes IRL-1 and IRL-2 (northern IRL Injection Wells) will receive carbon-amended Riverbank Extraction Well water if Cr(VI) concentrations in the Riverbank Extraction Wells exceed the cleanup goal; and IRL-3 and IRL-4 (southern IRL Injection Wells) will receive freshwater. Thus, the startup scenarios include IRL-3 and IRL-4 with the Freshwater Injection ON; and IRL ON includes only IRL-1 and IRL-2. Injection wells IRL-1 through IRL-4 will be constructed for flexibility to inject either/both freshwater or/and Riverbank Extraction Well water during the lifetime of the remedy. FW-1 (not depicted on the figures) is located west of the area shown.





## **Appendix B: Development of Groundwater Flow, Geochemical, and Solute Transport Models**

Topock Compressor Station  
Needles, California

Figures 7.4-11 and 7.4-12 depict the simulated Cr(VI) transport results for the two 2-year IM-3 transition schedules (Scenarios 1B and 2B) for model layers 2 and 4, respectively. Similar to the 1-year scenarios, the main difference that is apparent between these two 2-year scenarios is that the Cr(VI) plume migrates slightly farther to the east when the freshwater injection is turned on in month 12 (Scenario 1B) instead of month 18 (Scenario 2B). While it would still be ideal to activate the remedial pumping according to the faster 1-year transition schedule in the interest of reducing the total remedial timeframe, the solute transport modeling results for both 2-year transition scenarios indicate that they are also protective of the Colorado River and are viable IM-3 transition options.

## **8. Manganese Hyporheic Zone Model Results**

The geochemical model described in Section 5 was used in a one-dimensional reactive transport model to simulate the oxidative precipitation of manganese in the hyporheic zone (groundwater-surface-water mixing zone) as groundwater passing through the Site discharges into the Colorado River. The goal of this model is to establish reasonable bounds on the quantity of manganese that would be expected to enter the river from the floodplain under various remedy scenarios, relative to ambient conditions. Because  $Mn^{2+}$  concentrations, groundwater flow rates, and geochemical environments are complex and spatially variable, the goal is to limit the analysis to a simple (one-dimensional) mass balance approach.

### **8.1 Hyporheic Zone Model Domain, Parameters, and Execution**

The hyporheic zone model domain represents the last 5 feet of groundwater flow before discharging into the Colorado River, with the effluent cell boundary representing the river water interface. The model influent has the characteristics of the measured floodplain groundwater and the flow rate is constant. Within the model, dissolved Mn(II) interacts with the dissolved oxygen present in the groundwater-river water mixing zone resulting in low-solubility Mn(IV) oxides. The model was run until uniform dissolved Mn(II) concentrations were achieved throughout the domain, with conditions balanced by inward advection and oxidation within the mixing zone. After reaching steady state, the Mn(II) concentration at the effluent boundary is interpreted as the concentration of Mn(II) in the water discharging to the Colorado River.

#### **8.1.1 Flow and Transport Model Parameters**

The model domain consists of a one-dimensional 1-foot by 1-foot by 5-foot channel with flow along the long axis, discretized with a cell spacing of 0.05 feet (number of cells = 100). Consistent with the site-wide solute transport model, a dual-porosity domain was constructed with mobile porosity = 0.12, immobile porosity = 0.23, and mass transfer coefficient =  $0.001\text{ d}^{-1}$ , with dispersion turned off. Mn(II) transport is, therefore, governed by advection, mobile-immobile zone mass transfer, oxidation, and mixing within cells.

The flow rate was fixed based on the rate of discharge of groundwater that passes through the IRZ into the Colorado River (i.e., discharge rate of “treated plume water”), calculated from the site-wide groundwater flow model. This discharge rate was estimated over the approximately 2,800-foot stretch of the river that receives treated plume water. The groundwater flow model and site data predict a discharge rate of 34 gpm from this zone under ambient flow conditions, increasing to 140 gpm under IRZ active conditions. This increase in flow during remedy operation is caused by the upgradient injection of freshwater from Arizona. The actual discharge to the river during remedy operation will be affected by the riverbank extraction; however, this range in flow rates serves as a reasonable bound on anticipated conditions. Using the river bottom surface area over the IRZ stretch of the Colorado River (approximately 1.96 million square feet [ $\text{ft}^2$ ]), the specific discharge of groundwater across the river bottom interface is estimated at 0.0033 cubic feet ( $\text{ft}^3$ ) per day per

ft<sup>2</sup> and 0.014 ft<sup>3</sup> per day per ft<sup>2</sup> under ambient and IRZ active conditions, respectively. With a mobile porosity of 12%, this yields pore water seepage velocities of 0.028 feet per day and 0.12 feet per day under ambient and IRZ active conditions, respectively.

#### 8.1.2 Geochemical Model Parameters

To represent the hyporheic zone, a fixed dissolved oxygen concentration profile was assigned within the model domain to represent a steady-state groundwater-surface-water mixing profile, with the river water dissolved oxygen concentration assigned at the effluent (river interface) boundary and dissolved oxygen dropping to zero with distance into the sediment. Very limited information is available on the actual hyporheic zone thickness for the Colorado River at the Site. A pore-water characterization study conducted previously at the Site indicated that reducing conditions are present at a depth of 6 feet, based on dissolved iron and manganese concentrations. The chemistry at this 6-foot depth indicates that there is no river water influence at 6 feet (CH2M HILL 2006). The limit of surface-water mixing based on the daily fluctuation in river stage is 2 feet or less. In the hyporheic zone model, a shallow, step-like function was assumed for the dissolved oxygen profile. The assigned dissolved oxygen profile consisted of river water dissolved oxygen concentrations persisting to 1-foot, and then dropping linearly to zero between 1-foot and 2-feet, for a total hyporheic or mixing zone depth of 2 feet (see Figure 8.2-1). Quarterly monitoring results at the Site indicate that dissolved oxygen levels in the Colorado River vary seasonally between approximately 7 and 13 mg/L; however, rather than assuming a supersaturated dissolved oxygen content at the river interface, a uniform value of 8.4 mg/L for river water was assumed (nominal dissolved oxygen saturation in equilibrium with atmosphere).

Mn(II) oxidation to Mn(IV) occurs in the model in the presence of dissolved oxygen. Based on the literature observations discussed in Section 5.3, the oxidation rate was assumed first order with respect to Mn(II) concentration above 2.5 mg/L (i.e., independent of dissolved oxygen content above 30% dissolved oxygen saturation) and second order with respect to Mn(II) and dissolved oxygen (first order with respect to each) below 2.5 mg/L (Marble et al. 1999). The base-case pseudo-first order rate constant for Mn(II) was assigned as 0.083 h<sup>-1</sup> [Mn(II) half-life = 8.3 hours for dissolved oxygen greater than 2.5 mg/L], corresponding to the lowest hyporheic zone rate observed by Harvey and Fuller (1998). As a sensitivity test, the model was also run with a rate constant decreased by factors of 5 and 10 (half-lives of 42 and 83 hours for dissolved oxygen greater than 2.5 mg/L, respectively).

Influent groundwater geochemistry was based on average floodplain conditions, as listed in Section 5.3. All other aspects of the geochemical model [including aqueous speciation and Mn(II) sorption] followed the design outlined in Section 5. The model was run under the following three scenarios:

- 1) Average-Ambient: Mn(II) concentration set at the Site upper tolerance limit  
Mn(II) concentration = 1.3 mg/L  
Groundwater flux = 0.0033 ft<sup>3</sup> per day per ft<sup>2</sup>

- 2) IRZ-Active: Mn(II) concentration set at the upper end of the anticipated range at the riverbank  
Mn(II) concentration = 2.0 mg/L  
Groundwater flux = 0.014 ft<sup>3</sup> per day per ft<sup>2</sup>
- 3) Extreme IRZ-Active: Mn(II) concentration set at the maximum threshold value  
Mn(II) concentration = 3.0 mg/L  
Groundwater flux = 0.014 feet per day

The anticipated range and maximum threshold values for Mn(II) are defined in the Operations and Maintenance Manual Volume 2: Sampling and Analysis Plan (Appendix L of the 60% Basis of Design).

Each of the three model scenarios was evaluated using the base-case, 5 times reduced, and 10 times reduced Mn(II) oxidation rates. The model results were used to determine Mn(II) concentration at the river interface, mass flux of Mn(II) discharged to the river, and incremental Mn(II) concentration increase within the river, as described below. The hyporheic zone sensitivity runs consider a larger fractional range in oxidation half-life than what was investigated in the solute transport model (which accounts for manganese oxidation in the upland), where a half-life increase of 2X was tested. The higher range was used herein to specifically determine how slow the rate needed to be to observe a non-zero manganese concentration at the river interface.

## **8.2 Results**

Steady-state manganese profiles for each of the model run scenarios are shown on Figure 8.2-1. In all cases (Scenarios 1, 2, and 3), the model predicts that dissolved Mn(II) is completely oxidized before groundwater discharges into the river when the base-case oxidation rate (half-life = 8.3 hours) is assumed, as reflected by steady-state Mn(II) concentrations that attenuate to effectively zero (less than 1 nanogram per liter [ng/L]) at the river interface. The model results, therefore, suggest that increasing groundwater fluxes and Mn(II) concentrations resulting from IRZ activity, even if Mn(II) concentrations are higher than anticipated, are not expected to result in higher concentrations of Mn(II) being discharged to the river using reasonable, hyporheic zone-specific Mn(II) oxidation rates.

Sensitivity runs were performed using Mn(II) oxidation half-lives increased by factors of 5 and 10. Under all three scenarios, increasing the Mn(II) half-life 5 times (half-life = 42 hours) results in Mn(II) concentrations below 10 µg/L (below typical analytical reporting limits). Under ambient conditions, Mn(II) concentrations are predicted to attenuate effectively to zero, while under IRZ active conditions, residual Mn(II) concentrations of between 3 and 6 µg/L are predicted with influent groundwater Mn(II) concentrations of 2 to 3 mg/L. When the oxidation half-life is increased by 1 order of magnitude over base-case (half-life = 83 hours), higher residual Mn(II) concentrations are predicted at the river interface. The concentration under ambient conditions is less than 1 µg/L, while under IRZ active conditions, concentrations between 80 and 120 µg/L are predicted. Therefore, under all conditions and oxidation rates tested, the model predicts that between 96

and 100% of the dissolved manganese entering the hyporheic zone in groundwater is oxidized before discharging to the river. These results are summarized in Table 8.2-1.

For model scenarios where non-zero manganese concentrations were predicted at the sediment-river interface, manganese discharge mass fluxes and incremental river concentration increases were estimated (Table 8.2-1). The manganese mass fluxes were calculated based on predicted river interface concentrations and the site-wide groundwater flow model discharge estimates of 34 and 140 gpm under ambient and IRZ active conditions, respectively. For comparison, results are also shown in the table assuming no hyporheic zone oxidation of manganese. Without oxidation, estimated mass fluxes of manganese to the river are on the order of 0.2 kilograms per day (kg/day) under ambient conditions over the IRZ stretch, going up to as high as 2.3 kg/day under extreme conditions. With oxidation, these mass fluxes drop to less than 0.1 kg/day under all conditions studied (less than 4% of influent manganese making it to the river). Incremental manganese concentration increases in the river were calculated based on the average river flow rate past the Site, estimated at 6.8 million gpm (CH2M HILL 2011). Based on model-estimated river interface concentrations and the calculated river dilution factors, the incremental concentration increase is less than 2.5 ng/L (less than 0.0025  $\mu\text{g/L}$ ) under all scenarios modeled, down from between 6 and 60 ng/L without oxidation. It is, therefore, predicted that any increase in Mn(II) concentration in the river will be orders of magnitude below detection, particularly after oxidation within the hyporheic zone.

## **9. Geochemical Reactive Transport Model Results and Sensitivity Analyses**

### **9.1 Solute Transport Model and Geochemical Reactive Transport Model Comparison**

To test the validity of the site-wide solute transport model in describing Cr(VI) reduction/removal and byproduct dynamics in the aquifer, a comparison was run between the MT3D solute transport model and the geochemical reactive transport model, implemented in PHT3D. The comparison was run within a one-dimensional domain representative of the flow path between the NTH IRZ and the river, as described below. The two models were identical with regard to flow parameters and influent conditions, differing only in how biogeochemical processes were captured by each of the models, described in detail in Sections 5 and 6 for the PHT3D and MT3D simulations, respectively.

#### **9.1.1 Model Comparison Domain and Geochemical Inputs**

The model domain used for the comparison involved a one-dimensional (1-foot by 1-foot by 750-foot) channel representing a flow path within model layer 1 starting upgradient of the NTH IRZ, then running through an NTH IRZ injection well, passing through the floodplain, and terminating near the riverbank. The total domain was 750 feet long in the direction of groundwater flow, with an injection well located 250 feet into the domain (500 feet from the effluent end). A 100-cell, variable-cell-spacing grid was used, with a refined grid in the vicinity of the injection well (2-foot cell spacing), getting gradually coarser with distance from the injection well (10-foot grid spacing at influent and effluent ends). The model domain is illustrated conceptually on Figure 9.1-1, although it should be emphasized that the model parameters were based on average floodplain conditions and the domain does not represent a specific injection well.

Constant head boundary conditions were assigned at the influent and effluent boundaries, with head difference and hydraulic conductivities calibrated to yield a groundwater seepage velocity of 1.75 feet per day under ambient conditions. The injection rate was then calibrated to yield a groundwater seepage velocity downgradient of the injection well of 2.3 feet per day. These groundwater velocities represent average floodplain values extracted from the site-wide flow and transport model. The resulting head profiles under active and ambient conditions are shown on Figure 9.1-1. Because the heads were calibrated to extracted groundwater velocities, it was not necessary to explicitly include a Riverbank Extraction Well near the effluent boundary. The model was executed for one single IRZ on/off cycle (6 months on, 18 months off) to illustrate how each model simulates Cr(VI) removal and byproduct transport with and without TOC injections.

The resulting model parameters for the flow domain are summarized below. Note that the calibrated injection rate is much smaller than the actual injection rate for any given well, because it only includes the effective injected rate into the 1-foot by 1-foot cross-section of the flow channel.

Domain length:	750 feet
Mobile porosity:	0.12
Immobile porosity:	0.23
Mass transfer coefficient:	0.001 d <sup>-1</sup>
Ambient groundwater velocity:	1.75 feet per day
IRZ-active groundwater velocity:	2.3 feet per day
IRZ well injection rate:	0.166 ft <sup>3</sup> per day
Head drop across 750-foot domain:	1.88 feet
Hydraulic conductivity:	70 feet per day
On cycle duration:	180 days
Off cycle duration:	540 days

The initial geochemical conditions within the domain were assigned based on average floodplain conditions, as listed in Section 5.3, with the exception of chromate, dissolved oxygen, and nitrate. For these parameters, higher concentrations were assigned upgradient of the injection well to reflect higher concentrations upgradient of the NTH IRZ within the Cr(VI) plume. The initial conditions for these parameters were as follows:

	<u>Upgradient</u>	<u>Floodplain</u>
Cr(VI)	15 mg/L	0
Dissolved oxygen	5 mg/L	2 mg/L
Nitrate	5 mg/L	2.6 mg/L

Dissolved oxygen and nitrate values were based on approximate averages along the NTH and the floodplain, while a high upgradient Cr(VI) value was used to appropriately test the limits of the models. The transition between upgradient and floodplain initial chemistry was made linearly over a distance of 60 feet, centered at the injection well. Influent geochemistry at the domain inlet was the same as the upgradient initial geochemistry.

As mentioned above, the solute transport (MT3D) and geochemical reactive transport (PHT3D) models differed only in the ways in which biogeochemical processes were captured. In particular, the geochemical reactive transport model explicitly included thermodynamic redox calculations for all major redox-active components (TOC, oxygen, chromium, nitrogen, manganese, oxygen, and sulfur; arsenic was assumed to be present as arsenite for simplicity); precipitation and dissolution reactions for chromium, manganese, and iron; and sorption of Mn(II) and Fe(II) described using the SCM. As in the solute transport model, sorption in the PHT3D simulation was only assumed to occur outside of the TOC footprint (TOC less than 0.1 mg/L). Arsenic sorption was not included; attenuation of arsenic was modeled using the first-order attenuation mechanism in both the MT3D and PHT3D simulations. Manganese byproduct generation in the PHT3D simulation was modeled as the kinetic reductive dissolution of pyrolusite as described in Section 5.3. However, due to numerical instabilities, the iron oxide dissolution release mechanism for arsenic described



in Section 5.4 could not be implemented in the reactive transport model; therefore, arsenic generation was linked to TOC degradation as in the solute transport model. It was demonstrated in Section 5.4 that the two mechanisms yield similar results.

#### 9.1.2 Transport Model Comparison Results

The geochemical reactive transport model results for the 1D IRZ domain are shown on Figures 9.1-2 and 9.1-3, with concentration profiles across the model domain given in 3- to 6-month increments. While the remedy is on (green curves), TOC exhibits an exponentially decaying profile downgradient of the injection well, governed by the 20-day biodegradation half-life. These profiles attenuate back to zero once the remedy is turned off. The oxidation of organic matter in the model is coupled to the reduction of Cr(VI), dissolved oxygen gas, and nitrate. The concentration profiles for these species indicate that reduction is complete and sustained, even in the presence of iron oxides and dissolved sulfate. The Cr(VI) plume does not migrate past the injection well, while dissolved oxygen and nitrate concentrations drop to zero within the TOC footprint. After Cr(VI), nitrate, and dissolved oxygen are completely consumed in the model, Fe(III)-oxides reductively dissolve to form dissolved/sorbed Fe(II) and Fe(II)-oxides (primarily magnetite in the model), which largely remain within the IRZ footprint. Sulfate is not significantly reduced in the model (results for iron and sulfate not shown). As groundwater moves through, the residual dissolved oxygen and nitrate, initially present in the floodplain, migrate out of the model domain. When the TOC injection is turned off after 6 months, continued reduction of Cr(VI), dissolved oxygen, and nitrate occurs due to the stored reducing capacity in the form of reduced iron minerals, primarily magnetite in the model. As this reducing capacity is depleted, the Cr(VI), dissolved oxygen, and nitrate fronts slowly creep forward, though it is clear that more than sufficient reducing capacity remains after the 18-month off-cycle. Aqueous manganese and arsenic are generated and travel downgradient, attenuating only after leaving the TOC footprint approximately 200 feet from the effluent end. Bicarbonate alkalinity increases in the model as a result of organic matter degradation, while pH fluctuations are minimal due to the soil buffering reaction incorporated in the model, in line with pilot test observations.

The comparative results of the 1D IRZ simulation using the geochemical reactive transport model and the MT3D solute transport model are shown for TOC, Cr(VI), Mn(II), and arsenic in Figure 9.1-4. The simulations are remarkably close, demonstrating that the incorporation of biogeochemical processes within the MT3D simulations is comparable to the more mechanistic descriptions included in the geochemical modeling. For manganese, the comparison demonstrates that approximation of generation and sorption using the TOC-linkage and fitted Freundlich sorption models are adequate compared to explicit reductive dissolution and surface complexation descriptions, respectively. For chromium, small deviations in the migration of the Cr(VI) front between MT3D and PHT3D simulations during the off-cycle are due to the vastly different approaches for capturing Cr(VI) reduction in the two models. However, the similarity is strong enough to confirm that the approach used in the site-wide solute transport model is adequate.



## 9.2 Geochemical Sensitivity Analysis

The geochemical model was also used to investigate the effects of variations in groundwater geochemistry on the different aspects of the treatment remedy. The effects of pH, alkalinity, and TDS were specifically investigated. As discussed in Section 3, these parameters are not expected to have a significant impact on organic matter biodegradation or Cr(VI) reductive precipitation given the ranges observed within the floodplain. It is anticipated that variability in groundwater chemistry would have the greatest impact on the adsorption of byproduct manganese, as ion sorption to charged surfaces is well known to be dependent on pH, ionic strength, and the presence of competing sorptive ions (e.g., Dzombak and Morel 1990; Appelo et al. 2002). The geochemical sensitivity analysis, therefore, focused on Mn(II) sorption, with the goal of helping to define appropriate sensitivity ranges for the site-wide solute transport model sensitivity analysis (Section 10) based on the geochemical variability observed in the floodplain.

The floodplain pH, alkalinity, TDS, and major ion concentrations are summarized below, with averages and standard deviations calculated from all available floodplain well data between 1997 and spring 2012.

	pH	Alkalinity	TDS	Ca	Mg	K	Na	SO <sub>4</sub>
Average	7.56	202	7204	318	83	29	2223	842
Standard Deviation	0.45	170	7006	273	166	91	1970	728
Average TDS ratio	---	---	---	0.044	0.011	0.004	0.309	0.12

The batch PHREEQC model run used to develop the Mn(II) Freundlich isotherm (described in Section 5.3.2) was run with a constant total Mn(II) concentration of 10 mg/L, separately varying pH, alkalinity, and TDS within observed ranges. To capture variations in the concentrations of individual major ions in the model, proportionality was assumed between each ion and the TDS concentration. The average ion:TDS ratio was calculated for each ion from the floodplain dataset and reported above. In the varying TDS model run, the concentration of each ion was varied in proportion to TDS. In this way, the TDS sensitivity analysis included both general ionic strength effects, as well as individual ion-competition effects (e.g., Ca<sup>2+</sup> and Mg<sup>2+</sup> competing with Mn<sup>2+</sup> for sorption sites).

The results of the sensitivity analysis are shown on Figure 9.2-1, with aqueous Mn(II) and resultant Freundlich sorption parameter ( $K_F$ , with  $n = 0.875$ ) plotted as a function of pH, alkalinity, and TDS. The analyses were carried out well past  $\pm 1$  standard deviation to reflect the full observed geochemical ranges. The results for Mn(II) sorption are in line with expectations for each geochemical parameter. Specifically, cation sorption increases with increasing pH due to the enhanced electrostatic attraction as the surface deprotonates, increasing alkalinity decreases sorption due to both surface site competition with bicarbonate



## **Appendix B: Development of Groundwater Flow, Geochemical, and Solute Transport Models**

Topock Compressor Station  
Needles, California

and Mn(II)-bicarbonate aqueous complex formation, and decreased sorption with increasing TDS due largely to ion competition for surface sites.

The solute transport model sensitivity analysis in Section 10 considers a  $K_F$  sensitivity range of 0.137 to 6.85, which completely encompasses the variation in  $K_F$  due to anticipated geochemical variability, particularly within  $\pm 1$  standard deviation, which is the range describing the majority of the floodplain. The sensitivity range considered in the solute transport model sensitivity analysis, therefore, adequately accounts for uncertainty and variability in groundwater chemistry, as well as additional uncertainty/variability in sorption site concentration.

## **10. Solute Transport Model Sensitivity Analysis**

A detailed sensitivity analysis was conducted to evaluate the relative impact various components of the groundwater flow and solute transport models have on the solute transport model results. The sensitivity analyses presented in this Appendix B include NTH IRZ well spacing, injected TOC concentrations, riverbank extraction rates, manganese sorption and generation, arsenic precipitation and generation, Cr(VI) sorption, conditioned remedy-produced water injection into NTH IRZ, IRL and freshwater injection oscillation, off-cycle NTH IRZ extraction, TOC half-life, NTH IRZ total rate, freshwater injection rate, intermediate late remedy recirculation wells, and IRL TOC injection. Results of each of these sensitivity analyses are presented for model layers 2 and 4 after 10 years and 30 years of simulated transport. These layers and timeframes were selected to provide representative results in the shallow and deep portions of the aquifer at short- and long-term intervals of the active remedy. Subsequent to the completion of the sensitivity analyses, the following remediation well modifications were incorporated into the 60% design:

- East Ravine Extraction Well ER-6 at the Site H bedrock location was incorporated into the 60% design.
- Transwestern Bench Extraction Wells TWB-1 and TWB-2 were relocated as a part of the overall Transwestern Bench layout coordination.

These modifications were not included in the sensitivity analyses; however, the sensitivity analyses are compared against the same baseline run and, therefore, the relative sensitivity of the adjusted parameters can still be evaluated.

### **10.1 NTH IRZ Well Spacing**

The NTH IRZ remedial wells are designed to create a reducing zone along the downgradient axis of the Cr(VI) plume that is simulated in the upper 4 model layers in the alluvial aquifer. The primary two NTH IRZ layouts evaluated consisted of 150-foot spacing and 75-foot spacing between NTH IRZ injection wells. In both scenarios, the total extraction and injection rates of the entire NTH IRZ are maintained at 300 gpm each, for a net flow difference of 0 gpm. In the 75-foot NTH IRZ spacing run, in order to reduce the potential for fouling of the NTH IRZ extraction wells, the well spacing was kept at 150 feet between the extraction well and the closest injection well. With respect to the 150-foot well spacing, initial model runs indicated that there was a potential for Cr(VI) breakthrough at two locations (between IRZ-15 and IRZ-17 and between IRZ-19 and IRZ-21). To reduce this potential, additional wells (IRZ-16 and IRZ-20) were added in these potential gap locations reducing the spacing in these areas to 75 feet for the 150-foot NTH IRZ spacing run. The relative impact of the 150-foot and 75-foot NTH IRZ layouts with respect to the Cr(VI) after 10 years of simulated transport in model layers 2 and 4 are displayed on Figures 10.1-1 and 10.1-2, respectively. These figures indicate that by year 10, the 75-foot and 150-foot NTH IRZ well spacings produced similar results and are successful in preventing significant Cr(VI) breakthrough. In model layer 2, there is slight Cr(VI) breakthrough in both layouts: between IRZ-17 and IRZ-19 for the 150-foot NTH IRZ spacing run, and near

IRZ-23 for the 75-foot spacing run. Despite this slight breakthrough, the Cr(VI) is reduced during the next active NTH IRZ cycle and does not progress further into the floodplain. Figures 10.1-3 and 10.1-4 depict the model layers 2 and 4 Cr(VI) results for the 75-foot and 150-foot NTH IRZ well spacing after 30 years of simulated transport. These 30-year figures indicate that both NTH IRZ well spacing layouts produce very similar results at later times in the simulated remedy. The solute transport modeling indicates there is no significant advantage in increasing the amount of NTH IRZ infrastructure with respect to the Cr(VI) transport.

The NTH IRZ well spacing was also evaluated with respect to manganese concentrations. Figures 10.1-5 and 10.1-6 depict the manganese byproduct generated for the 150-foot and 75-foot NTH IRZ well layouts in model layers 2 and 4 after 10 years of simulated transport. These two figures indicate that the two NTH IRZ well layouts results in similar manganese byproduct footprints. There are slight differences in that the 150-foot NTH IRZ spacing manganese byproduct extends slightly farther downgradient due to greater point injection rates, and the 75-foot NTH IRZ spacing manganese byproduct is more continuous laterally along the NTH IRZ due to lower point injection rates and an increased number of injection wells along the NTH IRZ. Figures 10.1-7 and 10.1-8 display the manganese byproduct footprints after 30 years of simulated transport in model layers 2 and 4 for the 150-foot and 75-foot NTH IRZ well spacing. These figures indicate that the resultant manganese byproduct is similar between the two NTH IRZ well layouts at later times in the active remedy. Similar to the 10-year results, at 30 years the 150-foot NTH IRZ well spacing simulated manganese byproduct extends slightly further downgradient than the 75-foot NTH IRZ well spacing scenario due to higher point injection rates. Both NTH IRZ well layouts indicate manganese byproduct above 130 µg/L shows up from the recirculated riverbank extracted water injected into IRL-1 and IRL-2.

Lastly, the NTH IRZ well spacing was also evaluated with respect to arsenic concentrations. The simulated arsenic byproduct generated for the 150-foot and 75-foot NTH IRZ well layouts never exceeded 5 µg/L within the model domain during the full 30-year simulation; therefore, no arsenic figures are presented for this sensitivity analysis.

In summary, the 150-foot NTH IRZ layout is the preferred design in that less infrastructure is required to maintain an NTH IRZ reducing zone. The 75-foot NTH IRZ well spacing locations should still be considered as future provisional wells in the event that observations indicate areas of weakness along the NTH IRZ.

## **10.2 Injected TOC Concentrations**

The next parameter evaluated with respect to Cr(VI) reduction and byproduct generation was the injected TOC concentration. The 150-foot NTH IRZ well spacing layout was utilized to evaluate a range of injected TOC concentrations from 50 mg/L to 150 mg/L. The impact of the injected TOC concentration on simulated Cr(VI) transport after 10 years for model layers 2 and 4 is depicted on Figures 10.2-1 and 10.2-2, respectively. Cr(VI) breakthrough occurs in model layers 2 and 4 at an injected TOC concentration of 50 mg/L, but there are only minor differences in the solute transport results for Cr(VI) at the 100 mg/L and 150

mg/L TOC injection concentrations. The Cr(VI) transport results after 30 years of simulated transport in model layers 2 and 4 are shown on Figures 10.2-3 and 10.2-4 respectively. The 30-year Cr(VI) results indicate that there is not a significant difference between the three TOC concentration level scenarios at later times in the remedy. This indicates that the benefit of the 100 mg/L or 150 mg/L TOC concentrations is more beneficial at early remedy times compared to the 50 mg/L TOC concentrations because there is a greater potential for Cr(VI) breakthrough past the NTH IRZ into the floodplain at the lower TOC concentration when the upgradient Cr(VI) plume has the greatest extent and highest concentrations.

The sensitivity of byproduct manganese was also evaluated with respect to the TOC concentration of injected water. Figures 10.2-5 and 10.2-6 show the byproduct generated manganese after 10 years of simulated transport in model layers 2 and 4, respectively, for TOC injection concentrations of 50 mg/L, 100 mg/L, and 150 mg/L. A direct correlation between TOC concentration and byproduct is apparent in that a 50% increase or decrease in TOC concentration results in a 50% increase or decrease in the magnitude of byproduct manganese concentration. After 10 years of simulated transport, the maximum manganese concentration is less than 2 mg/L and occurs in model layer 4 with a 150 mg/L TOC injection concentration. The 30-year manganese byproduct TOC injection concentration sensitivity simulation results for model layer 2 and 4 are shown on Figures 10.2-7 and 10.2-8, respectively. The direct relationship between TOC injection concentration and manganese byproduct concentrations is still apparent 30 years into the simulated remedy. By year 30, the maximum manganese concentration is still less than 2 mg/L and occurs in model layer 4 with a TOC injection concentration of 150 mg/L.

The sensitivity of arsenic was also evaluated with respect to the TOC concentration of injected water. After 10 years of byproduct arsenic generation, byproduct arsenic downgradient of the IRZs is still below 5 µg/L for all three simulated TOC injection concentrations. The arsenic concentrations after 30 years of simulated transport for model layers 2 and 4 are displayed on Figures 10.2-9 and 10.2-10, respectively. The only simulation where byproduct arsenic is present above 5 µg/L is in model layer 2 and 4 under the high TOC injection concentration (150 mg/L TOC). Small lobes of byproduct arsenic are visible in the immediate vicinity of a few of the NTH IRZ injection wells; however, concentrations are still below the maximum contaminant level of 10 µg/L. These simulated byproduct arsenic concentrations will attenuate in the floodplain prior to reaching the Riverbank Extraction Wells.

During implementation of the NTH IRZ remedial design, Cr(VI) and byproduct concentrations should be closely monitored to evaluate the effectiveness of the system. Injected TOC concentration should be lowered to a level to produce minimal byproducts while still generating an effective reducing zone to treat the Cr(VI).

This sensitivity analysis suggests that the TOC injection concentration should be at a high enough concentration to maintain a sufficient reducing zone for Cr(VI) remediation, but excessive TOC concentrations will lead to generation of additional manganese byproduct. If reduced TOC concentrations

are still preferred, increases can be made to TOC injection rates, or the duration of the off-cycle NTH IRZ period can be reduced to maintain the continuous reducing zone.

### **10.3 Riverbank Extraction Rates**

The Riverbank Extraction Wells in the remedial system were designed with the goal of providing hydraulic capture of the Cr(VI) groundwater concentrations, accelerating cleanup of the floodplain, enhancing the flow of contaminated groundwater through the NTH IRZ line [Cr(VI) located upgradient (west) of the NTH IRZ is anticipated to be treated by the NTH IRZ], and control migration of IRZ-generated byproducts toward the Colorado River in the deeper part of the aquifer. A range of riverbank extraction rates were evaluated from 0 gpm to 300 gpm. Figures 10.3-1 and 10.3-2 depict the impact of riverbank extraction rates of 0 gpm, 150 gpm, and 300 gpm on simulated Cr(VI) transport after 10 years for model layers 2 and 4, respectively. This sensitivity analysis indicates that the northern extent of the plume is significantly larger in the 0 gpm riverbank extraction as compared to the 300 gpm riverbank extraction scenario. The Cr(VI) impact initialized in the floodplain in model layer 4 is also more quickly extracted in the highest 300 gpm riverbank extraction scenario. One potential negative impact of a higher riverbank extraction that is apparent is that the higher velocity induced by the higher extraction rates could potentially lead to Cr(VI) breakthrough past the NTH IRZ line. This is apparent by comparing the 0 gpm riverbank extraction to the 300 gpm extraction in model layer 2 after 10 years of simulated transport (Figure 10.3-1). There are small fingers of Cr(VI) that progress past the NTH IRZ in the 300 gpm scenario, while the 0 gpm scenario does exhibit minimal Cr(VI) breakthrough. Despite the breakthrough under 300 gpm, the Cr(VI) fingers are attenuated during the next NTH IRZ 6-month active cycle. Figures 10.3-3 and 10.3-4 depict the impact of riverbank extraction rates of 0 gpm, 150 gpm, and 300 gpm on simulated Cr(VI) transport after 30 years for model layers 2 and 4, respectively. The model layer 2 results indicate that by year 30, the 300 gpm riverbank extraction scenario results in an approximate 50% reduction in Cr(VI) mass as compared to the 0 gpm riverbank extraction scenario. Similarly, the model layer 4 results at 30 years for the 300 gpm riverbank extraction have a much smaller Cr(VI) footprint than the 0 gpm scenario. Additionally, in model layer 4 at 30 years, Cr(VI) is present underneath the river, whereas the floodplain Cr(VI) is predominantly removed by the 150 gpm and 300 gpm riverbank extraction scenarios.

Figures 10.3-5 and 10.3-6 display the simulated manganese byproduct under the three different riverbank extraction rates (0 gpm, 150 gpm, and 300 gpm) after 10 years in model layers 2 and 4, respectively. In all three scenarios, the same amount of manganese is generated; however, due to the different velocities in the floodplain, the manganese distribution differs between the three riverbank extraction scenarios. The 0 gpm riverbank extraction rate results in higher concentrations but over a smaller footprint, while the 300 gpm riverbank extraction scenario results in a larger footprint with lower concentrations. The 30-year results for the manganese byproduct riverbank extraction sensitivity analysis for model layers 2 and 4 are shown on Figures 10.3-7 and 10.3-8, respectively. Due to the lack of hydraulic influence of the Riverbank Extraction Wells in the 0 gpm riverbank extraction scenario, the byproduct manganese has extended further under the

river in model layer 2, while the byproduct manganese has similar extents in model layer 4. By year 30, manganese byproduct also begins to show in the upland IRL wells that receive the riverbank extraction water, with the largest footprint associated with the 300 gpm riverbank extraction scenario.

Arsenic was simulated under the 0 gpm, 150 gpm, and 300 gpm riverbank extraction scenarios for 30 years. Despite fluctuations in riverbank extraction rates, arsenic byproduct still does not exceed 5 µg/L in the floodplain during the full 30-year simulation; therefore, no figures are shown for this sensitivity analysis with respect to arsenic.

In summary, higher riverbank extraction rates result in a faster removal of floodplain groundwater impacted with Cr(VI). However, the negative impact of elevated riverbank extraction rates would be spreading the manganese byproduct footprint farther in the floodplain, potentially drawing down of the naturally occurring shallow reducing rind, and developing areas of weakness in the NTH IRZ reducing zone due to faster local groundwater velocities. Therefore, the transport model simulations recommend a starting operational riverbank extraction of 150 gpm and utilize field observations to adjust this rate as necessary.

#### **10.4 Manganese Sorption, Generation, and Oxidation**

To evaluate the sensitivity of the solute transport model to the manganese geochemical parameters, an analysis was performed varying the sorption, generation, and oxidation terms in the solute transport model within a reasonable range (see Sections 6.2.6 and 6.2.7). Manganese sorption was simulated using the non-linear Freundlich isotherm ( $C^* = KC^N$ ), where K and N are constants that were varied to align with observed field data consistent with the geochemical sensitivity analysis presented in Section 9.2. In all three sorption scenarios, the N exponent was held constant at 0.875, while the K multiplier was varied. The base manganese sorption scenario utilized a K value of 1.37, the decreased manganese sorption scenario utilized a K value of 0.137, and the increased manganese sorption scenario used a K value of 6.85. The simulated 10-year manganese byproduct sensitivity run results for model layers 2 and 4 are shown on Figures 10.4-1 and 10.4-2, respectively. These figures indicate that manganese sorption is a fairly sensitive parameter based upon the variations in simulated manganese byproduct distributions. The decreased sorption scenario has a significantly larger manganese footprint downgradient of the NTH IRZ and TCS injection wells. Additionally, the decreased manganese sorption run results in manganese byproduct showing up in the two IRL injection wells that receive riverbank extracted water impacted by manganese byproducts. By year 30, the manganese sorption sensitivity runs still indicate significant differences in manganese byproduct footprints in model layers 2 and 4 (Figures 10.4-3 and 10.4-4, respectively). The increased sorption scenario has a significantly smaller manganese footprint than the other two scenarios, and little to no manganese byproduct has arrived in the two upland IRL injection wells receiving water from the Riverbank Extraction Wells.



The next manganese parameter evaluated through sensitivity analysis is the manganese generation term. The generation term was developed as a stoichiometric ratio that relates carbon degradation to manganese byproduct mobilization (generation). The base scenario has a stoichiometric carbon to manganese generation ratio of 0.016, meaning for every 1 mg/L of TOC that degrades, 0.016 mg/L of manganese is generated in the solute transport model. The decreased and increased stoichiometric generation ratios are 0.005 and 0.05, respectively. Figures 10.4-5 and 10.4-6 display the 10-year results of the manganese byproduct generation sensitivity in model layers 2 and 4, respectively. The impact of the variation in byproduct manganese generation is apparent in that by year 10, the decreased generation run has a maximum manganese concentration of 0.3 mg/L, the base generation maximum manganese is 1.1 mg/L, and the increased generation maximum manganese concentration is 3.4 mg/L. The extent of the manganese footprint also has a direct relationship to the generation parameter. Figures 10.4-7 and 10.4-8 display the manganese byproduct generation results after 30 years of simulated transport in model layers 2 and 4, respectively. By year 30, both the base and increased generation runs have manganese footprints around the two upgradient IRL injection wells that receive water from the Riverbank Extraction Wells. While the footprints expanded between years 10 and 30, the magnitude of the maximum manganese byproduct concentration did not increase significantly. The maximum manganese byproduct concentrations for the decreased, base, and increased generation runs are 0.35 mg/L, 1.13 mg/L, and 3.5 mg/L, respectively.

The final manganese parameter evaluated was the manganese oxidation rate. The only area that is impacted by manganese oxidation with respect to simulated byproduct manganese is the manganese injected into the two upland IRL injection wells that originated from the Riverbank Extraction Wells. The base manganese oxidation rate was simulated using a 30-day half-life in the solute transport model. The increased oxidation half-life simulated was 60 days, while the decreased oxidation half-life was 15 days. The 10-year manganese oxidation sensitivity results are shown on Figures 10.4-9 and 10.4-10 for model layers 2 and 4, respectively. Because manganese oxidation is only simulated in the uplands and by year 10, no manganese is injected into IRL wells IRL-1 and IRL-2 above 130 µg/L, there is no difference between the three different oxidation rates. However, by year 30, manganese shows up in IRL-1 and IRL-2 above 130 µg/L and the relative impact of the oxidation rate variation is apparent in model layers 2 and 4 (Figures 10.4-11 and 10.4-12). These figures suggest a direct relationship between the oxidation rate and radial footprint of the upland manganese byproduct. Doubling the half-life results in a radial manganese footprint that is approximately twice as large, while reducing the oxidation half-life by half results in an approximate 50% decrease in radial footprint.

### **10.5 Arsenic Precipitation, Generation, and Sorption**

To evaluate the sensitivity of the solute transport model to the arsenic geochemical parameters, an analysis was performed by varying the arsenic precipitation, generation, and sorption terms in the solute transport model within a reasonable range. Within the solute transport submodel, the only locations where arsenic sorption is simulated is downgradient of the maximum extent of the 1 mg/L TOC footprint of the NTH IRZ



and TCS carbon-amended injection wells. The 1 mg/L TOC IRZ footprints indicate areas where ferrous iron is potentially available to coprecipitate with the byproduct arsenic. Arsenic precipitation was simulated as a half-life in the solute transport model. The base arsenic precipitation rate was simulated using a 30-day half-life in the solute transport model. The increased precipitation half-life simulated was 60 days, while the decreased precipitation half-life was 15 days. In all of these half-life simulations, there is no simulated arsenic greater than 5 µg/L downgradient of the NTH IRZ or the TCS carbon-amended injection wells for the full 30-year simulation period. Therefore, the arsenic precipitation rate is not a sensitive parameter in the solute transport model and figures were not generated for this sensitivity analysis.

The next arsenic parameter varied was the arsenic generation term. Similar to manganese, the generation term was developed as a stoichiometric ratio that relates carbon degradation to arsenic byproduct mobilization (generation). The base scenario has a stoichiometric carbon to arsenic generation ratio of 0.000108, meaning for every 1 mg/L of TOC that degrades, 0.108 µg/L of arsenic is generated in the solute transport model. The decreased and increased stoichiometric generation ratios are 0.00005 and 0.00018, respectively. The 10-year results indicate all byproduct arsenic is still below 5 µg/L for all three generation rates; therefore, figures were not generated. However, the 30-year results for model layers 2 and 4 (Figures 10.5-1 and 10.5-2, respectively) indicate that arsenic is present at concentrations between 5 and 10 µg/L downgradient of the NTH IRZ for the increased arsenic generation run. Despite the generation of this small arsenic distribution, this simulated arsenic will be attenuated prior to reaching the Riverbank Extraction Wells.

The final arsenic parameter evaluated is the arsenic sorption rate. Similar to manganese, arsenic sorption was simulated using the non-linear Freundlich isotherm ( $C^* = KC^N$ ), where K and N are constants that were varied to align with observed field data consistent with the geochemical sensitivity analysis presented in Section 9.2. In all three sorption scenarios, the N exponent was held constant at 0.465, while the K multiplier was varied. The base arsenic sorption scenario utilized a K value of 2.77, the decreased arsenic sorption scenario utilized a K value of 0.277, and the increased arsenic sorption scenario used a K value of 13.85. Despite the variations in the arsenic sorption rate, byproduct arsenic concentrations remained below 5 µg/L for the full 30-year simulation period; therefore, no figures were generated for this sensitivity analysis.

## 10.6 Chromium Sorption

To evaluate the sensitivity of the solute transport model results to the Cr(VI) sorption parameter, the distribution coefficient ( $K_d$ ) of Cr(VI) was doubled. The base  $K_d$  of 0.05 L/kg was increased to a  $K_d$  of 0.5 L/kg. The resulting impact on the Cr(VI) transport after 10 years of transport in model layers 2 and 4 is depicted on Figures 10.6-1 and 10.6-2, respectively. Increasing the Cr(VI)  $K_d$  by an order of magnitude results in a fairly significant retardation of Cr(VI) transport. This is even more apparent by the results after 30 years of simulated transport in model layers 2 and 4 as shown on Figures 10.6-3 and 10.6-4, respectively. While this increase in Cr(VI) retardation would suggest significantly longer remediation timeframes, this is

not a likely scenario as the understanding of groundwater flow and plume development suggests a Cr(VI)  $K_d$  of 0.5 L/kg would be excessive. This sensitivity analysis was done for comparative purposes to gauge the relative impact of Cr(VI) sorption.

### **10.7 Conditioned Remedy-Produced Water NTH IRZ Injection**

To evaluate the sensitivity of the solute transport model to the addition of conditioned remedy-produced water to NTH IRZ, an analysis was performed by injecting conditioned remedy-produced water at a combined total average rate of 10 gpm into the 16 NTH IRZ injection wells. The 10 gpm was divided evenly over the 16 NTH IRZ injection wells and 5 mg/L TOC was added to the conditioned remedy-produced water for treatment. The resulting impact on the Cr(VI) transport after 10 years of transport in model layers 2 and 4 is depicted on Figures 10.7-1 and 10.7-2, respectively. These results indicate that the conditioned remedy-produced water injected into the NTH IRZ injection wells during the 18-month NTH IRZ off-cycle has little to no impact on the simulated Cr(VI) impact. Even by year 30, as shown on Figures 10.7-3 and 10.7-4, there is minimal impact of the conditioned remedy-produced water injection in the simulated model layers 2 and 4 Cr(VI) results. This indicates that the 10 gpm conditioned remedy-produced water injection distributed over the 16 NTH IRZ injection wells does not create a hydraulic barrier and allows for continued Cr(VI) reduction.

The impact of the conditioned remedy-produced water injection on the simulated manganese byproduct after 10 years in model layers 2 and 4 is shown on Figures 10.7-5 and 10.7-6, respectively. These results indicate there is only a small difference between the runs in that there is a very slight increase in the manganese footprint due to the conditioned remedy-produced water injected during the NTH IRZ off-cycle. The 30-year conditioned remedy-produced water sensitivity manganese byproduct results for model layers 2 and 4 are shown on Figures 10.7-7 and 10.7-8, respectively. Similar to the 10-year results, the 30-year results indicate only a very slight increase in the manganese byproduct footprint in the conditioned remedy-produced water injection run. Due to the limited differences in the simulated manganese byproduct distribution, the simulated manganese byproduct is not sensitive to the addition of the 10 gpm conditioned remedy-produced water off-cycle NTH IRZ injection.

The impact of the conditioned remedy-produced water injection on the simulated arsenic was also evaluated. After 30 years of simulation, arsenic concentrations remained below 5  $\mu\text{g/L}$  downgradient of the NTH IRZ throughout the model domain; therefore, no figures were generated for this sensitivity analysis.

### **10.8 IRL/Freshwater Oscillation**

In order to potentially mitigate the impact of Cr(VI) or byproducts from either the riverbank extracted water or the HNWR-1 freshwater source injected into the IRLs, a scenario was evaluated where the injection pattern was varied for the four IRL wells. For the first 10 years of this run, IRL-1 and IRL-2 receive 75 gpm each from the Riverbank Extractions Wells, while IRL-3 and IRL-4 receive 100 gpm and 200 gpm, respectively,

from the HNWR-1 freshwater source. From years 10 to 20 this injection pattern is rearranged so that IRL-1, IRL-2, and IRL-3 receive 100 gpm each from the HNWR-1 freshwater source, while IRL-4 receives the full 150 gpm from the Riverbank Extraction Well. From years 20 to 30, the IRL injection pattern is consistent with the first 10-year pattern. The Cr(VI) IRL/freshwater oscillation sensitivity run results after 20 years of transport in model layers 2 and 4 are presented on Figures 10.8-1 and 10.8-2, respectively. Because there is no riverbank extracted water with a Cr(VI) concentration above 32  $\mu\text{g/L}$ , these results are very similar. The only slight difference that is apparent is the model layer 4 Cr(VI) plume downgradient of IRL-4 is slightly larger in the IRL/freshwater oscillation scenario because the rate injected into IRL-4 was reduced from 200 gpm to 150 gpm, resulting into a slightly lower hydraulic push in this area. The 30-year simulated Cr(VI) results for the IRL/freshwater oscillation sensitivity in model layers 2 and 4 are depicted on Figures 10.8-3 and 10.8-4, respectively. Similar to the 10 year results, the riverbank extracted water is still below 32  $\mu\text{g/L}$ , so the only slight difference that is apparent is the extent of the model layer 4 plume downgradient of IRL-4 due to the reduced injection in IRL-4 from years 10 to 20.

The simulated manganese byproduct was also evaluated with respect to the IRL/freshwater oscillation scenario. The 20-year simulated manganese byproduct results for the IRL/freshwater oscillation sensitivity run in model layers 2 and 4 are shown on Figures 10.8-5 and 10.8-6, respectively. The 20-year results indicate that manganese byproduct is present in the riverbank extracted water above 130  $\mu\text{g/L}$  and is injected into the upland wells. The impact of the IRL/freshwater oscillation is evident in the year 30 results for model layers 2 and 4 (Figures 10.8-7 and 10.8-8, respectively). The 30-year results indicate that the manganese byproduct that was present near IRL-4 in year 20 has attenuated by year 30 due to the oscillation of the IRL-4 water source from riverbank extracted water back to freshwater from HNWR-1. This sensitivity analysis indicates that an IRL/freshwater oscillation schedule could potentially be beneficial in controlling manganese byproduct distribution in the uplands.

Lastly, the simulated arsenic was evaluated with respect to the IRL/freshwater oscillation scenario. No arsenic generated with respect to the NTH IRZ exceeded 5  $\mu\text{g/L}$  during the full 30-year simulation period; therefore, no figures were generated for this sensitivity analysis.

### **10.9 Off-Cycle NTH IRZ Extraction**

In order to address the simulated low levels of Cr(VI) that migrate past the northern NTH IRZ Extraction Wells, an analysis was conducted to reduce this potential by operating the northern NTH IRZ Extraction Wells at a reduced rate during the simulated 18-month NTH IRZ off-cycle. For this analysis during the 18-month off-cycle, the NTH IRZ Extraction Wells were operated at half the rate they operate during the NTH IRZ on-cycle. The 10-year simulated Cr(VI) results in model layers 2 and 4 for this analysis are presented on Figures 10.9-1 and 10.9-2, respectively. There is limited difference in the model layer 2 results because the Cr(VI) plume has attenuated to south of the northern three NTH IRZ Extraction Wells by year 10. However, the 10-year model layer 4 results indicate this off-cycle-reduced extraction is effective in reducing the

breakthrough of the Cr(VI) past the NTH IRZ. The 30-year simulated Cr(VI) NTH IRZ off-cycle extraction rates for model layers 2 and 4 are presented on Figures 10.9-3 and 10.9-4, respectively. While both the base run and the NTH IRZ off-cycle extraction do not exhibit Cr(VI) breakthrough past the NTH IRZ line, the Cr(VI) distribution is slightly smaller in the NTH IRZ off-cycle extraction due to the slight increase in gradient from the base run.

The manganese byproduct was also evaluated with respect to the incorporation of the off-cycle NTH IRZ extraction. The 10-year results for this evaluation in model layers 2 and 4 are presented on Figures 10.9-5 and 10.9-6, respectively. The hydraulic impact of the off-cycle NTH IRZ extraction is apparent in that the northern portion of the manganese byproduct does not extend as far downgradient into the floodplain as in the base run. This slight deflection in the manganese byproduct footprint is also present by year 30 as shown on Figures 10.9-7 and 10.9-8 for model layers 2 and 4, respectively. These results indicate that off-cycle NTH IRZ extraction does not have a significant impact on the byproduct manganese.

Finally, arsenic was evaluated with respect to the incorporation of the off-cycle NTH IRZ extraction. The full 30-year simulated arsenic results indicate that the simulated arsenic is not impacted by off-cycle NTH IRZ extraction because floodplain arsenic is below 5 µg/L. Therefore, figures were not generated for arsenic evaluation for this sensitivity analysis.

#### **10.10 TOC Half-Life Sensitivity**

To evaluate the sensitivity of the solute transport model to the half-life of TOC, the base TOC half-life of 20 days was decreased to 10 days and increased to 30 days. The impact of the TOC half-life variation was first evaluated with respect to the simulated Cr(VI). Figures 10.10-1 and 10.10-2 display the simulated Cr(VI) results after 10 years of simulated transport in model layers 2 and 4, respectively. The TOC half-life has a noticeable impact on Cr(VI) in that it determines the persistence of the reducing downgradient of the NTH IRZ. When the TOC half-life is reduced to 10 days, the IRZ degrades away twice as quickly and Cr(VI) breakthrough occurs. This Cr(VI) breakthrough results in an increased Cr(VI) concentration in the Riverbank Extraction Wells that is injected into IRL-1 and IRL-2. This leads to a Cr(VI) impact above 32 µg/L in the uplands. To prevent this Cr(VI) breakthrough and uplands impact, the duration of the NTH IRZ on-/off-cycles can be adjusted to maintain the reducing zone downgradient of the NTH IRZ. TOC can also be added to the Cr(VI)-impacted riverbank extracted water to minimize upland Cr(VI) impacts. Both the base (20-day) and increased (30-day) TOC half-lives provide a sustained reducing zone to reduce the potential of Cr(VI) breakthrough. By year 30, the simulated Cr(VI) results for the three TOC half-lives in model layers 2 and 4 are fairly similar, as shown on Figures 10.10-3 and 10.10-4, respectively. The decreased TOC half-life has a slightly higher Cr(VI) distribution in the immediate vicinity of the NTH IRZ. Cr(VI) concentrations that were present in the uplands at year 10 have been attenuated by year 30. In the event that field observations after remedy design startup support a TOC half-life towards the faster end of the range, potential gaps in the NTH IRZ can be addressed by increased injection or increased TOC concentrations.

The manganese byproduct generation was also evaluated with respect to the variations in TOC half-lives. Figures 10.10-5 and 10.10-6 display the simulated manganese byproduct results for the three different TOC half-lives after 10 years of simulated transport in model layers 2 and 4, respectively. The most apparent difference is that an increased TOC half-life of 30 days results in a larger manganese byproduct footprint than the other two lower TOC half-lives. This is due to the TOC persisting longer, allowing it to migrate farther downgradient, expanding the manganese byproduct footprint. This further migration of the manganese byproduct leads to elevated manganese concentrations being extracted from the riverbank extraction wells and injection into the uplands. The 30-year manganese byproducts results for this analysis for model layers 2 and 4 are presented on Figures 10.10-7 and 10.10-8, respectively. By year 30, the results indicate the three TOC half-lives impact on byproduct manganese is not as pronounced as after only 10 years.

Arsenic was also evaluated with respect to the three TOC half-lives. The simulated arsenic results for the full 30-year simulation period indicate that the simulated arsenic is not impacted by fluctuations in TOC half-life because floodplain arsenic is below 5 µg/L. Simulated arsenic figures were, therefore, not generated for this sensitivity analysis.

#### **10.11 NTH IRZ Rate Sensitivity**

In order to evaluate the impact of the total NTH IRZ injection/extraction rates, a sensitivity analysis was conducted by varying the total NTH IRZ injection/extraction rates using the rates 150 gpm, 300 gpm, and 600 gpm. In all three scenarios, the net rate is still 0 gpm, as the total NTH IRZ extraction is equal to the total NTH IRZ injected. The simulated Cr(VI) results after 10 years of simulated transport in model layers 2 and 4 for the NTH IRZ rate sensitivity analysis are presented on Figures 10.11-1 and 10.11-2, respectively. The decreased NTH IRZ rate results indicate there is a greater potential for Cr(VI) breakthrough. Both the 300 gpm and 600 gpm NTH IRZ rate scenarios indicate minimal Cr(VI) breakthrough occurs. The 600 gpm NTH IRZ rate indicates a slightly smaller Cr(VI) impact upgradient of the NTH IRZ, primarily due to the increased extraction from the central NTH IRZ Extraction Well. The 30-year Cr(VI) results for model layers 2 and 4 for the NTH IRZ rate sensitivity analysis are shown on Figures 10.11-3 and 10.11-4, respectively. By year 30, the three NTH IRZ rate analysis Cr(VI) results are very similar, as the Cr(VI) plume upgradient of the NTH IRZ has similar extents. This indicates the NTH IRZ rate is more sensitive at early times when the extent of the Cr(VI) plume footprint is the largest. This analysis also indicates that there is no significant advantage of trying to increase the NTH IRZ rate from 300 gpm to 600 gpm.

The NTH IRZ rate sensitivity analysis was also run with respect to manganese byproduct. The 10-year simulated manganese byproduct results for model layers 2 and 4 are presented on Figures 10.11-5 and 10.11-6, respectively. These results indicate that the magnitude and extent of the manganese byproduct generated is directly related to the NTH IRZ rate. This is due to the fact that an increase in NTH IRZ injection rates results in an increase in injected TOC. The 30-year simulated manganese byproduct results for model

layers 2 and 4 are presented on Figures 10.11-7 and 10.11-8, respectively. An increase in injected TOC in turn generates more manganese downgradient of the NTH IRZ. This shows the potential negative impact of increasing the total NTH IRZ rate. Therefore, the NTH IRZ should be kept to an effective minimal rate to achieve a continuous Cr(VI) reducing zone and minimize the amount of byproduct generated.

Arsenic was also evaluated with respect to the variations in NTH IRZ rates. The simulated arsenic results for the full 30-year simulation period indicate that the simulated arsenic is not impacted by fluctuations in NTH IRZ rates because floodplain arsenic remains 5 µg/L. Simulated arsenic figures were, therefore, not generated for this sensitivity analysis.

#### **10.12 Freshwater Injection Rate Sensitivity**

To evaluate the sensitivity of the solute transport model to the freshwater injection rate, a range of freshwater injection rates were evaluated from 225 gpm to 650 gpm. Figures 10.12-1 and 10.12-2 depict the impact of freshwater injection rates of 225 gpm, 450 gpm, and 650 gpm on simulated Cr(VI) transport after 10 years for model layers 2 and 4, respectively. This sensitivity analysis indicates that the extent of the Cr(VI) plume is inversely related to the freshwater injection rate. This demonstrates that increasing the freshwater injection rate results in a greater hydraulic push of the Cr(VI) plume through the NTH IRZ. Despite this increase in freshwater injection/hydraulic gradient, the NTH IRZ is still effective in preventing Cr(VI) breakthrough into the floodplain. Figures 10.12-3 and 10.12-4 depict the impact of freshwater injection rates of 225 gpm, 450 gpm, and 650 gpm on simulated Cr(VI) transport after 30 years for model layers 2 and 4, respectively. These 30-year figures demonstrate the importance of the freshwater injection relative to the remedial system performance, as there is a measurable difference in remaining Cr(VI) mass between the three freshwater injection scenarios.

Byproduct manganese was also evaluated relative to the three freshwater injection rates. The manganese byproduct results in model layers 2 and 4 after 10 years of simulated transport are shown on Figures 10.12-5 and 10.12-6, respectively. These figures indicate that differences in freshwater injection rates have a slight impact on the byproduct manganese downgradient of the NTH IRZ. While the total byproduct manganese generated between the three freshwater injection scenarios is similar, the distribution of the manganese byproduct varies. Higher freshwater injection rates result in a slightly large manganese byproduct footprint with lower peak manganese concentrations as compared to the lower freshwater injection rates. The 30-year simulated byproduct manganese results for model layers 2 and 4 are shown on Figures 10.12-7 and 10.12-8, respectively. These figures indicate a similar manganese byproduct pattern as observed in the simulated 10-year results.

The impact of the freshwater injection rate was also evaluated relative to the simulated arsenic. The full 30-year simulation results indicate there is no impact on the arsenic generated in the NTH IRZ reducing zone



because arsenic concentrations remain below the minimum contour interval of 5 µg/L. Arsenic figures were, therefore, not generated for this sensitivity analysis.

### **10.13 Intermediate Recirculation Well Sensitivity**

In order to optimize the performance of the remedial design, a scenario was evaluated that introduced additional wells at later times in the remedy to try to target areas of lingering Cr(VI). This scenario addressed this by introducing a recirculation well pair at year 20 that injected carbon-amended water into the northern central portion of the plume (IRL-7) and an extraction well in the southern central portion of the plume (IRL-6). This simulated intermediate recirculation loop extracted and injected at rates of 100 gpm. The 30-year simulated Cr(VI) results are shown on Figures 10.13-1 and 10.13-2, respectively. These results indicate this intermediate recirculation well pair was successful in reducing the remaining footprint of the Cr(VI) plume. One potential negative impact of this scenario is that the southern extraction well has the potential to reverse the flow direction away from the NTH IRZ, which will limit Cr(VI) reduction in this area.

This intermediate recirculation well pair was also evaluated relative to manganese byproduct. Figures 10.13-3 and 10.13-4 display the 30-year simulated byproduct manganese results in model layers 2 and 4, respectively, after the intermediate recirculation well pair was activated in year 20. These figures indicate a local manganese byproduct radial footprint surrounds the northern injection well. Additionally, manganese generated at the TCS injection wells migrates in a northerly direction towards the southern extraction well. These byproduct manganese impacts are within the footprint of the plume and do not extend a significant distance after 10 years of active recirculation.

Finally, the intermediate recirculation well pair was evaluated relative to arsenic. Figures 10.13-5 and 10.13-6 display the 30-year simulated arsenic results in model layers 2 and 4, respectively, after the intermediate recirculation well pair was activated in year 20. The primary impact is there is a slight arsenic footprint generated around the northern carbon-amended injection well with a concentration between 5 and 10 µg/L.

### **10.14 IRL TOC Injection Sensitivity**

To evaluate the potential impact of amending the riverbank extracted water with TOC to address elevated Cr(VI) concentrations extracted from the floodplain, a scenario was setup that would inject 50 mg/L of TOC with the riverbank extracted water into IRL-1 and IRL-2 for a period of approximately 4.5 years. After 4.5 years, the carbon amendment was ceased and riverbank extracted water was continually injected into IRL-1 and IRL-2 for the remainder of the remedy. Figures 10.14-1 and 10.14-2 display the Cr(VI) results after 5 years of simulated transport. Because riverbank Cr(VI) does not exceed 32 µg/L, only the TOC footprint is visible emanating from IRL-1 and IRL-2. Figures 10.14-3 and 10.14-4 display the Cr(VI) results after 10 years of simulated transport in model layers 2 and 4, respectively. By year 10, the TOC injected into IRL-1 and IRL-2 has fully degraded and the Cr(VI) results for the base run and IRL TOC scenario are identical.

Because the Cr(VI) results are identical at year 10, year 30 results are identical as well and were not necessary to present for this scenario.

The TOC addition to IRL-1 and IRL-2 was also evaluated with respect to byproduct manganese. Figures 10.14-5 and 10.14-6 display the manganese byproduct results after 5 years of simulated transport in model layers 2 and 4, respectively. These figures indicate that the injection of TOC into IRL-1 and IRL-2 for 4.5 years resulted in a local reducing zone, and manganese byproduct is generated downgradient of these wells. Figures 10.14-7 and 10.14-8 show the manganese byproduct results after 10 years of simulated transport in model layers 2 and 4, respectively. These figures indicate that by year 10, after 5.5 years of riverbank extracted water without TOC, manganese concentrations that were visible in year 5 have almost been fully attenuated downgradient of IRL-1 and IRL-2. Therefore, the solute transport model indicates that short-term TOC injection to treat riverbank extracted water will not have a long-term impact with respect to manganese byproduct in the uplands. Arsenic was also evaluated with respect to the short-term addition of carbon to IRL-1 and IRL-2. Despite simulated fluctuations of the TOC footprint, there is simulated arsenic that exceeds 5 µg/L. Therefore, arsenic figures were not generated for this sensitivity analysis.

#### **10.15 TOC/Hexavalent Chromium Trigger Sensitivity**

In order to evaluate the sensitivity of the Cr(VI) remediation simulation to the simulated TOC/Cr(VI) precipitation trigger (concentration of TOC that activates chromium reduction in the solute transport model), this trigger was increased an order of magnitude from 0.1 mg/L to 1 mg/L. The TOC/Cr(VI) precipitation trigger was previously evaluated in Section 7.4 during the transient and transition modeling where the initial trigger was increased to 10 mg/L TOC over the first 6 months to simulate the development of the NTH IRZ reducing zone during the IM-3 transition and then maintained at 0.1 mg/L TOC to represent the established reducing zone. This sensitivity analysis is designed to simulate a long-term increase in the trigger value with it sustained at 1 mg/L TOC throughout the duration of the remedy. In addition to this trigger increase, the NTH IRZ on-/off-cycle was adjusted to a 12-month on/12-month off cycle. Figures 10.15-1 and 10.15-2 display the simulated Cr(VI) results after 10 years in model layers 2 and 4, respectively. These 10-year results indicate that increasing the TOC trigger an order of magnitude results in some hexavalent breakthrough along the NTH IRZ. Despite this breakthrough, much of this Cr(VI) that extends into the floodplain will be reduced during the next active TOC injection cycle. By year 30, the simulated Cr(VI) results are comparable in model layer 2 as shown on Figure 10.15-3. In model layer 4 (Figure 10.15-4), there is more residual Cr(VI) in the floodplain after 30 years when the trigger is 1.0 mg/L TOC. In these two figures, the primary difference is the Cr(VI) breakthrough that occurs in the central portion of the NTH IRZ line. However, the use of this 1.0 mg/L TOC trigger for the full simulation underestimates the established reducing capacity that would occur during the NTH IRZ off-cycle. As discussed in Section 7.4, reducing the TOC trigger to 0.1 mg/L during the NTH IRZ simulated off-cycle to represent a more established reducing zone minimizes the breakthrough of Cr(VI).



## **11. Uncertainty**

As with all mathematical models of natural systems, the groundwater flow and solute transport model is limited by factors, such as scale, accuracy of the estimated hydraulic properties and/or boundary conditions, and the underlying simplifications and assumptions incorporated into the model. These factors result in limitations to the model's appropriate uses and to the interpretations that may be made of the simulation results.

Several strategies were employed to address the uncertainties inherent to the predictive model. As discussed in Section 4, the flow model was calibrated against: (a) long-term average groundwater levels that incorporate seasonal/other fluctuations in the system flow conditions, (b) average monthly floodplain levels responding to fluctuating river levels, (c) short-term responses to pump testing events, and (d) plume development over time, and the autocalibration program PEST was employed to refine the calibration and to reduce effects of uncertainty in each calibration target. This calibration procedure resulted in a highly heterogeneous distribution of hydraulic conductivity to better represent the natural system. Note that density-dependent flows (resulting from potential deviations in temperature and salinity) were not simulated because these will have a negligible impact on system flows and the remedy design when compared to the natural heterogeneity of the aquifer.

With respect to the solute transport model, uncertainty associated with subsurface heterogeneity was addressed by simulating the system as a dual-domain model, allowing for interaction between the mobile and immobile portions of the aquifer (see Section 6.2.1). Uncertainty was further addressed by conducting a detailed sensitivity analysis on various solute transport parameters [i.e., Cr(VI) partition coefficient, manganese generation/attenuation rate, and arsenic generation/attenuation rate] as discussed in Section 6.2 and 10. This sensitivity analysis can be utilized to address the uncertainty in the model by providing a range of remedial impacts and relative impacts of byproducts.



## **Appendix B: Development of Groundwater Flow, Geochemical, and Solute Transport Models**

Topock Compressor Station  
Needles, California

### **12. Conclusions**

Based on the various sensitivity analyses and solute transport runs, the solute transport model indicates that the proposed remedial design as described in Section 6.4 and shown on Figure 6.4-1 is effective in remediating the current Cr(VI) plume distribution while minimizing the potential adverse impacts from byproduct generation. This solute transport model can be utilized as a tool to evaluate potential remedial options, but the implemented remedial system must be closely monitored to measure the effectiveness of this proposed approach. During installation and implementation of the remedial design, the additional hydrogeologic and groundwater quality data can be utilized to update the groundwater flow and transport models to improve their effectiveness as evaluation tools.

### **13. References**

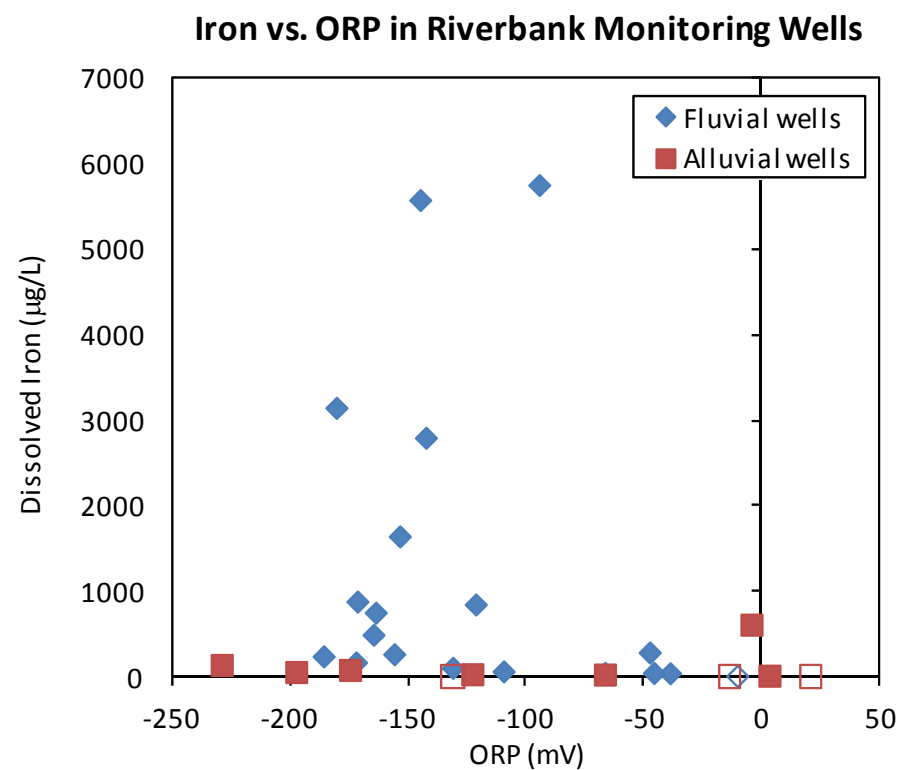
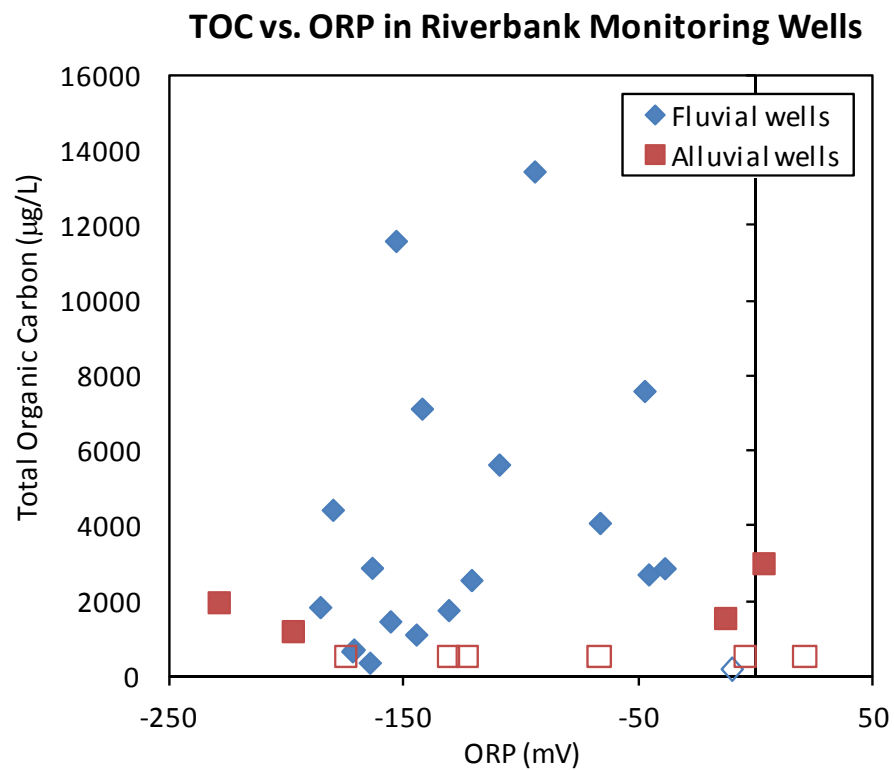
- Appelo, C.A.J., M.J.J. van der Weiden, C. Tournassat, and L. Charlet. 2002. Surface complexation of ferrous iron and carbonate on ferrihydrite and the mobilization of arsenic. *Environmental Science & Technology* 36: 3096-3103.
- ARCADIS. 2008. Floodplain Reductive Zone In-Situ Pilot Test Final Completion Report. March 5, 2008.
- ARCADIS. 2009. Upland Reductive Zone In-Situ Pilot Test Final Completion Report. March 3, 2009.
- ARCADIS. 2009b. Third Quarter 2009 Monitoring Report for the Upland Reductive Zone In-Situ Pilot Test. December 15, 2009.
- CH2M HILL. 2011. Second Quarter 2011 Interim Measures Performance Monitoring and Site-Wide Groundwater and Surface Water Monitoring Report, PG&E Topock Compressor Station, Needles, California. August 15, 2011.
- CH2M HILL. 2009a. RCRA Facility Investigation/Remedial Investigation Report, Volume 2: Hydrogeologic Characterization and Results of Groundwater and Surface Water Investigation. February 11, 2009.
- CH2M HILL. 2009b. Corrective Measures/Feasibility Study Report for Chromium in Groundwater, PG&E Topock Compressor Station, Needles, California. December 11, 2009.
- CH2M HILL. 2006. Pore Water and Seepage Study Report, PG&E Topock Compressor Station, Needles, California. March 13, 2006.
- CH2M HILL. 2005a. Summary of Results—Aerobic Zone Hexavalent Chromium Core Testing, PG&E Topock Compressor Station, Needles, California. May 20, 2005.
- CH2M HILL. 2005b. Groundwater Model Update Report, PG&E Topock Compressor Station, Needles, California. July 29, 2005.
- Dixit, S. and Hering, J. 2003. Comparison of arsenic(V) and arsenic(III) sorption onto iron oxide minerals: Implications for arsenic mobility. *Environmental Science & Technology*, 37, 4182-4189.
- Dzombak, D.A., and Morel, F.M. 1990. *Surface Complexation Modeling: Hydrous Ferric Oxide*. New York: Wiley-Interscience. 393pp.

- Eary, L.E. and D. Rai. 1987. Kinetics of chromium (III) oxidation to chromium (VI) by reaction with manganese dioxide. *Environmental Science and Technology* 21: 1187-1193.
- Essington, M.E. *Soil and Water Chemistry, An Integrative Approach*. New York: CRC Press. 534pp.
- Feehley, C.E., C. Zheng, and F.J. Molz. 2000. *A dual-domain mass transfer approach for modeling solute transport in heterogeneous aquifers: Application to the macrodispersion experiment (MADE) site*. *Water Resources Research* 36, no. 9: 2501–2515.
- Flach, G.P., S.A. Crisman, and F.J. Molz III, 2004. Comparison of Single-Domain and Dual-Domain Subsurface Transport Models. *Ground Water* 42, no. 6: 815-828.
- Fuller, C.C. and Harvery, J.W. 2000. *Reactive Uptake of Trace Metals in the Hyporheic Zone of a Mining-Contaminated Stream, Pinal Creek, Arizona*. *Environmental Science and Technology* 34(7): 1150-1155.
- Gandy, C.J., J.W.N. Smith, and A.P. Jarvis. 2006. Attenuation of mining-derived pollutants in the hyporheic zone: A review. *Science of the Total Environment*, 373(2-3), 435-446.
- Gillham, R.W., E.A. Sudicky, J.A. Cherry, and E.O. Frind. 1984. *An advection-diffusion concept for solute transport in heterogeneous unconsolidated geological deposits*. *Water Resources Research* 20, no.3: 369-378
- Gleyzes, C., Teller, S., Astruc, M. 2002. *Fractionation studies of trace elements in contaminated soils and sediments: a review of sequential extraction procedures*. *Trends in Analytical Chemistry* 21(6-7), 451-467.
- Harvey, J.W., and Fuller, C.C. 1998. Effect of enhanced manganese oxidation in the hyporheic zone on basin-scale geochemical mass balance. *Water Resources Research*, 34(4), 623-636.
- Harvey, C.F., and S.M. Gorelick. 2000. *Rate-limited mass transfer or macrodispersion: Which dominates plume evolution at the macrodispersion experiment (MADE) site?* *Water Resources Research* 36, no. 3: 637–650.
- Hemker, C.J. 2006. MicroFEM, version 3.60. Groundwater flow modeling software, available at <http://www.microfem.com>.
- Howard, K. A., B.E. John, and J.E. Nielson. 1997. *Preliminary Geological Map of Eastern and Northern Parts of the Topock 7.5-minute Quadrangle, Arizona and California*, United States Geological Survey Open-File report 95-534

- Hwang, I., B. Batchelor, M.A. Schlautman, and R. Wang. 2002. Effects of ferrous iron and molecular oxygen on chromium(VI) redox kinetics in the presence of aquifer solids. *Journal of Hazardous Materials B92*: 143-159.
- Julian, H.E., M.J. Boggs, C. Zheng, and C.E. Feehley. 2001. *Numerical simulation of a natural gradient tracer experiment for the natural attenuation study: Flow and physical transport*. *Ground Water* 39, no. 4: 534-545.
- Kay, J.T., Conklin, M.H., Fuller, C.C., and O'Day, P.A. 2001. Processes of nickel and cobalt uptake by a manganese oxide forming sediment in Pinal Creek, Globe Mining District, Arizona. *Environmental Science & Technology*, 35(24), 4719-4725.
- Kosmulski, M., S. Durand-Vidal, E. Maczka, and J.B. Rosenholm. 2004. Morphology of synthetic goethite particles. *Journal of Colloid and Interface Science* 271: 261-269.
- Manceau, A. 1995. The mechanism of anion adsorption on Fe oxides: Evidence for the bonding of arsenate tetrahedral on free Fe(O,OH)<sub>6</sub> edges. *Geochimica et Cosmochimica Acta*, 59: 3647-3653.
- Marble, J.C., Corley, T.L., Conklin, M.H., and Fuller, C.C. 1999. Environmental factors affecting oxidation of manganese in Pinal Creek, Arizona. U.S. Geological Survey Water-Resources Investigations Report 99-4018A, Volume 1, Section C.
- McDonald, M. G., and A. W. Harbaugh, 1988. *A Modular Three-Dimensional Finite-Difference Ground-Water Flow Model, Techniques of Water-Resources Investigations, Book 6, Chapter A1*. U. S. Geological Survey. Reston, Virginia.
- Metzger, D.G., Loeltz, O.J. 1973. *Geohydrology of the Needles Area, Arizona, California, and Nevada*. U.S. Geological Professional Paper 486-J
- Molz, F.J., C. Zheng, S.M. Gorelick, and C.F. Harvey. 2006. *Comment on "Investigating the Macrodispersion Experiment (MADE) site in Columbus, Mississippi, using a three-dimensional inverse flow and transport model" by Heidi Christiansen Barlebo, Mary C. Hill, and Dan Rosbjerg*. *Water Resources Research*. 42 no. 6 W06603
- Morel, F.M.M. and J.G. Hering. 1993. *Principles and Applications of Aquatic Chemistry*. John Wiley & Sons, Inc., New York.
- Morgan, J.J. 2005. Kinetics of reaction between O<sub>2</sub> and Mn(II) species in aqueous solutions. *Geochimica et Cosmochimica Acta* 69(1): 35-48.

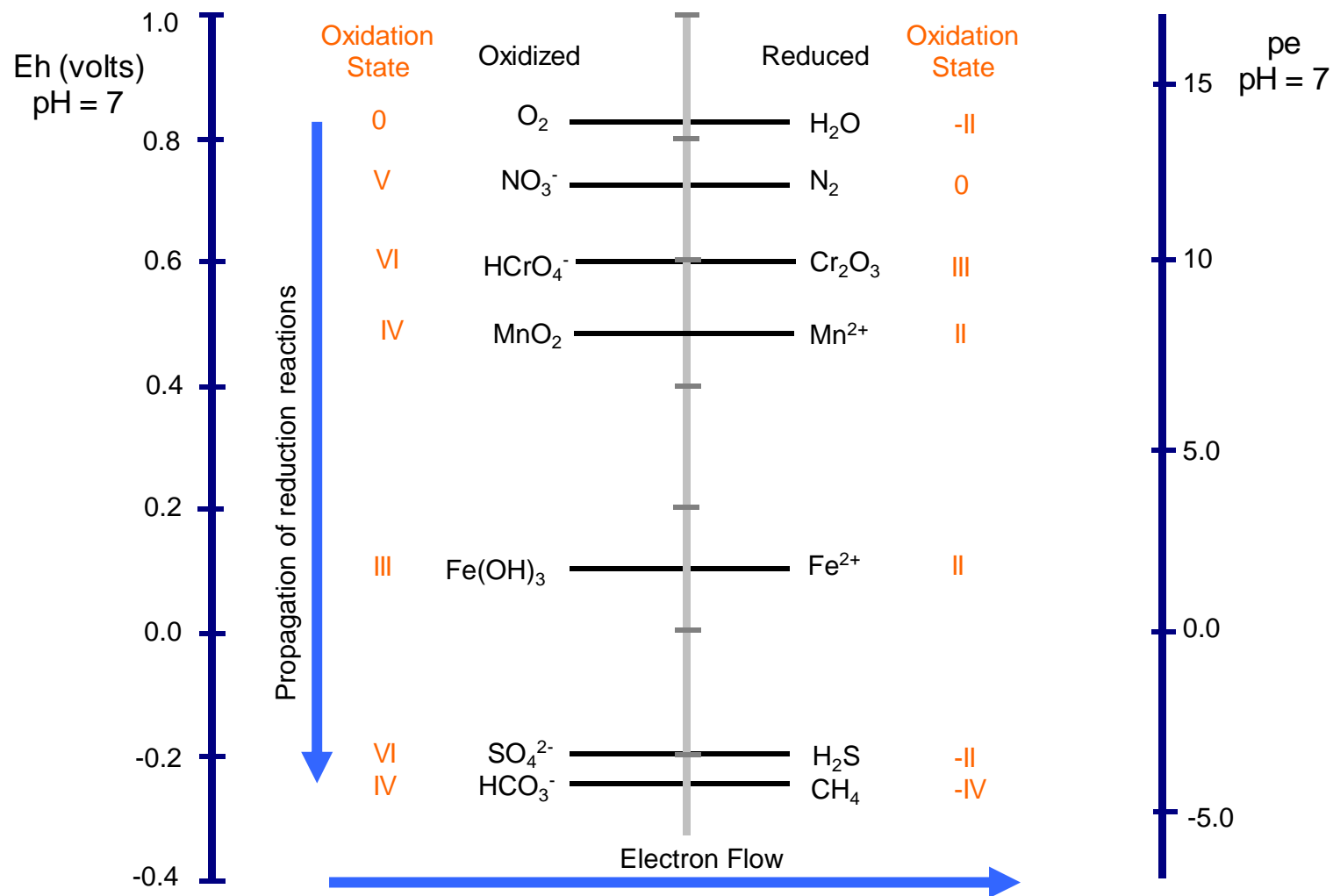
- Parkhurst, D., and C.A.J. Appelo. 1999. User's guide to PHREEQC (Version 2) – A computer program for speciation, batch-reaction, one-dimensional transport, and inverse geochemical calculations. U.S. Geological Survey Water Resources Investigations Report 99-4259.
- Payne, F.C., J.A. Quinnan, and S.T. Potter. 2008. Remediation Hydraulics. CRC Press, Boca Raton, Florida.
- Potter, S.T., Moreno-Barbero, E., and Divine, C.E. 2008. MODALL: A practical tool for designing and optimizing capture systems. *Ground Water*, 46(2): 335-340.
- Prommer, H., D.A. Barry, and C. Zheng. 2003. MODFLOW/MT3DMS based reactive multicomponent transport modeling. *Ground Water* 41(2): 247-257.
- Sass, B.M., and D. Rai. 1987. Solubility of amorphous chromium(III)-iron(III) hydroxide solid solutions. *Inorganic Chemistry* 26: 2228-2232.
- Smedley, P.L., and Kinniburgh, D.G. 2002. A review of the source, behaviour and distribution of arsenic in natural waters. *Applied Geochemistry* 17: 517–568
- U.S. Environmental Protection Agency. 1999. Understanding Variation in Partition Coefficient,  $K_d$ , Values, Volume II: Review of Geochemistry and Available  $K_d$  Values for Cadmium, Cesium, Chromium, Lead, Plutonium, Radon, Strontium, Thorium, Tritium, and Uranium. Appendix E.
- U.S. Geological Survey 1999. Parkhurst, D.L. and Appelo, C.A.J. User's Guide to PHREEQC (Version 2) – A Computer Program for Speciation, Batch-Reaction, One-Dimensional Transport, and Inverse Geochemical Calculations. United States Geological Survey Water-Resources Investigations Report 99-4259.
- Van Geen, A., A.P. Robertson, and J.O. Leckie. 1994. Complexation of carbonate species at the goethite surface: Implications for adsorption of metal ions in natural waters. *Geochimica et Cosmochimica Acta*, 58: 2073-2086.
- Zheng, C. 1990. *MT3D: A Modular Three-Dimensional Transport Model for Simulation of Advection, Dispersion, and Chemical Reactions of Contaminants in Groundwater Systems*. Prepared for the U.S. Environmental Protection Agency. Robert S. Kerr Environmental Research Laboratory, Ada, Oklahoma. Developed by S.S. Papadopoulos & Associates, Inc., Rockville, Maryland.
- Zheng, C., and G. D. Bennett. 2002. *Applied Contaminant Transport Modeling Second Edition*, John Wiley & Sons, New York, 621 pp.
- Zheng, C., and P. Wang. 1999. *MT3DMS: A Modular Three-Dimensional Multispecies Transport Model for Simulation of Advection, Dispersion, and Chemical Reactions of Contaminants in Groundwater Systems*. Prepared for the U.S. Army Corps of Engineers, Washington, DC. University of Alabama, Tuscaloosa.





Note: Open symbols are below detection and are plotted as one-half the reported detection limit for the respective sampling events.



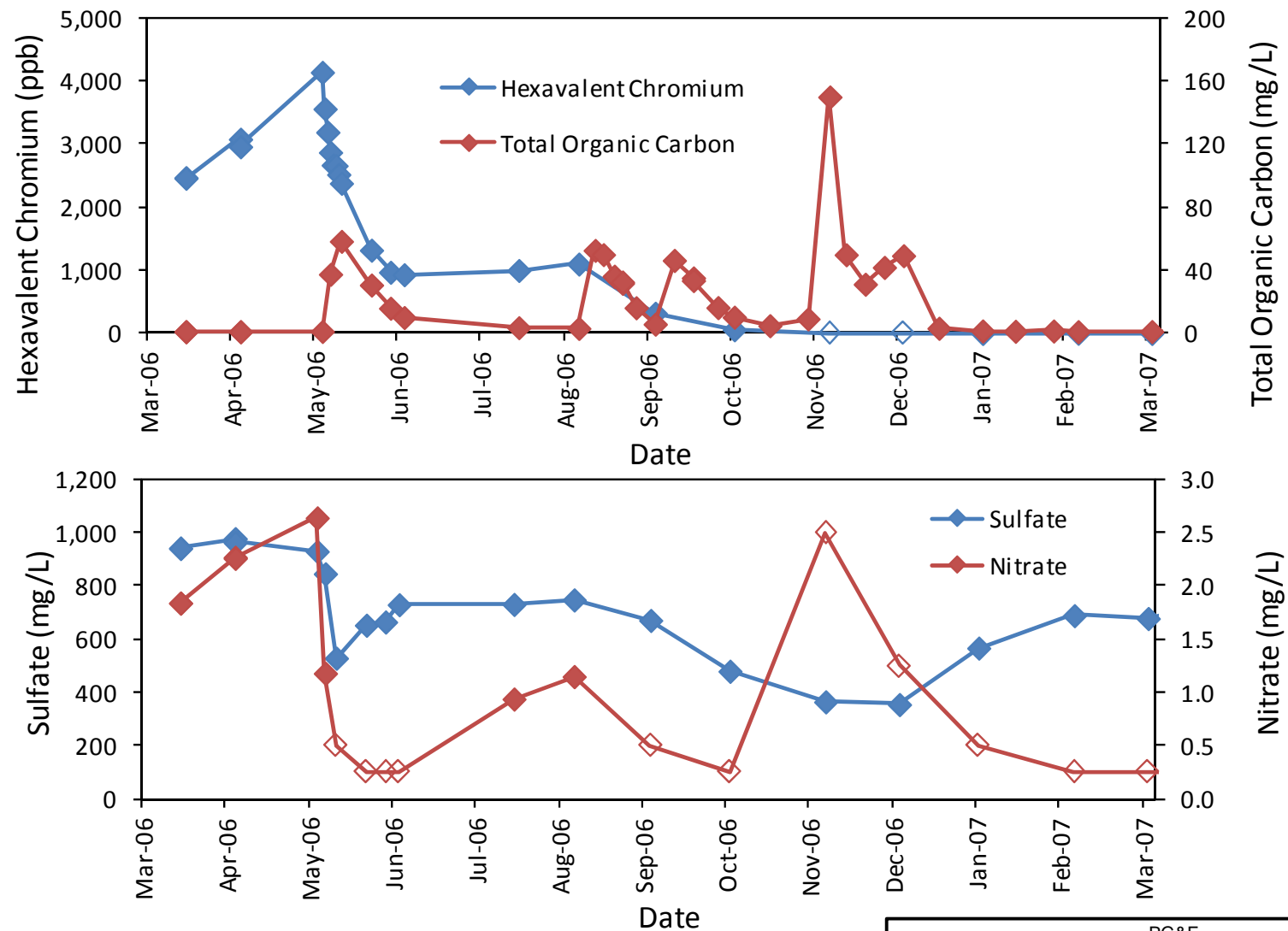


PG&E  
TOPOCK COMPRESSOR STATION  
NEEDLES, CALIFORNIA  
MODELING APPENDIX

## REDOX LADDER



FIGURE  
2.4-1



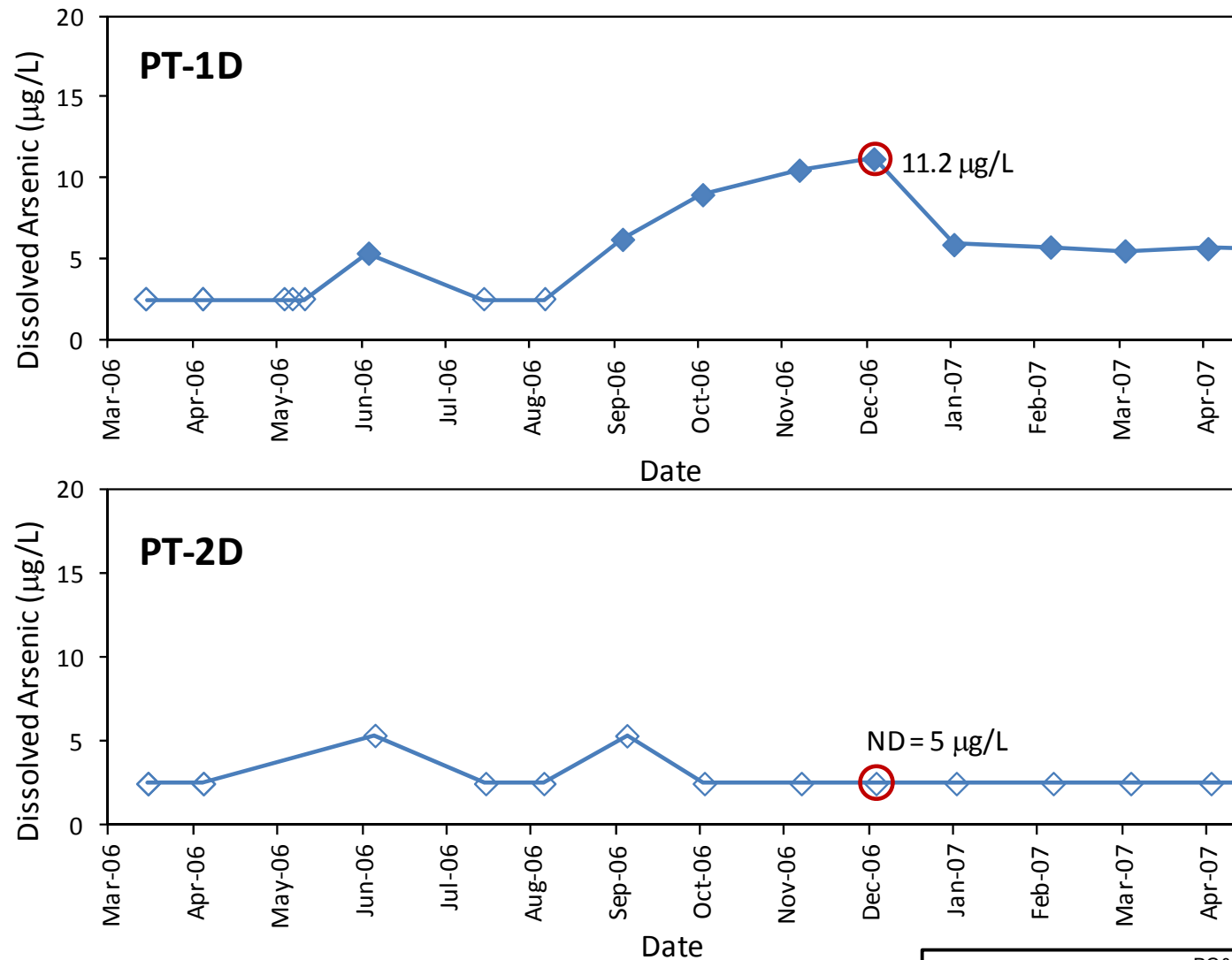
Note: Open symbols are below detection and are plotted as one-half the reported detection limit for the respective sampling event.

PG&E  
TOPOCK COMPRESSOR STATION  
NEEDLES, CALIFORNIA  
MODELING APPENDIX

FLOODPLAIN ISPT RESULTS FOR PT-1D,  
INJECTION EVENTS 1-4



FIGURE  
3.4-1



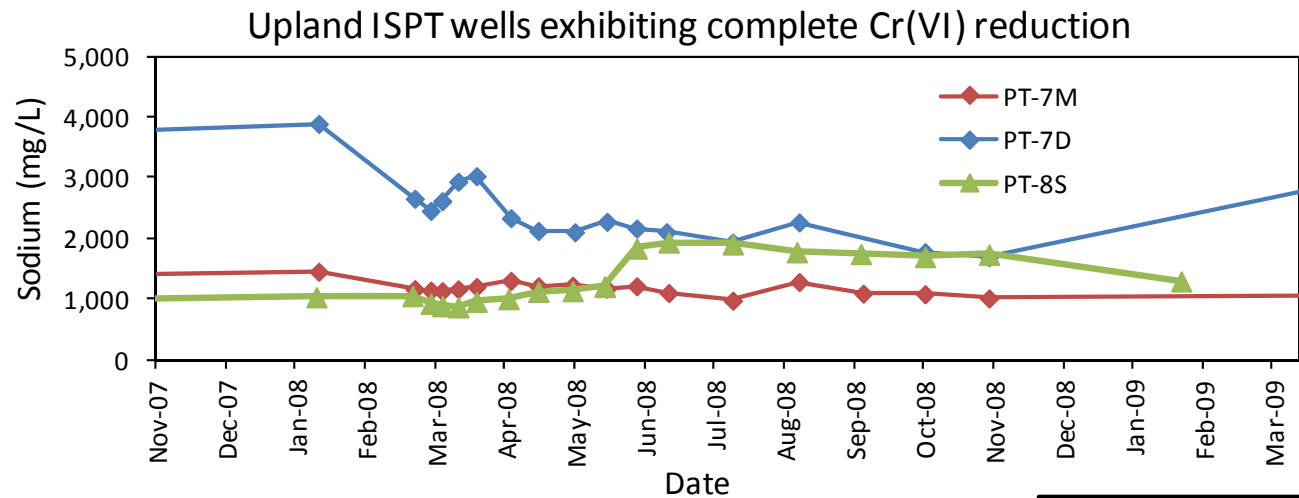
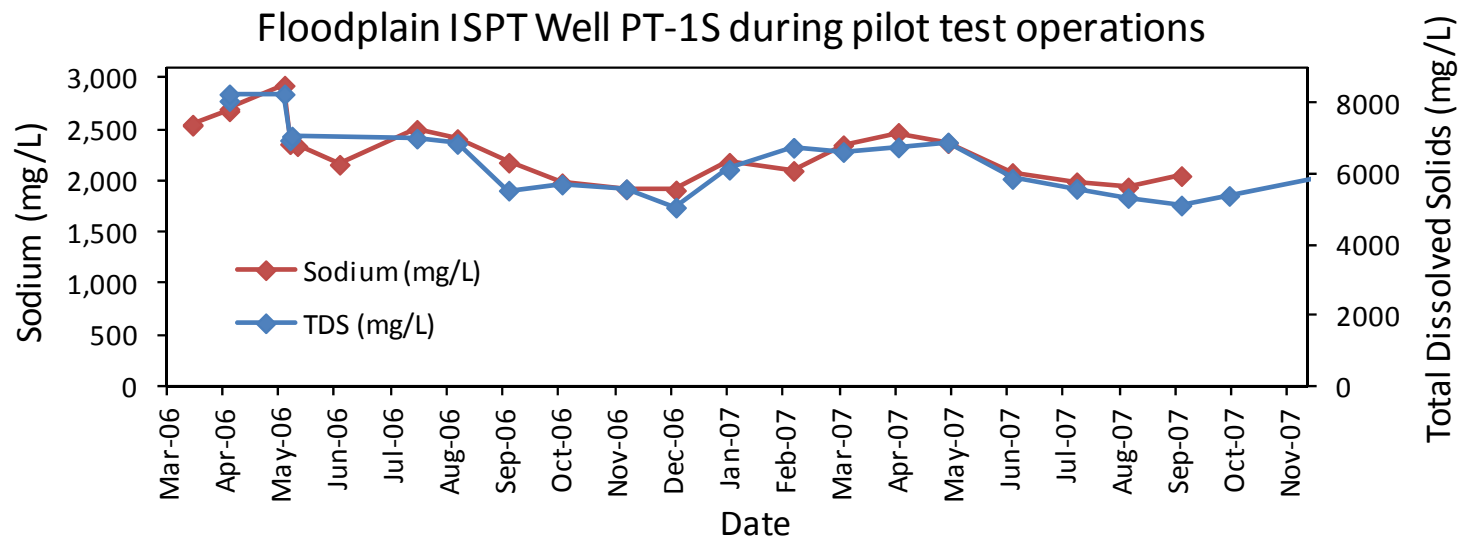
Note: Open symbols are below detection and are plotted as one-half the reported detection limit for the respective sampling event.

PG&E  
TOPOCK COMPRESSOR STATION  
NEEDLES, CALIFORNIA  
MODELING APPENDIX

ARSENIC CONCENTRATIONS  
OBSERVED IN PT-1D AND PT-2D,  
INJECTION EVENTS 1-4



FIGURE  
3.4-2

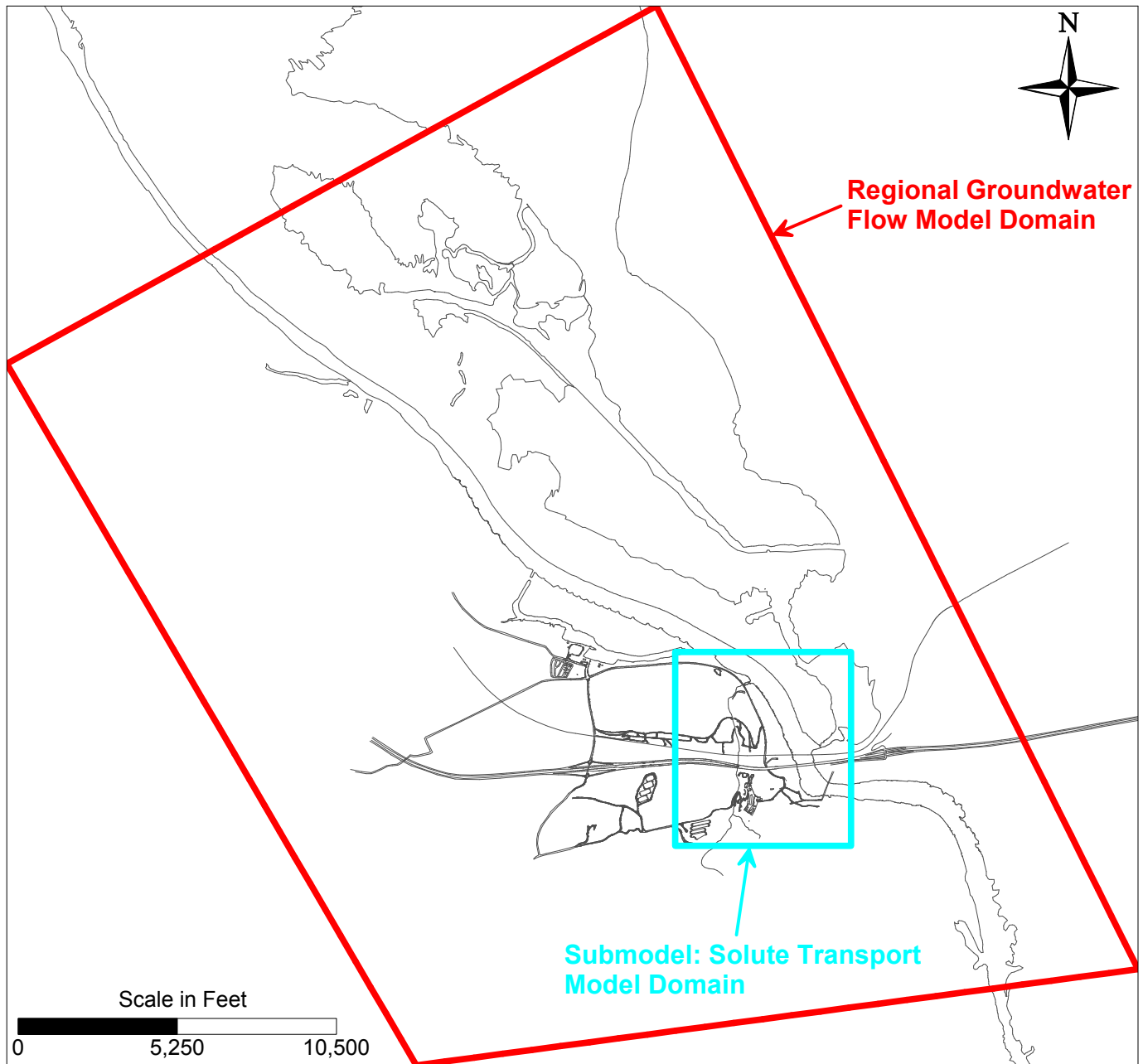


PG&E  
TOPOCK COMPRESSOR STATION  
NEEDLES, CALIFORNIA  
MODELING APPENDIX

TDS AND SODIUM CONCENTRATIONS IN  
FLOODPLAIN AND UPLAND ISPT WELLS



FIGURE  
3.5-1

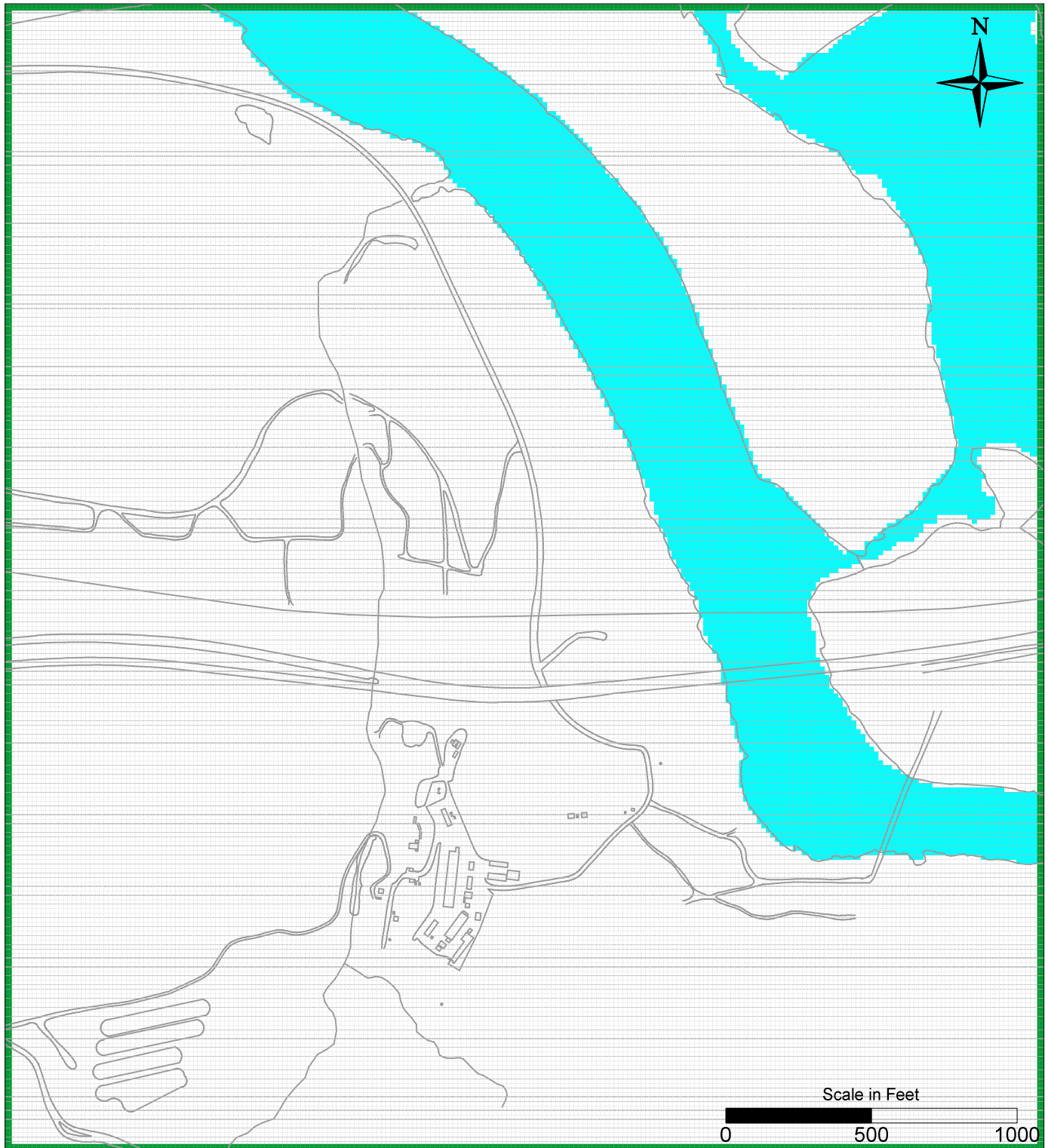


PG&E  
TOPOCK COMPRESSOR STATION  
NEEDLES, CALIFORNIA  
MODELING APPENDIX

REGIONAL MODEL AND SUBMODEL  
DOMAIN EXTENTS



FIGURE  
4-1



**LEGEND**

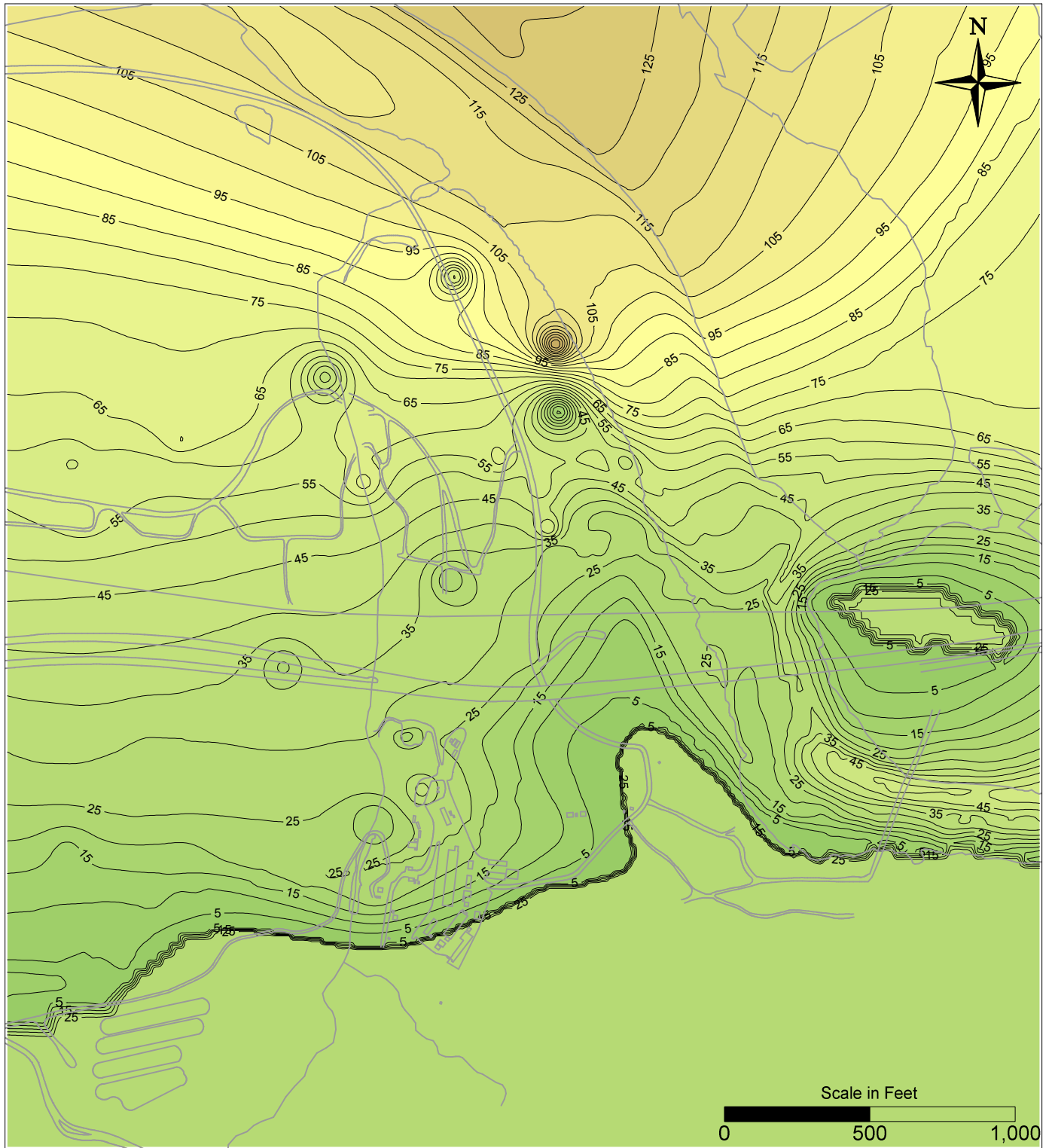
- Finite Difference Grid Cell
- Constant Flux Boundary Cell
- River Boundary Cell

PG&E  
TOPOCK COMPRESSOR STATION  
NEEDLES, CALIFORNIA  
MODELING APPENDIX

SUBMODEL DOMAIN AND  
FINITE DIFFERENCE GRID



FIGURE  
**4.2-1**



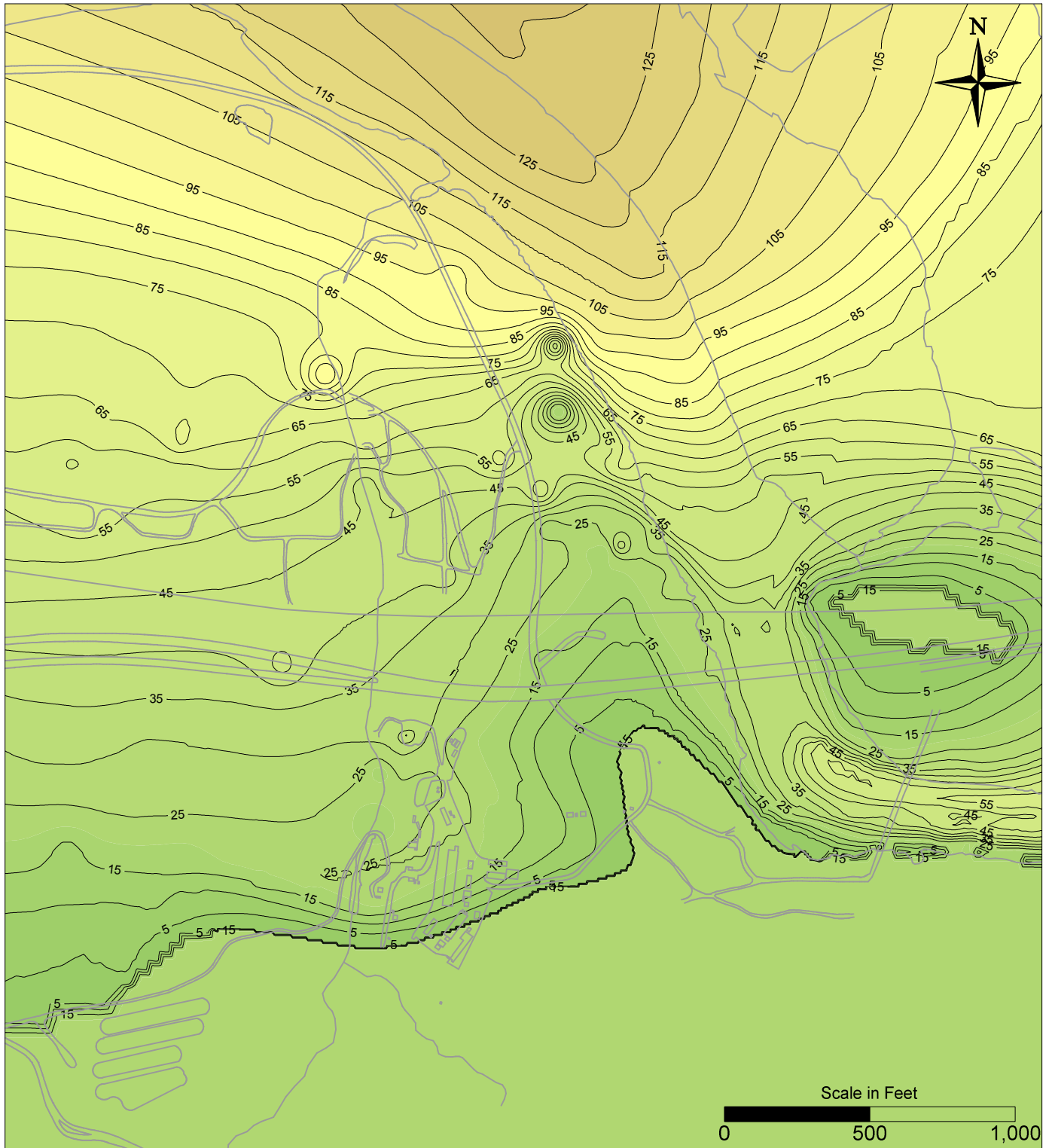
PG&E  
TOPOCK COMPRESSOR STATION  
NEEDLES, CALIFORNIA  
MODELING APPENDIX

THICKNESS MODEL LAYER 1



FIGURE  
4.2-2





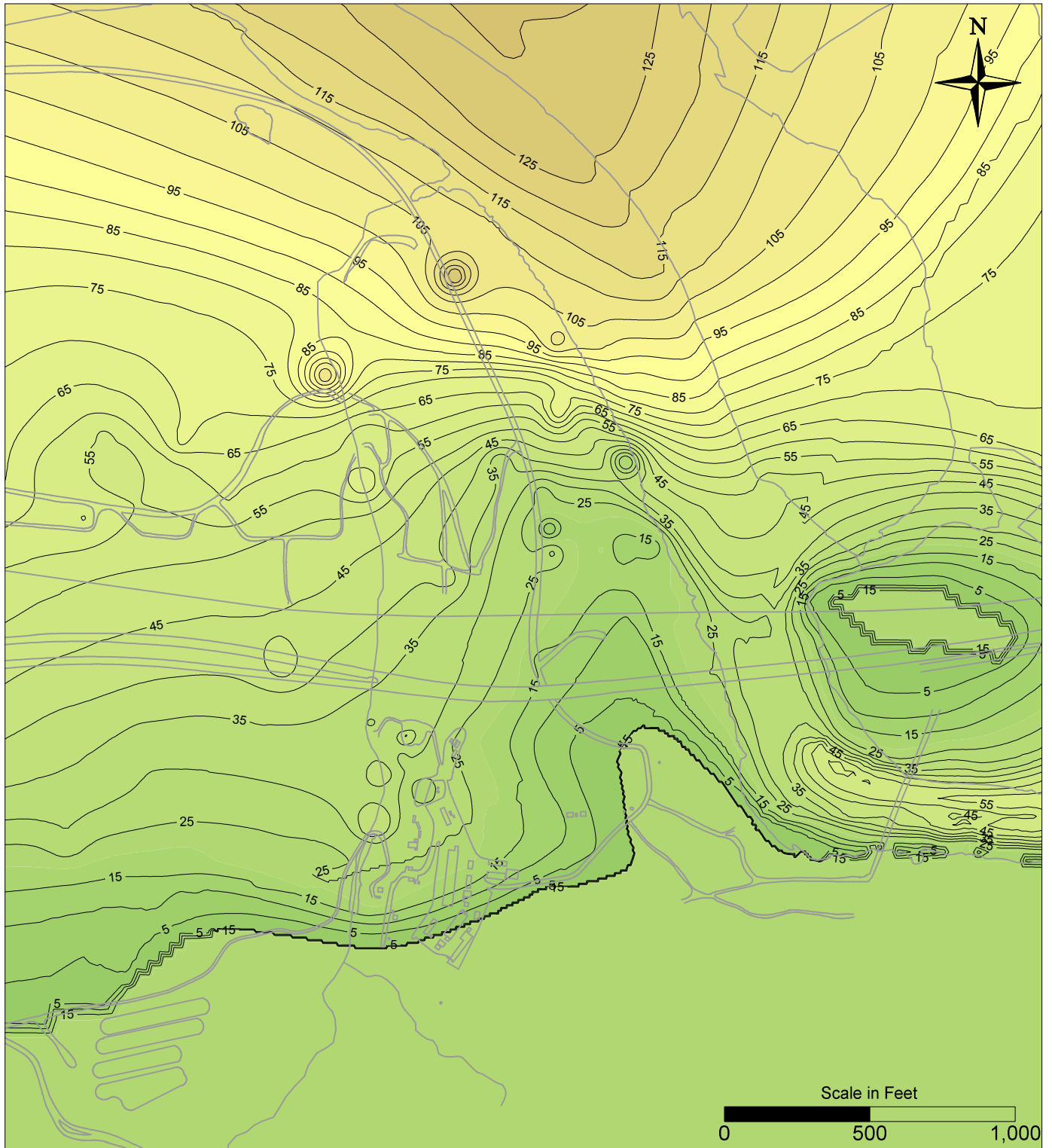
PG&E  
TOPOCK COMPRESSOR STATION  
NEEDLES, CALIFORNIA  
MODELING APPENDIX

THICKNESS MODEL LAYER 2



FIGURE  
4.2-3



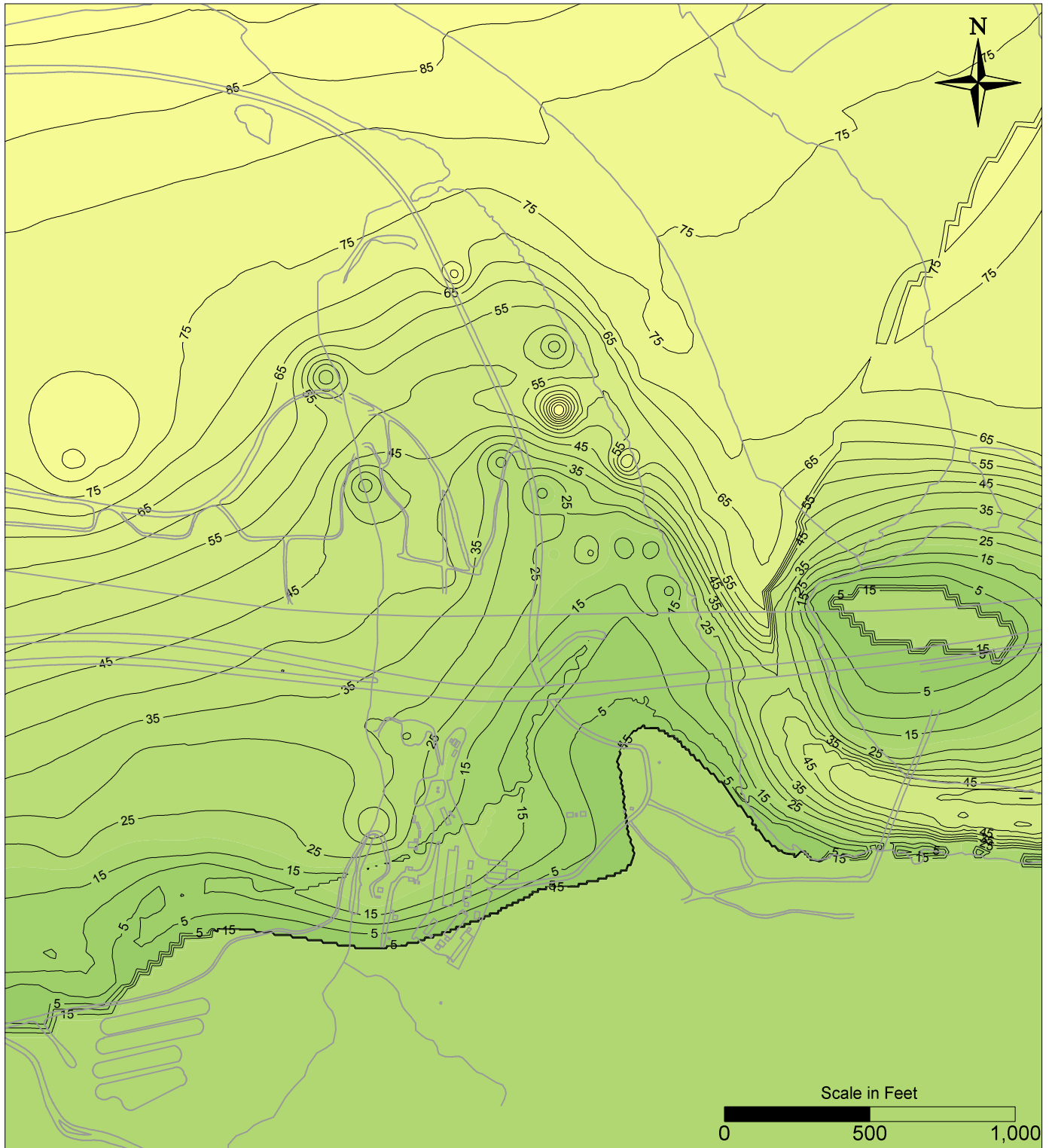


PG&E  
TOPOCK COMPRESSOR STATION  
NEEDLES, CALIFORNIA  
MODELING APPENDIX

THICKNESS MODEL LAYER 3



FIGURE  
4.2-4

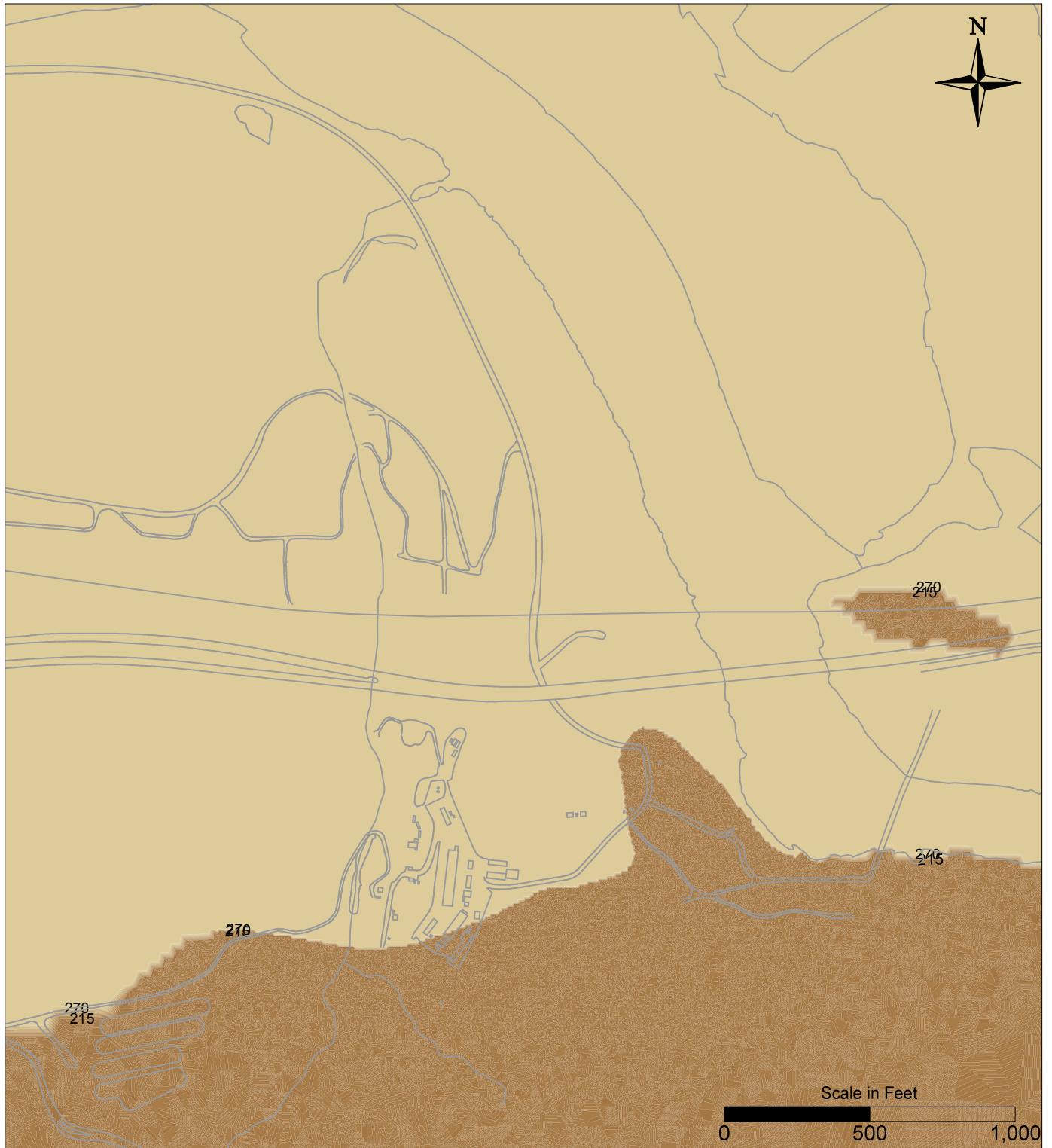


PG&E  
TOPEAK COMPRESSOR STATION  
NEEDLES, CALIFORNIA  
MODELING APPENDIX

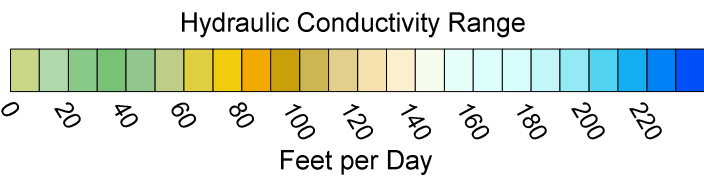
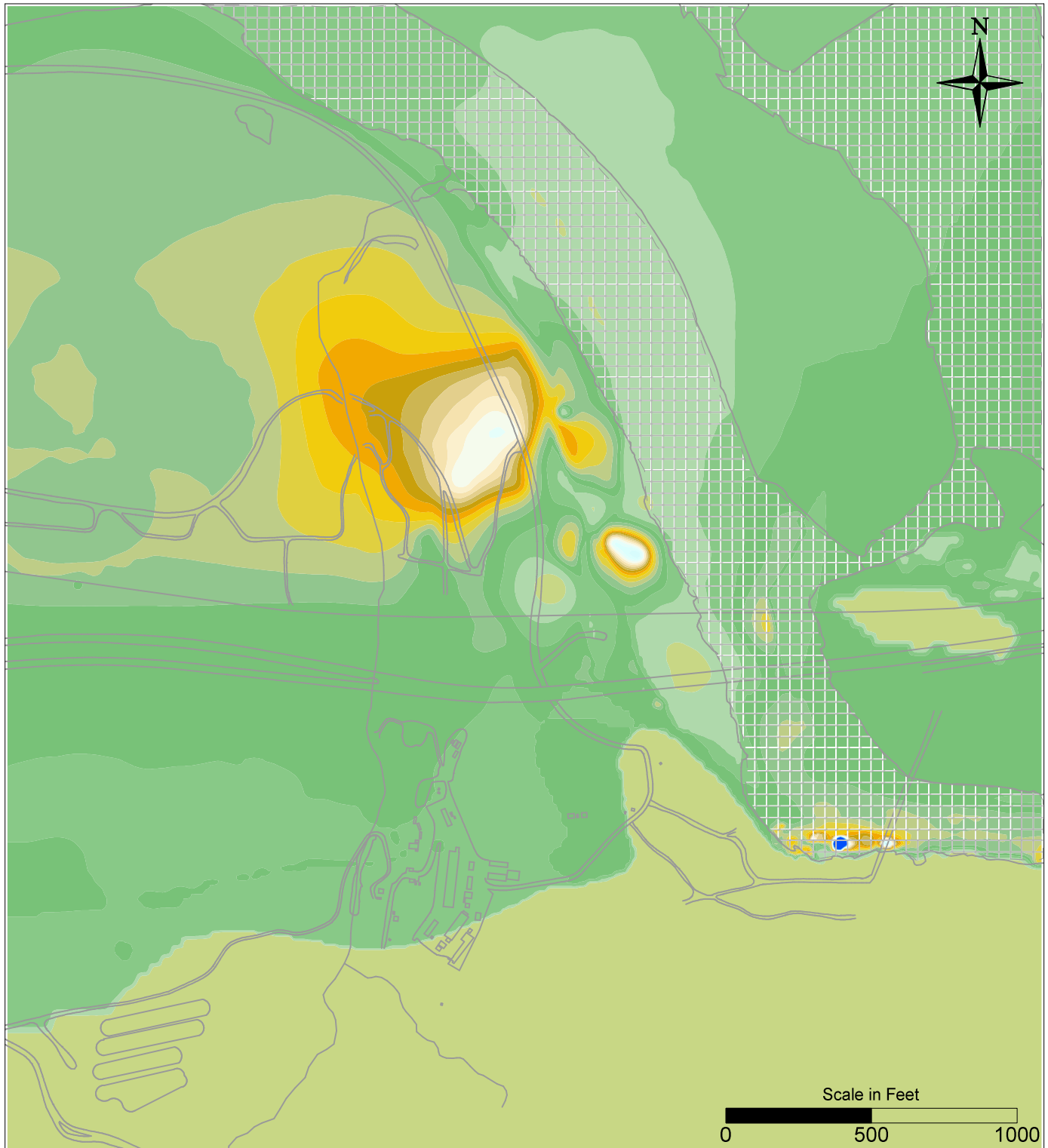
THICKNESS MODEL LAYER 4



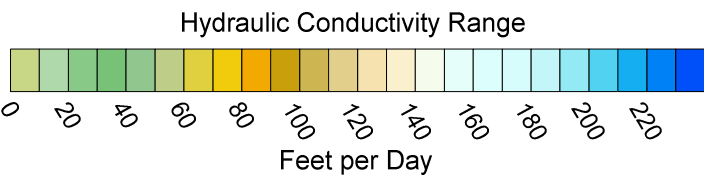
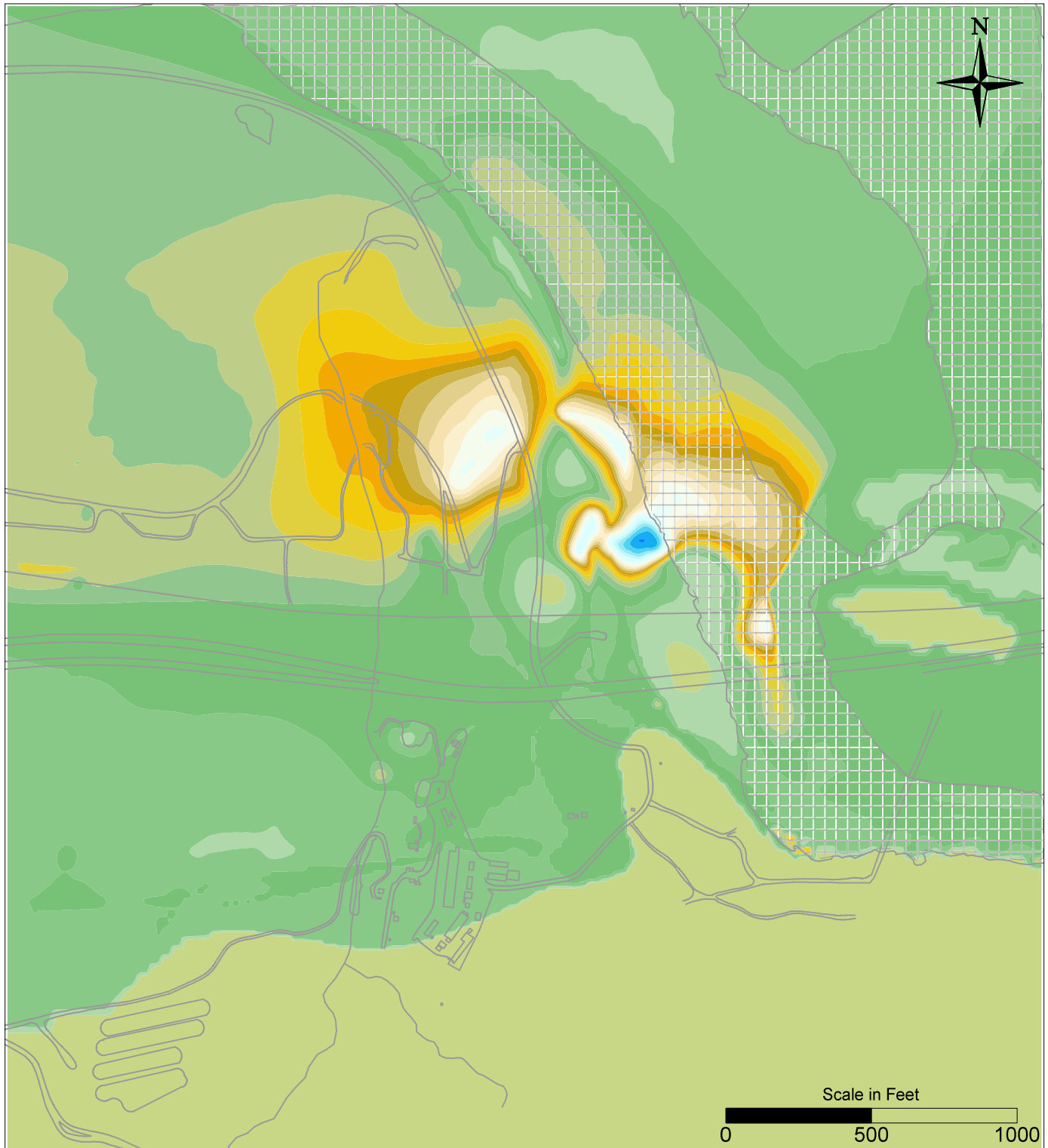
FIGURE  
4.2-5



PG&E TOPOCK COMPRESSOR STATION NEEDLES, CALIFORNIA MODELING APPENDIX	
THICKNESS MODEL LAYER 5	
	FIGURE <b>4.2-6</b>

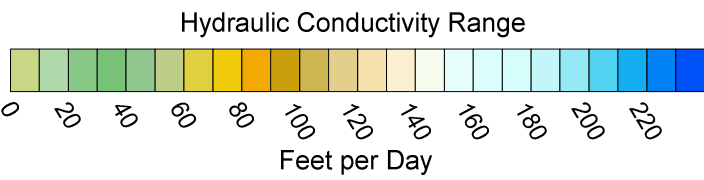
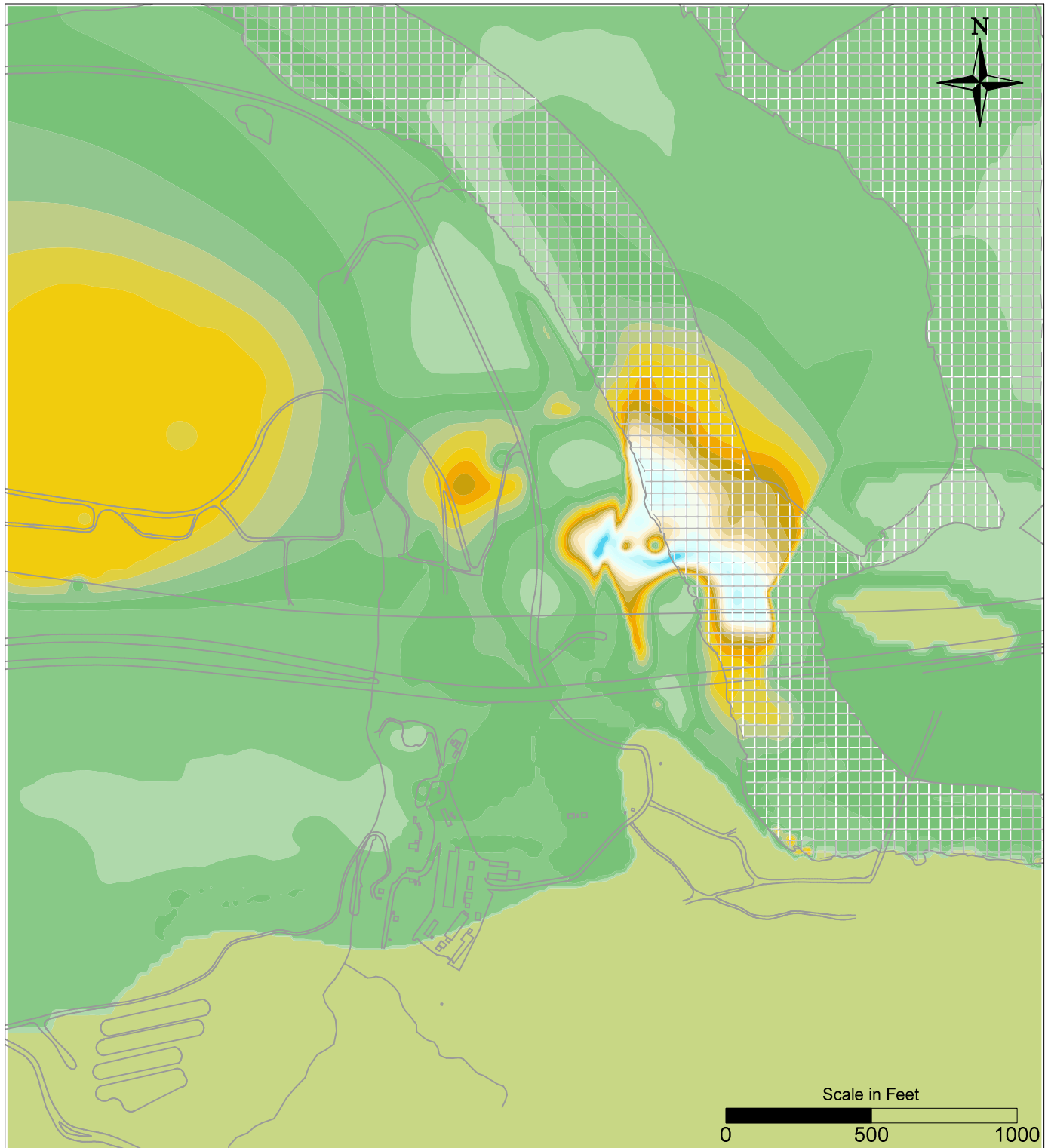


PG&E TOPOCK COMPRESSOR STATION NEEDLES, CALIFORNIA MODELING APPENDIX	
HYDRAULIC CONDUCTIVITY MODEL LAYER 1	
	FIGURE <b>4.5-1</b>

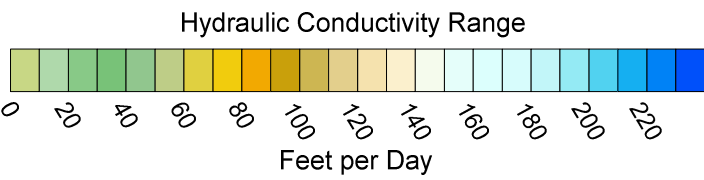
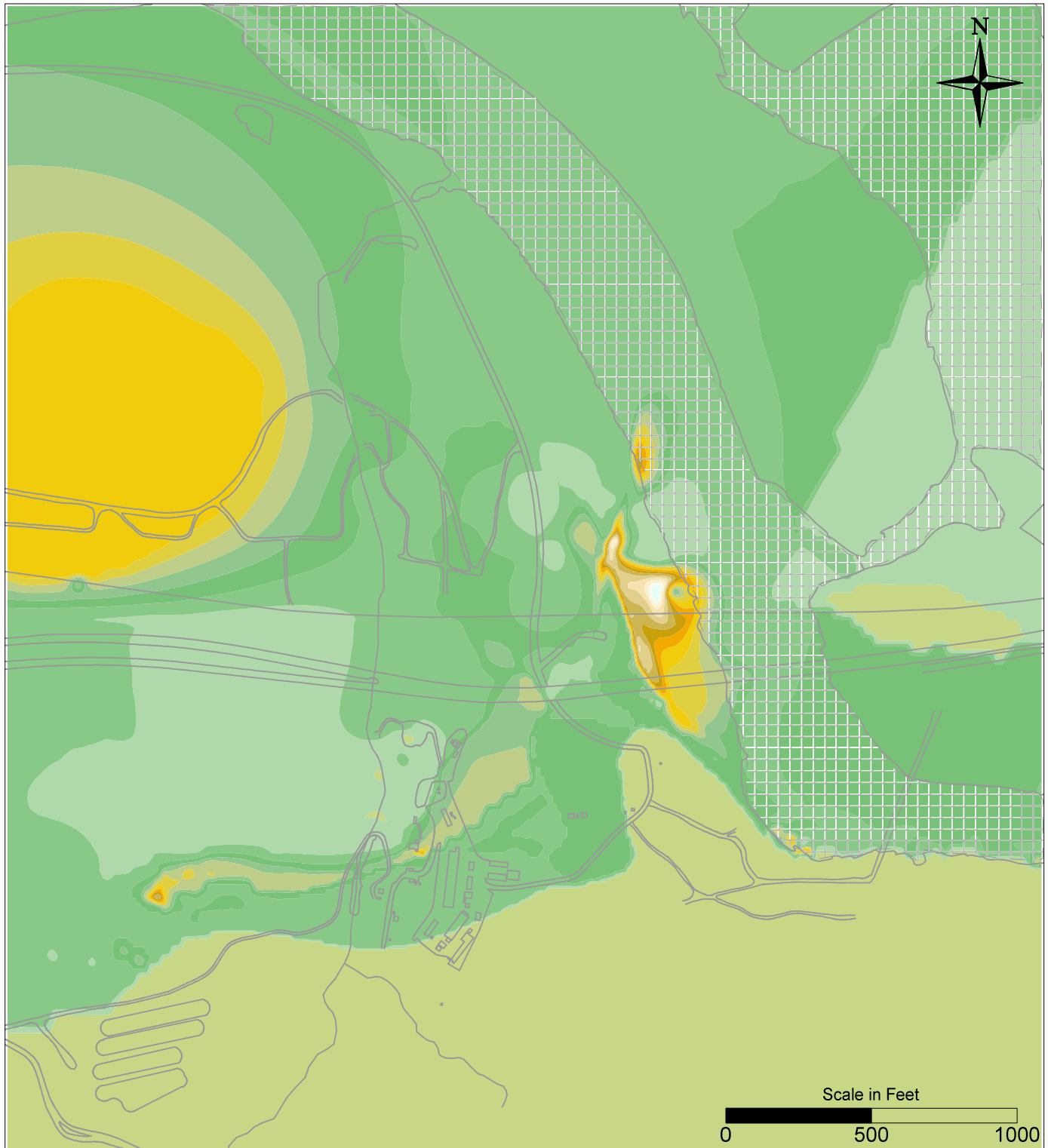


PG&E TOPOCK COMPRESSOR STATION NEEDLES, CALIFORNIA MODELING APPENDIX	
HYDRAULIC CONDUCTIVITY MODEL LAYER 2	
	FIGURE <b>4.5-2</b>



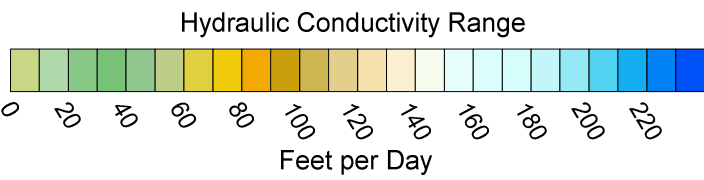
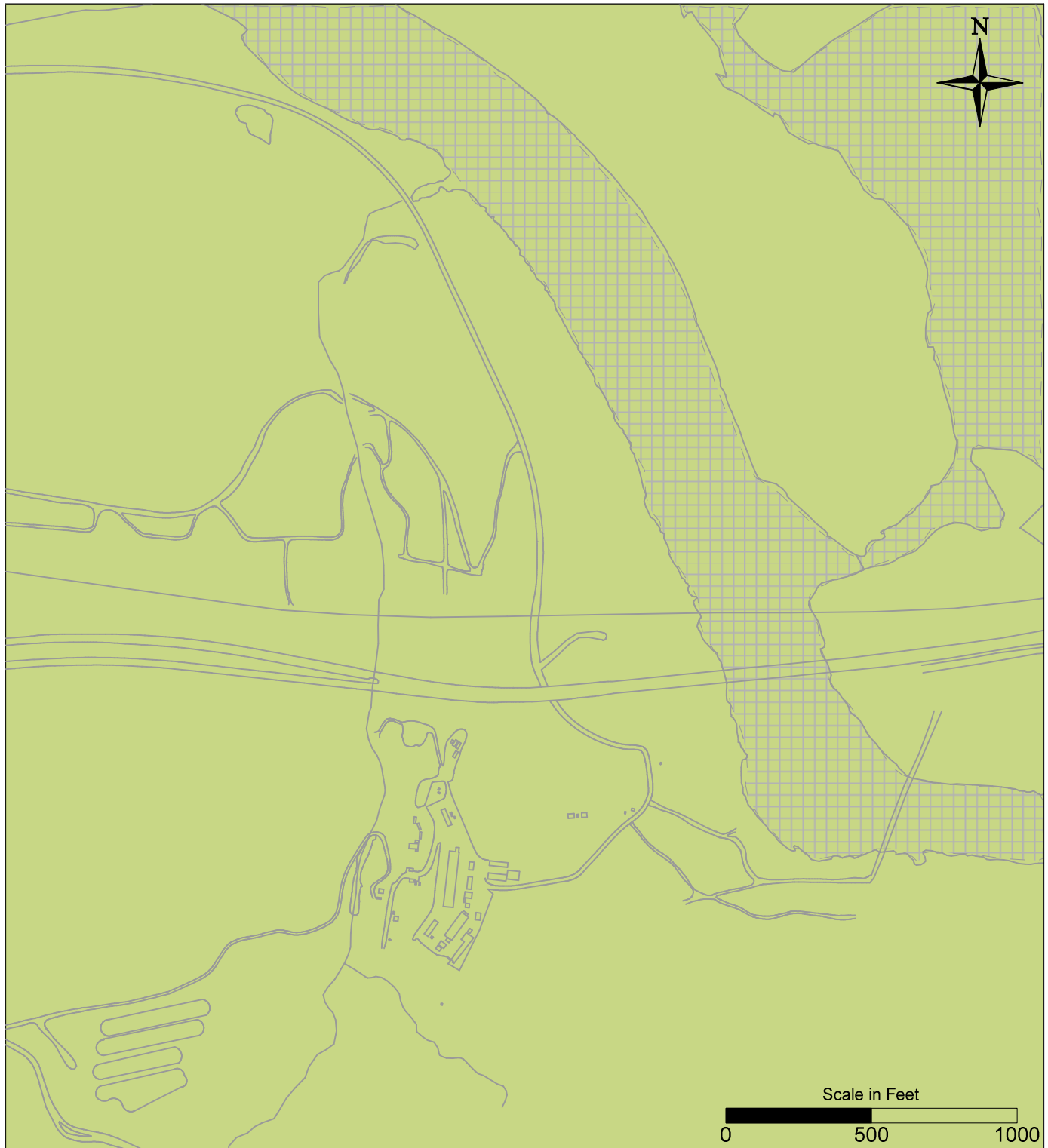


PG&E TOPOCK COMPRESSOR STATION NEEDLES, CALIFORNIA MODELING APPENDIX	
HYDRAULIC CONDUCTIVITY MODEL LAYER 3	
	FIGURE <b>4.5-3</b>

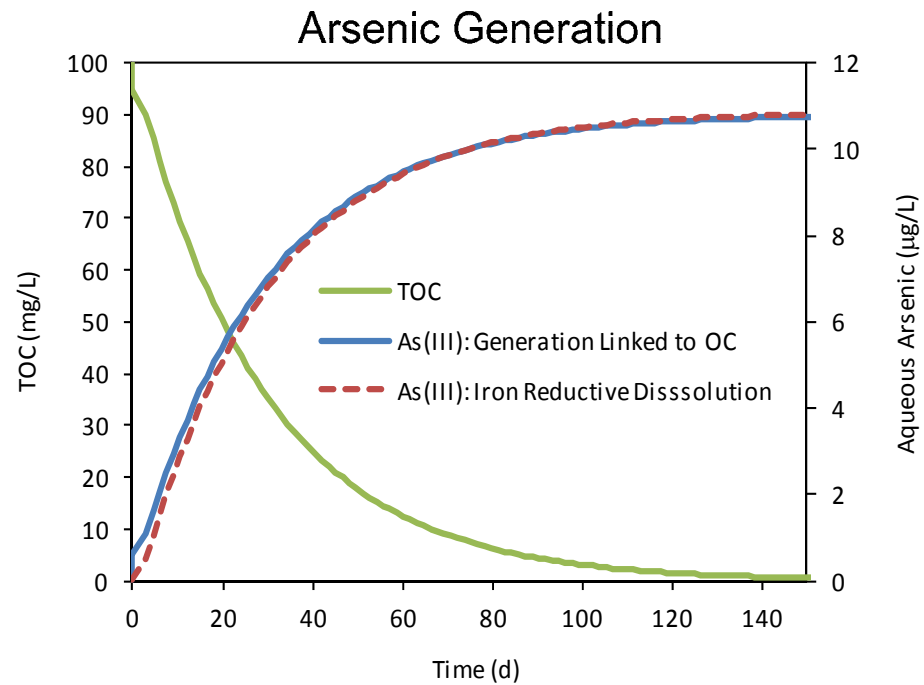
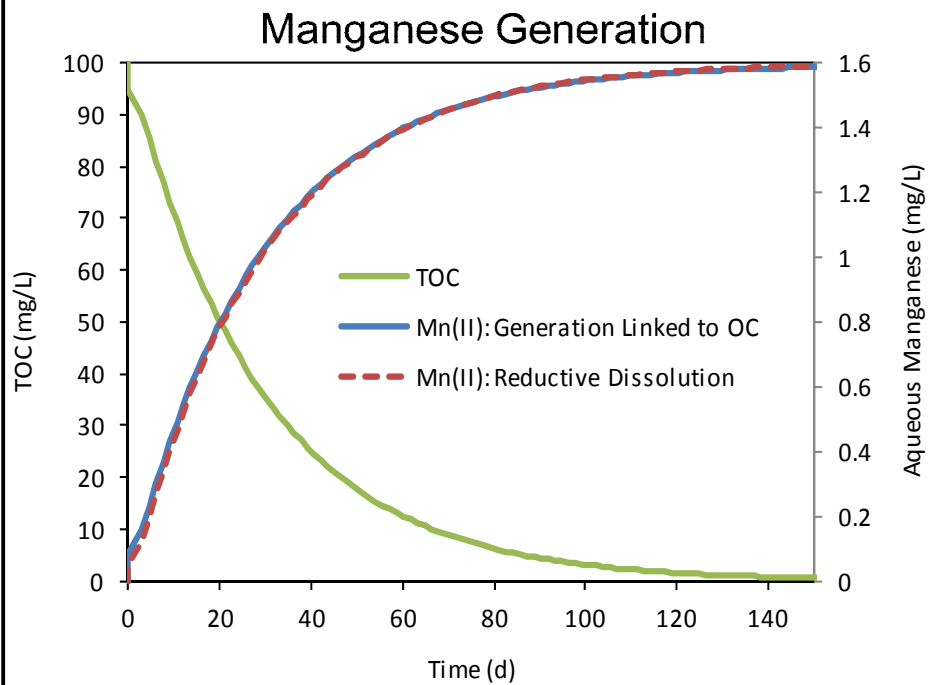


PG&E TOPOCK COMPRESSOR STATION NEEDLES, CALIFORNIA MODELING APPENDIX	
HYDRAULIC CONDUCTIVITY MODEL LAYER 4	
	FIGURE <b>4.5-4</b>





PG&E TOPOCK COMPRESSOR STATION NEEDLES, CALIFORNIA MODELING APPENDIX	
HYDRAULIC CONDUCTIVITY MODEL LAYER 5	
	FIGURE <b>4.5-5</b>

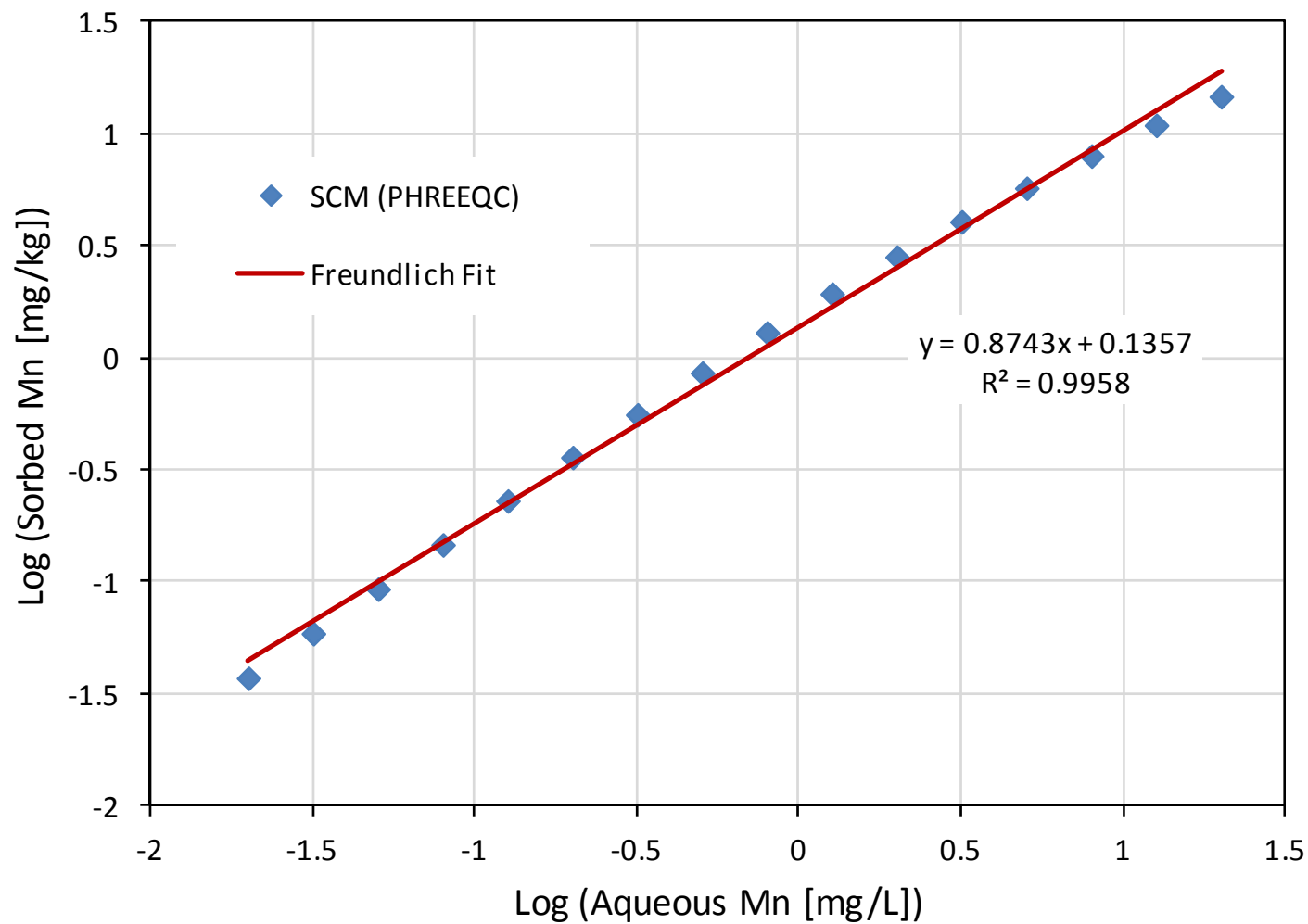


PG&E  
TOPOCK COMPRESSOR STATION  
NEEDLES, CALIFORNIA  
MODELING APPENDIX

#### BATCH MANGANESE AND ARSENIC GENERATION COMPARISONS



FIGURE  
5.3-1

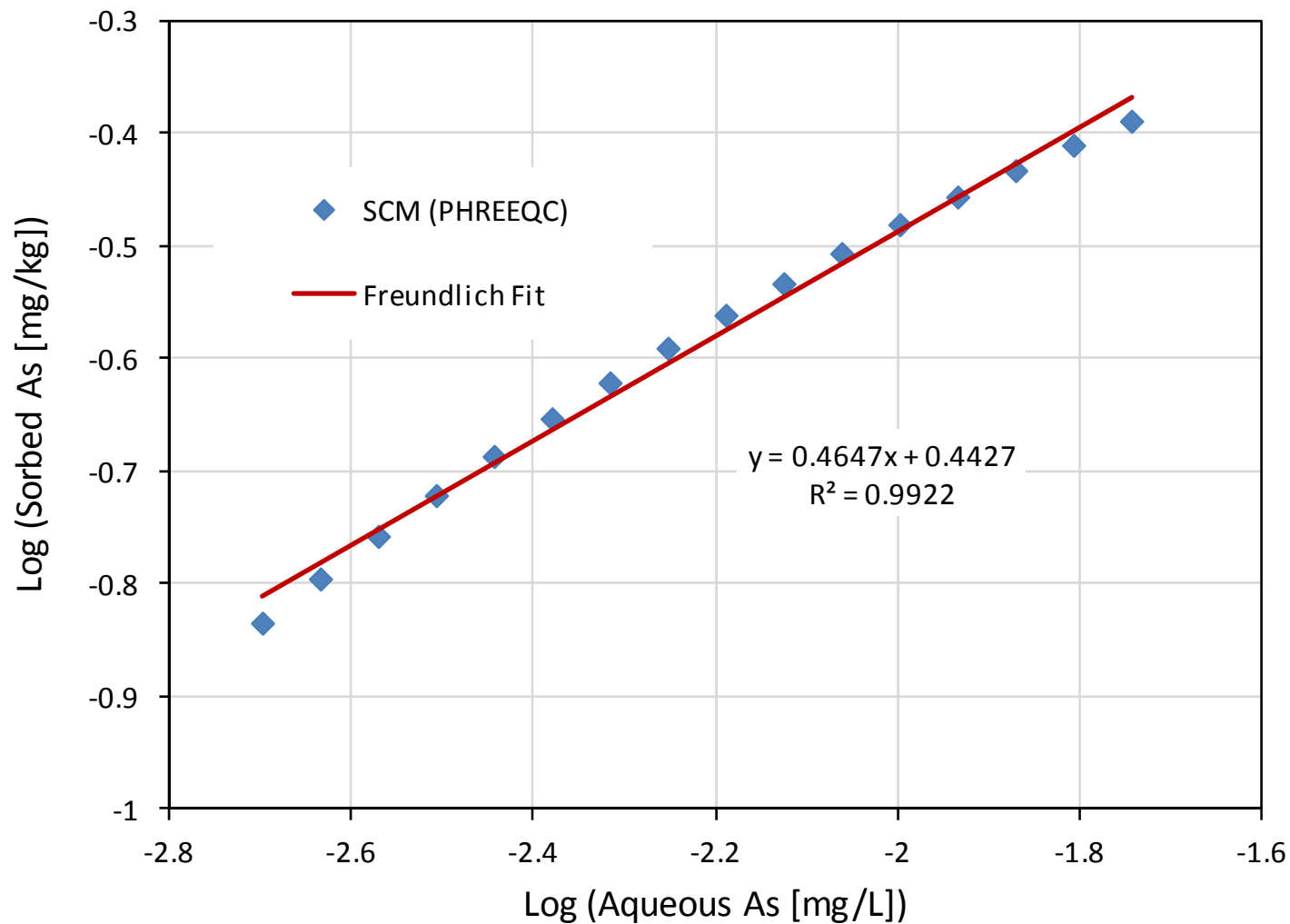


PG&E  
TOPOCK COMPRESSOR STATION  
NEEDLES, CALIFORNIA  
MODELING APPENDIX

MANGANESE SURFACE COMPLEXATION  
MODEL RESULTS AND FITTED  
FREUNDLICH ISOTHERM



FIGURE  
5.3-2

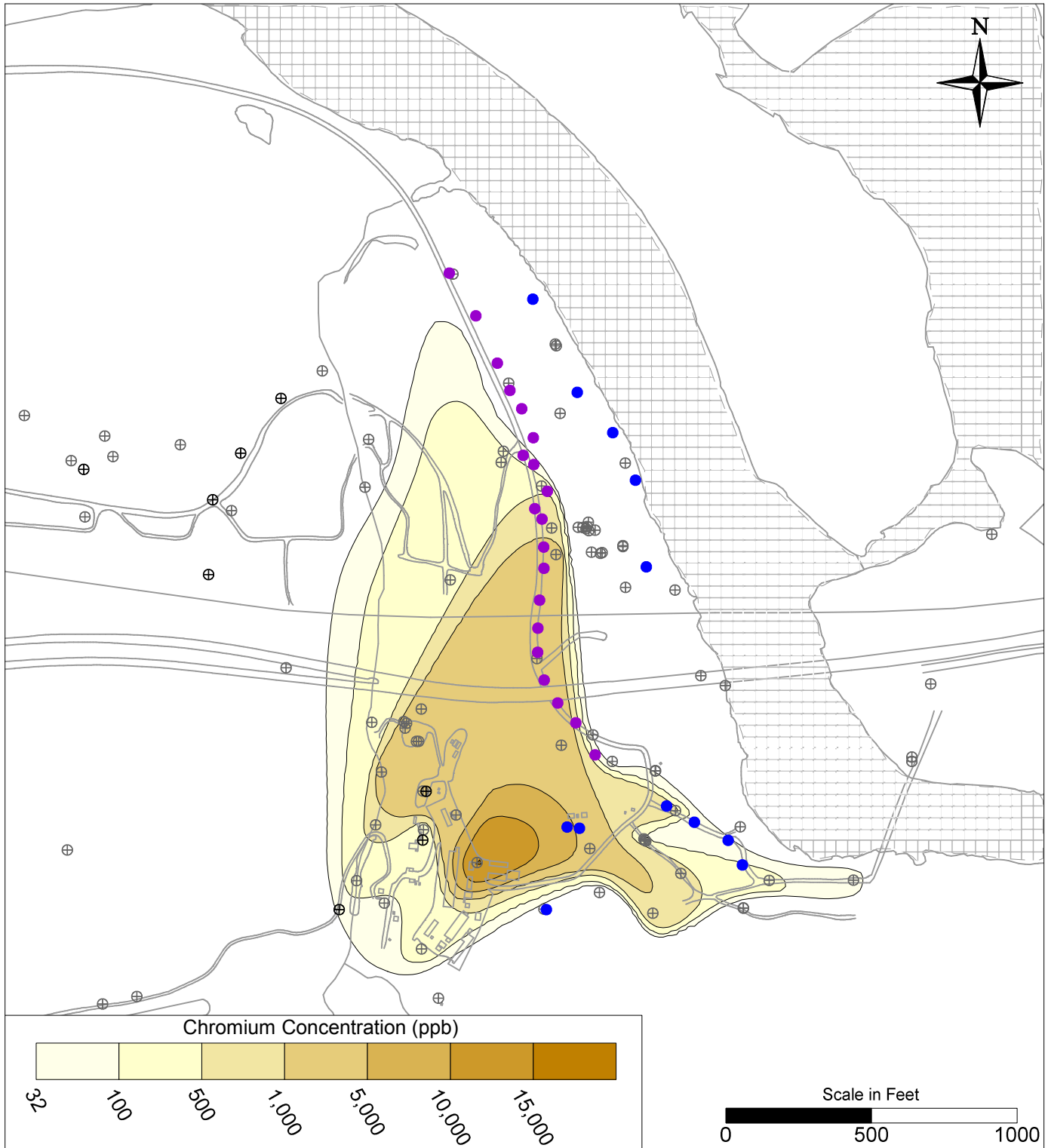


PG&E  
TOPOCK COMPRESSOR STATION  
NEEDLES, CALIFORNIA  
MODELING APPENDIX

ARSENATE SURFACE COMPLEXATION  
MODEL RESULTS AND FITTED  
FREUNDLICH ISOTHERM



FIGURE  
5.4-1



# **LEGEND**

- IRZ WELLS
- ⊕ UPGRADIENT INJECTION WELLS
- EXTRACTION WELLS
- ⊕ MONITORING WELLS

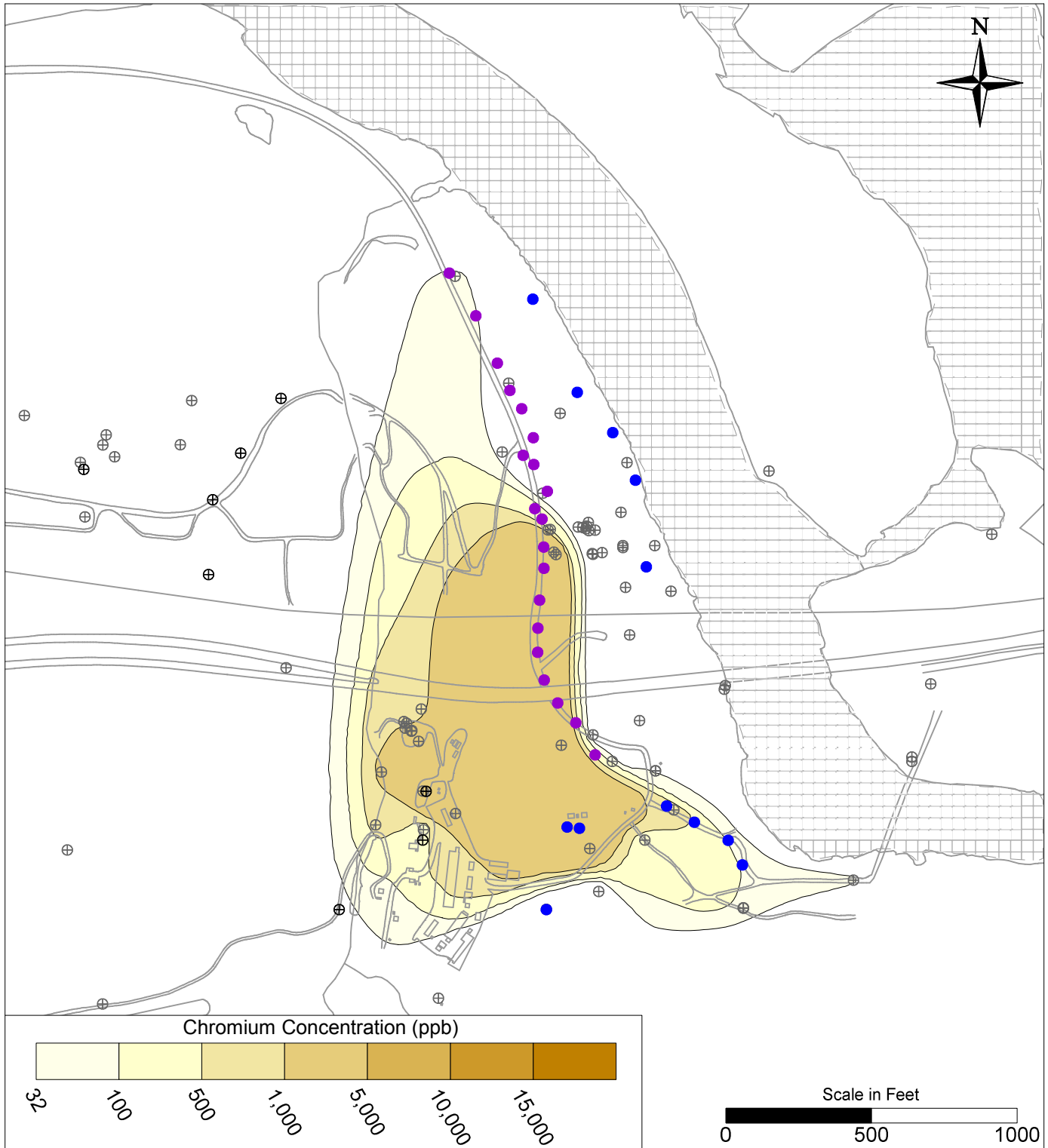
PG&E  
TOPOCK COMPRESSOR STATION  
NEEDLES, CALIFORNIA  
MODELING APPENDIX

INITIAL HEXAVALENT CHROMIUM  
CONCENTRATION DISTRIBUTION  
MODEL LAYER 1



FIGURE

6.2-1



# **LEGEND**

- IRZ WELLS
- ⊕ UPGRADIENT INJECTION WELLS
- EXTRACTION WELLS
- ⊕ MONITORING WELLS

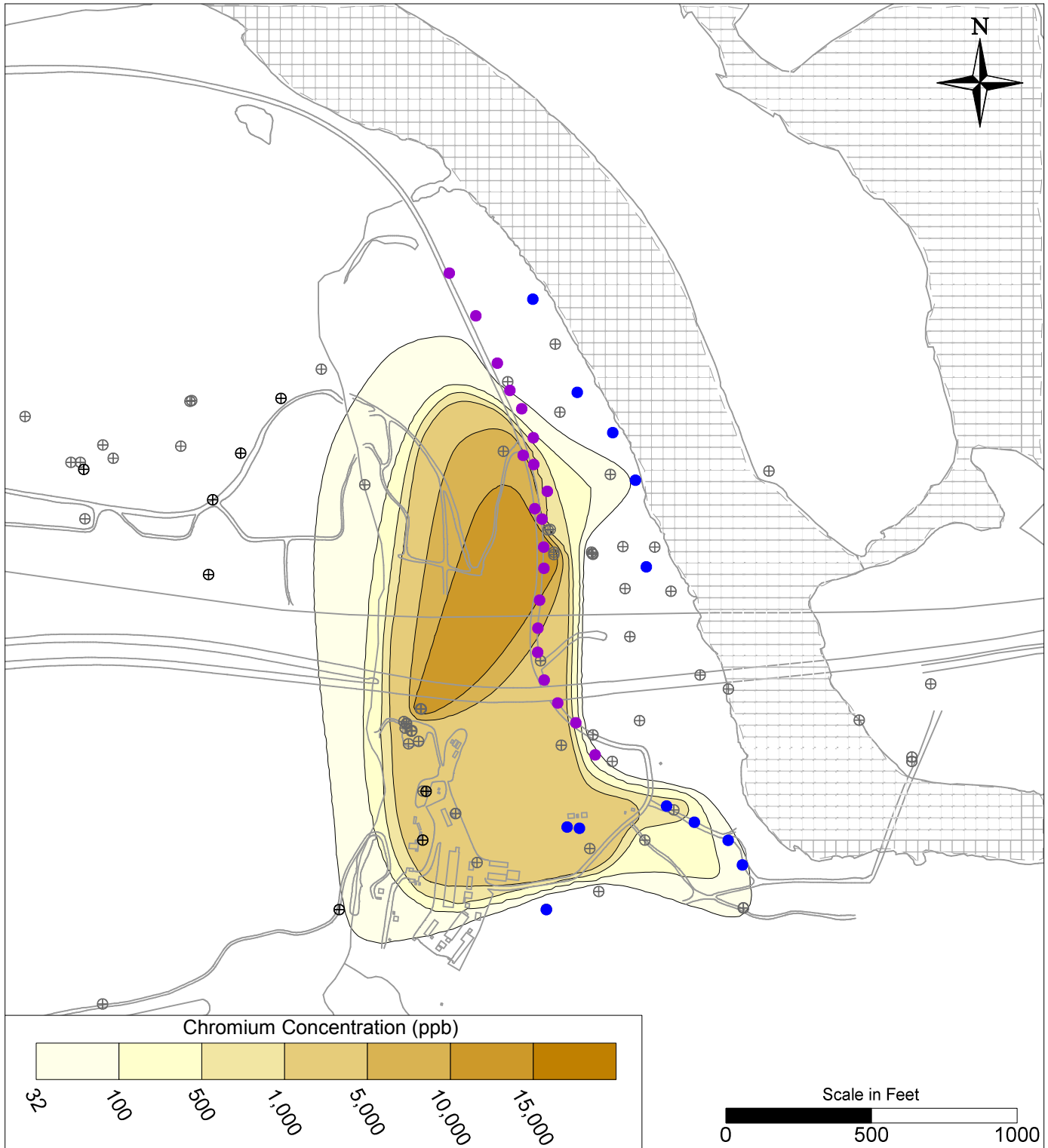
PG&E  
TOPOCK COMPRESSOR STATION  
NEEDLES, CALIFORNIA  
MODELING APPENDIX

INITIAL HEXAVALENT CHROMIUM  
CONCENTRATION DISTRIBUTION  
MODEL LAYER 2



FIGURE

6.2-2



**LEGEND**

- IRZ WELLS
- ⊕ UPGRADIENT INJECTION WELLS
- EXTRACTION WELLS
- ⊕ MONITORING WELLS

PG&E  
TOPOCK COMPRESSOR STATION  
NEEDLES, CALIFORNIA  
MODELING APPENDIX

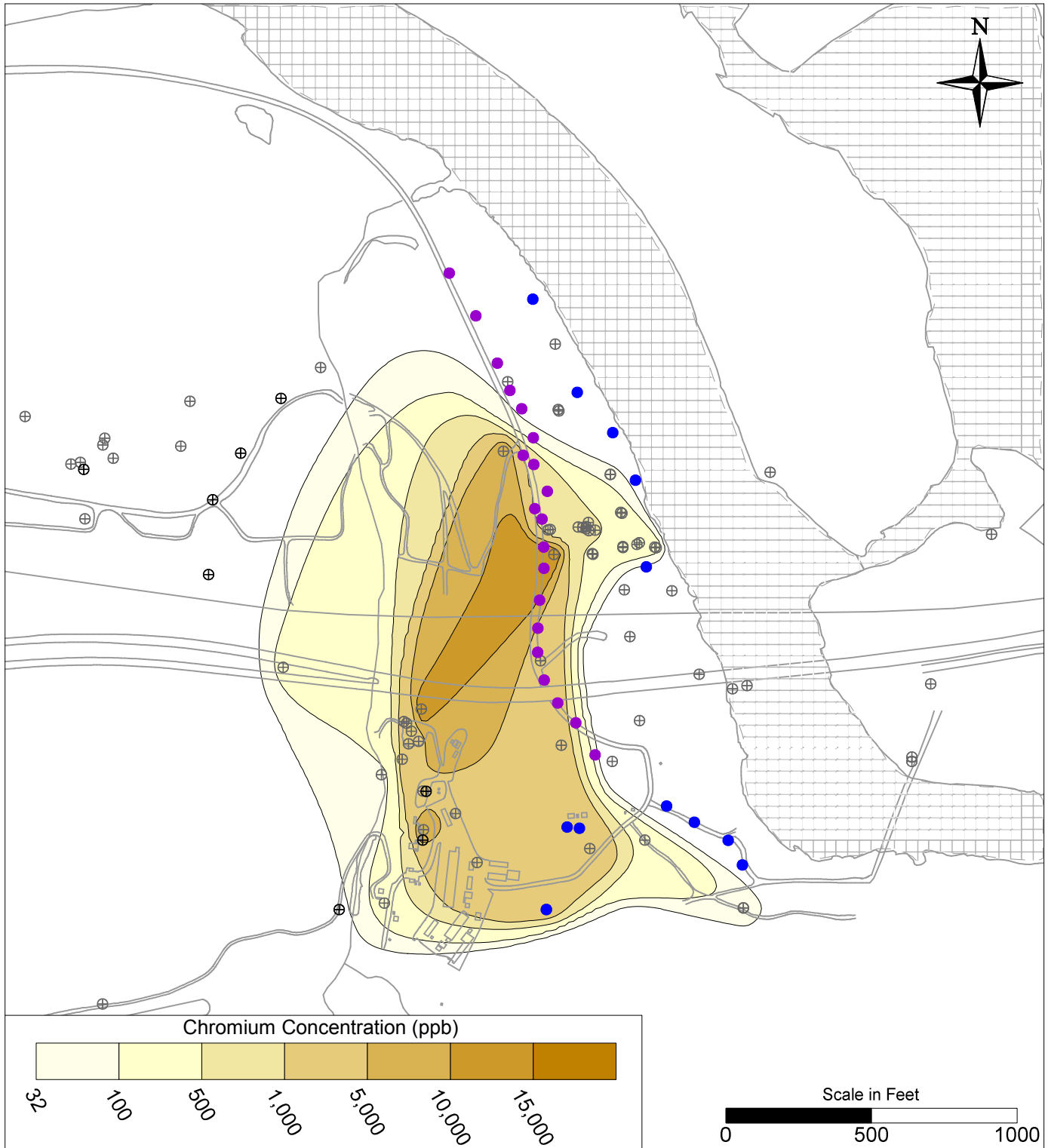
INITIAL HEXAVALENT CHROMIUM  
CONCENTRATION DISTRIBUTION  
MODEL LAYER 3



FIGURE

6.2-3





**LEGEND**

- IRZ WELLS
- ⊕ UPGRADIENT INJECTION WELLS
- EXTRACTION WELLS
- ⊕ MONITORING WELLS

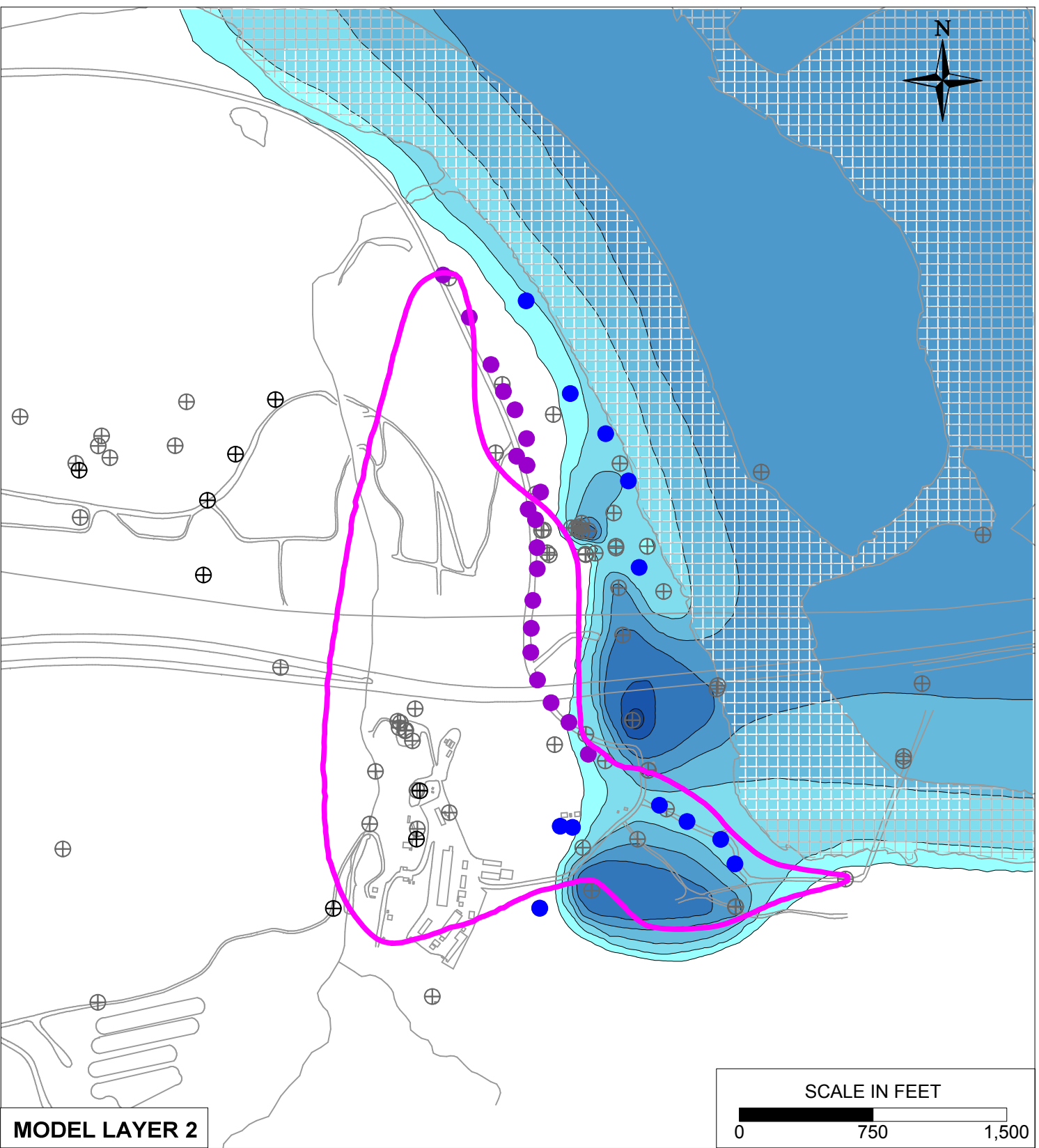
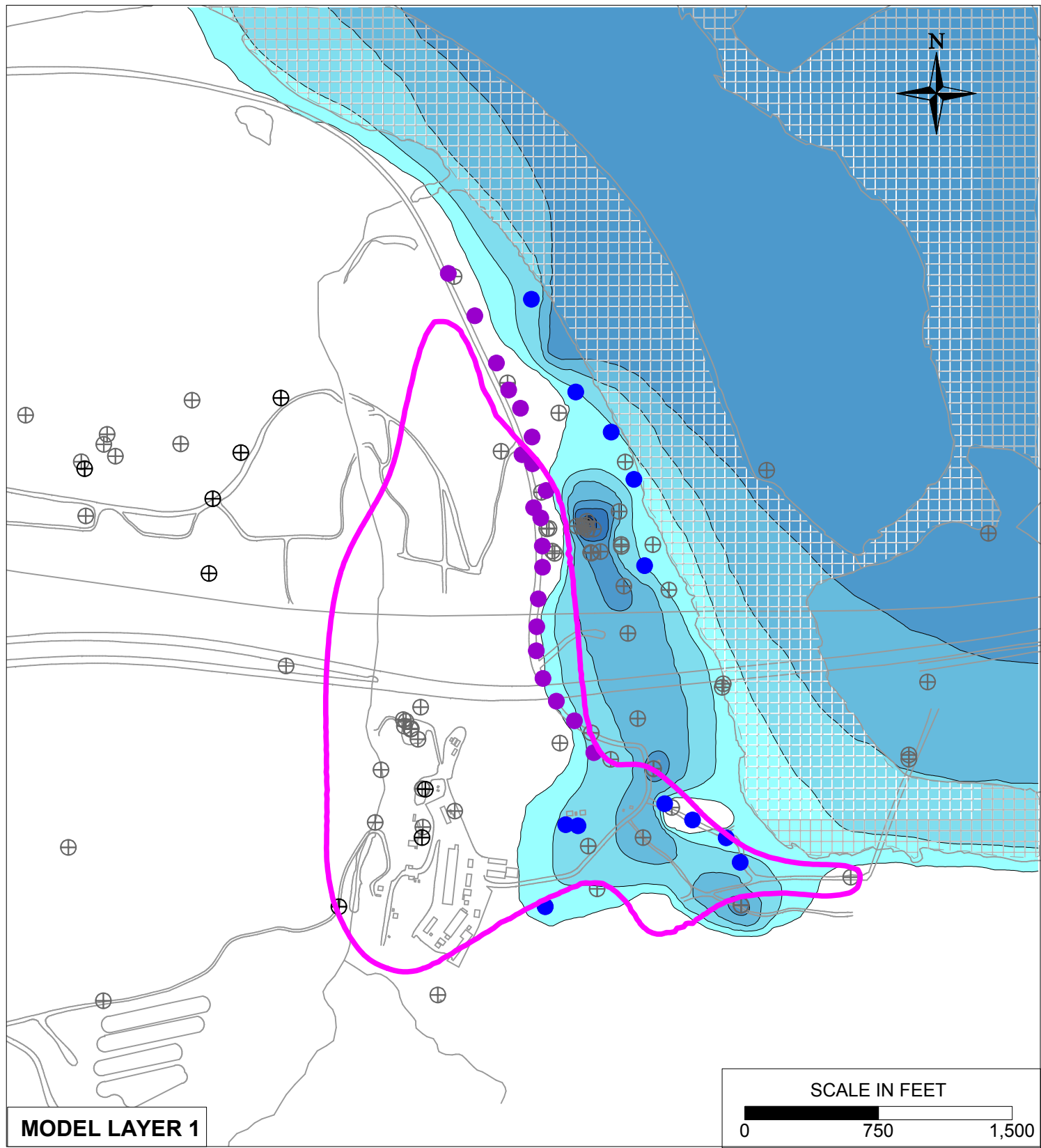
PG&E  
TOPOCK COMPRESSOR STATION  
NEEDLES, CALIFORNIA  
MODELING APPENDIX

INITIAL HEXAVALENT CHROMIUM  
CONCENTRATION DISTRIBUTION  
MODEL LAYER 4



FIGURE

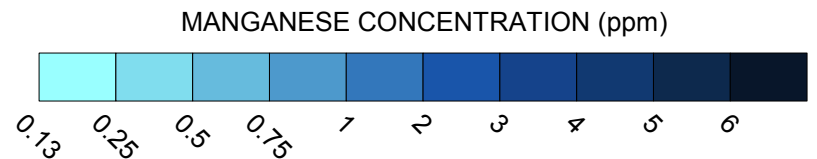
6.2-4



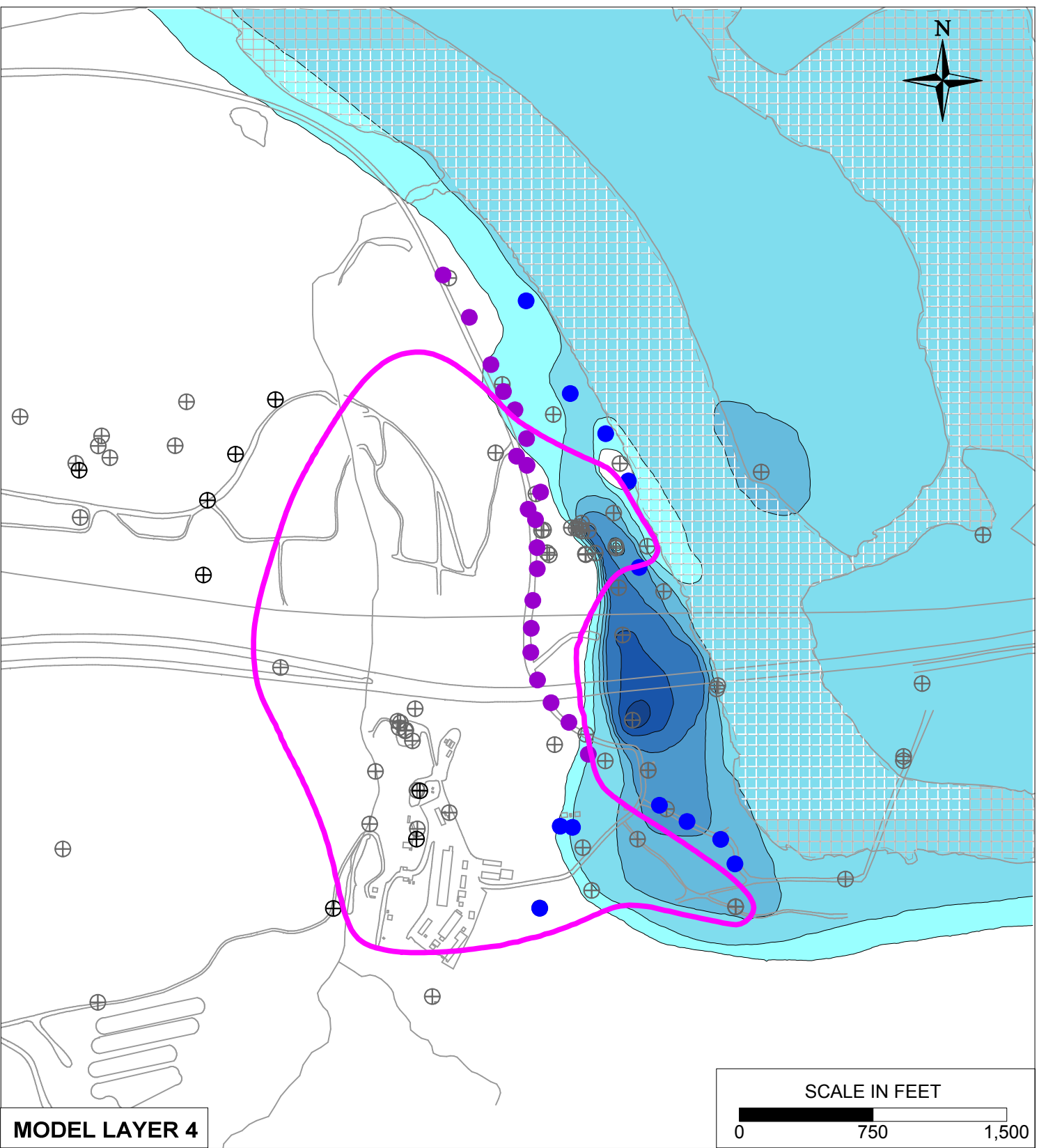
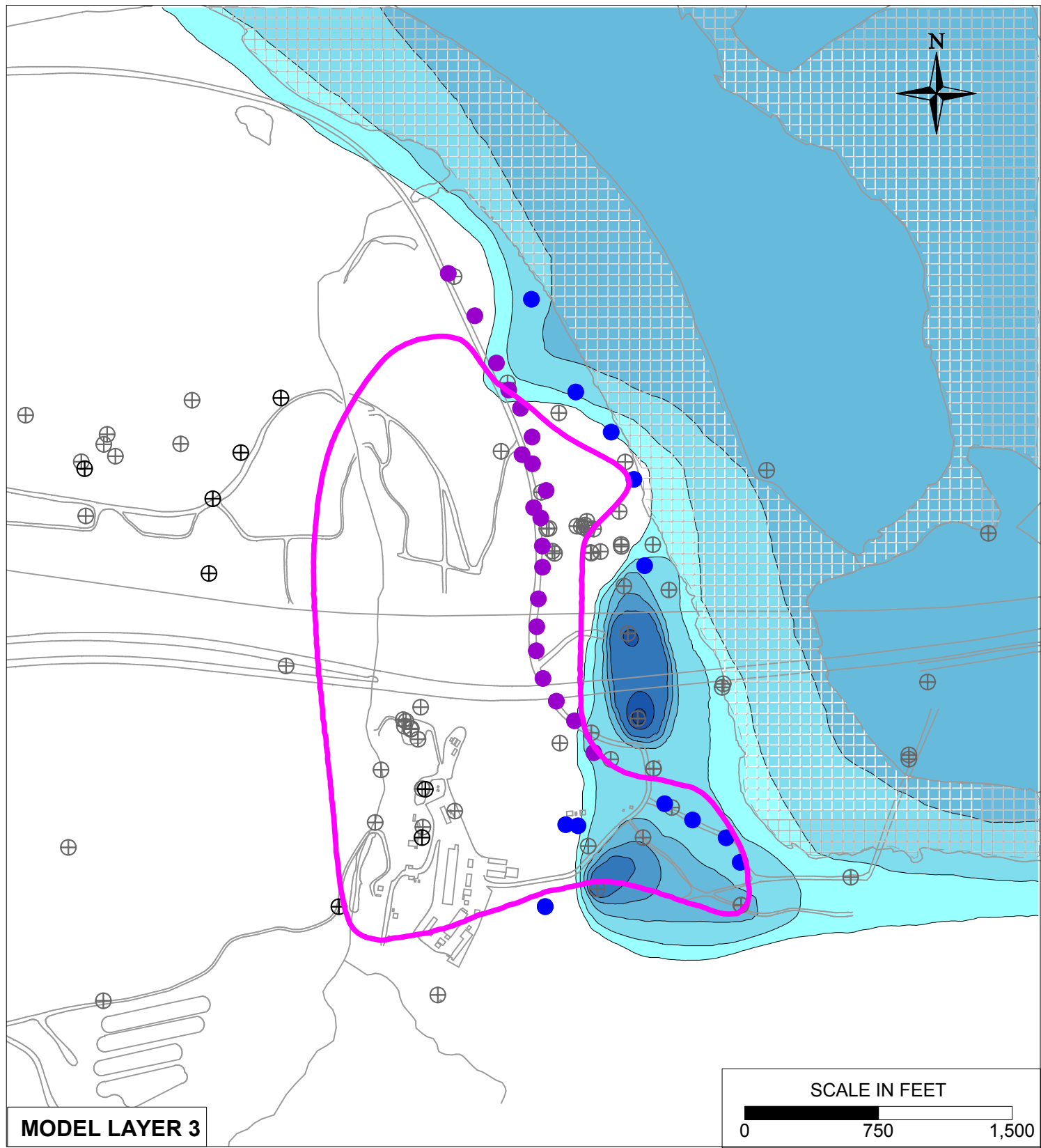
**LEGEND**

- IRZ WELLS
- ⊕ UPGRADIENT INJECTION WELLS
- EXTRACTION WELLS
- ⊕ MONITORING WELLS

— HEXAVALENT CHROMIUM GROUNDWATER PLUME FOOTPRINT



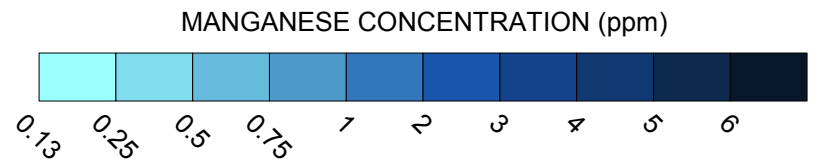
PG&E TOPOCK COMPRESSOR STATION NEEDLES, CALIFORNIA MODELING APPENDIX	
DELINEATION OF AVERAGE FLOODPLAIN MANGANESE CONCENTRATIONS IN GROUNDWATER (JULY 1997 - DECEMBER 2011) IN MODEL LAYERS 1 AND 2	
	<b>FIGURE</b> <b>6.2-5</b>



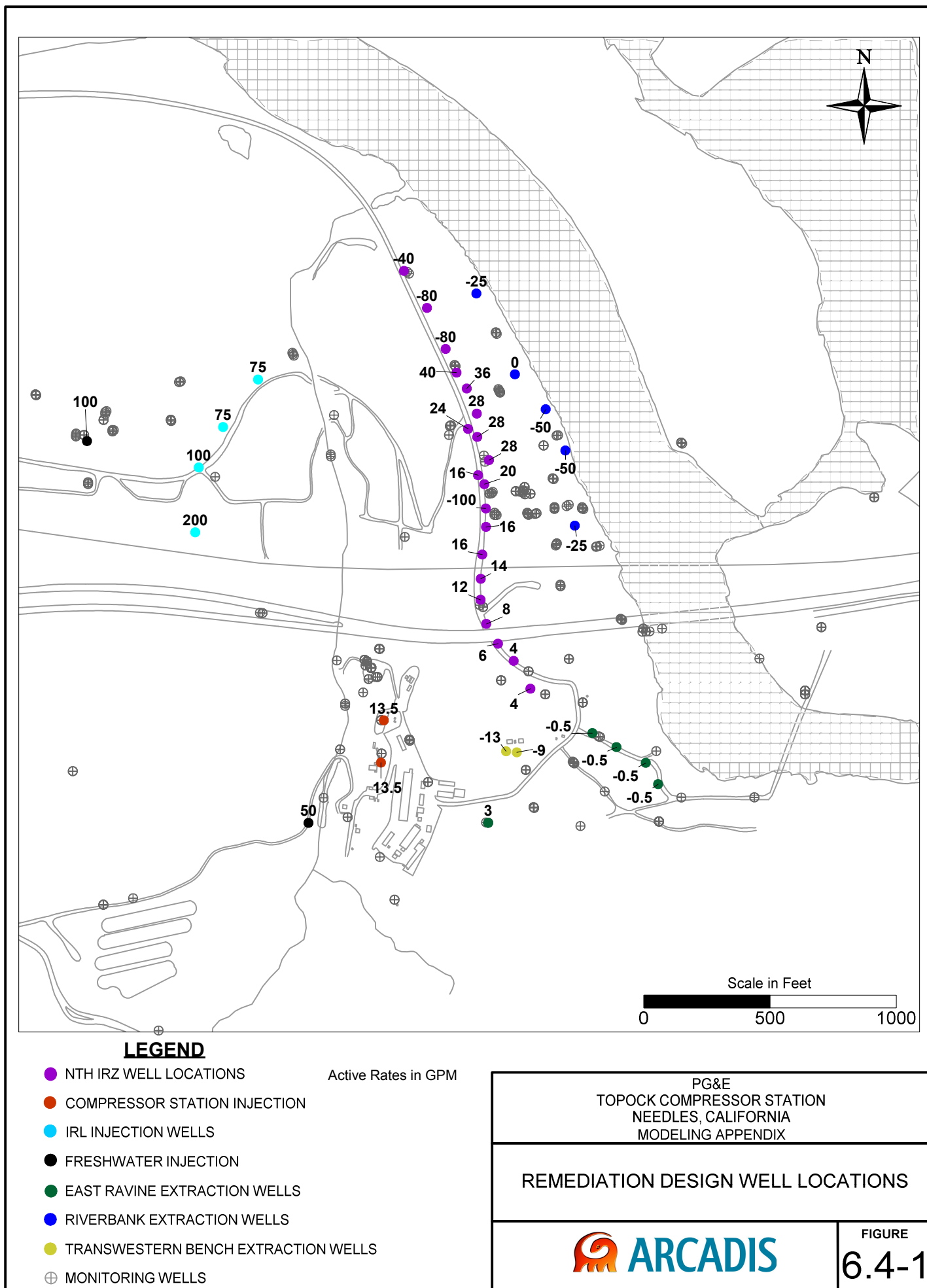
**LEGEND**

- IRZ WELLS
- ⊕ UPGRADE INJECTION WELLS
- EXTRACTION WELLS
- ⊕ MONITORING WELLS

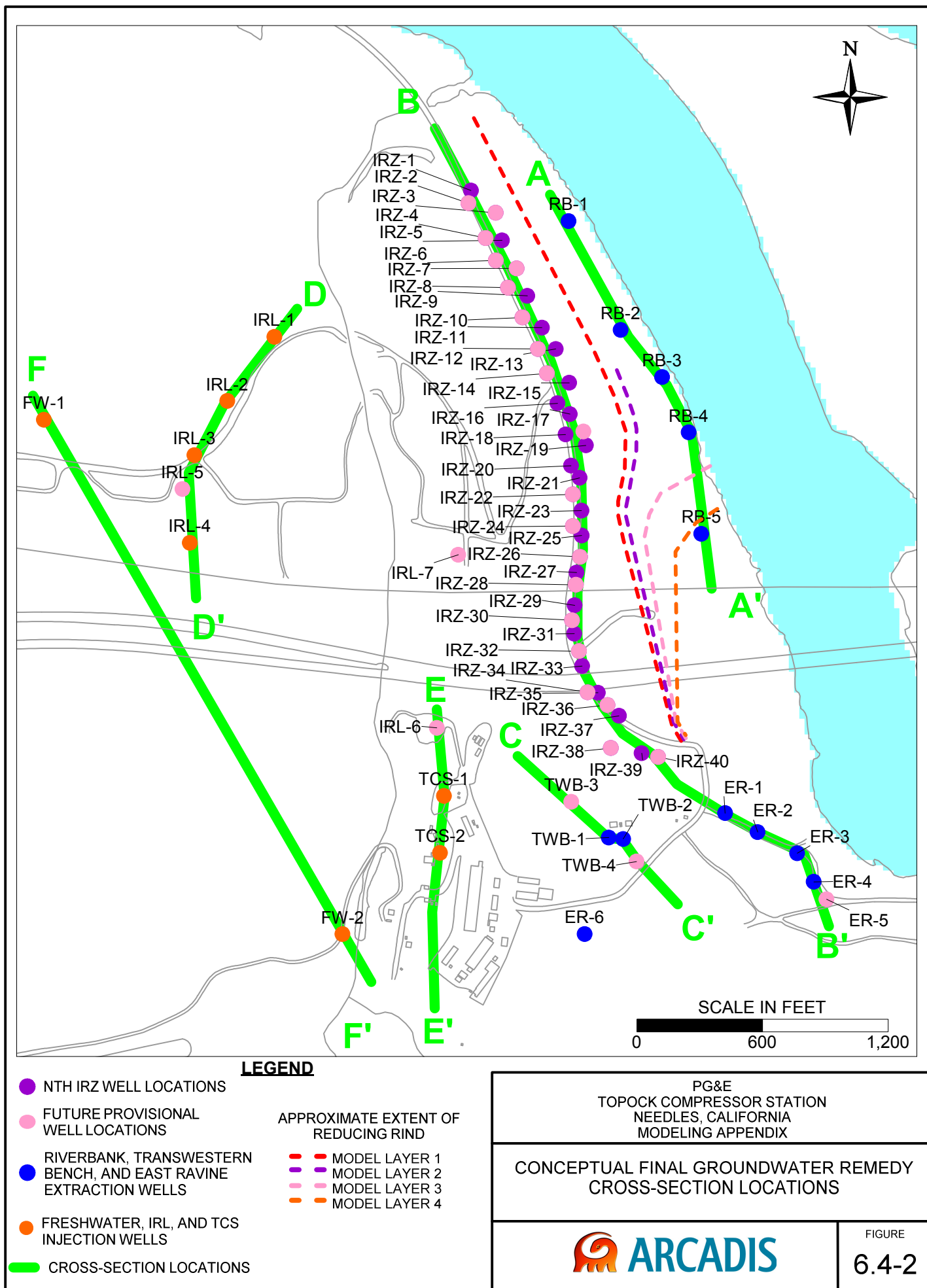
— HEXAVALENT CHROMIUM GROUNDWATER PLUME FOOTPRINT

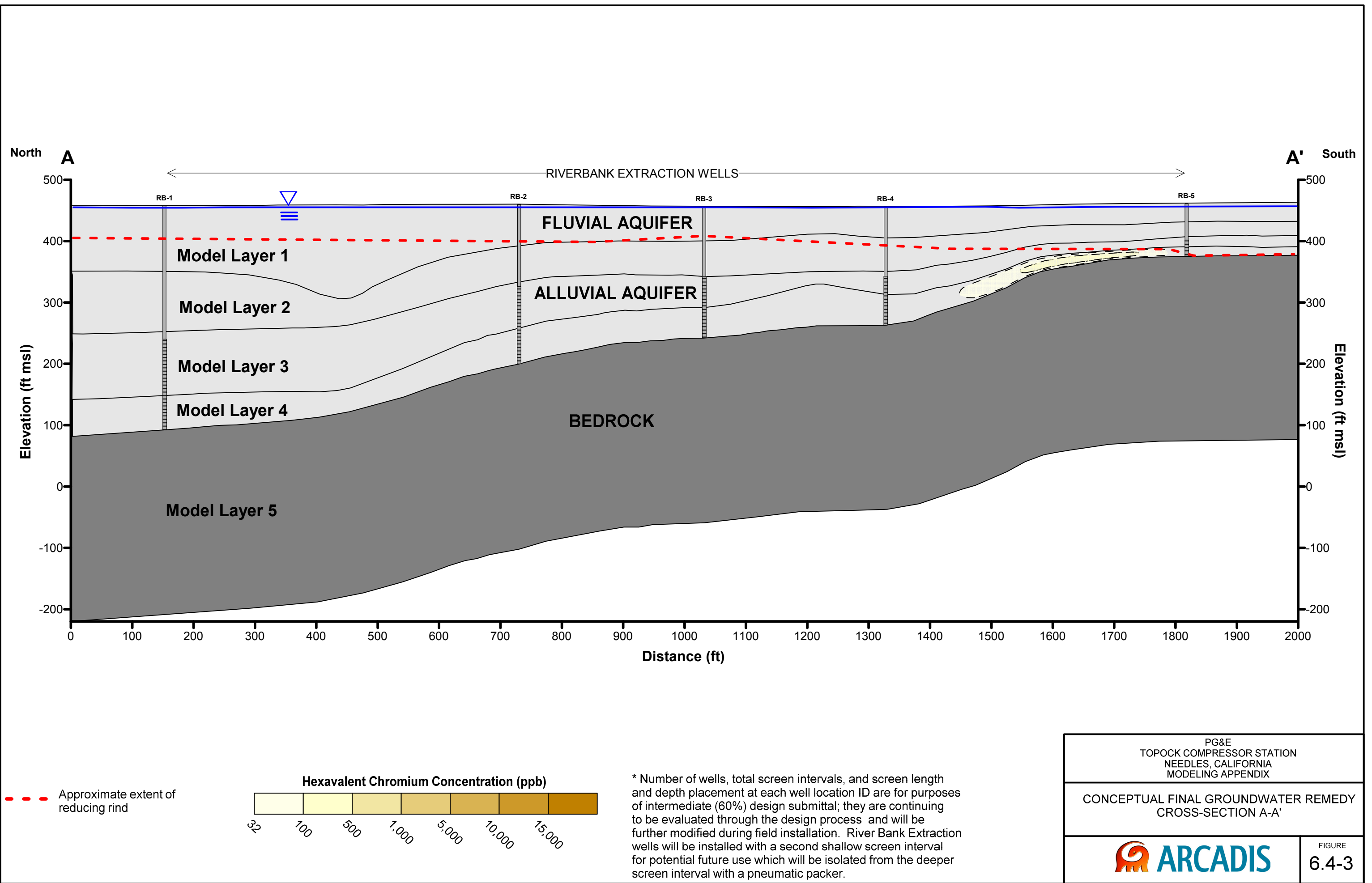


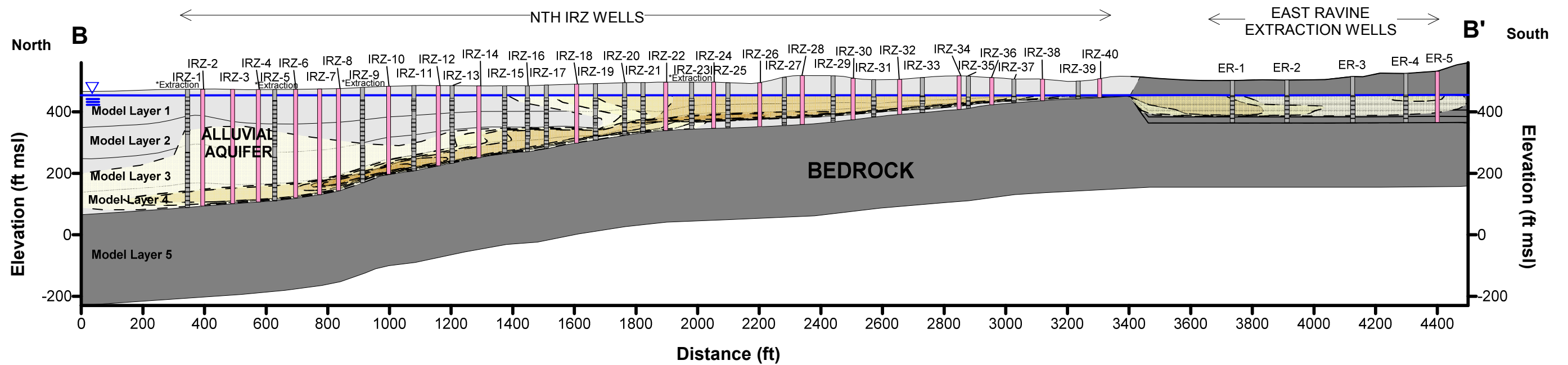
PG&E TOPOCK COMPRESSOR STATION NEEDLES, CALIFORNIA MODELING APPENDIX	
DELINEATION OF AVERAGE FLOODPLAIN MANGANESE CONCENTRATIONS IN GROUNDWATER (JULY 1997 - DECEMBER 2011) IN MODEL LAYERS 3 AND 4	
	FIGURE <b>6.2-6</b>



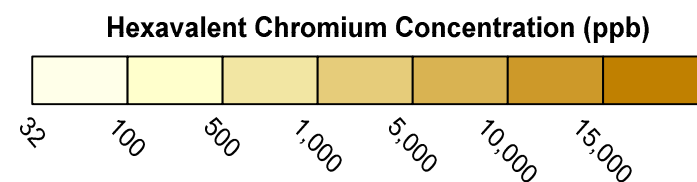








\* Number of wells, total screen intervals, and screen length and depth placement at each well location ID are for purposes of intermediate (60%) design submittal; they are continuing to be evaluated through the design process and will be further modified during field installation. One well location ID may consist of multiple wells or screens, and one well screen interval may include more than one model layer. A maximum of two discrete screen intervals will be included per individual well. Dual screen wells will consist of one well with two discrete screen intervals separated by a packer. Some well location IDs include two dual screen wells which will be installed in separate boreholes. Wells IRZ-1, 5, and 9 are constructed with a dedicated pump for each well screen with the intervals separated using a pneumatic packer. IRZ-23 well design and operation will target extraction of groundwater from all four model layers without being screened across all layers. East Ravine extraction wells are not expected to produce significant water and automated pump cycling could be required.



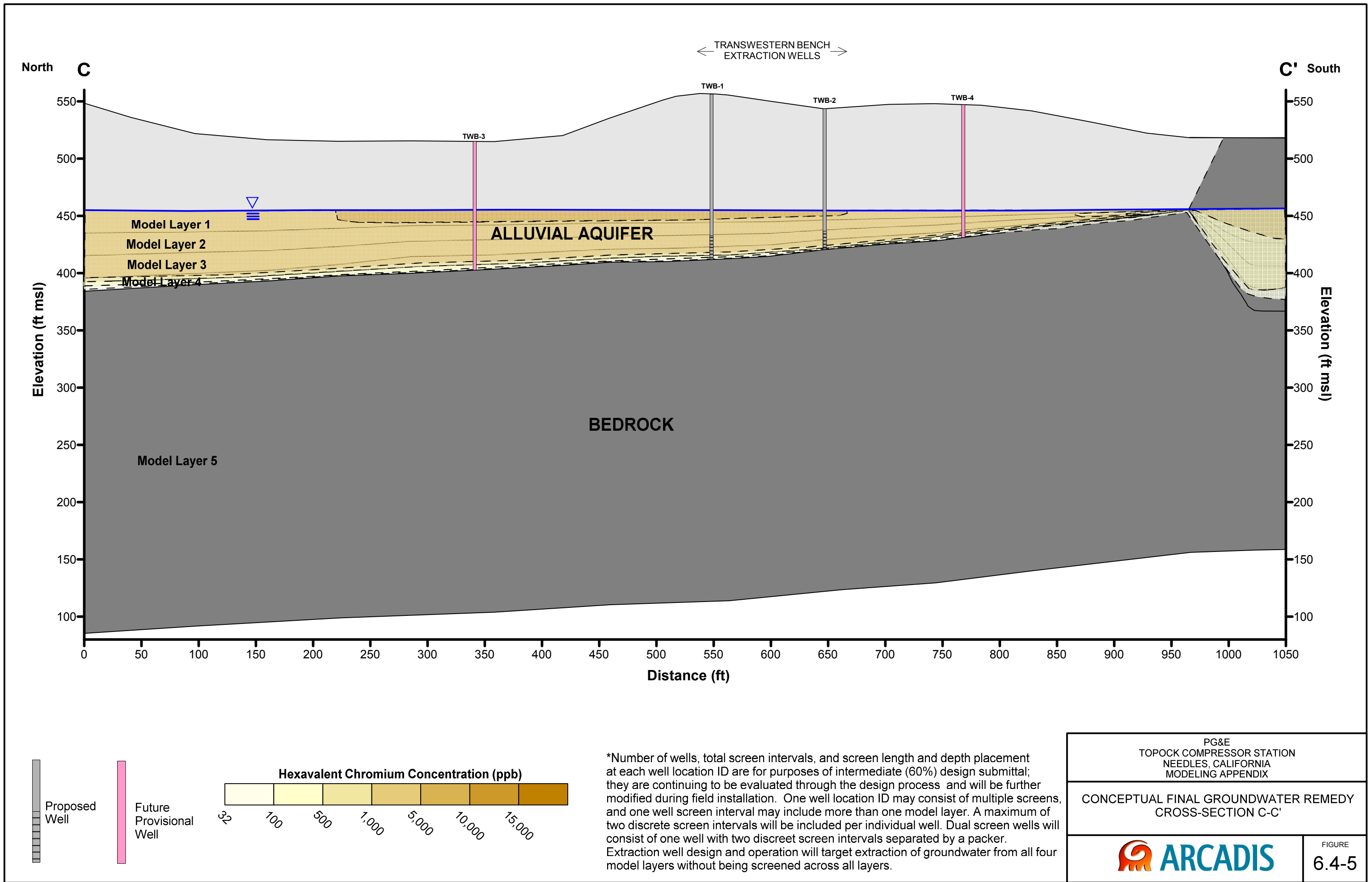
Proposed Well

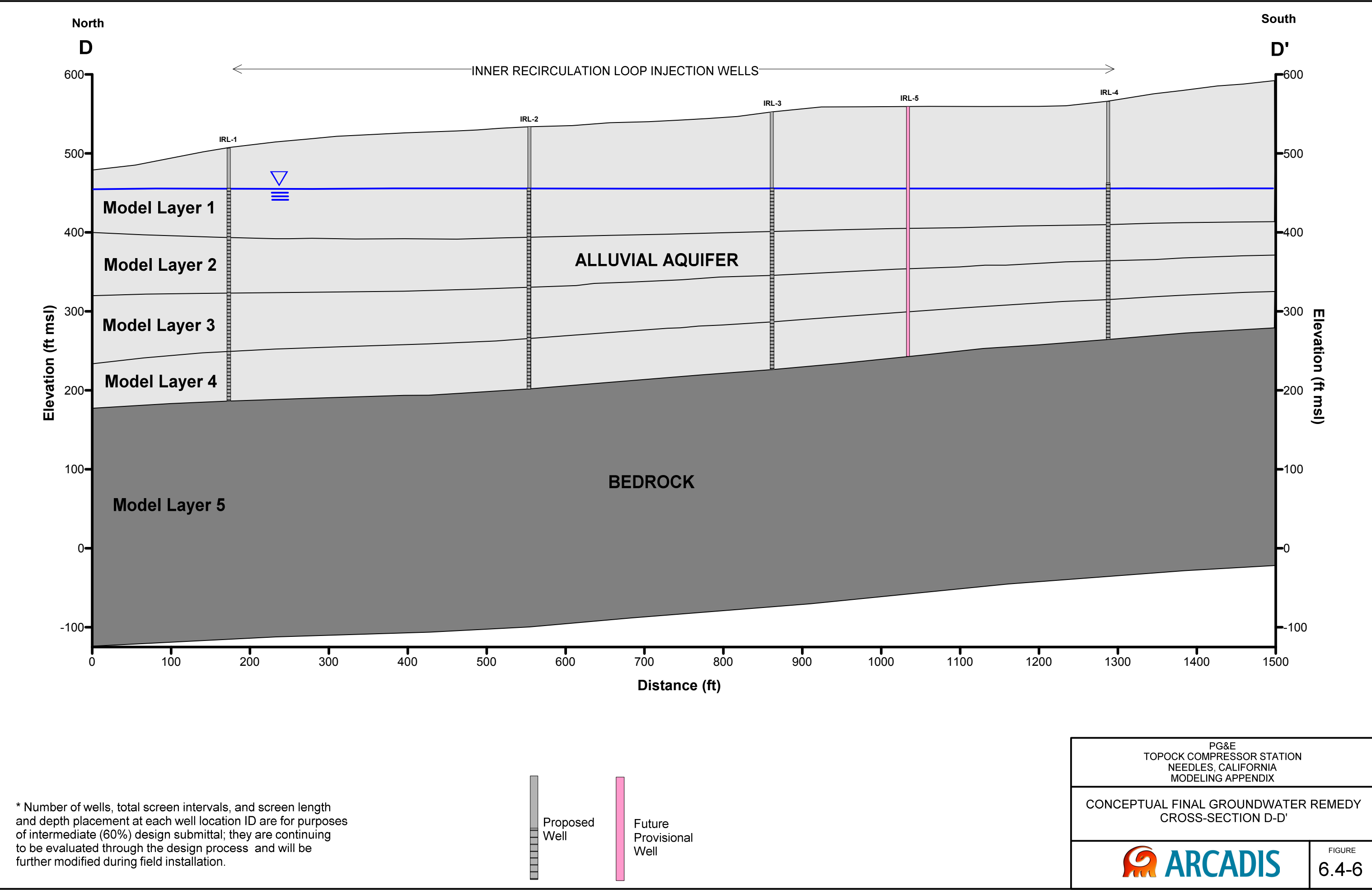


Future Provisional Well

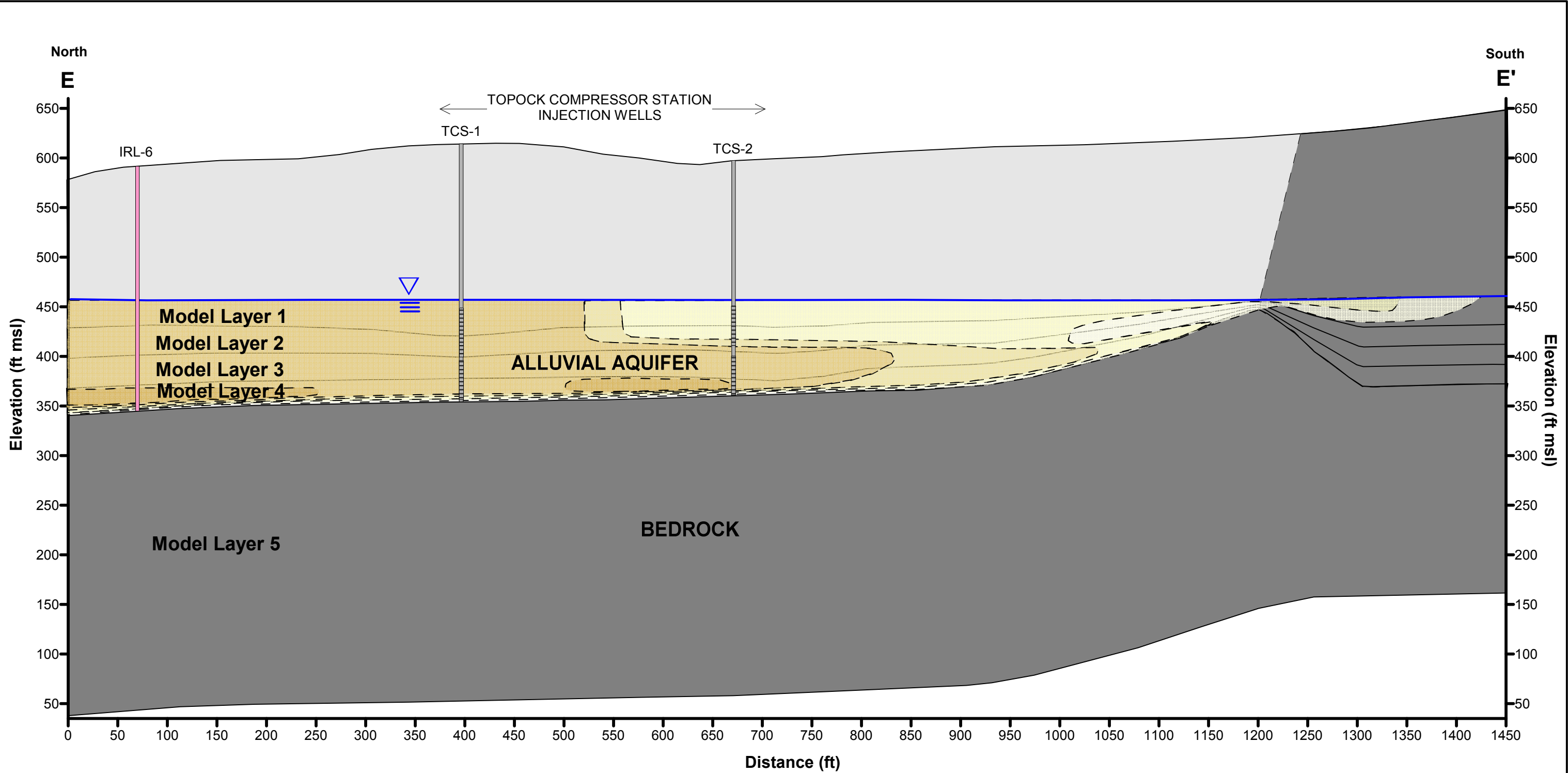
PG&E TOPOCK COMPRESSOR STATION NEEDLES, CALIFORNIA MODELING APPENDIX	
CONCEPTUAL FINAL GROUNDWATER REMEDY CROSS-SECTION B-B'	
	FIGURE 6.4-4







\* Number of wells, total screen intervals, and screen length and depth placement at each well location ID are for purposes of intermediate (60%) design submittal; they are continuing to be evaluated through the design process and will be further modified during field installation.

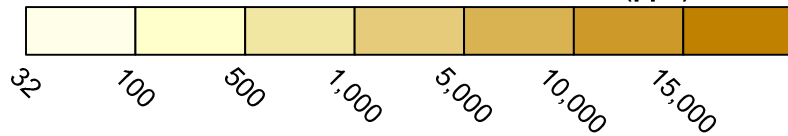


Proposed  
Well



Future  
Provisional  
Well

Hexavalent Chromium Concentration (ppb)



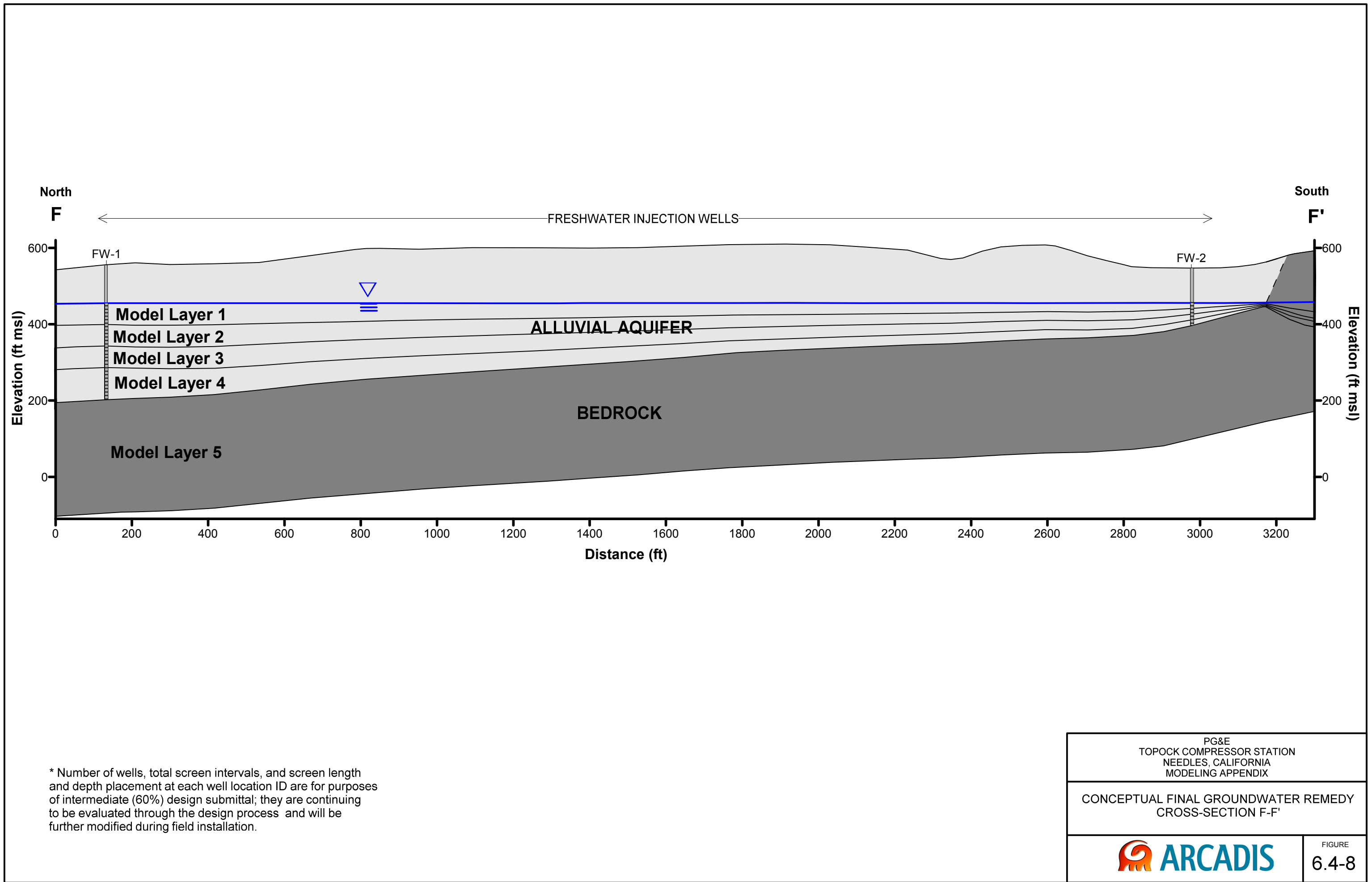
\*Number of wells, total screen intervals, and screen length and depth placement at each well location ID are for purposes of intermediate (60%) design submittal; they are continuing to be evaluated through the design process and will be further modified during field installation. One well location ID may consist of multiple screens, and one well screen interval may include more than one model layer. A maximum of two discrete screen intervals will be included per individual well. Dual screen wells will consist of one well with two discrete screen intervals separated by a packer.

PG&E  
TOPOCK COMPRESSOR STATION  
NEEDLES, CALIFORNIA  
MODELING APPENDIX

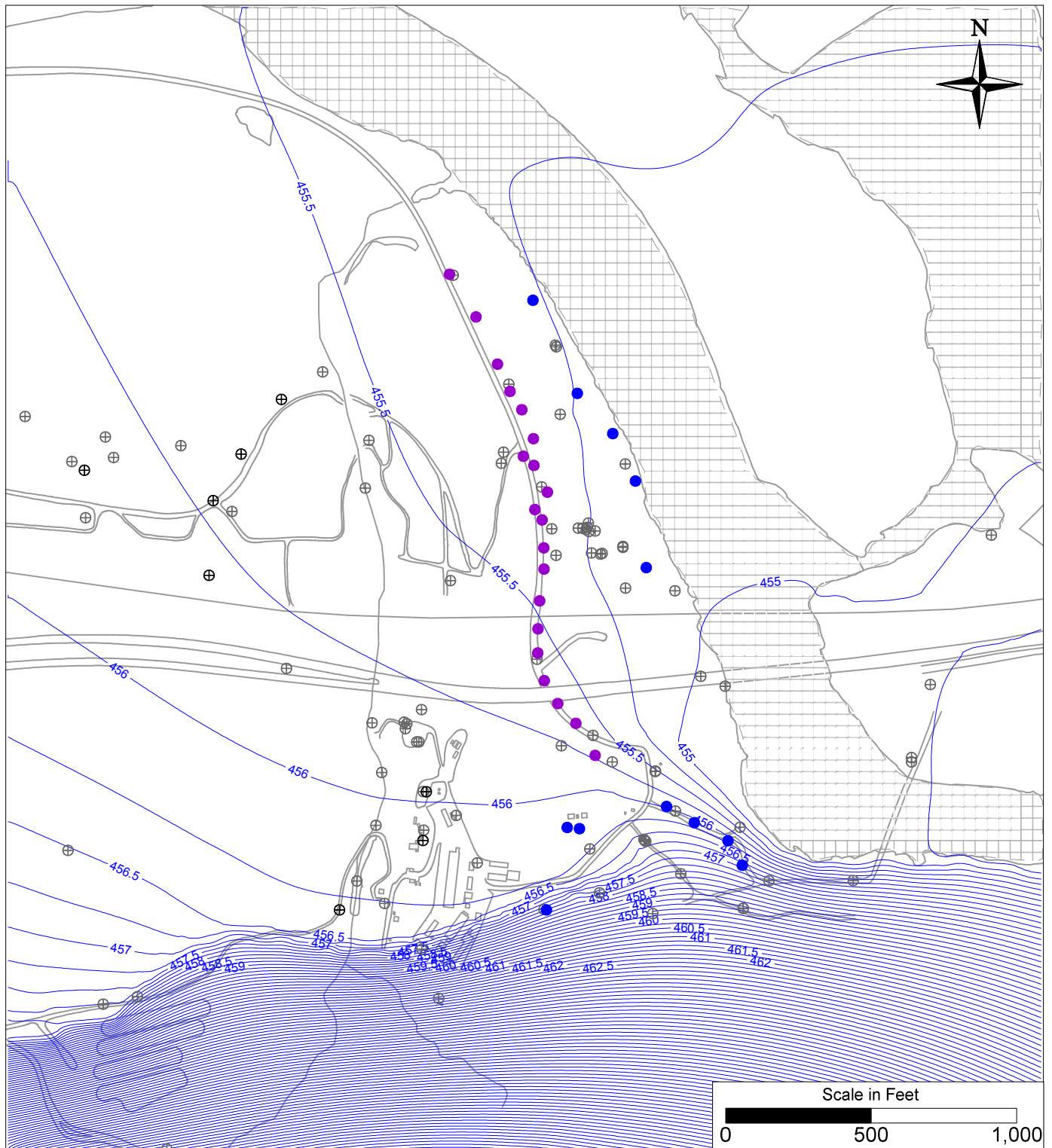
CONCEPTUAL FINAL GROUNDWATER REMEDY  
CROSS-SECTION E-E'



FIGURE  
6.4-7



\* Number of wells, total screen intervals, and screen length and depth placement at each well location ID are for purposes of intermediate (60%) design submittal; they are continuing to be evaluated through the design process and will be further modified during field installation.



### LEGEND

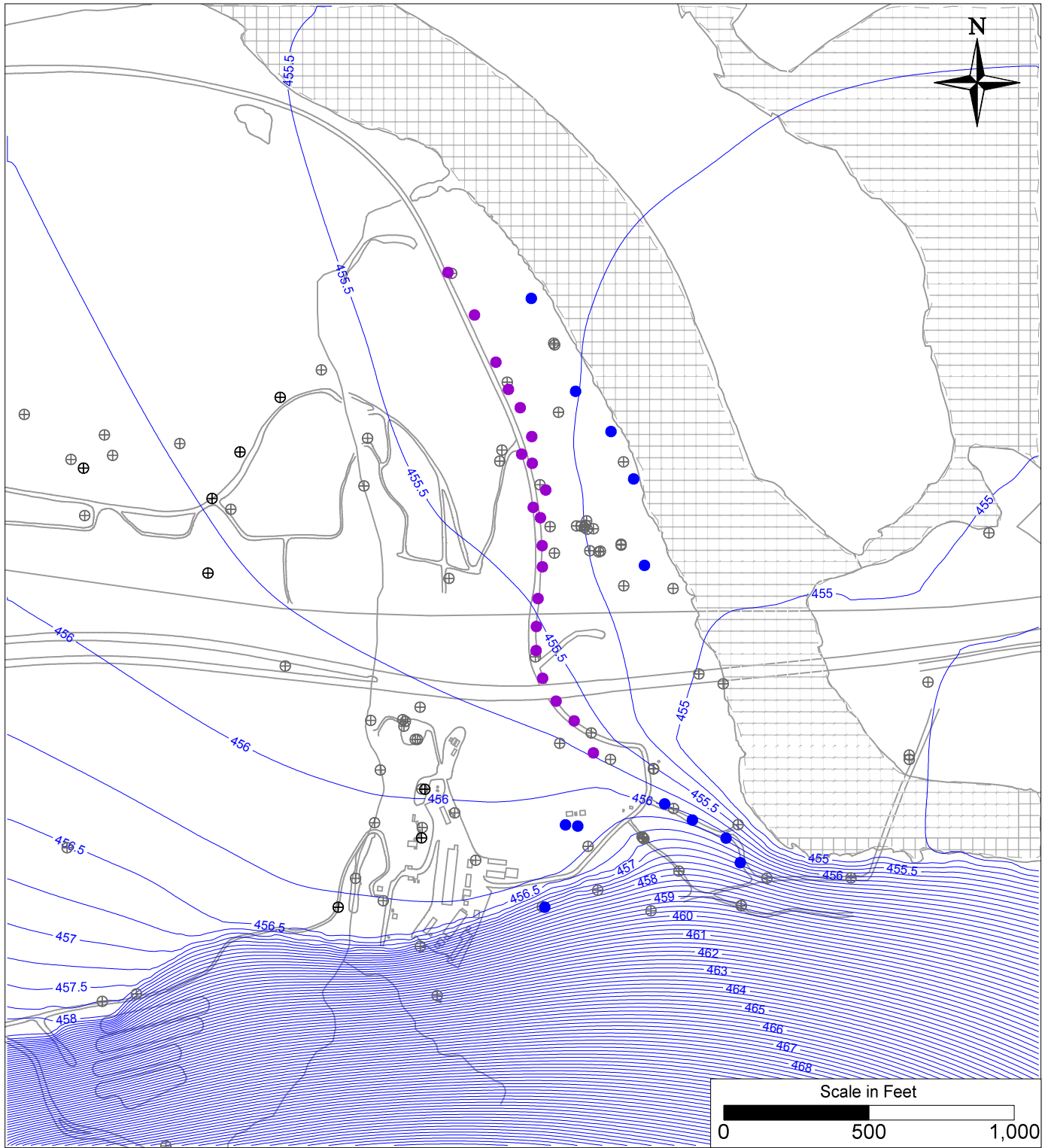
- IRZ WELLS
- ⊕ UPGRADIENT INJECTION WELLS
- EXTRACTION WELLS
- ⊕ MONITORING WELLS
- 460- SIMULATED GROUNDWATER LEVELS (FT MSL)

PG&E  
TOPOCK COMPRESSOR STATION  
NEEDLES, CALIFORNIA  
MODELING APPENDIX

**SIMULATED GROUNDWATER CONTOURS  
UNDER AMBIENT FLOW CONDITIONS  
IN MODEL LAYER 1**



FIGURE  
6.5-1



### LEGEND

- IRZ WELLS
- ⊕ UPGRADIENT INJECTION WELLS
- EXTRACTION WELLS
- ⊕ MONITORING WELLS
- 460— SIMULATED GROUNDWATER LEVELS (FT MSL)

PG&E  
TOPOCK COMPRESSOR STATION  
NEEDLES, CALIFORNIA  
MODELING APPENDIX

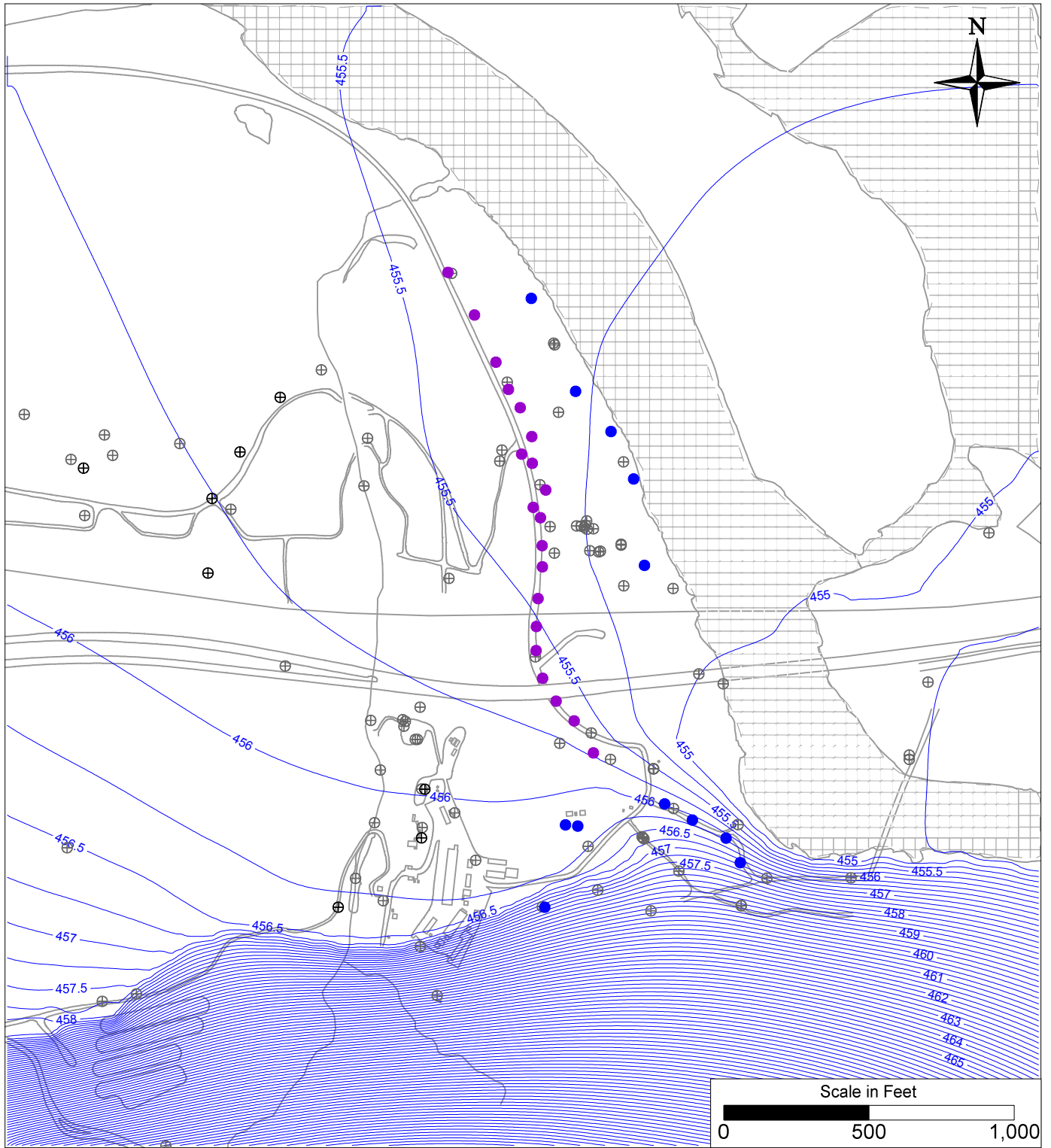
SIMULATED GROUNDWATER CONTOURS  
UNDER AMBIENT FLOW CONDITIONS  
IN MODEL LAYER 2



FIGURE

6.5-2





# **LEGEND**

- IRZ WELLS
- ⊕ UPGRADIENT INJECTION WELLS
- EXTRACTION WELLS
- ⊕ MONITORING WELLS
- 460— SIMULATED GROUNDWATER LEVELS (FT MSL)

PG&E  
TOPOCK COMPRESSOR STATION  
NEEDLES, CALIFORNIA  
MODELING APPENDIX

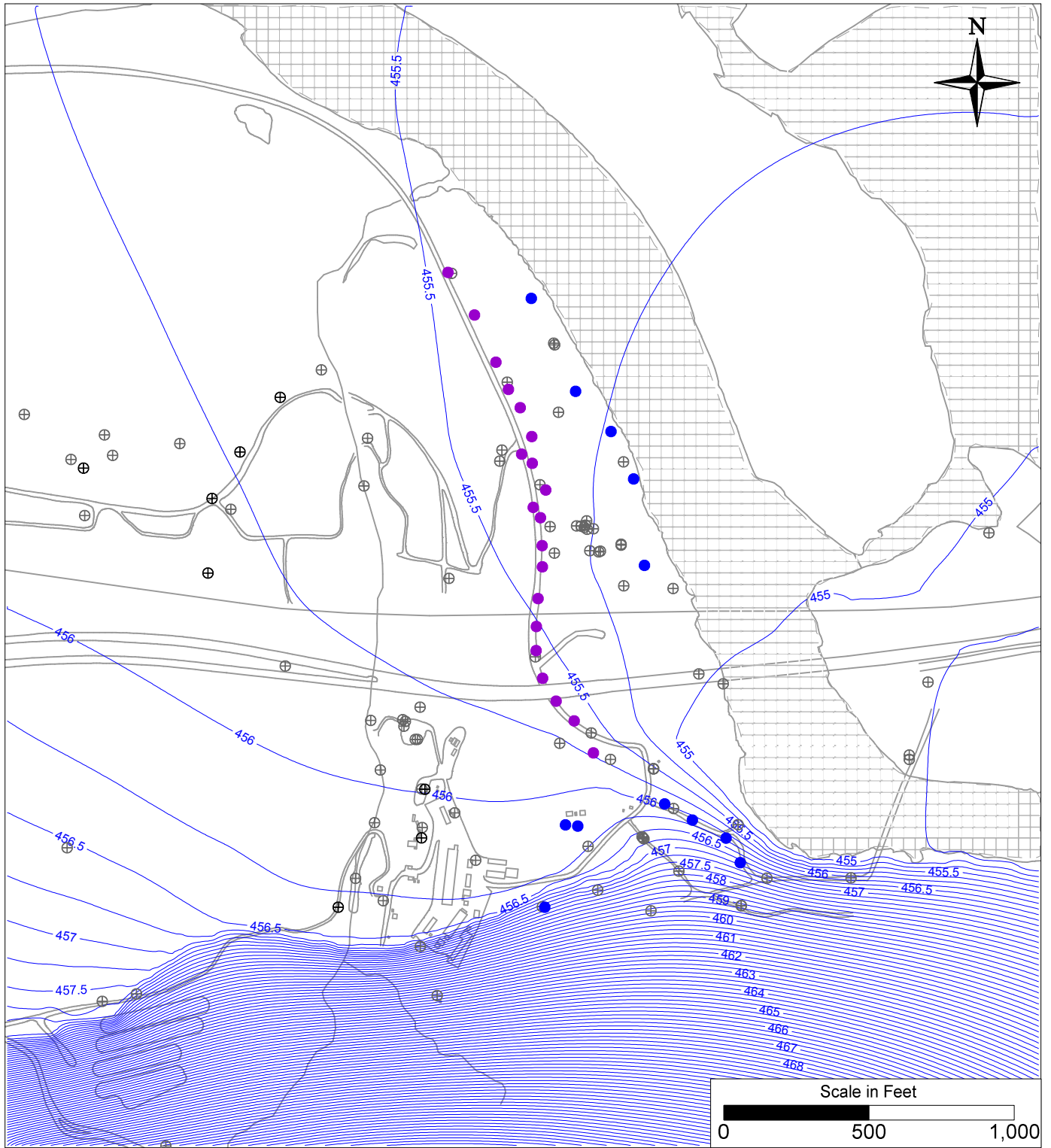
**SIMULATED GROUNDWATER CONTOURS  
UNDER AMBIENT FLOW CONDITIONS  
IN MODEL LAYER 3**



FIGURE

**6.5-3**





# **LEGEND**

- IRZ WELLS
- ⊕ UPGRADIENT INJECTION WELLS
- EXTRACTION WELLS
- ⊕ MONITORING WELLS
- 460— SIMULATED GROUNDWATER LEVELS (FT MSL)

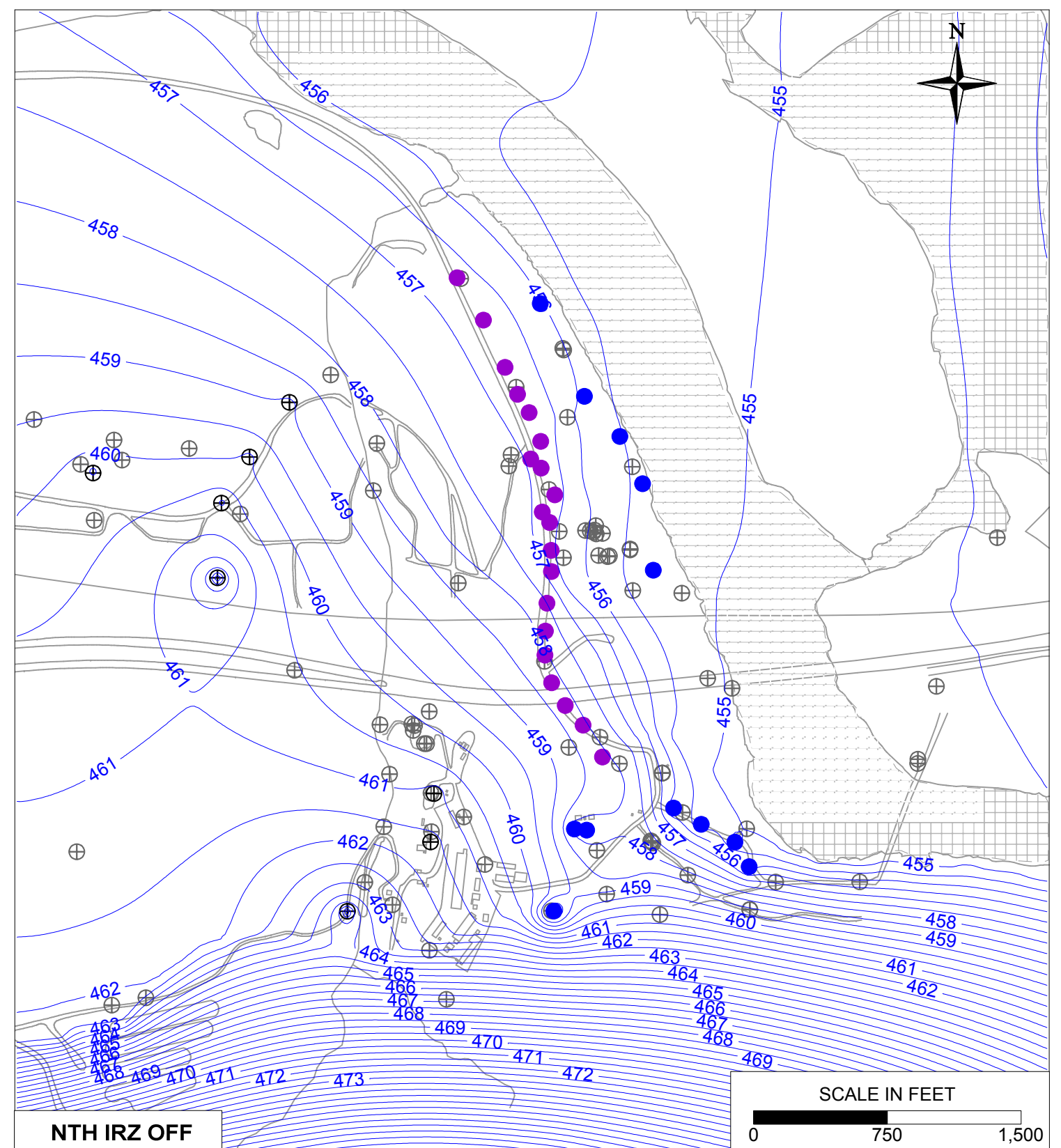
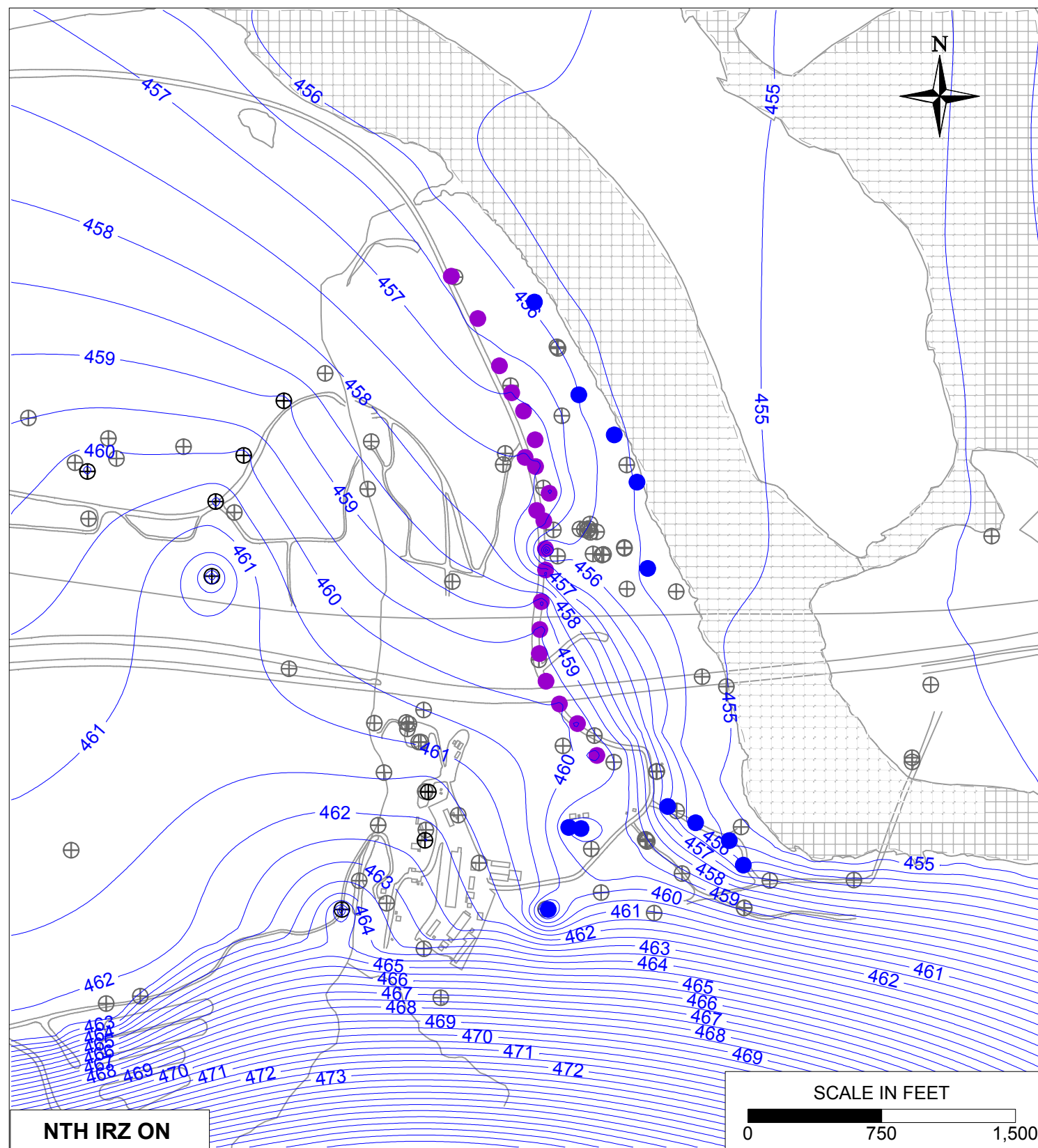
PG&E  
TOPOCK COMPRESSOR STATION  
NEEDLES, CALIFORNIA  
MODELING APPENDIX

**SIMULATED GROUNDWATER CONTOURS  
UNDER AMBIENT FLOW CONDITIONS  
IN MODEL LAYER 4**



FIGURE

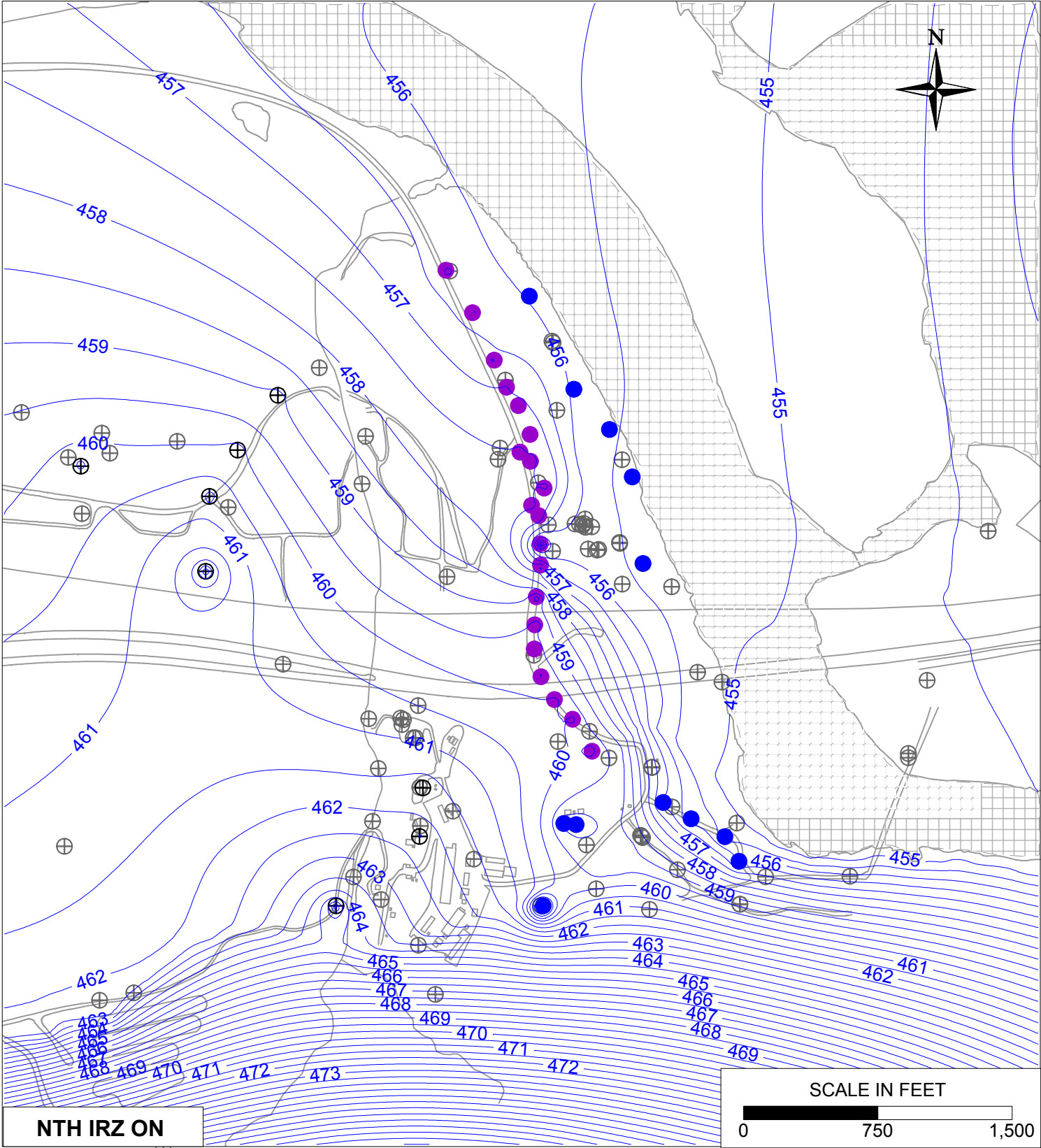
**6.5-4**



- LEGEND**
- IRZ WELLS
  - ⊕ UPGRADIENT INJECTION WELLS
  - EXTRACTION WELLS
  - ⊕ MONITORING WELLS
  - 460— SIMULATED GROUNDWATER LEVELS (FT MSL)

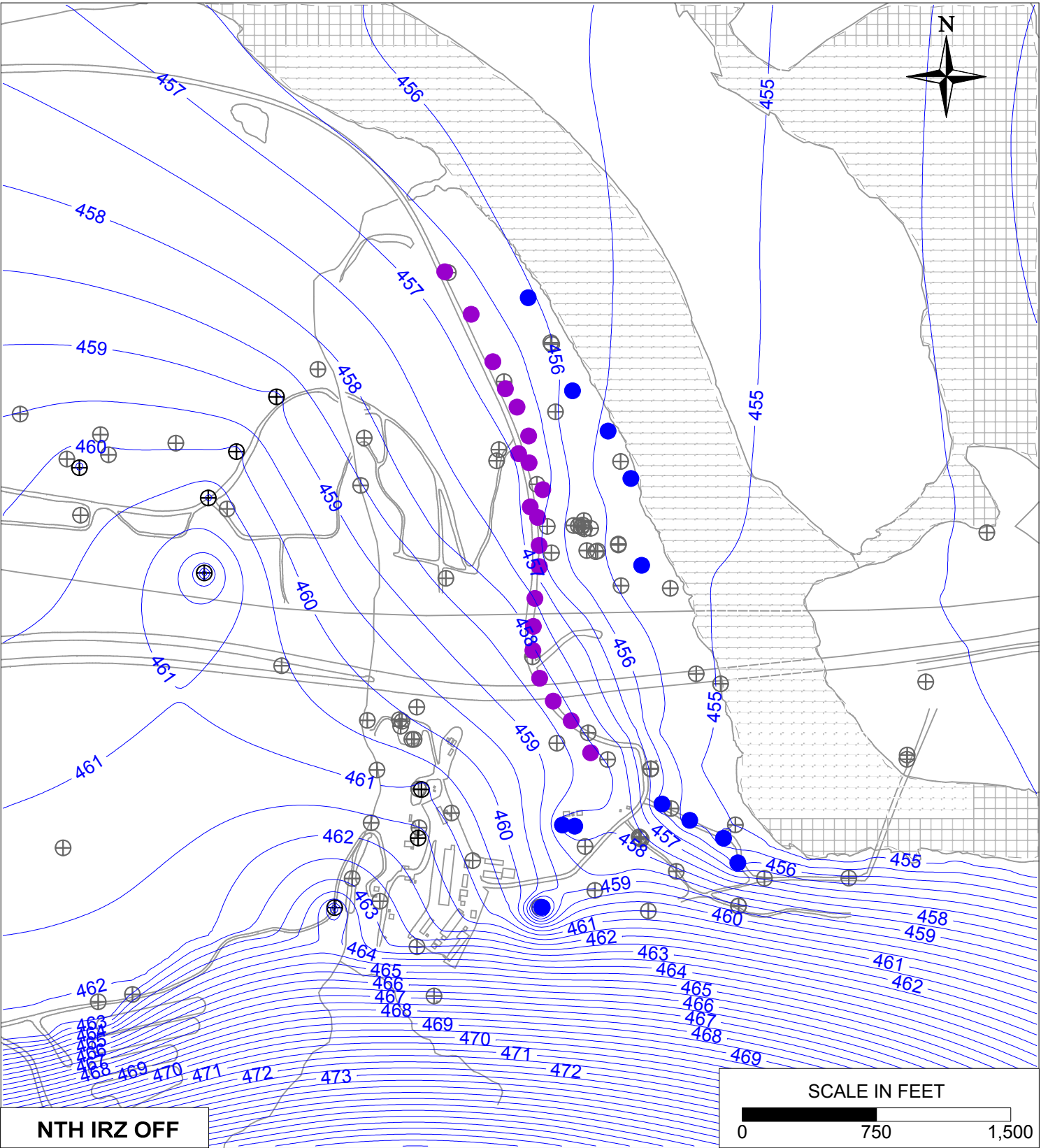
PG&E TOPOCK COMPRESSOR STATION NEEDLES, CALIFORNIA MODELING APPENDIX	
SIMULATED GROUNDWATER CONTOURS UNDER ACTIVE REMEDY FLOW CONDITIONS IN MODEL LAYER 1	
	FIGURE <span style="font-size: 24pt; font-weight: bold;">6.5-5</span>




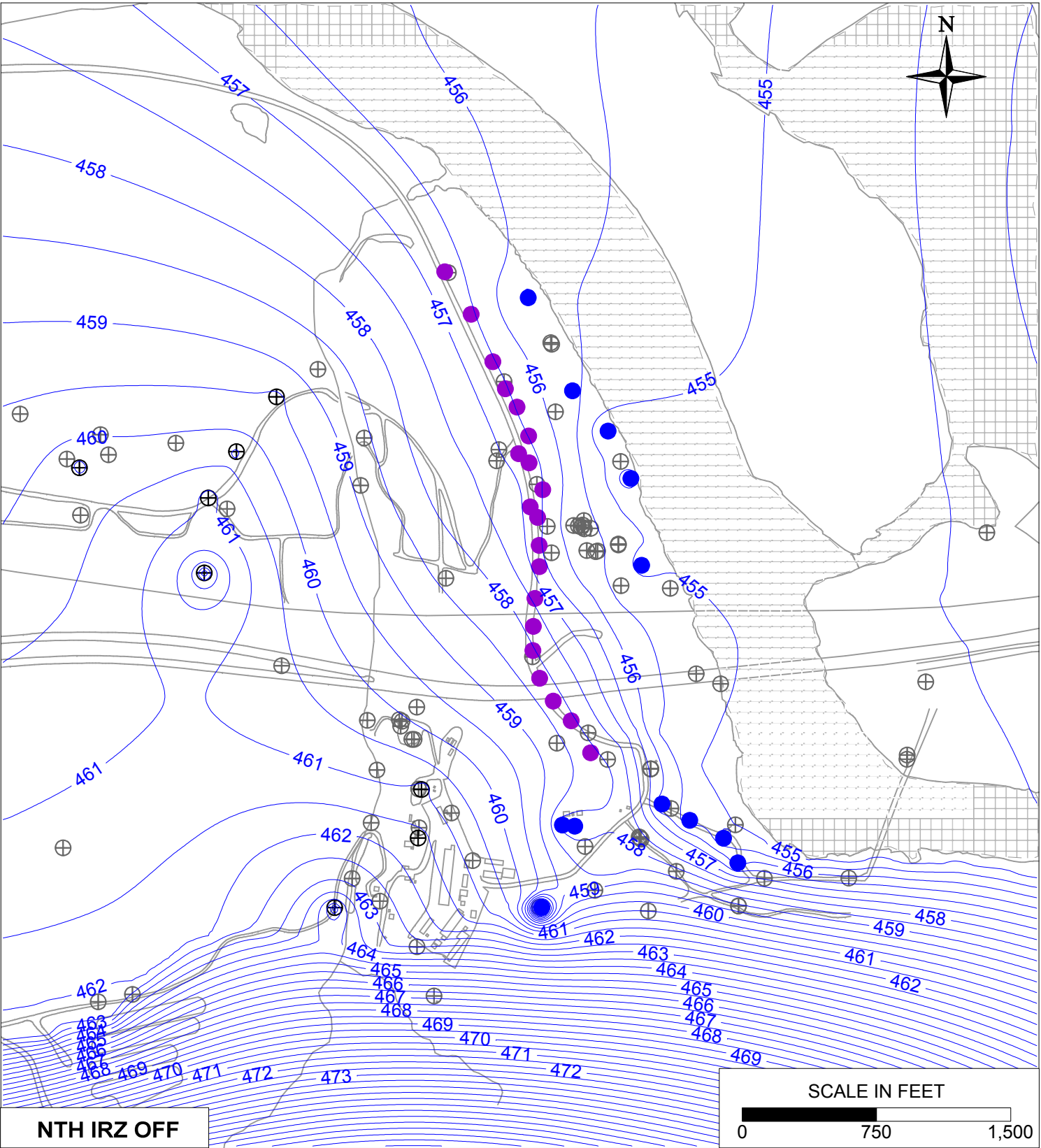
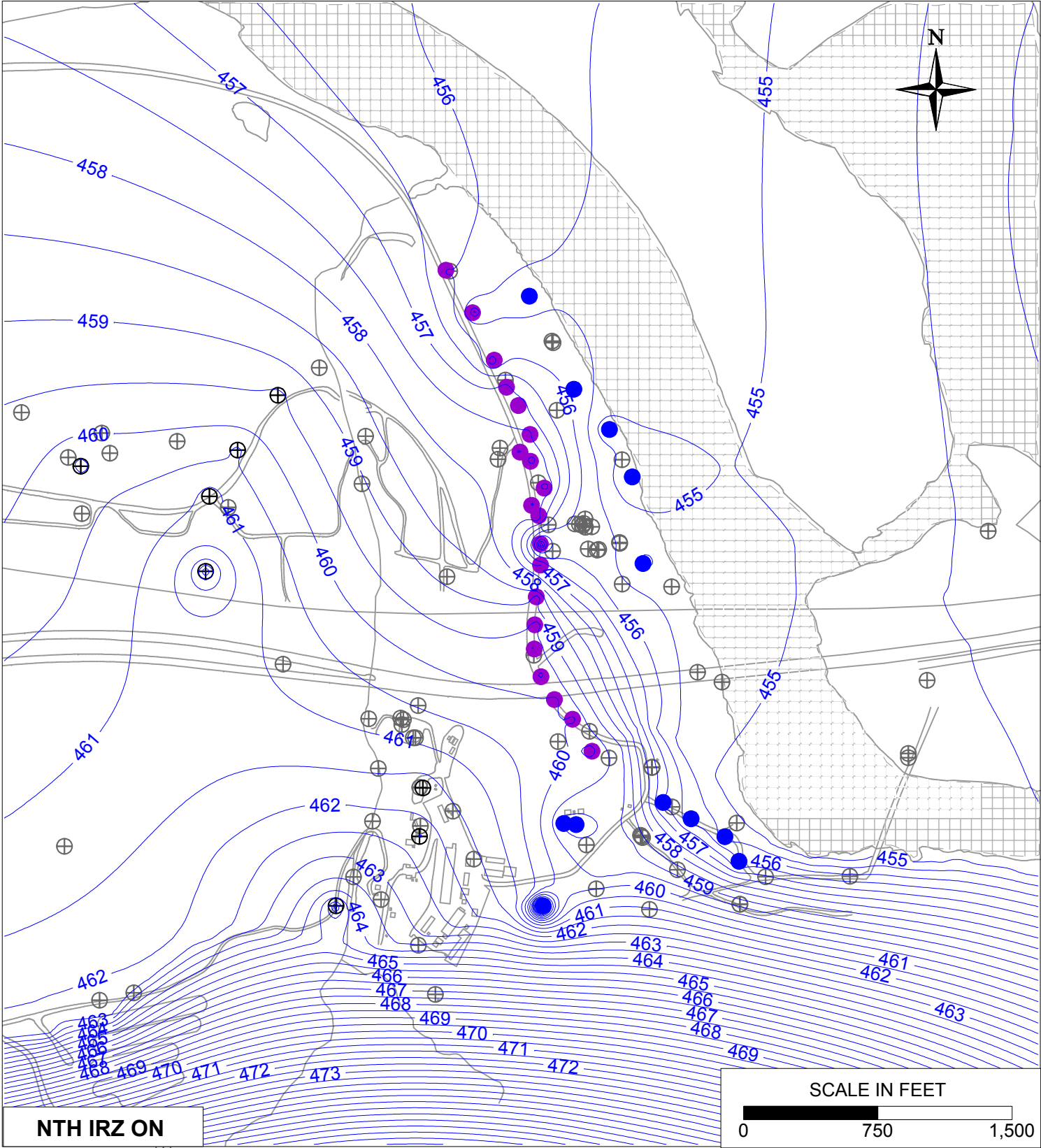


**LEGEND**


- IRZ WELLS
- ⊕ UPGRADIENT INJECTION WELLS
- EXTRACTION WELLS
- ⊕ MONITORING WELLS
- 460— SIMULATED GROUNDWATER LEVELS (FT MSL)



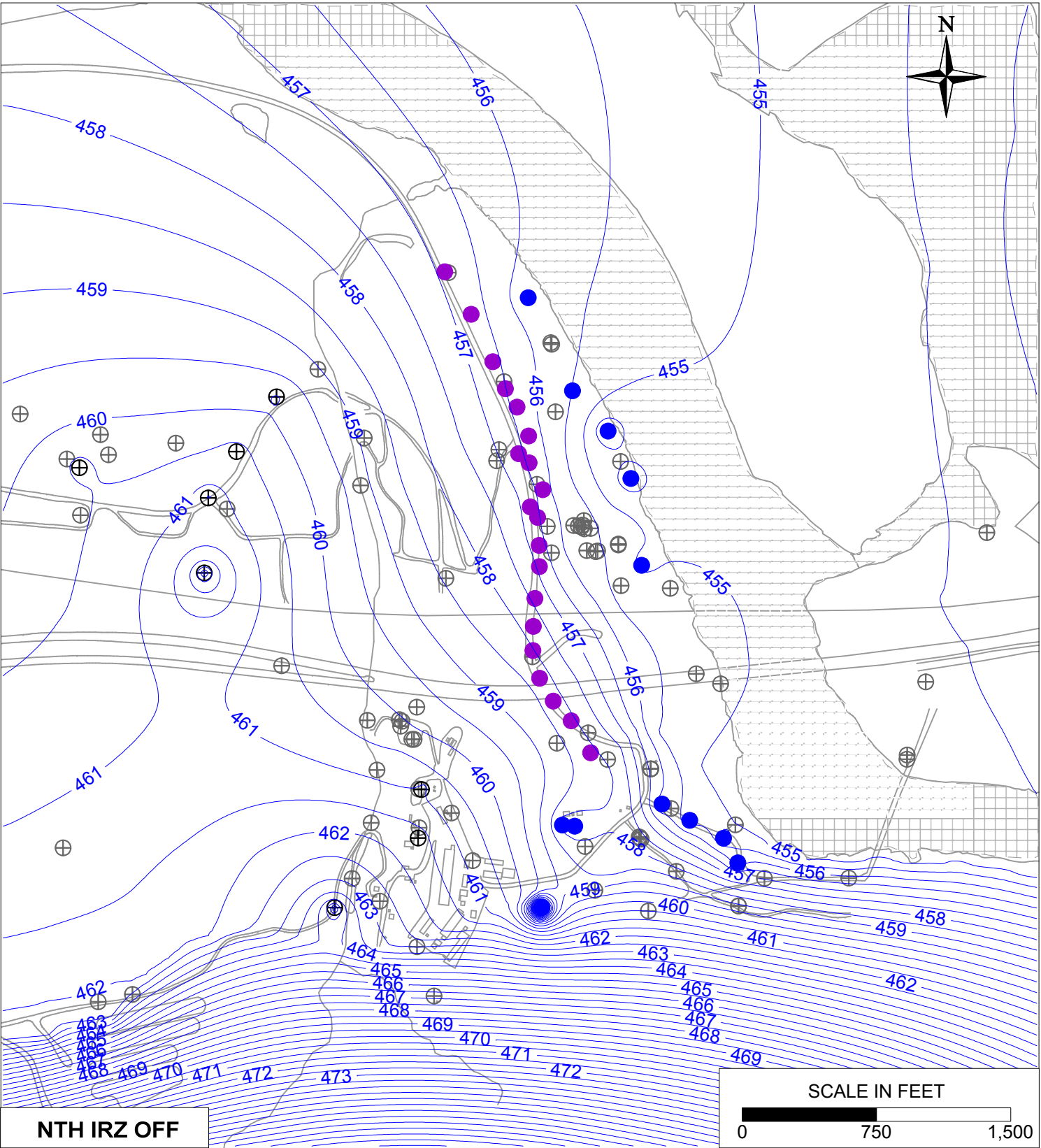
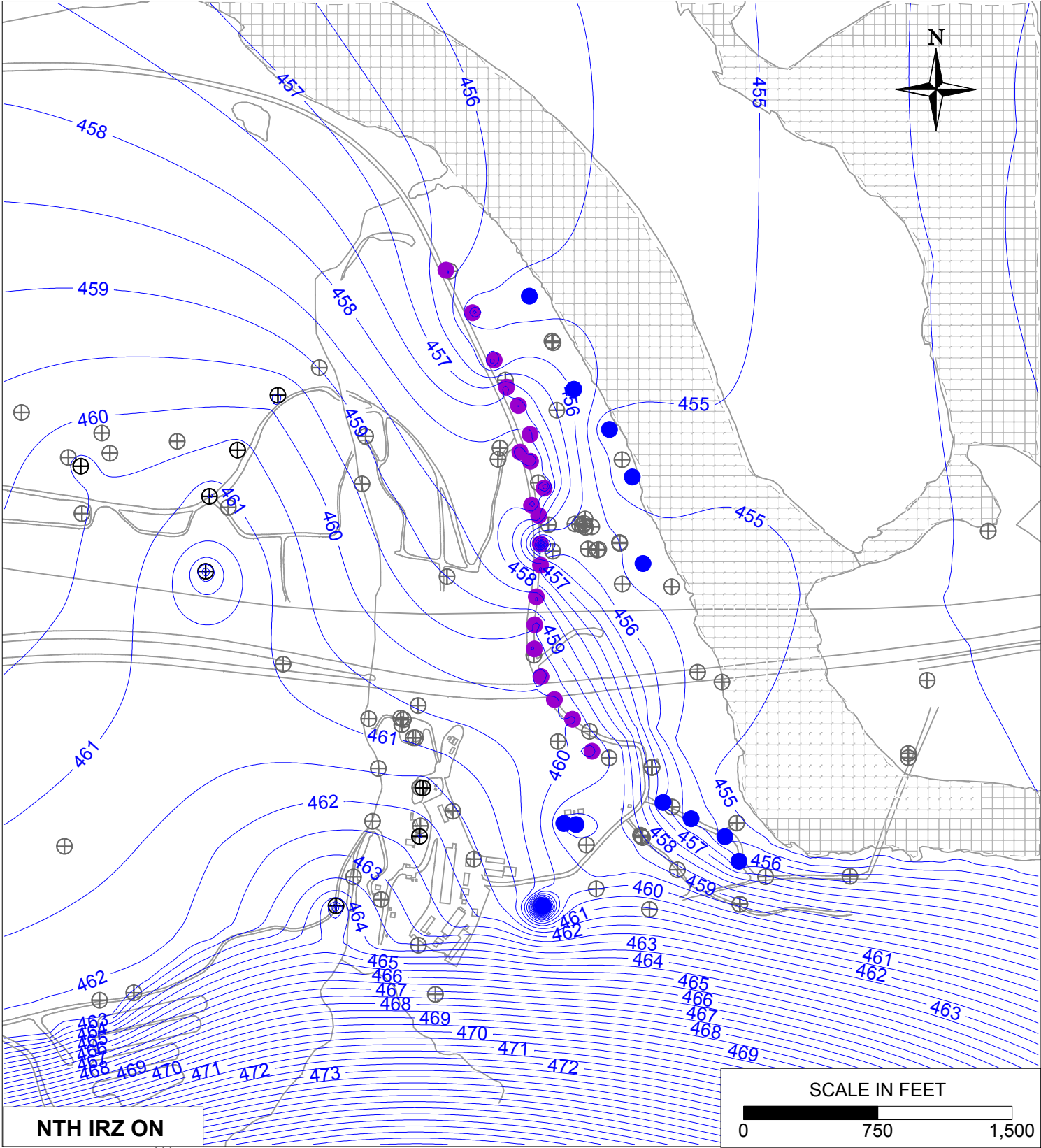
PG&E TOPOCK COMPRESSOR STATION NEEDLES, CALIFORNIA MODELING APPENDIX	
SIMULATED GROUNDWATER CONTOURS UNDER ACTIVE REMEDY FLOW CONDITIONS IN MODEL LAYER 2	
	FIGURE <b>6.5-6</b>




- LEGEND**
- IRZ WELLS
  - ⊕ UPGRADIENT INJECTION WELLS
  - EXTRACTION WELLS
  - ⊕ MONITORING WELLS
  - 460- SIMULATED GROUNDWATER LEVELS (FT MSL)

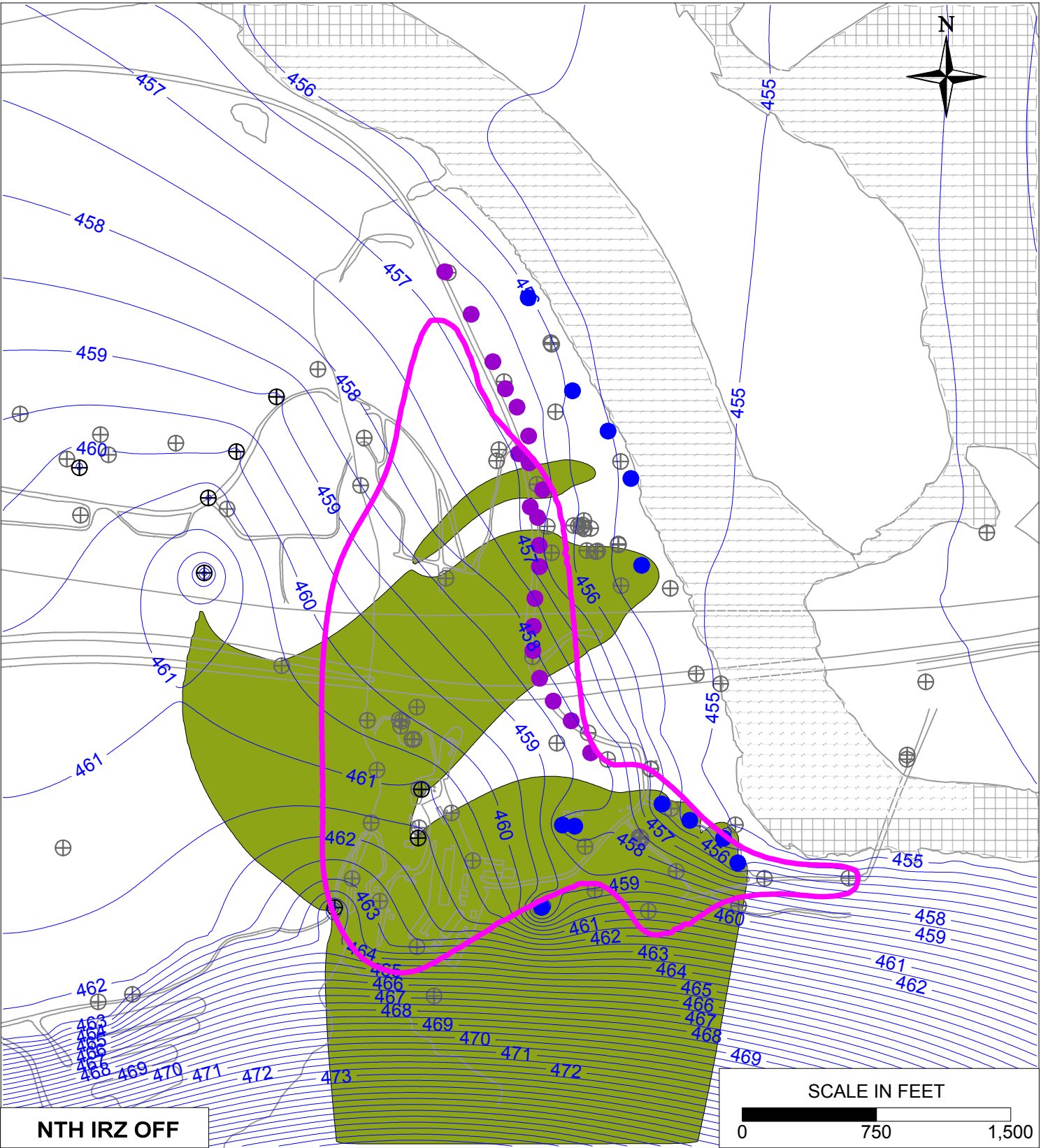
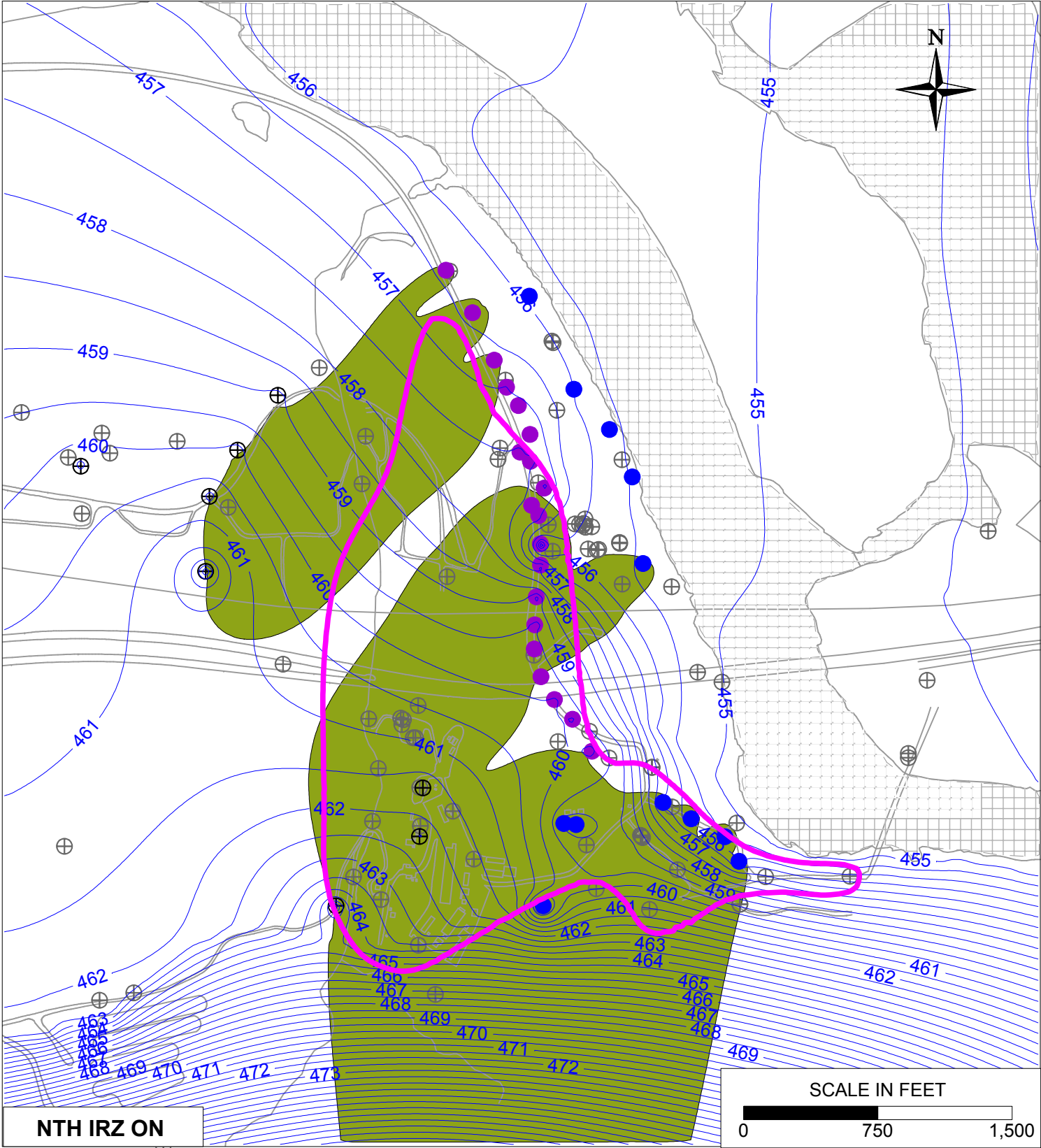
PG&E TOPOCK COMPRESSOR STATION NEEDLES, CALIFORNIA MODELING APPENDIX	
SIMULATED GROUNDWATER CONTOURS UNDER ACTIVE REMEDY FLOW CONDITIONS IN MODEL LAYER 3	
	FIGURE <b>6.5-7</b>





- LEGEND**
- IRZ WELLS
  - ⊕ UPGRADIENT INJECTION WELLS
  - EXTRACTION WELLS
  - ⊕ MONITORING WELLS
  - 460- SIMULATED GROUNDWATER LEVELS (FT MSL)

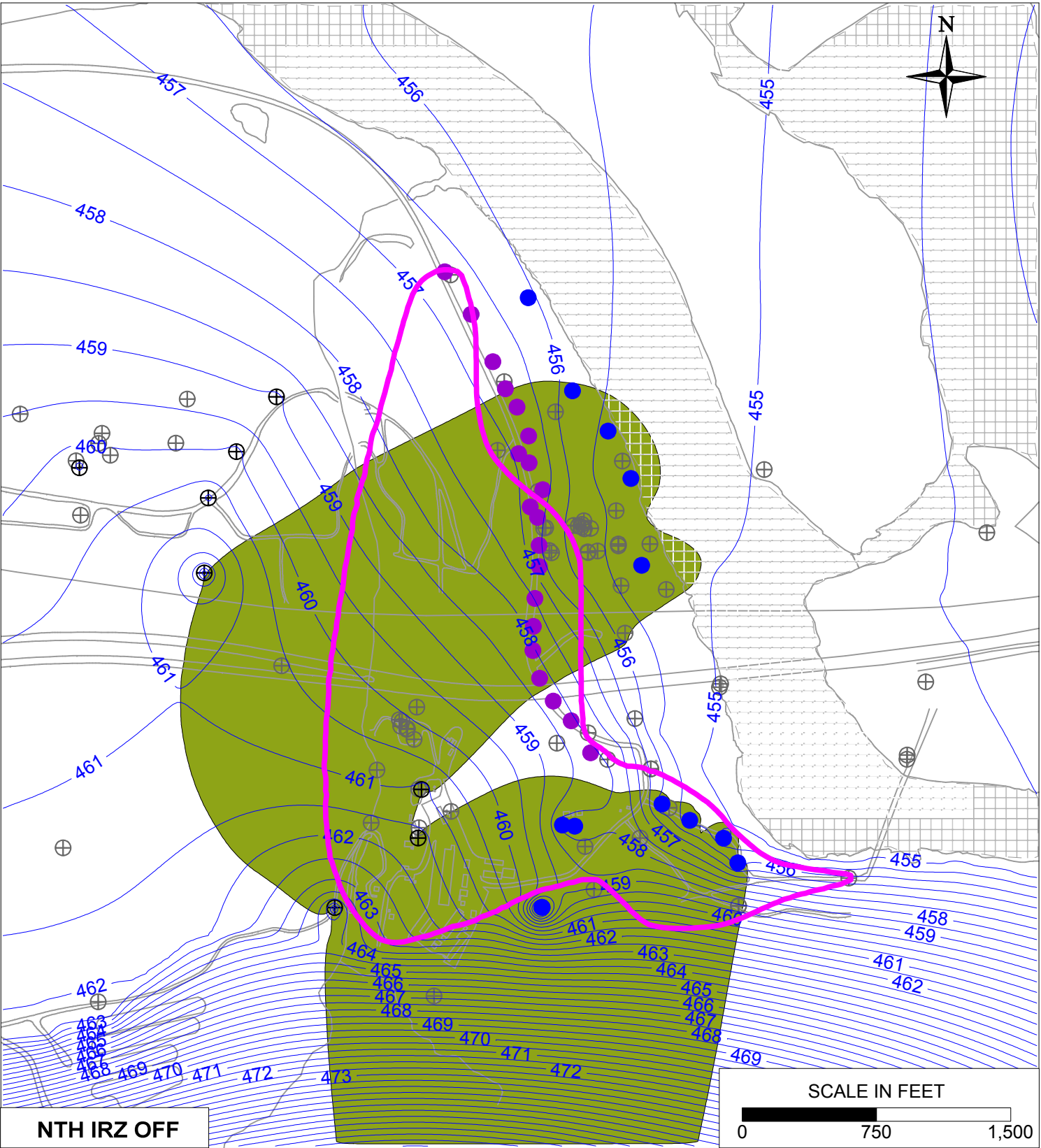
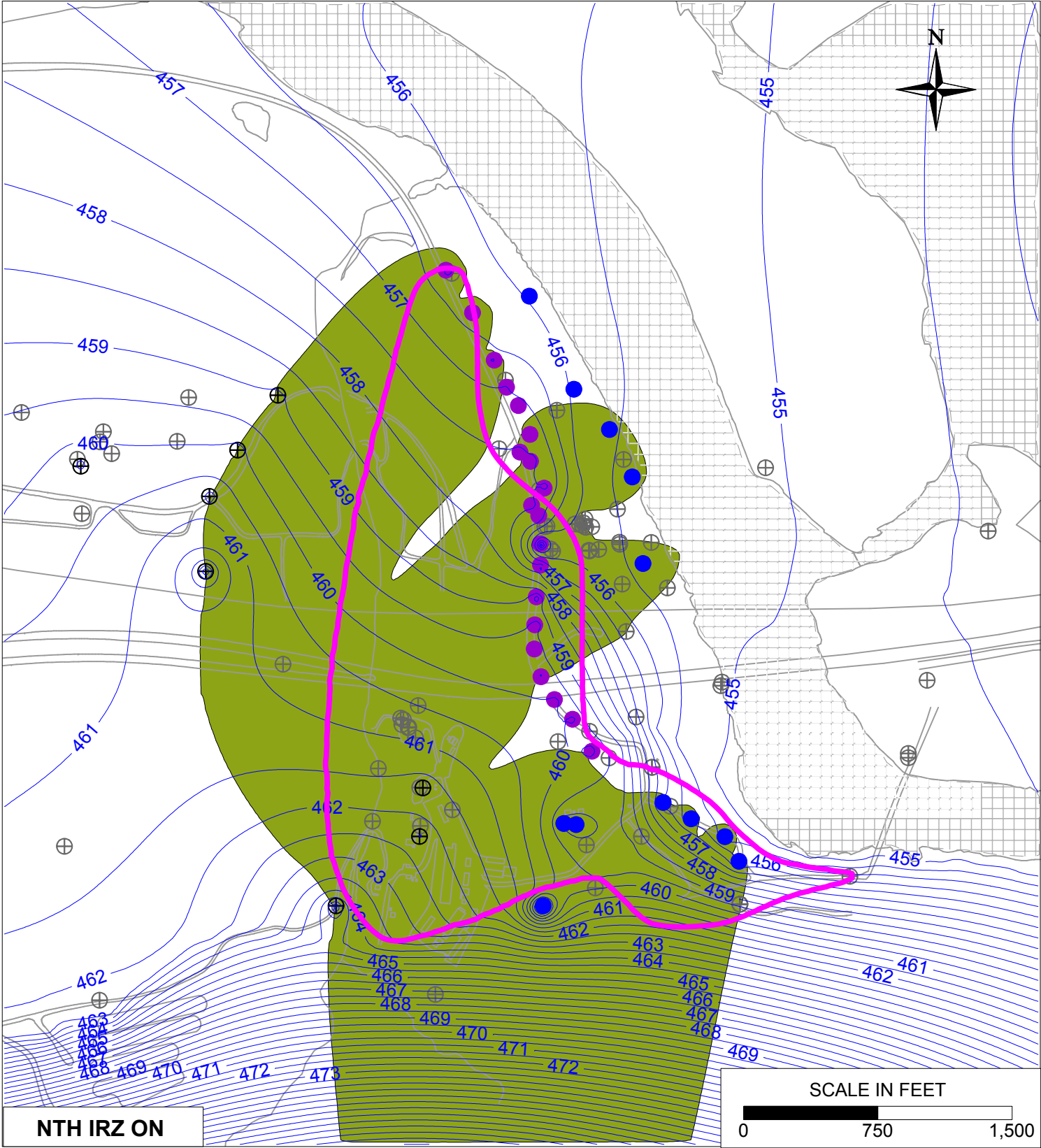
PG&E TOPOCK COMPRESSOR STATION NEEDLES, CALIFORNIA MODELING APPENDIX	
SIMULATED GROUNDWATER CONTOURS UNDER ACTIVE REMEDY FLOW CONDITIONS IN MODEL LAYER 4	
	FIGURE 6.5-8



**LEGEND**

- IRZ WELLS
- ⊕ UPGRADIENT INJECTION WELLS
- EXTRACTION WELLS
- ⊕ MONITORING WELLS
- 460— SIMULATED GROUNDWATER LEVELS (FT MSL)
- MAGENTA LINE — HEXAVALENT CHROMIUM GROUNDWATER PLUME FOOTPRINT
- SIMULATED GROUNDWATER CAPTURE ZONE





**LEGEND**

- IRZ WELLS
- ⊕ UPGRAIDENT INJECTION WELLS
- EXTRACTION WELLS
- ⊕ MONITORING WELLS
- 460— SIMULATED GROUNDWATER LEVELS (FT MSL)
- MAGENTA — HEXAVALENT CHROMIUM GROUNDWATER PLUME FOOTPRINT
- SIMULATED GROUNDWATER CAPTURE ZONE

PG&E  
TOPOCK COMPRESSOR STATION  
NEEDLES, CALIFORNIA  
MODELING APPENDIX

SIMULATED GROUNDWATER CAPTURE  
UNDER ACTIVE REMEDY FLOW CONDITIONS  
IN MODEL LAYER 2


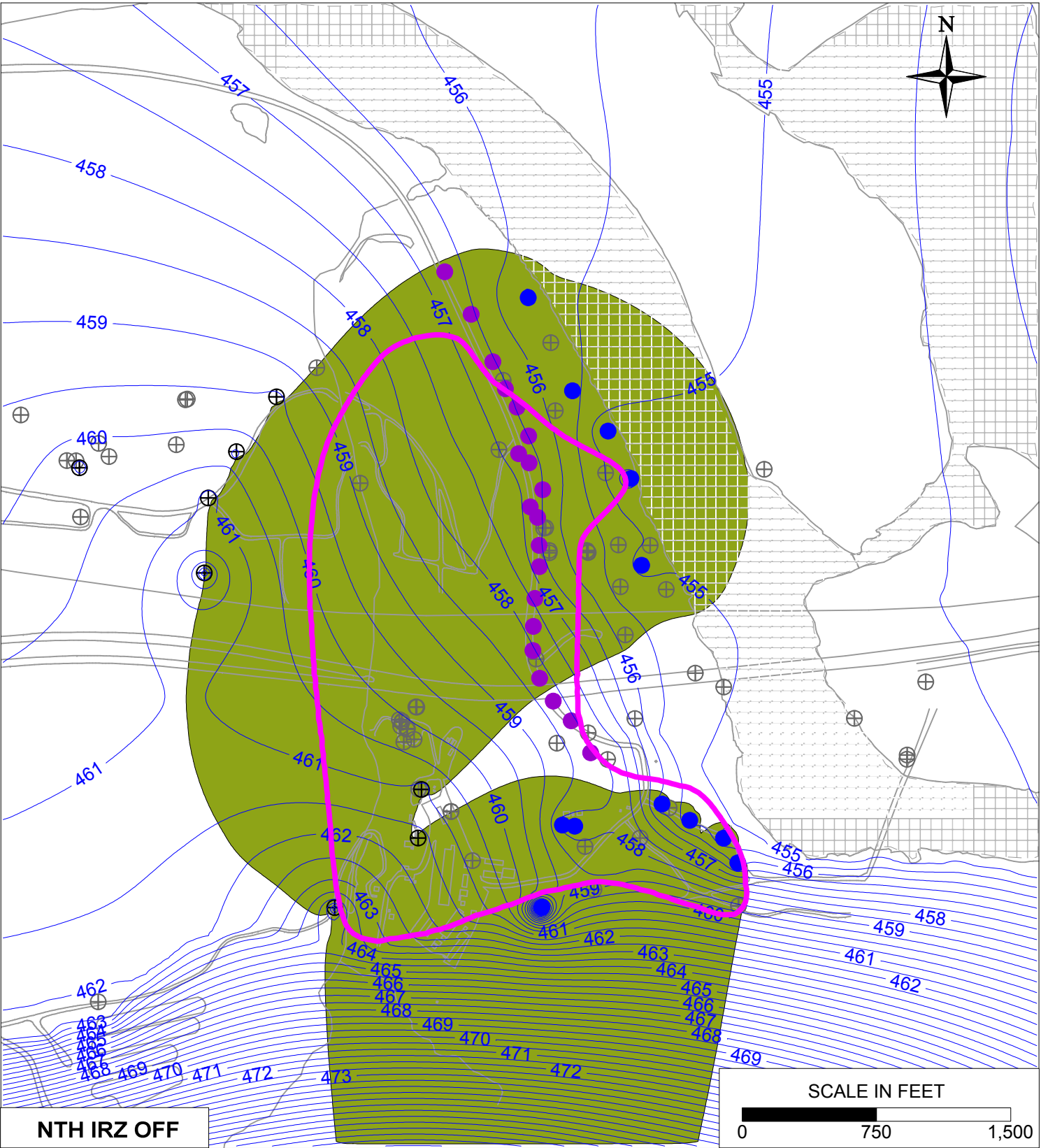
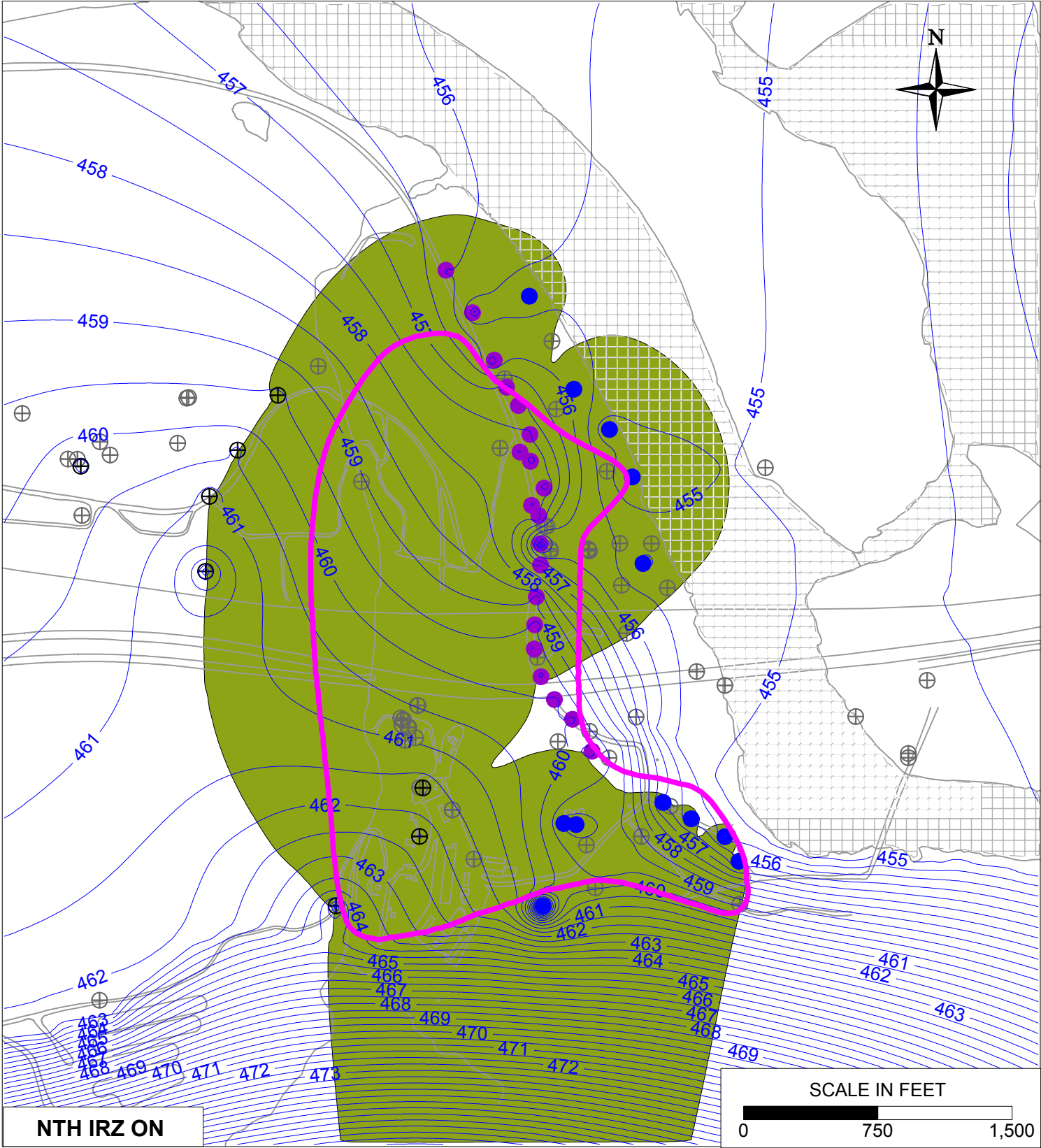
 **ARCADIS**

FIGURE  
**6.5-10**





**LEGEND**

- IRZ WELLS
- ⊕ UPGRADIENT INJECTION WELLS
- EXTRACTION WELLS
- ⊕ MONITORING WELLS
- 460— SIMULATED GROUNDWATER LEVELS (FT MSL)
- MAGENTA — HEXAVALENT CHROMIUM GROUNDWATER PLUME FOOTPRINT
- SIMULATED GROUNDWATER CAPTURE ZONE

PG&E  
TOPOCK COMPRESSOR STATION  
NEEDLES, CALIFORNIA  
MODELING APPENDIX

SIMULATED GROUNDWATER CAPTURE  
UNDER ACTIVE REMEDY FLOW CONDITIONS  
IN MODEL LAYER 3


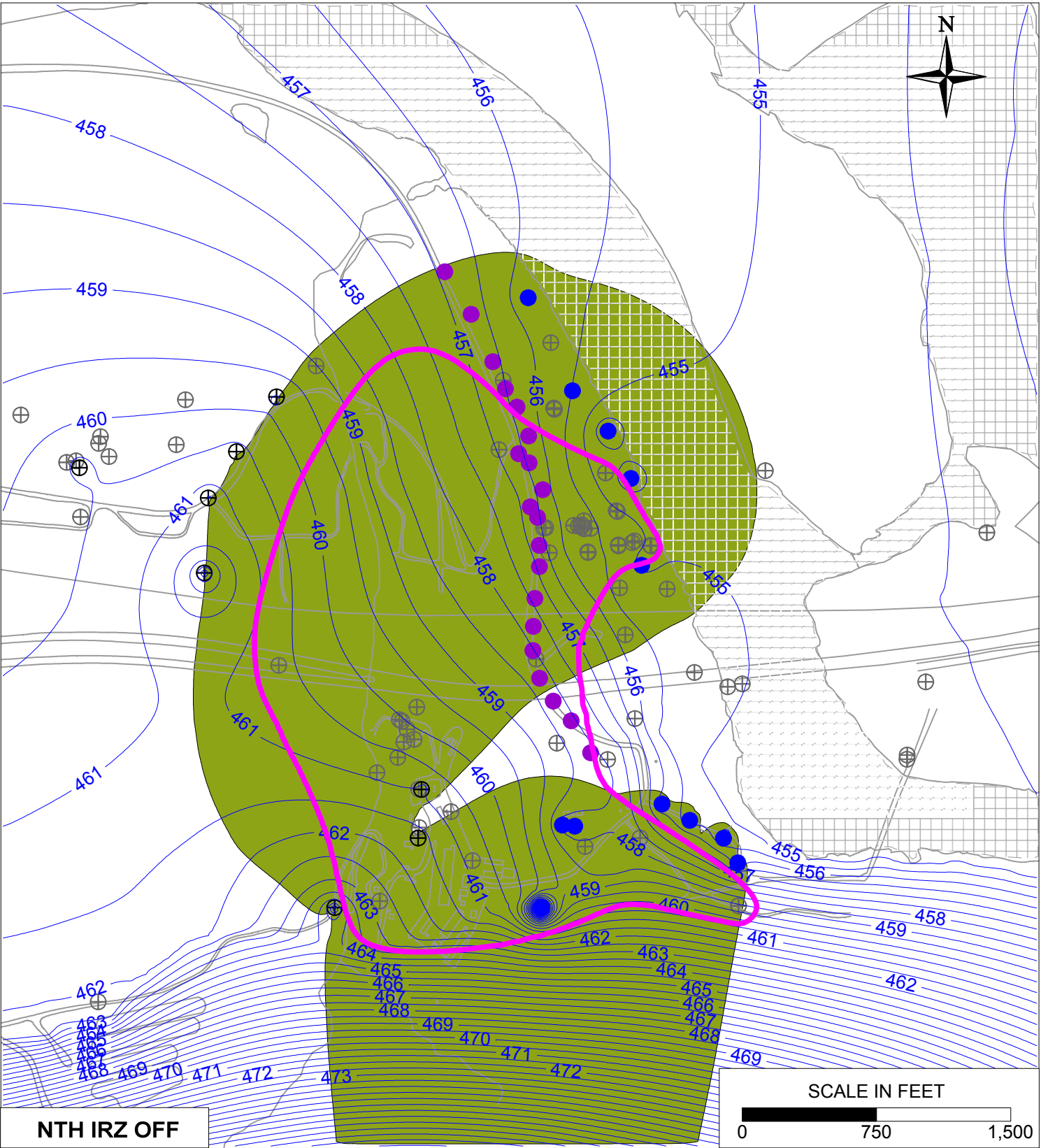
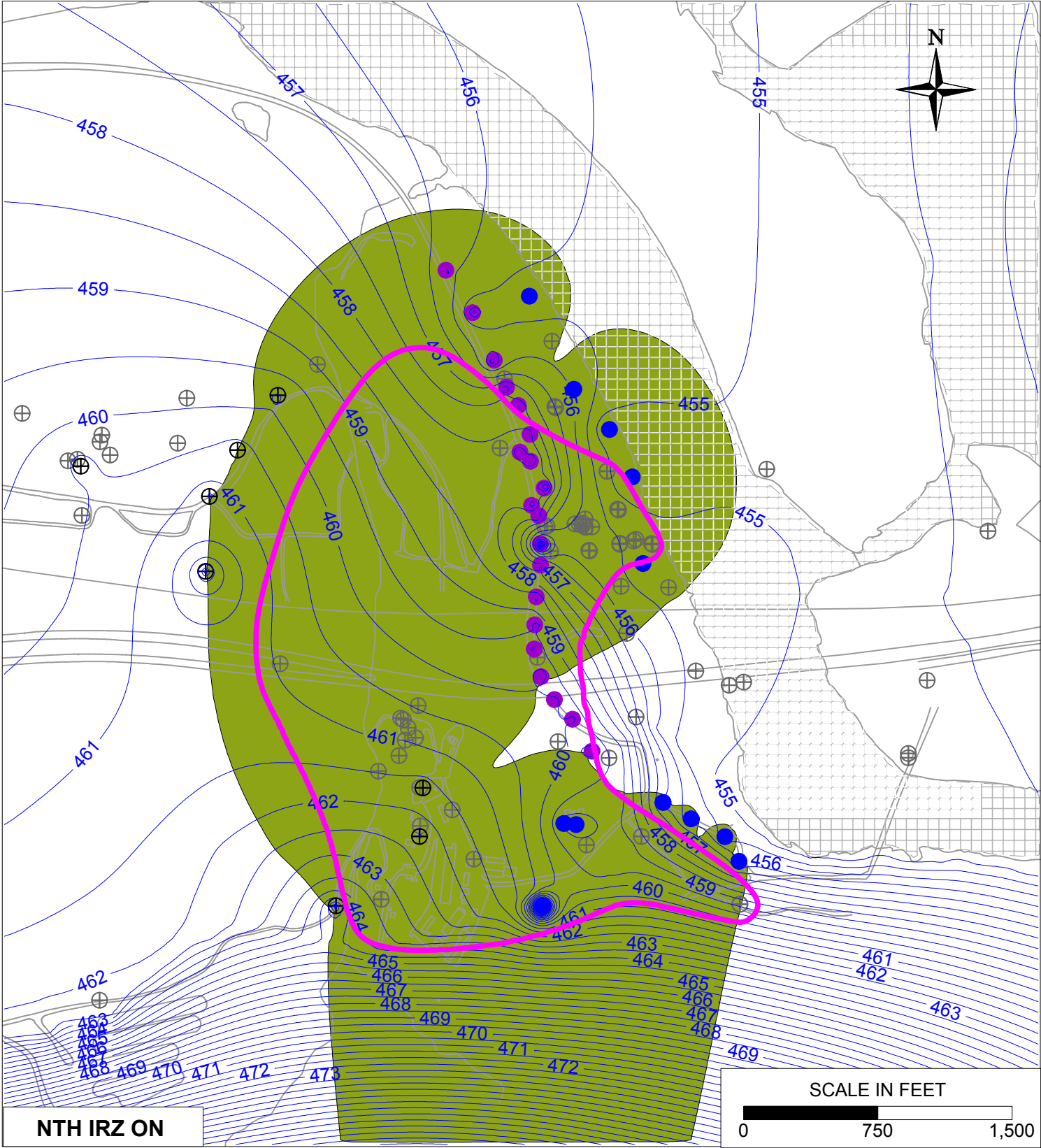


FIGURE  
6.5-11





**LEGEND**

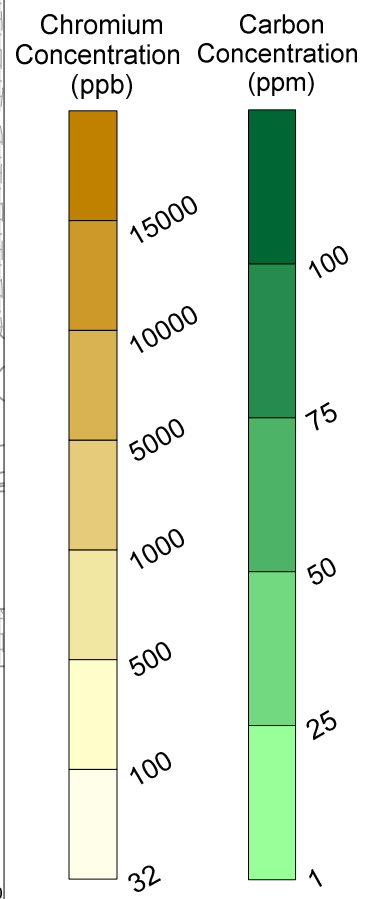
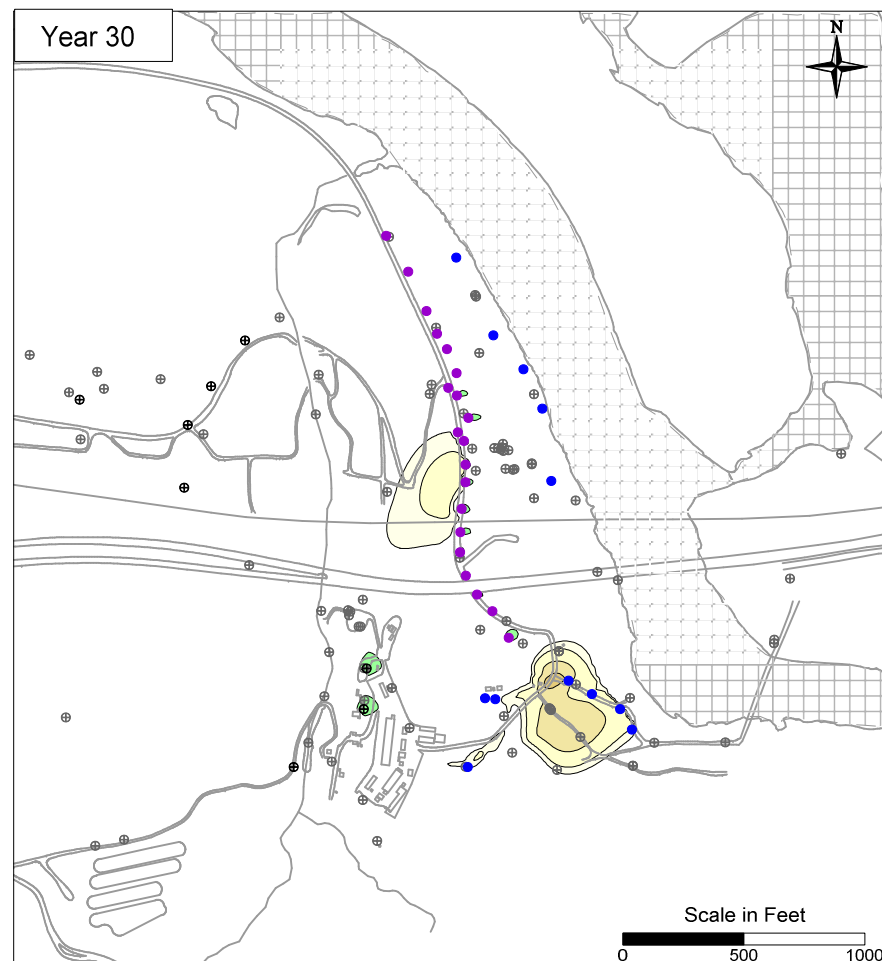
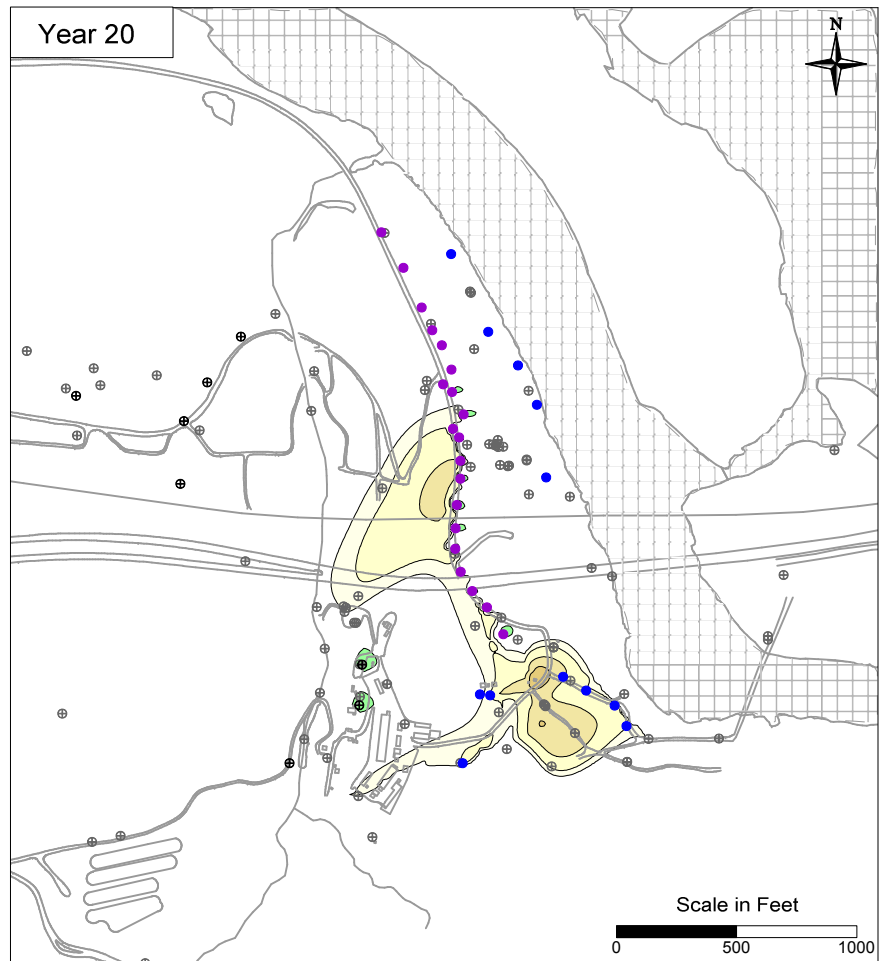
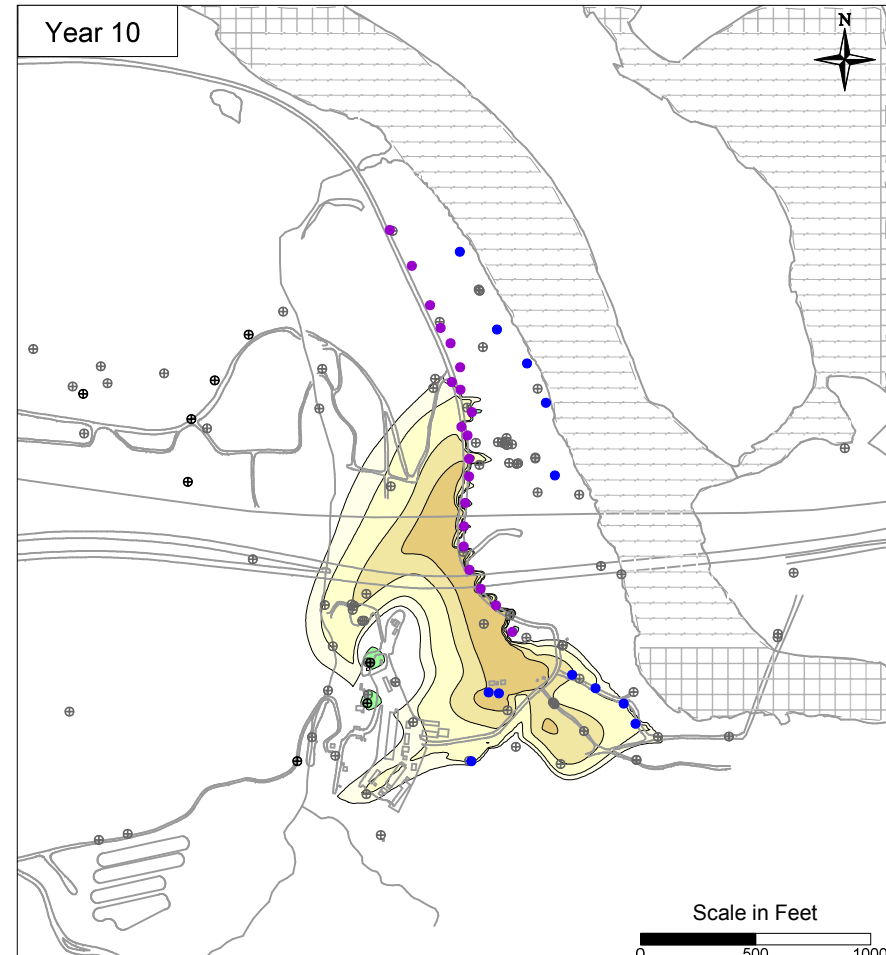
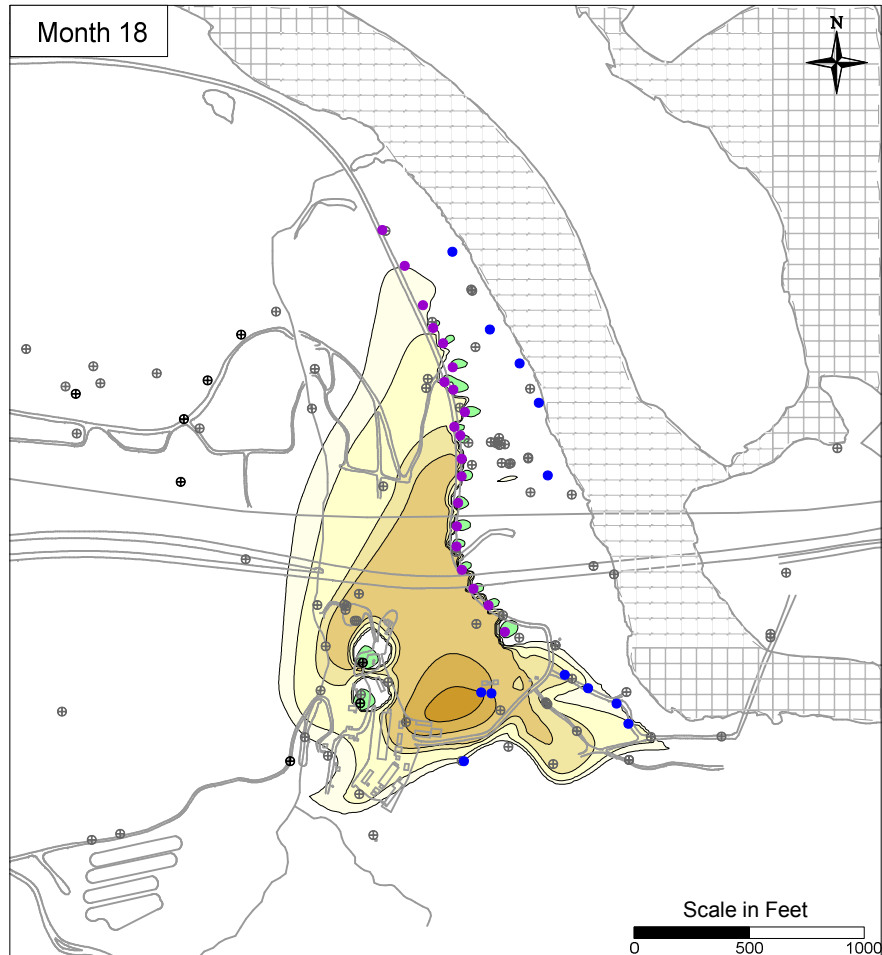
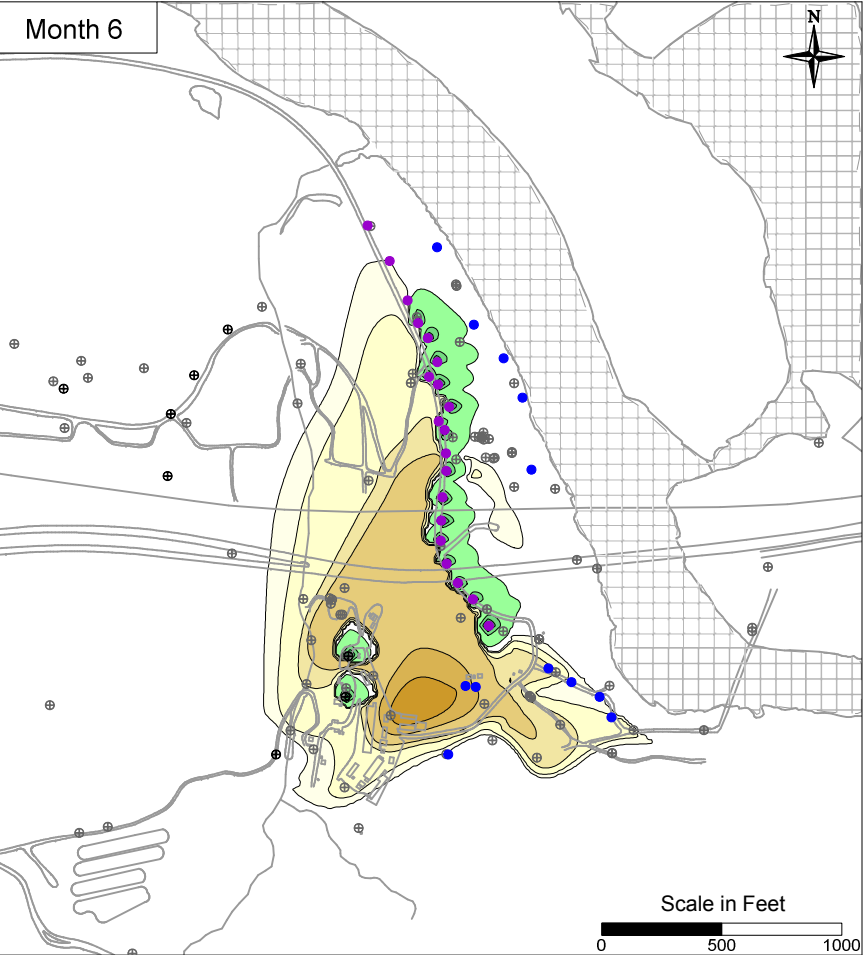
- IRZ WELLS
- ⊕ UPGRADIENT INJECTION WELLS
- EXTRACTION WELLS
- ⊕ MONITORING WELLS
- 460— SIMULATED GROUNDWATER LEVELS (FT MSL)
- HEXAVALENT CHROMIUM GROUNDWATER PLUME FOOTPRINT
- SIMULATED GROUNDWATER CAPTURE ZONE

PG&E  
TOPOCK COMPRESSOR STATION  
NEEDLES, CALIFORNIA  
MODELING APPENDIX

SIMULATED GROUNDWATER CAPTURE  
UNDER ACTIVE REMEDY FLOW CONDITIONS  
IN MODEL LAYER 4

ARCADIS

FIGURE  
6.5-12



**LEGEND**

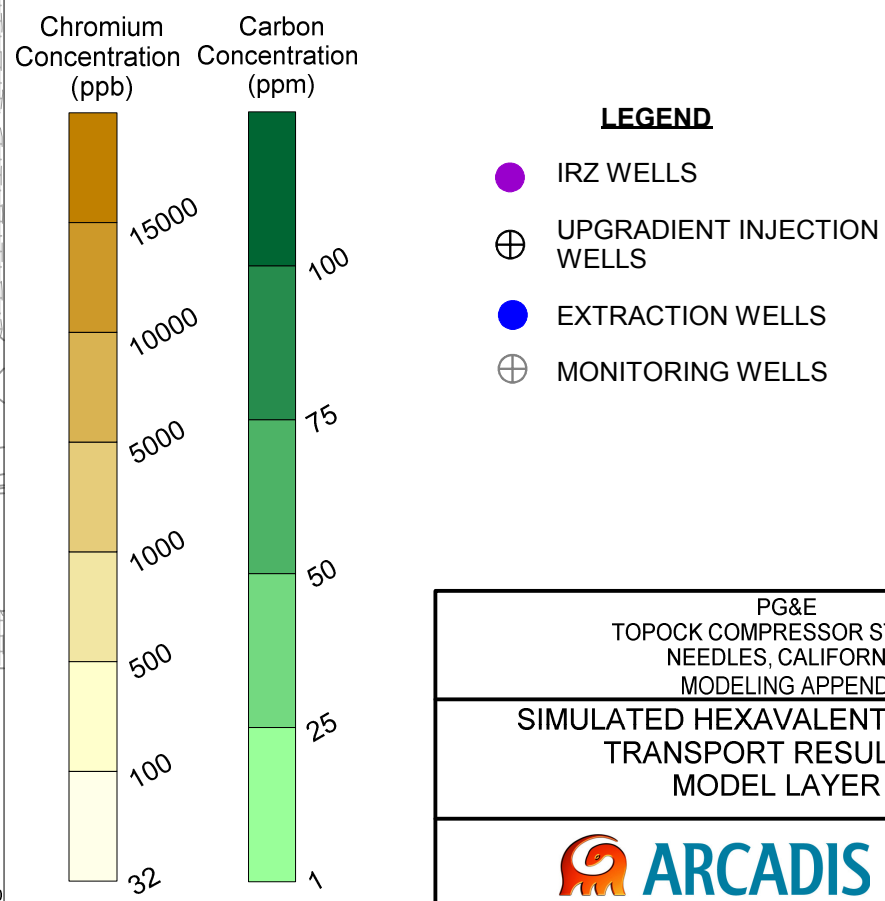
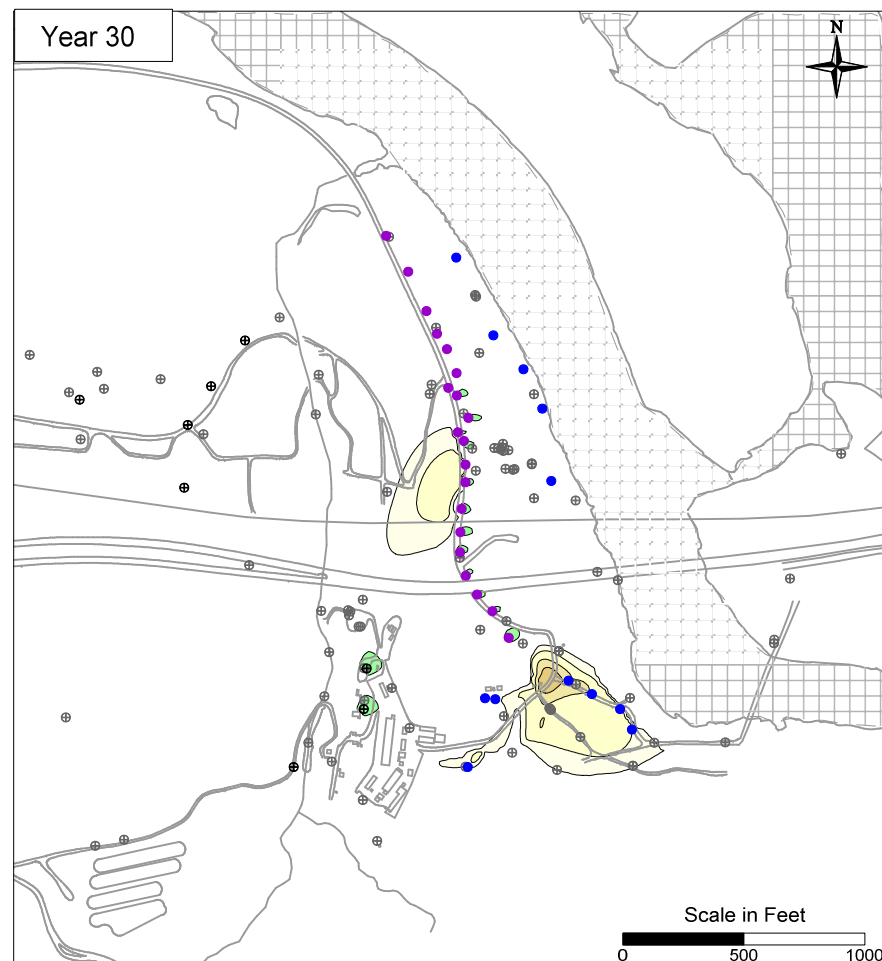
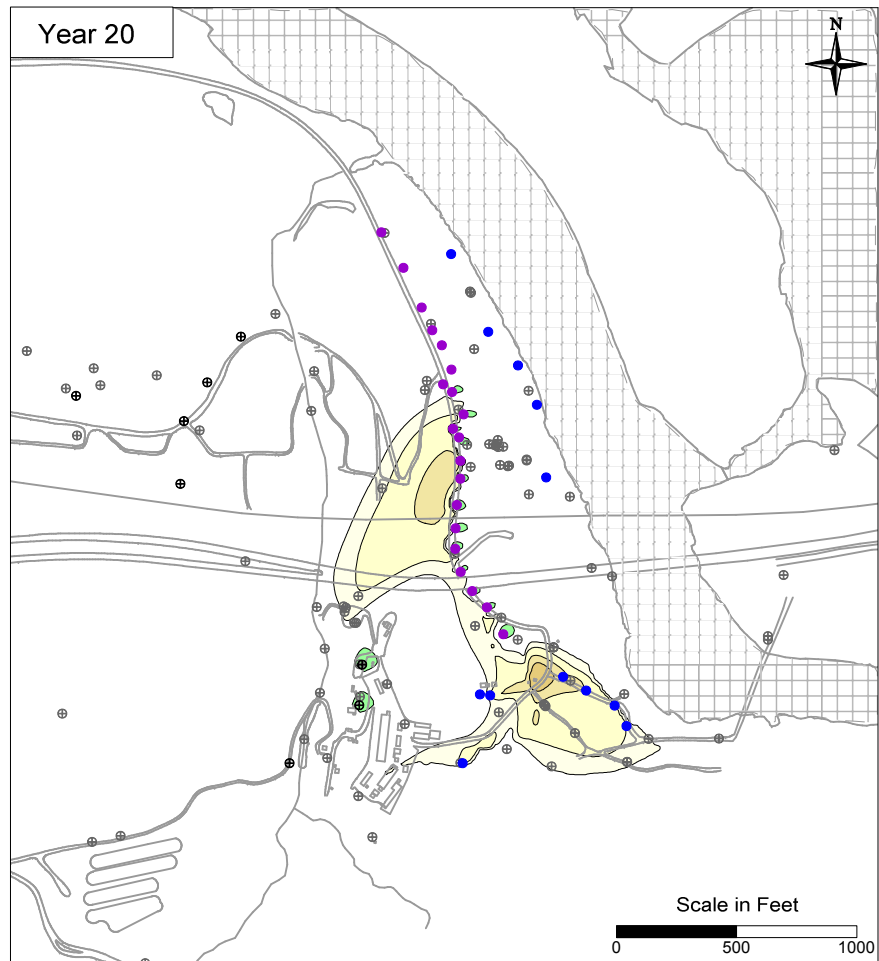
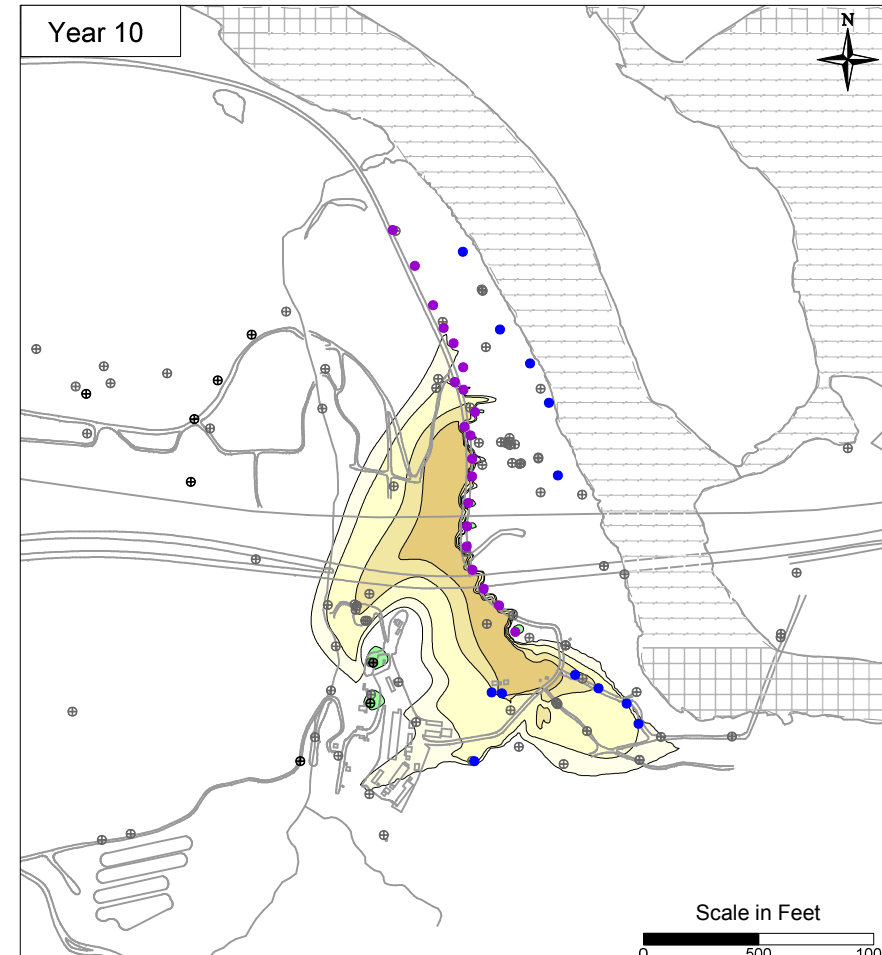
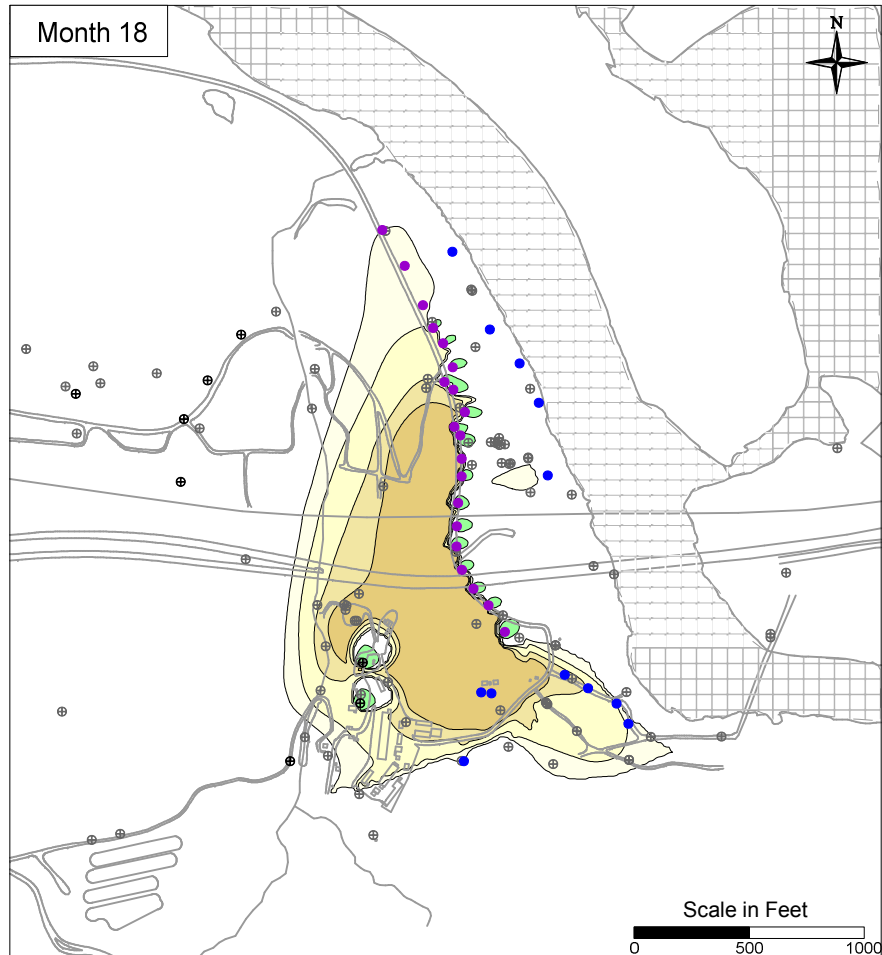
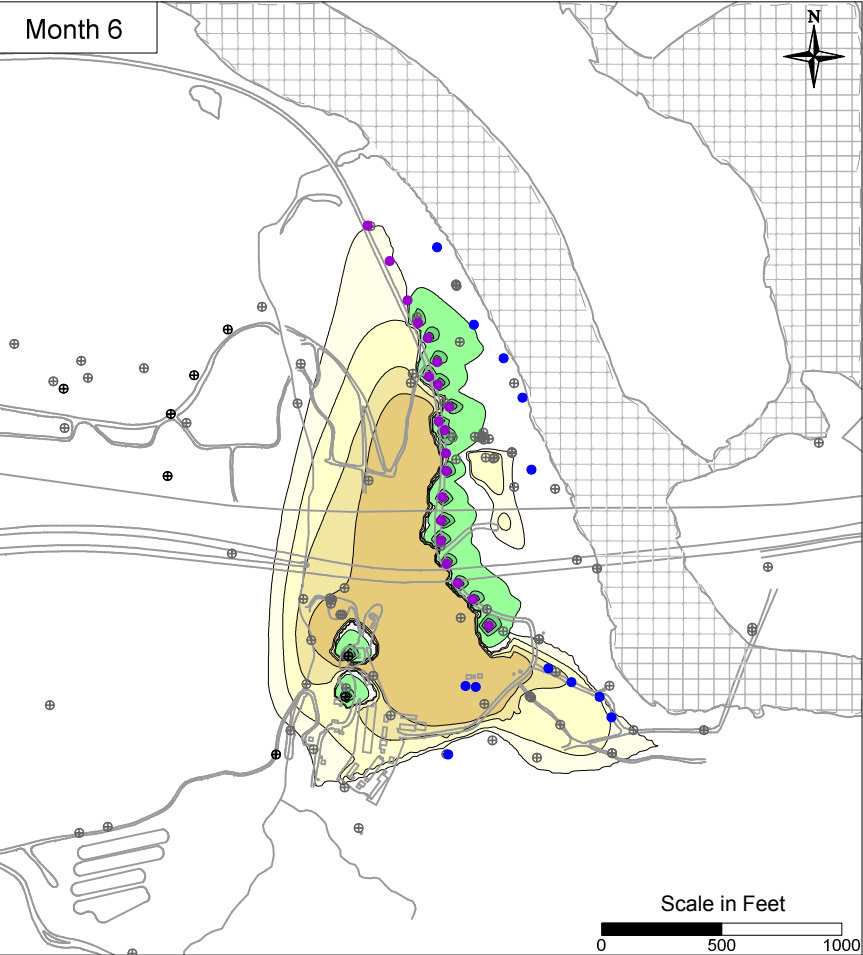
- IRZ WELLS
- UPGRADIENT INJECTION WELLS
- EXTRACTION WELLS
- MONITORING WELLS

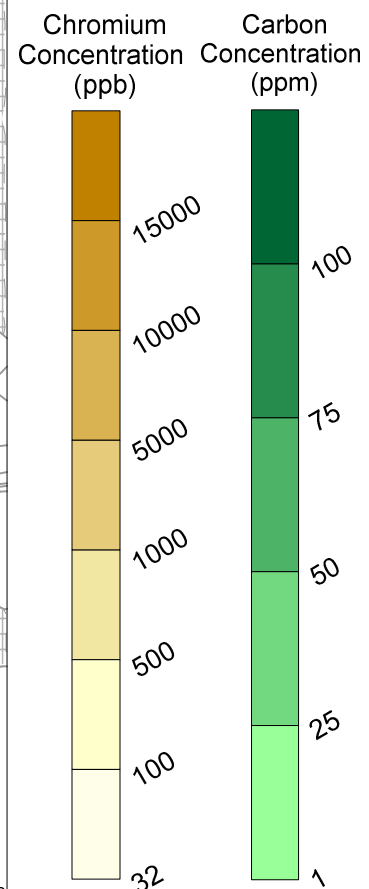
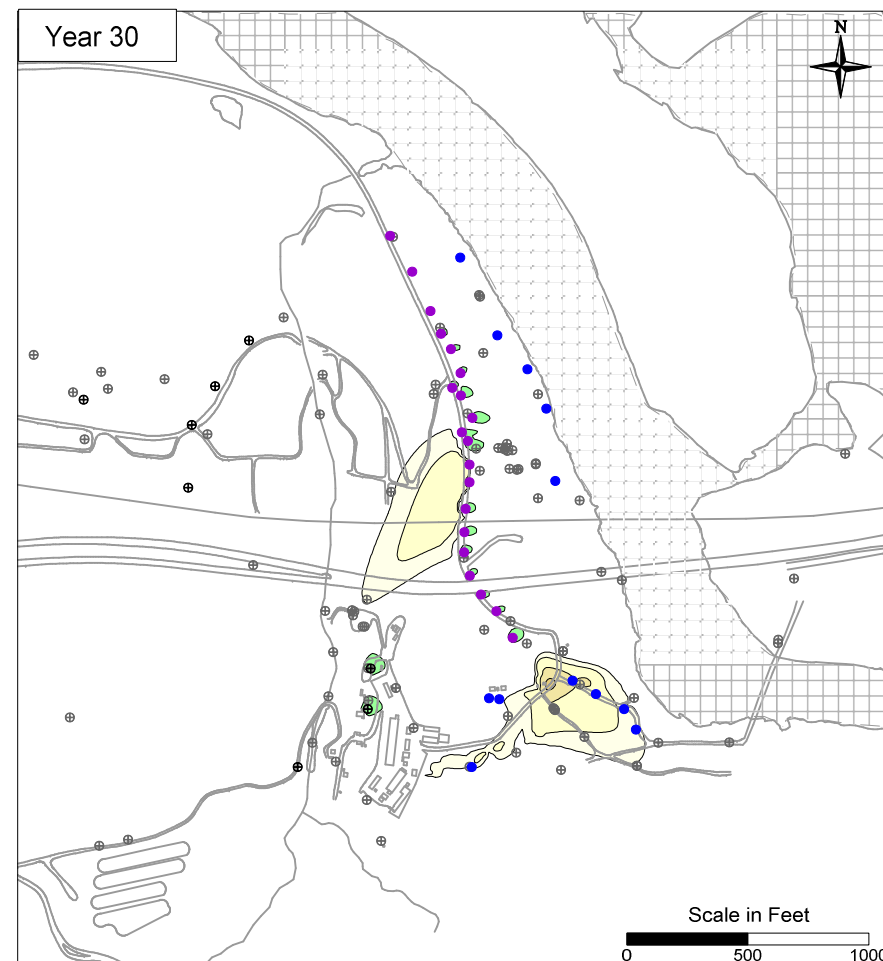
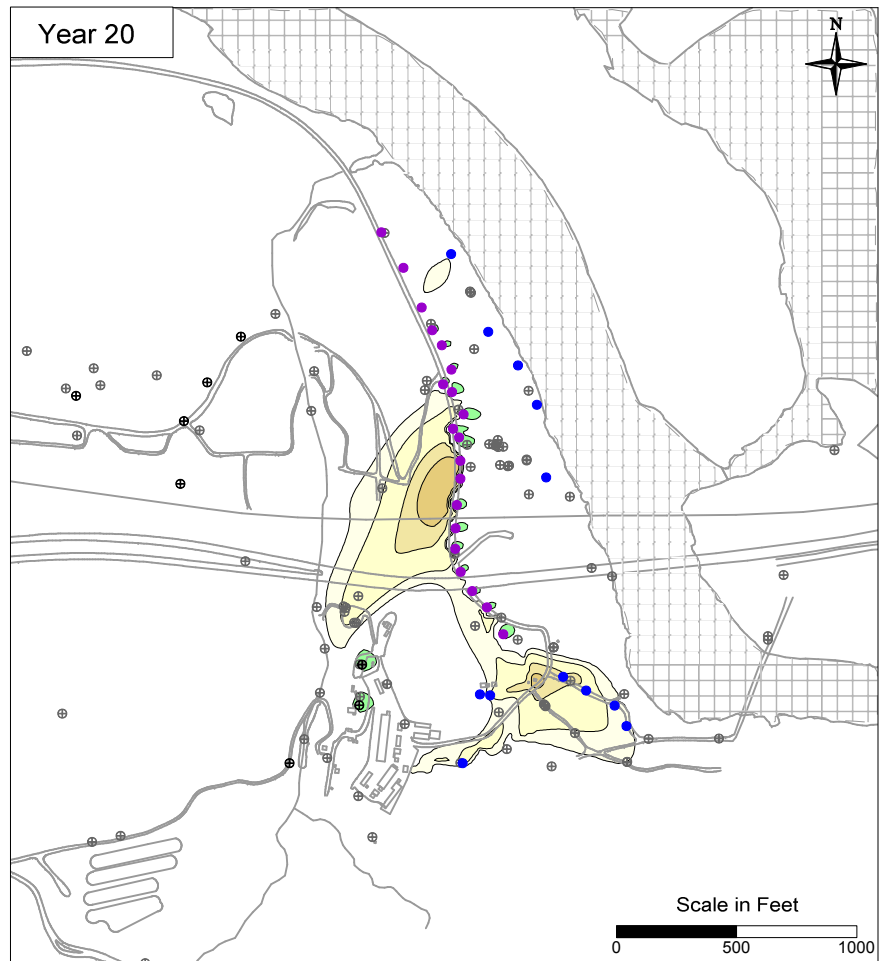
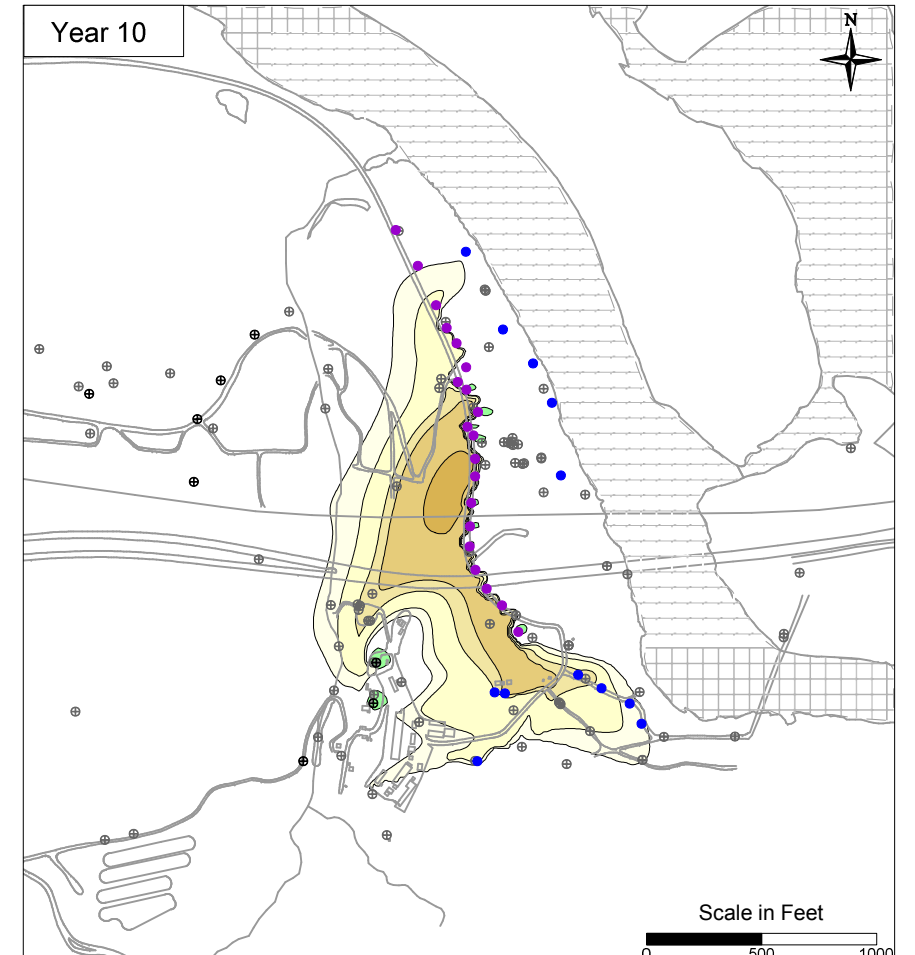
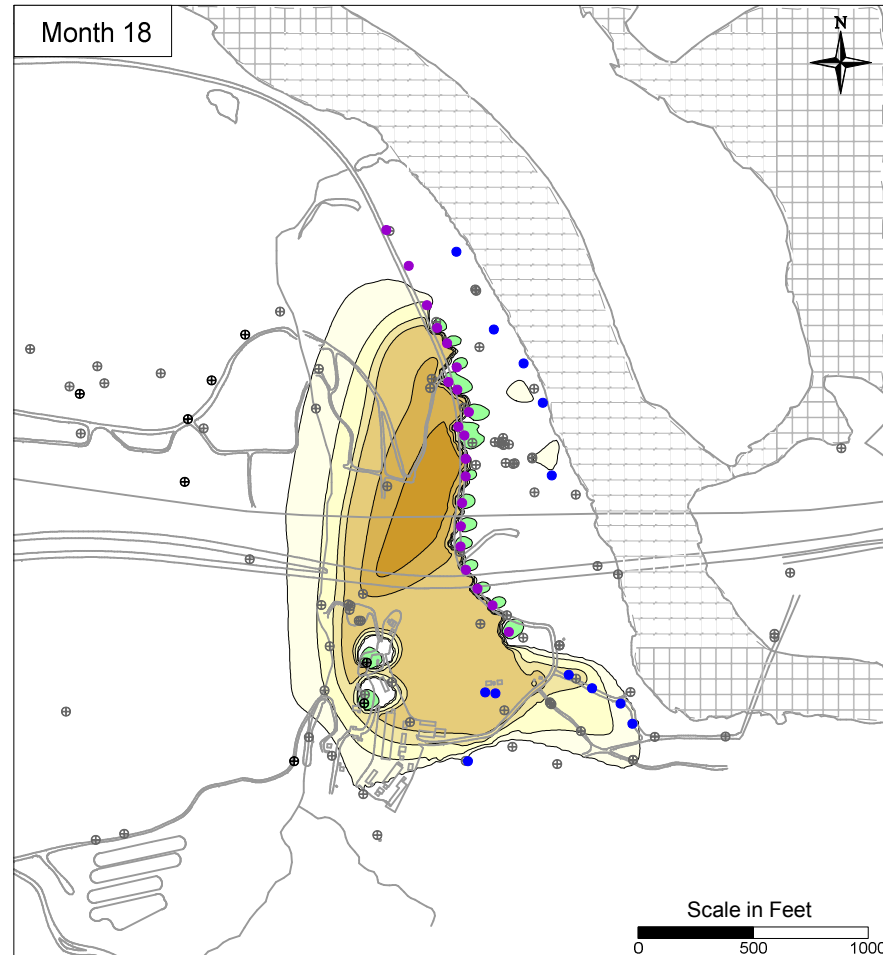
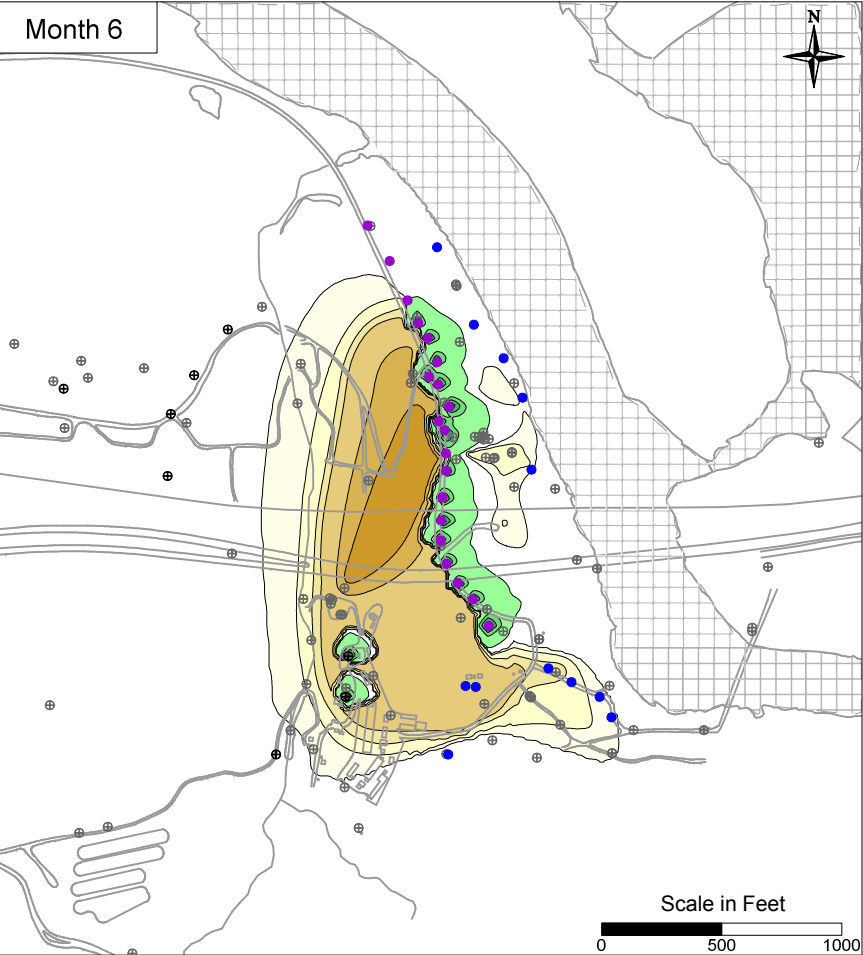
PG&E  
TOPOCK COMPRESSOR STATION  
NEEDLES, CALIFORNIA  
MODELING APPENDIX  
SIMULATED HEXAVALENT CHROMIUM  
TRANSPORT RESULTS IN  
MODEL LAYER 1



FIGURE  
7.1-1







**LEGEND**

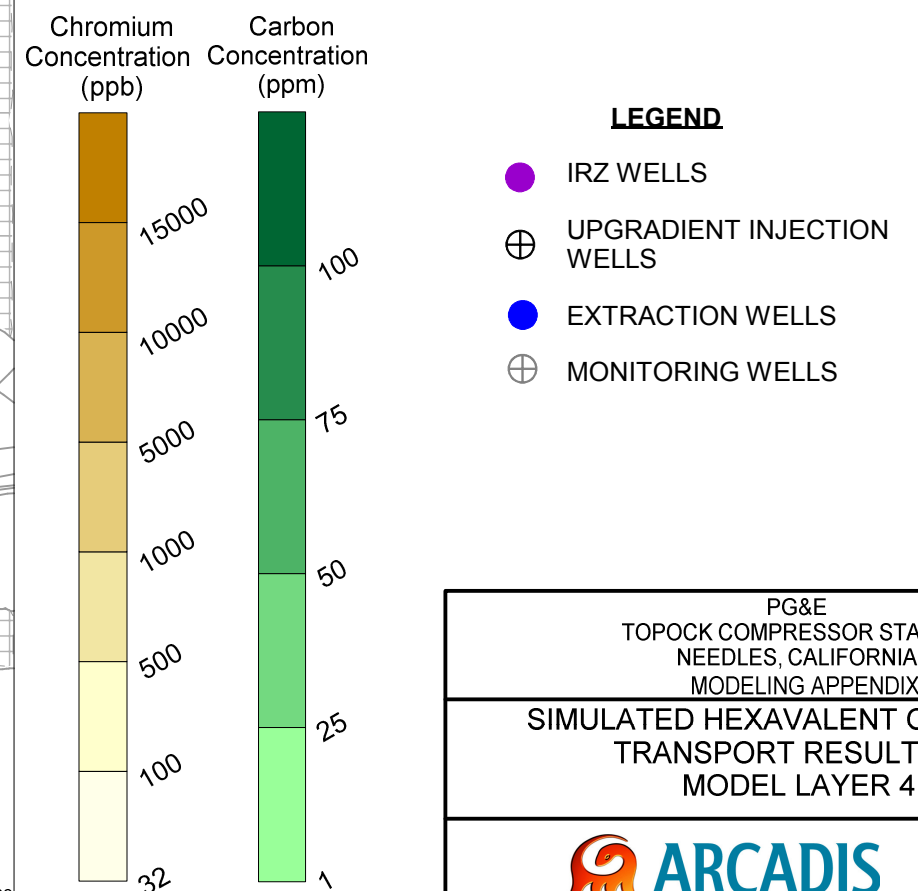
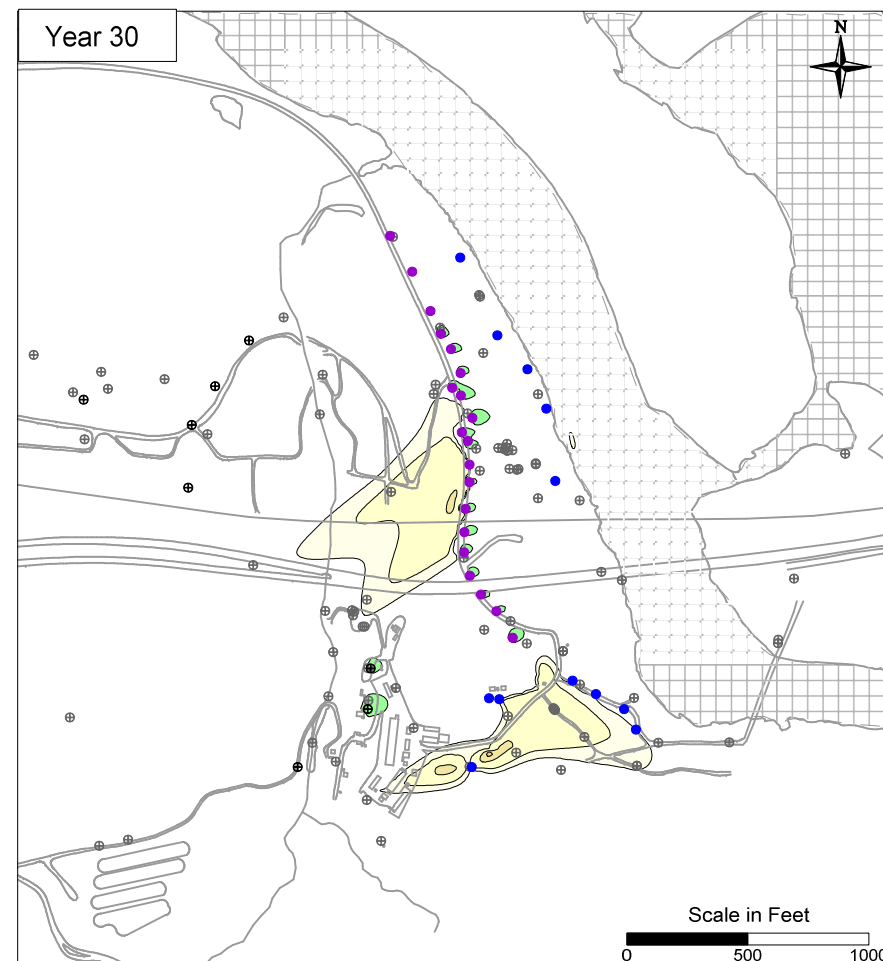
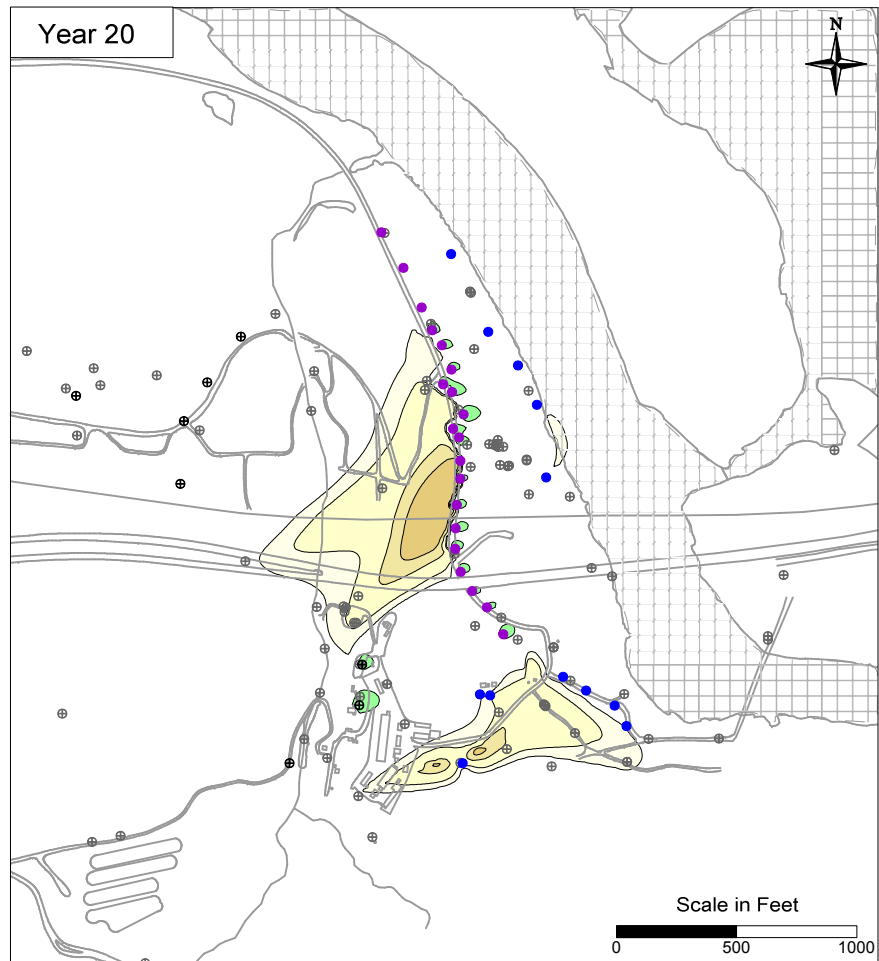
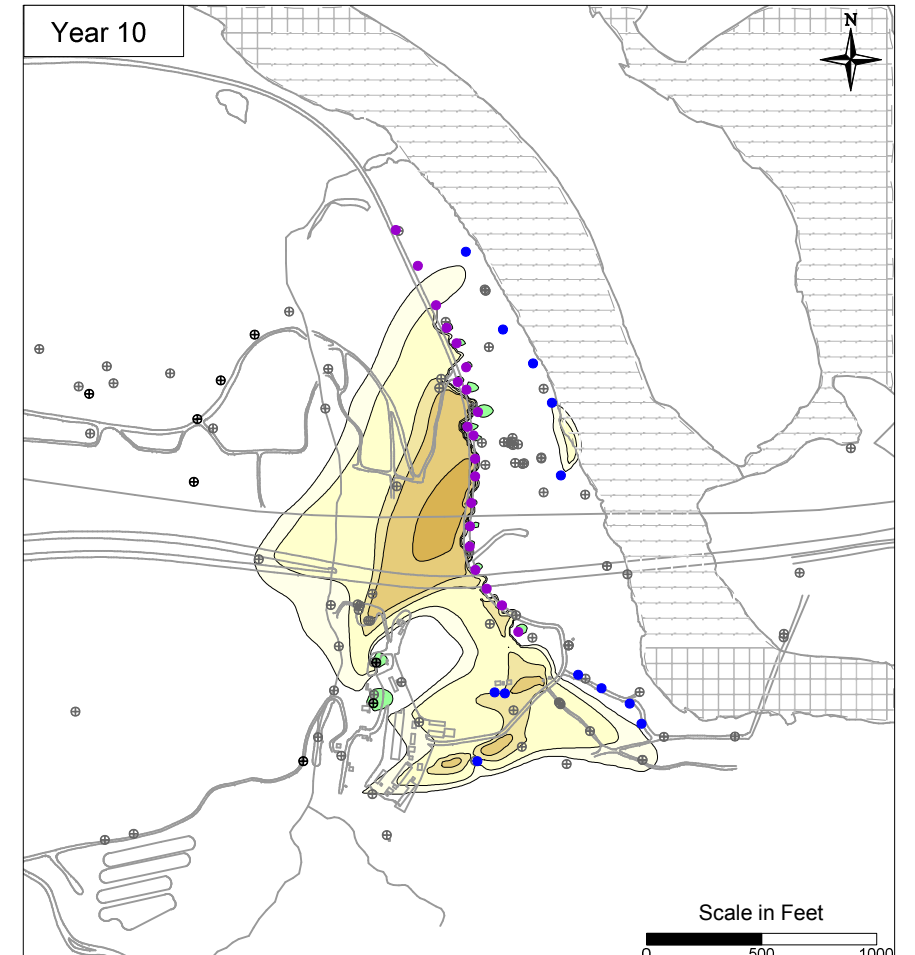
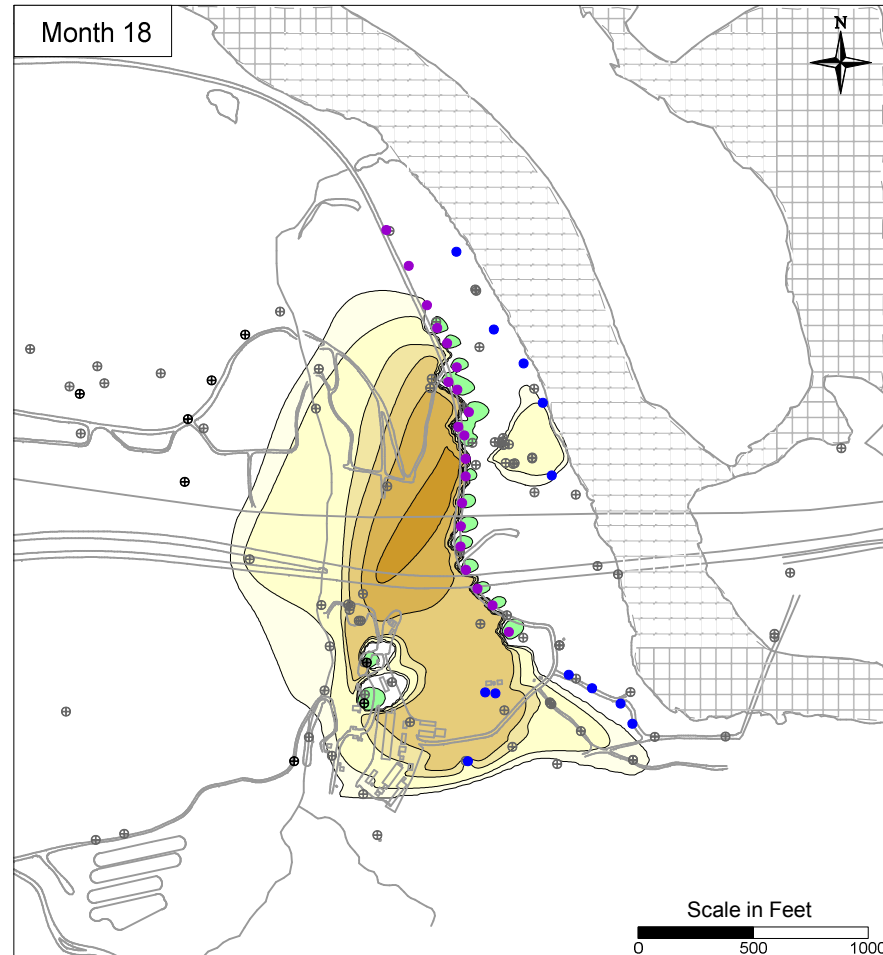
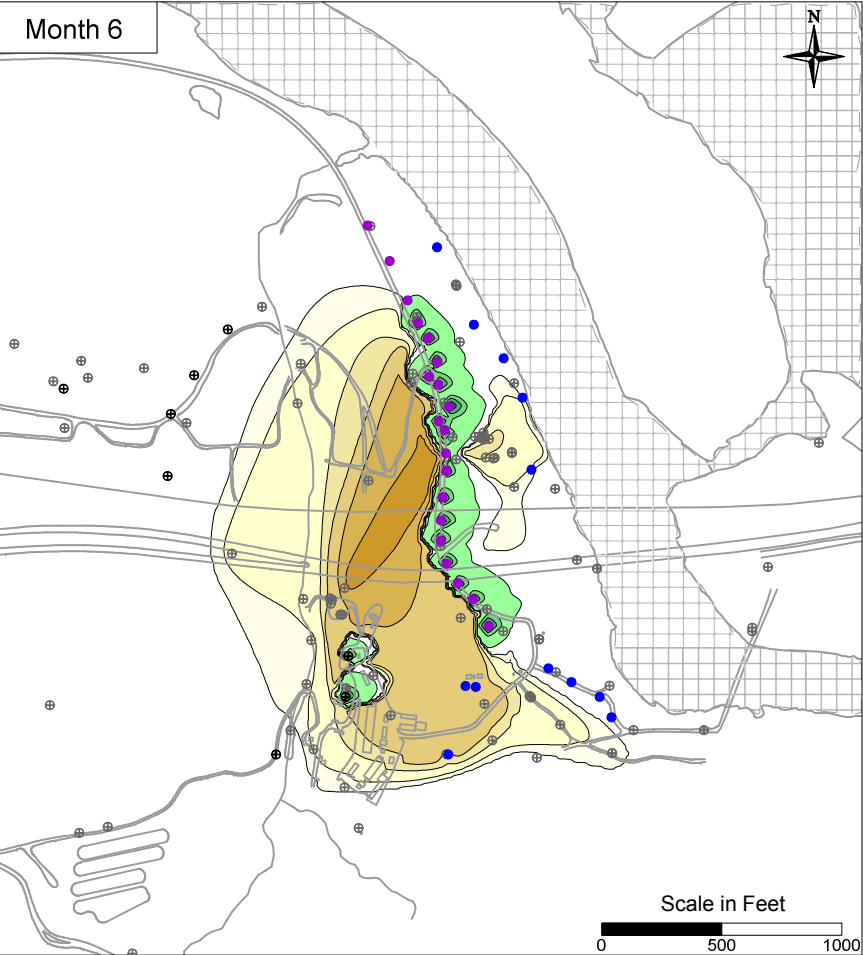
- IRZ WELLS
- UPGRADIENT INJECTION WELLS
- EXTRACTION WELLS
- MONITORING WELLS

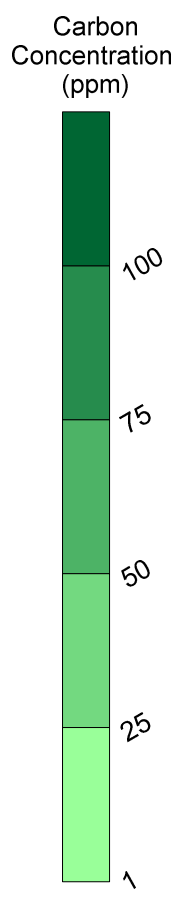
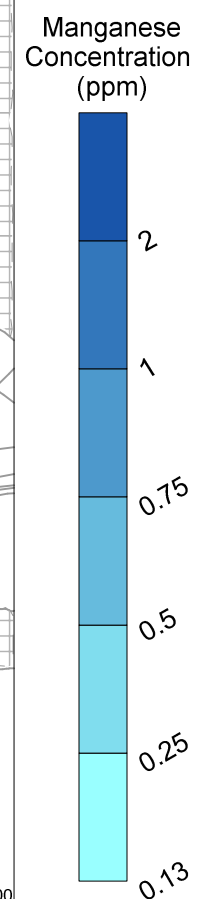
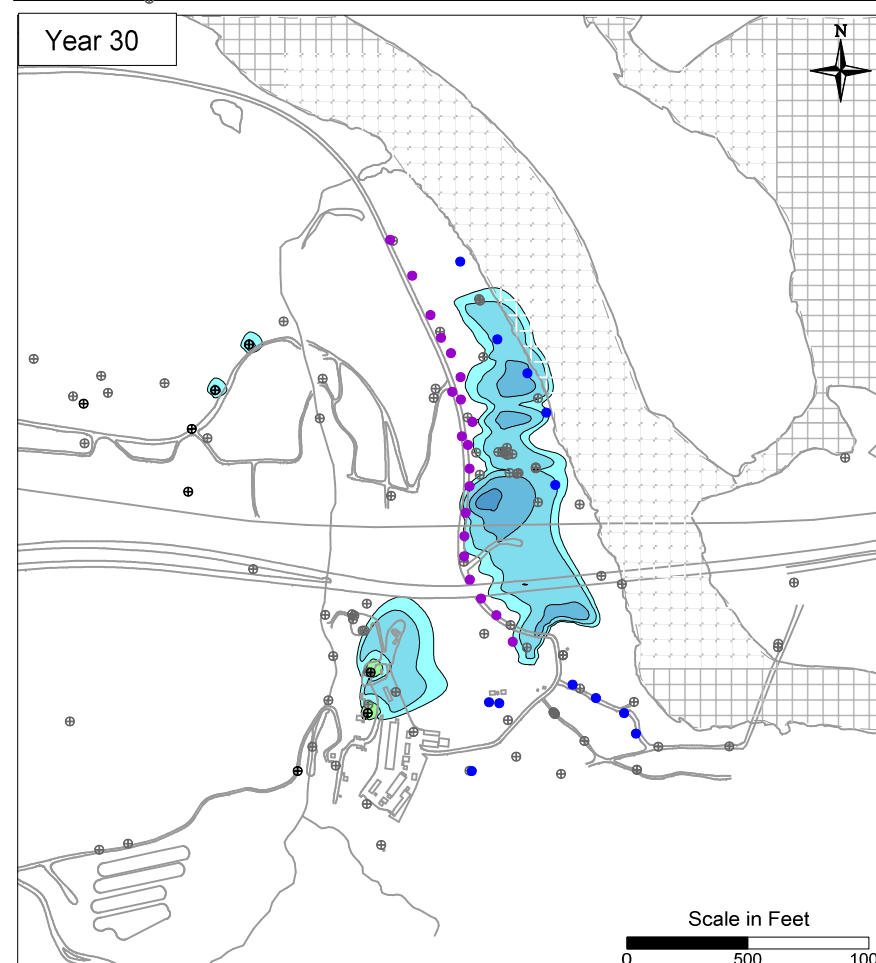
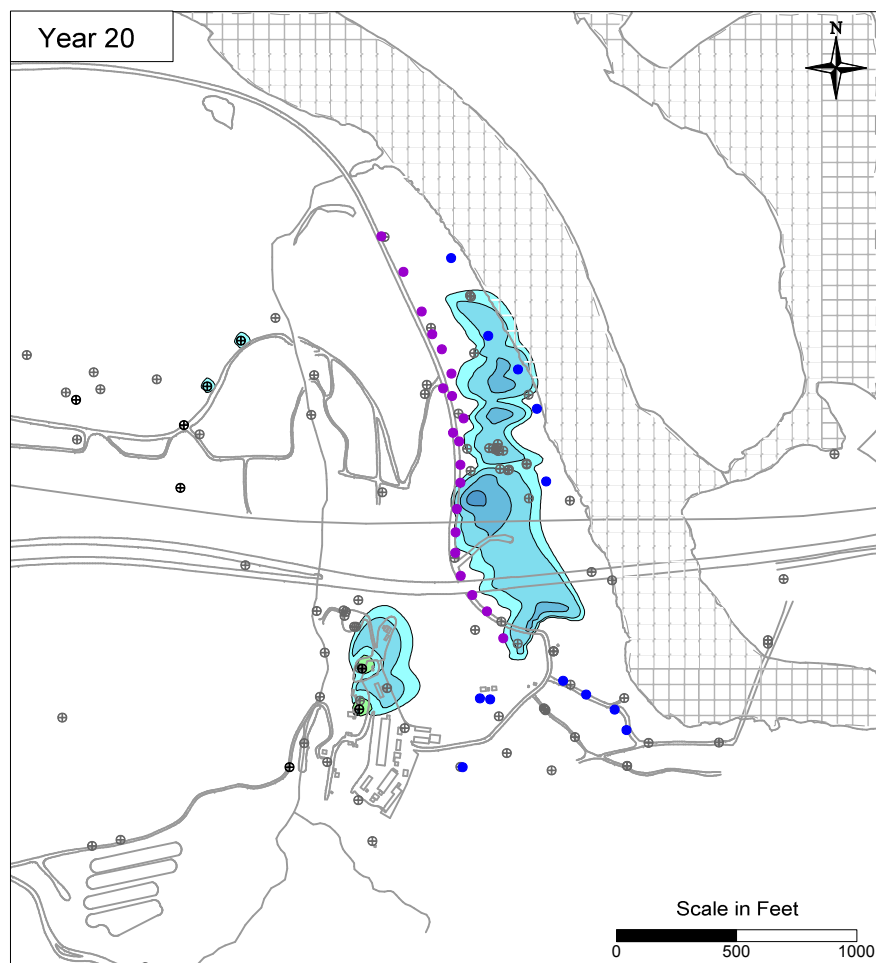
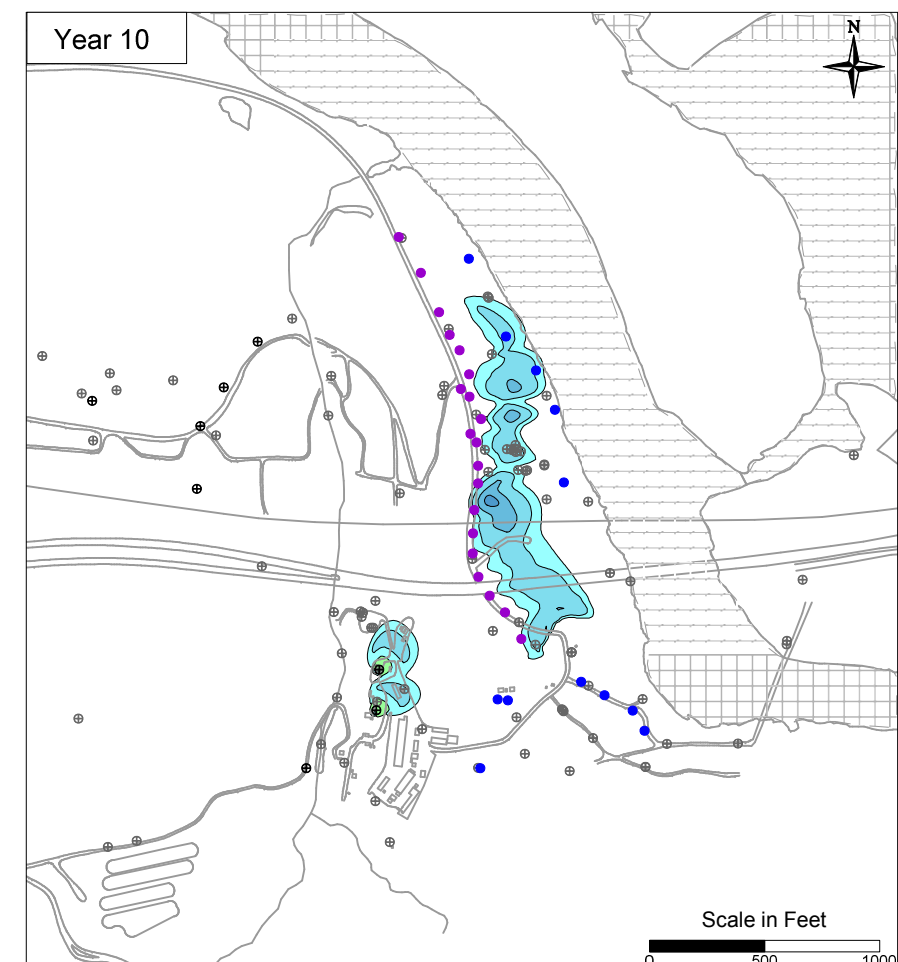
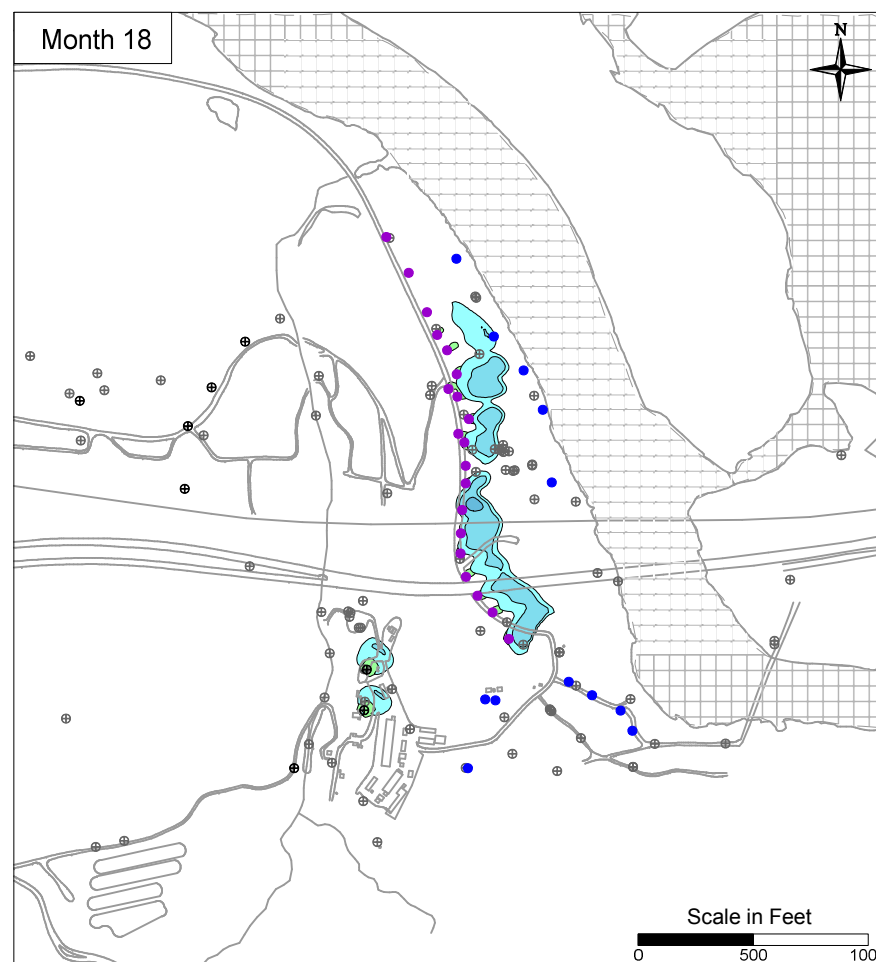
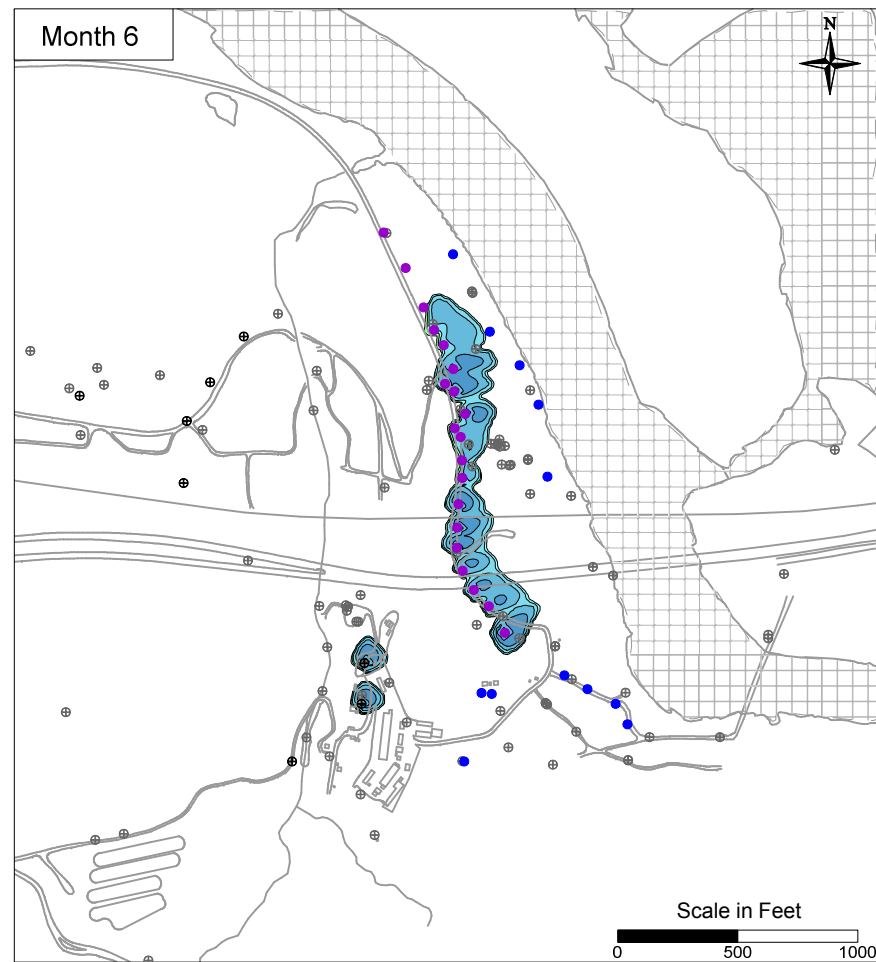
PG&E  
TOPOCK COMPRESSOR STATION  
NEEDLES, CALIFORNIA  
MODELING APPENDIX  
SIMULATED HEXAVALENT CHROMIUM  
TRANSPORT RESULTS IN  
MODEL LAYER 3



FIGURE  
7.1-3



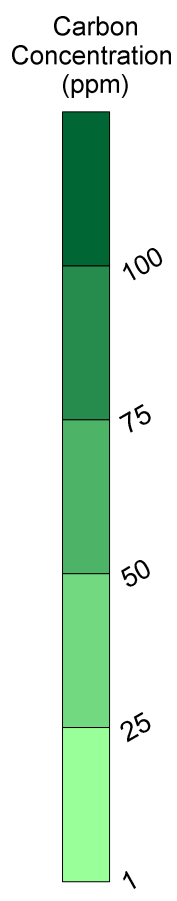
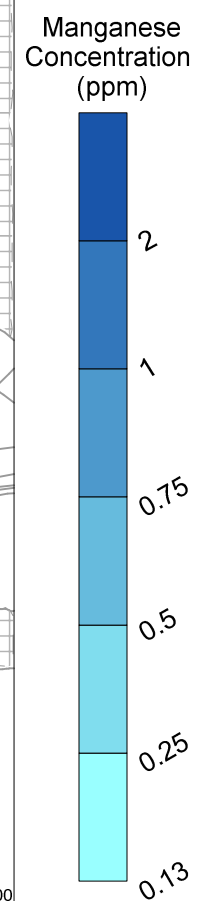
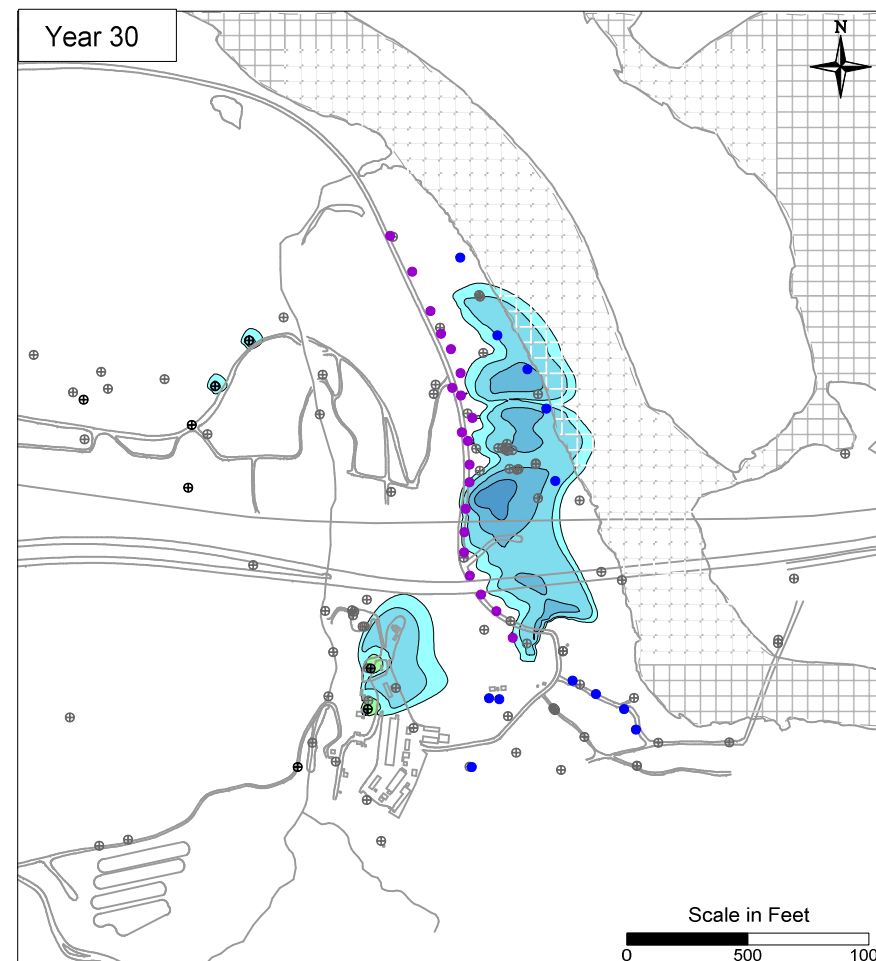
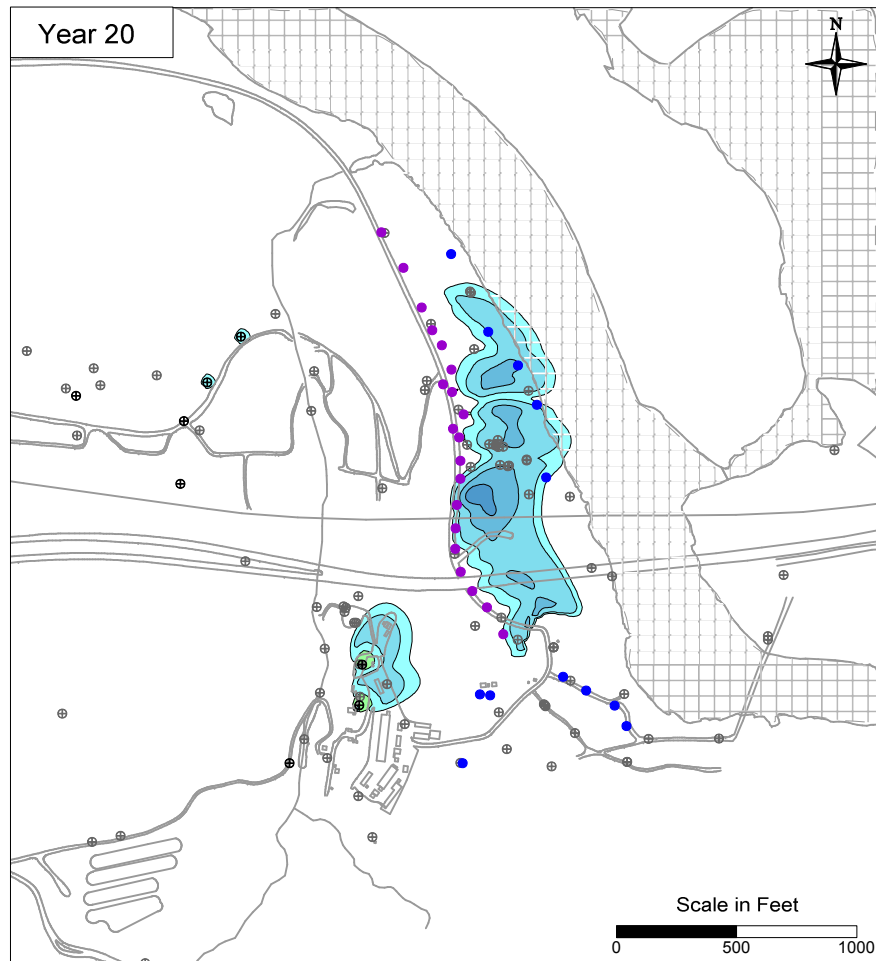
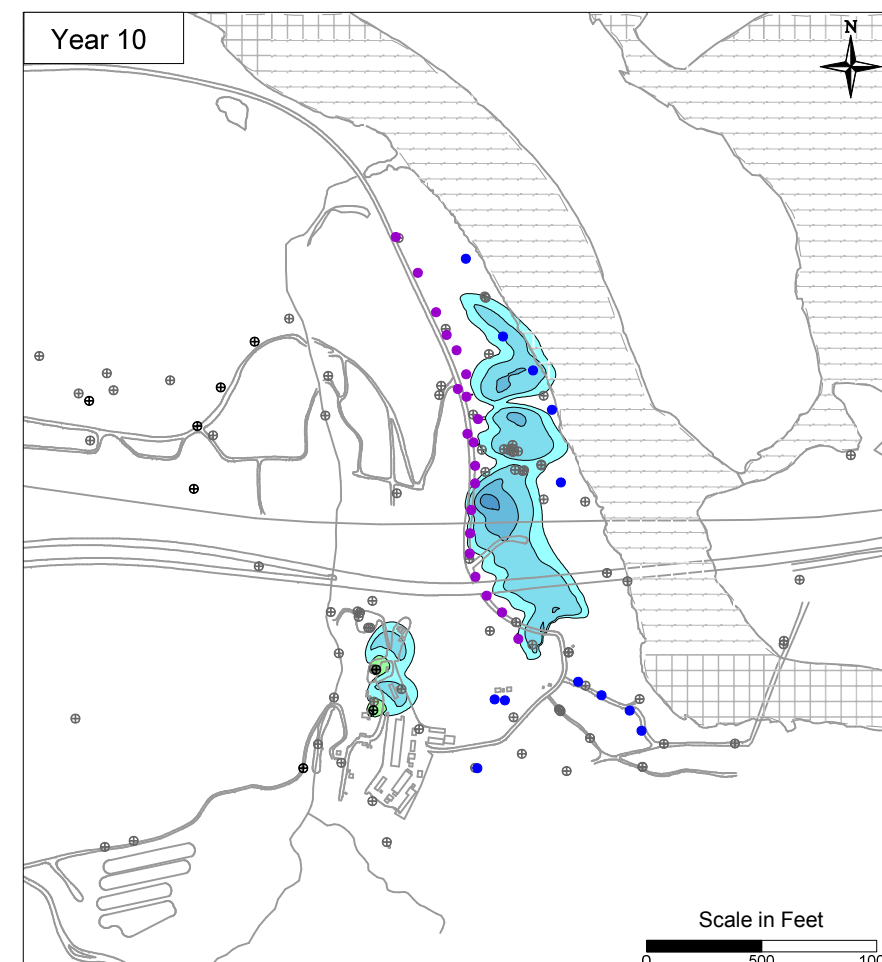
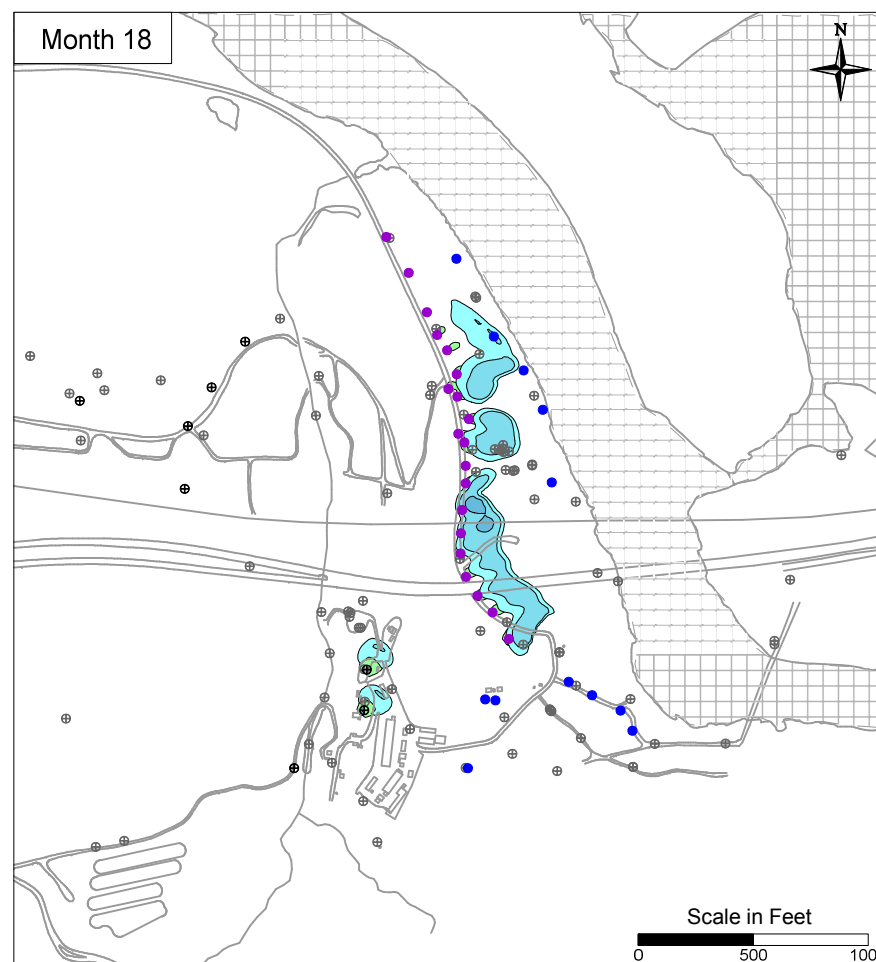
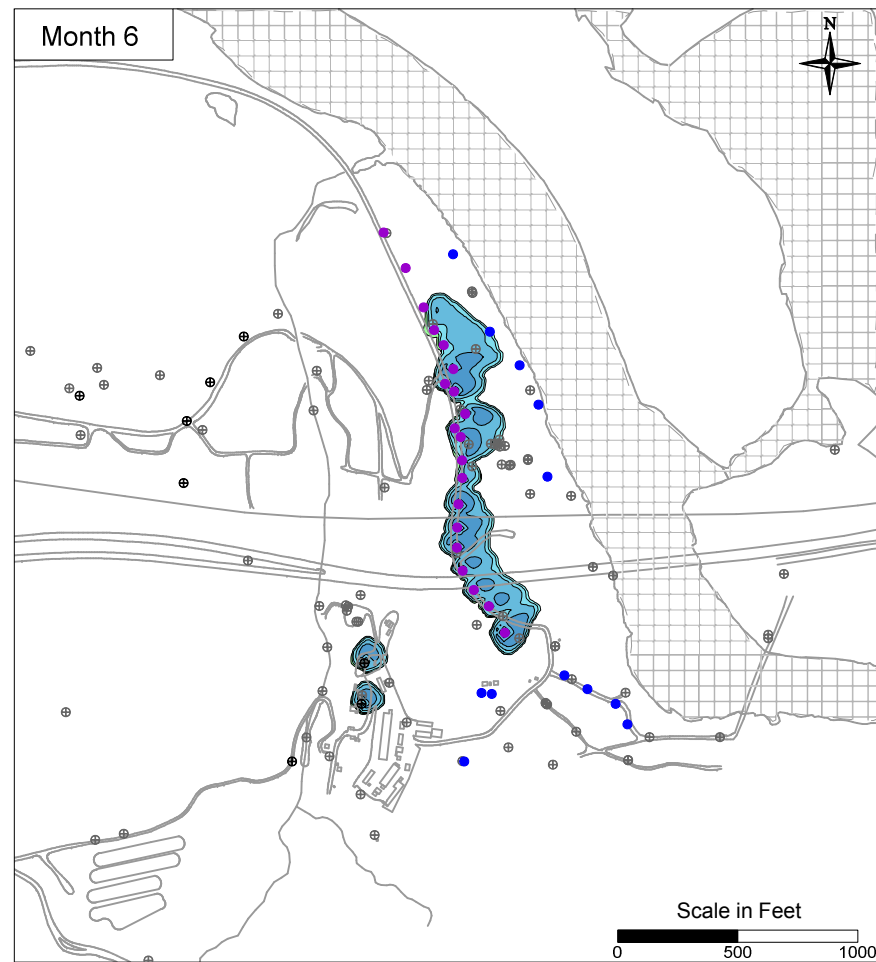




**LEGEND**

- IRZ WELLS
- ⊕ UPGRADE INJECTION WELLS
- EXTRACTION WELLS
- ⊕ MONITORING WELLS





**LEGEND**

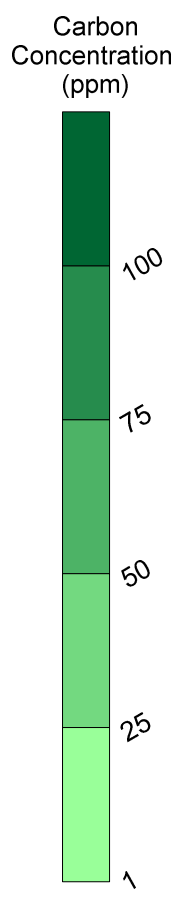
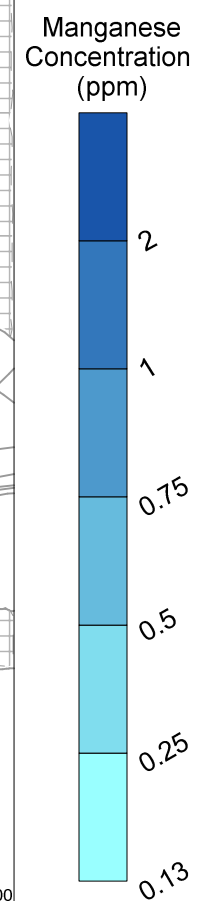
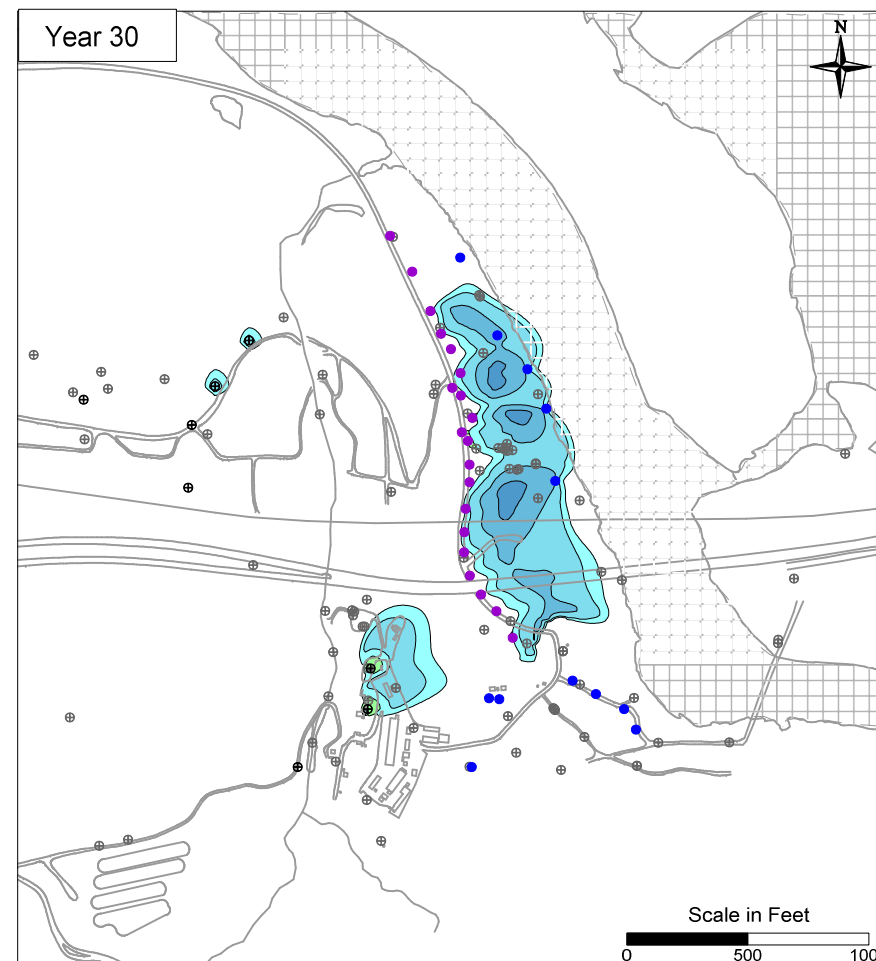
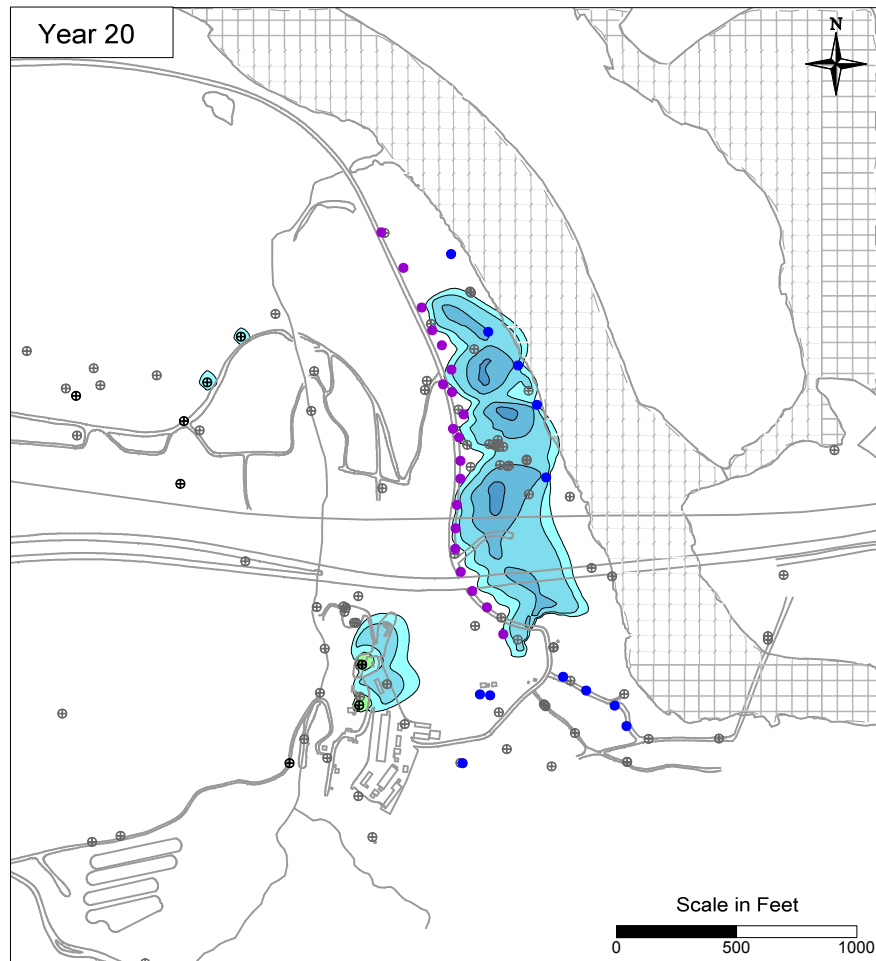
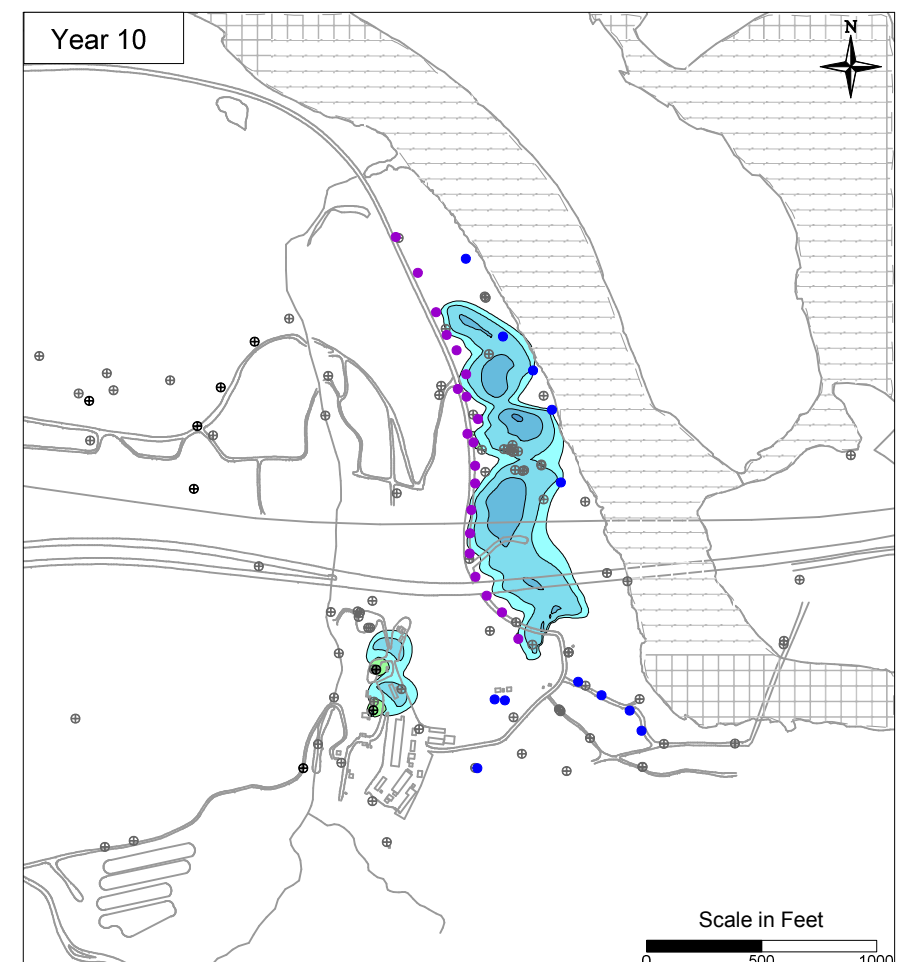
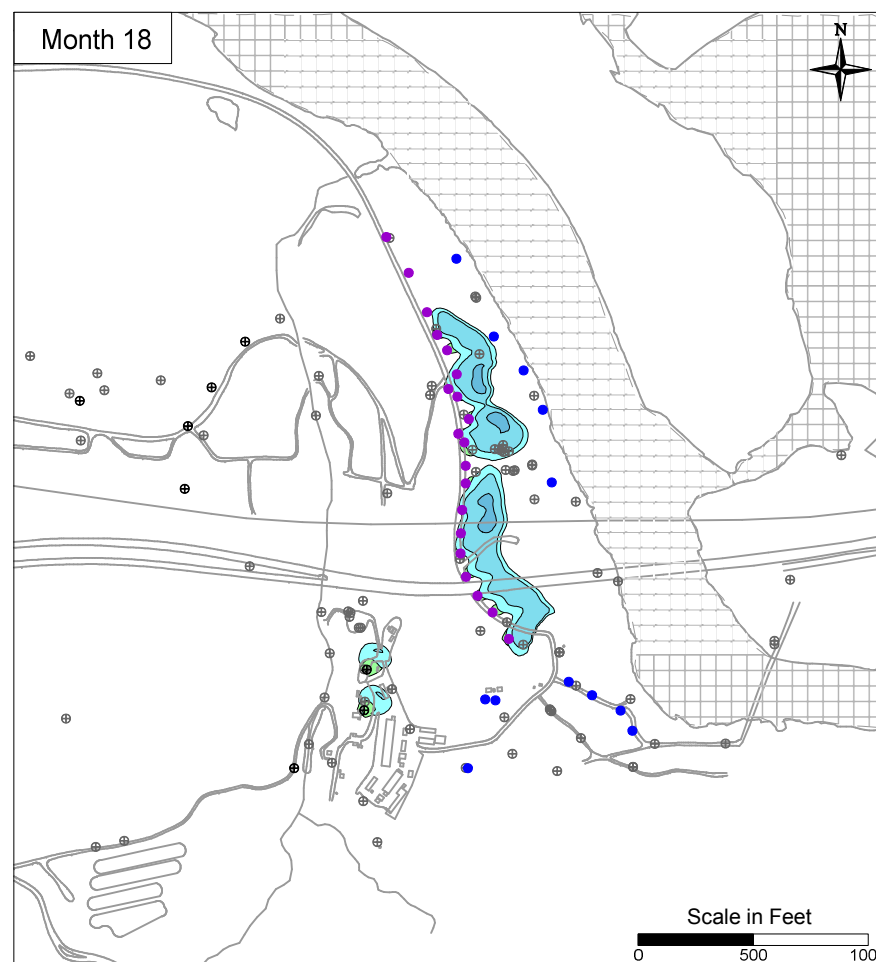
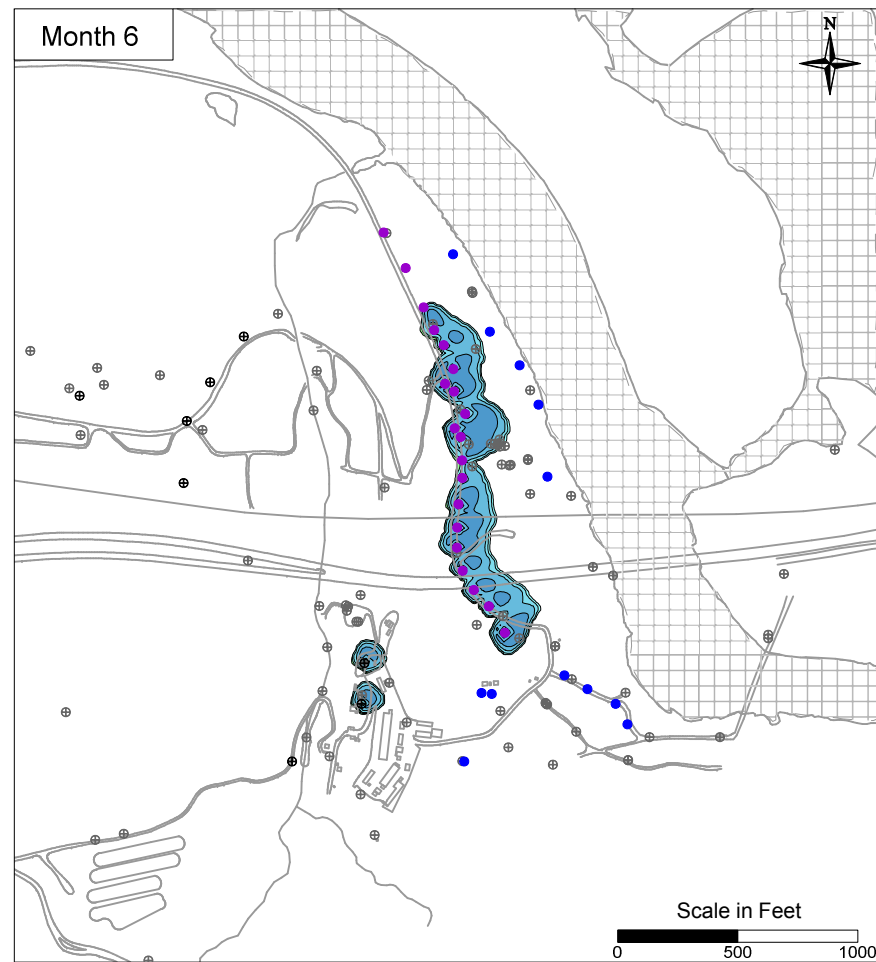
- IRZ WELLS
- ⊕ UPGRADE INJECTION WELLS
- EXTRACTION WELLS
- ⊕ MONITORING WELLS

PG&E  
TOPOCK COMPRESSOR STATION  
NEEDLES, CALIFORNIA  
MODELING APPENDIX

SIMULATED IRZ GENERATED MANGANESE  
BYPRODUCT TRANSPORT RESULTS IN  
MODEL LAYER 2



FIGURE  
7.2-2



**LEGEND**

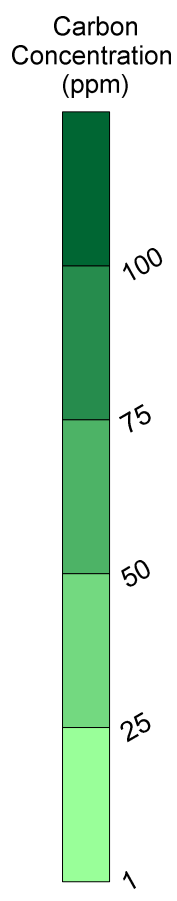
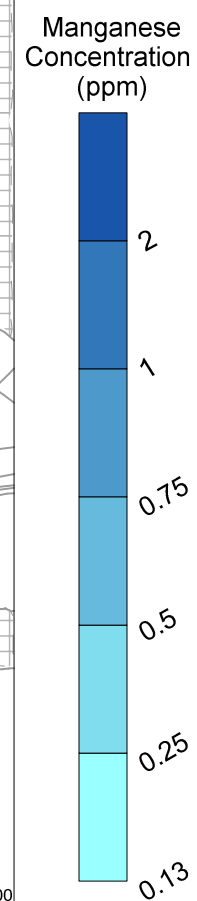
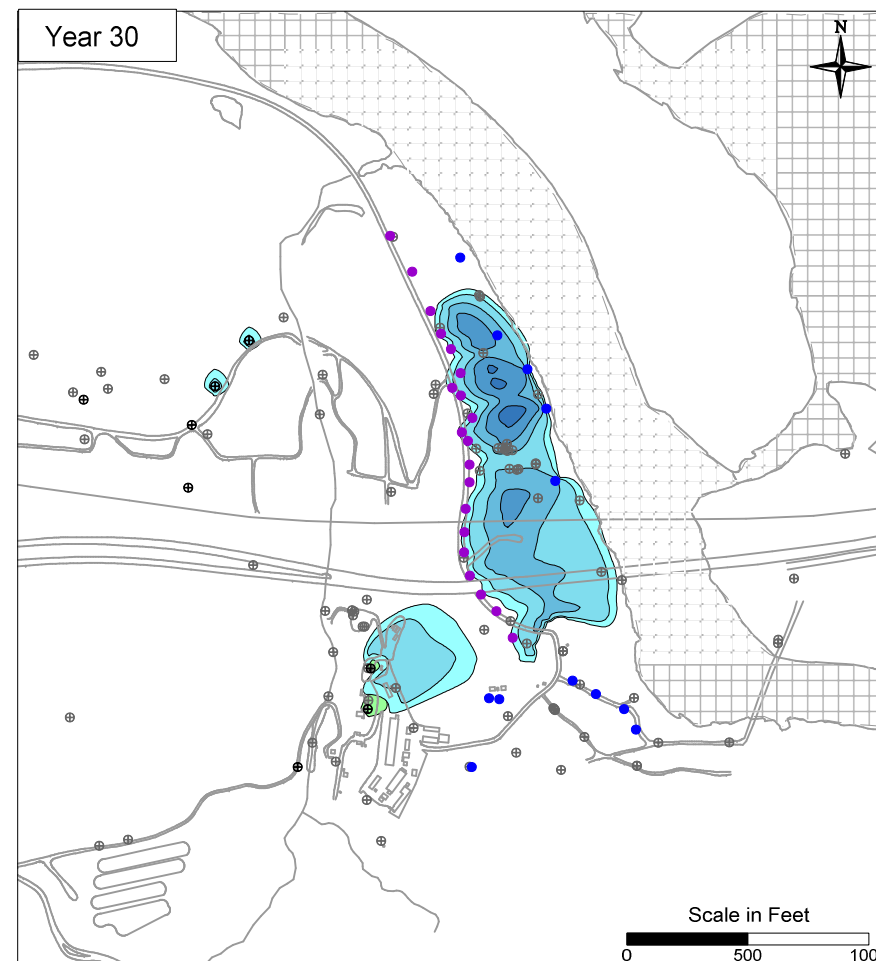
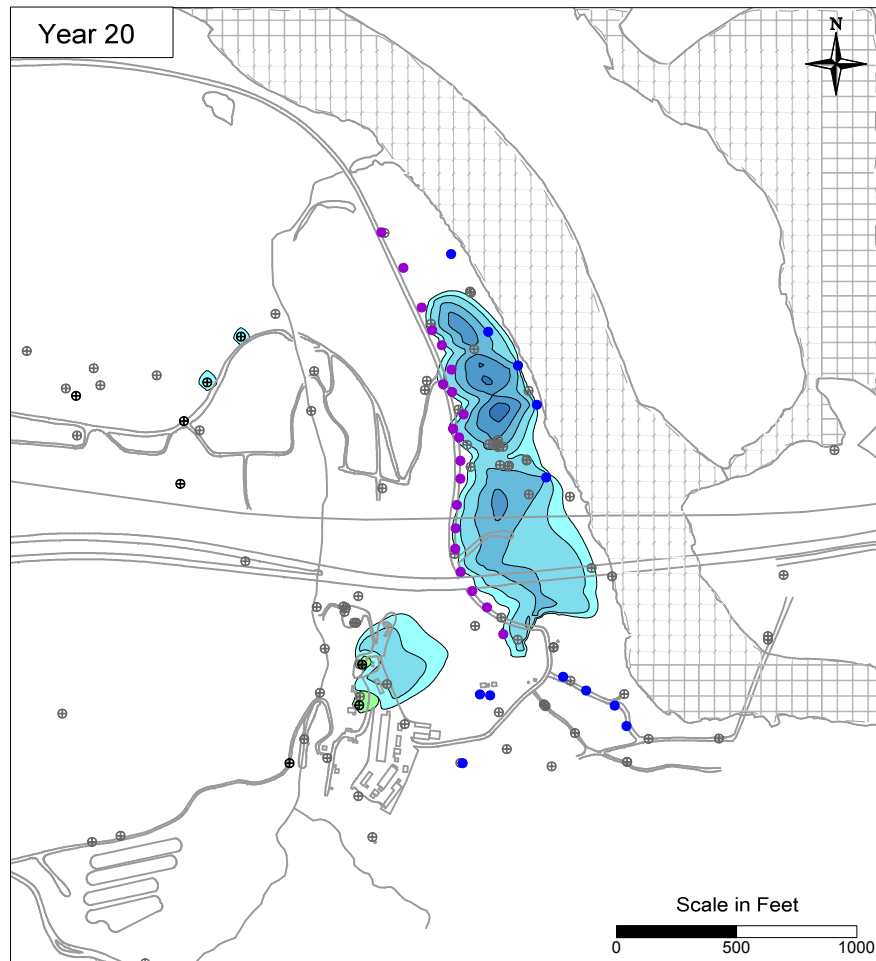
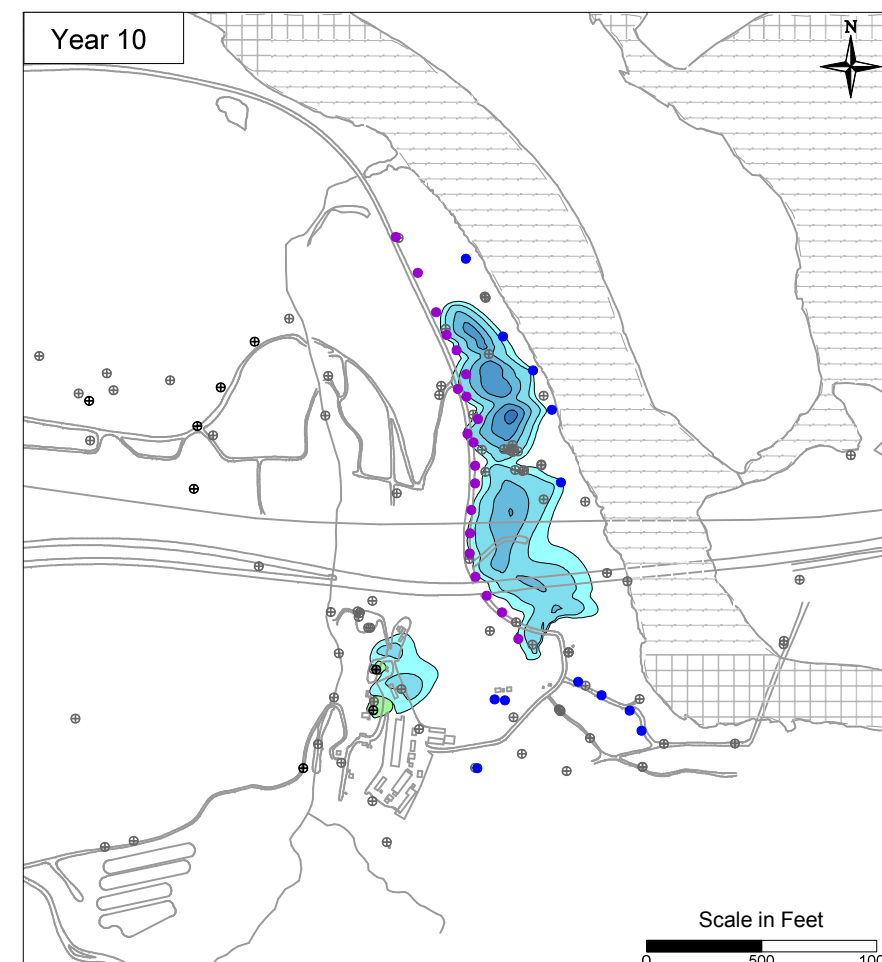
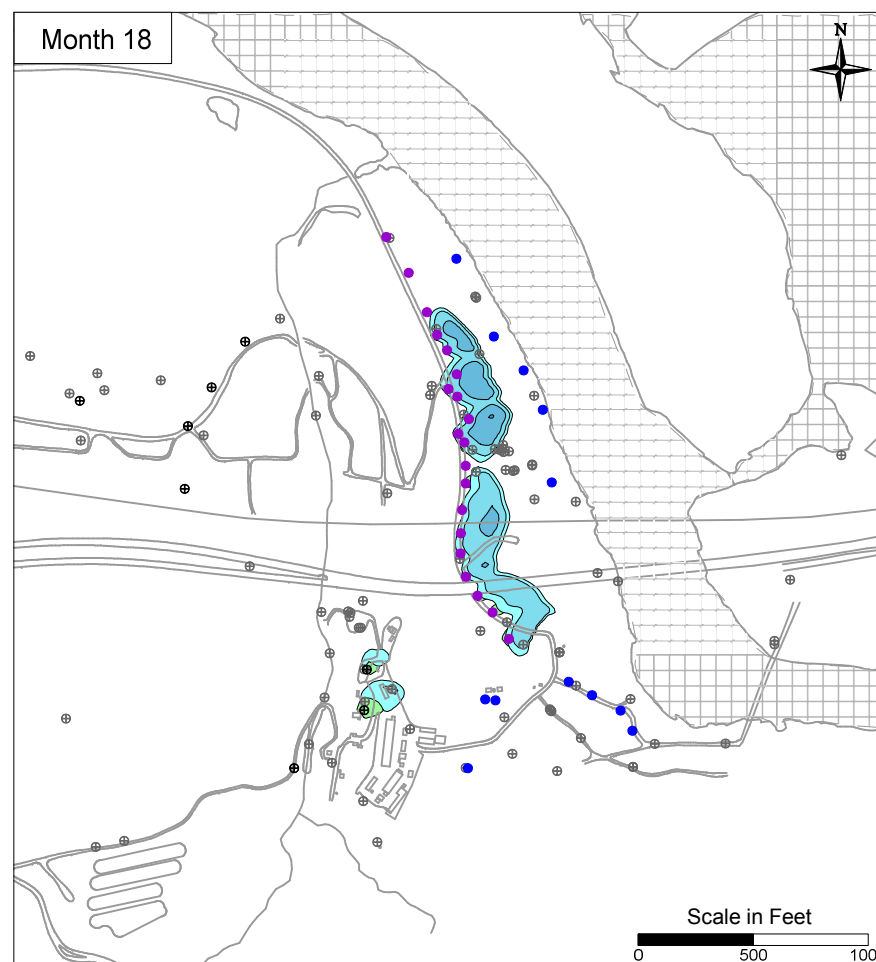
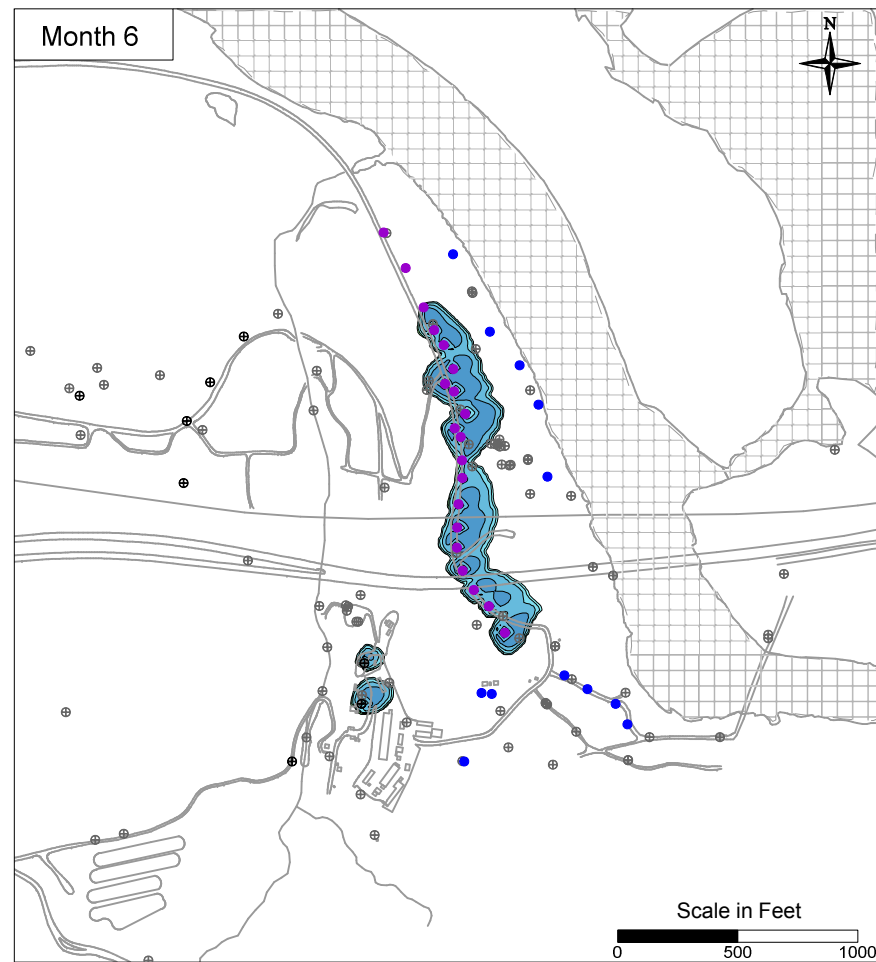
- IRZ WELLS
- ⊕ UPGRADIENT INJECTION WELLS
- EXTRACTION WELLS
- ⊕ MONITORING WELLS

PG&E  
TOPOCK COMPRESSOR STATION  
NEEDLES, CALIFORNIA  
MODELING APPENDIX

SIMULATED IRZ GENERATED MANGANESE  
BYPRODUCT TRANSPORT RESULTS IN  
MODEL LAYER 3



FIGURE  
7.2-3



**LEGEND**

- IRZ WELLS
- ⊕ UPGRAIDENT INJECTION WELLS
- EXTRACTION WELLS
- ⊕ MONITORING WELLS

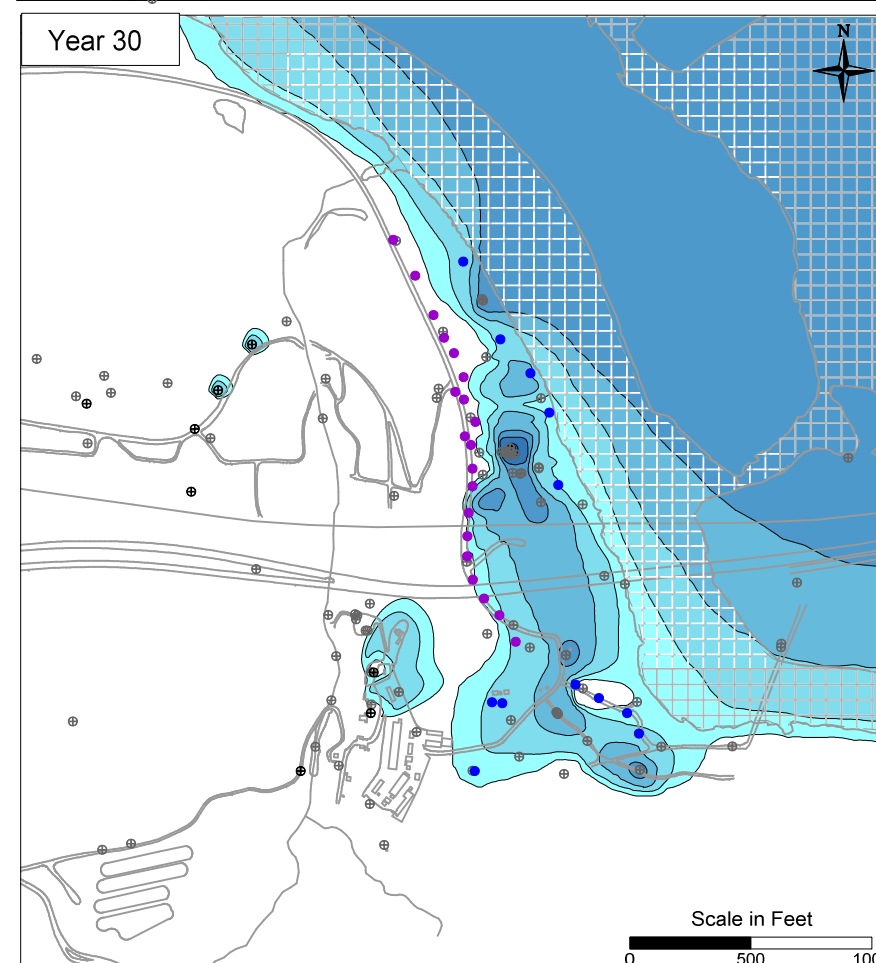
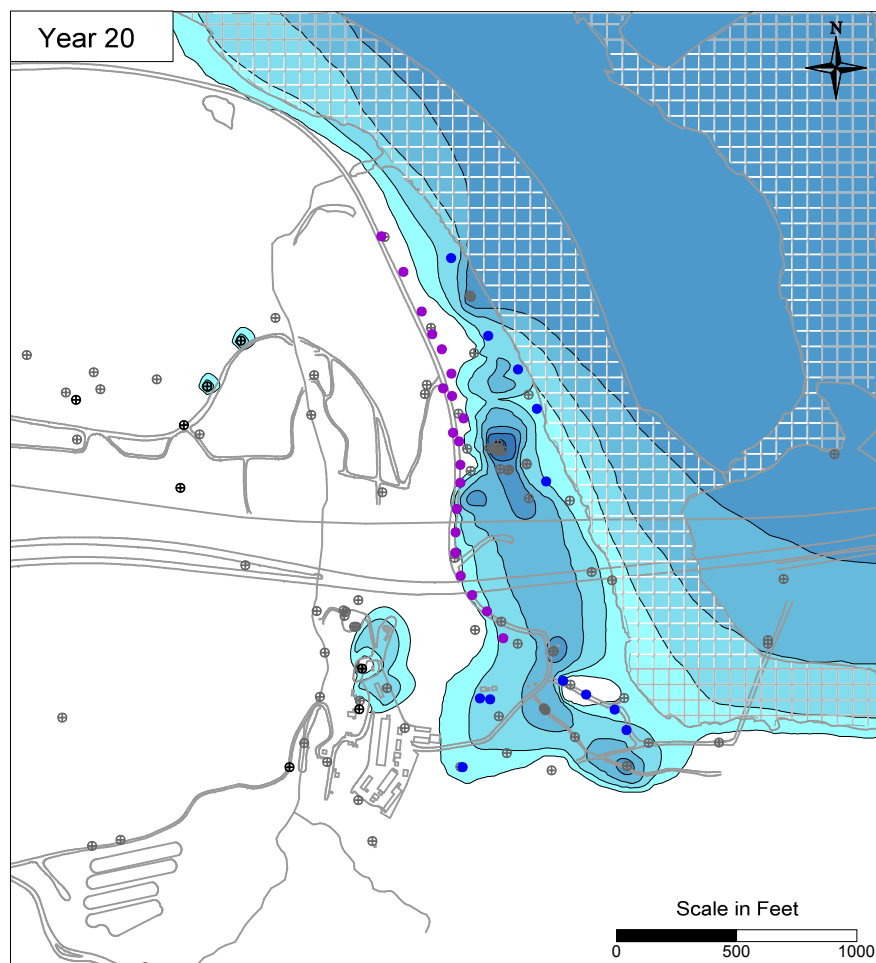
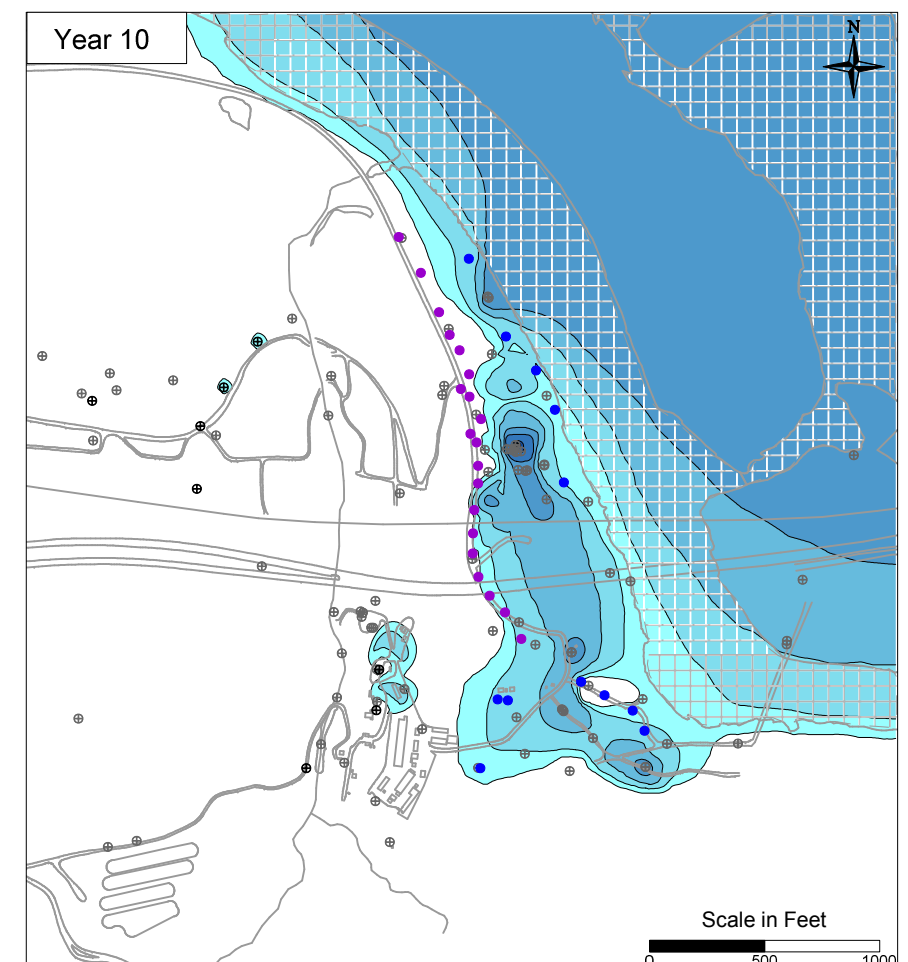
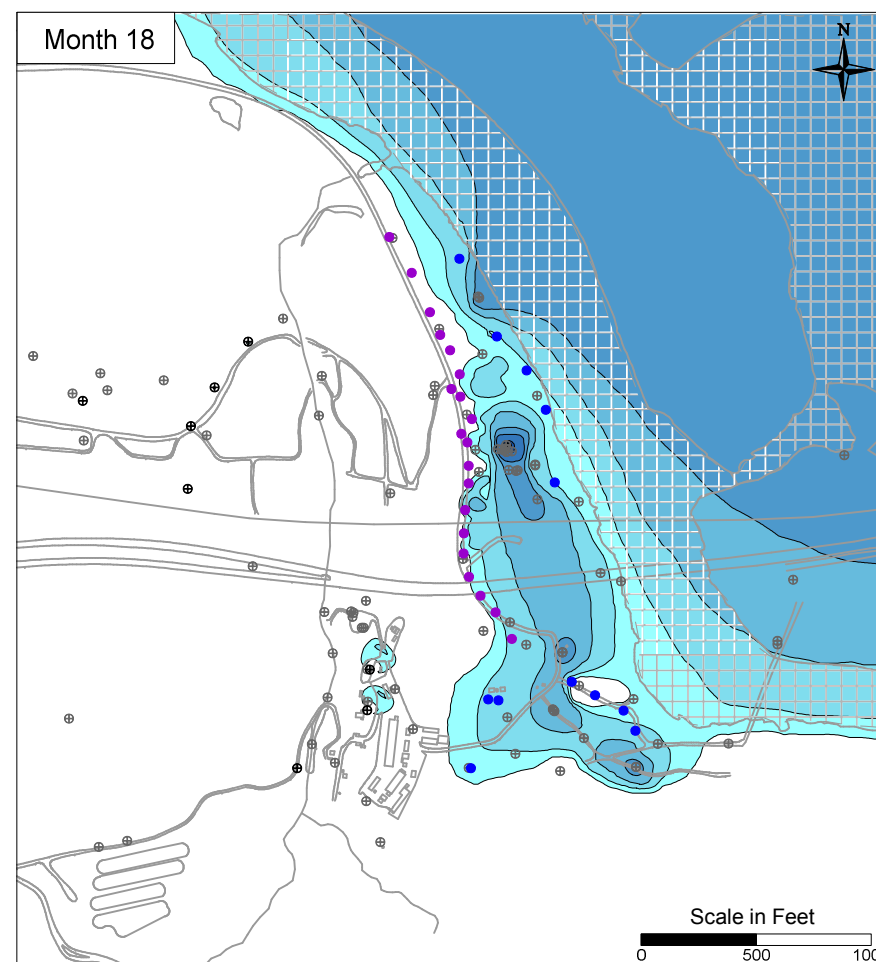
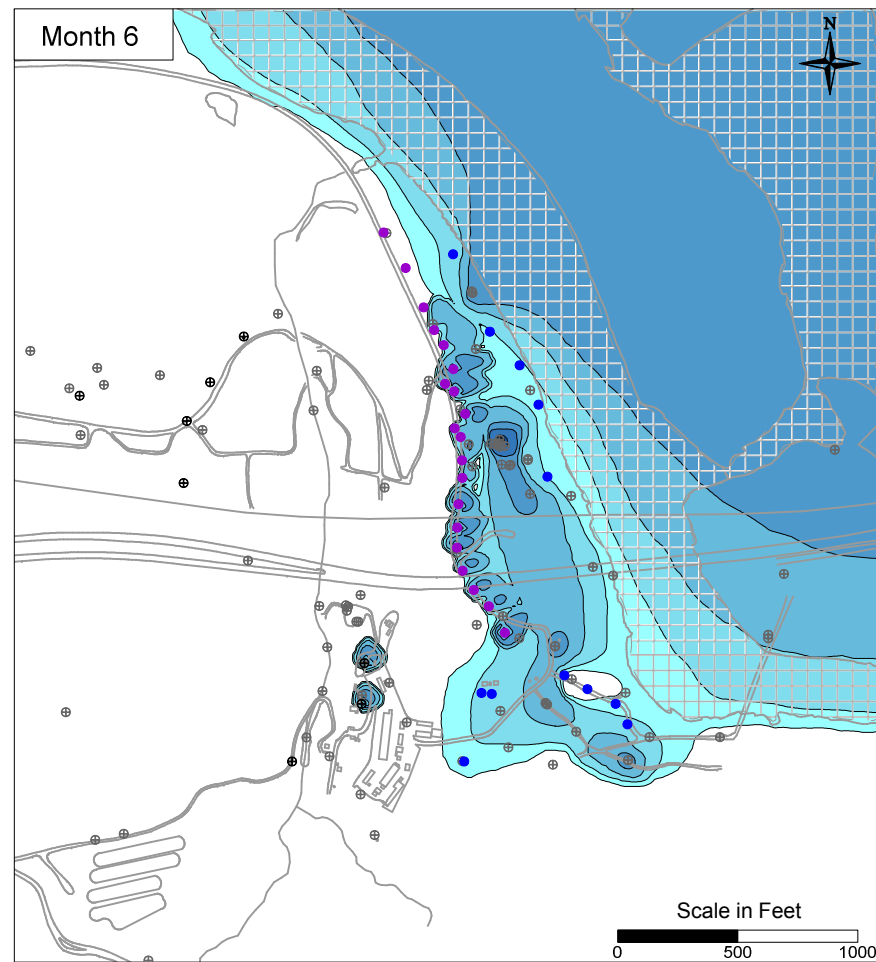
PG&E  
TOPOCK COMPRESSOR STATION  
NEEDLES, CALIFORNIA  
MODELING APPENDIX

SIMULATED IRZ GENERATED MANGANESE  
BYPRODUCT TRANSPORT RESULTS IN  
MODEL LAYER 4

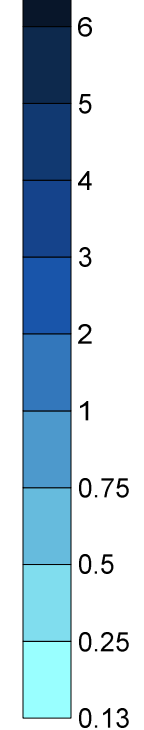


FIGURE  
7.2-4





Manganese  
Concentration  
(ppm)



**LEGEND**

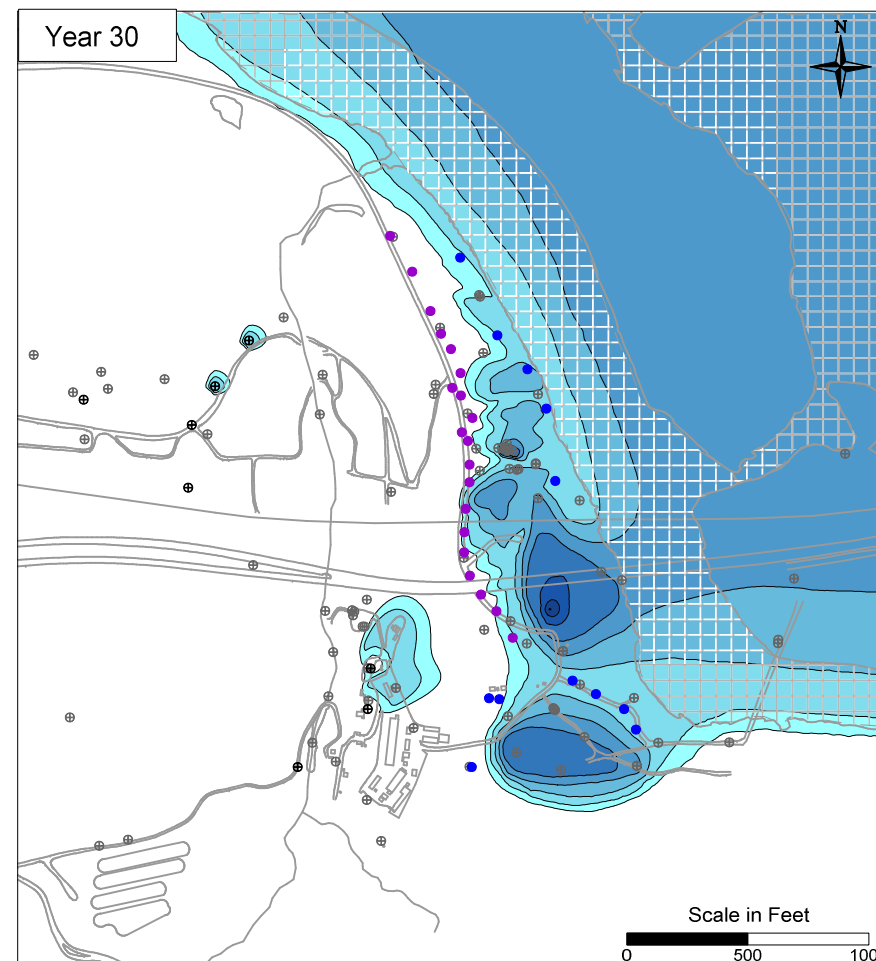
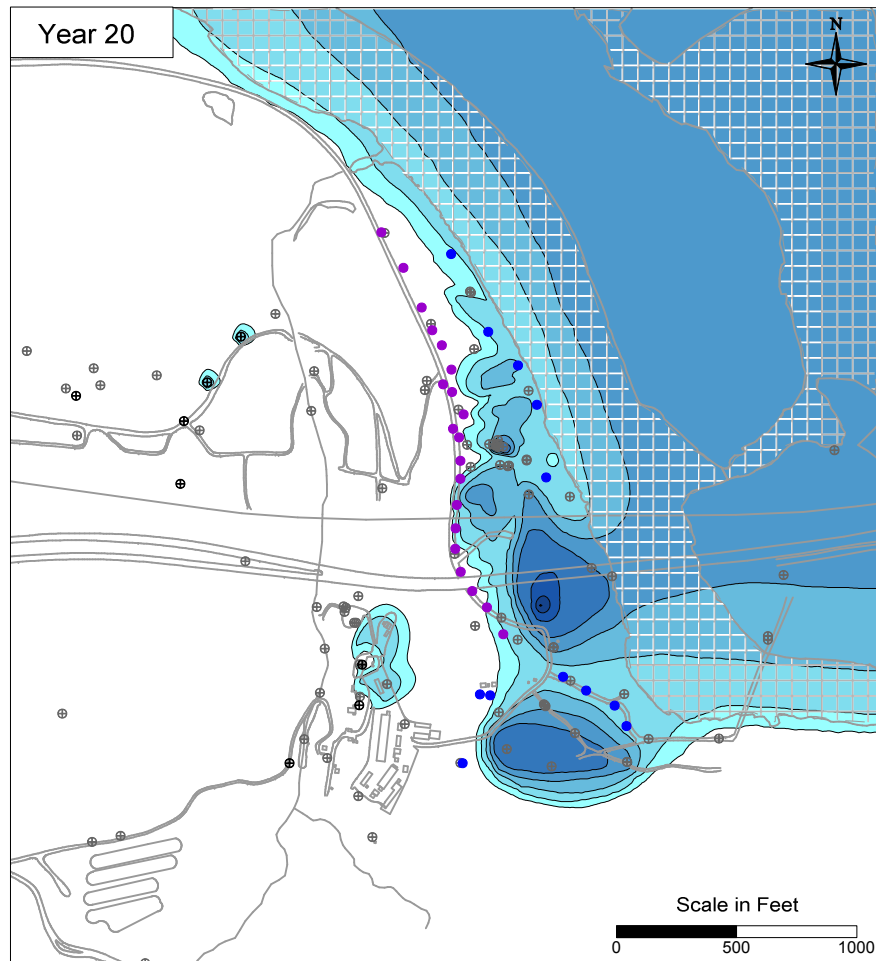
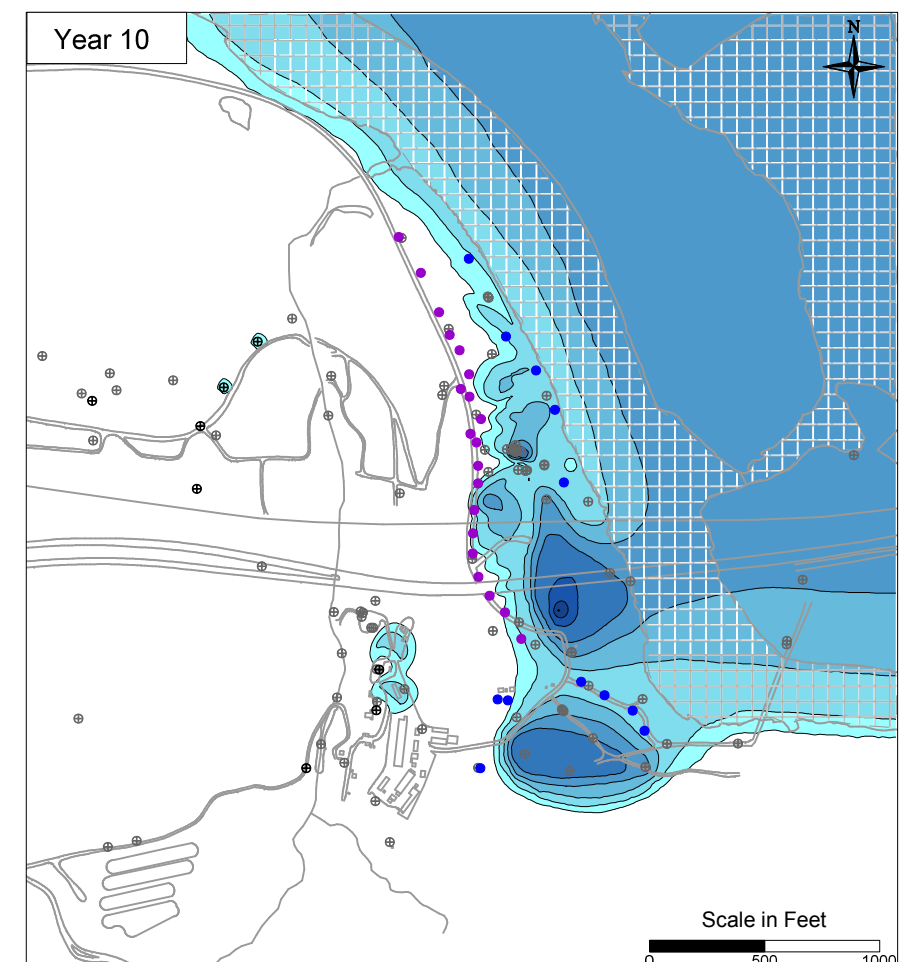
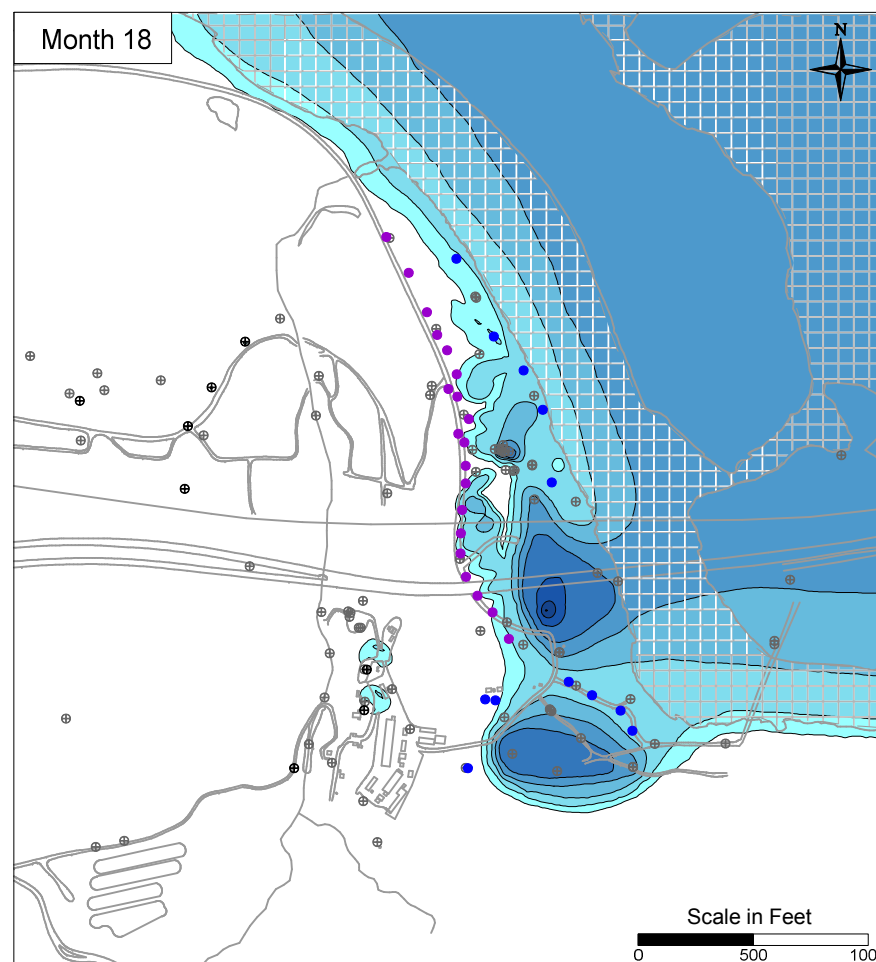
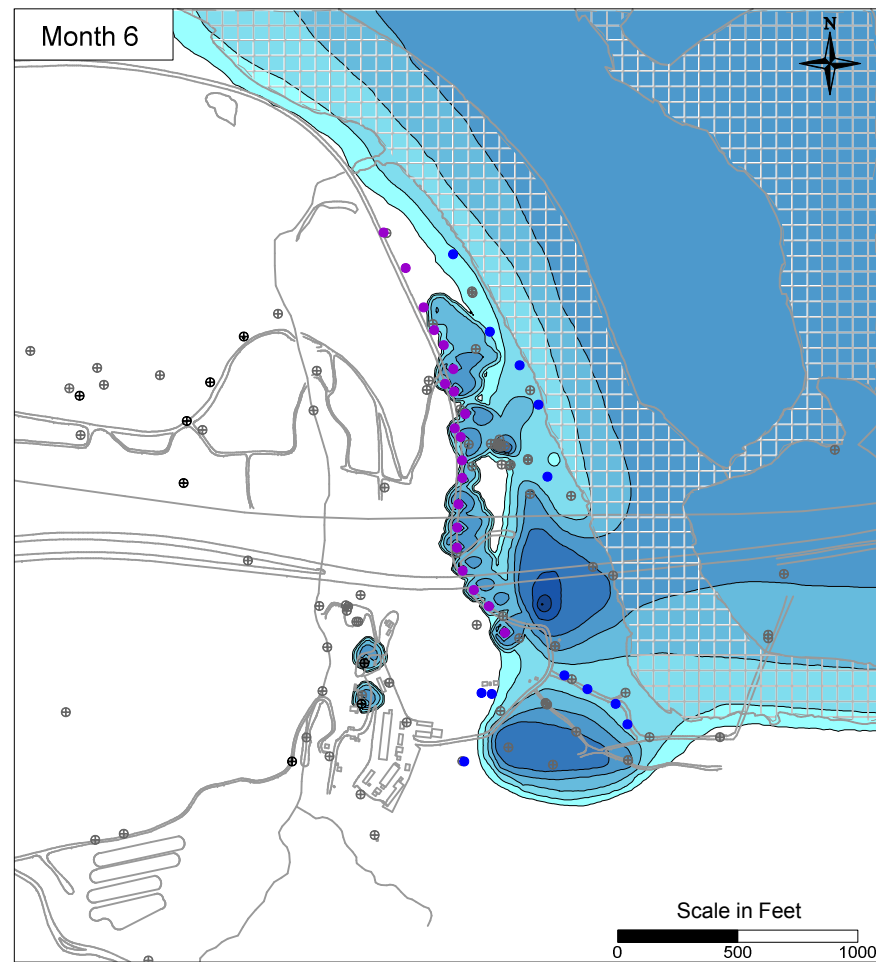
- IRZ WELLS
- ⊕ UPGRADE INJECTION WELLS
- EXTRACTION WELLS
- ⊕ MONITORING WELLS

PG&E  
TOPOCK COMPRESSOR STATION  
NEEDLES, CALIFORNIA  
MODELING APPENDIX

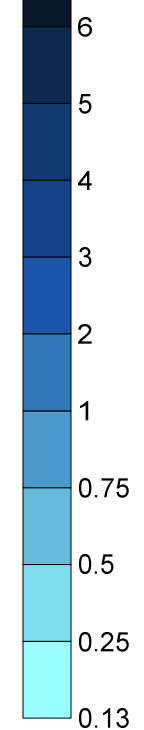
SIMULATED MAXIMUM IRZ GENERATED  
MANGANESE BYPRODUCT AND NATURALLY  
OCCURRING AVERAGE FLOODPLAIN  
MANGANESE IN MODEL LAYER 1



FIGURE  
7.2-5



Manganese  
Concentration  
(ppm)



**LEGEND**

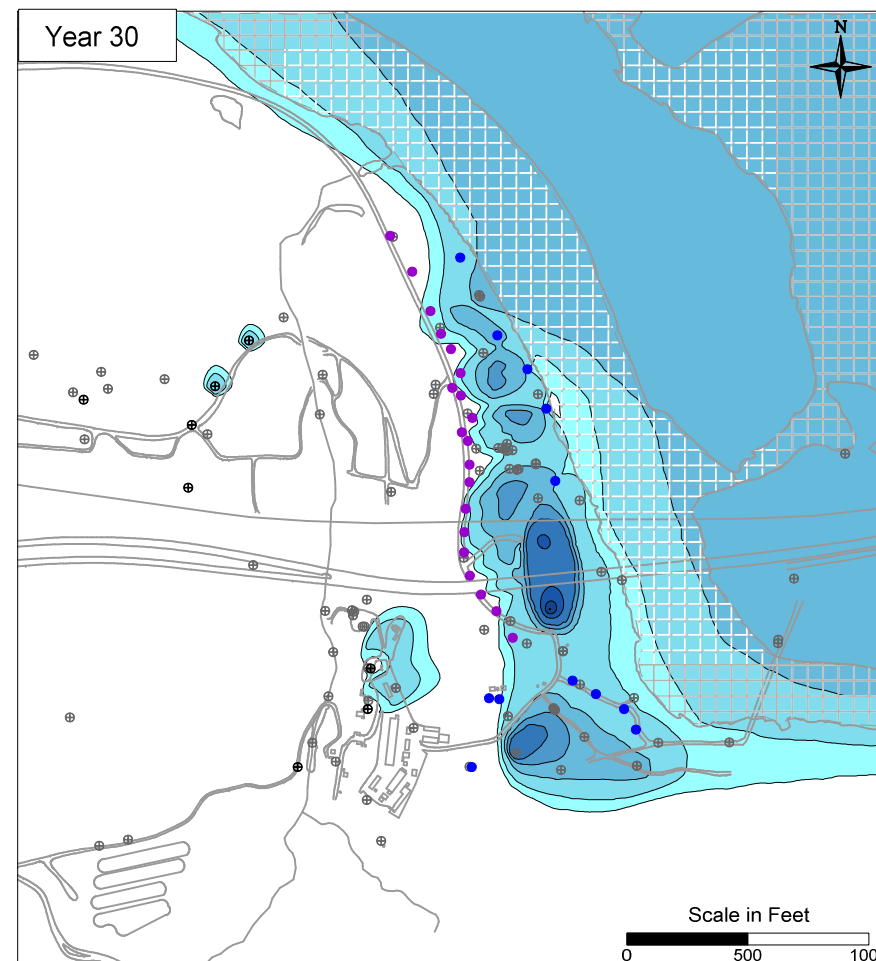
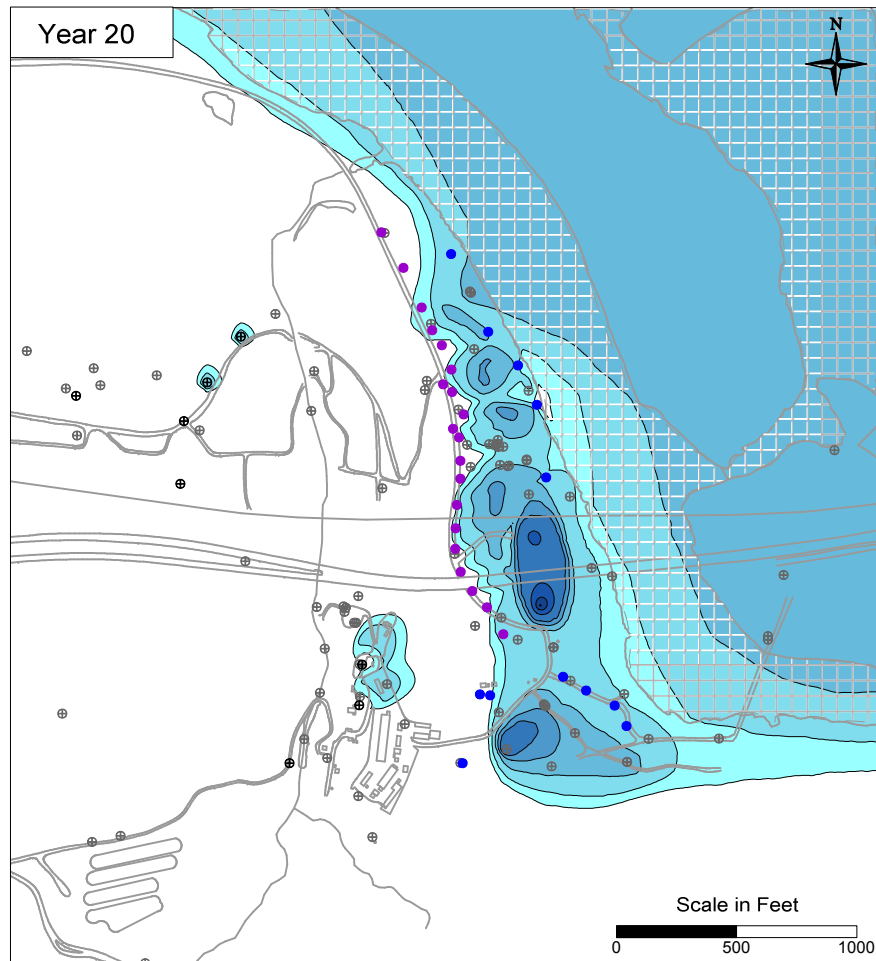
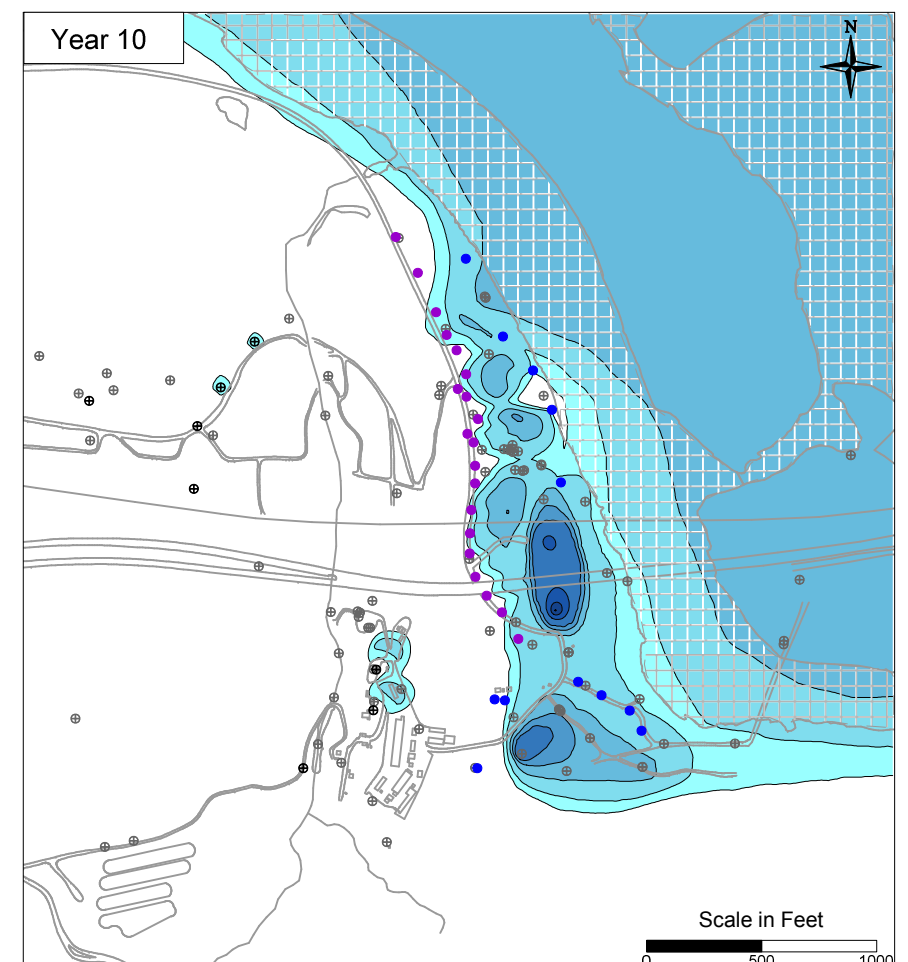
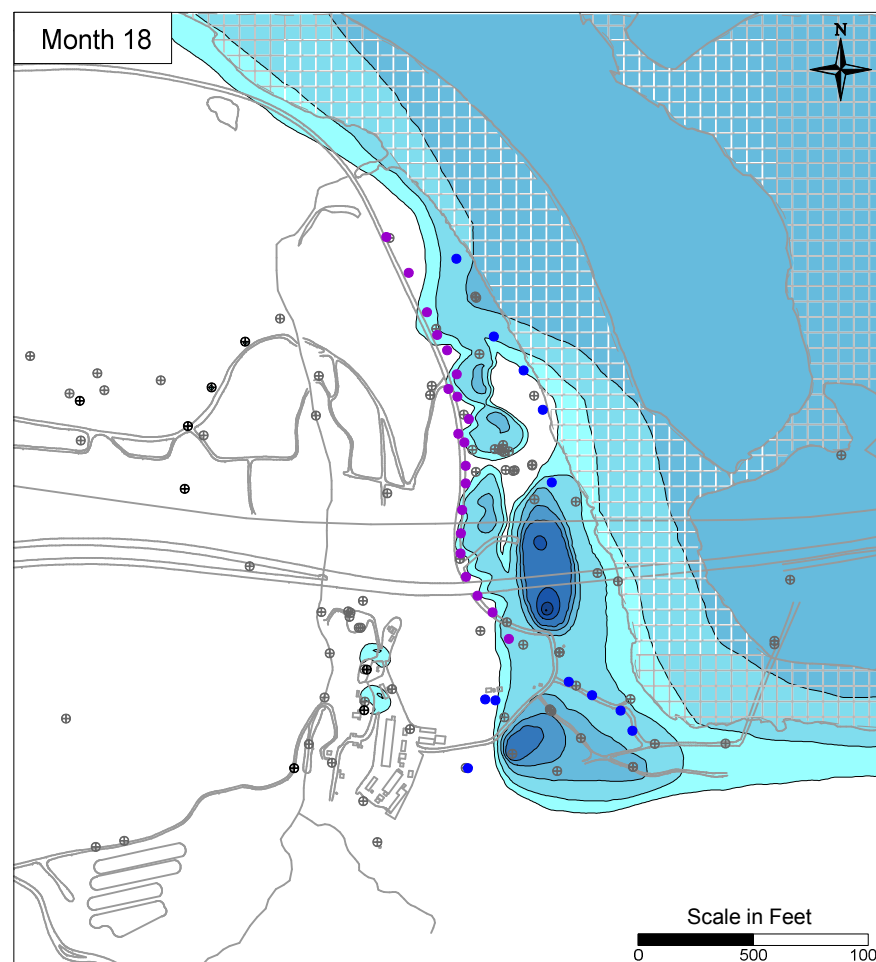
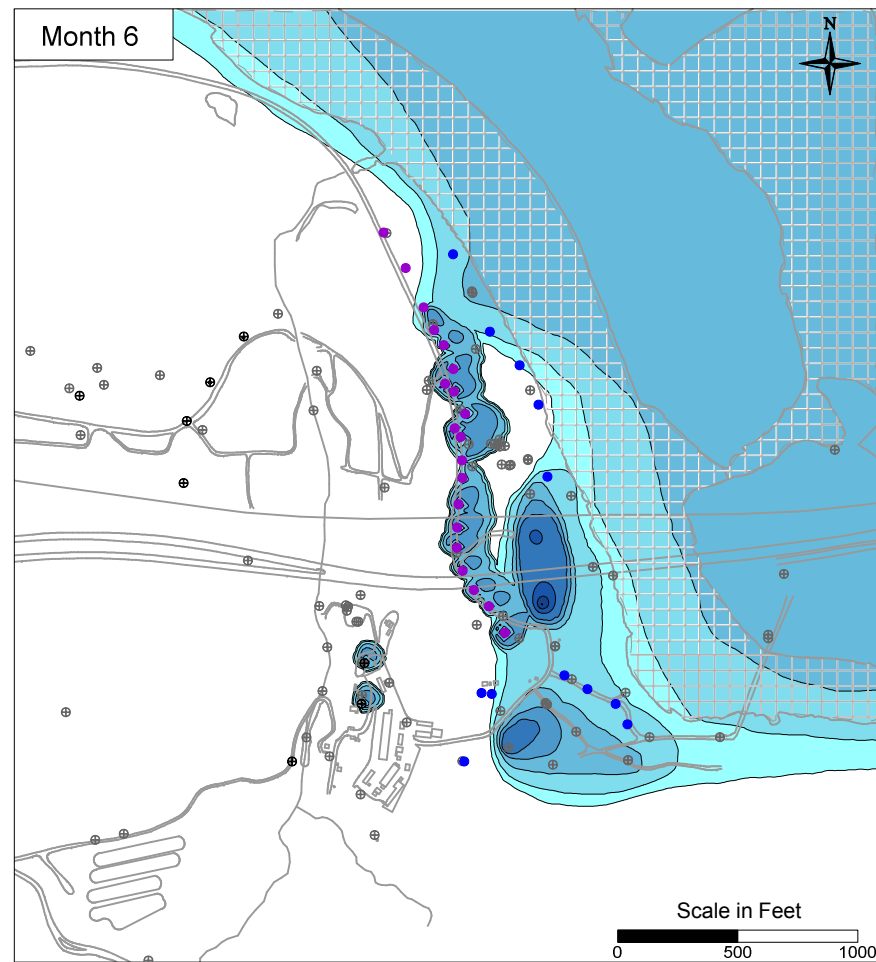
- IRZ WELLS
- ⊕ UPGRADIENT INJECTION WELLS
- EXTRACTION WELLS
- ⊕ MONITORING WELLS

PG&E  
TOPOCK COMPRESSOR STATION  
NEEDLES, CALIFORNIA  
MODELING APPENDIX  
SIMULATED MAXIMUM IRZ GENERATED  
MANGANESE BYPRODUCT AND NATURALLY  
OCCURRING AVERAGE FLOODPLAIN  
MANGANESE IN MODEL LAYER 2

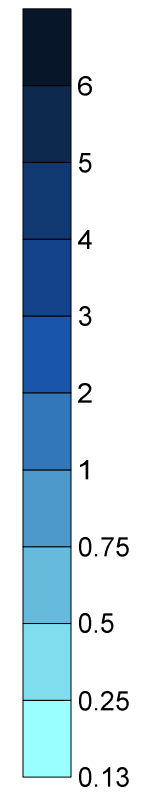


FIGURE  
7.2-6





Manganese  
Concentration  
(ppm)



**LEGEND**

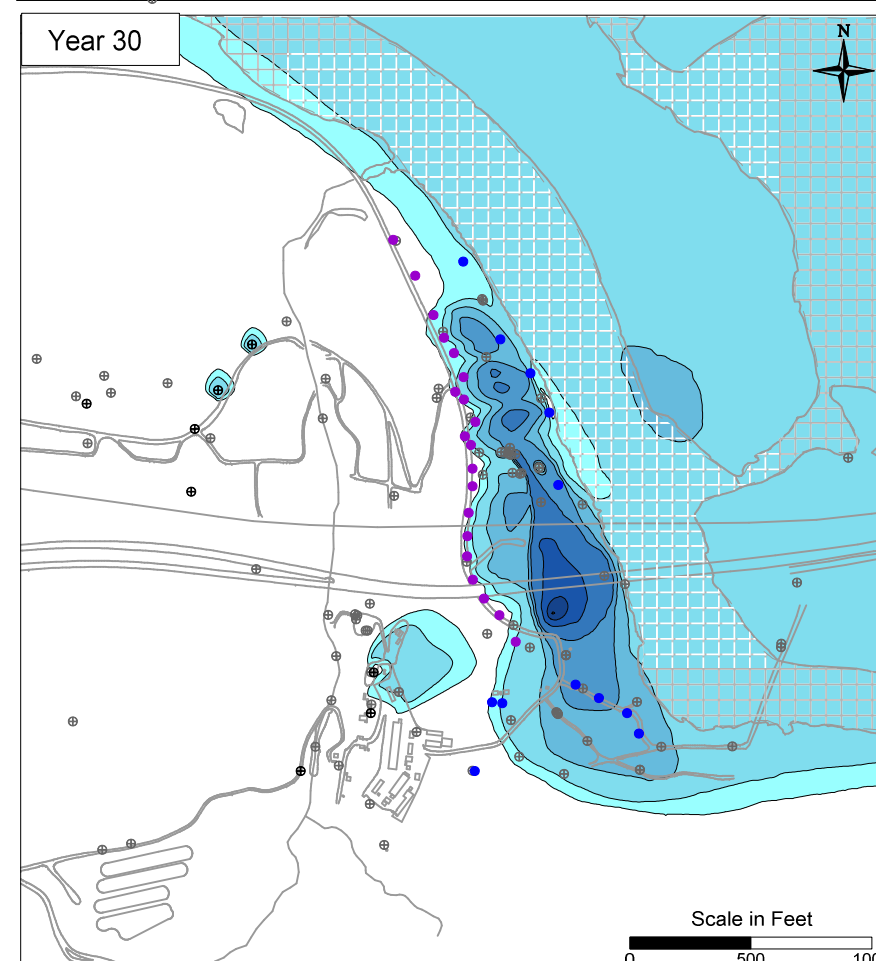
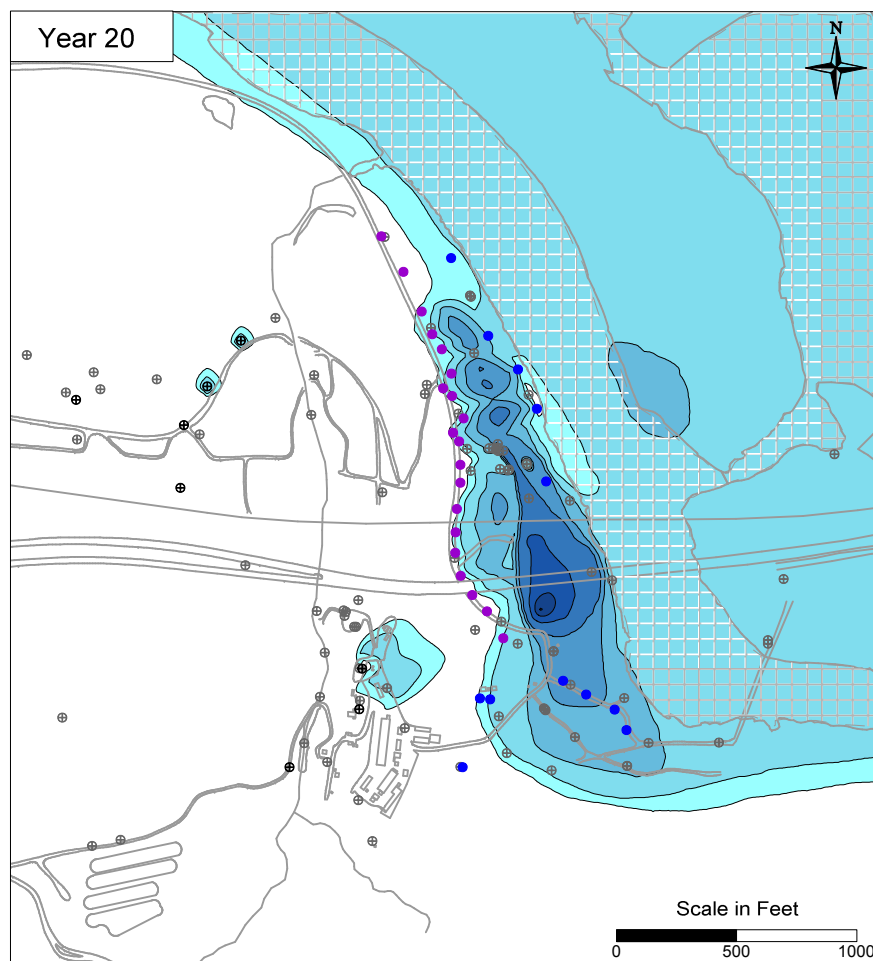
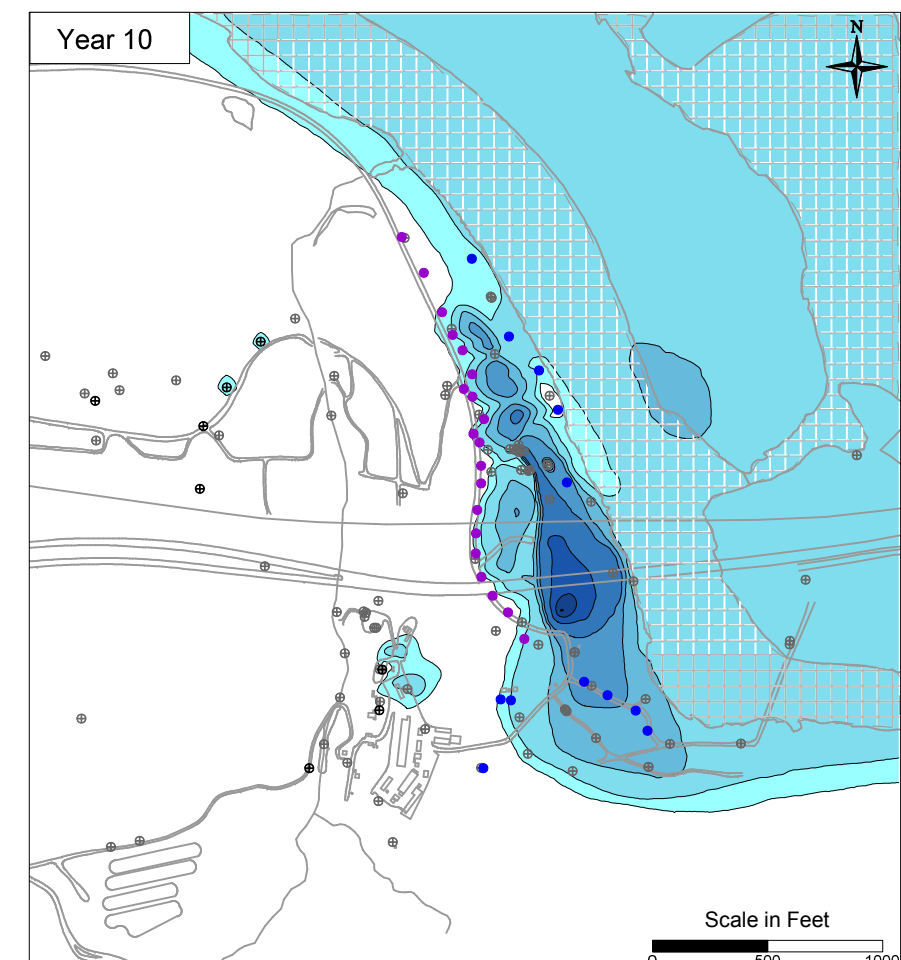
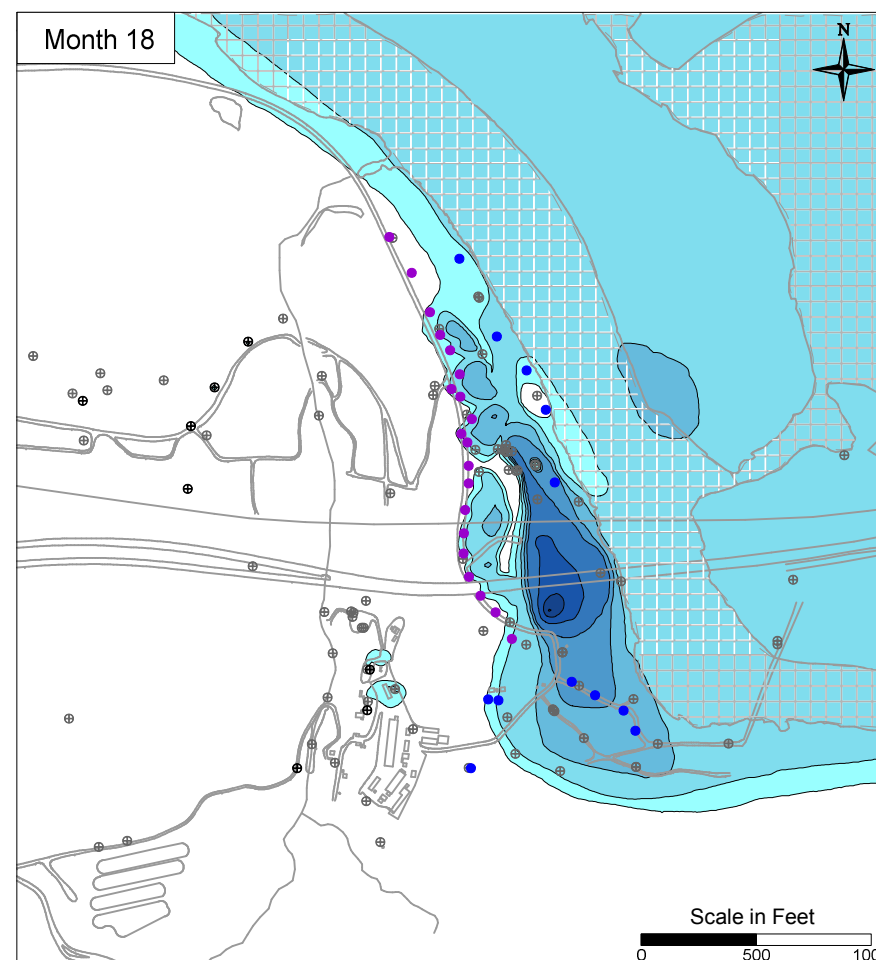
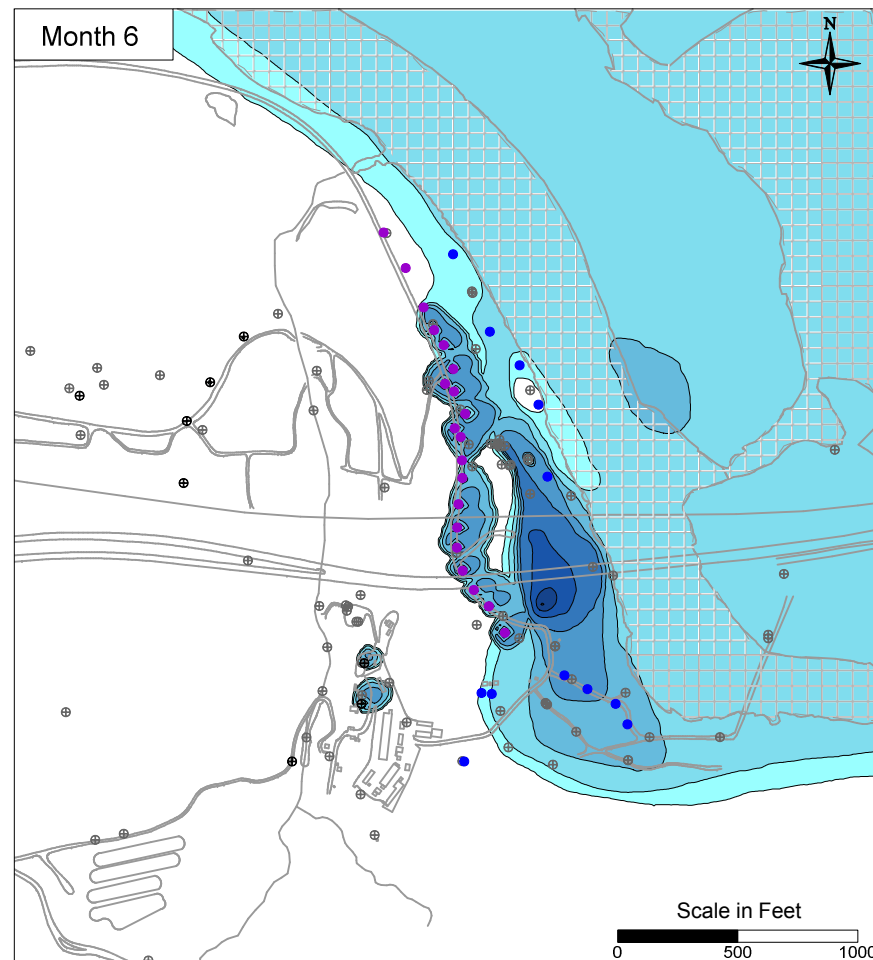
- IRZ WELLS
- ⊕ UPGRADE INJECTION WELLS
- EXTRACTION WELLS
- ⊕ MONITORING WELLS

PG&E  
TOPOCK COMPRESSOR STATION  
NEEDLES, CALIFORNIA  
MODELING APPENDIX  
SIMULATED MAXIMUM IRZ GENERATED  
MANGANESE BYPRODUCT AND NATURALLY  
OCCURRING AVERAGE FLOODPLAIN  
MANGANESE IN MODEL LAYER 3

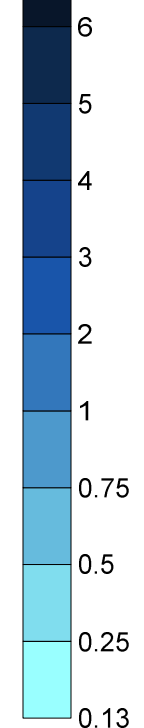


FIGURE  
7.2-7





Manganese  
Concentration  
(ppm)



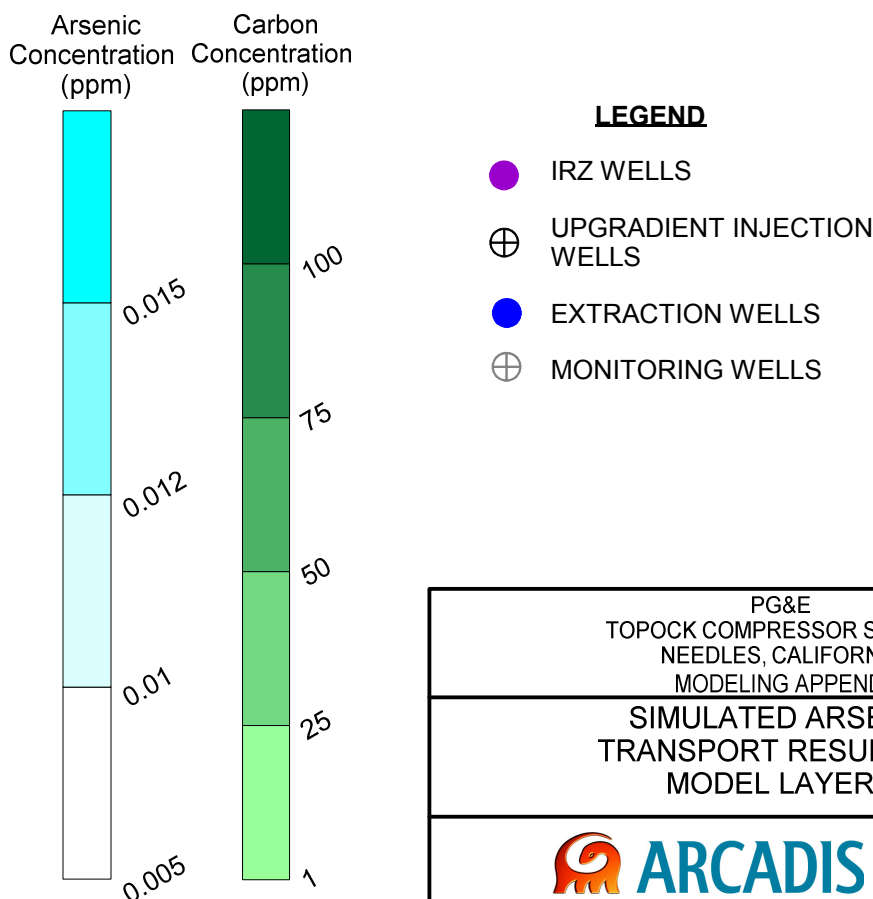
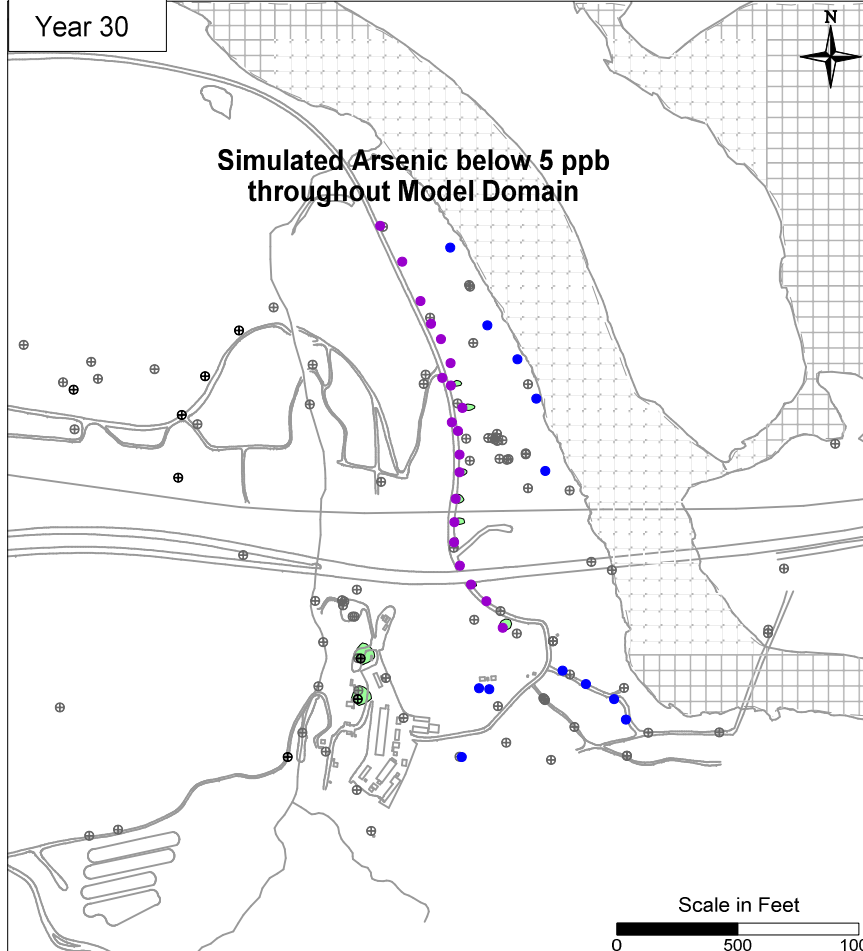
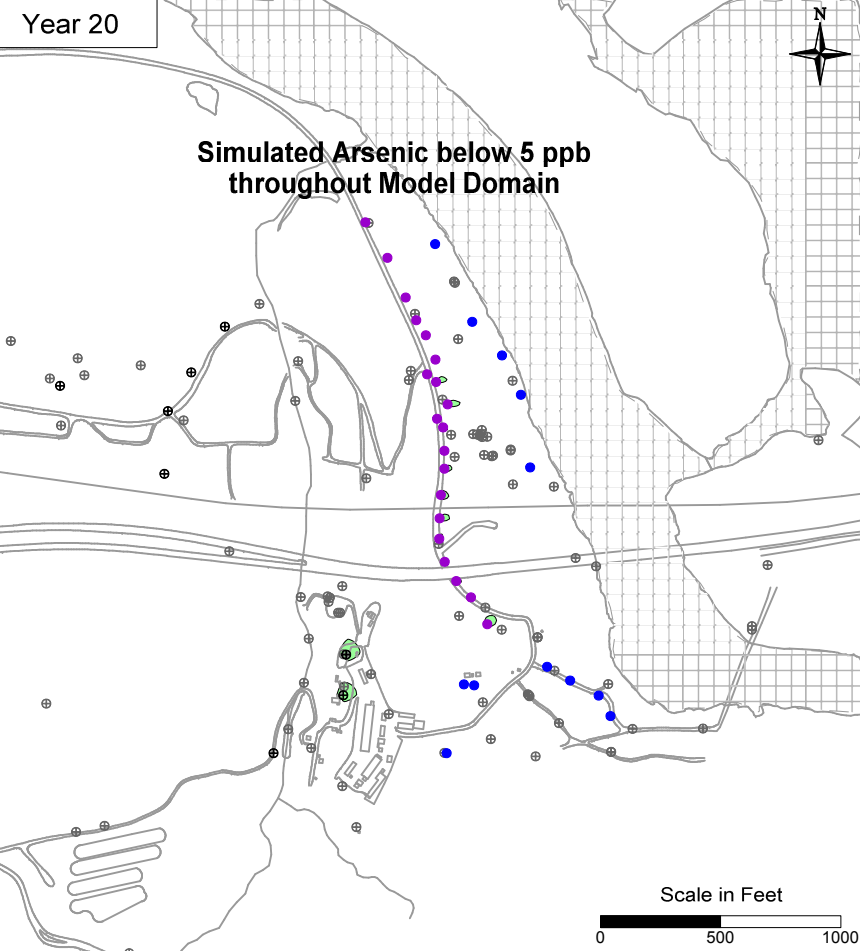
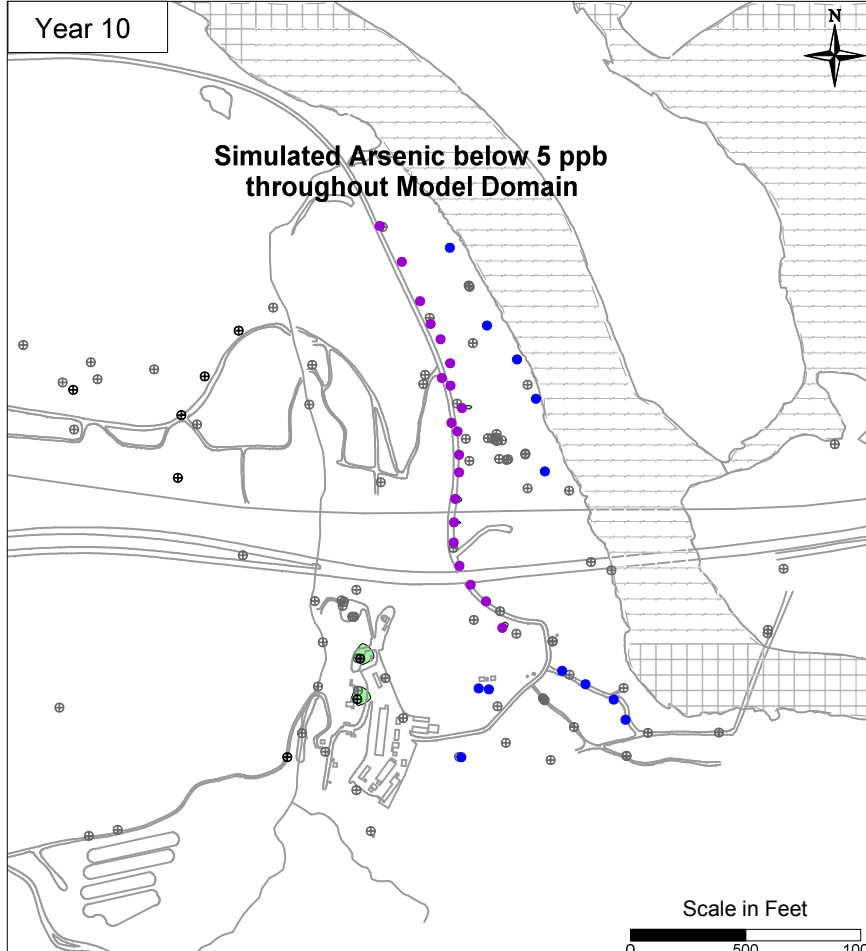
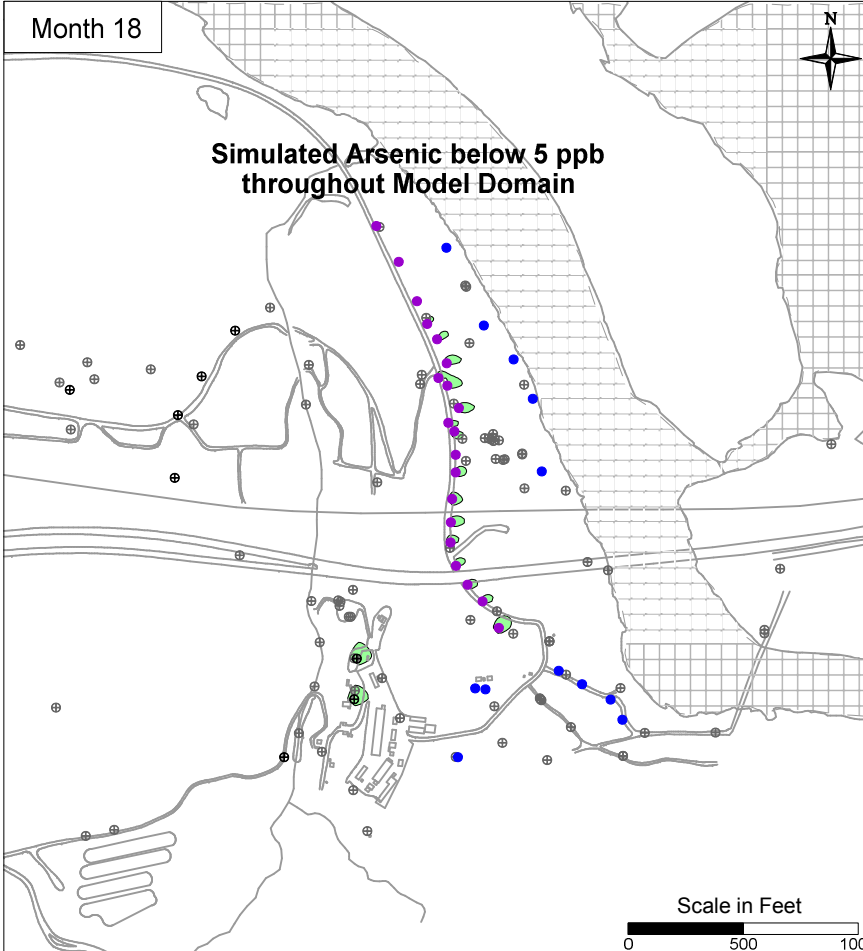
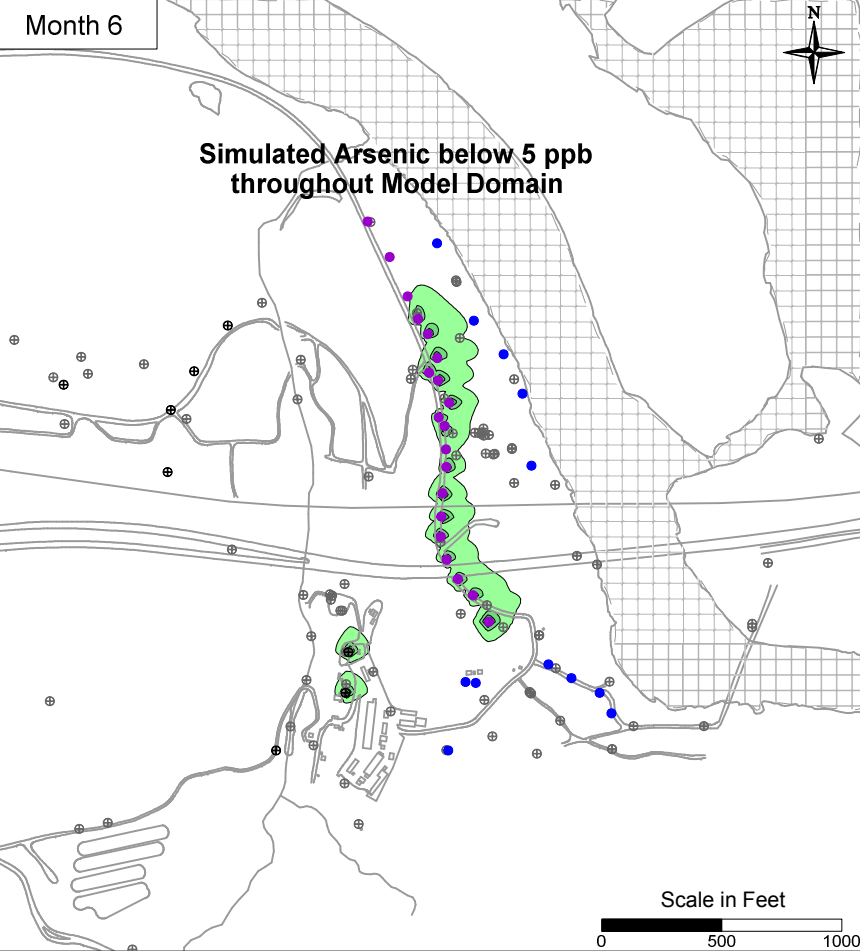
**LEGEND**

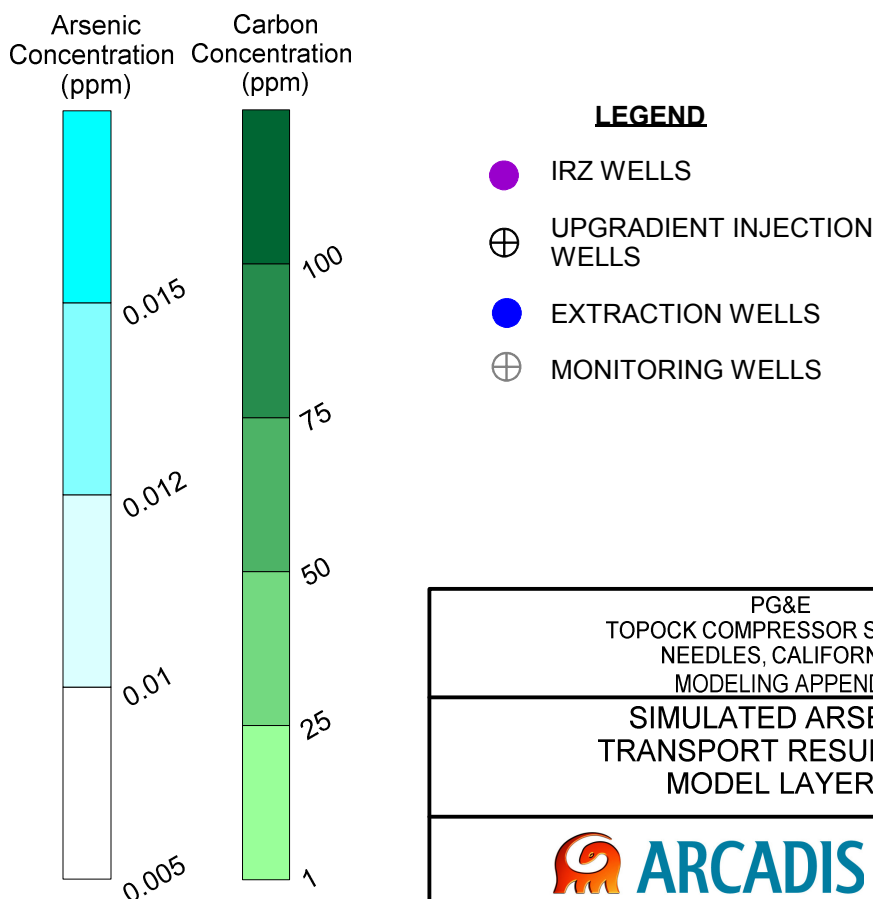
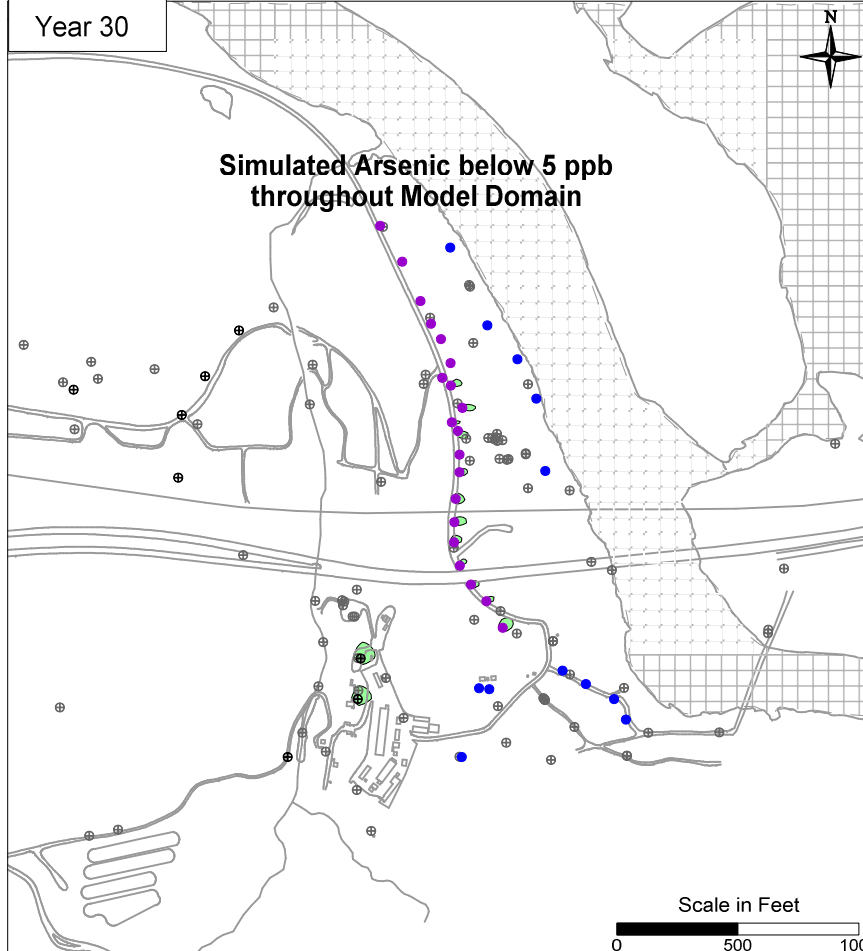
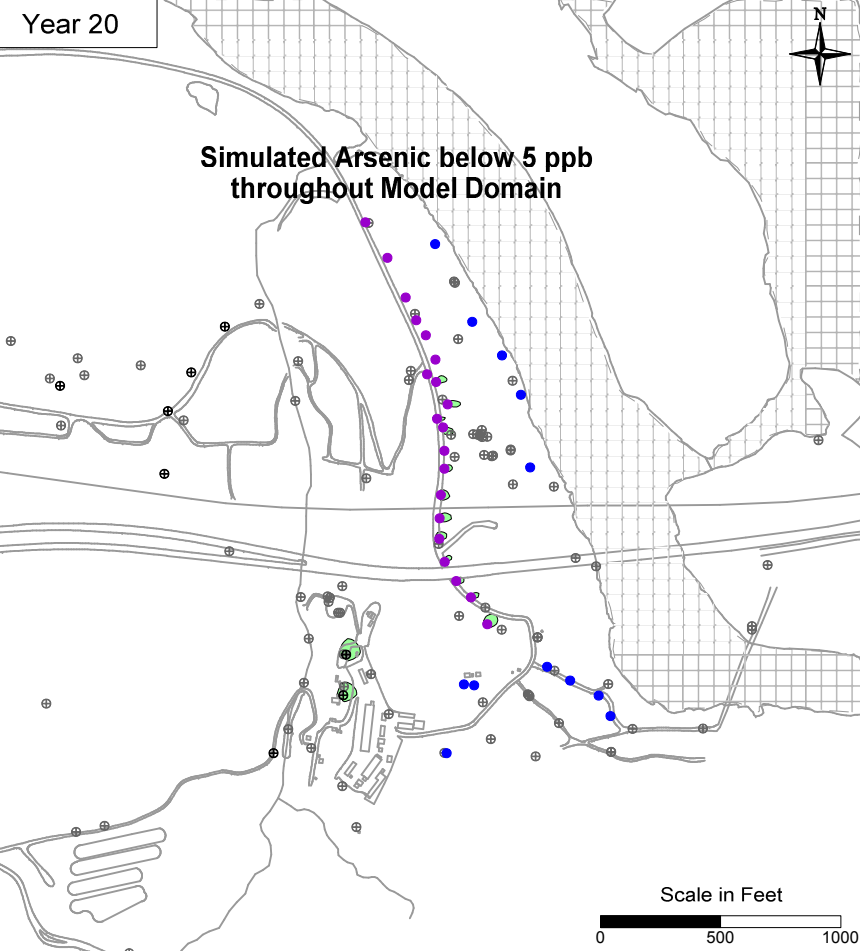
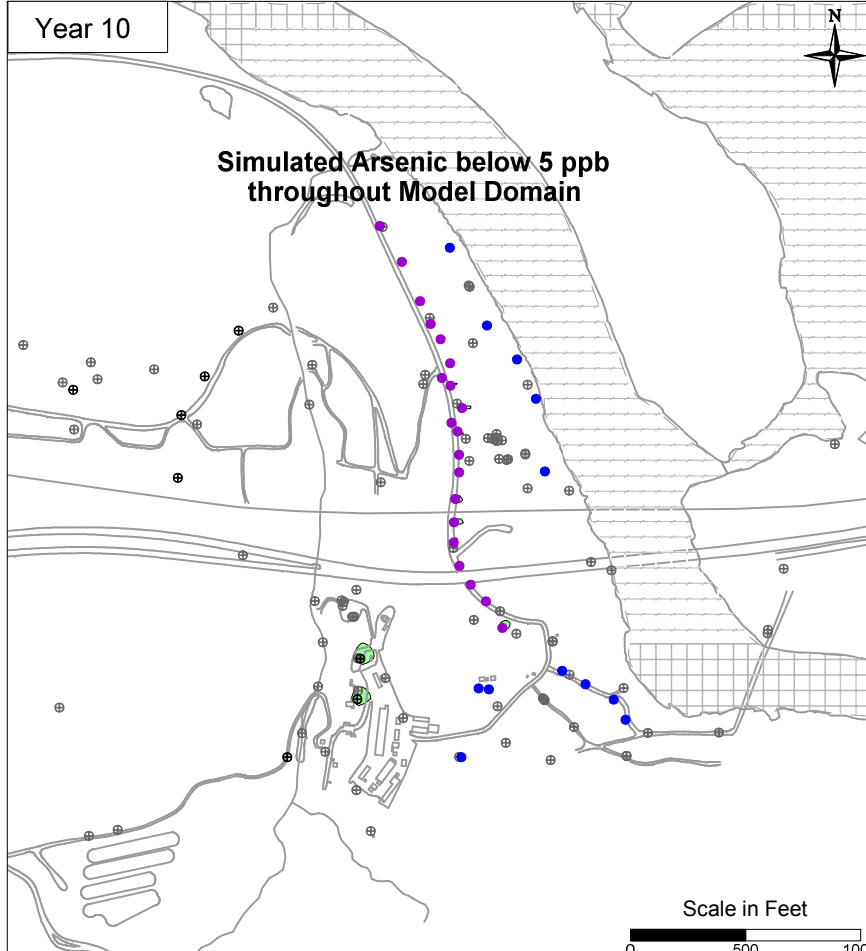
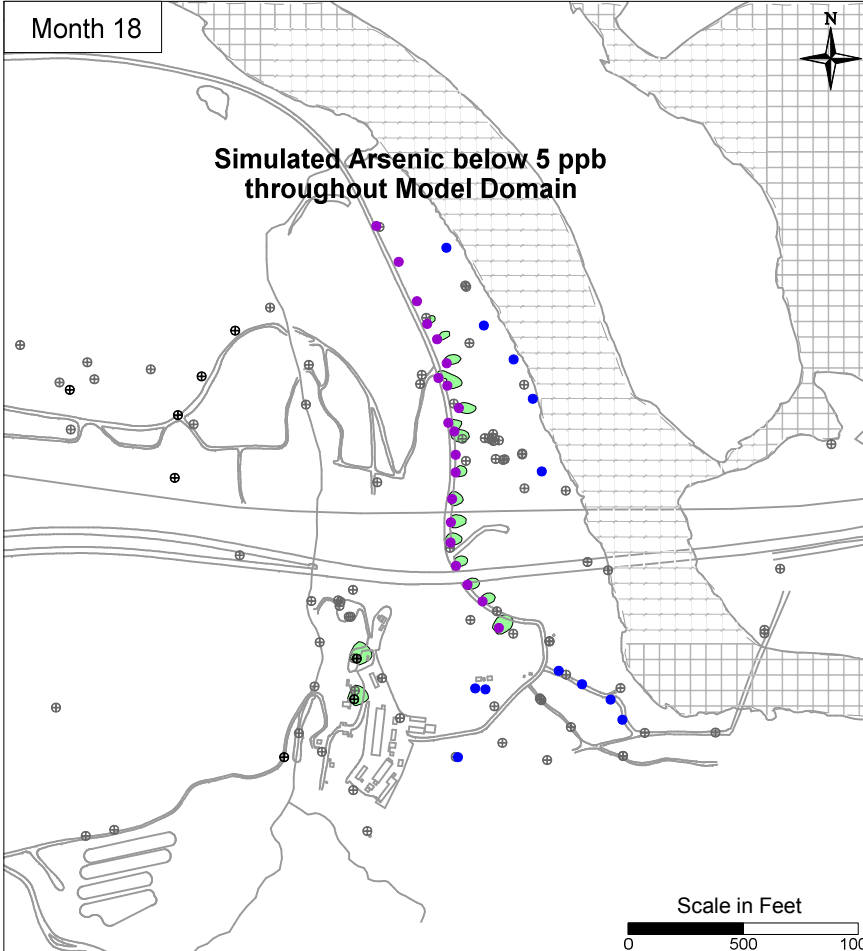
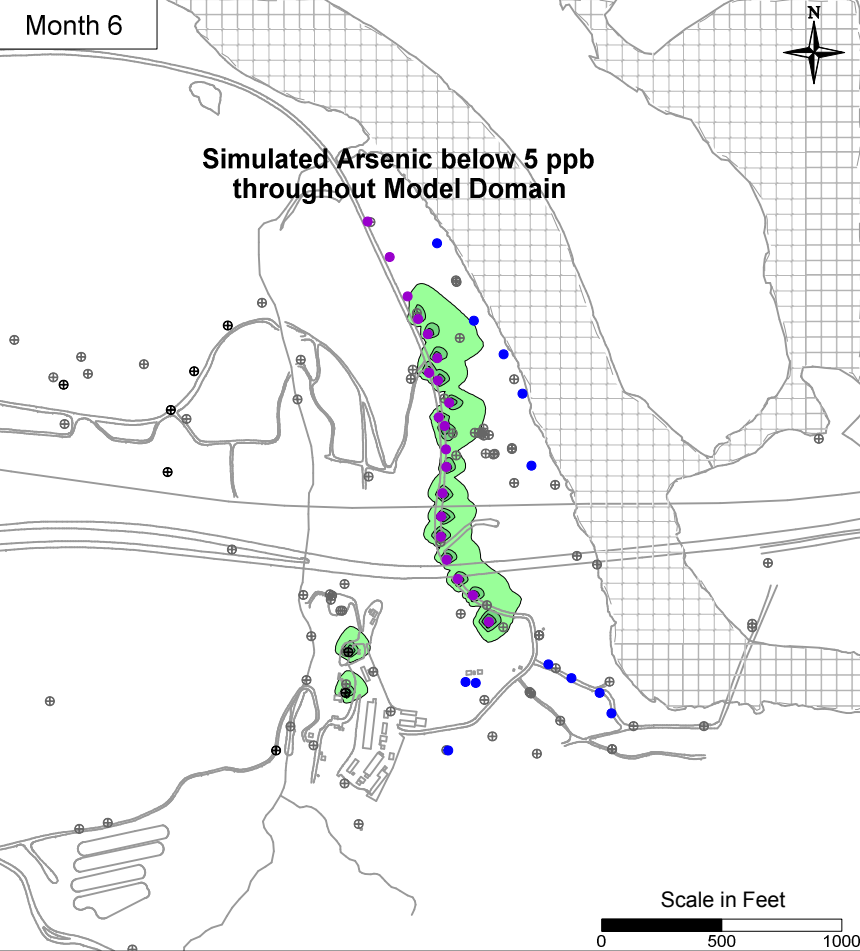
- IRZ WELLS
- ⊕ UPGRADIENT INJECTION WELLS
- EXTRACTION WELLS
- ⊕ MONITORING WELLS

PG&E  
TOPOCK COMPRESSOR STATION  
NEEDLES, CALIFORNIA  
MODELING APPENDIX  
SIMULATED MAXIMUM IRZ GENERATED  
MANGANESE BYPRODUCT AND NATURALLY  
OCCURRING AVERAGE FLOODPLAIN  
MANGANESE IN MODEL LAYER 4

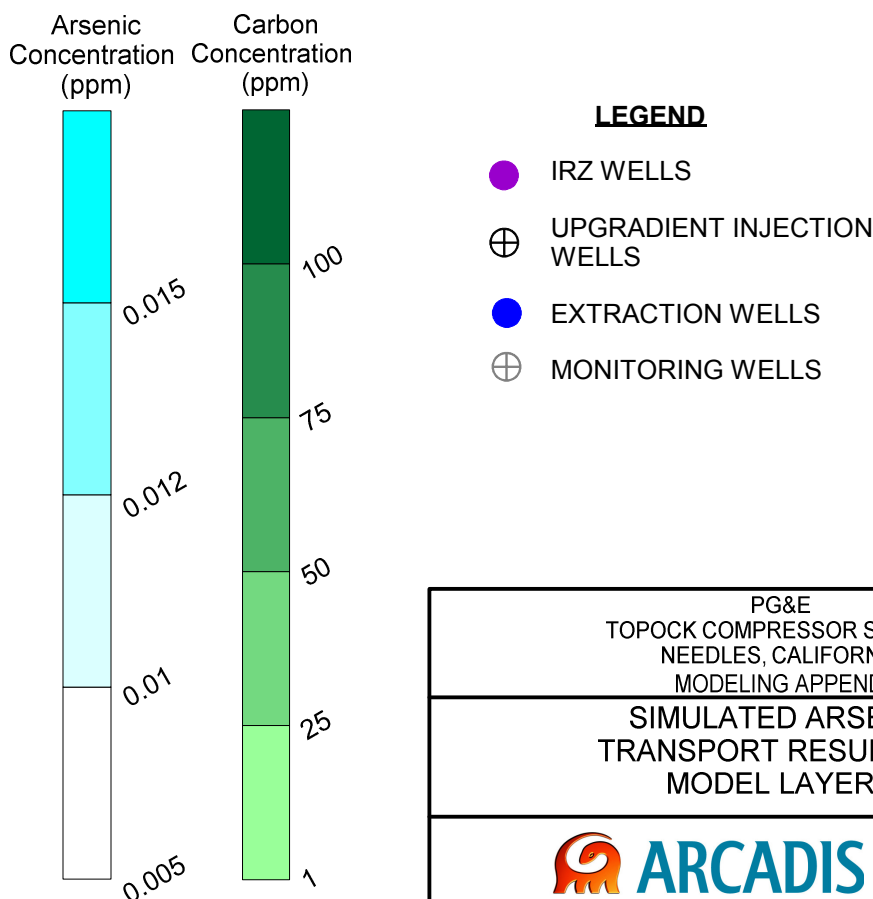
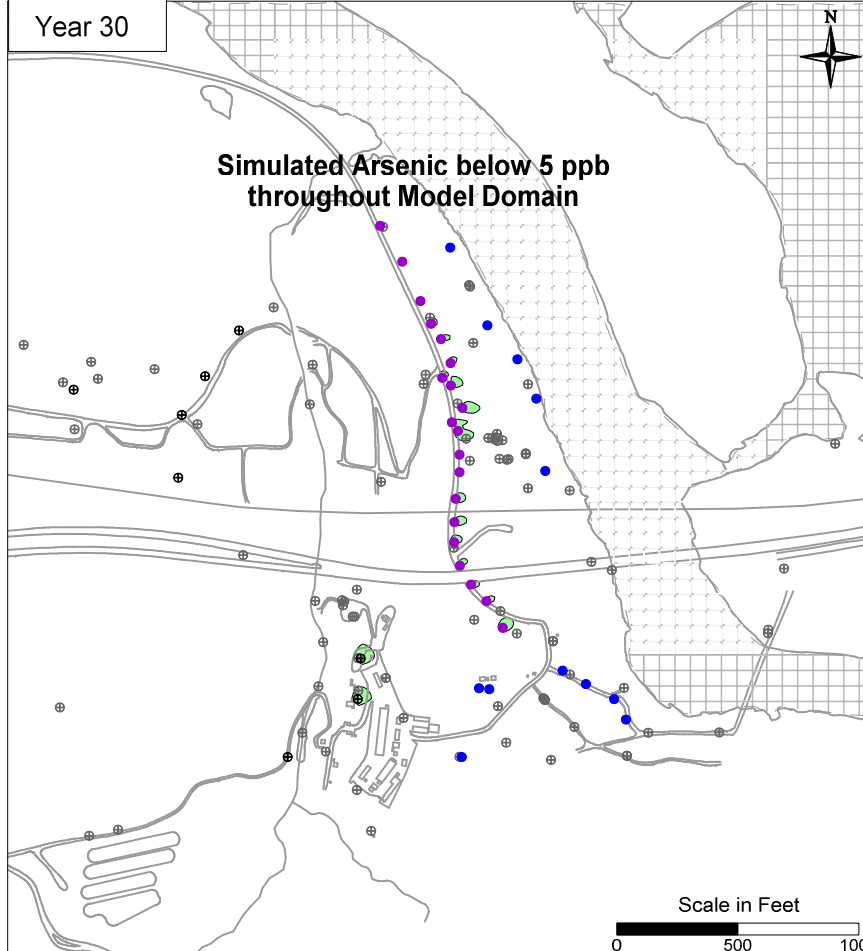
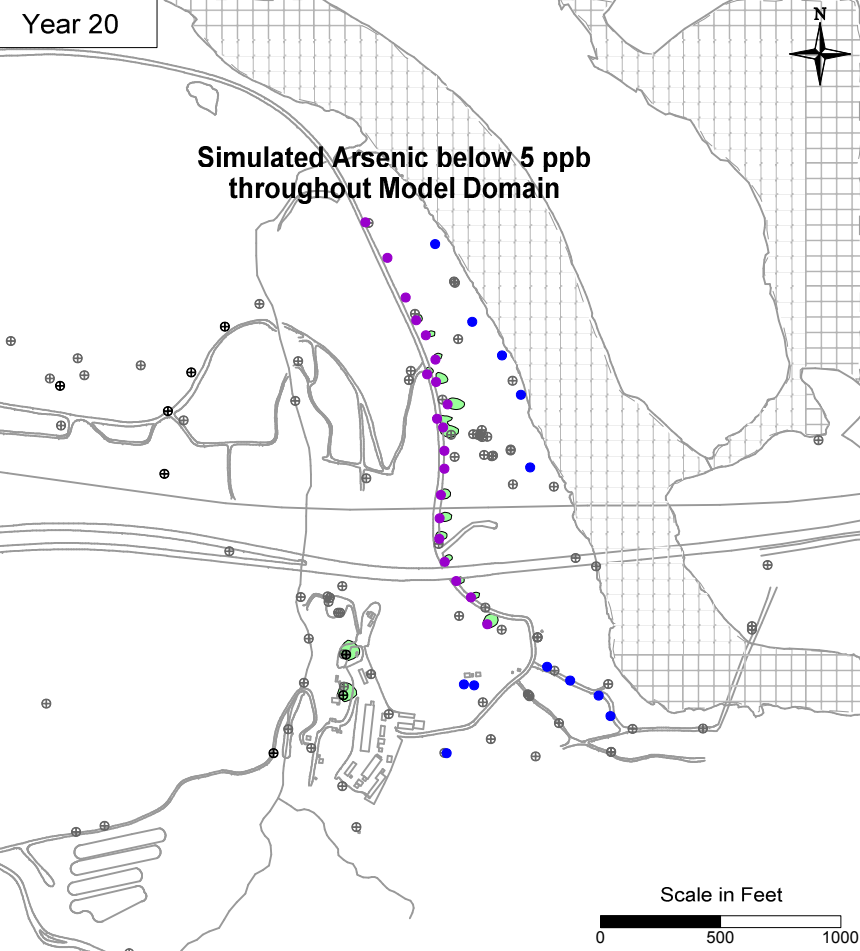
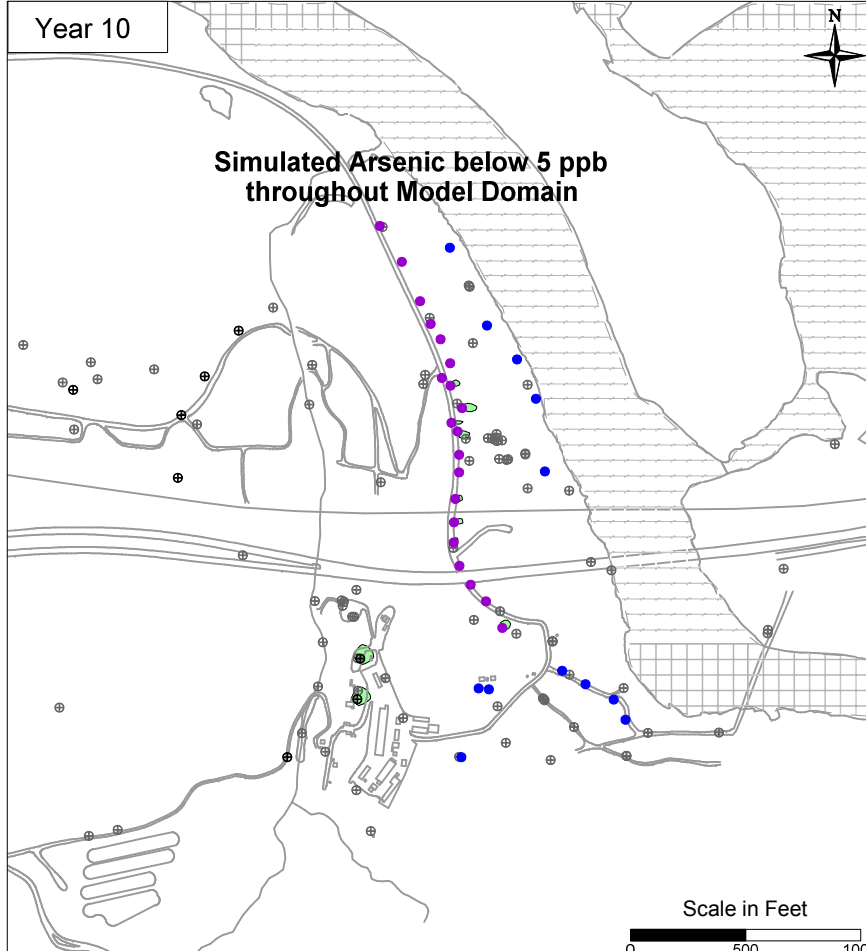
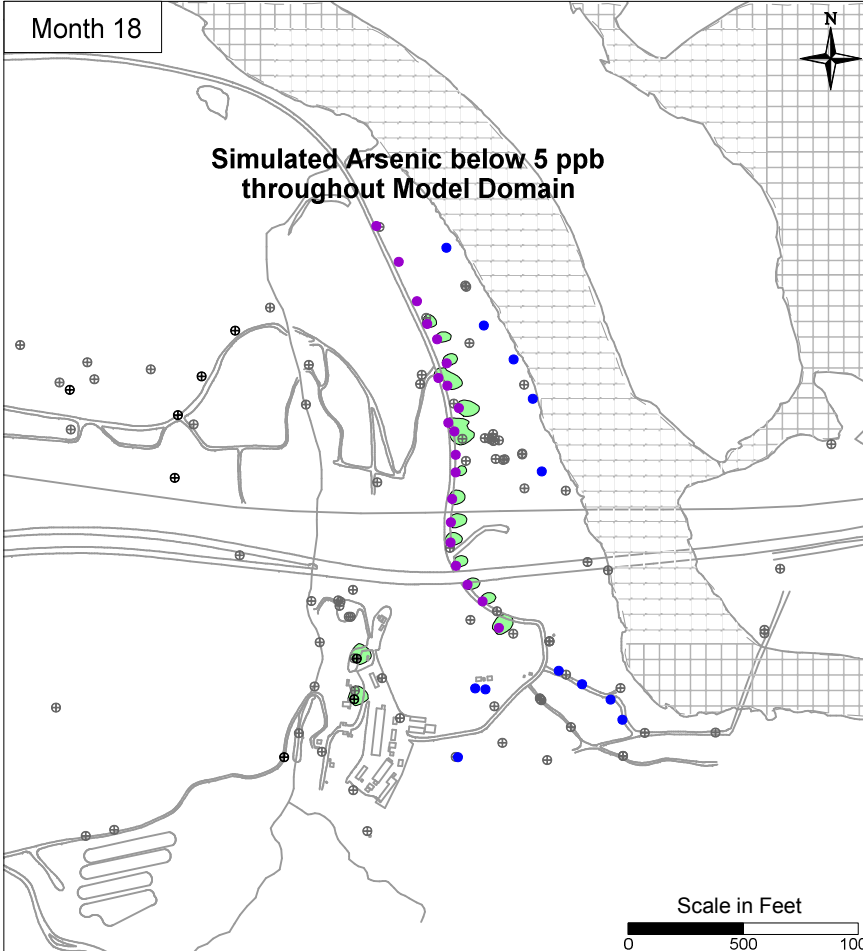
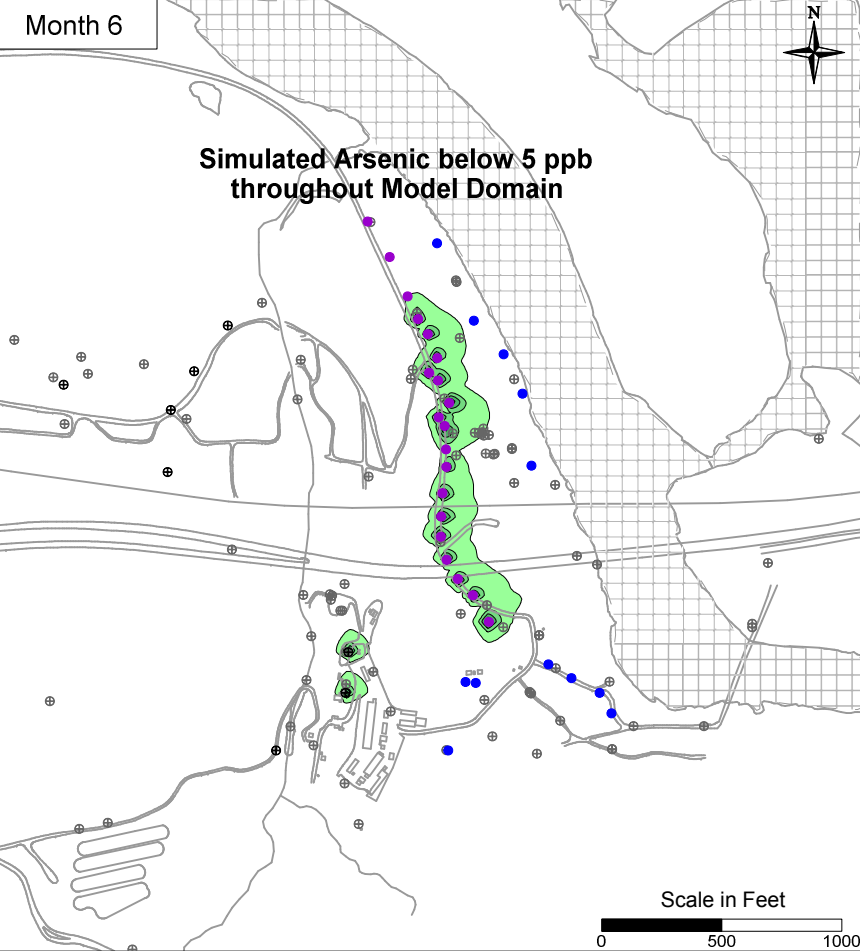


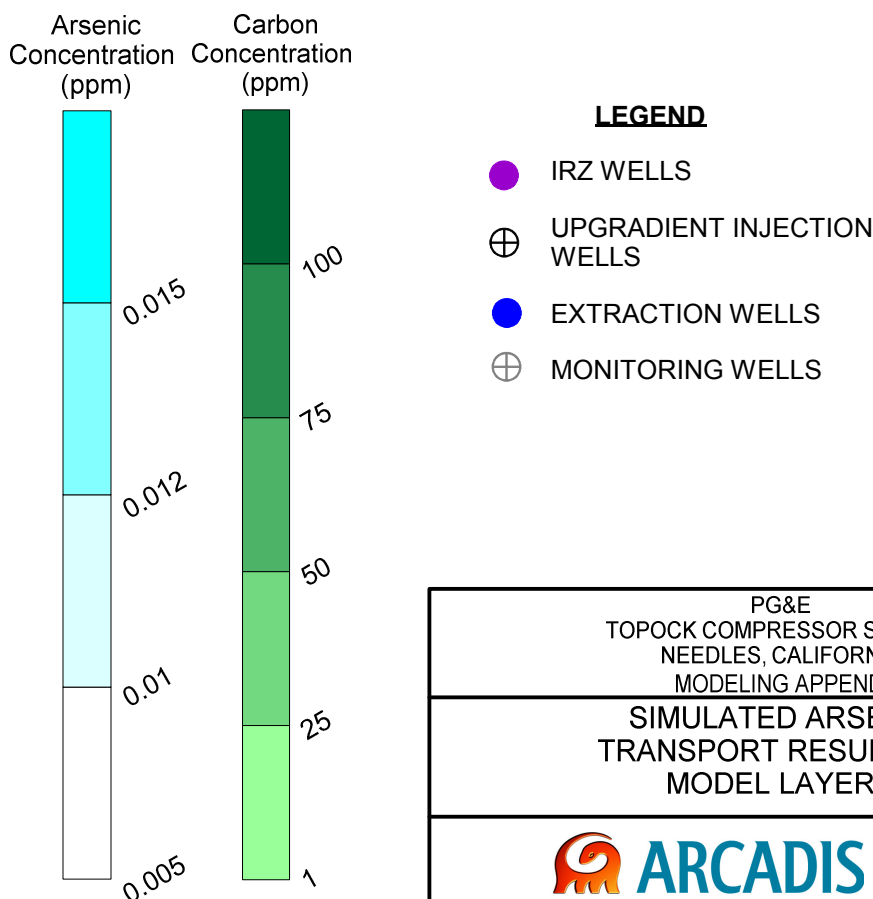
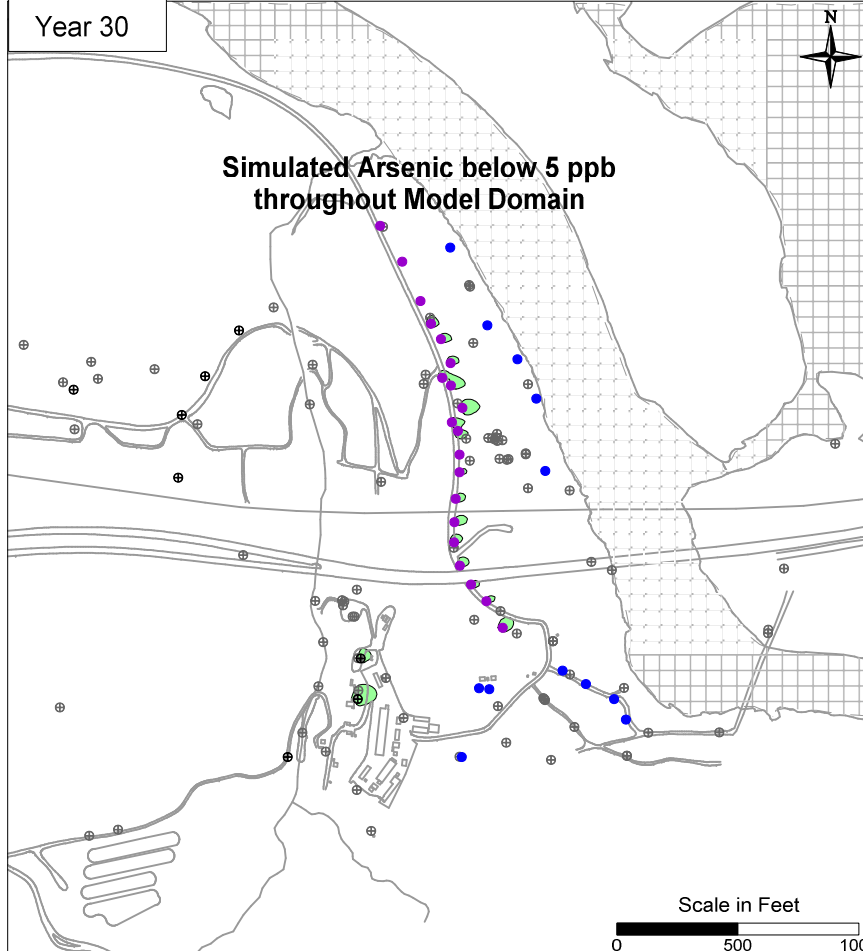
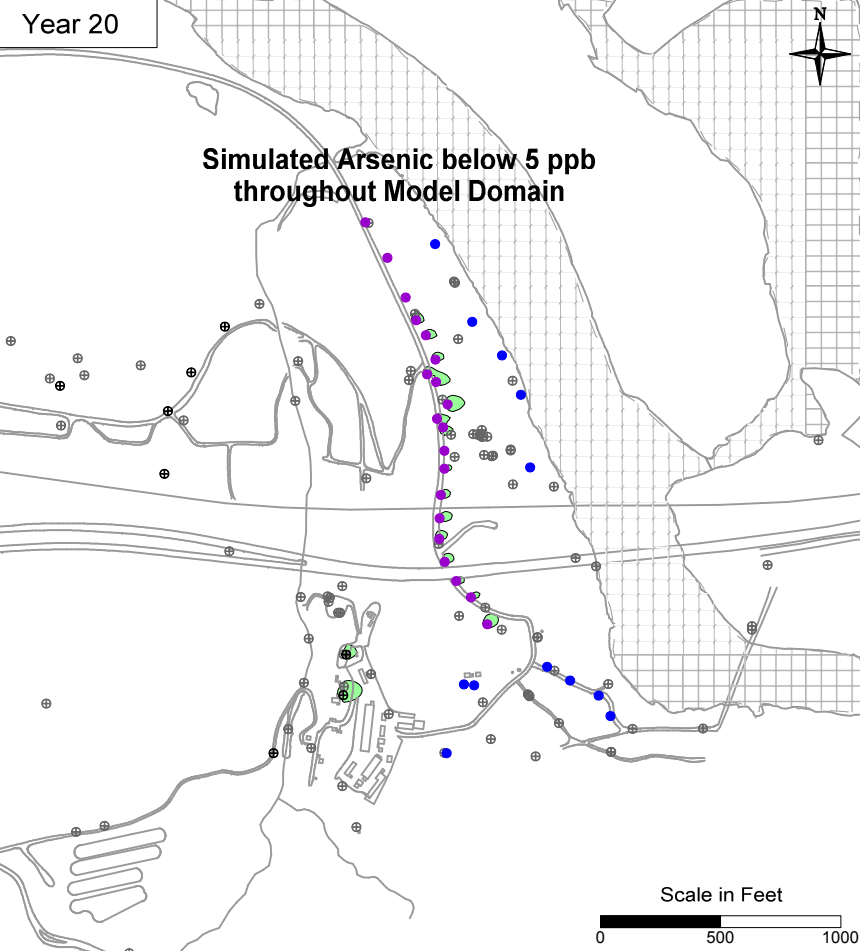
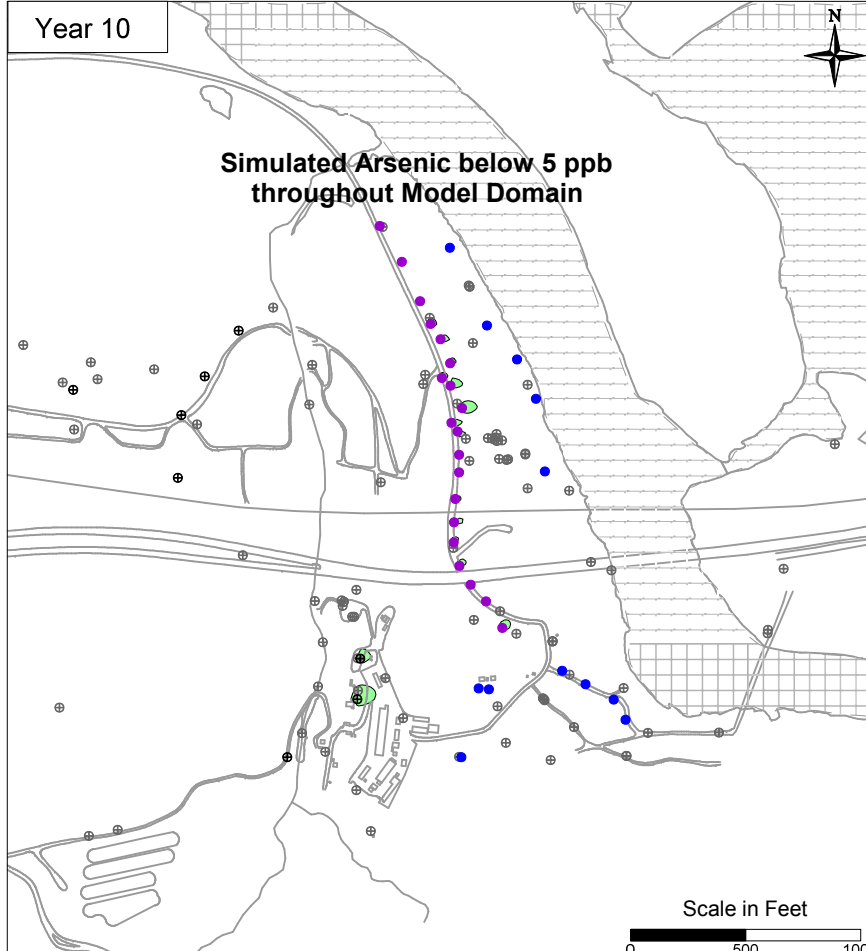
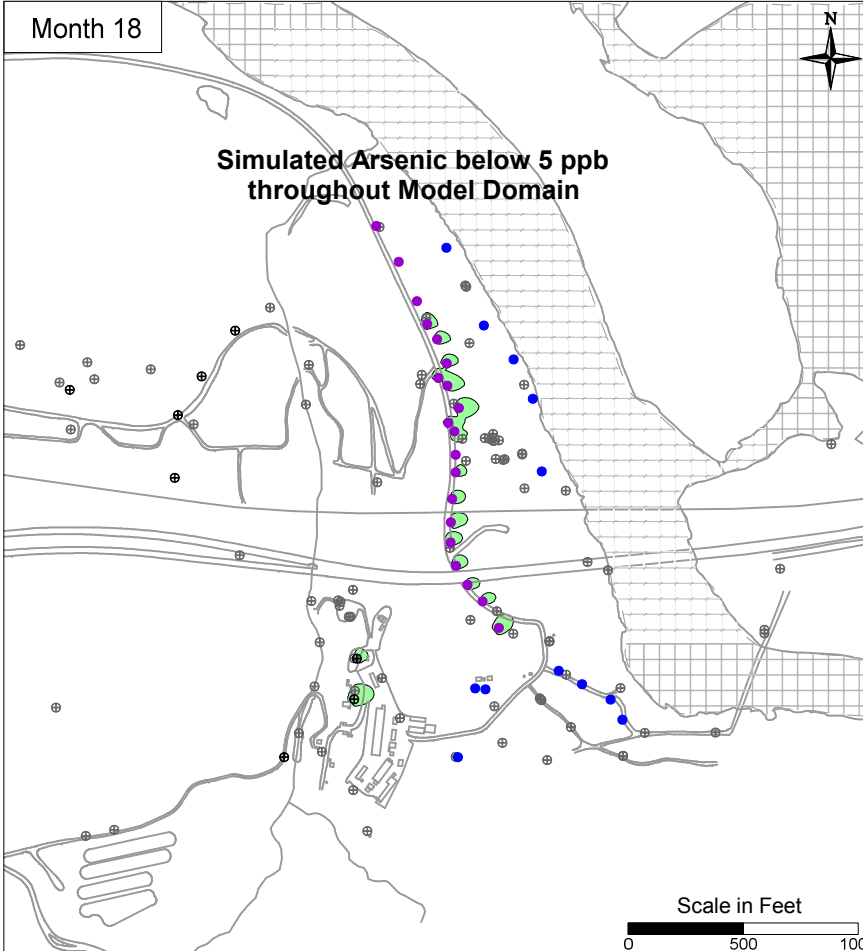
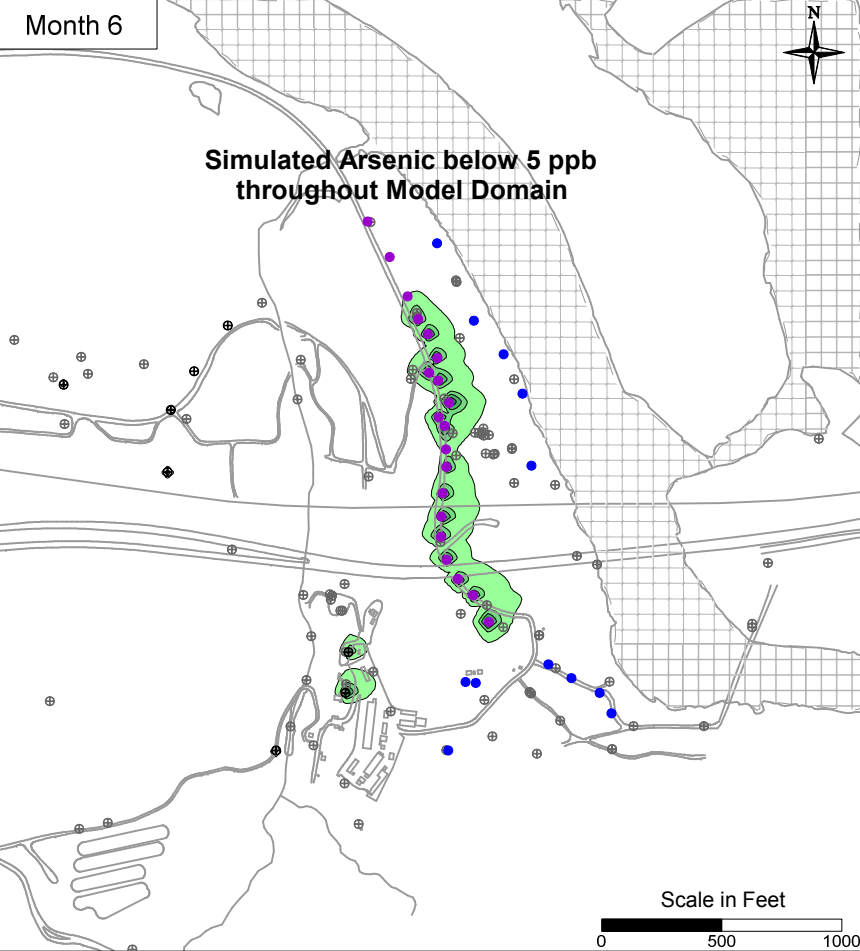
FIGURE  
7.2-8



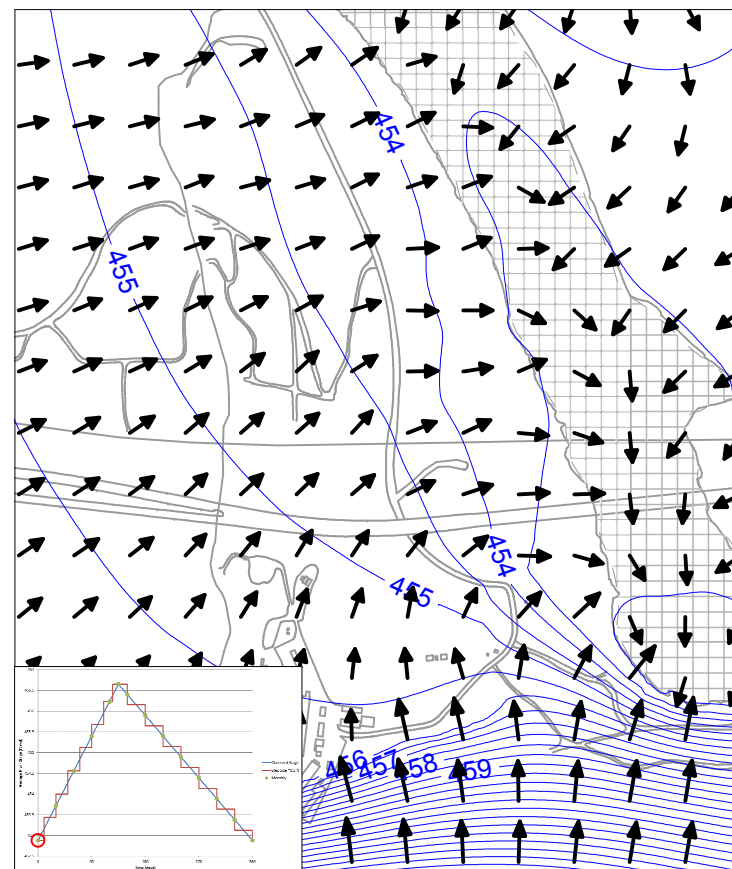




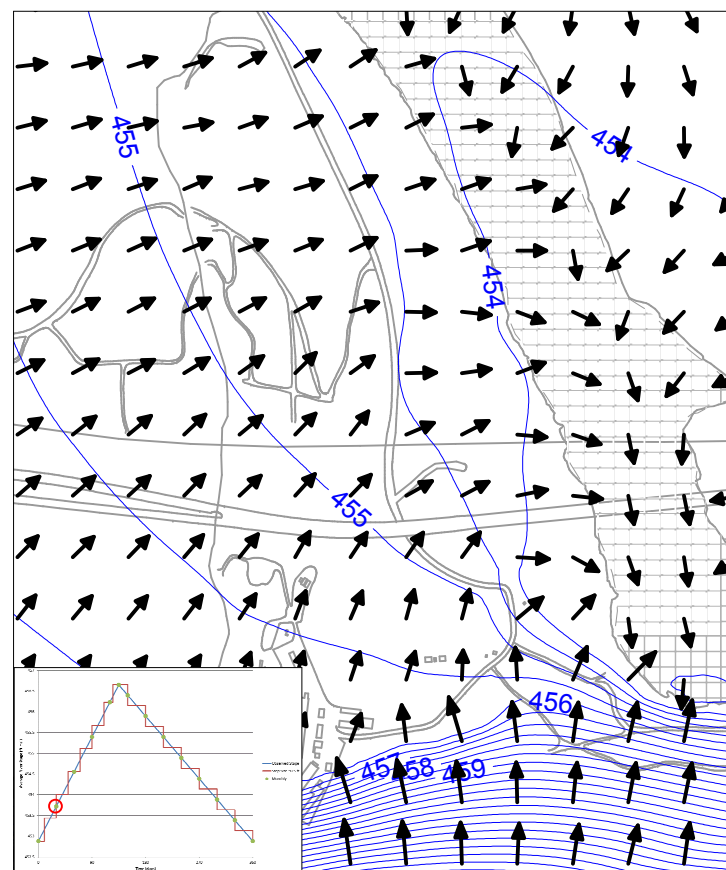




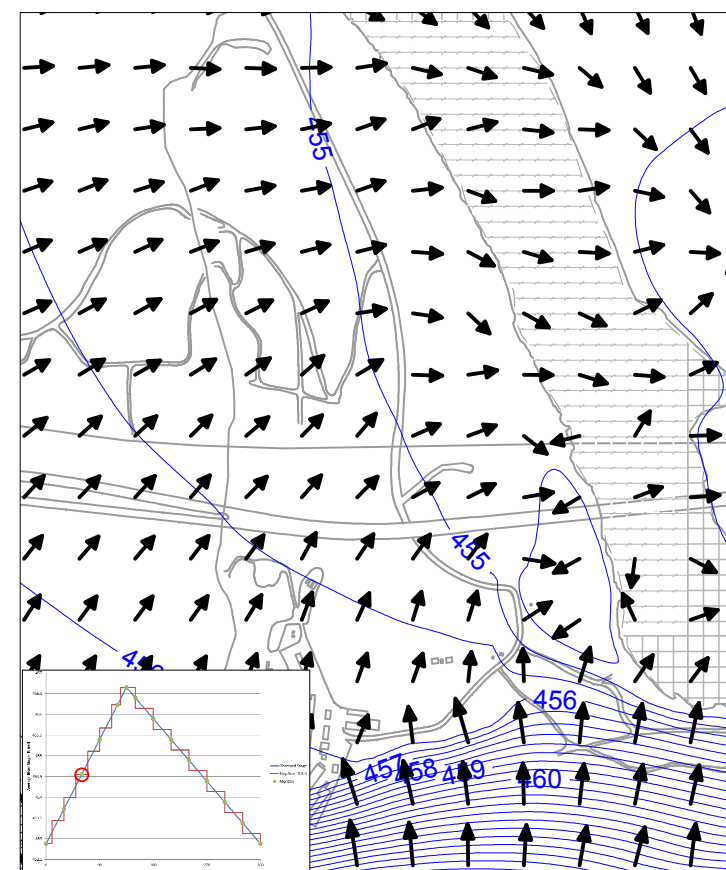




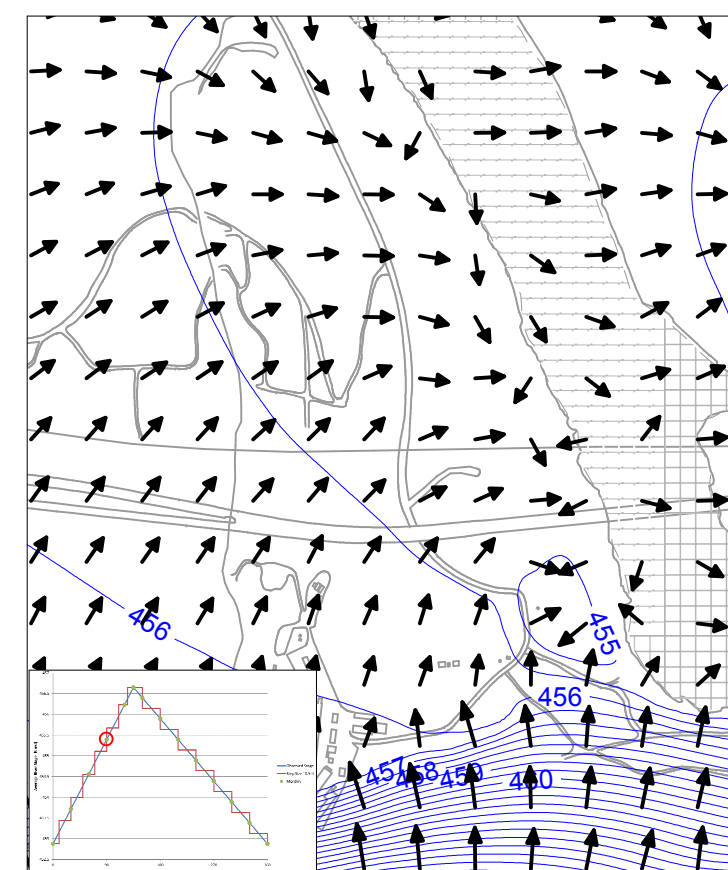
TRANSIENT MONTH 0



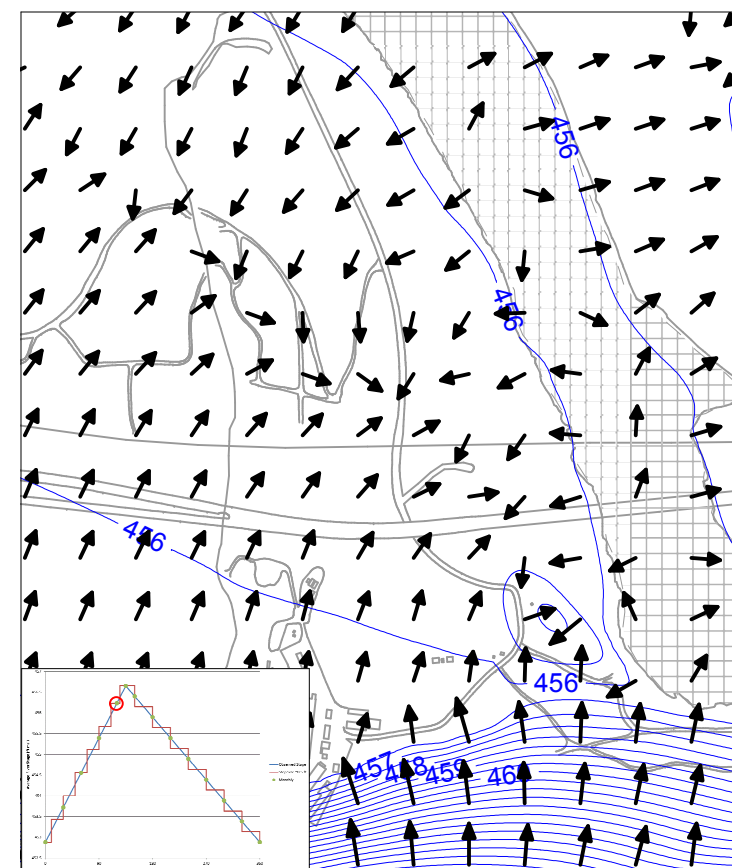
TRANSIENT MONTH 1



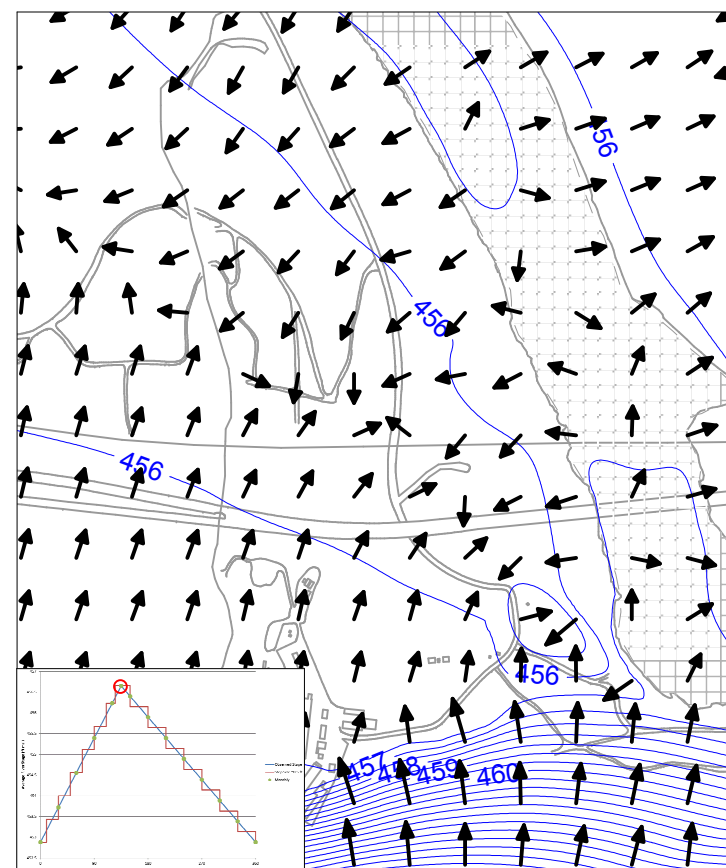
TRANSIENT MONTH 2



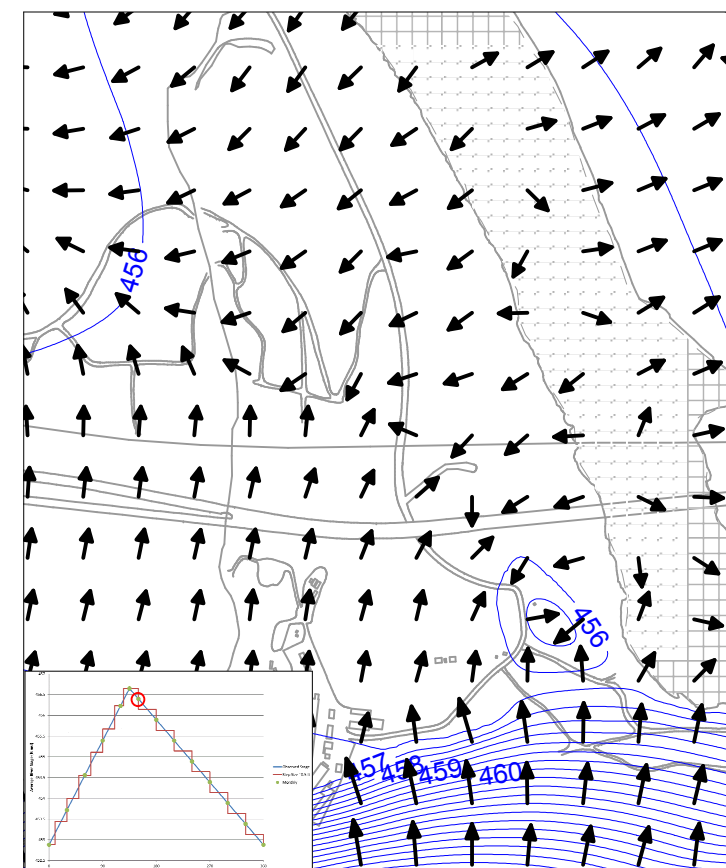
TRANSIENT MONTH 3



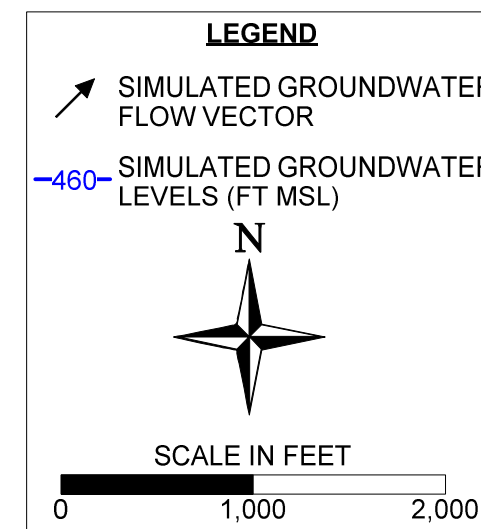
TRANSIENT MONTH 4



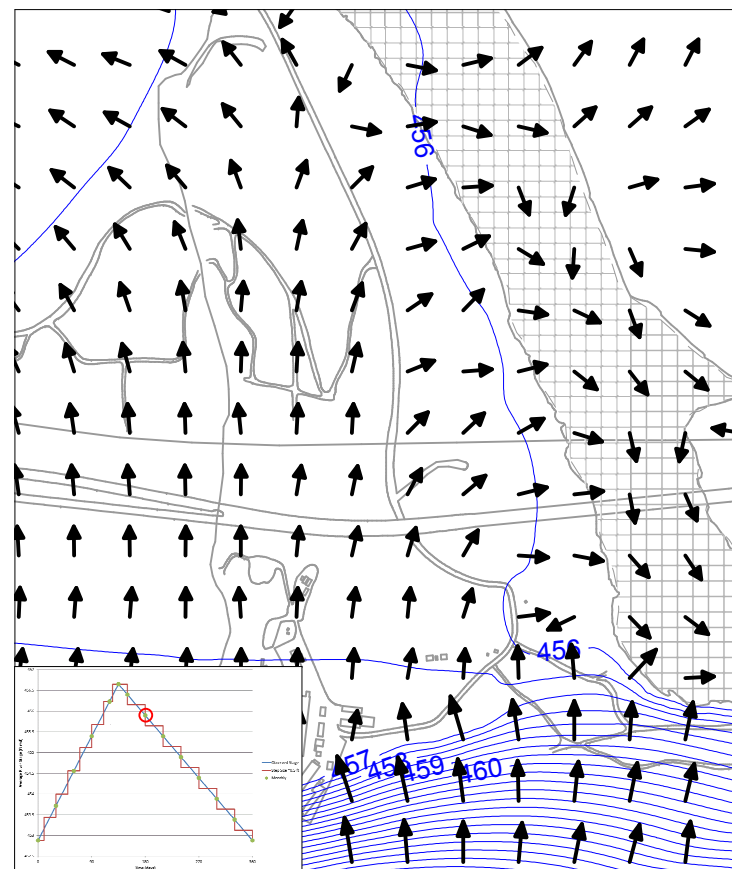
TRANSIENT MONTH 4.5



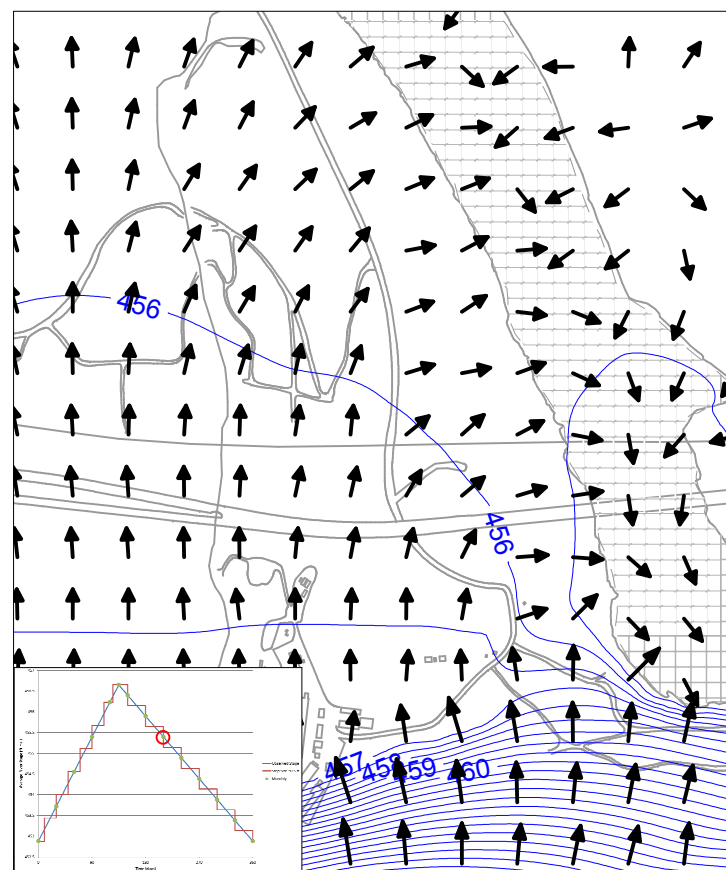
TRANSIENT MONTH 5



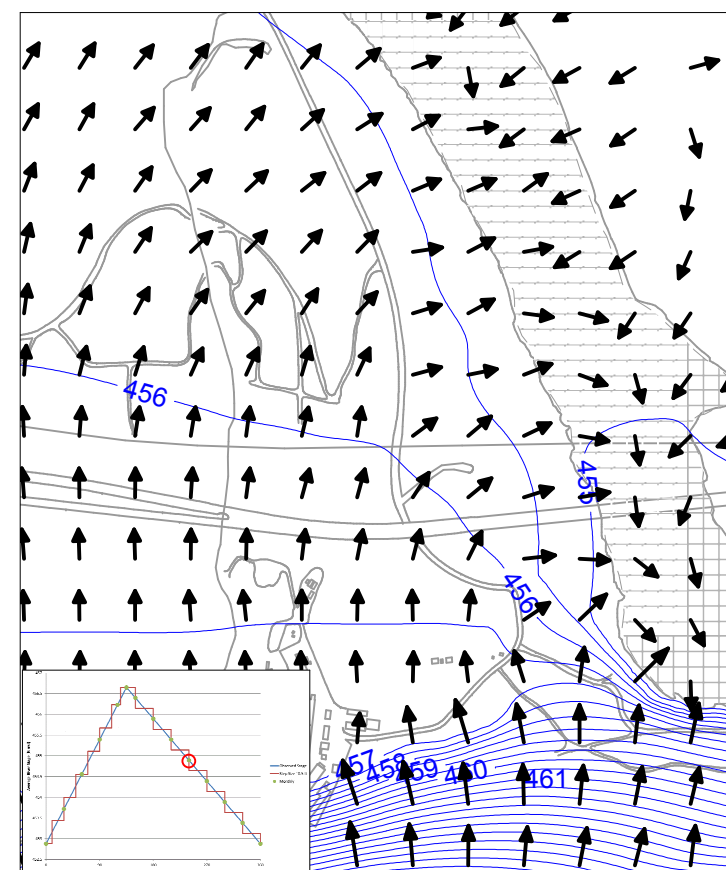




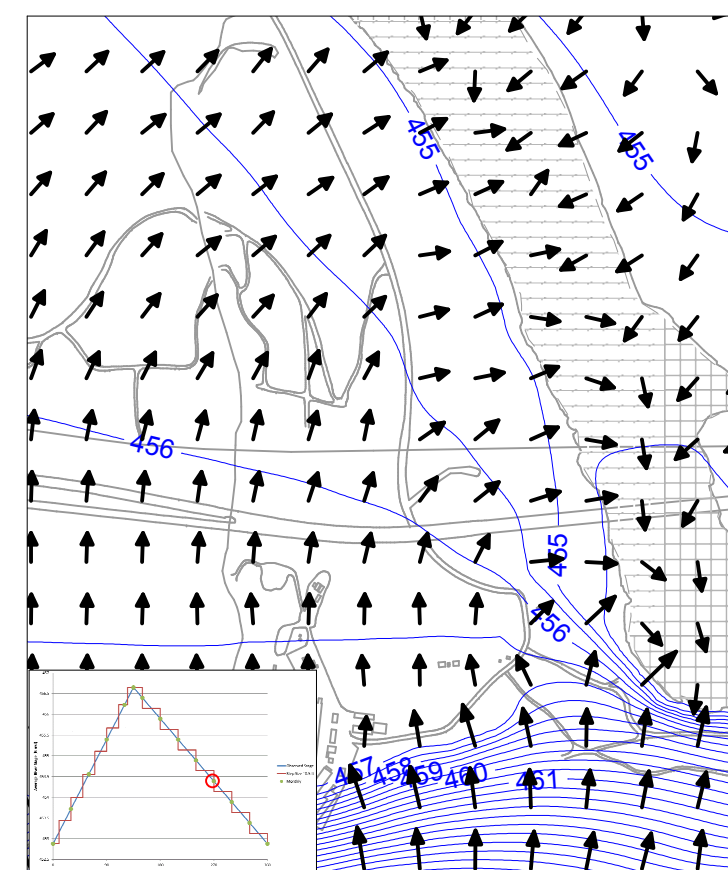
TRANSIENT MONTH 6



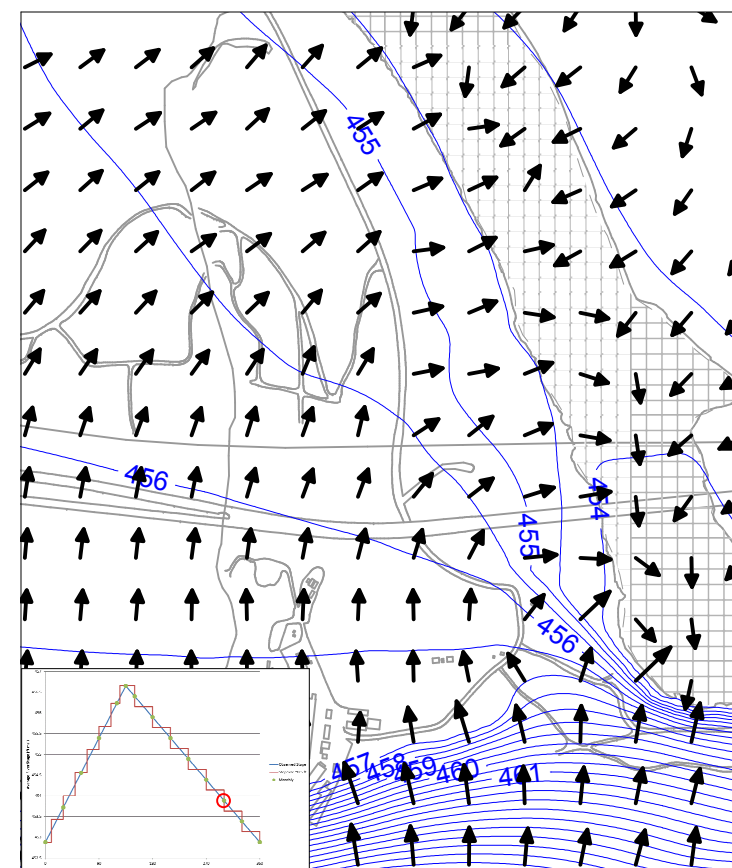
TRANSIENT MONTH 7



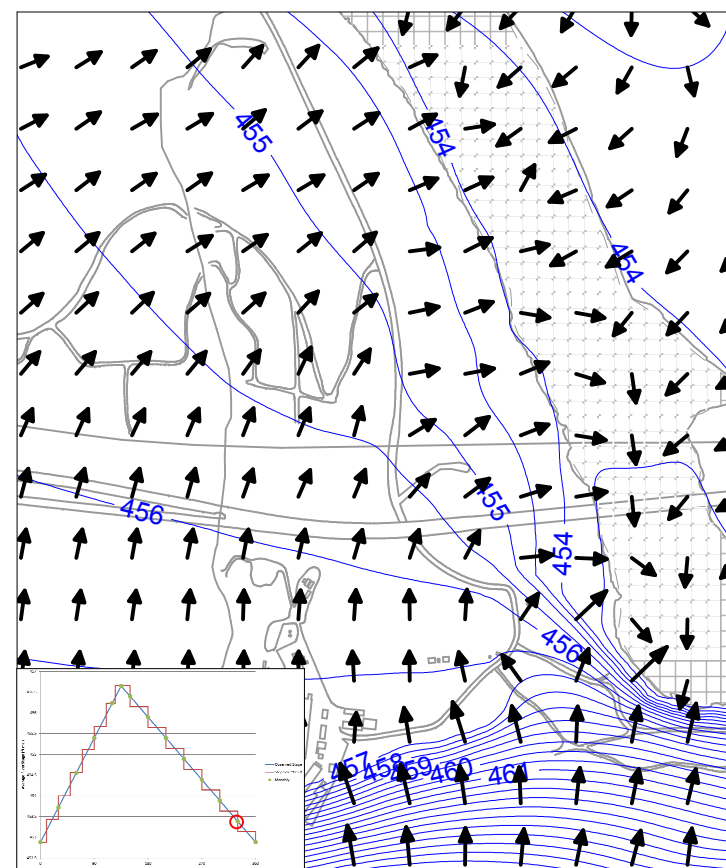
TRANSIENT MONTH 8



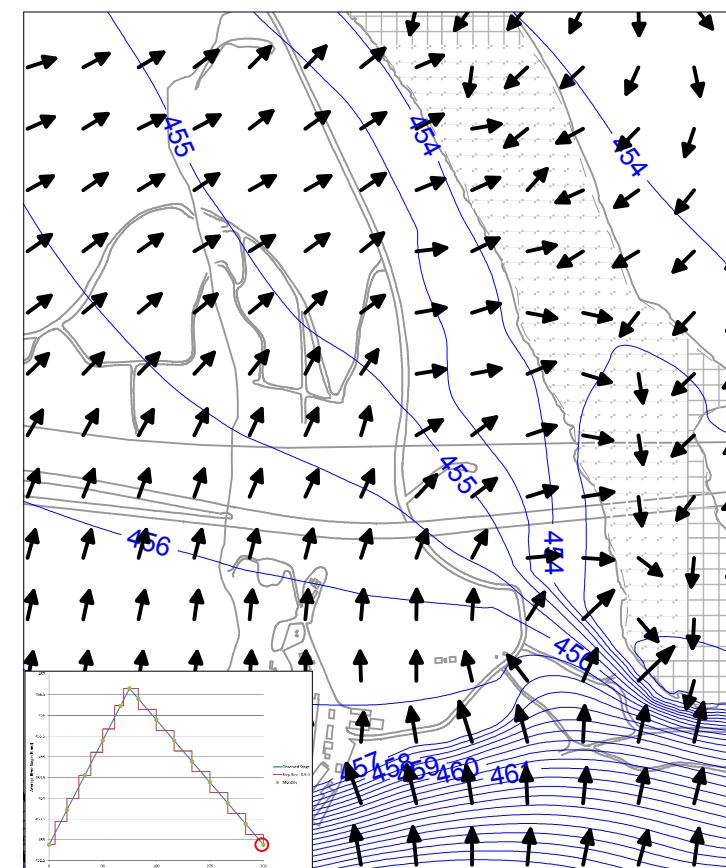
TRANSIENT MONTH 9



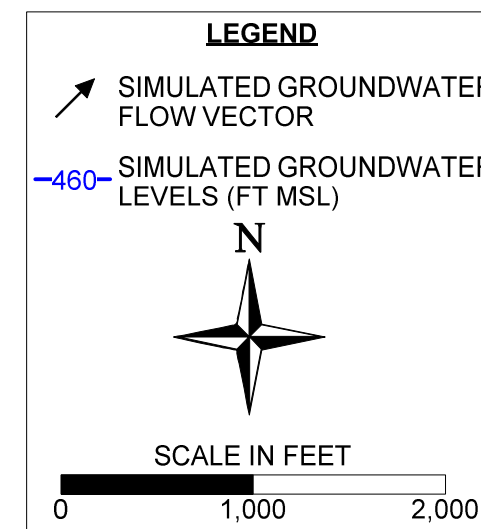
TRANSIENT MONTH 10



TRANSIENT MONTH 11



TRANSIENT MONTH 12

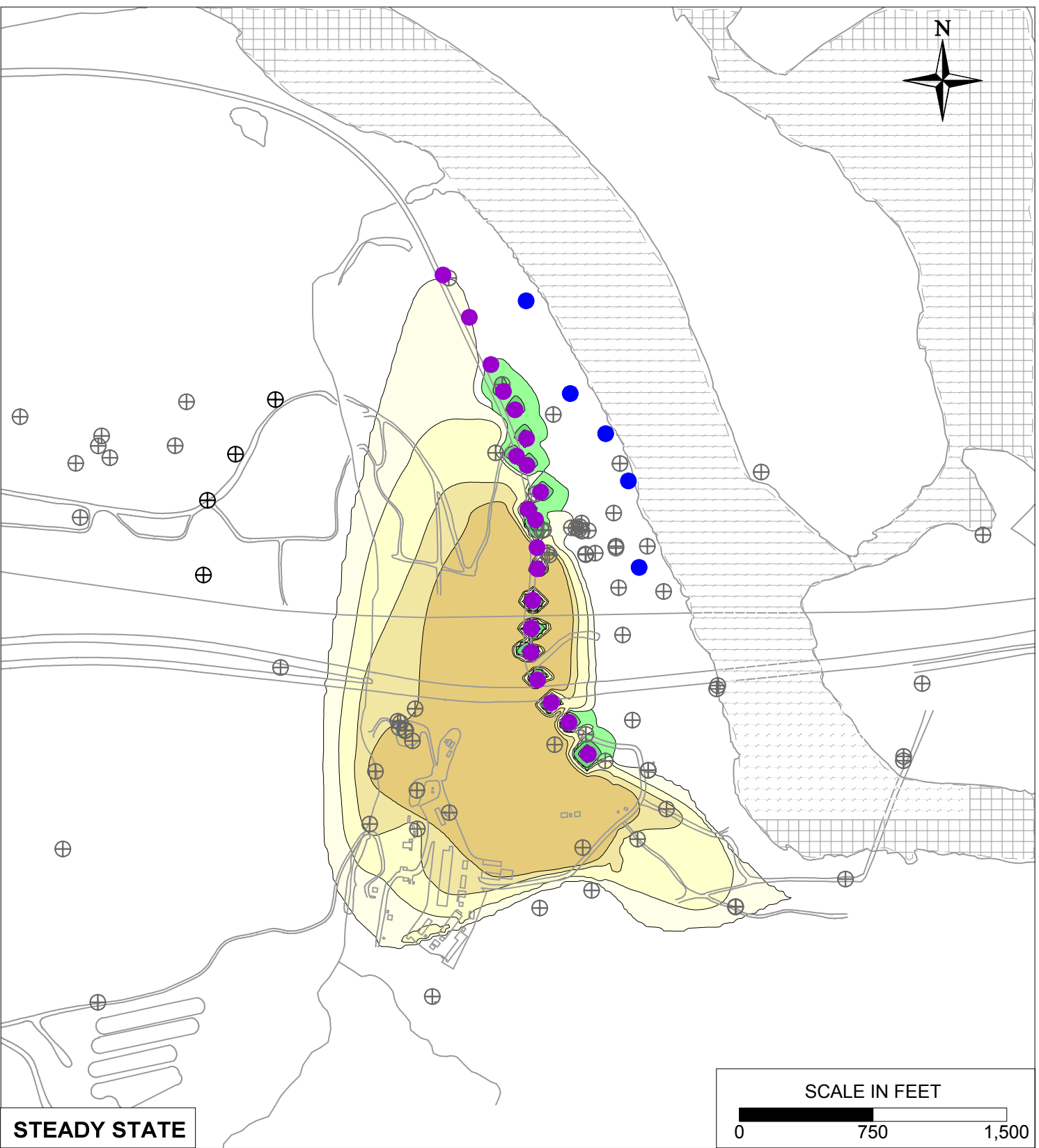
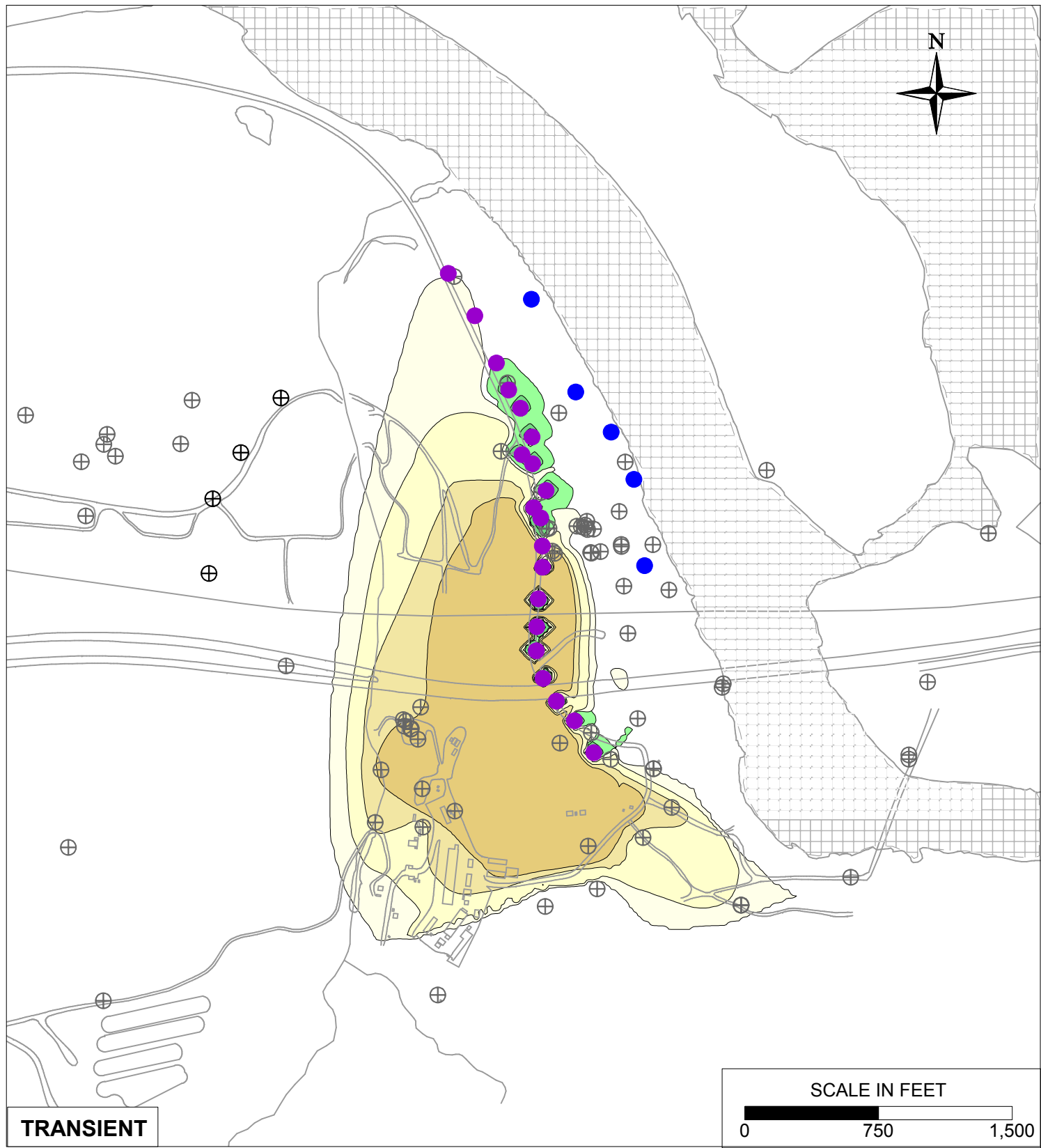


PG&E  
TOPOCK COMPRESSOR STATION  
NEEDLES, CALIFORNIA  
MODELING APPENDIX

SIMULATED TRANSIENT WATER LEVELS  
AND FLOW VECTORS IN MODEL LAYER 1  
MONTHS 6 TO 12

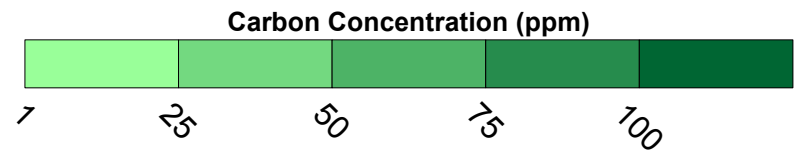
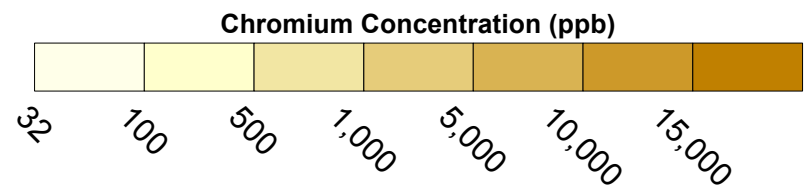


FIGURE  
7.4-2



**LEGEND**

- IRZ WELLS
- ⊕ UPGRADIENT INJECTION WELLS
- EXTRACTION WELLS
- ⊕ MONITORING WELLS



PG&E  
TOPOCK COMPRESSOR STATION  
NEEDLES, CALIFORNIA  
MODELING APPENDIX

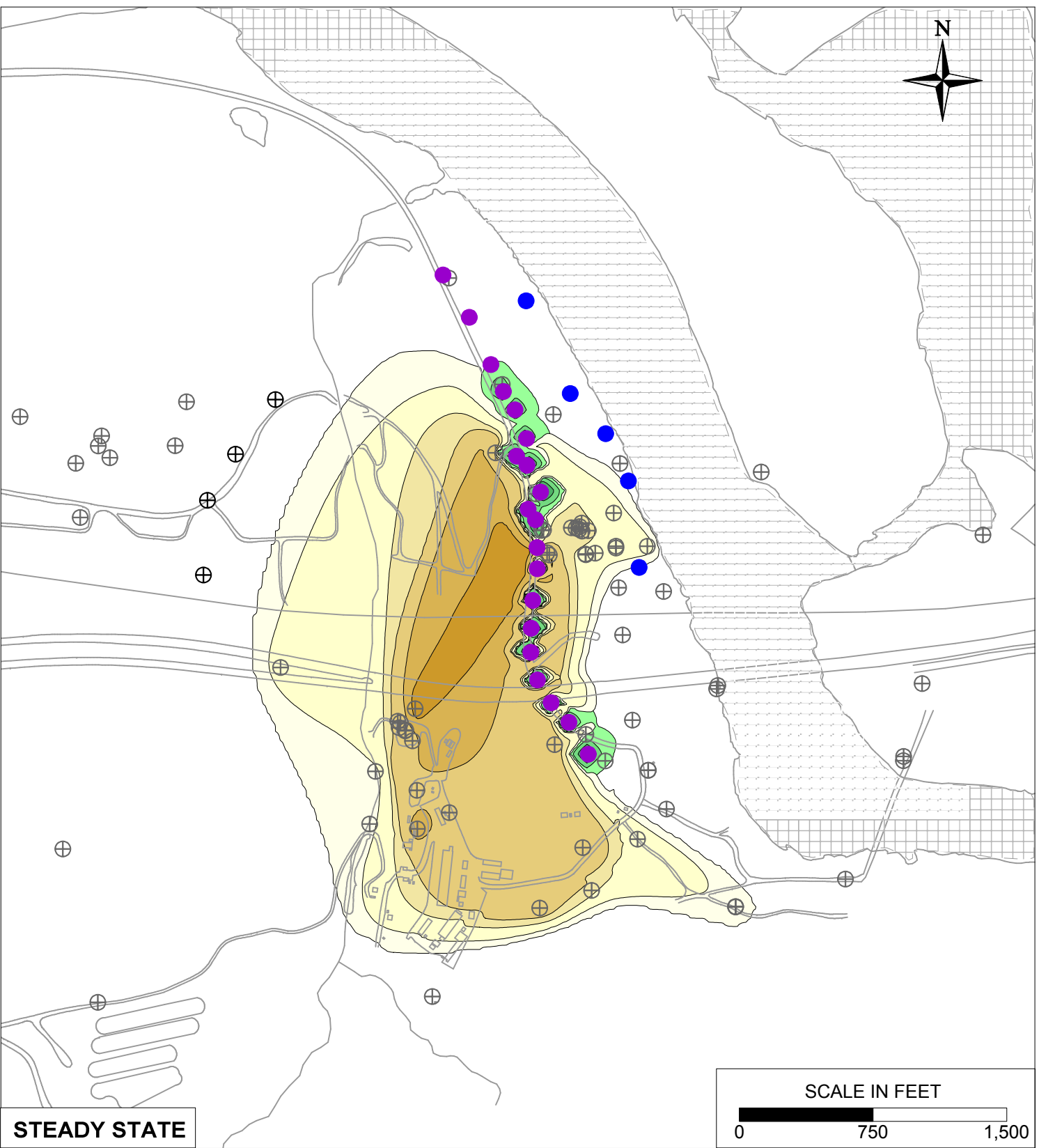
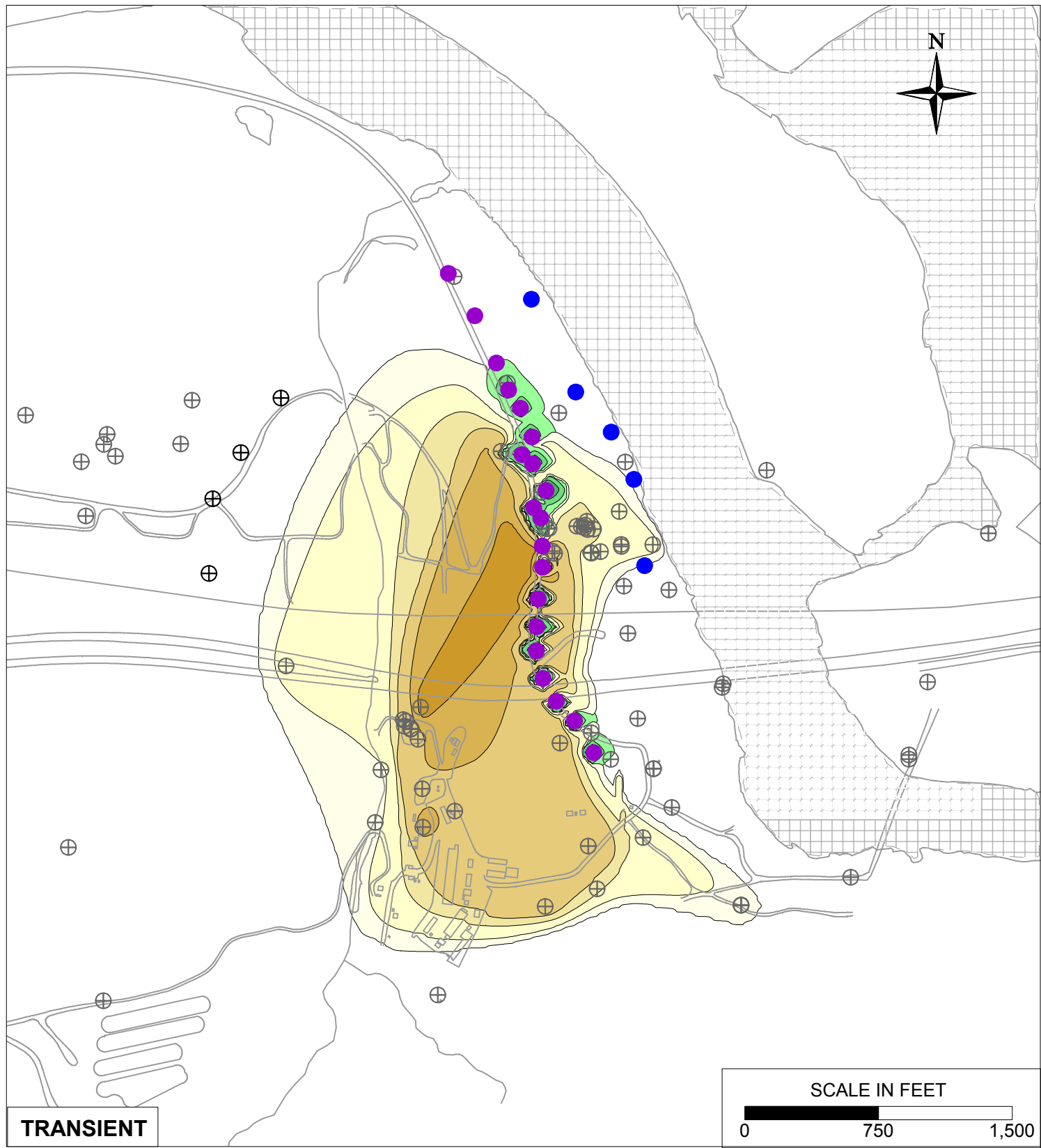
TRANSIENT AND STEADY STATE SIMULATED  
CHROMIUM TRANSPORT RESULTS AFTER  
3 MONTHS TRANSITION IN MODEL LAYER 2



FIGURE

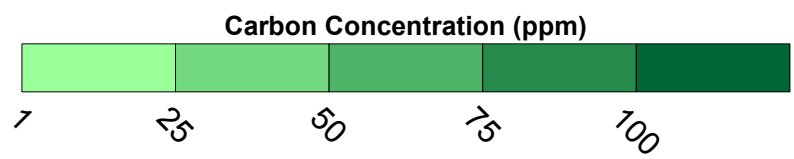
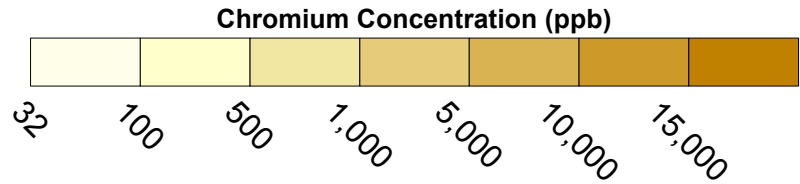
7.4-3





**LEGEND**

- IRZ WELLS
- ⊕ UPGRADIENT INJECTION WELLS
- EXTRACTION WELLS
- ⊕ MONITORING WELLS

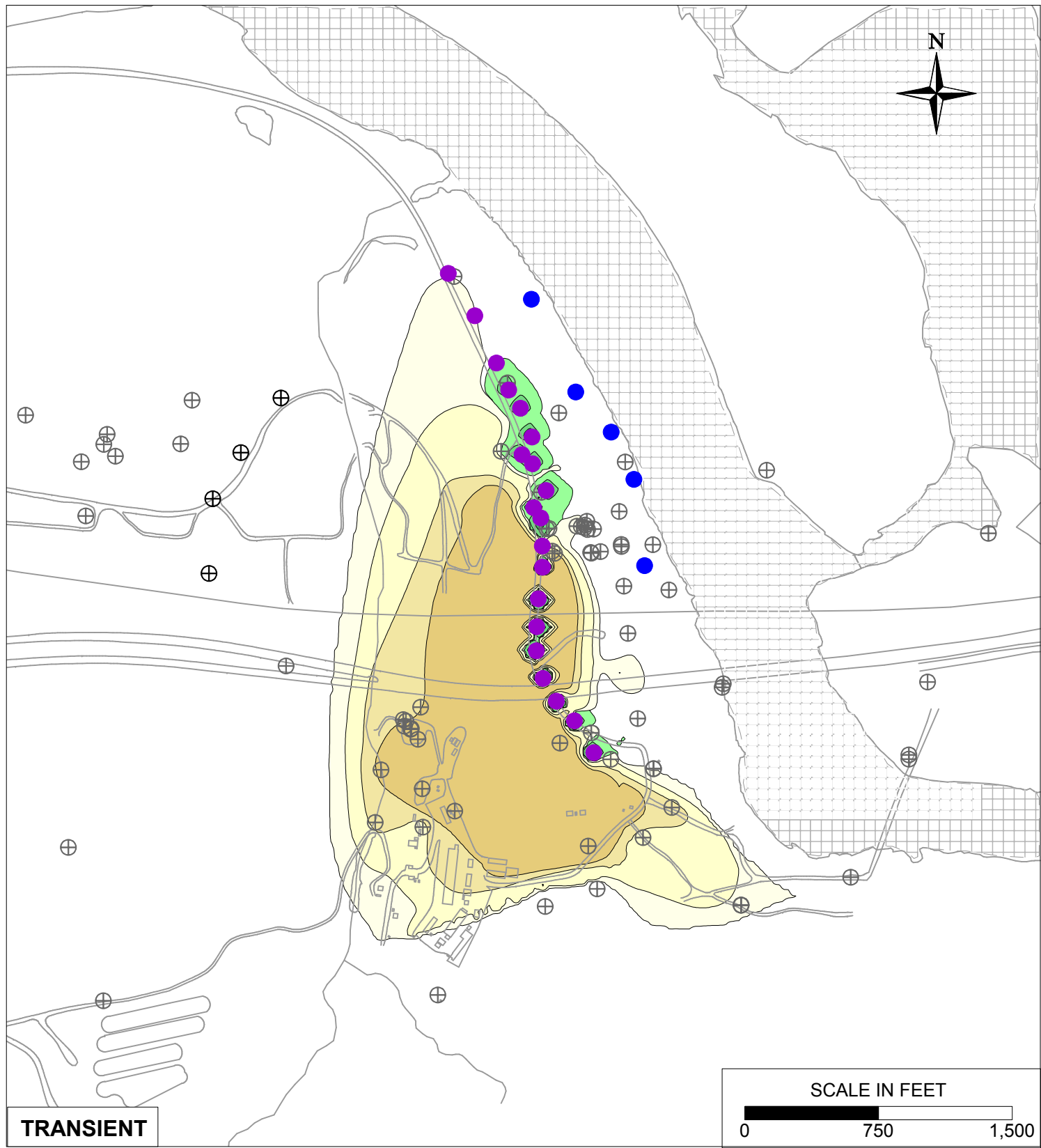


PG&E  
TOPOCK COMPRESSOR STATION  
NEEDLES, CALIFORNIA  
MODELING APPENDIX

TRANSIENT AND STEADY STATE SIMULATED  
CHROMIUM TRANSPORT RESULTS AFTER  
3 MONTHS TRANSITION IN MODEL LAYER 4



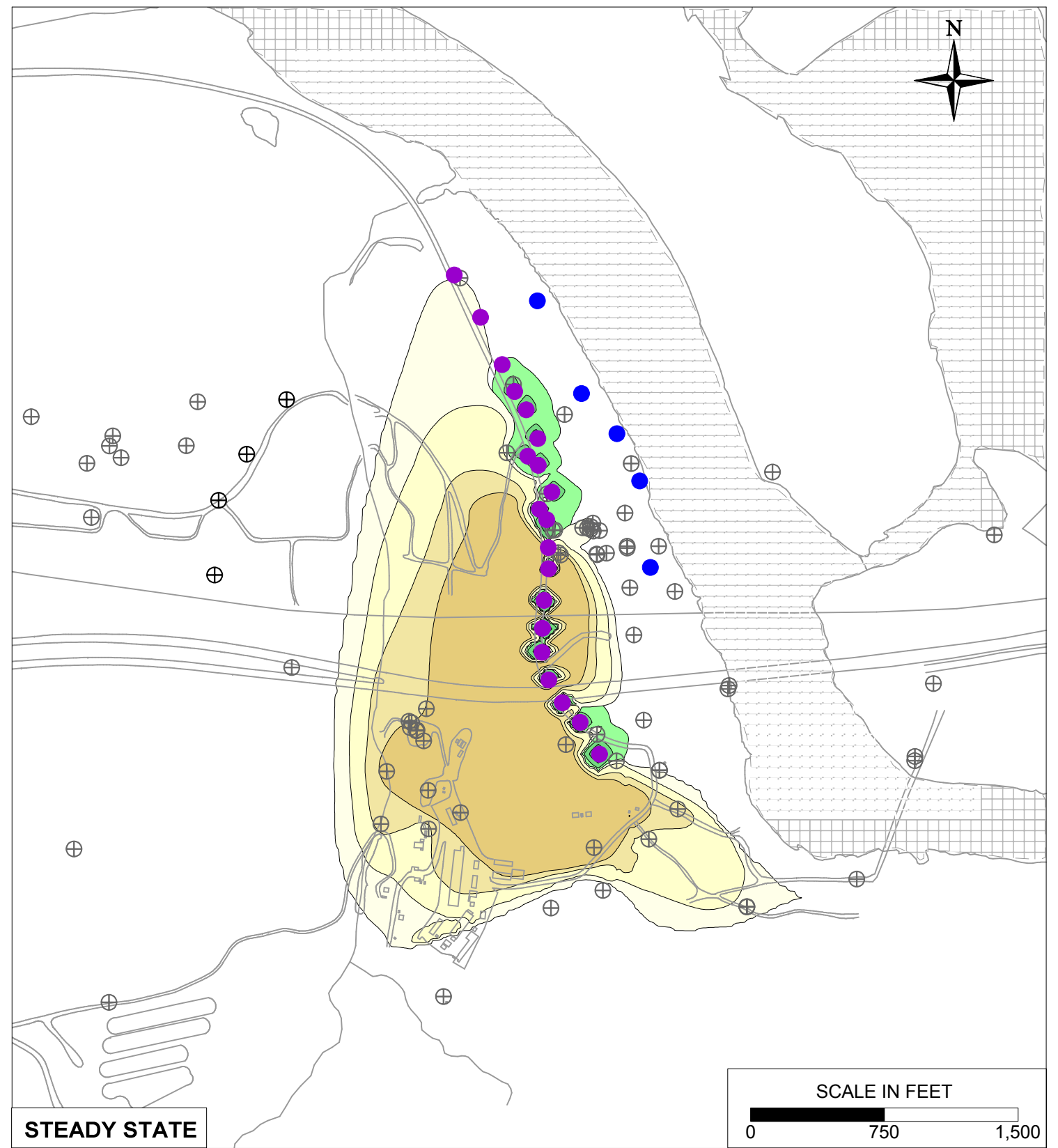
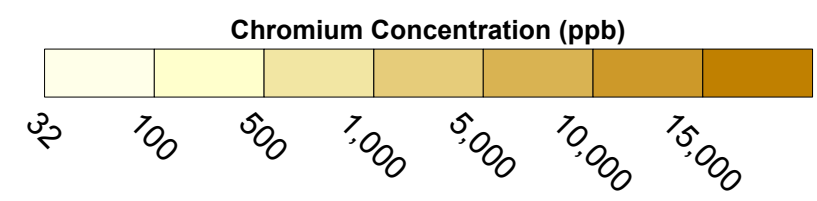
FIGURE  
**7.4-4**



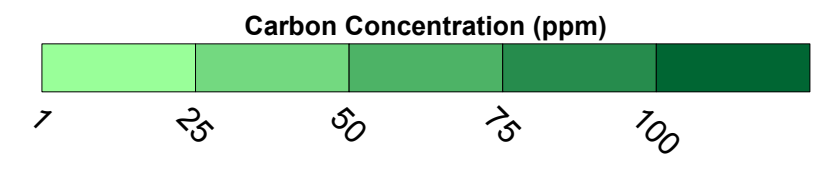
**TRANSIENT**

**LEGEND**

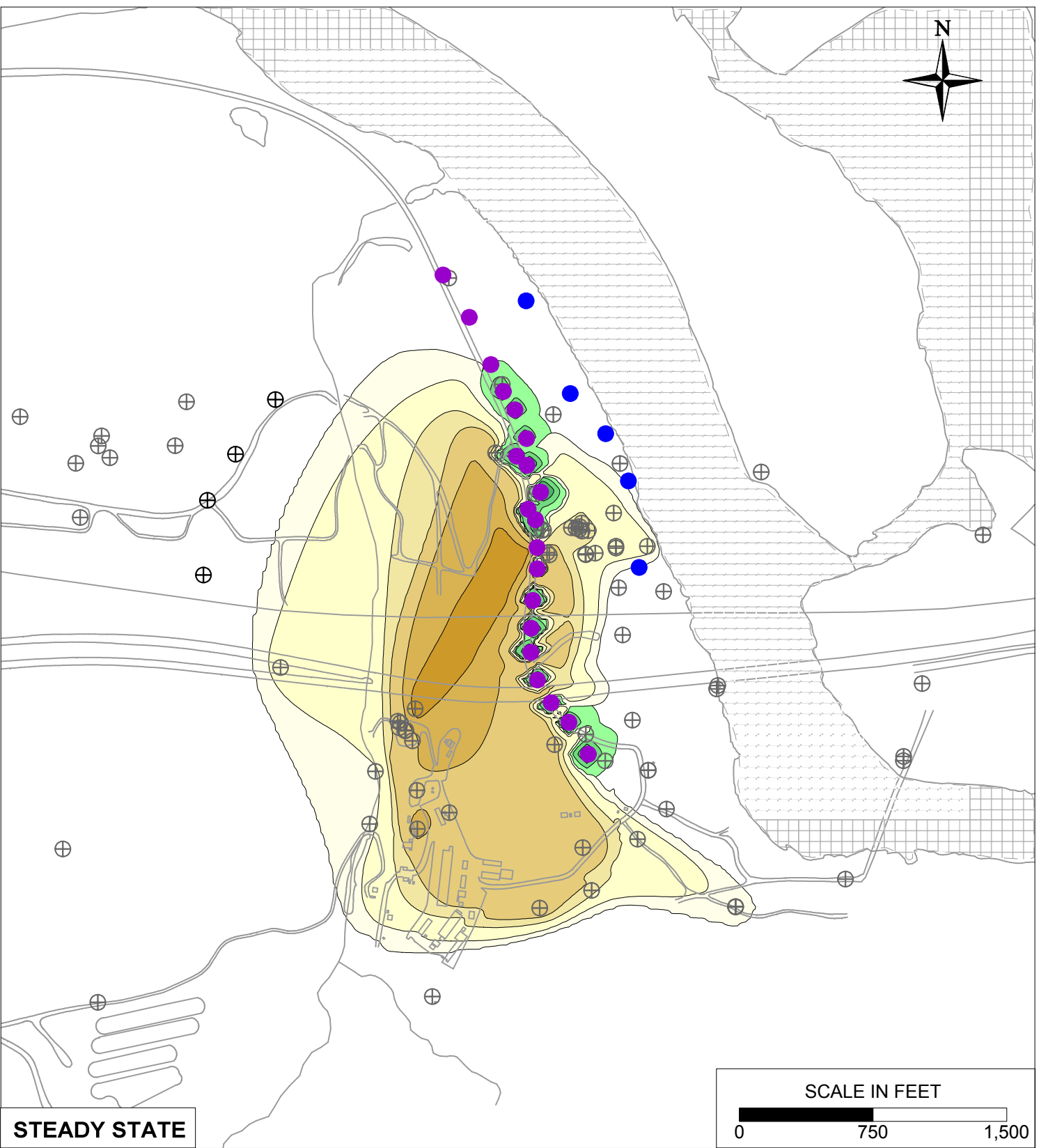
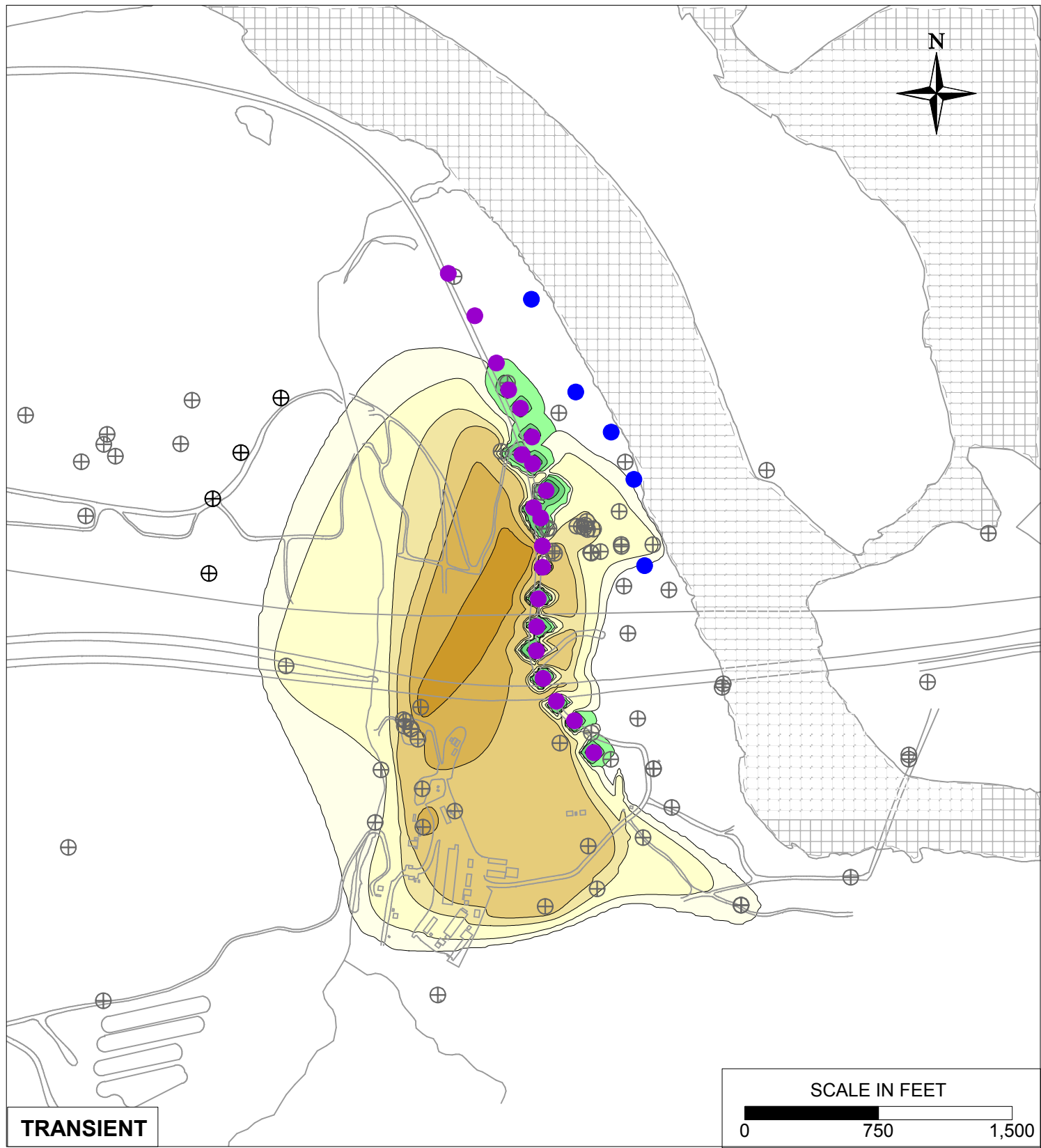
- IRZ WELLS
- ⊕ UPGRADIENT INJECTION WELLS
- EXTRACTION WELLS
- ⊕ MONITORING WELLS



**STEADY STATE**

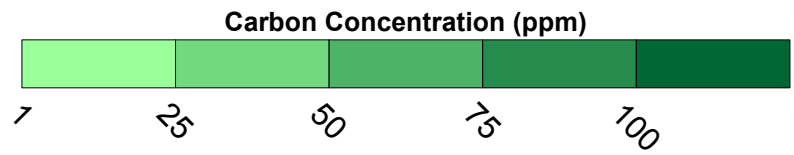
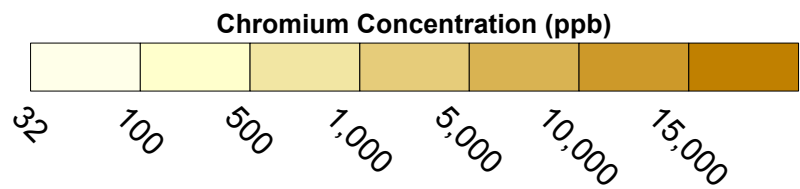


PG&E TOPOCK COMPRESSOR STATION NEEDLES, CALIFORNIA MODELING APPENDIX	
TRANSIENT AND STEADY STATE SIMULATED CHROMIUM TRANSPORT RESULTS AFTER 6 MONTHS TRANSITION IN MODEL LAYER 2	
	FIGURE <span style="font-size: 24pt; font-weight: bold;">7.4-5</span>



**LEGEND**

- IRZ WELLS
- ⊕ UPGRADIENT INJECTION WELLS
- EXTRACTION WELLS
- ⊕ MONITORING WELLS



PG&E  
TOPOCK COMPRESSOR STATION  
NEEDLES, CALIFORNIA  
MODELING APPENDIX

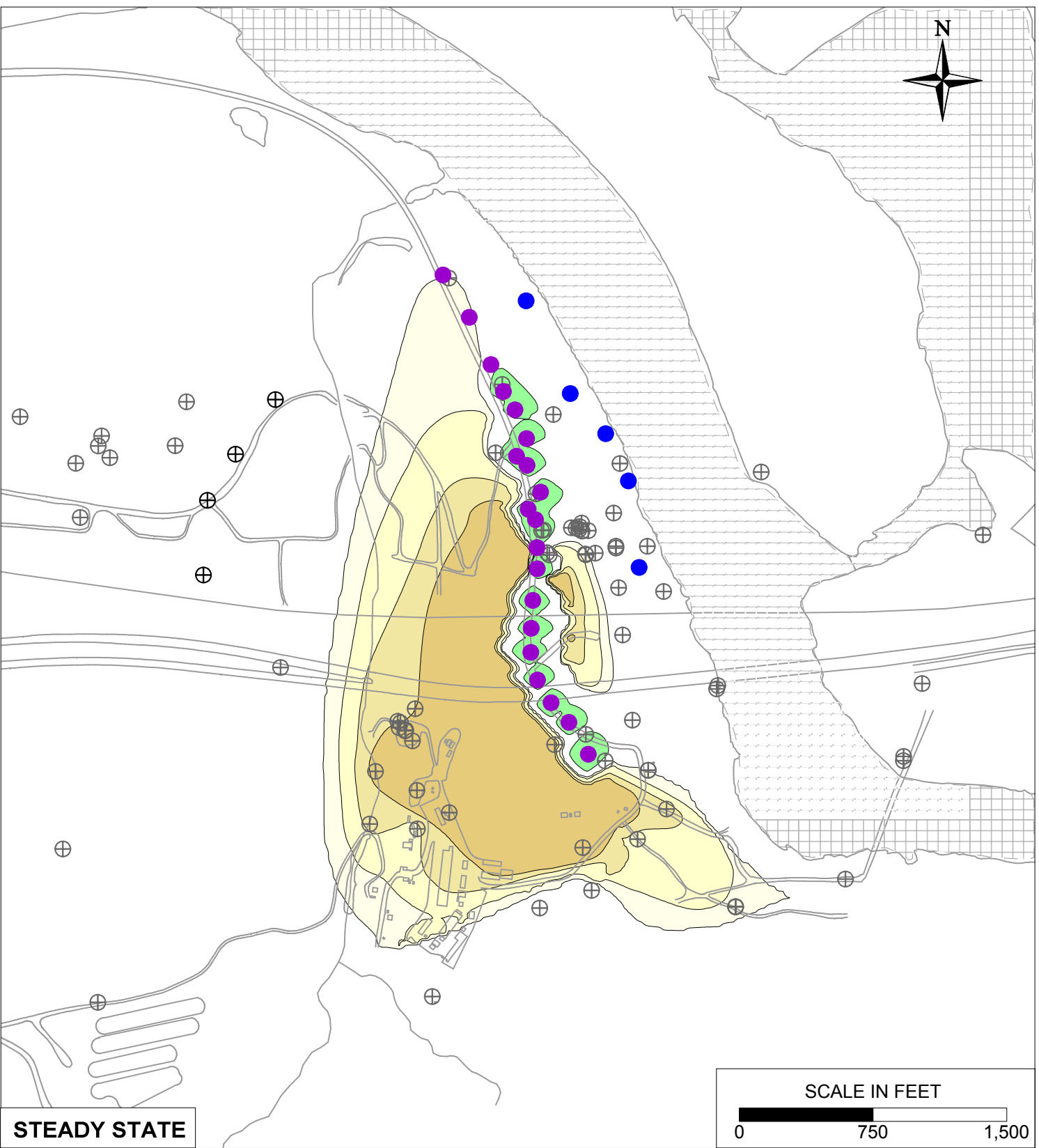
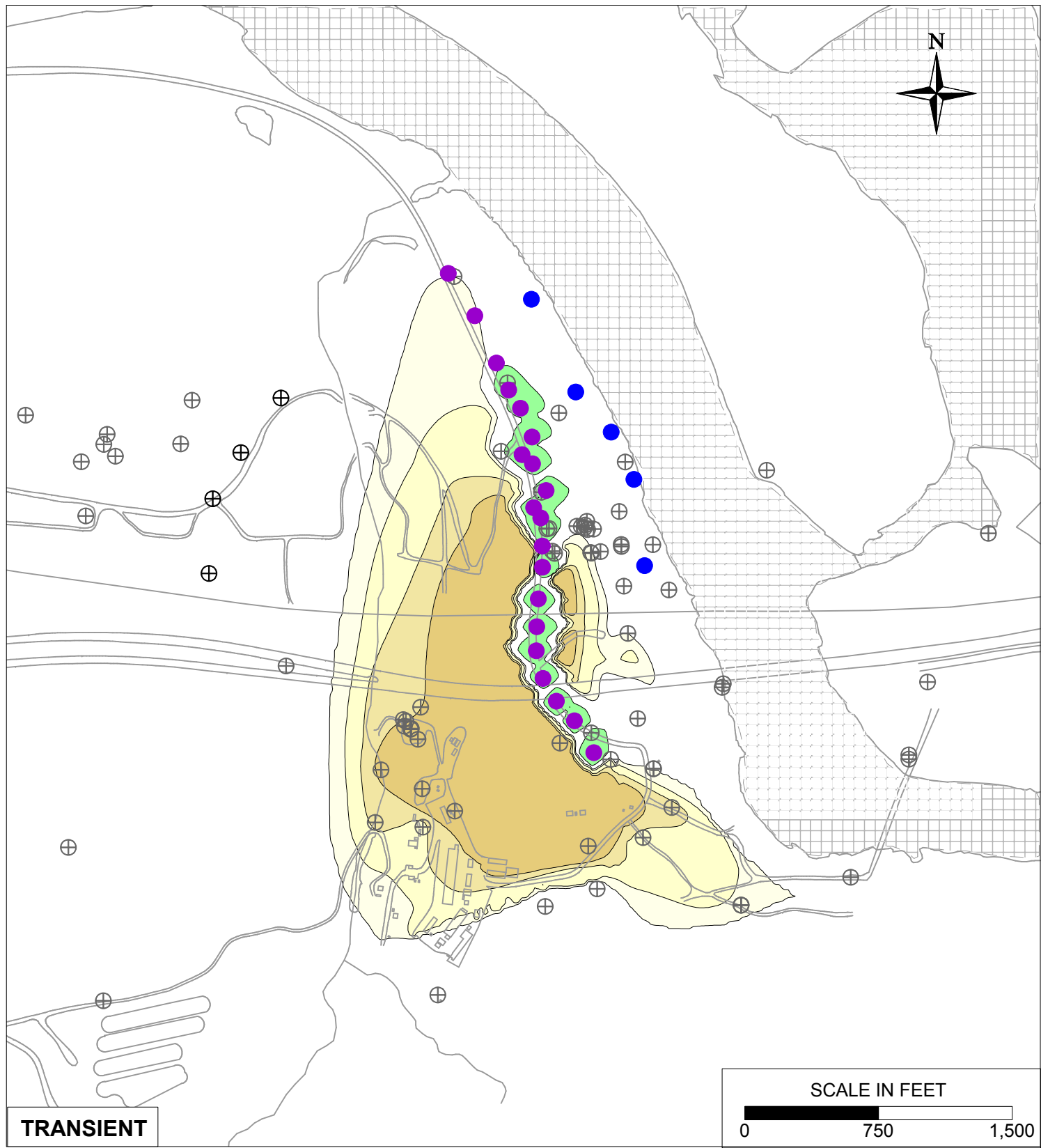
TRANSIENT AND STEADY STATE SIMULATED  
CHROMIUM TRANSPORT RESULTS AFTER  
6 MONTHS TRANSITION IN MODEL LAYER 4



FIGURE

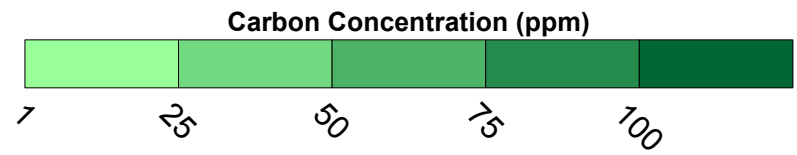
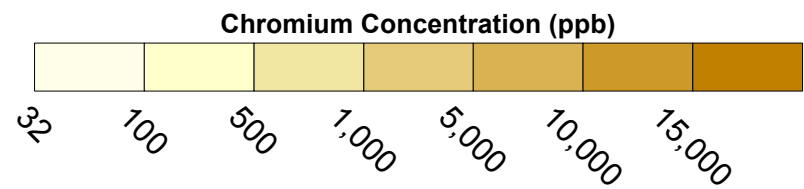
7.4-6





**LEGEND**

- IRZ WELLS
- ⊕ UPGRADIENT INJECTION WELLS
- EXTRACTION WELLS
- ⊕ MONITORING WELLS



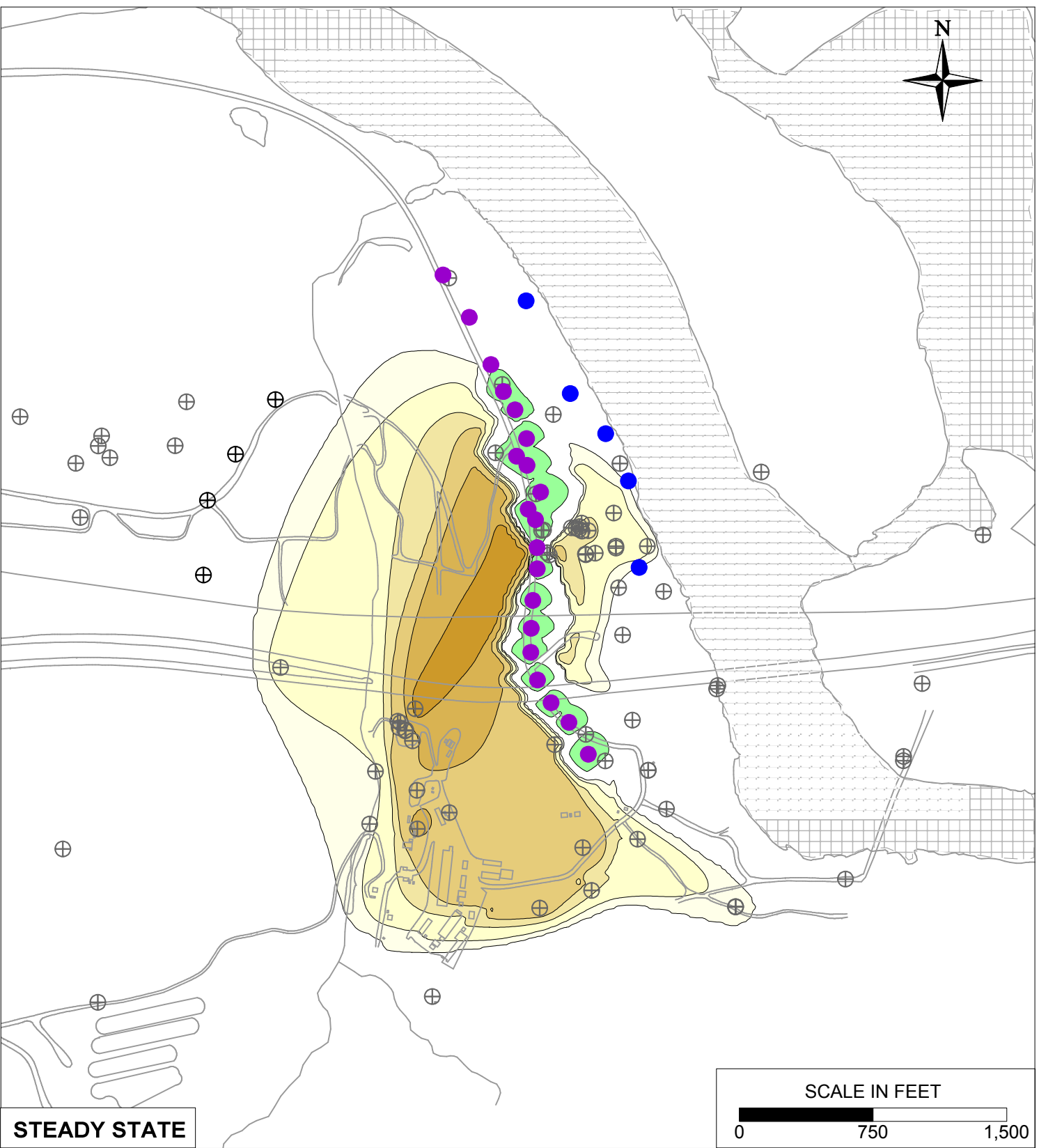
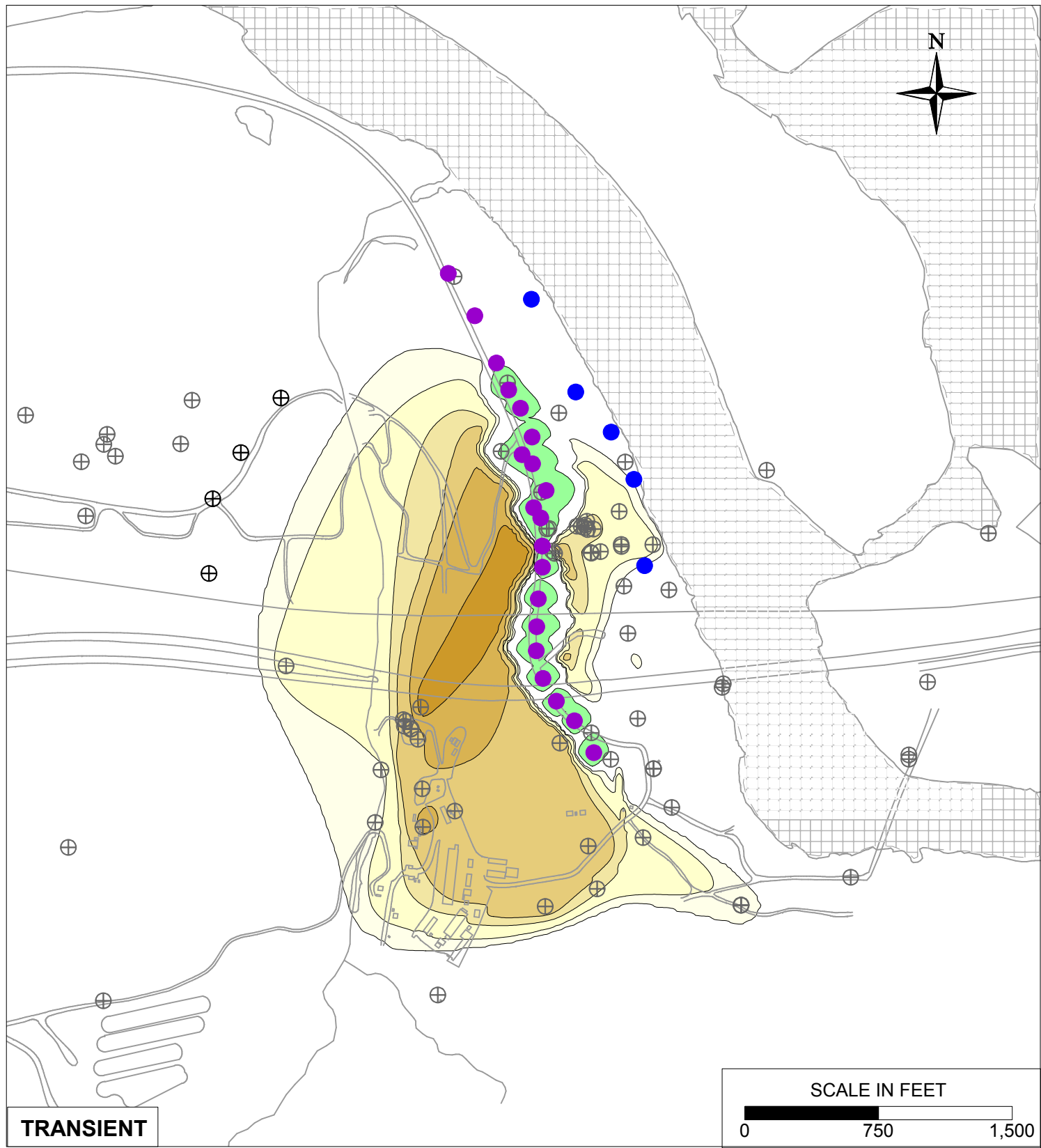
PG&E  
TOPOCK COMPRESSOR STATION  
NEEDLES, CALIFORNIA  
MODELING APPENDIX

TRANSIENT AND STEADY STATE SIMULATED  
CHROMIUM TRANSPORT RESULTS AFTER  
9 MONTHS TRANSITION IN MODEL LAYER 2



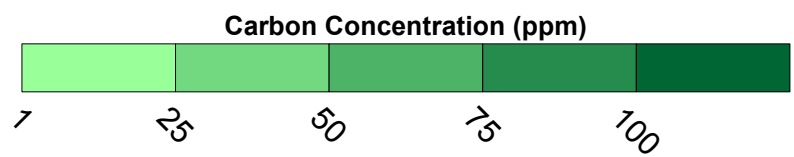
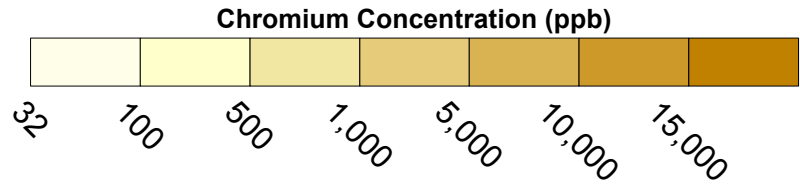
FIGURE

7.4-7



**LEGEND**

- IRZ WELLS
- ⊕ UPGRADIENT INJECTION WELLS
- EXTRACTION WELLS
- ⊕ MONITORING WELLS



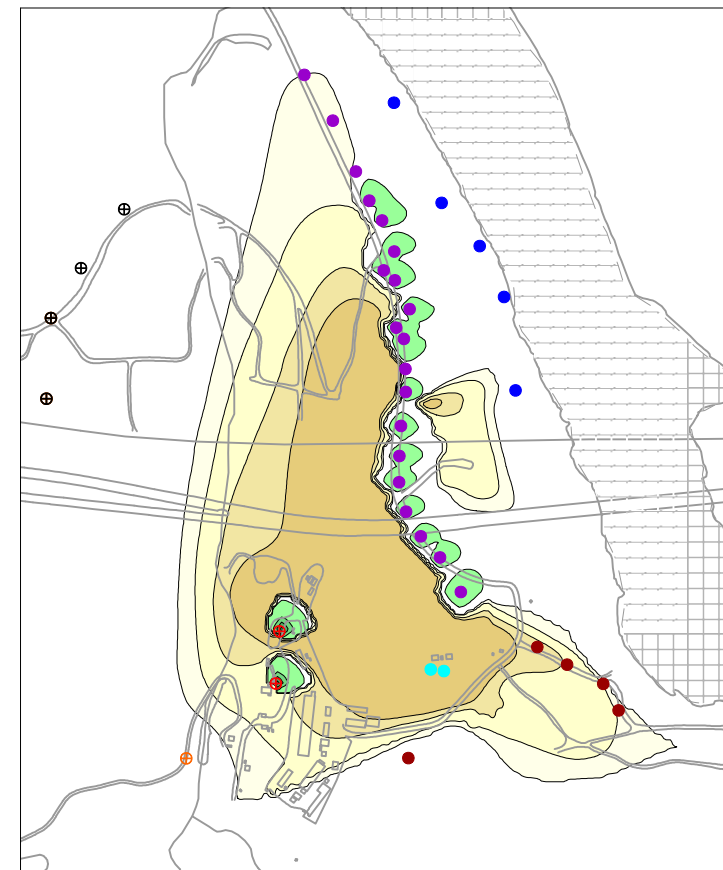
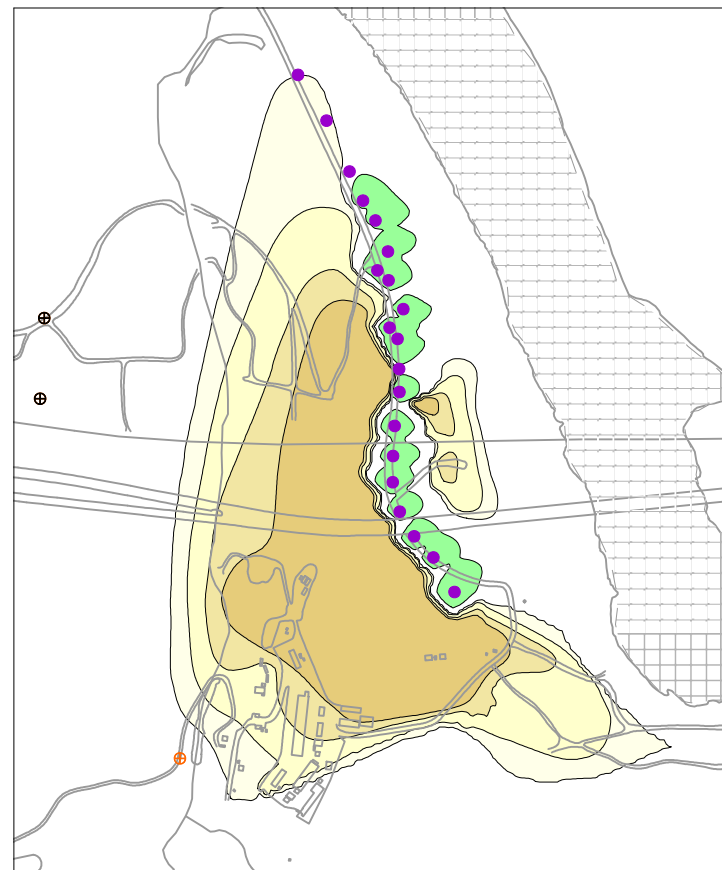
PG&E  
TOPOCK COMPRESSOR STATION  
NEEDLES, CALIFORNIA  
MODELING APPENDIX

TRANSIENT AND STEADY STATE SIMULATED  
CHROMIUM TRANSPORT RESULTS AFTER  
9 MONTHS TRANSITION IN MODEL LAYER 4



FIGURE  
7.4-8





**LEGEND**

- NTH IRZ WELLS
- RIVERBANK EXTRACTION WELLS
- IRL INJECTION WELLS
- FRESHWATER INJECTION WELLS
- TCS INJECTION WELLS
- TRANSWESTERN BENCH EXTRACTION WELLS
- EAST RAVINE EXTRACTION WELLS

**\*Note:** The intermediate nominal scenario assumes IRL-1 and IRL-2 (northern wells) will receive carbon-amended River Bank extraction well water if hexavalent chromium concentrations in the River Bank extraction wells exceed the clean-up goal; and IRL-3 and IRL-4 (southern wells) will receive freshwater. Therefore, the startup scenarios include IRL-3 and IRL-4 with the FW ON; IRL ON includes only IRL-1 and IRL-2. Injection wells IRL-1 through IRL-4 will be constructed for flexibility to inject either/both freshwater or/and River Bank extraction well water during the lifetime of the remedy. FW-1 (not shown) is located west of the area shown.

**SCALE IN FEET**

0 1,000 2,000

1A

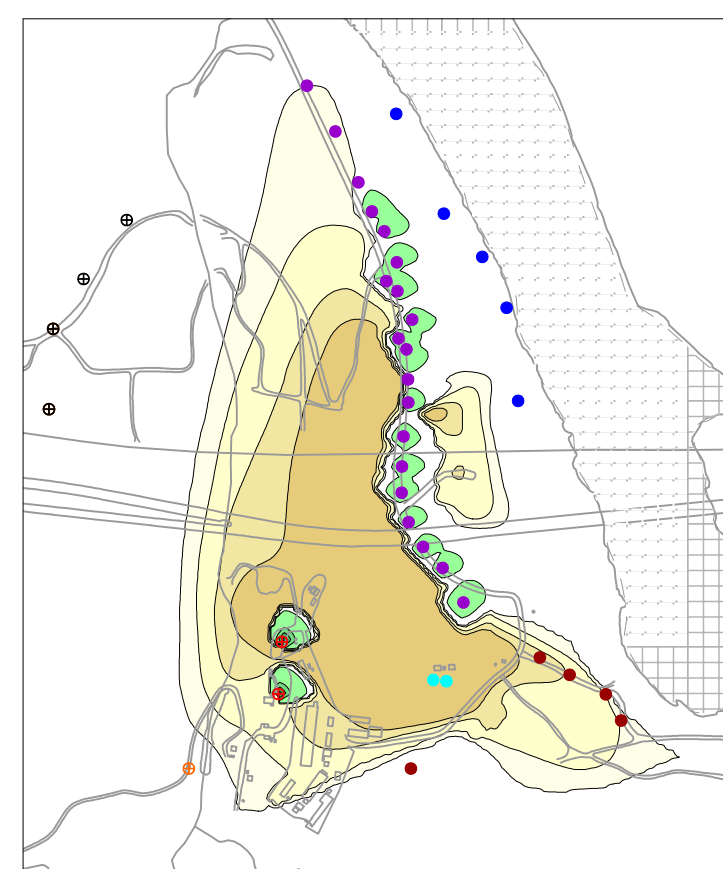
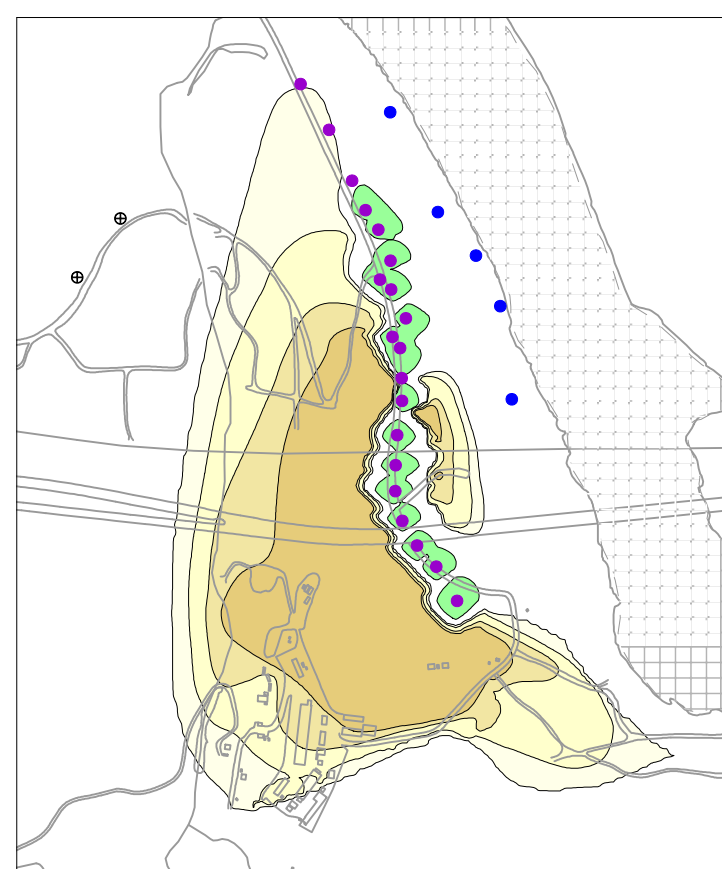
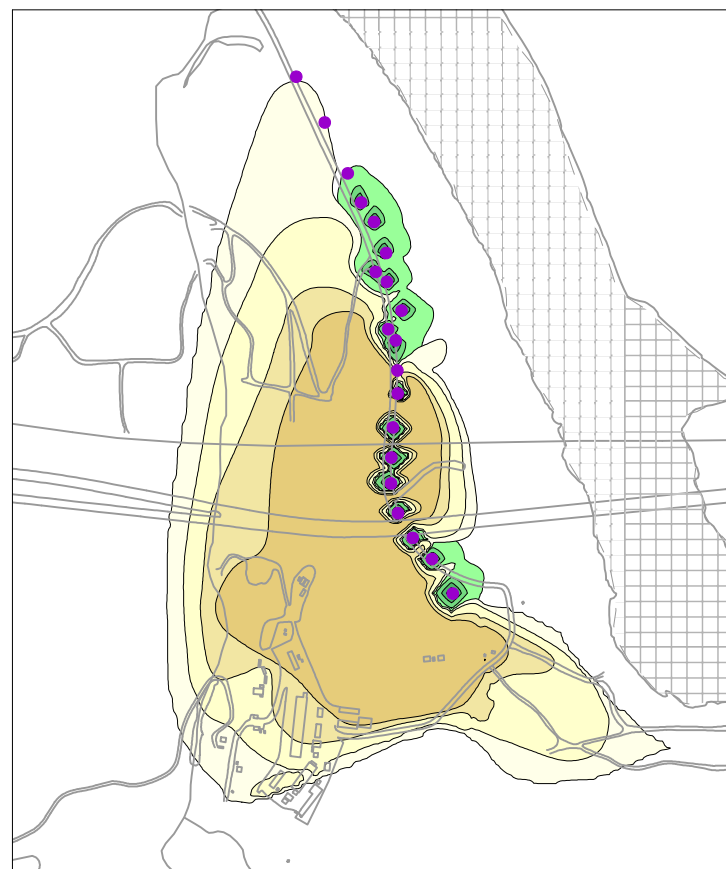
Transition Month 6  
NTH IRZ ON

Transition Month 9  
FW ON

Transition Month 12  
FW, TCS Recirculation Loop, & IRL ON

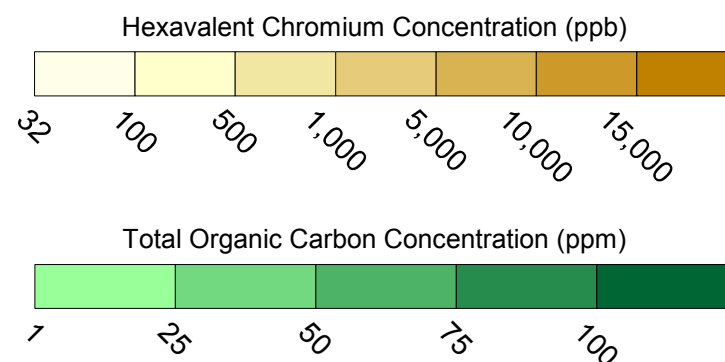
**SCENARIO 1A START UP SCHEDULE**

Months 0-6: NTH IRZ ON  
Months 6-9: NTH IRZ OFF and FW ON  
Months 9-12: NTH IRZ OFF and FW,  
TCS Recirculation Loop, & IRL ON



**SCENARIO 2A START UP SCHEDULE**

Months 0-6: NTH IRZ ON  
Months 6-9: NTH IRZ OFF and IRL ON  
Months 9-12: NTH IRZ OFF and FW,  
TCS Recirculation Loop, & IRL ON



2A

Transition Month 6  
NTH IRZ ON

Transition Month 9  
IRL ON

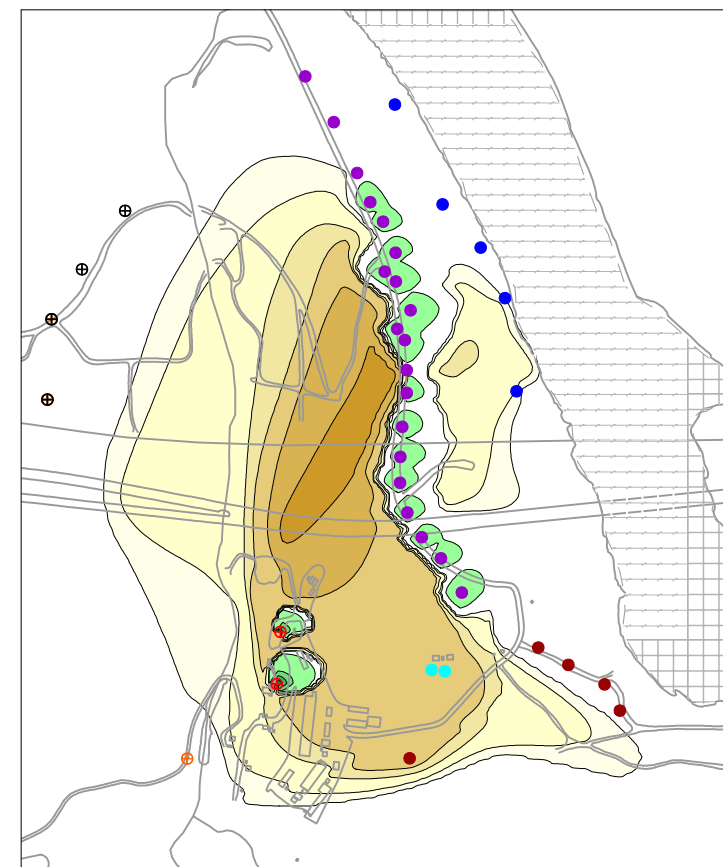
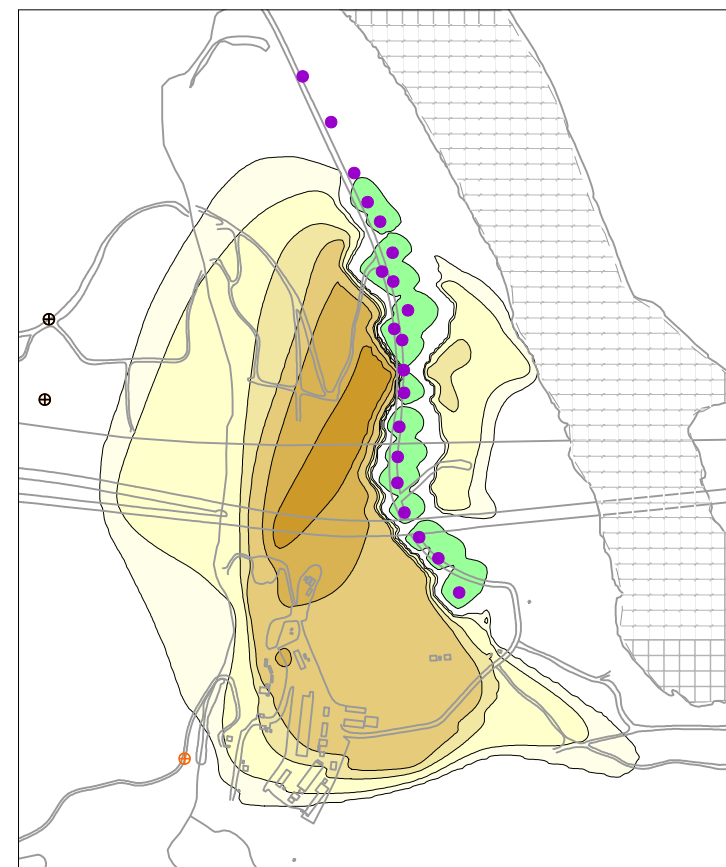
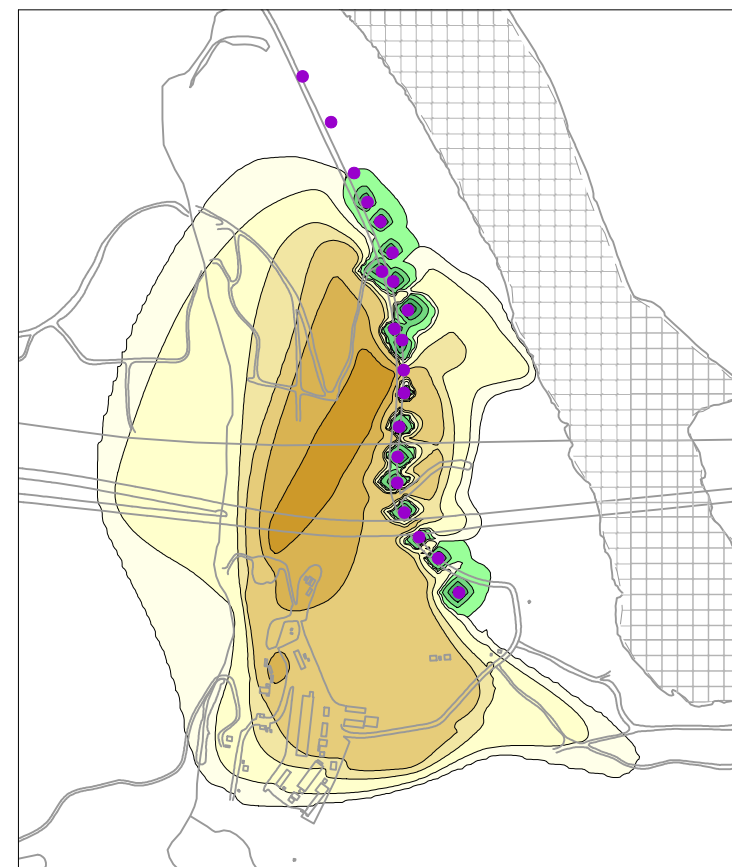
Transition Month 12  
IRL, FW, & TCS Recirculation Loop ON

PG&E  
TOPOCK COMPRESSOR STATION  
NEEDLES, CALIFORNIA  
MODELING APPENDIX

**SIMULATED HEXAVALENT CHROMIUM  
TRANSPORT IN MODEL LAYER 2 FOR  
1 YEAR START UP SCENARIOS**

**ARCADIS**

FIGURE  
7.4-9



**LEGEND**

- NTH IRZ WELLS
- RIVERBANK EXTRACTION WELLS
- IRL INJECTION WELLS
- FRESHWATER INJECTION WELLS
- TCS INJECTION WELLS
- TRANSWESTERN BENCH EXTRACTION WELLS
- EAST RAVINE EXTRACTION WELLS

\*Note: The intermediate nominal scenario assumes IRL-1 and IRL-2 (northern wells) will receive carbon-amended River Bank extraction well water if hexavalent chromium concentrations in the River Bank extraction wells exceed the clean-up goal; and IRL-3 and IRL-4 (southern wells) will receive freshwater. Therefore, the startup scenarios include IRL-3 and IRL-4 with the FW ON; IRL ON includes only IRL-1 and IRL-2. Injection wells IRL-1 through IRL-4 will be constructed for flexibility to inject either/both freshwater or/and River Bank extraction well water during the lifetime of the remedy. FW-1 (not shown) is located west of the area shown.

**SCALE IN FEET**

0 1,000 2,000

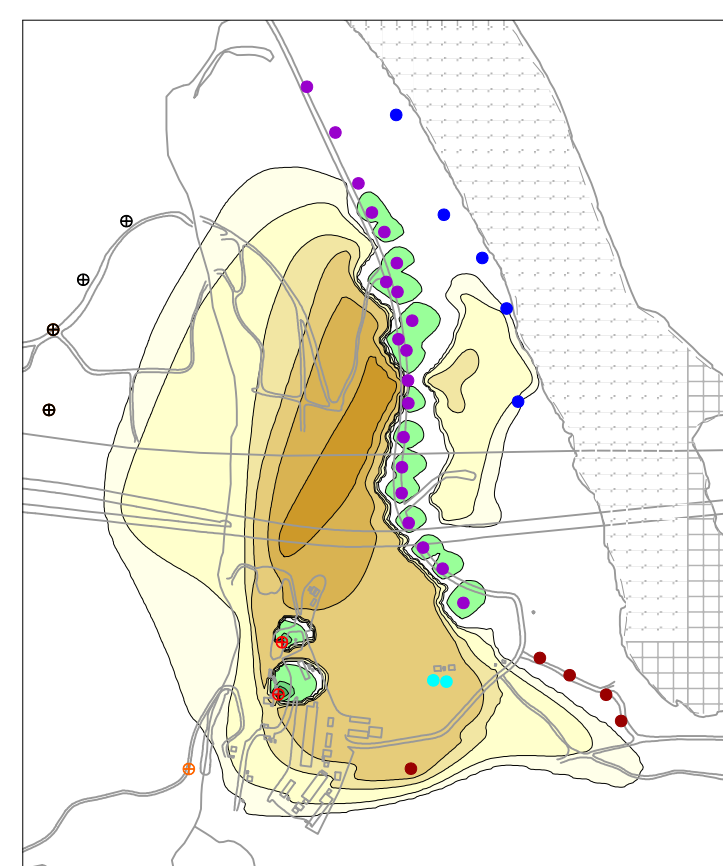
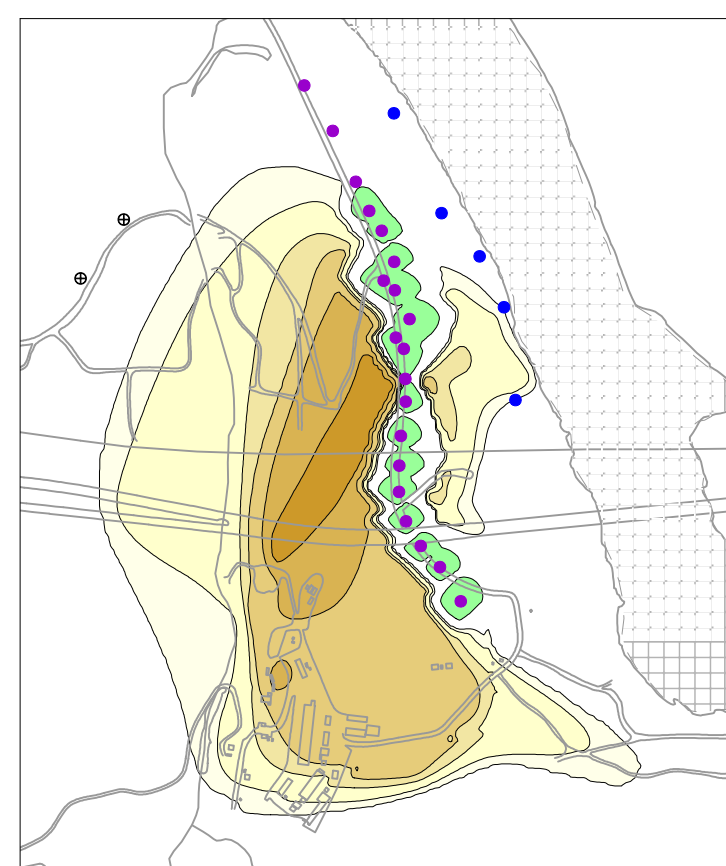
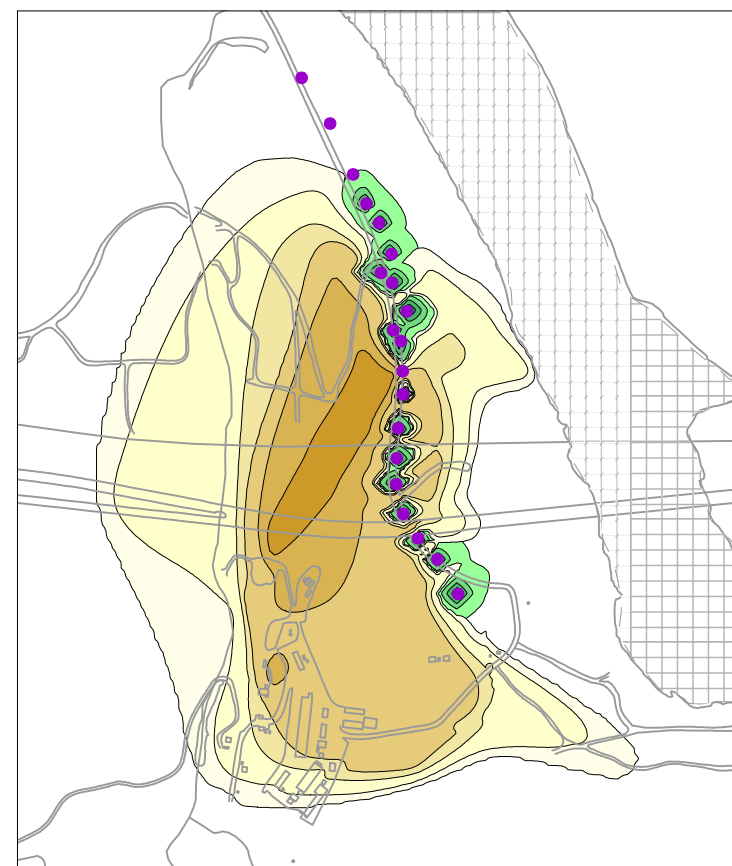
1A

Transition Month 6  
NTH IRZ ON

Transition Month 9  
FW ON

Transition Month 12  
FW, TCS Recirculation Loop, & IRL ON

**SCENARIO 1A START UP SCHEDULE**  
 Months 0-6: NTH IRZ ON  
 Months 6-9: NTH IRZ OFF and FW ON  
 Months 9-12: NTH IRZ OFF and FW,  
 TCS Recirculation Loop, & IRL ON



**SCENARIO 2A START UP SCHEDULE**  
 Months 0-6: NTH IRZ ON  
 Months 6-9: NTH IRZ OFF and IRL ON  
 Months 9-12: NTH IRZ OFF and FW,  
 TCS Recirculation Loop, & IRL ON

Hexavalent Chromium Concentration (ppb)

32 100 500 1,000 5,000 10,000 15,000

Total Organic Carbon Concentration (ppm)

1 25 50 75 100

2A

Transition Month 6  
NTH IRZ ON

Transition Month 9  
IRL ON

Transition Month 12  
IRL, FW, & TCS Recirculation Loop ON

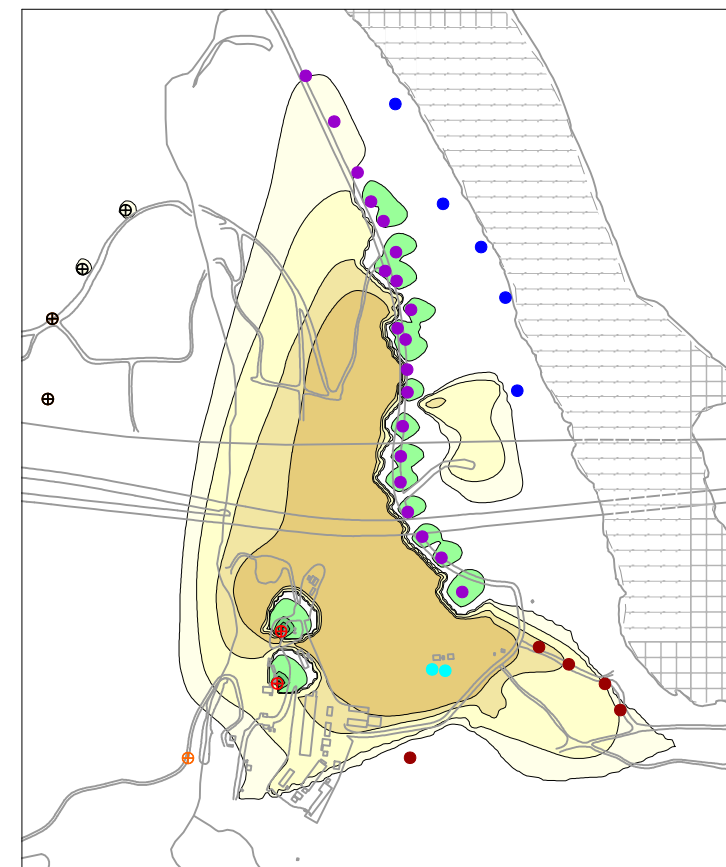
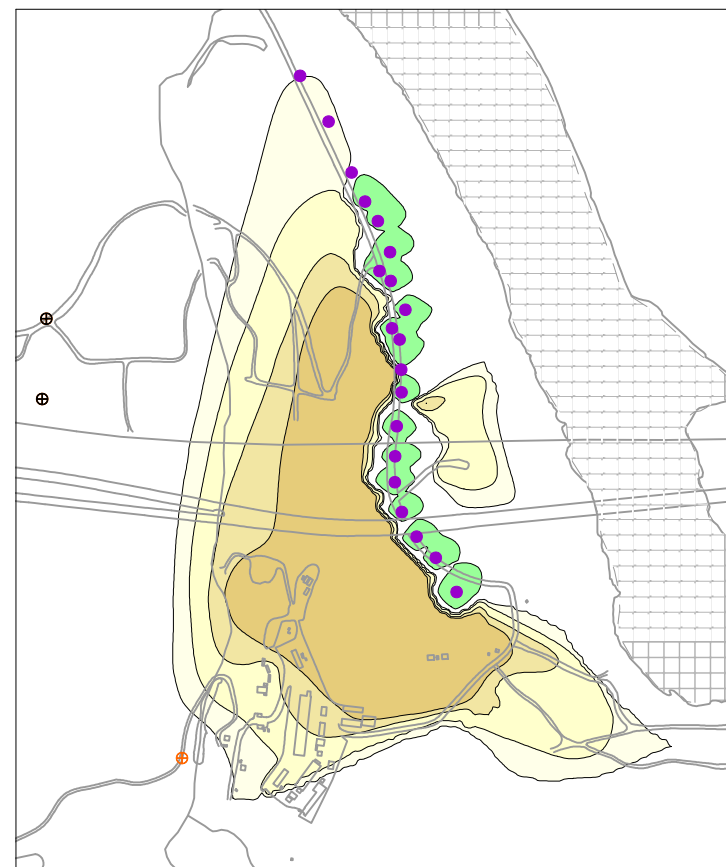
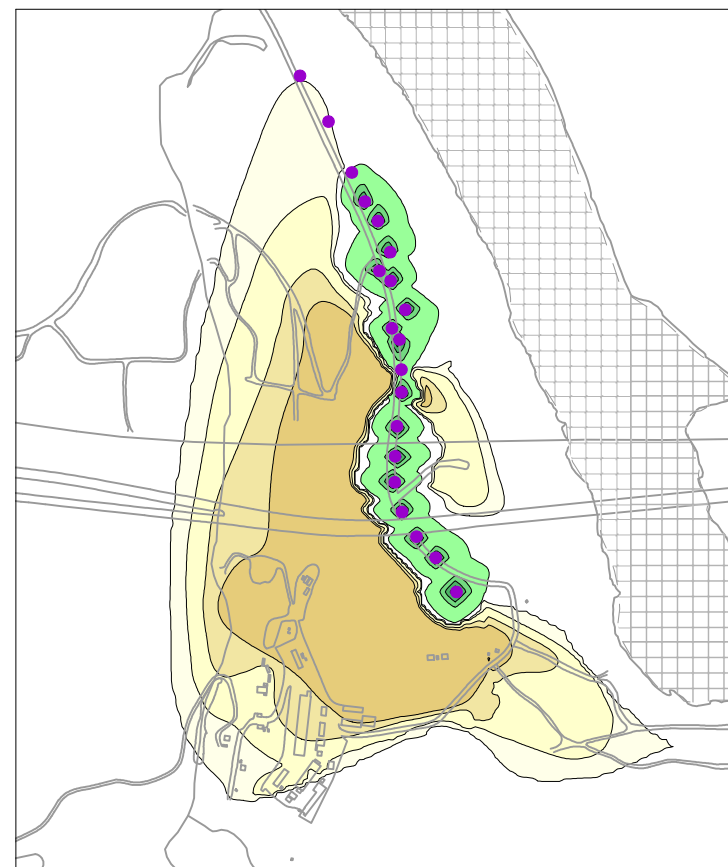
PG&E  
 TOPOCK COMPRESSOR STATION  
 NEEDLES, CALIFORNIA  
 MODELING APPENDIX

SIMULATED HEXAVALENT CHROMIUM  
 TRANSPORT IN MODEL LAYER 4 FOR  
 1 YEAR START UP SCENARIOS

**ARCADIS**

FIGURE  
 7.4-10





**LEGEND**

- NTH IRZ WELLS
- RIVERBANK EXTRACTION WELLS
- IRL INJECTION WELLS
- FRESHWATER INJECTION WELLS
- TCS INJECTION WELLS
- TRANSWESTERN BENCH EXTRACTION WELLS
- EAST RAVINE EXTRACTION WELLS

\*Note: The intermediate nominal scenario assumes IRL-1 and IRL-2 (northern wells) will receive carbon-amended River Bank extraction well water if hexavalent chromium concentrations in the River Bank extraction wells exceed the clean-up goal; and IRL-3 and IRL-4 (southern wells) will receive freshwater. Therefore, the startup scenarios include IRL-3 and IRL-4 with the FW ON; IRL ON includes only IRL-1 and IRL-2. Injection wells IRL-1 through IRL-4 will be constructed for flexibility to inject either/both freshwater or/and River Bank extraction well water during the lifetime of the remedy. FW-1 (not shown) is located west of the area shown.

**SCALE IN FEET**

0 1,000 2,000

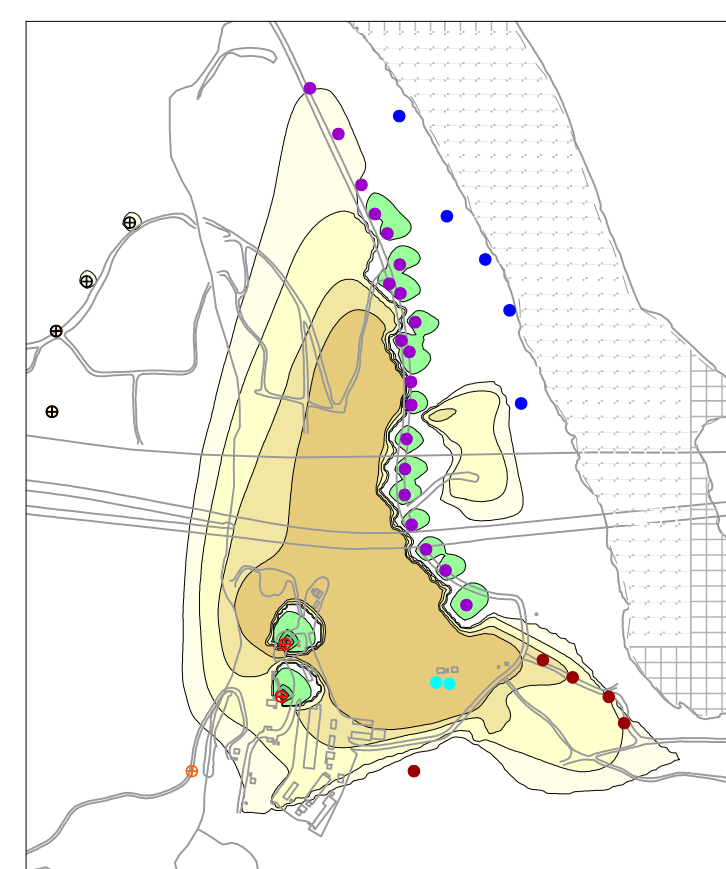
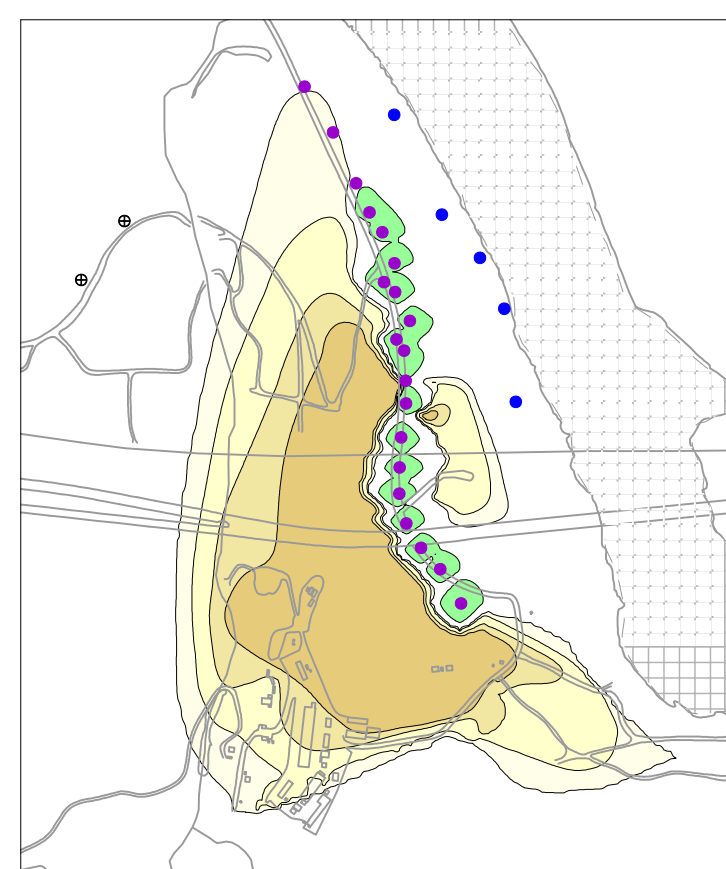
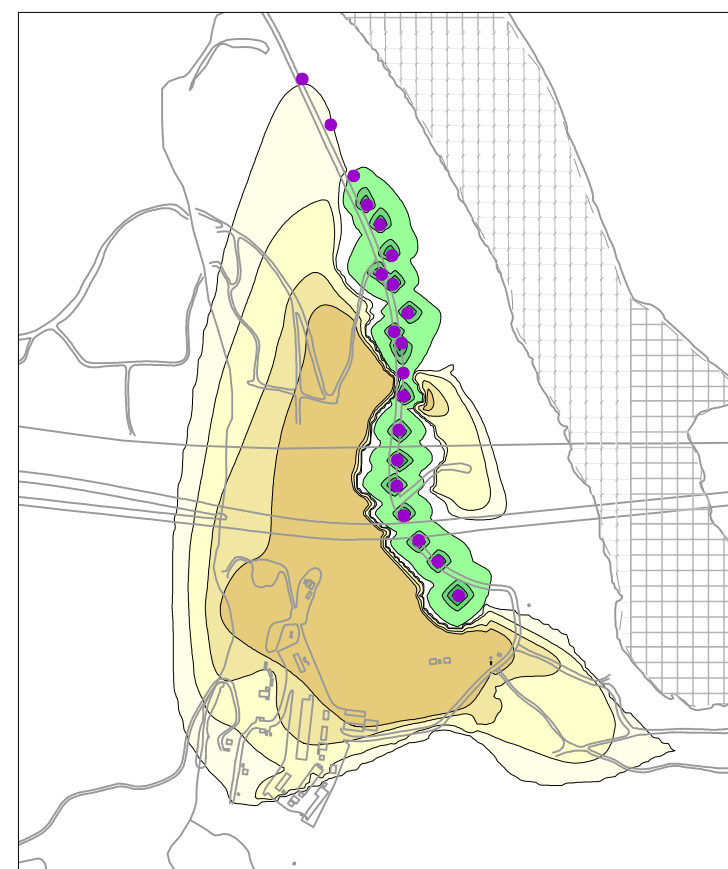
1B

Transition Month 12  
NTH IRZ ON

Transition Month 18  
FW ON

Transition Month 24  
FW, TCS Recirculation Loop, & IRL ON

**SCENARIO 1B START UP SCHEDULE**  
Months 0-12: NTH IRZ ON  
Months 12-18: NTH IRZ OFF and FW ON  
Months 18-24: NTH IRZ OFF and FW,  
TCS Recirculation Loop, & IRL ON



**SCENARIO 2B START UP SCHEDULE**  
Months 0-12: NTH IRZ ON  
Months 12-18: NTH IRZ OFF and IRL ON  
Months 18-24: NTH IRZ OFF and FW,  
TCS Recirculation Loop, & IRL ON

Hexavalent Chromium Concentration (ppb)

32 100 500 1,000 5,000 10,000 15,000

Total Organic Carbon Concentration (ppm)

7 25 50 75 100

2B

Transition Month 12  
NTH IRZ ON

Transition Month 18  
IRL ON

Transition Month 24  
IRL, FW, & TCS Recirculation Loop ON

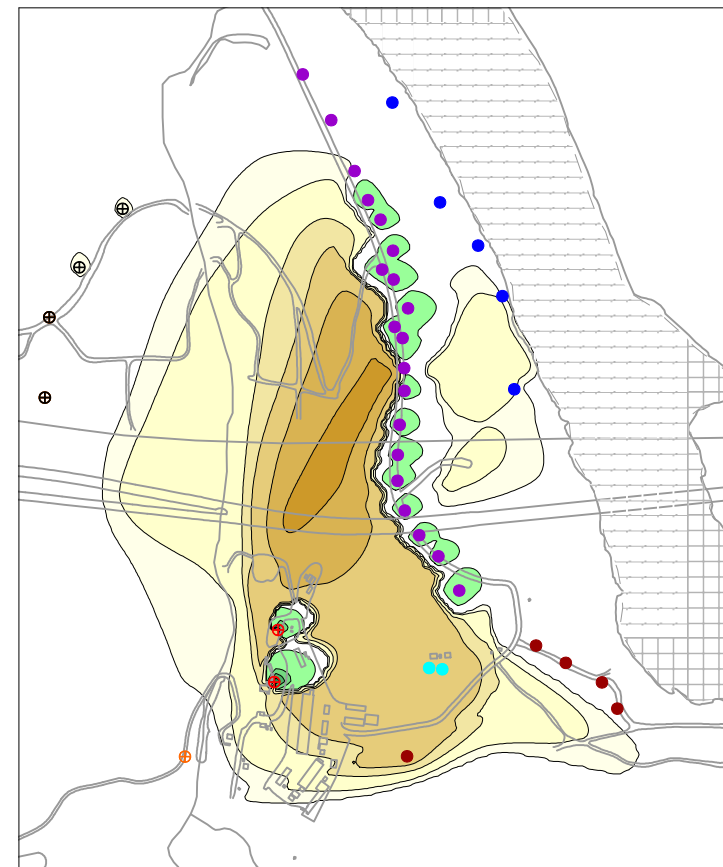
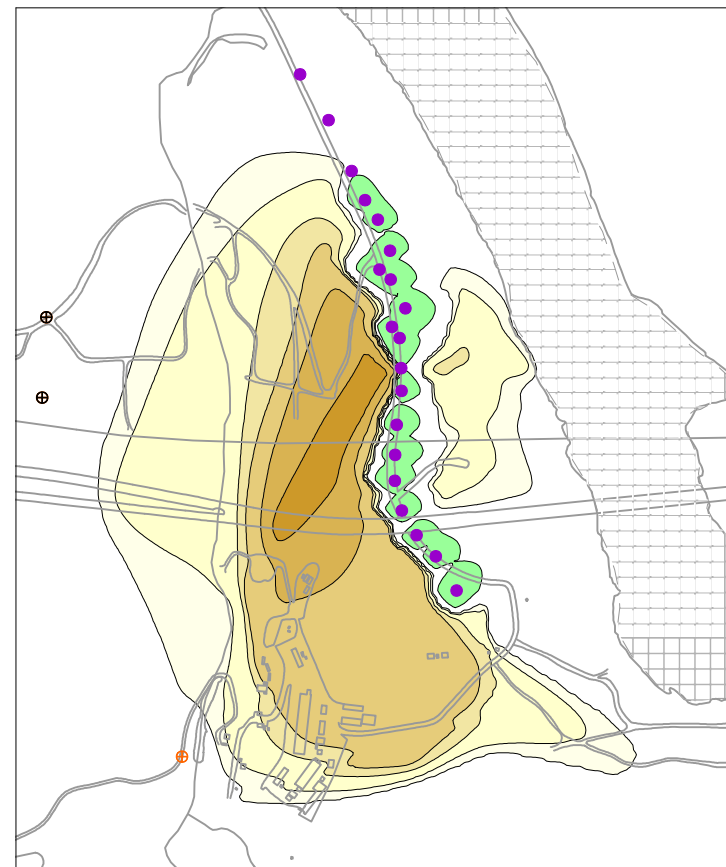
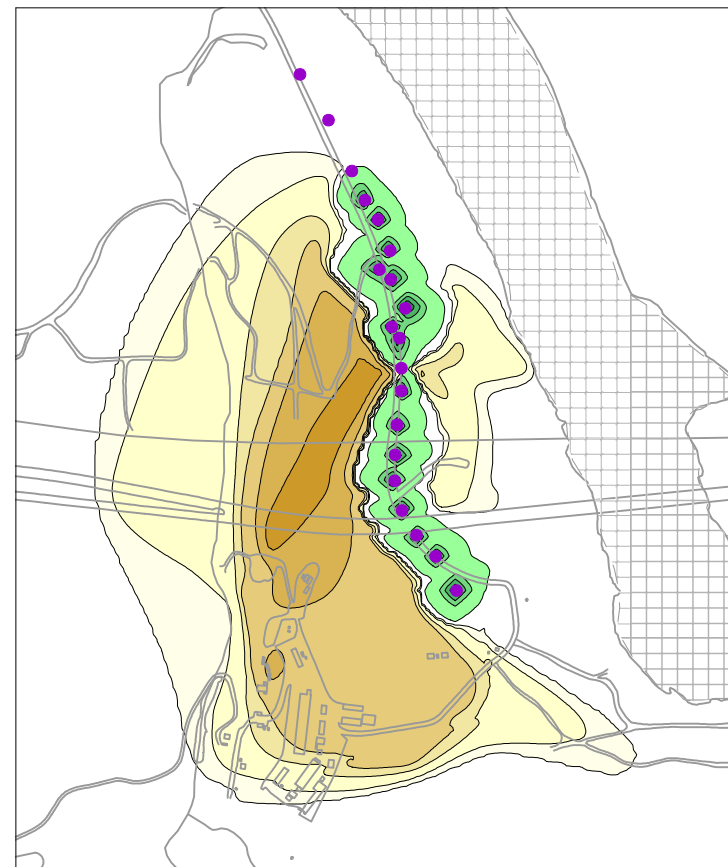
PG&E  
TOPOCK COMPRESSOR STATION  
NEEDLES, CALIFORNIA  
MODELING APPENDIX

**SIMULATED HEXAVALENT CHROMIUM  
TRANSPORT IN MODEL LAYER 2 FOR  
2 YEAR START UP SCENARIOS**

**ARCADIS**

FIGURE  
7.4-11





**LEGEND**

- NTH IRZ WELLS
- RIVERBANK EXTRACTION WELLS
- IRL INJECTION WELLS
- FRESHWATER INJECTION WELLS
- TCS INJECTION WELLS
- TRANSWESTERN BENCH EXTRACTION WELLS
- EAST RAVINE EXTRACTION WELLS

**\*Note:** The intermediate nominal scenario assumes IRL-1 and IRL-2 (northern wells) will receive carbon-amended River Bank extraction well water if hexavalent chromium concentrations in the River Bank extraction wells exceed the clean-up goal; and IRL-3 and IRL-4 (southern wells) will receive freshwater. Therefore, the startup scenarios include IRL-3 and IRL-4 with the FW ON; IRL ON includes only IRL-1 and IRL-2. Injection wells IRL-1 through IRL-4 will be constructed for flexibility to inject either/both freshwater or/and River Bank extraction well water during the lifetime of the remedy. FW-1 (not shown) is located west of the area shown.

**SCALE IN FEET**

0 1,000 2,000

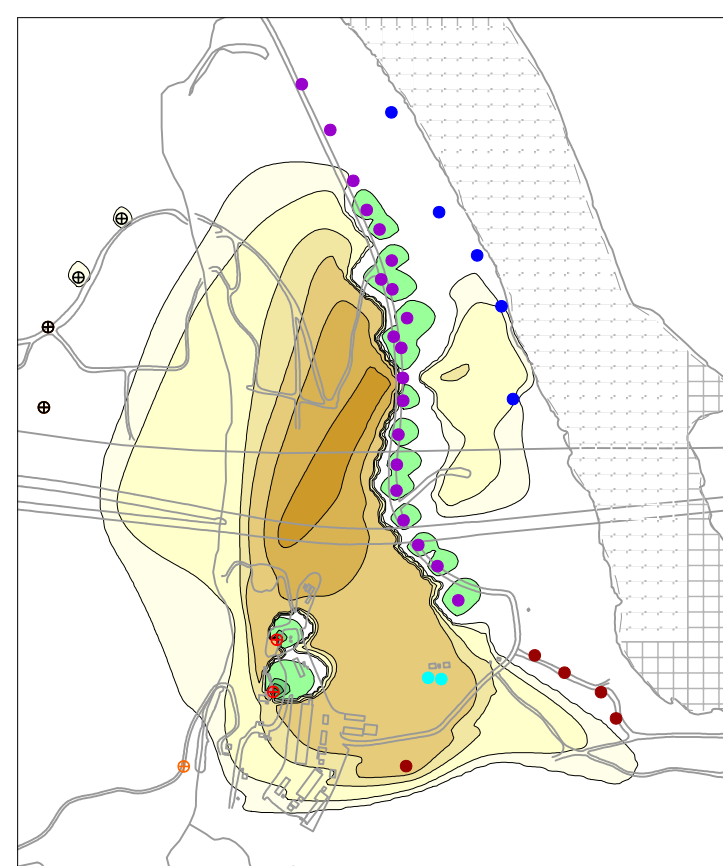
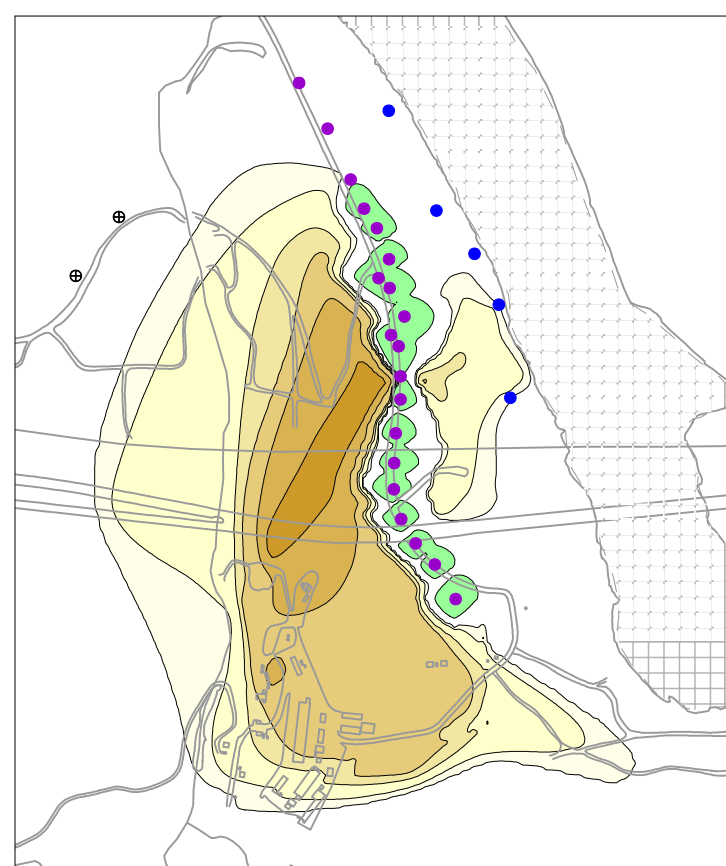
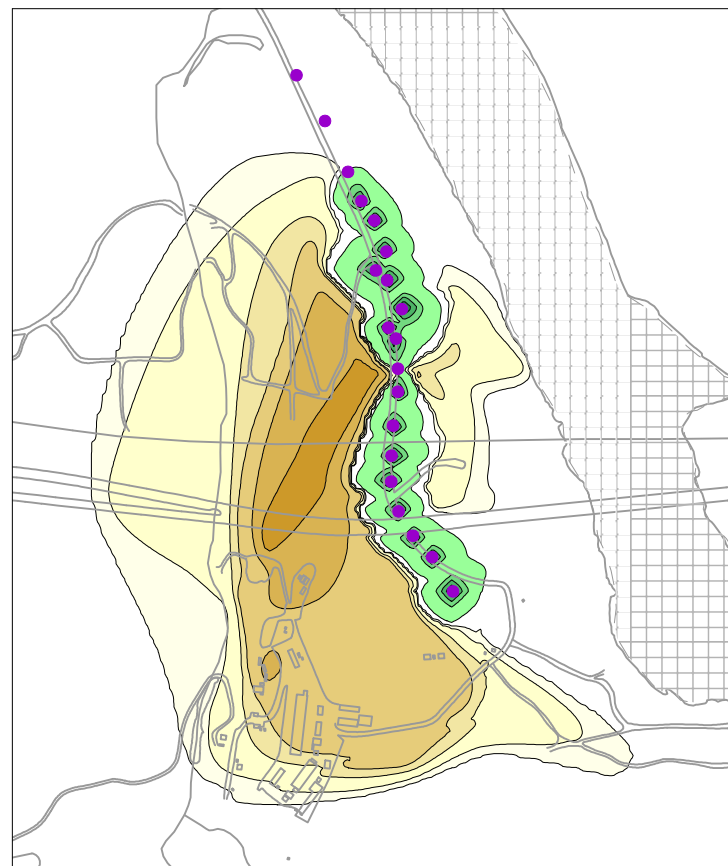
1B

Transition Month 12  
NTH IRZ ON

Transition Month 18  
FW ON

Transition Month 24  
FW, TCS Recirculation Loop, & IRL ON

**SCENARIO 1B START UP SCHEDULE**  
 Months 0-12: NTH IRZ ON  
 Months 12-18: NTH IRZ OFF and FW ON  
 Months 18-24: NTH IRZ OFF and FW,  
 TCS Recirculation Loop, & IRL ON



**SCENARIO 2B START UP SCHEDULE**  
 Months 0-12: NTH IRZ ON  
 Months 12-18: NTH IRZ OFF and IRL ON  
 Months 18-24: NTH IRZ OFF and FW,  
 TCS Recirculation Loop, & IRL ON

Hexavalent Chromium Concentration (ppb)

32 100 500 1,000 5,000 10,000 15,000

Total Organic Carbon Concentration (ppm)

1 25 50 75 100

2B

Transition Month 12  
NTH IRZ ON

Transition Month 18  
IRL ON

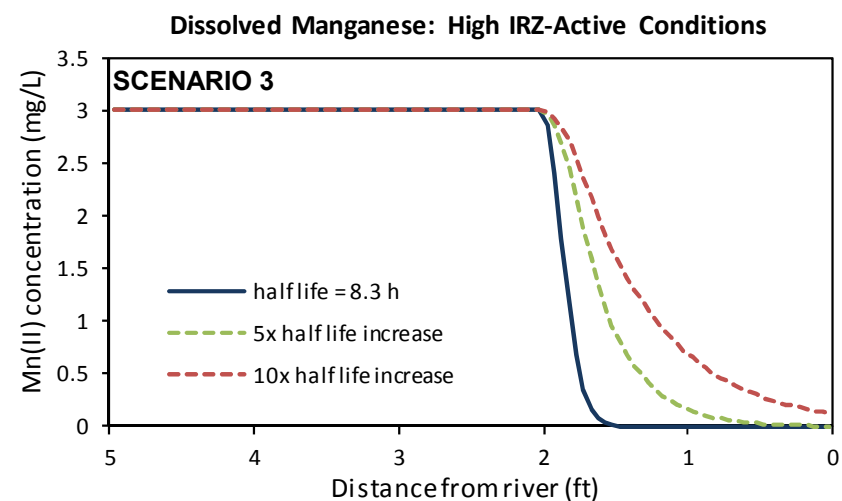
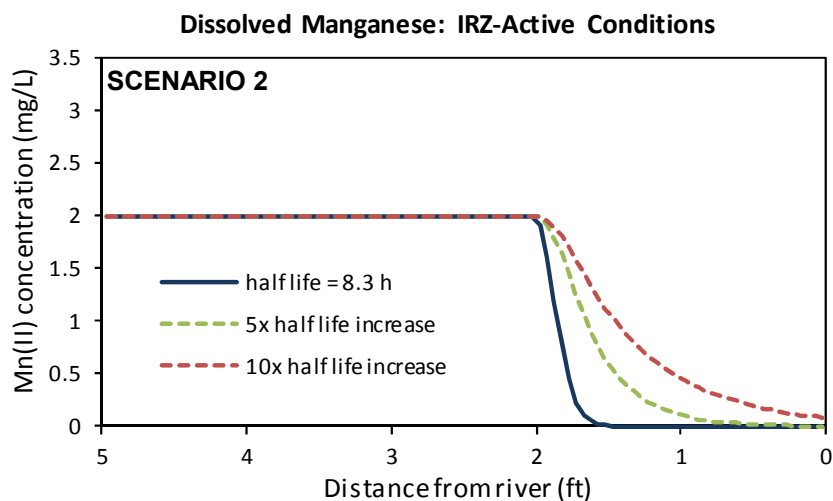
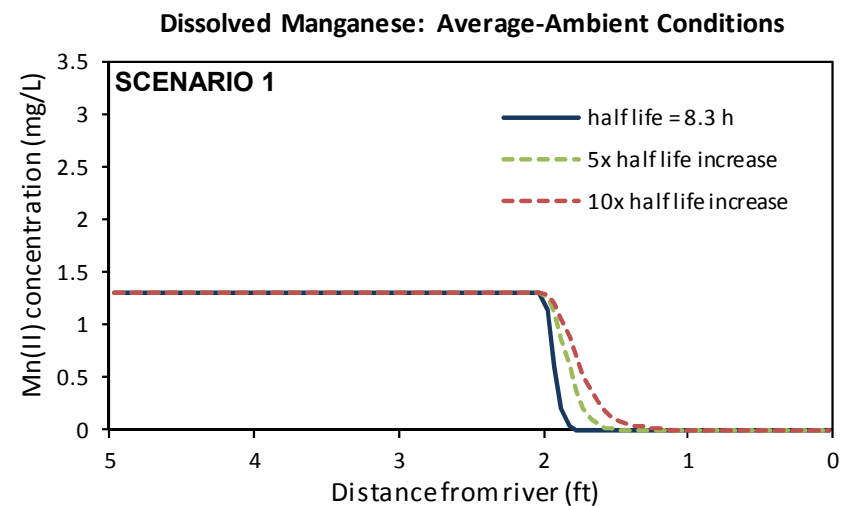
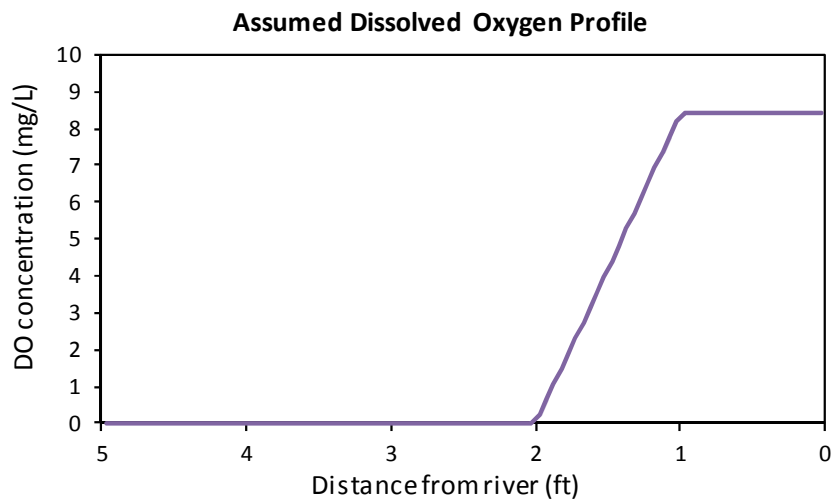
Transition Month 24  
IRL, FW, & TCS Recirculation Loop ON

PG&E  
TOPOCK COMPRESSOR STATION  
NEEDLES, CALIFORNIA  
MODELING APPENDIX

SIMULATED HEXAVALENT CHROMIUM  
TRANSPORT IN MODEL LAYER 4 FOR  
2 YEAR START UP SCENARIOS

**ARCADIS**

FIGURE  
7.4-12



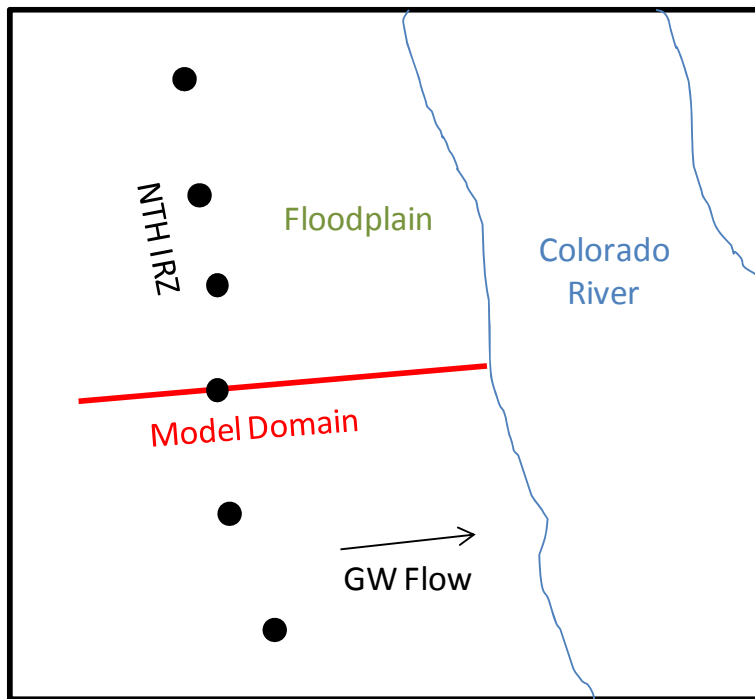
PG&E  
TOPOCK COMPRESSOR STATION  
NEEDLES, CALIFORNIA  
MODELING APPENDIX

Mn(II) OXIDATION IN THE  
HYPORHEIC ZONE

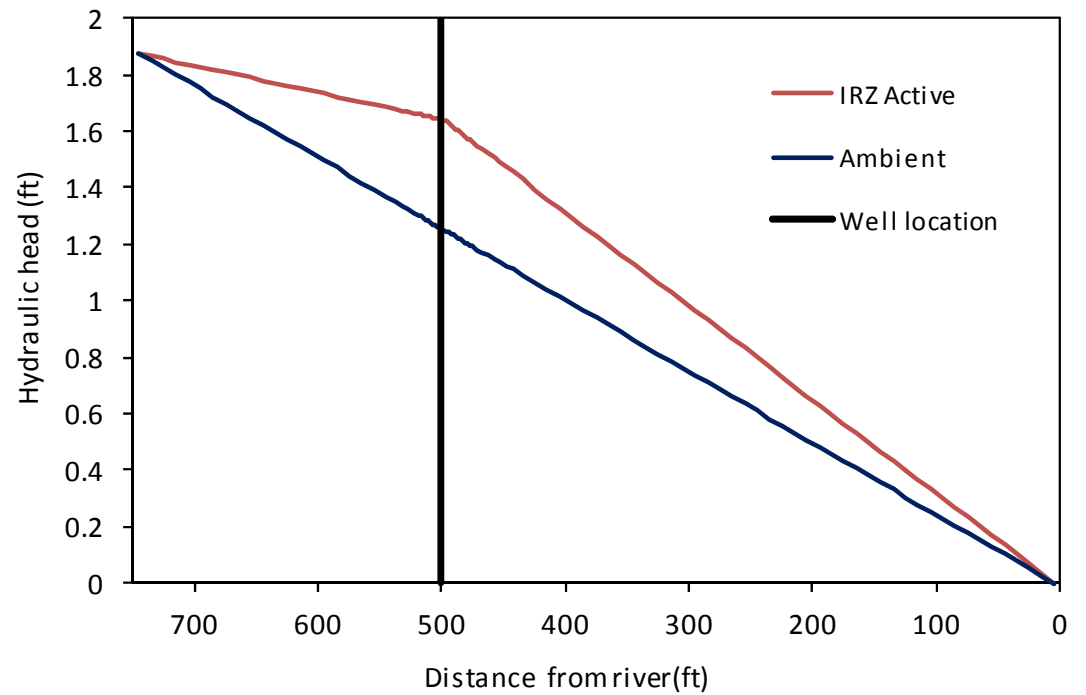


FIGURE  
8.2-1

# One-Dimensional, Hypothetical NTH IRZ Model Domain



## Hydraulic Head Profiles, Active vs. Ambient Conditions

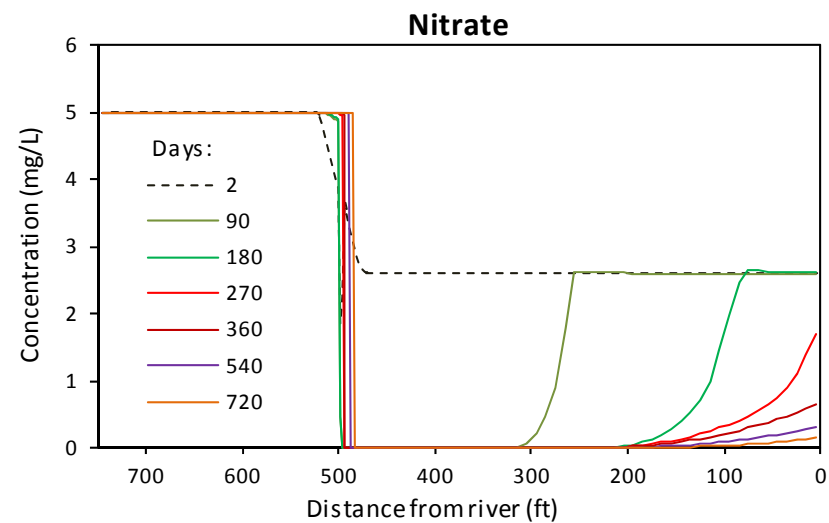
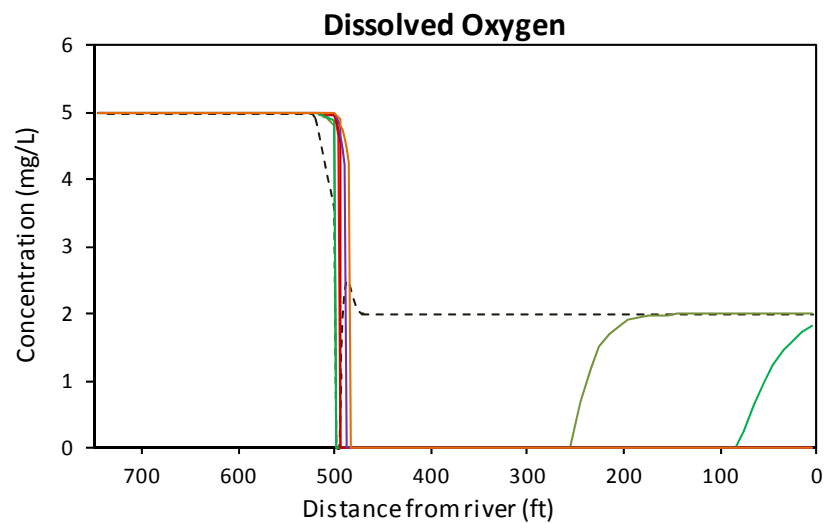
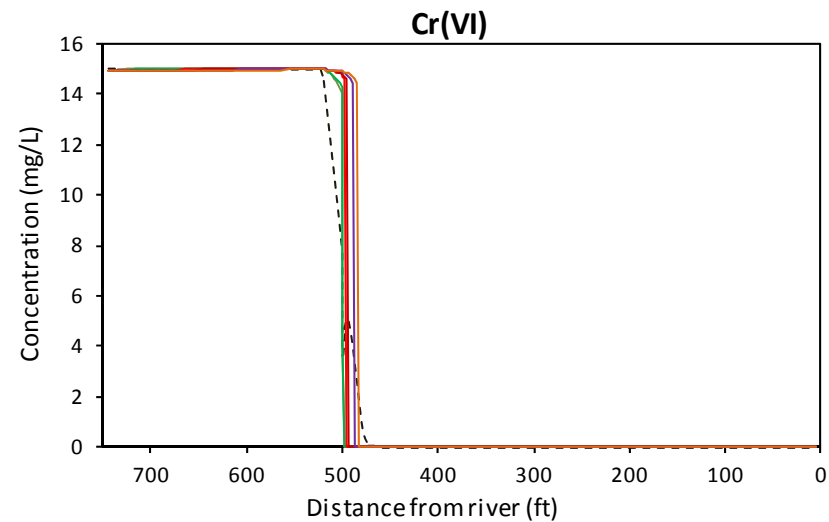
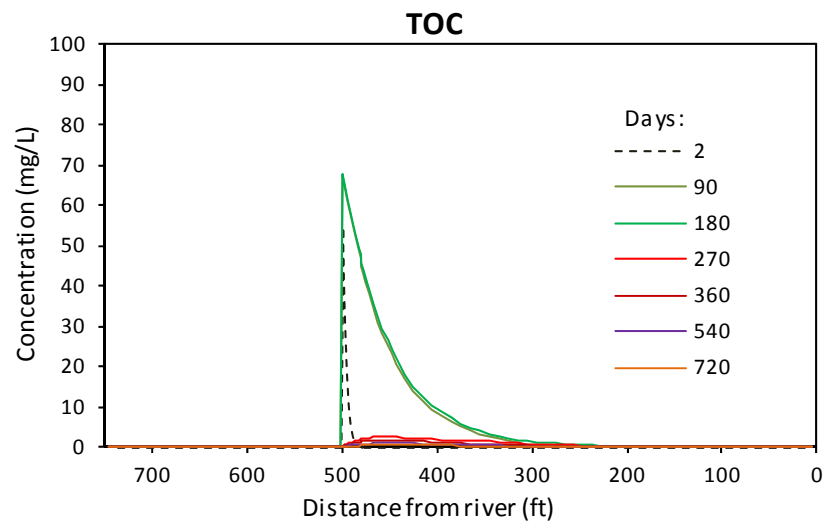


PG&E  
TOPOCK COMPRESSOR STATION  
NEEDLES, CALIFORNIA  
MODELING APPENDIX

HYPOTHETICAL IRZ MODEL DOMAIN AND  
CALIBRATED HYDRAULIC HEAD PROFILE



FIGURE  
9.1-1

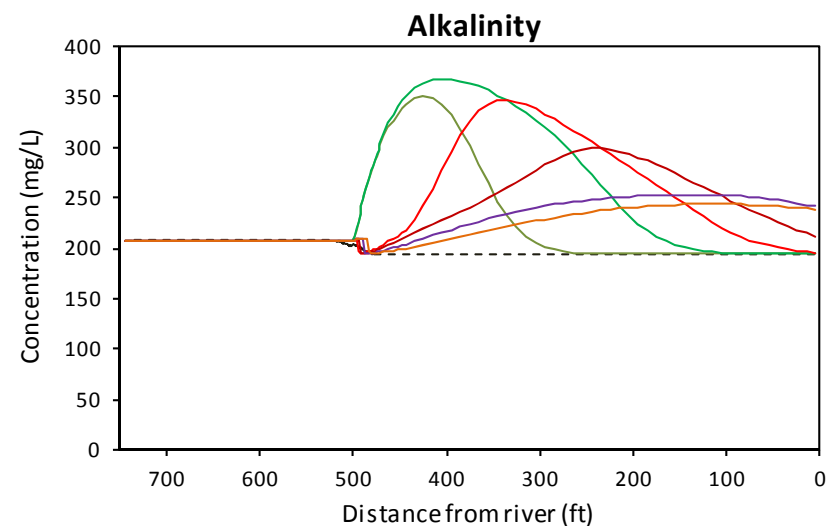
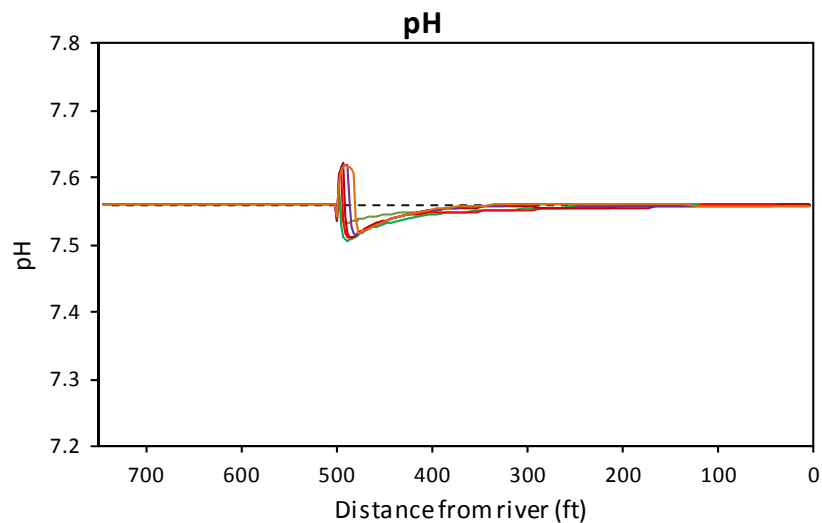
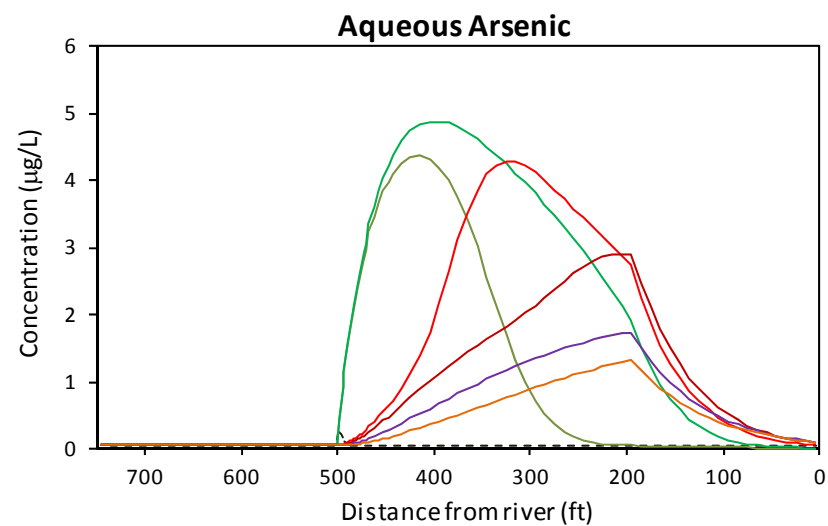
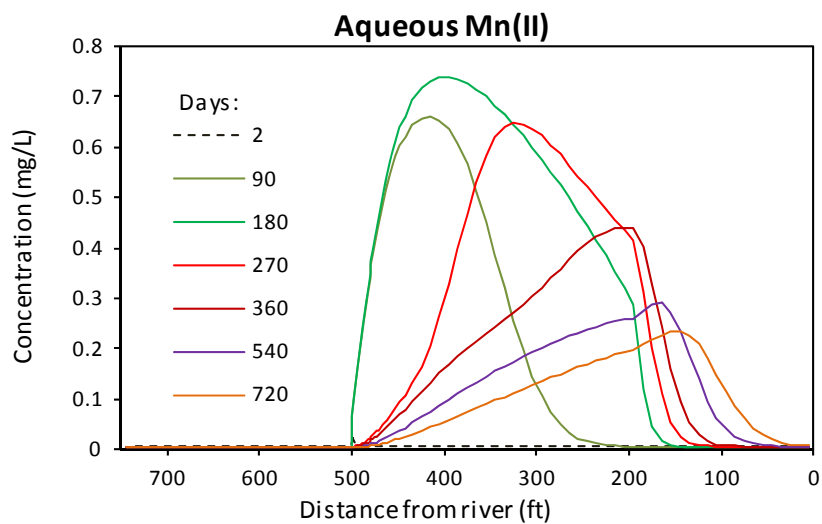


PG&E  
TOPOCK COMPRESSOR STATION  
NEEDLES, CALIFORNIA  
MODELING APPENDIX

GEOCHEMICAL REACTIVE TRANSPORT  
MODEL RESULTS FOR THE 1D IRZ SYSTEM:  
TOC, Cr(VI), DO, AND NITRATE



FIGURE  
**9.1-2**



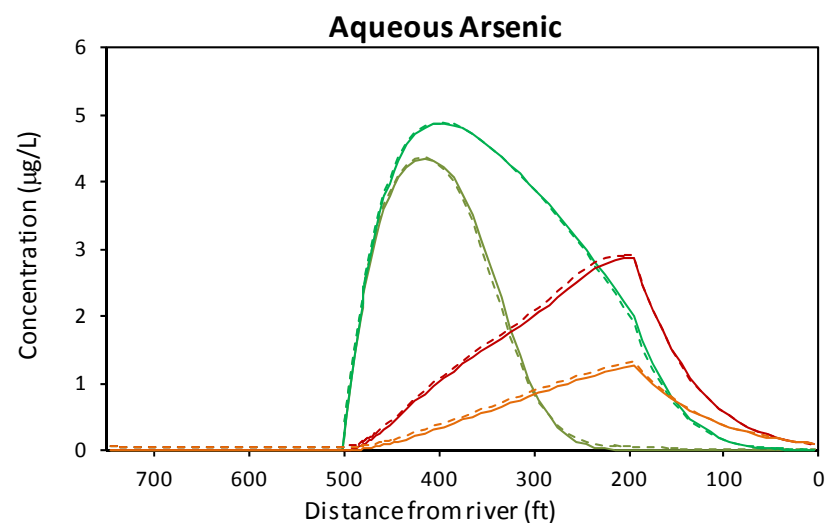
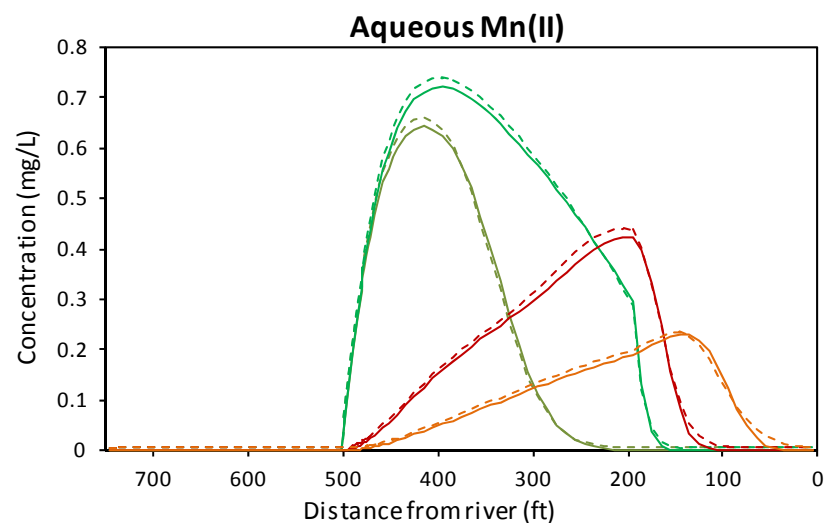
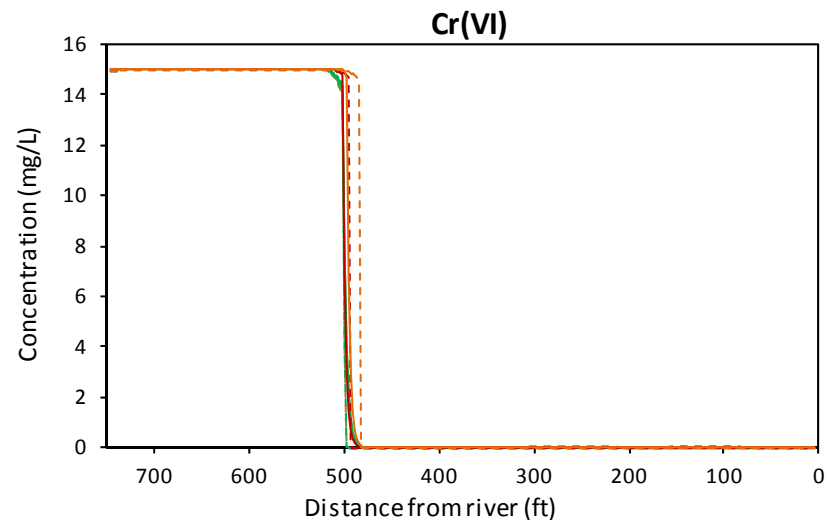
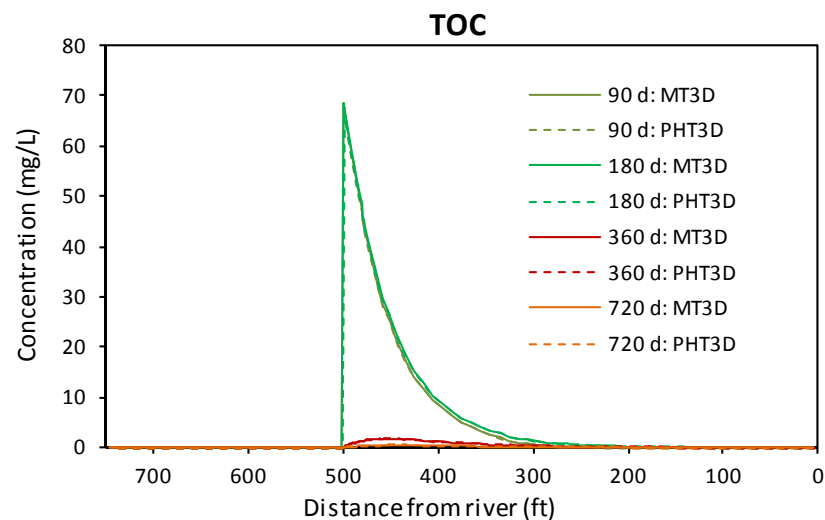
PG&E  
TOPOCK COMPRESSOR STATION  
NEEDLES, CALIFORNIA  
MODELING APPENDIX

GEOCHEMICAL REACTIVE TRANSPORT  
MODEL RESULTS FOR THE 1D IRZ SYSTEM:  
Mn, As, pH, AND ALKALINITY



FIGURE  
9.1-3



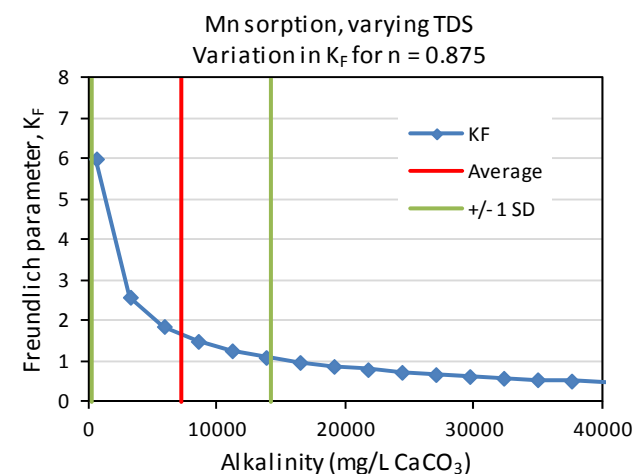
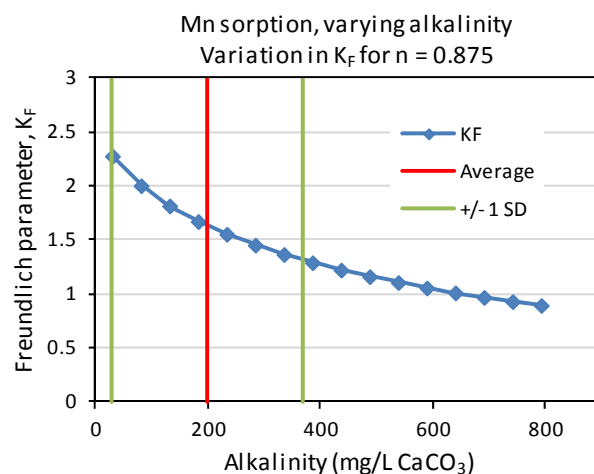
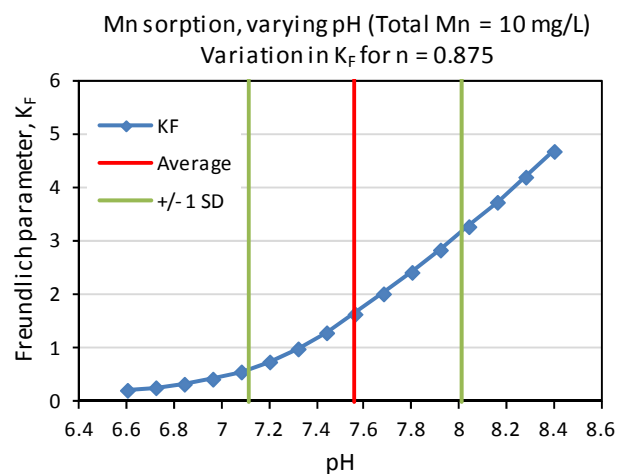
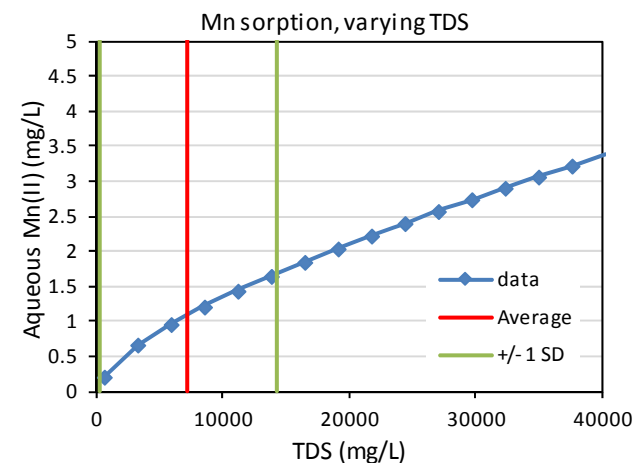
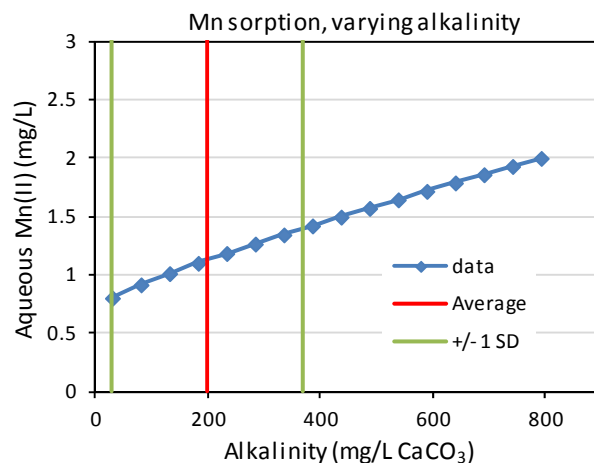
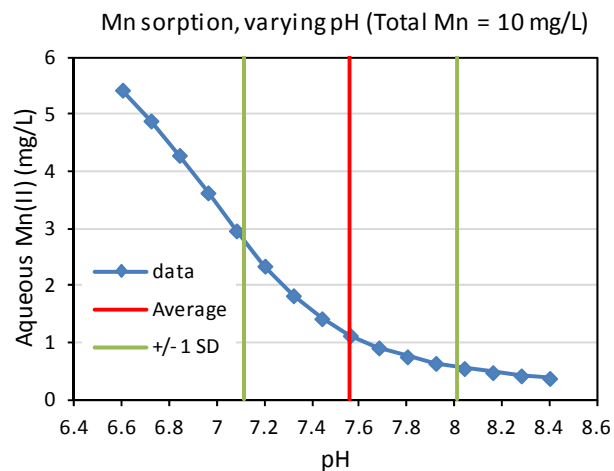


PG&E  
TOPOCK COMPRESSOR STATION  
NEEDLES, CALIFORNIA  
MODELING APPENDIX

COMPARISON OF PHT3D AND MT3D  
SIMULATION RESULTS FOR THE  
1D IRZ SYSTEM



FIGURE  
9.1-4

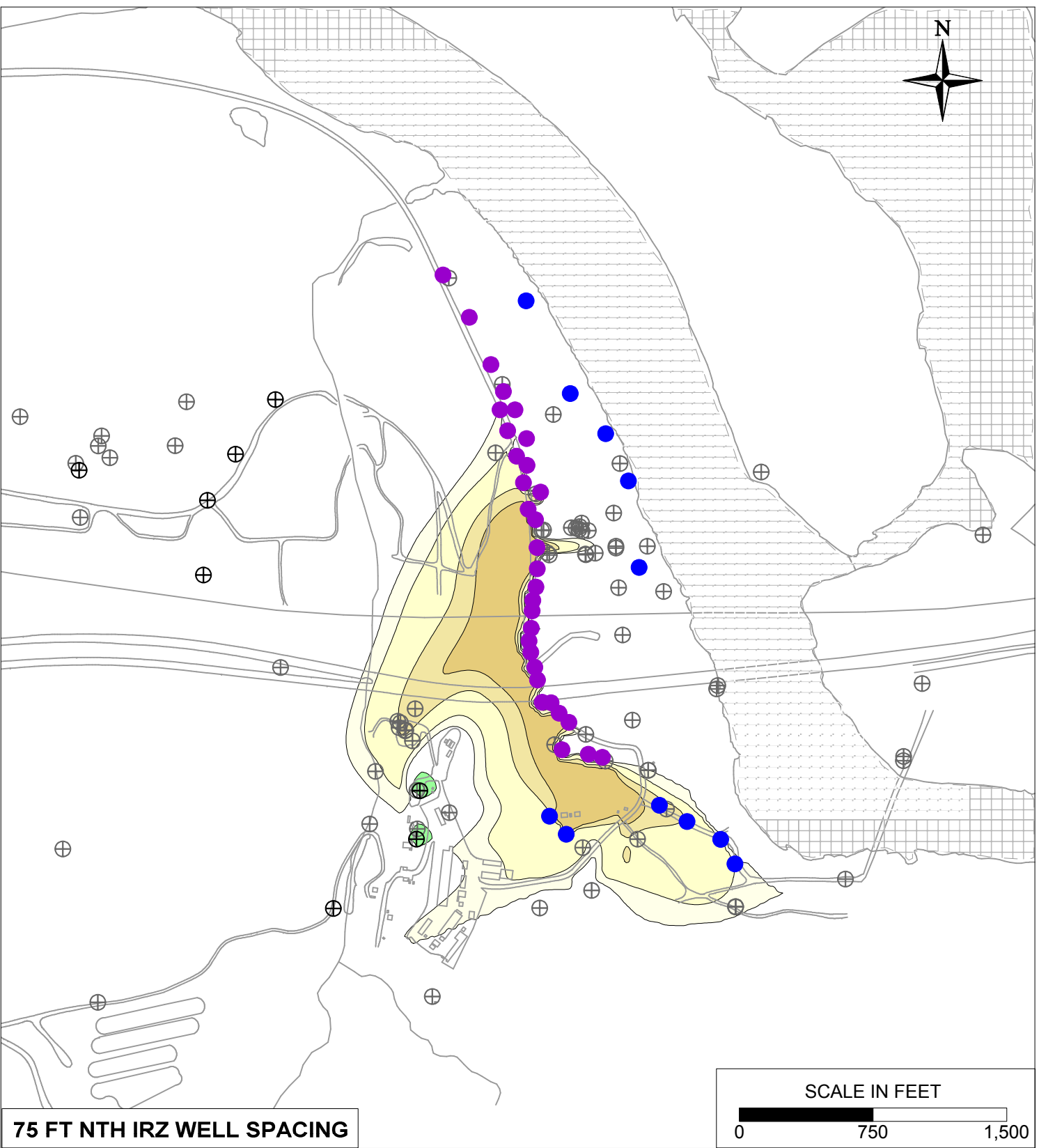
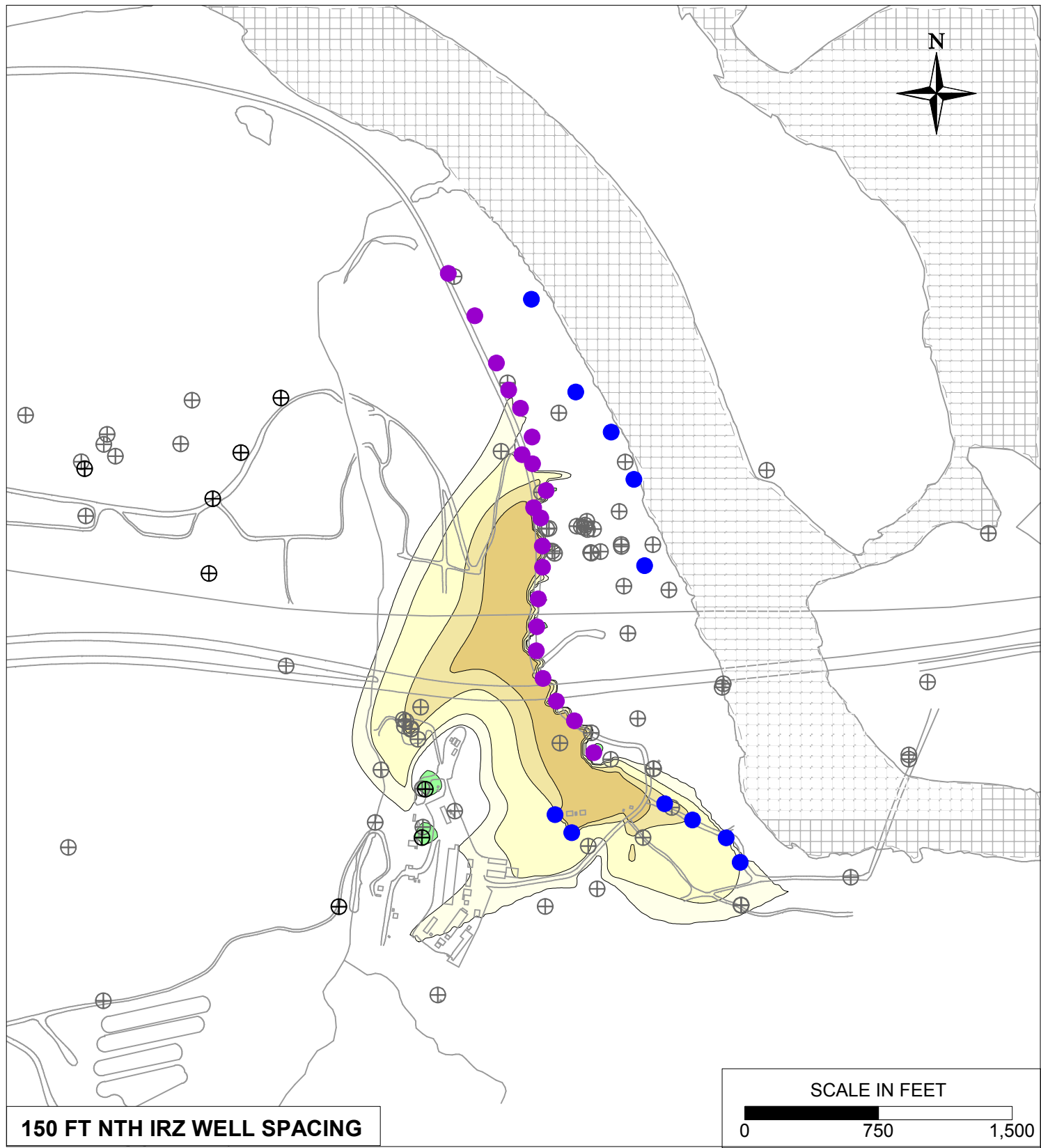


PG&E  
TOPOCK COMPRESSOR STATION  
NEEDLES, CALIFORNIA  
MODELING APPENDIX

VARIATION IN MANGANESE SORPTION WITH  
AQUEOUS GEOCHEMICAL CONDITIONS

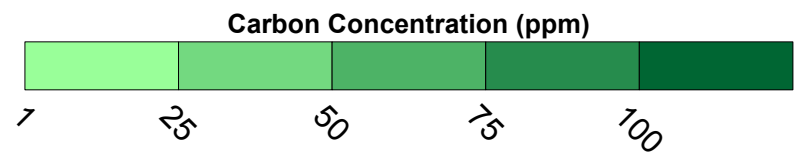
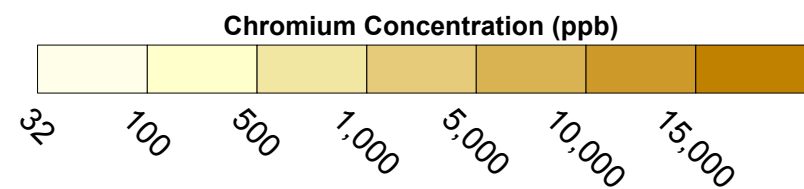


FIGURE  
9.2-1

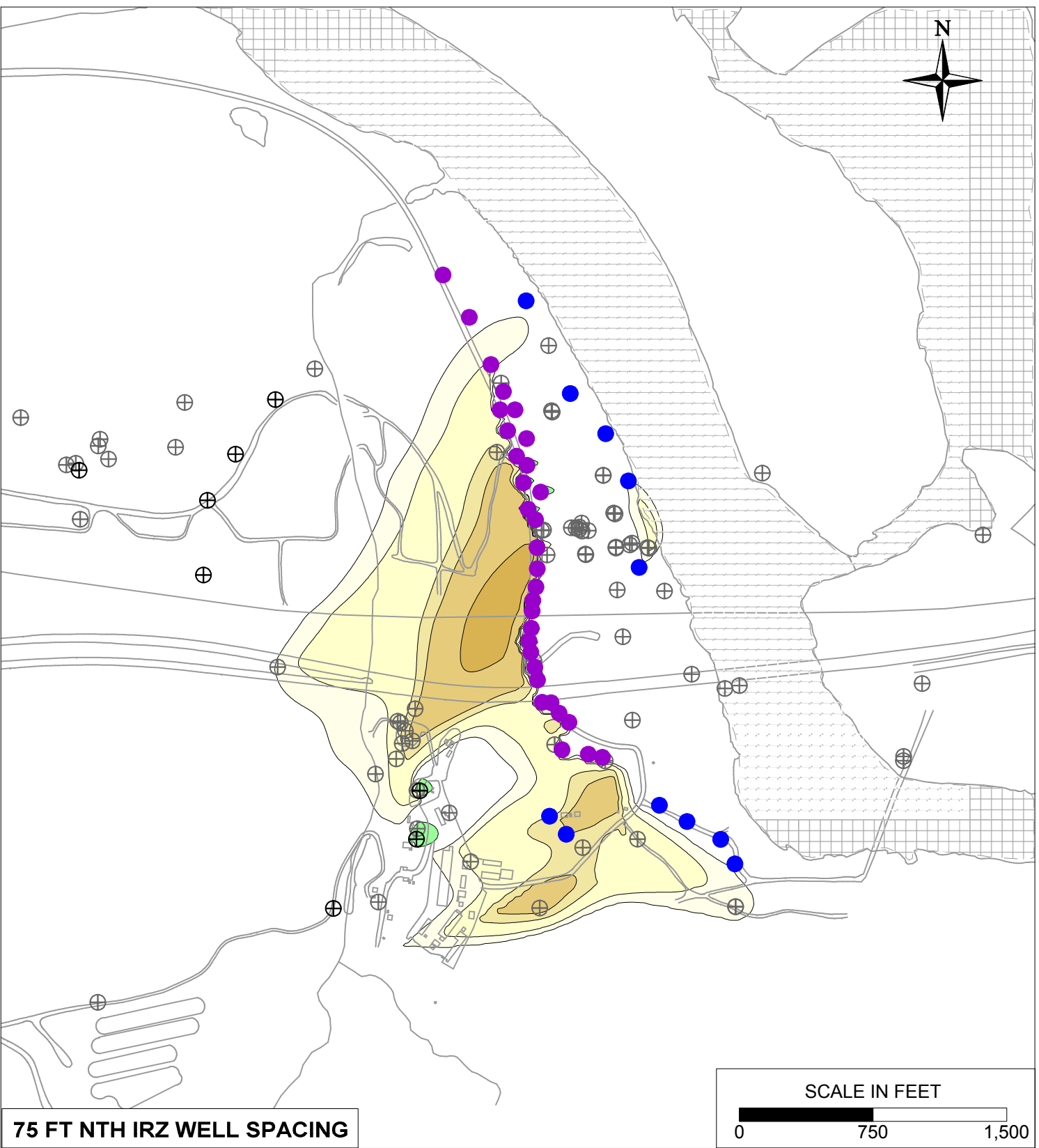
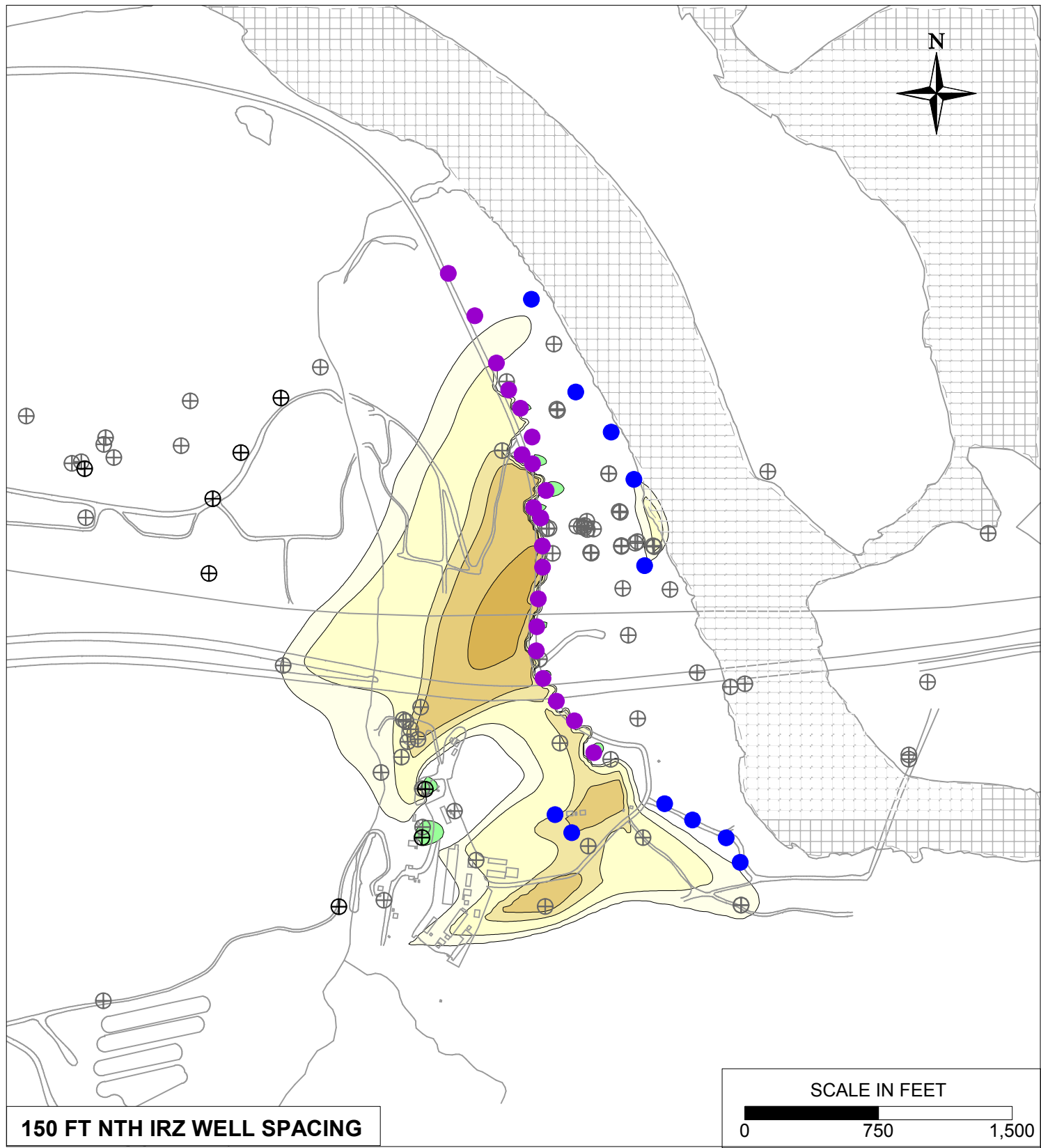


**LEGEND**

- IRZ WELLS
- ⊕ UPGRADIENT INJECTION WELLS
- EXTRACTION WELLS
- ⊕ MONITORING WELLS

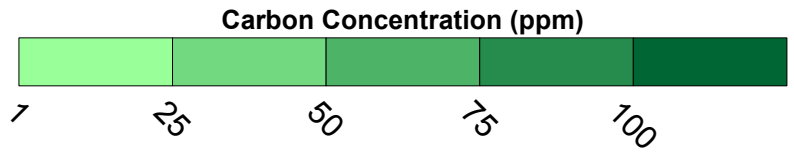
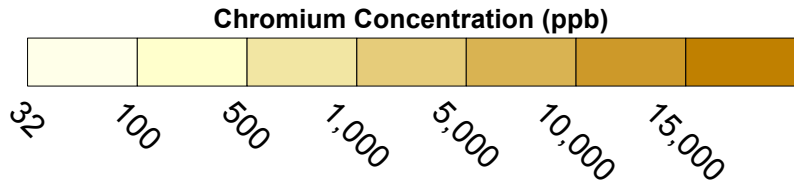


PG&E TOPOCK COMPRESSOR STATION NEEDLES, CALIFORNIA MODELING APPENDIX	
NTH IRZ WELL SPACING SENSITIVITY: 150 FT AND 75 FT SPACING WITH HEXAVALENT CHROMIUM TRANSPORT RESULTS FOR YEAR 10 IN MODEL LAYER 2	
	FIGURE <b>10.1-1</b>

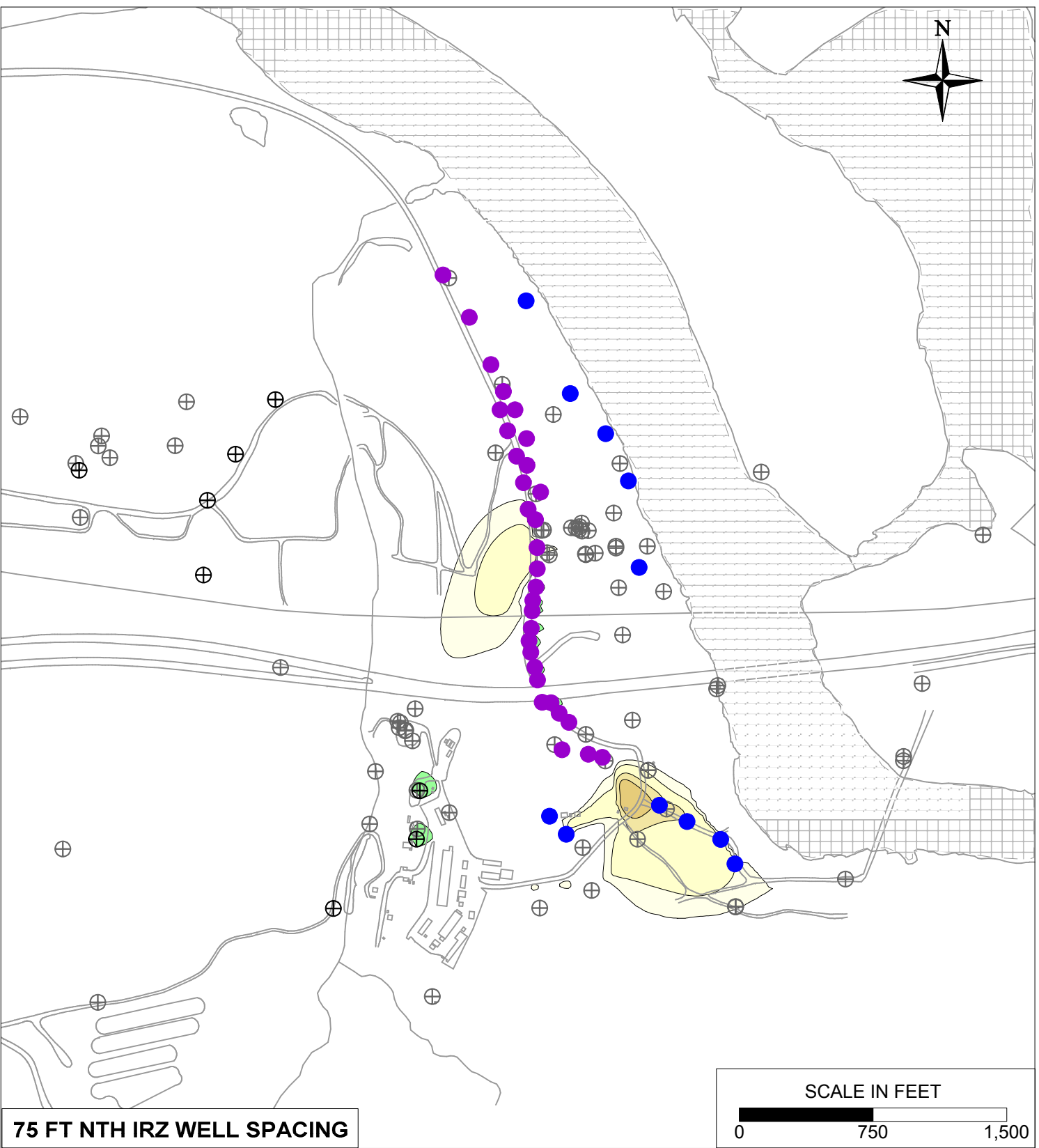
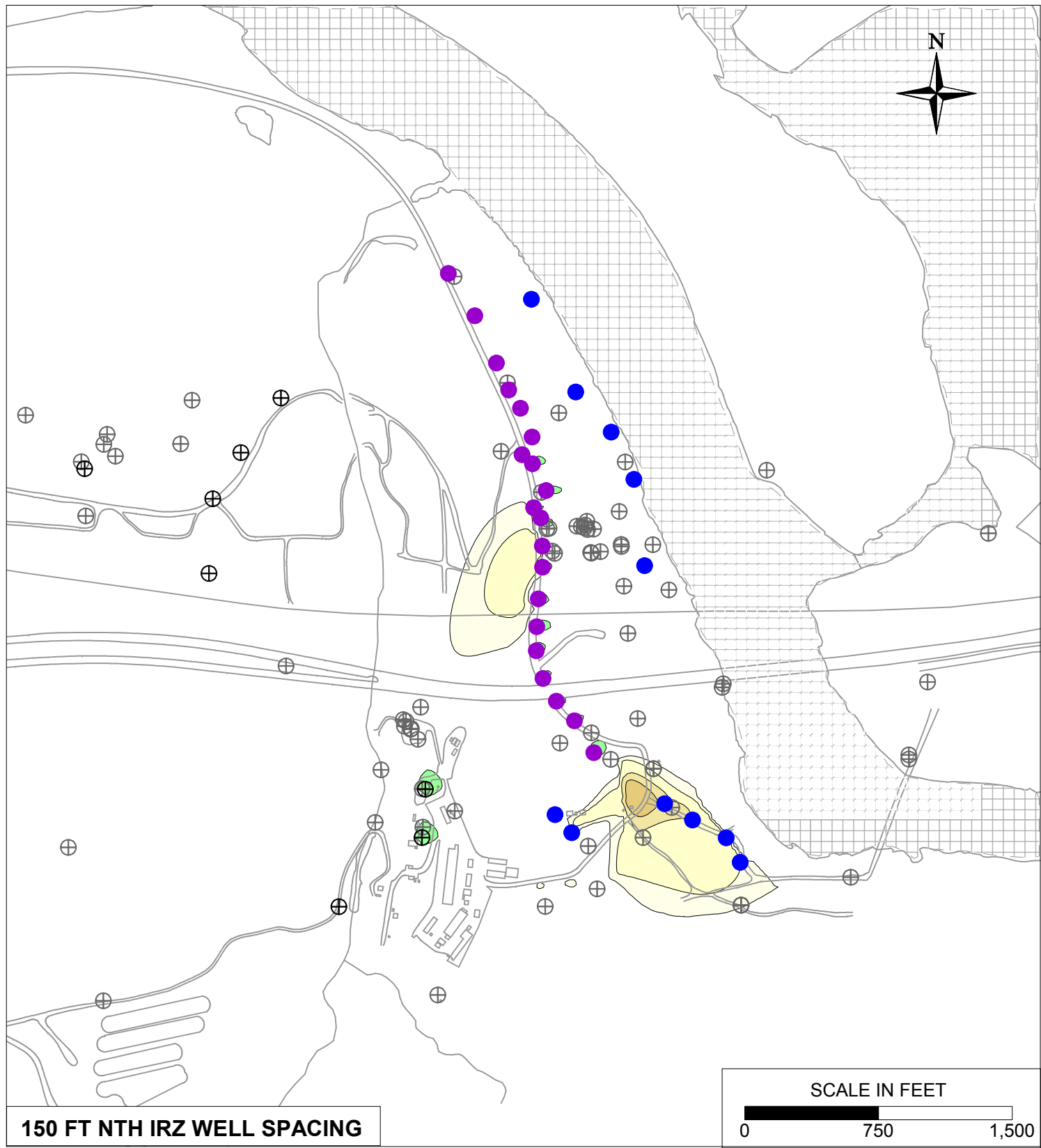


**LEGEND**

- IRZ WELLS
- ⊕ UPGRADIENT INJECTION WELLS
- EXTRACTION WELLS
- ⊕ MONITORING WELLS

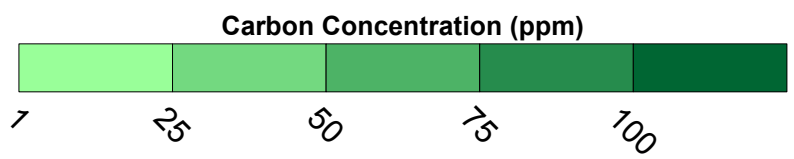
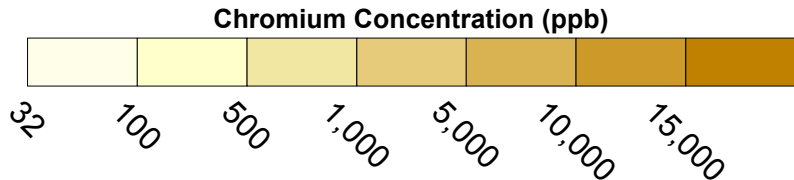


PG&E TOPOCK COMPRESSOR STATION NEEDLES, CALIFORNIA MODELING APPENDIX	
NTH IRZ WELL SPACING SENSITIVITY: 150 FT AND 75 FT SPACING WITH HEXAVALENT CHROMIUM TRANSPORT RESULTS FOR YEAR 10 IN MODEL LAYER 4	
	FIGURE <b>10.1-2</b>



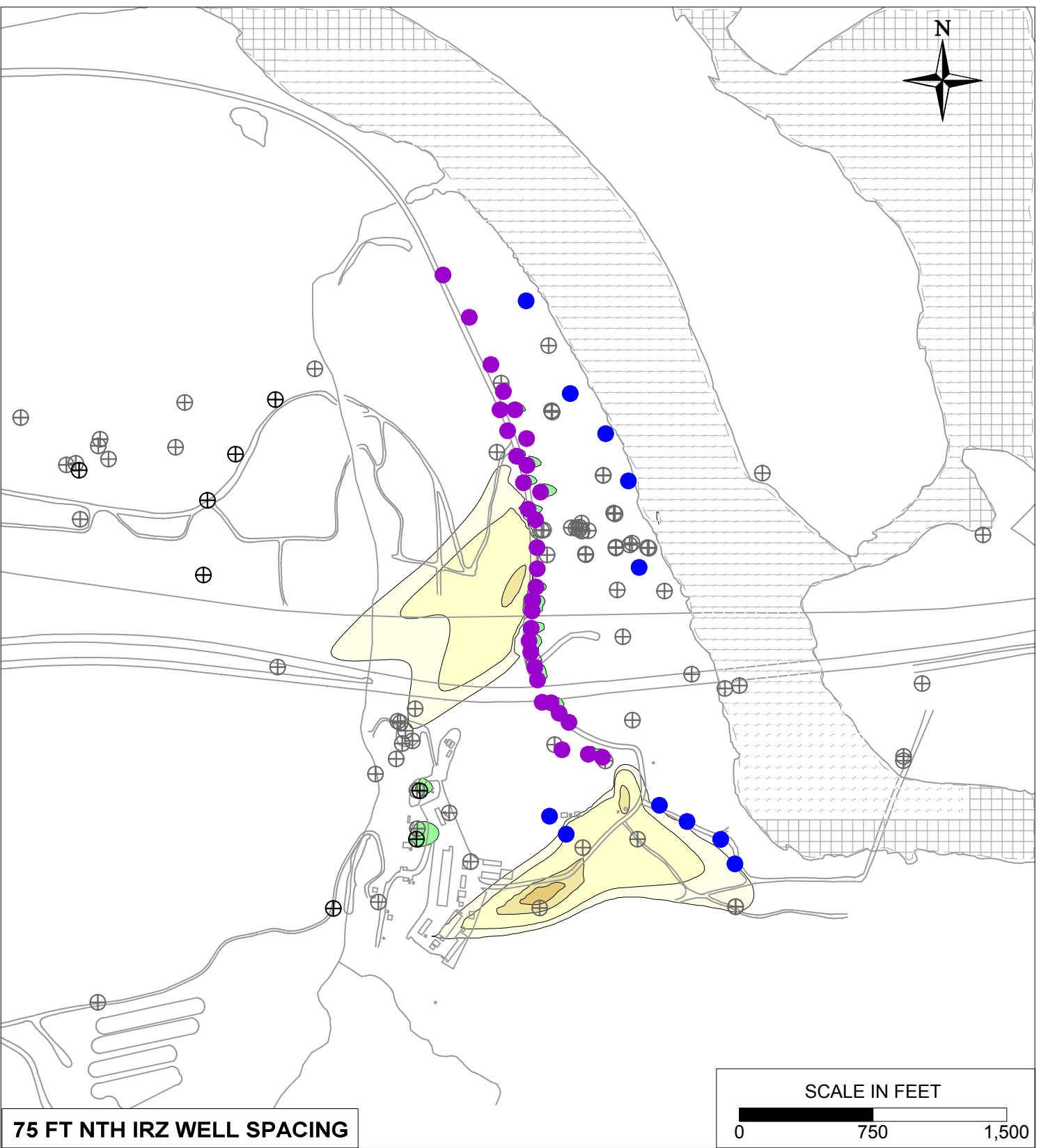
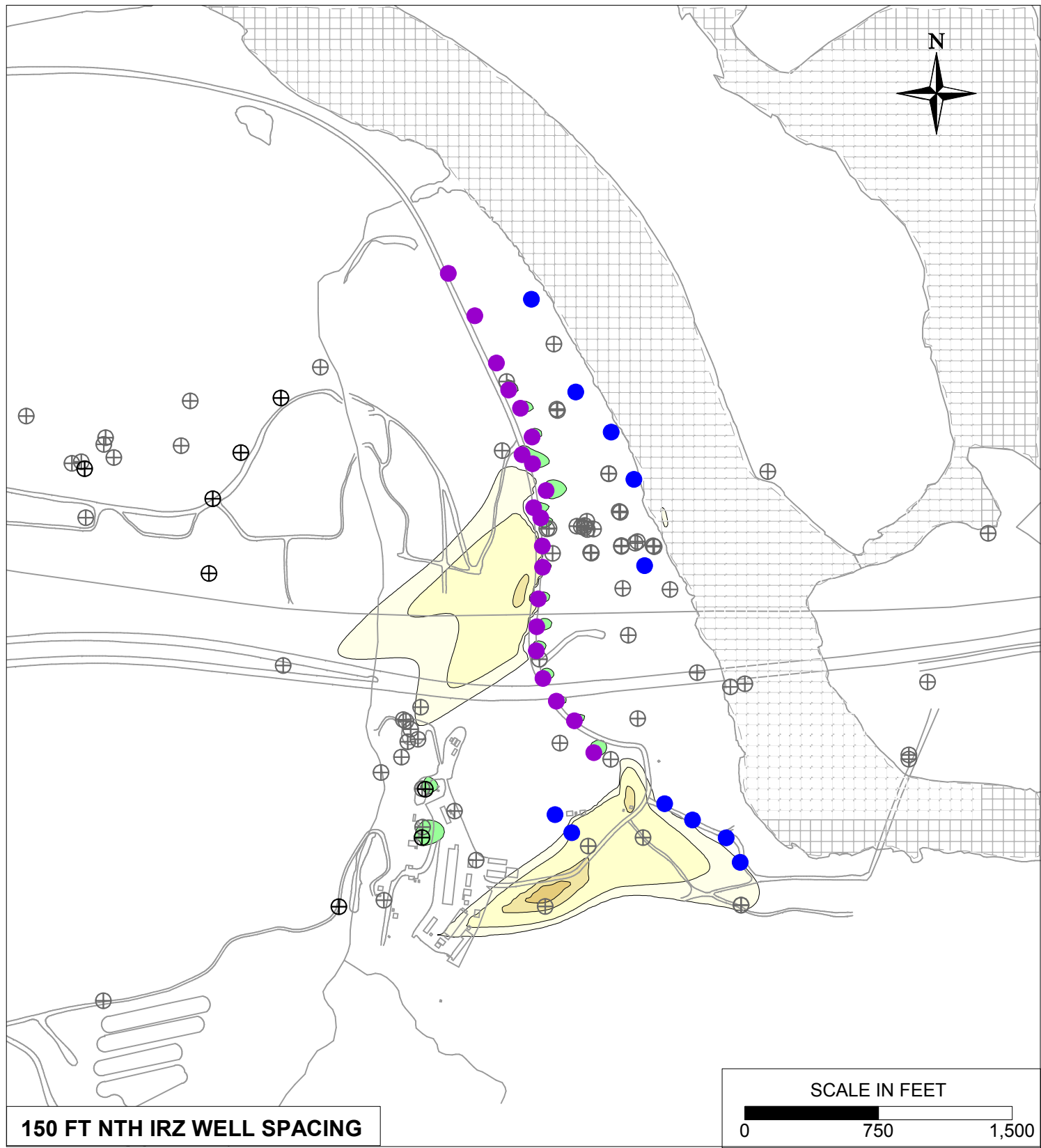
**LEGEND**

- IRZ WELLS
- ⊕ UPGRADIENT INJECTION WELLS
- EXTRACTION WELLS
- ⊕ MONITORING WELLS



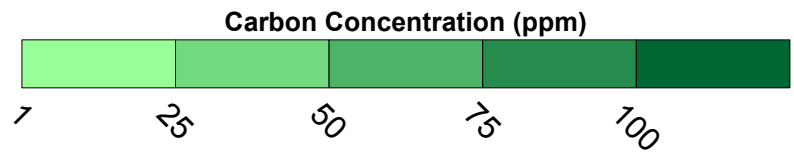
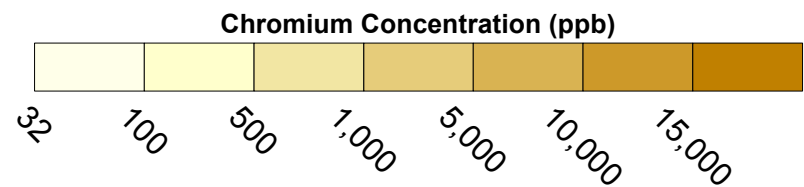
PG&E TOPOCK COMPRESSOR STATION NEEDLES, CALIFORNIA MODELING APPENDIX	
NTH IRZ WELL SPACING SENSITIVITY: 150 FT AND 75 FT SPACING WITH HEXAVALENT CHROMIUM TRANSPORT RESULTS FOR YEAR 30 IN MODEL LAYER 2	
	FIGURE <b>10.1-3</b>





**LEGEND**

- IRZ WELLS
- ⊕ UPGRADIENT INJECTION WELLS
- EXTRACTION WELLS
- ⊕ MONITORING WELLS



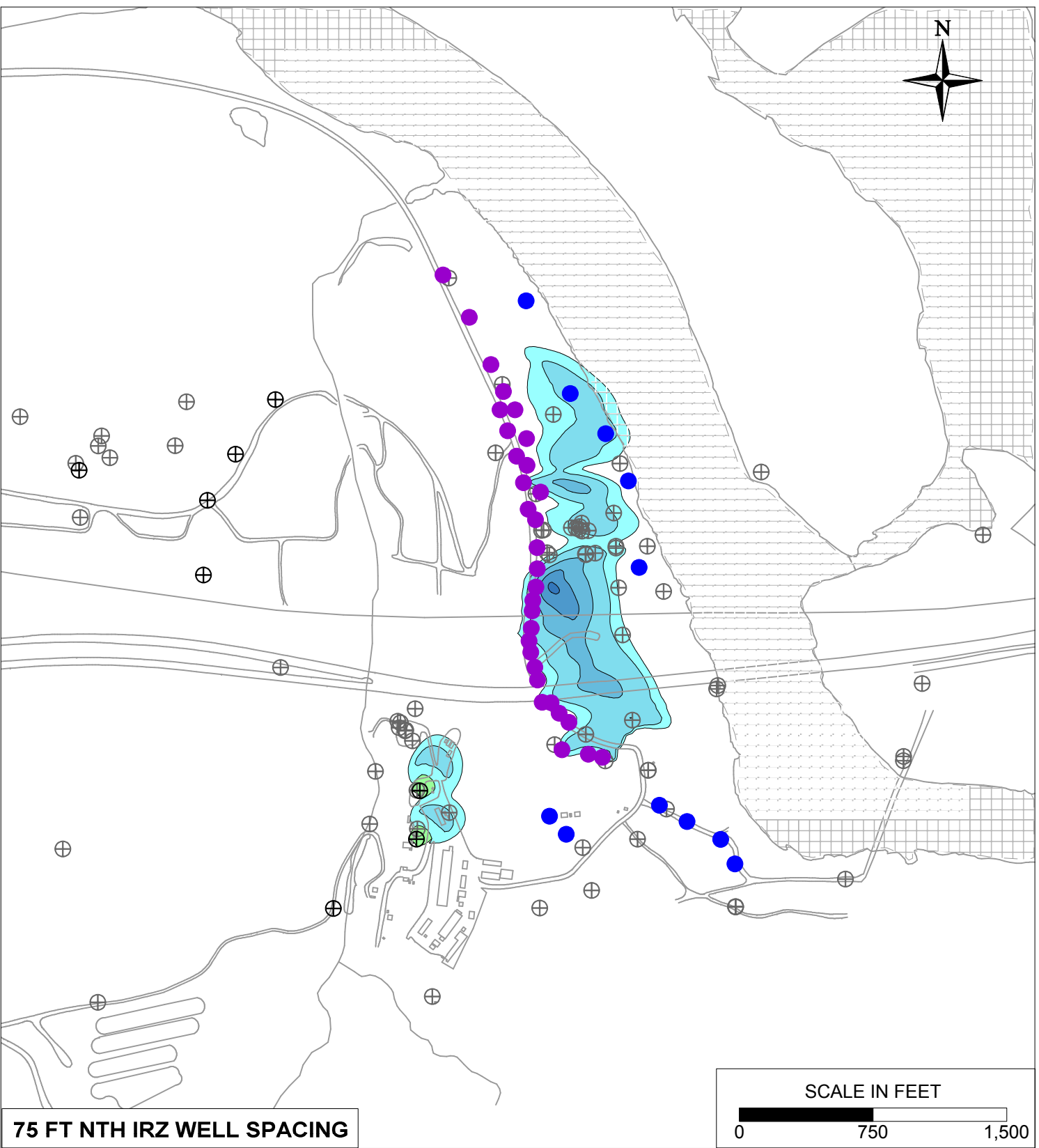
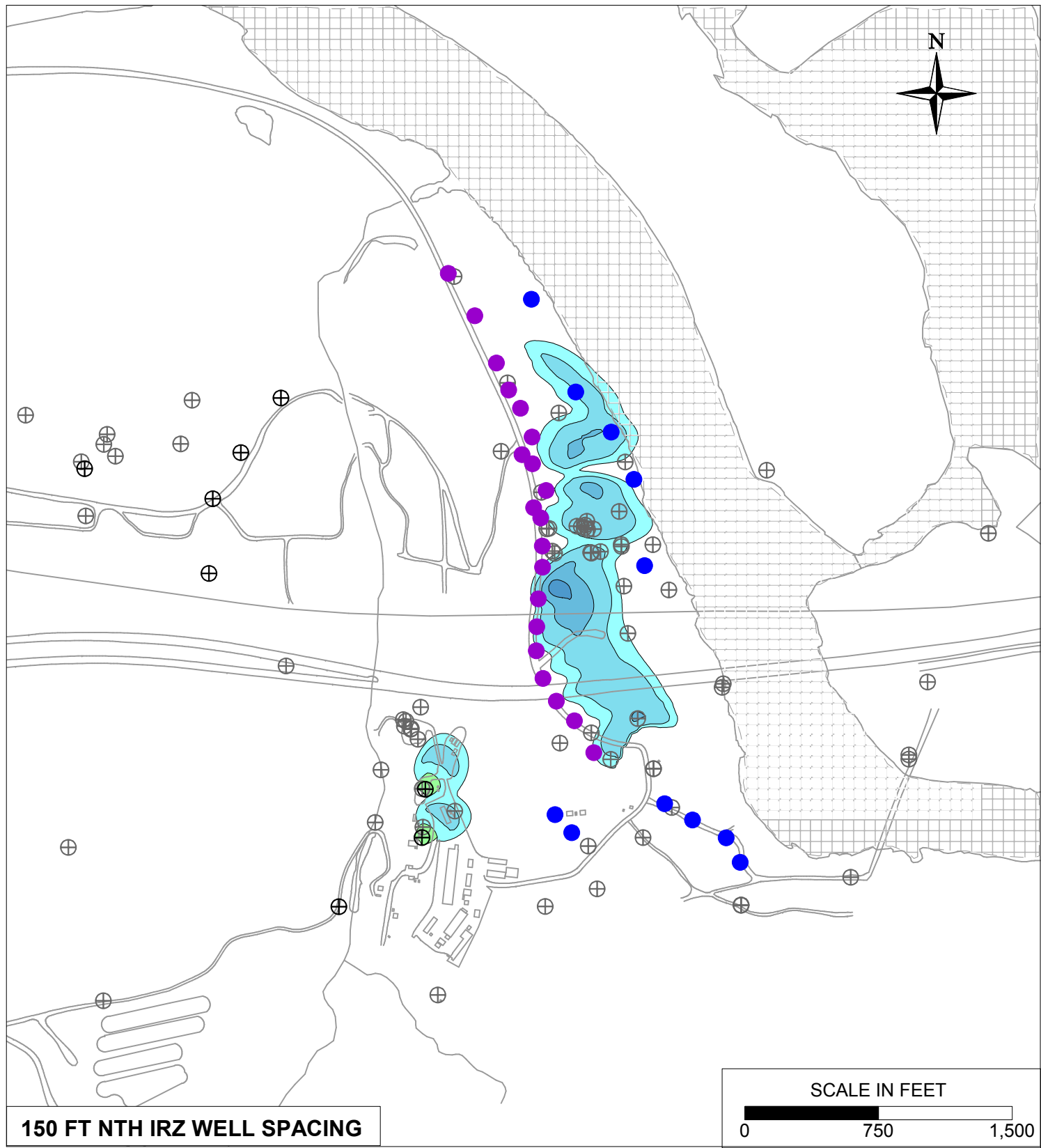
PG&E  
TOPOCK COMPRESSOR STATION  
NEEDLES, CALIFORNIA  
MODELING APPENDIX

NTH IRZ WELL SPACING SENSITIVITY:  
150 FT AND 75 FT SPACING WITH  
HEXAVALENT CHROMIUM TRANSPORT  
RESULTS FOR YEAR 30 IN MODEL LAYER 4



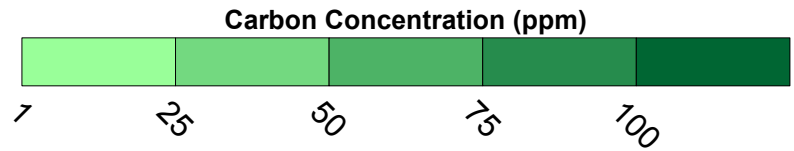
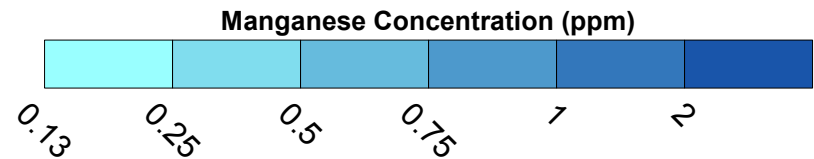
FIGURE

10.1-4



**LEGEND**

- IRZ WELLS
- ⊕ UPGRADIENT INJECTION WELLS
- EXTRACTION WELLS
- ⊕ MONITORING WELLS



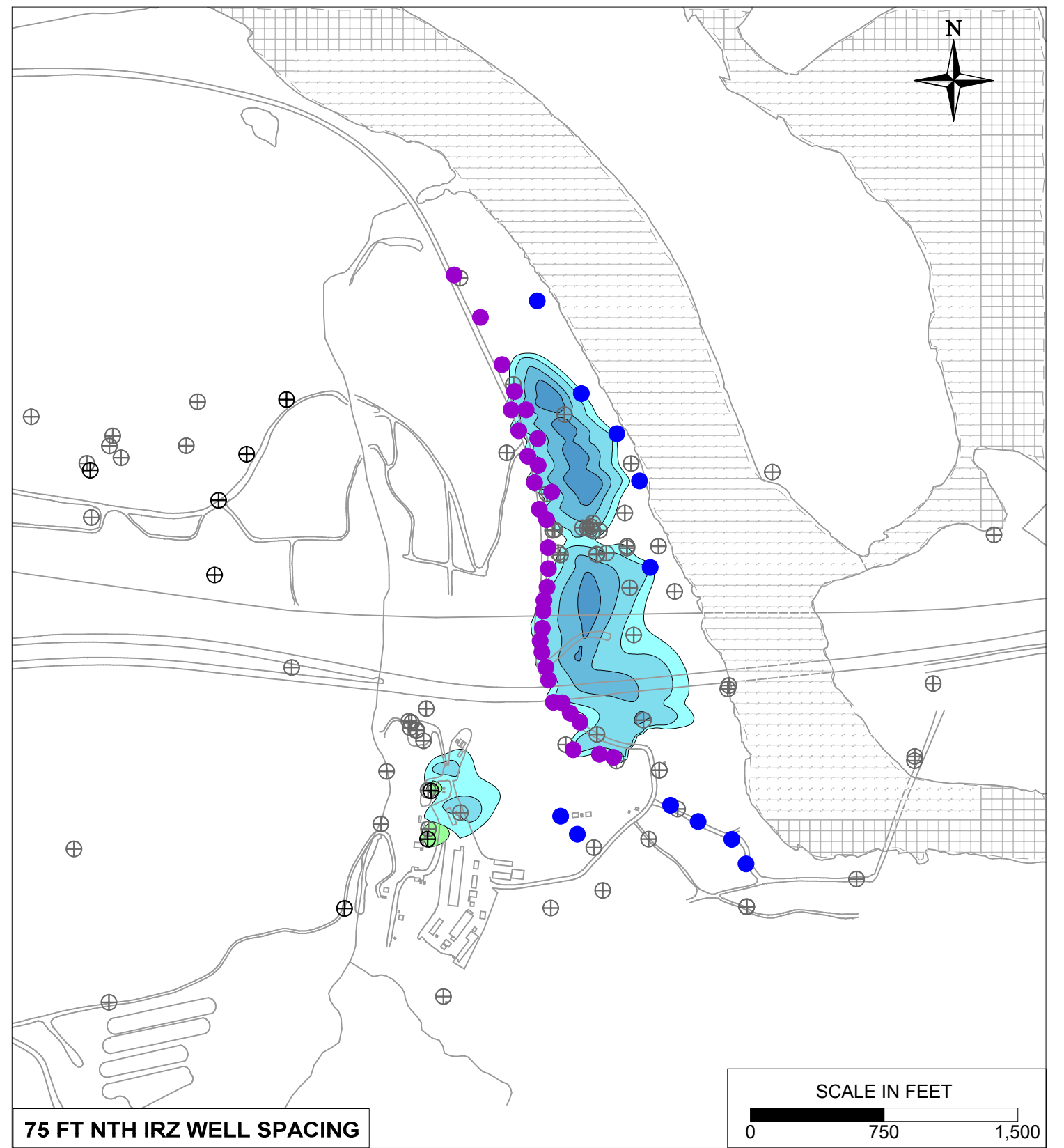
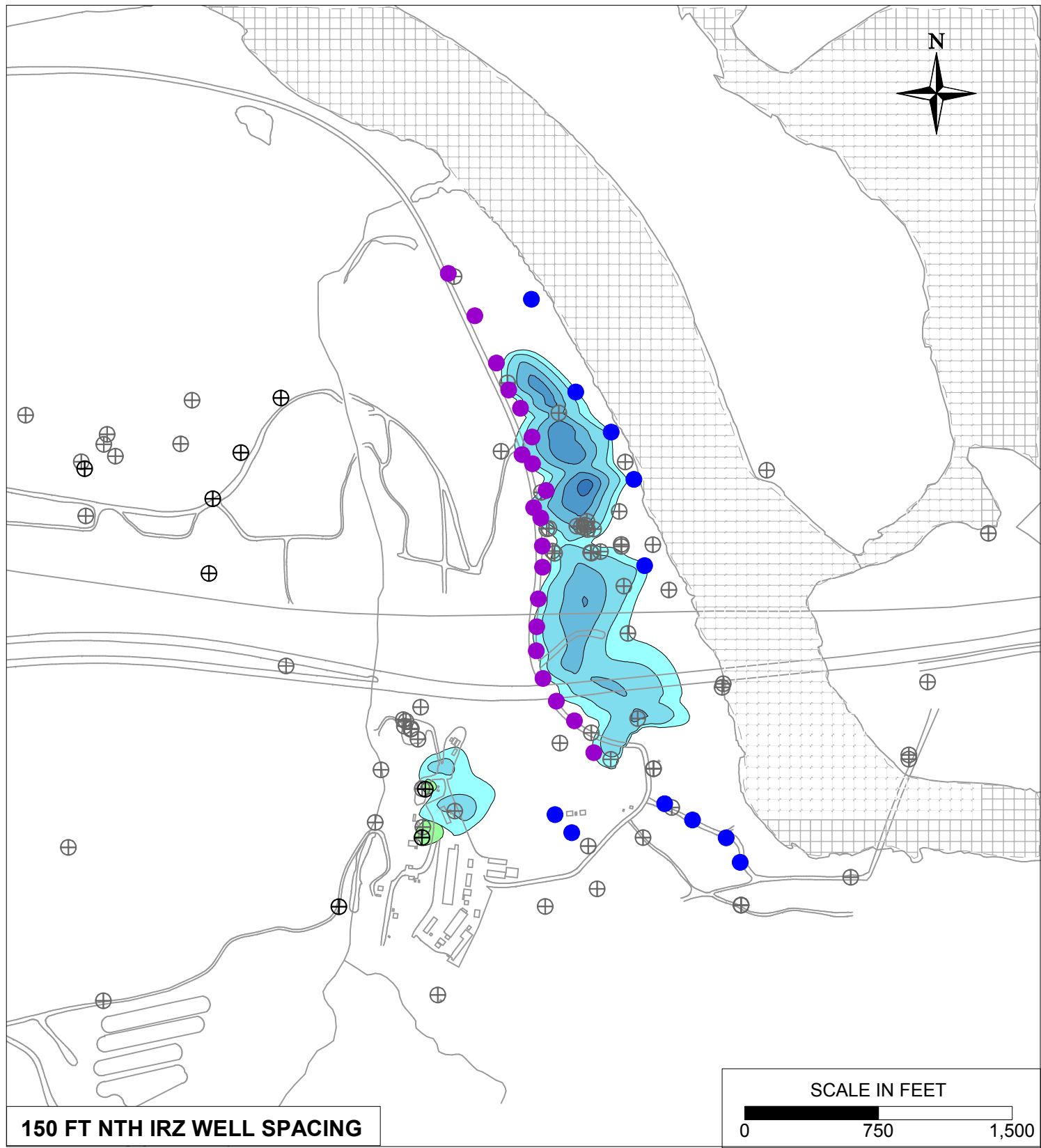
PG&E  
TOPOCK COMPRESSOR STATION  
NEEDLES, CALIFORNIA  
MODELING APPENDIX

NTH IRZ WELL SPACING SENSITIVITY:  
150 FT AND 75 FT SPACING WITH  
MANGANESE TRANSPORT RESULTS  
FOR YEAR 10 IN MODEL LAYER 2



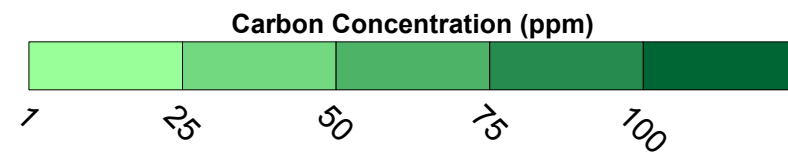
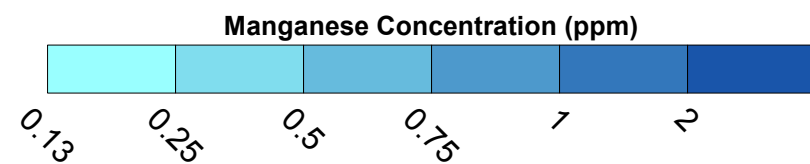
FIGURE

10.1-5



**LEGEND**

- IRZ WELLS
- ⊕ UPGRADIENT INJECTION WELLS
- EXTRACTION WELLS
- ⊕ MONITORING WELLS



PG&E  
TOPOCK COMPRESSOR STATION  
NEEDLES, CALIFORNIA  
MODELING APPENDIX

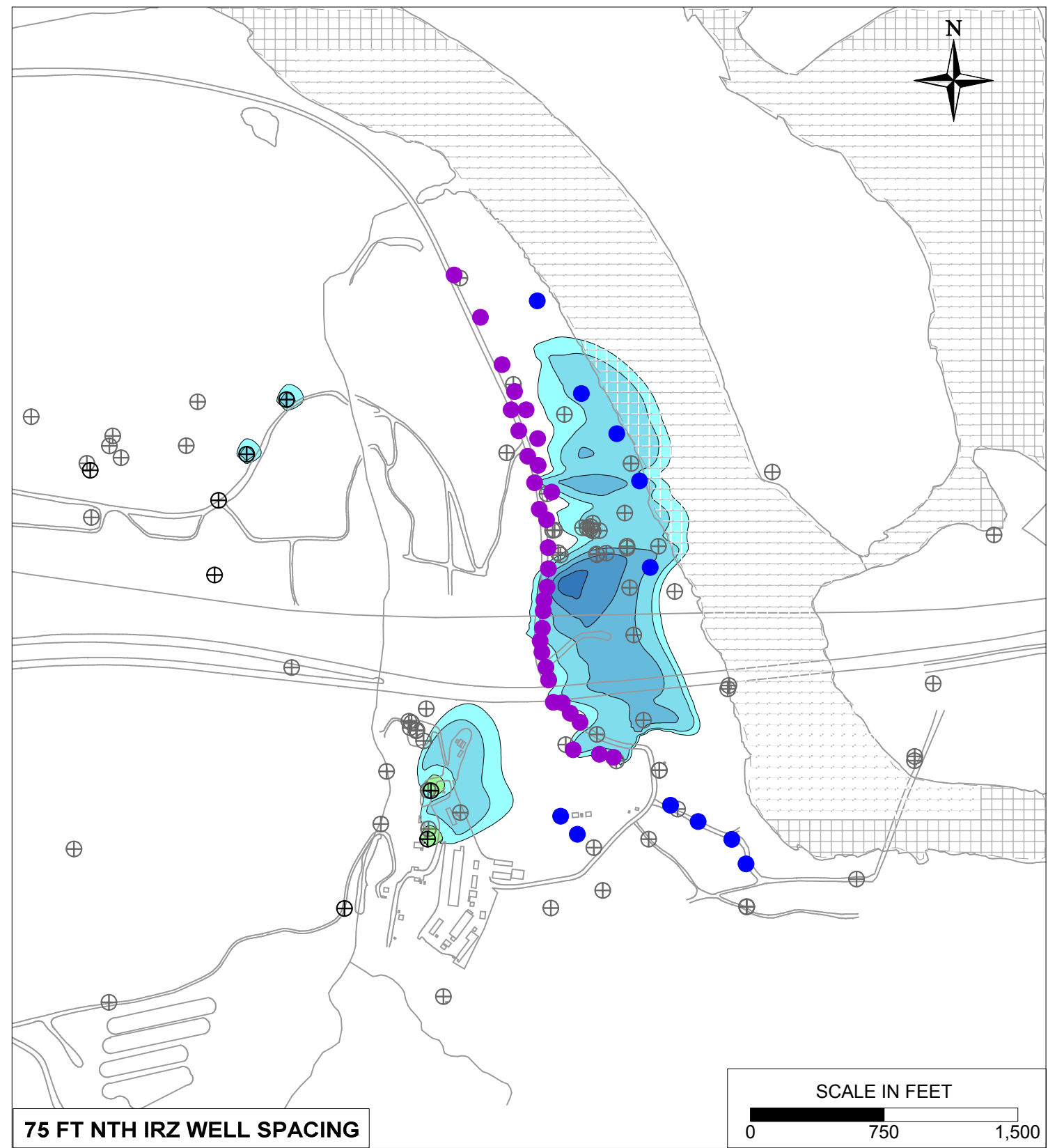
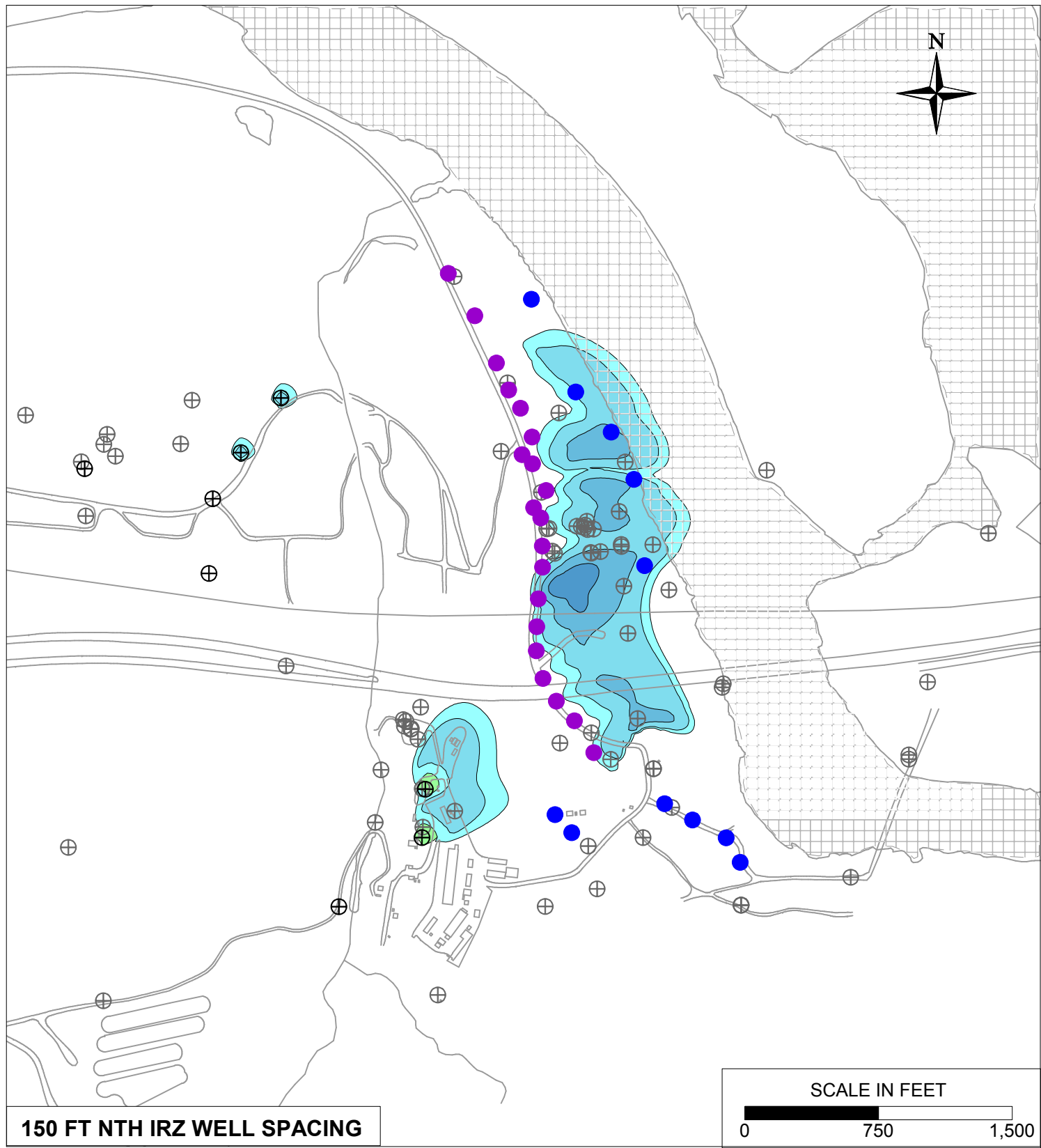
NTH IRZ WELL SPACING SENSITIVITY:  
150 FT AND 75 FT SPACING WITH  
MANGANESE TRANSPORT RESULTS  
FOR YEAR 10 IN MODEL LAYER 4



FIGURE

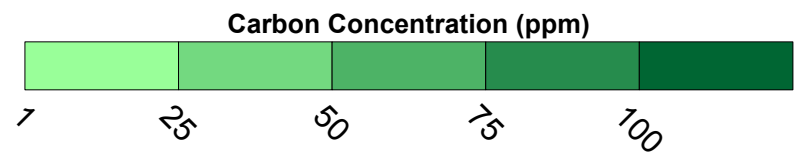
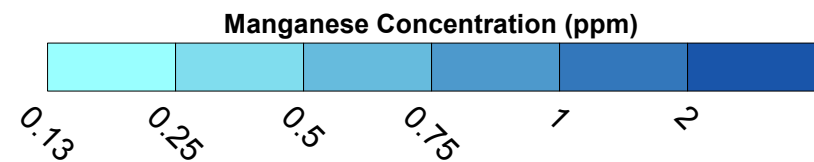
10.1-6





**LEGEND**

- IRZ WELLS
- ⊕ UPGRADIENT INJECTION WELLS
- EXTRACTION WELLS
- ⊕ MONITORING WELLS



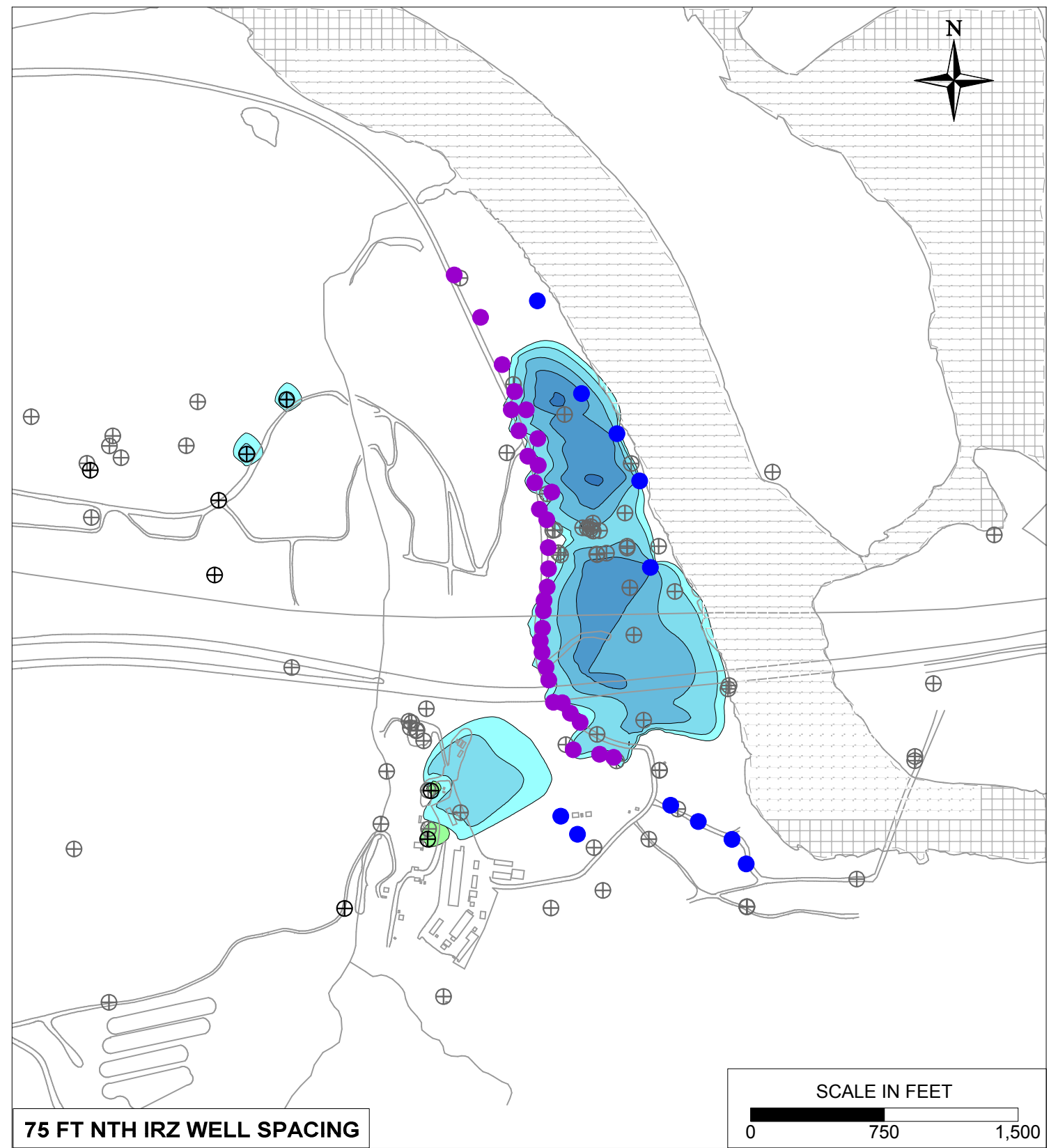
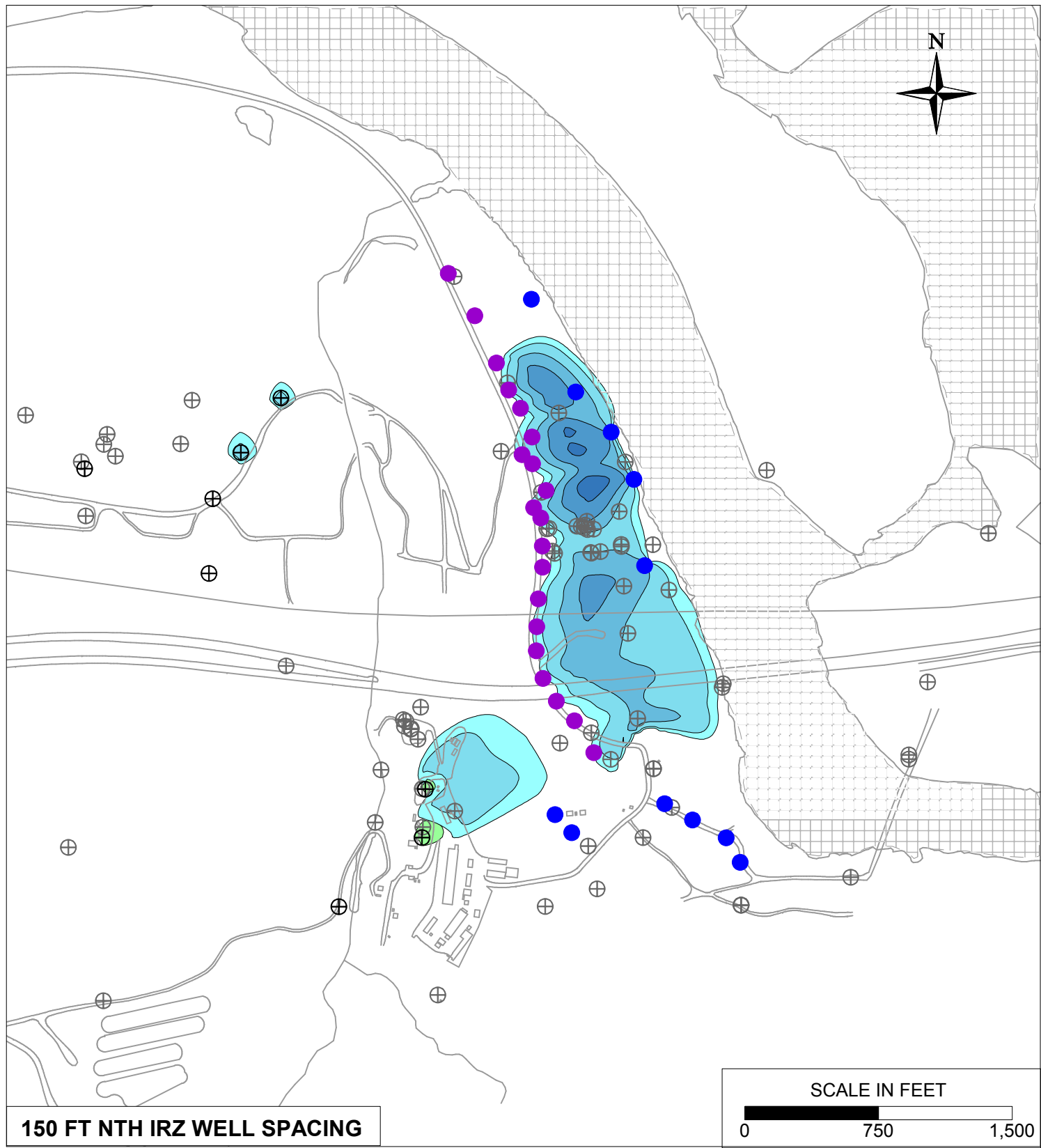
PG&E  
TOPOCK COMPRESSOR STATION  
NEEDLES, CALIFORNIA  
MODELING APPENDIX

NTH IRZ WELL SPACING SENSITIVITY:  
150 FT AND 75 FT SPACING WITH  
MANGANESE TRANSPORT RESULTS  
FOR YEAR 30 IN MODEL LAYER 2



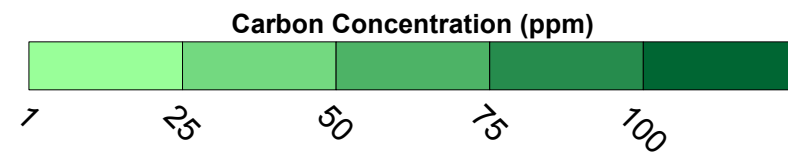
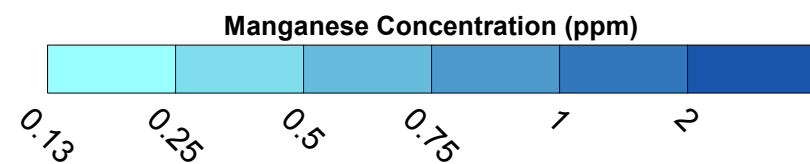
FIGURE

10.1-7



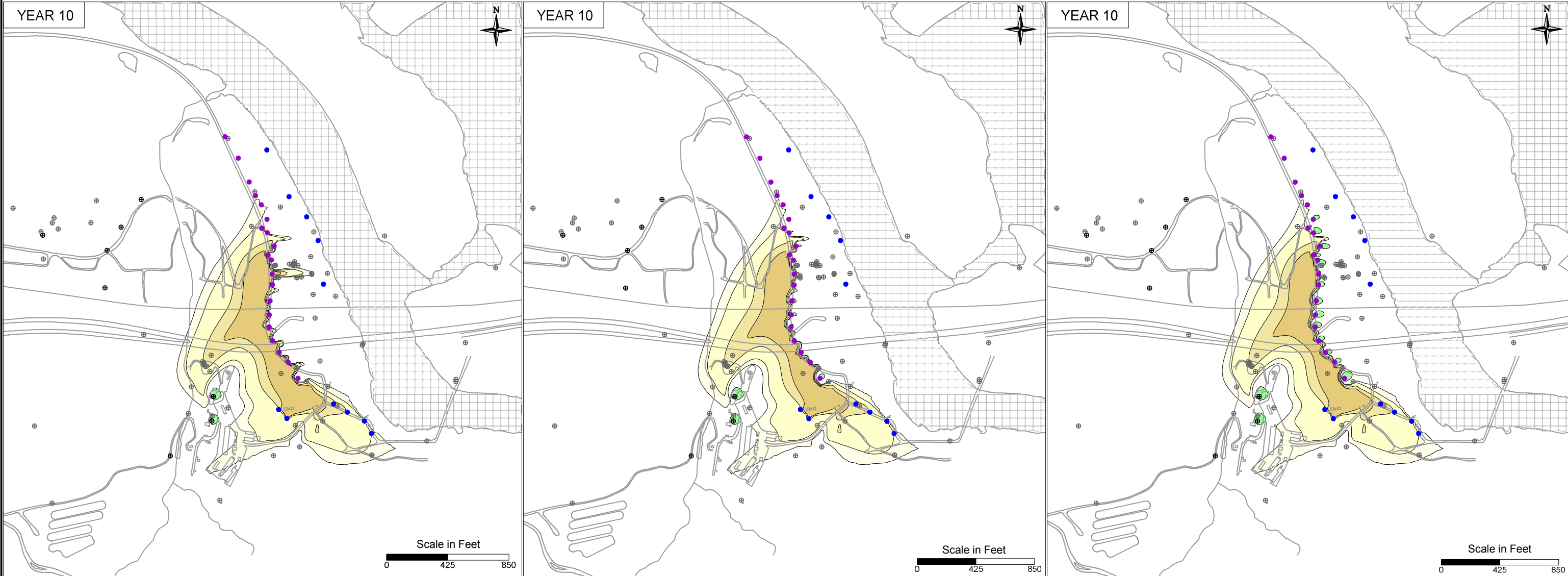
**LEGEND**

- IRZ WELLS
- ⊕ UPGRADIENT INJECTION WELLS
- EXTRACTION WELLS
- ⊕ MONITORING WELLS



PG&E TOPOCK COMPRESSOR STATION NEEDLES, CALIFORNIA MODELING APPENDIX	
NTH IRZ WELL SPACING SENSITIVITY: 150 FT AND 75 FT SPACING WITH MANGANESE TRANSPORT RESULTS FOR YEAR 30 IN MODEL LAYER 4	
	FIGURE <b>10.1-8</b>





LOW TOC = 50 ppm

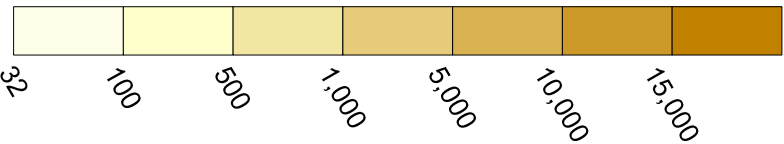
BASE TOC = 100 ppm

HIGH TOC = 150 ppm

**LEGEND**

- IRZ WELLS
- UPGRADIENT INJECTION WELLS
- EXTRACTION WELLS
- MONITORING WELLS

Chromium Concentration (ppb)



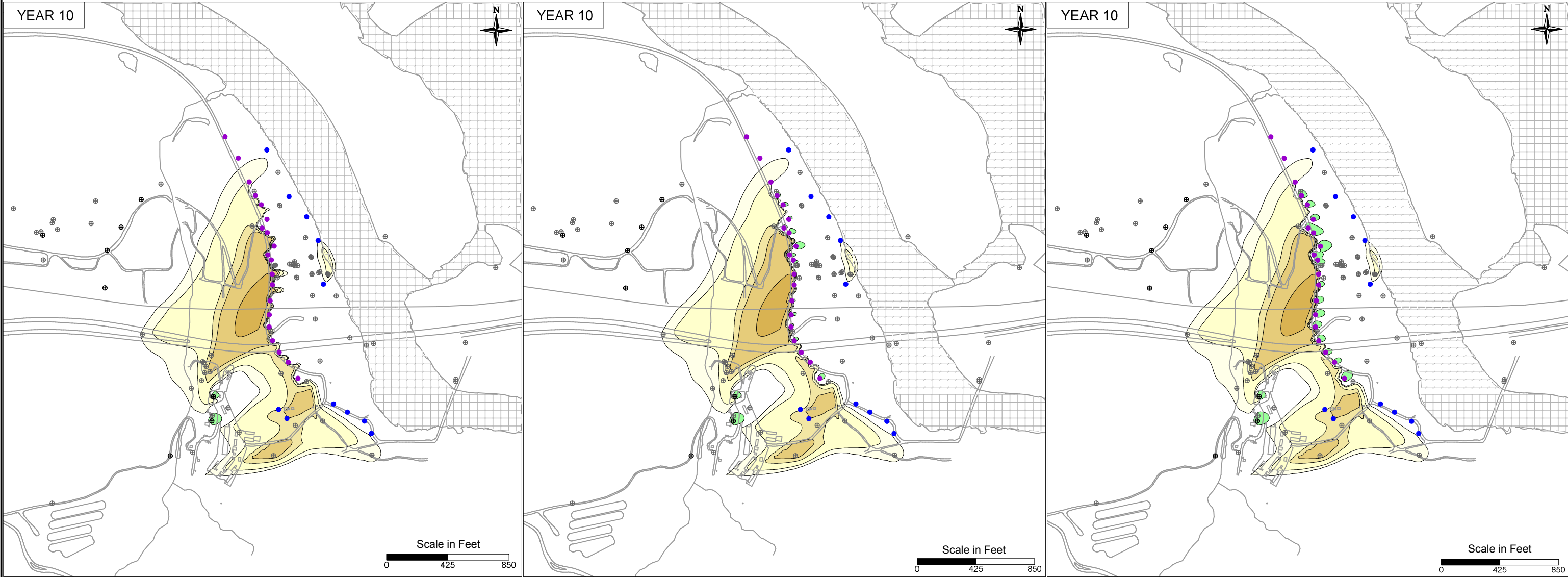
Carbon Concentration (ppm)



PG&E  
TOPOCK COMPRESSOR STATION  
NEEDLES, CALIFORNIA  
MODELING APPENDIX

TOC CONCENTRATION SENSITIVITY: SIMULATED  
HEXAVALENT CHROMIUM TRANSPORT RESULTS  
FOR YEAR 10 IN MODEL LAYER 2





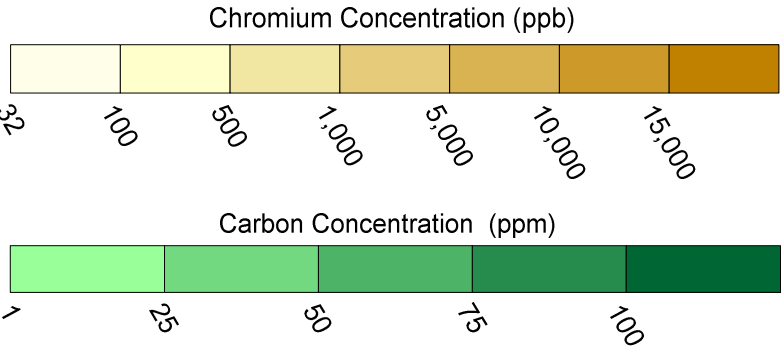
LOW TOC = 50 ppm

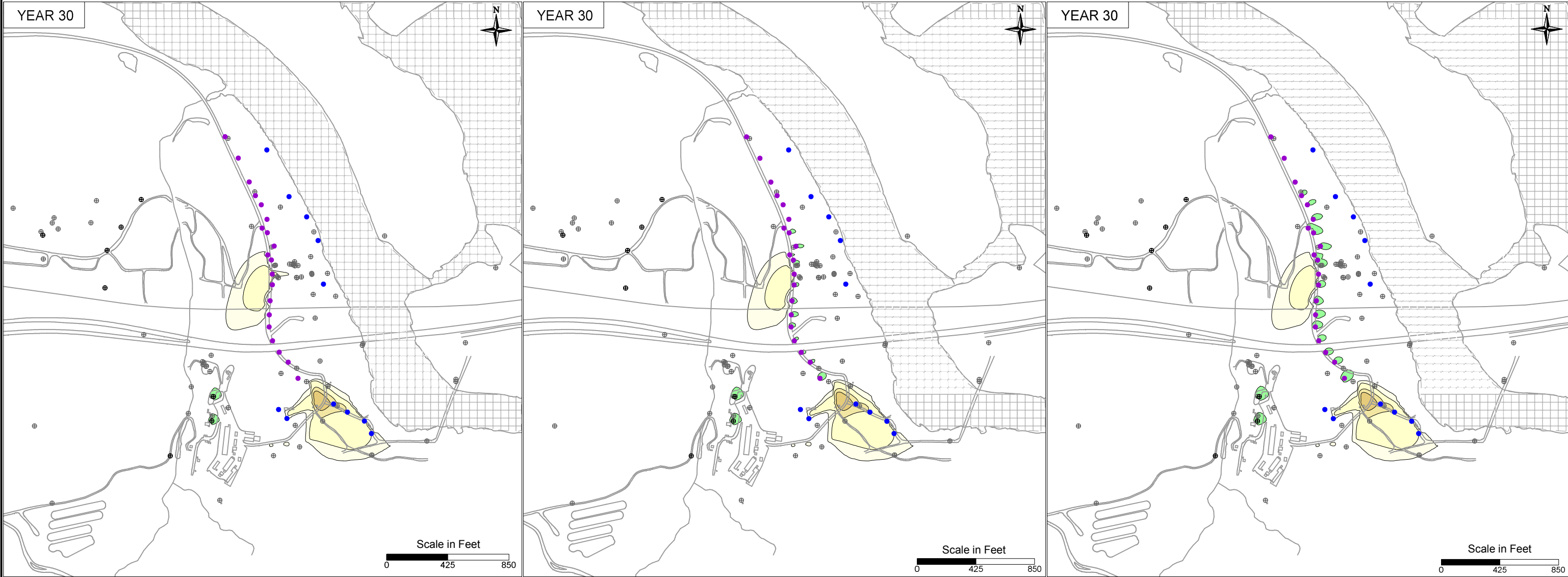
BASE TOC = 100 ppm

HIGH TOC = 150 ppm

**LEGEND**

- IRZ WELLS
- ⊕ UPGRADIENT INJECTION WELLS
- EXTRACTION WELLS
- ⊕ MONITORING WELLS





LOW TOC = 50 ppm

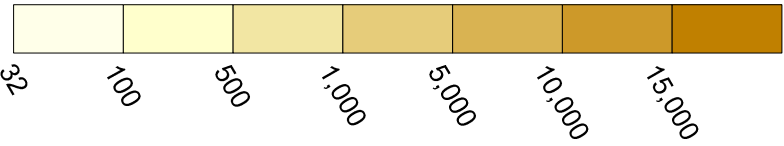
BASE TOC = 100 ppm

HIGH TOC = 150 ppm

**LEGEND**

- IRZ WELLS
- ⊕ UPGRADIENT INJECTION WELLS
- EXTRACTION WELLS
- ⊕ MONITORING WELLS

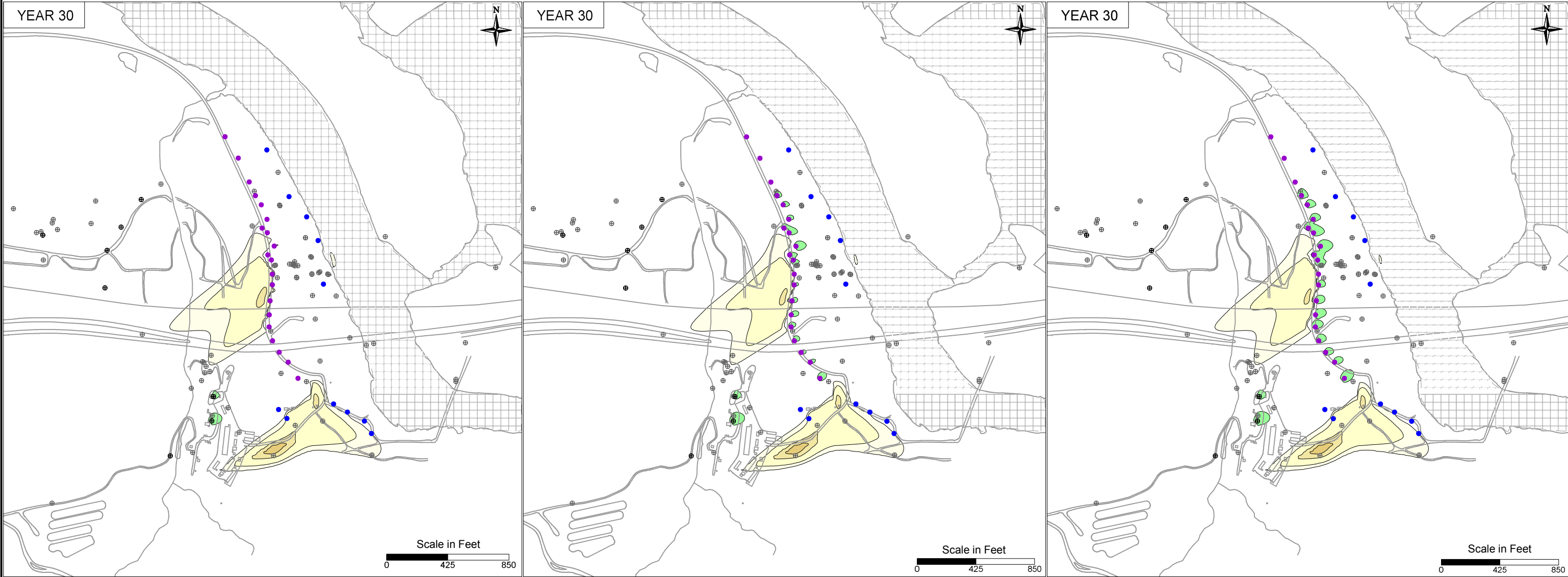
Chromium Concentration (ppb)



Carbon Concentration (ppm)



PG&E TOPOCK COMPRESSOR STATION NEEDLES, CALIFORNIA MODELING APPENDIX	
TOC CONCENTRATION SENSITIVITY: SIMULATED HEXAVALENT CHROMIUM TRANSPORT RESULTS FOR YEAR 30 IN MODEL LAYER 2	
	FIGURE 10.2-3



LOW TOC = 50 ppm

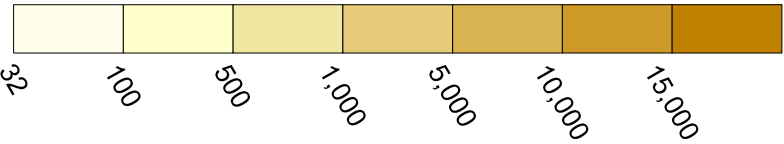
BASE TOC = 100 ppm

HIGH TOC = 150 ppm

**LEGEND**

- IRZ WELLS
- ⊕ UPGRADIENT INJECTION WELLS
- EXTRACTION WELLS
- ⊕ MONITORING WELLS

Chromium Concentration (ppb)

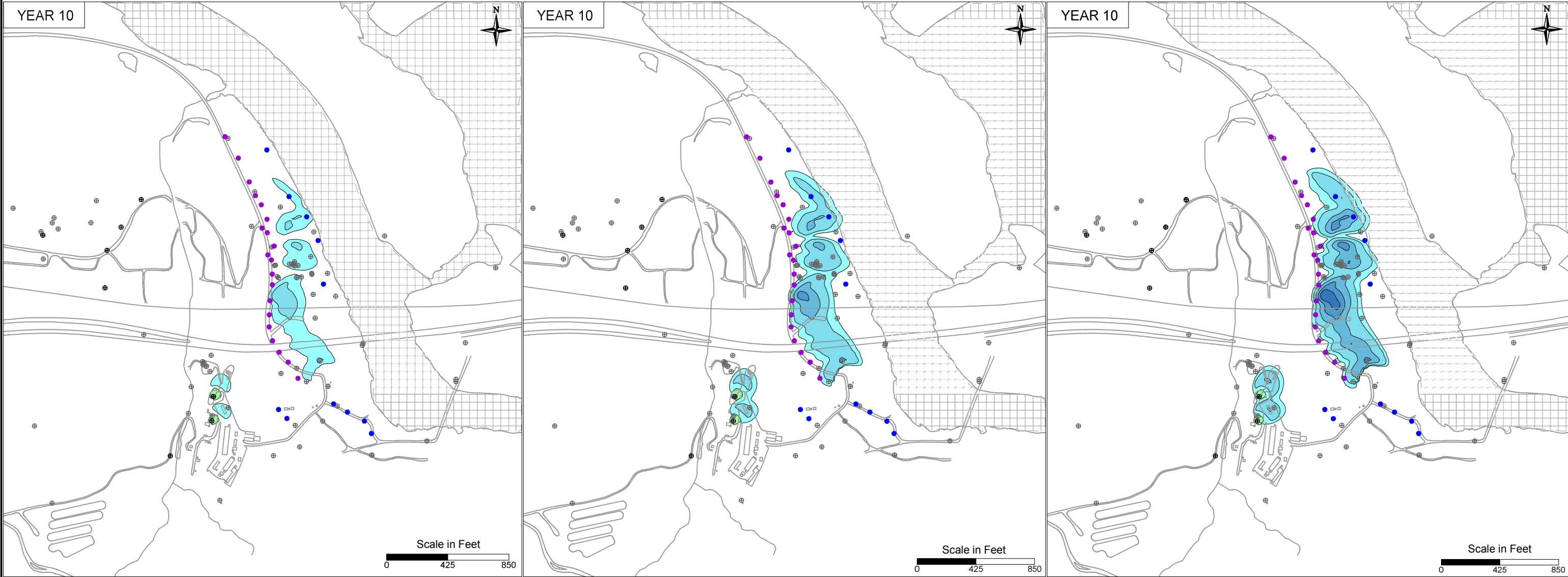


Carbon Concentration (ppm)



PG&E TOPOCK COMPRESSOR STATION NEEDLES, CALIFORNIA MODELING APPENDIX	
TOC CONCENTRATION SENSITIVITY: SIMULATED HEXAVALENT CHROMIUM TRANSPORT RESULTS FOR YEAR 30 IN MODEL LAYER 4	
	FIGURE 10.2-4





LOW TOC = 50 PPM

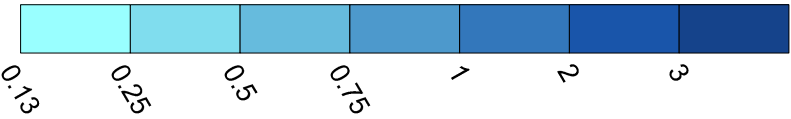
BASE TOC = 100 PPM

HIGH TOC = 150 PPM

**LEGEND**

- IRZ WELLS
- ⊕ UPGRADIENT INJECTION WELLS
- EXTRACTION WELLS
- ⊕ MONITORING WELLS

Manganese Concentration (ppm)



Carbon Concentration (ppm)



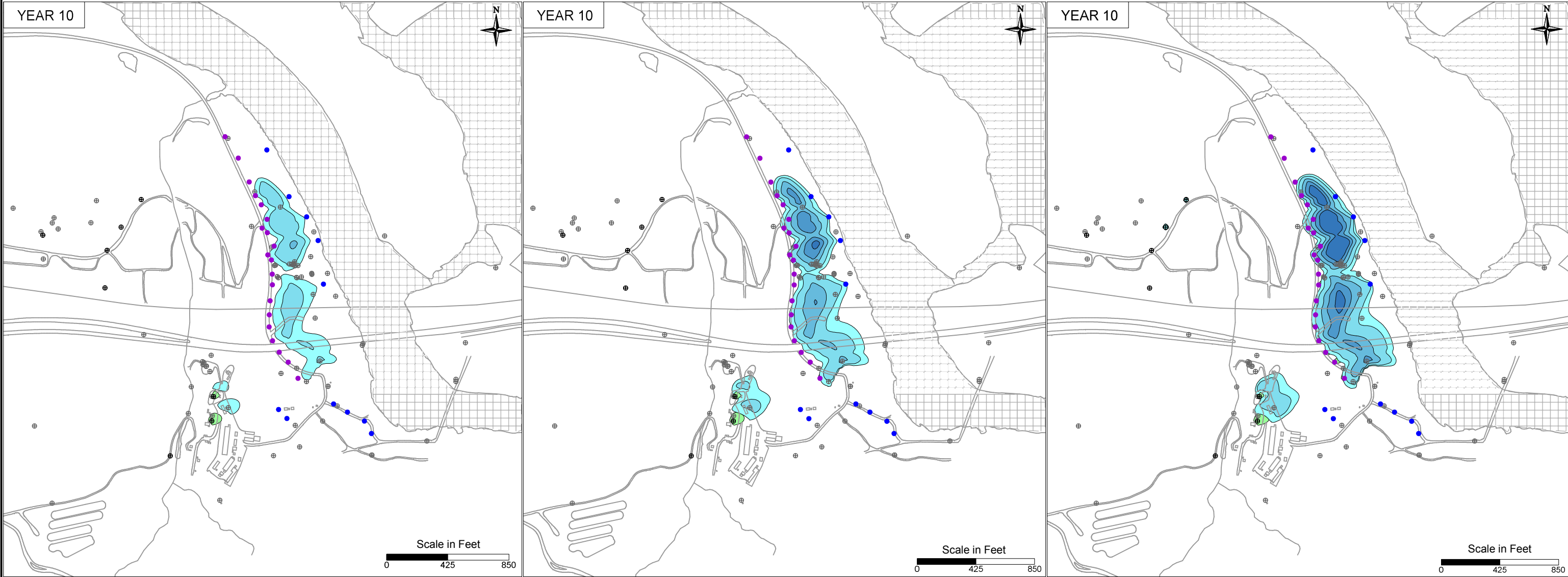
PG&E  
TOPOCK COMPRESSOR STATION  
NEEDLES, CALIFORNIA  
MODELING APPENDIX

TOC CONCENTRATION SENSITIVITY:  
SIMULATED MANGANESE TRANSPORT  
RESULTS IN MODEL LAYER 2



FIGURE  
10.2-5

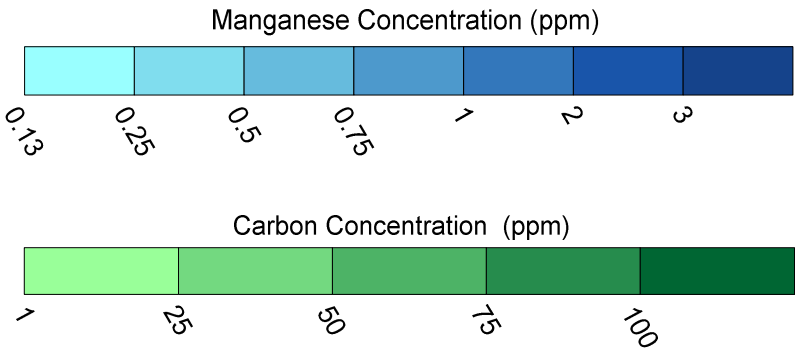




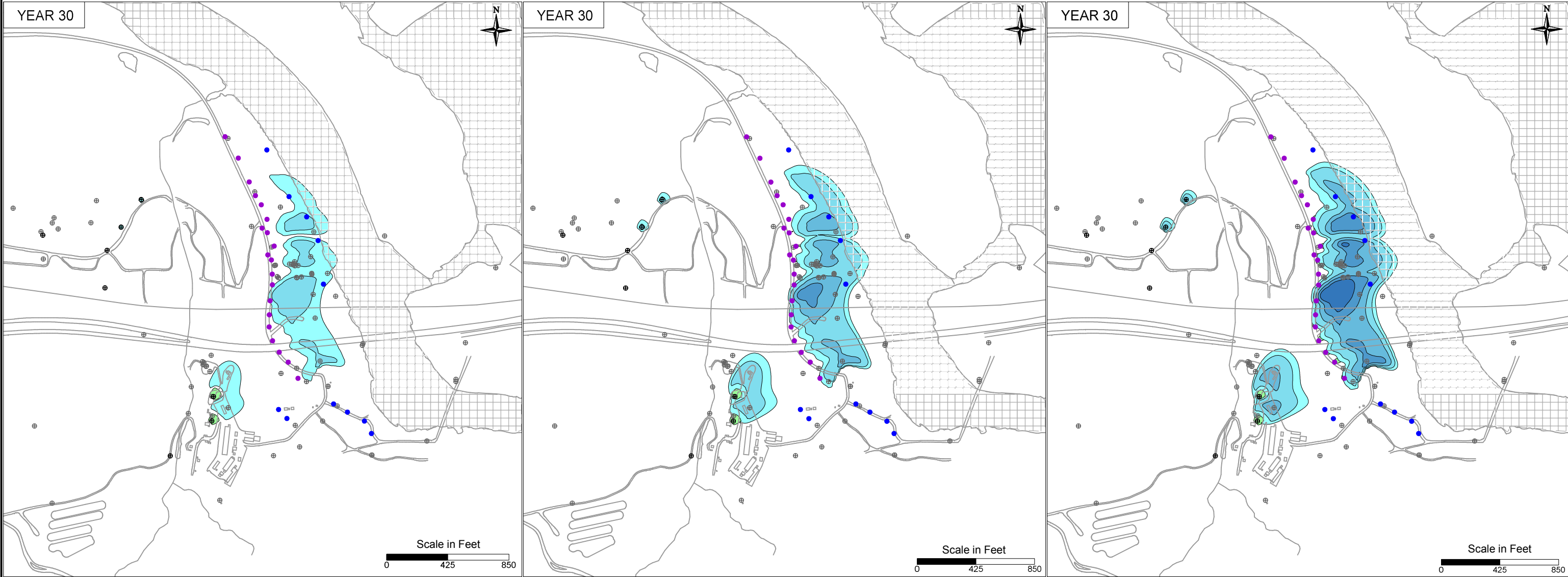
LOW TOC = 50 PPM

BASE TOC = 100 PPM

HIGH TOC = 150 PPM



- LEGEND**
- IRZ WELLS
  - UPGRADIENT INJECTION WELLS
  - EXTRACTION WELLS
  - MONITORING WELLS



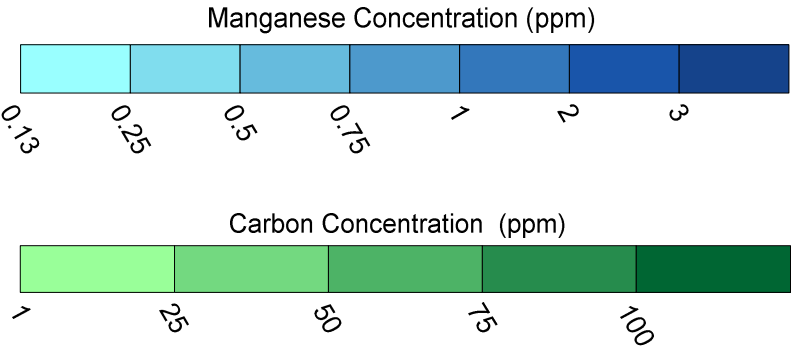
LOW TOC = 50 PPM

BASE TOC = 100 PPM

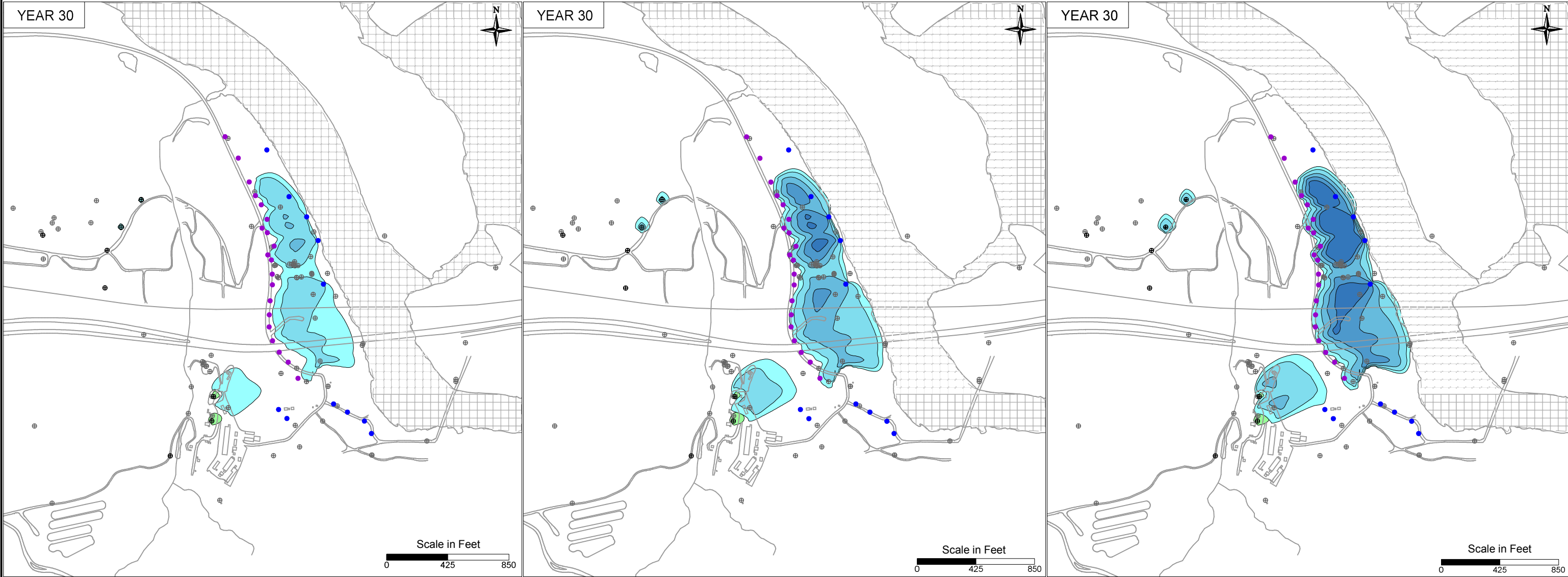
HIGH TOC = 150 PPM

**LEGEND**

- IRZ WELLS
- UPGRADIENT INJECTION WELLS
- EXTRACTION WELLS
- MONITORING WELLS



PG&E TOPOCK COMPRESSOR STATION NEEDLES, CALIFORNIA MODELING APPENDIX	
TOC CONCENTRATION SENSITIVITY: SIMULATED MANGANESE TRANSPORT RESULTS IN MODEL LAYER 2	
	FIGURE 10.2-7



LOW TOC = 50 PPM

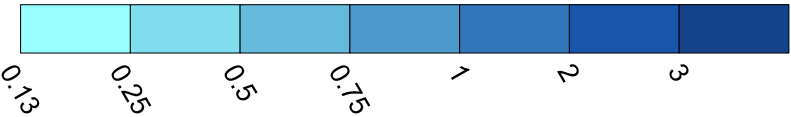
BASE TOC = 100 PPM

HIGH TOC = 150 PPM

**LEGEND**

- IRZ WELLS
- ⊕ UPGRADIENT INJECTION WELLS
- EXTRACTION WELLS
- ⊕ MONITORING WELLS

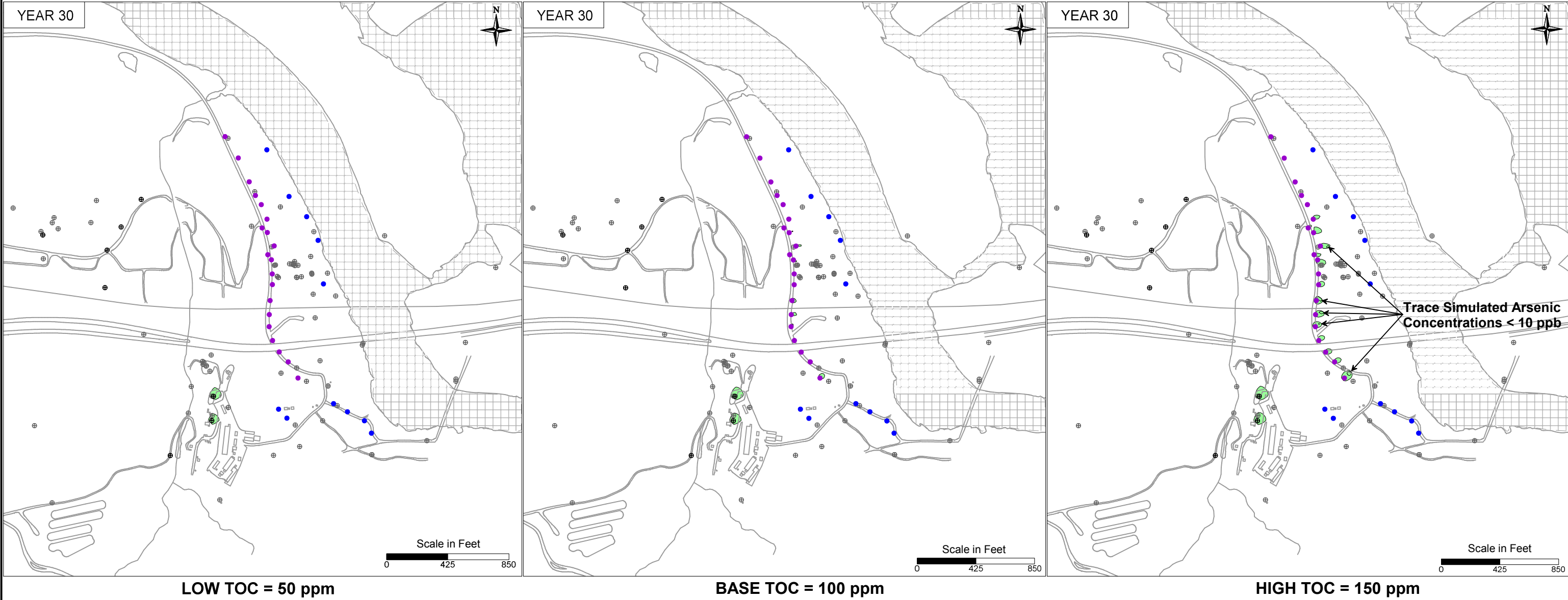
Manganese Concentration (ppm)



Carbon Concentration (ppm)

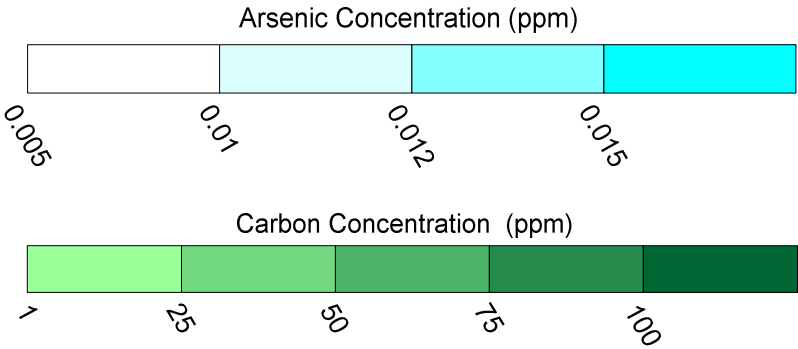


PG&E TOPOCK COMPRESSOR STATION NEEDLES, CALIFORNIA MODELING APPENDIX	
TOC CONCENTRATION SENSITIVITY: SIMULATED MANGANESE TRANSPORT RESULTS IN MODEL LAYER 4	
	FIGURE 10.2-8

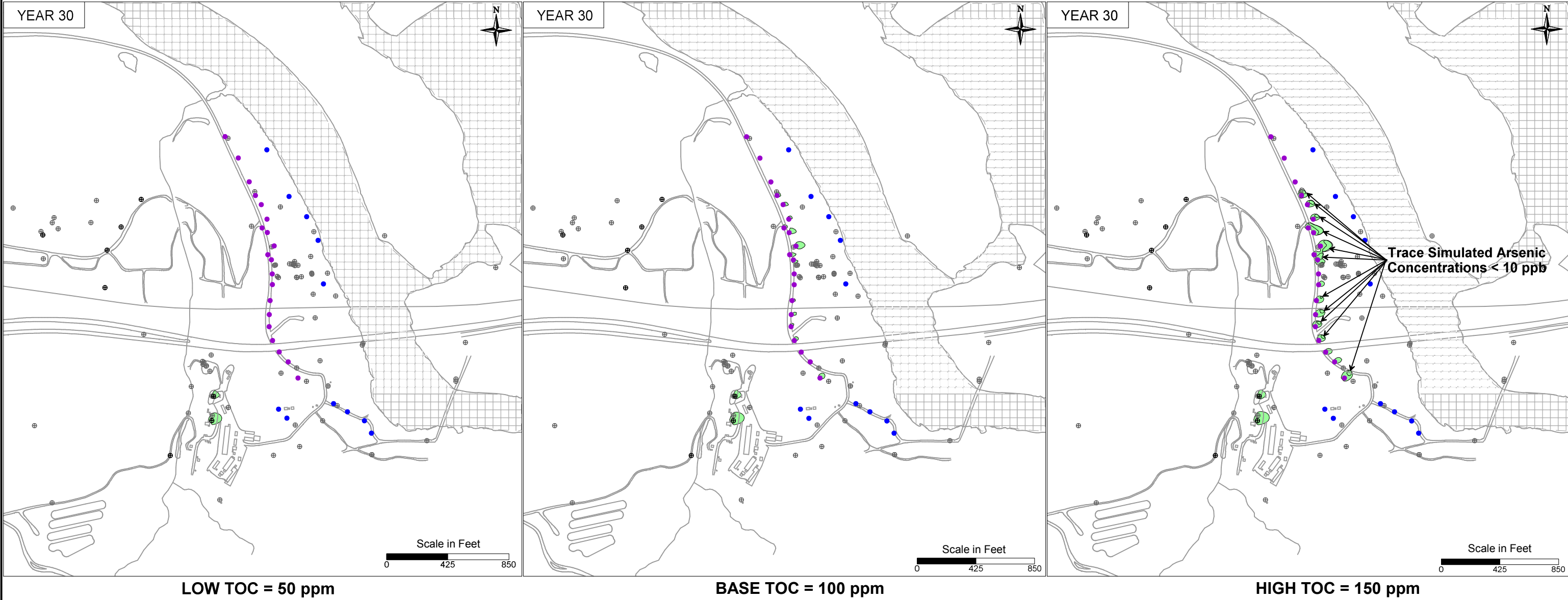


**LEGEND**

- IRZ WELLS
- UPGRADIENT INJECTION WELLS
- EXTRACTION WELLS
- MONITORING WELLS

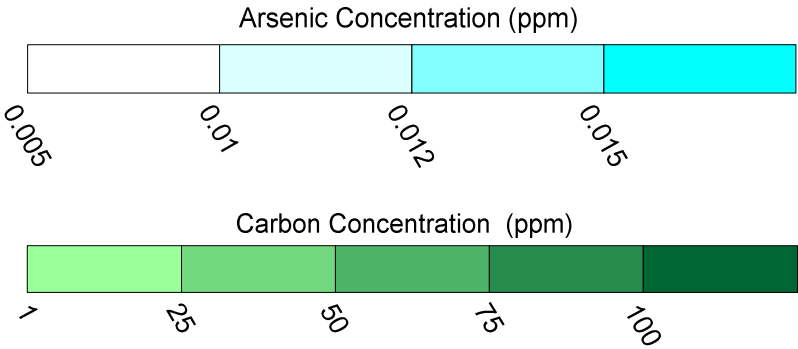




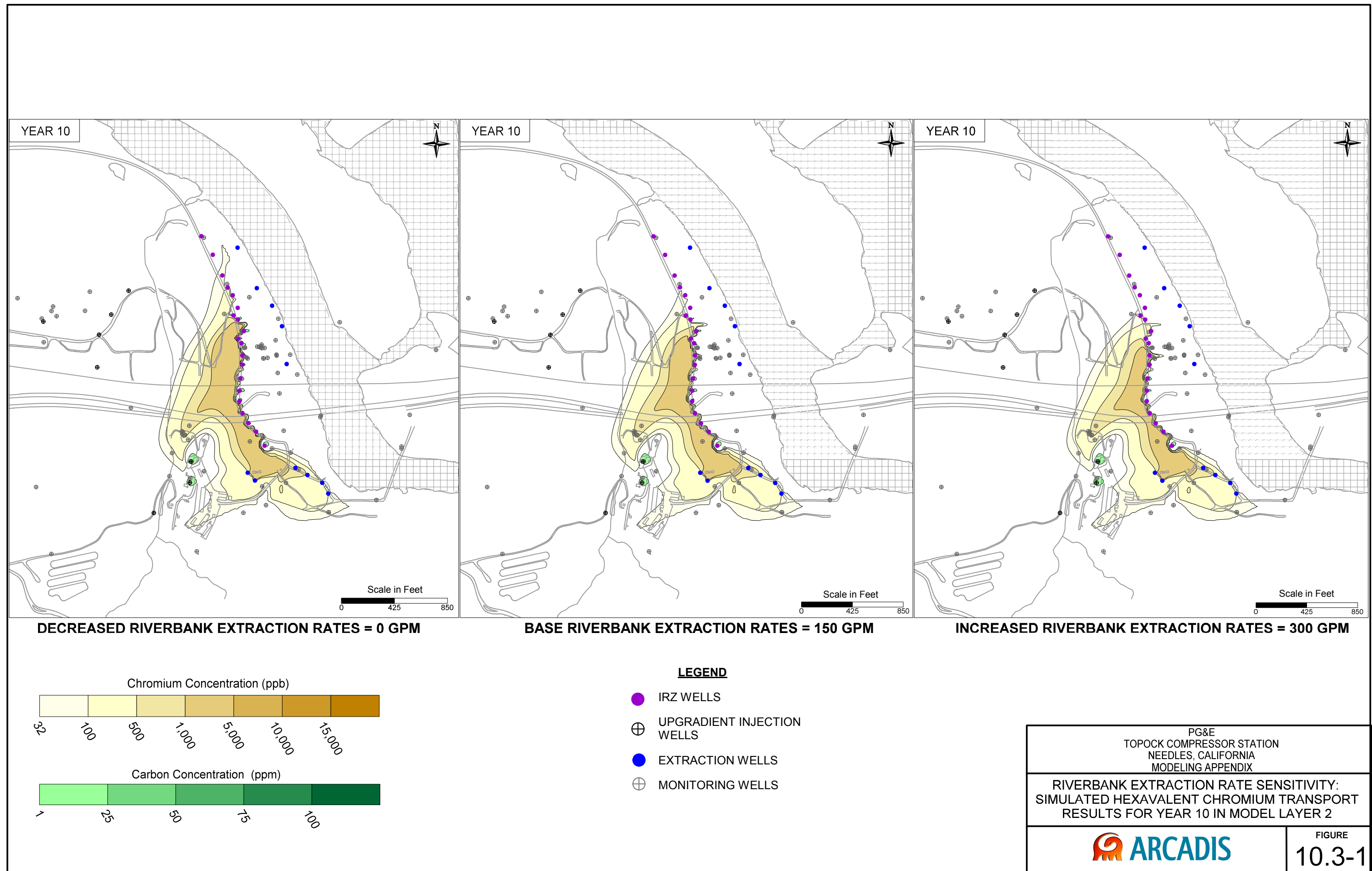


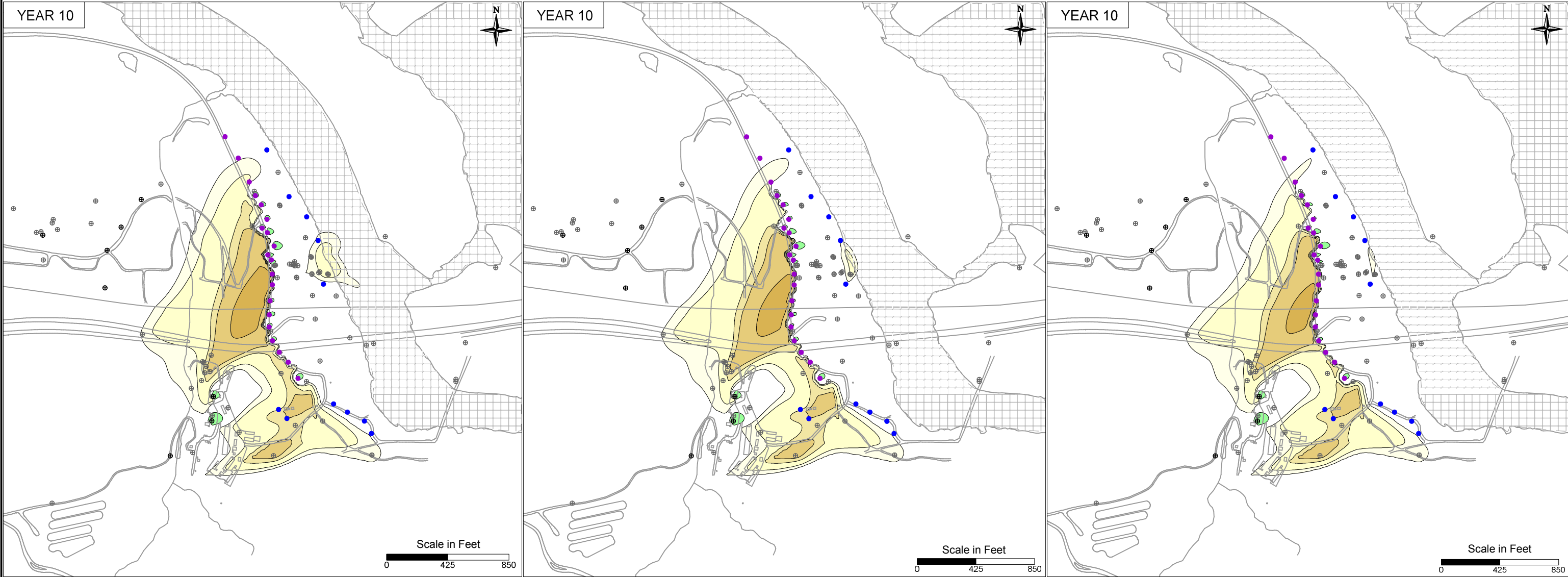
**LEGEND**

- IRZ WELLS
- UPGRADIENT INJECTION WELLS
- EXTRACTION WELLS
- MONITORING WELLS





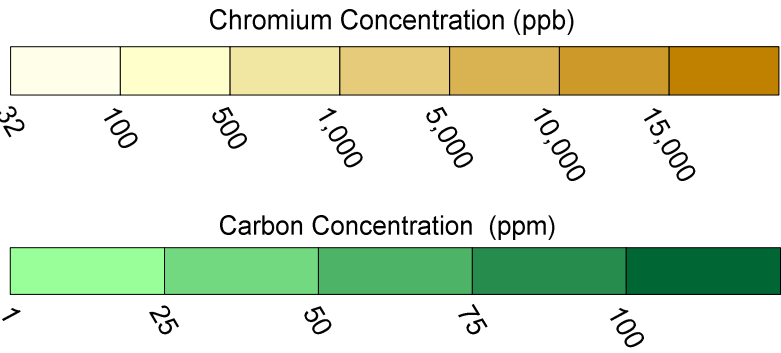




DECREASED RIVERBANK EXTRACTION RATES = 0 GPM

BASE RIVERBANK EXTRACTION RATES = 150 GPM

INCREASED RIVERBANK EXTRACTION RATES = 300 GPM



**LEGEND**

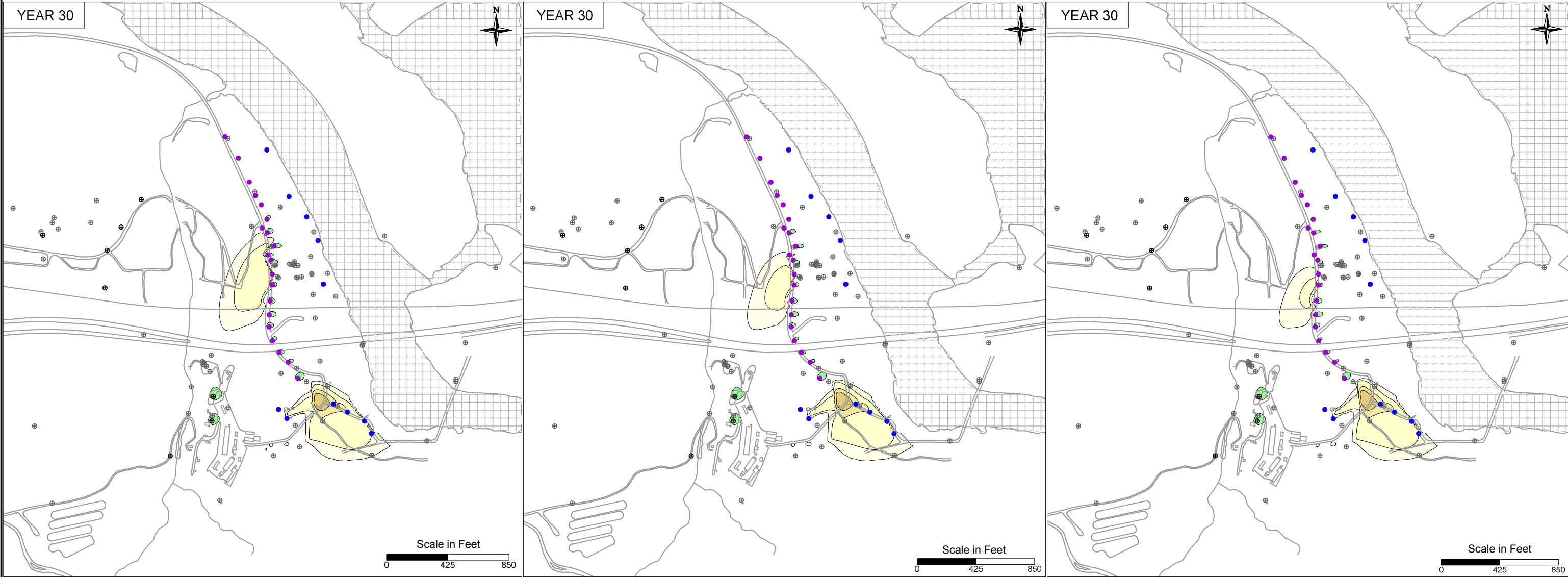
- IRZ WELLS
- UPGRADIENT INJECTION WELLS
- EXTRACTION WELLS
- MONITORING WELLS

PG&E  
TOPOCK COMPRESSOR STATION  
NEEDLES, CALIFORNIA  
MODELING APPENDIX

RIVERBANK EXTRACTION RATE SENSITIVITY:  
SIMULATED HEXAVALENT CHROMIUM TRANSPORT  
RESULTS FOR YEAR 10 IN MODEL LAYER 4

ARCADIS

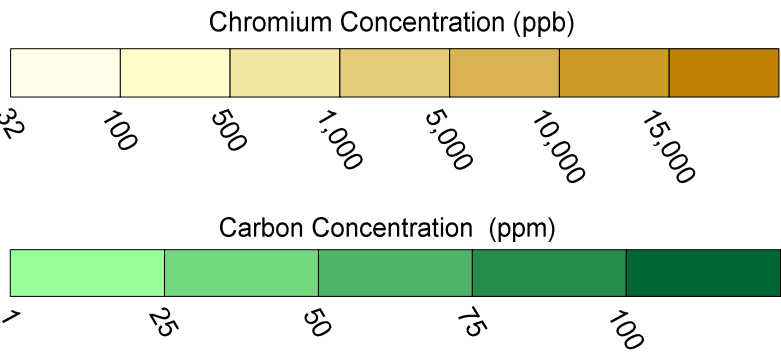
FIGURE  
10.3-2



DECREASED RIVERBANK EXTRACTION RATES = 0 GPM

BASE RIVERBANK EXTRACTION RATES = 150 GPM

INCREASED RIVERBANK EXTRACTION RATES = 300 GPM

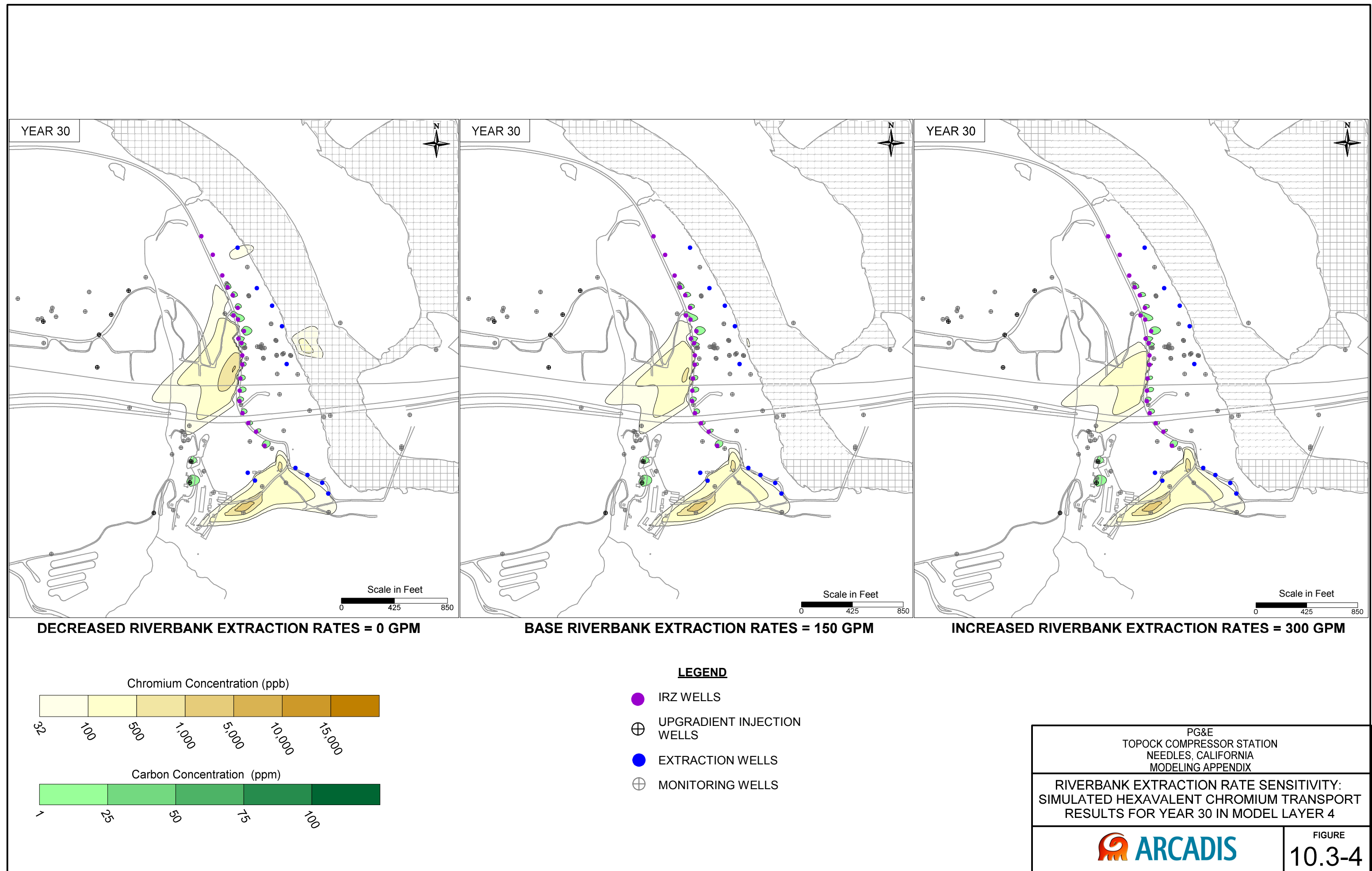


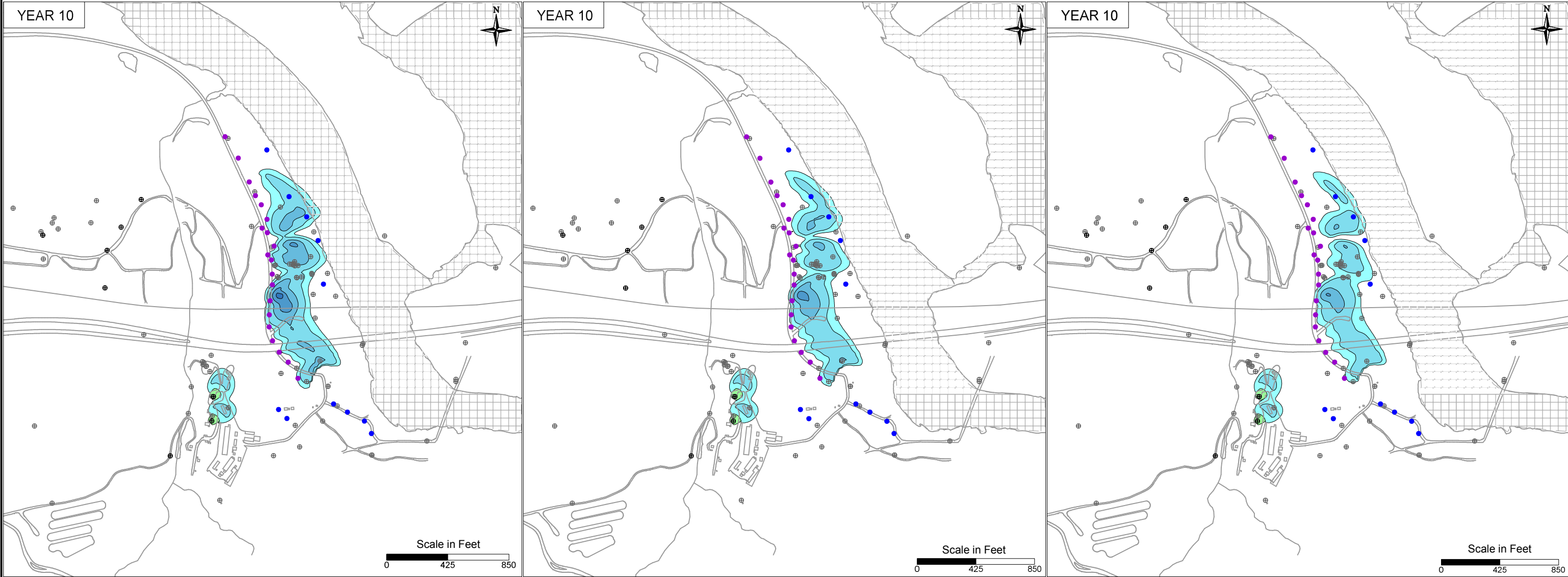
**LEGEND**

- IRZ WELLS
- ⊕ UPGRADIENT INJECTION WELLS
- EXTRACTION WELLS
- ⊕ MONITORING WELLS

PG&E TOPOCK COMPRESSOR STATION NEEDLES, CALIFORNIA MODELING APPENDIX	
RIVERBANK EXTRACTION RATE SENSITIVITY: SIMULATED HEXAVALENT CHROMIUM TRANSPORT RESULTS FOR YEAR 30 IN MODEL LAYER 2	
	FIGURE 10.3-3







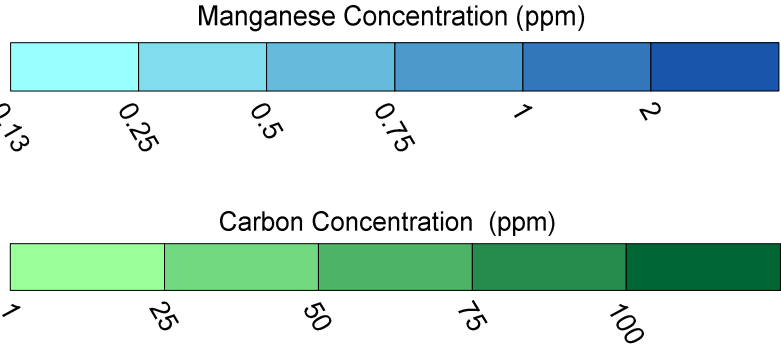
DECREASED RIVERBANK EXTRACTION RATES = 0 GPM

BASE RIVERBANK EXTRACTION RATES = 150 GPM

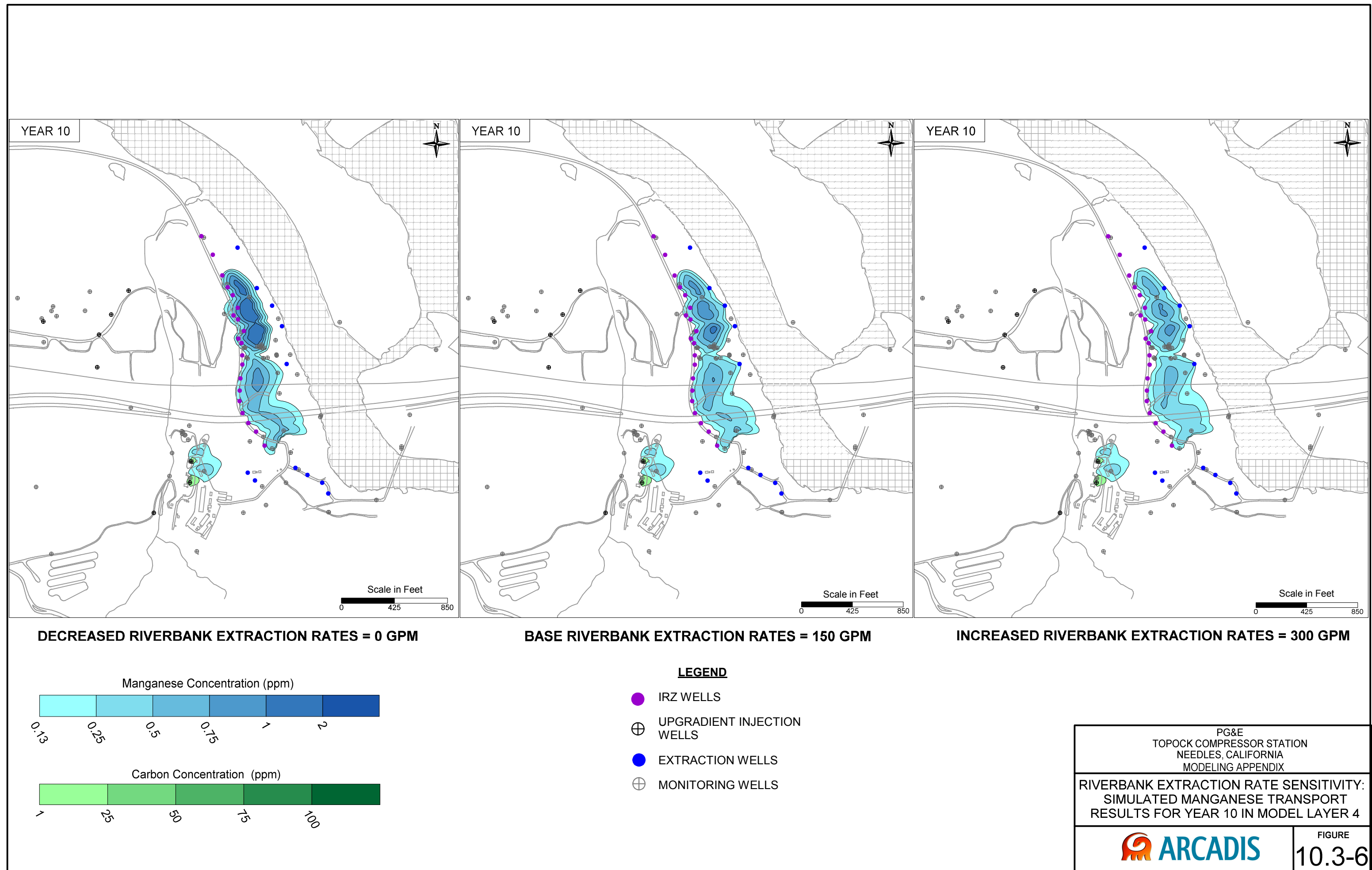
INCREASED RIVERBANK EXTRACTION RATES = 300 GPM

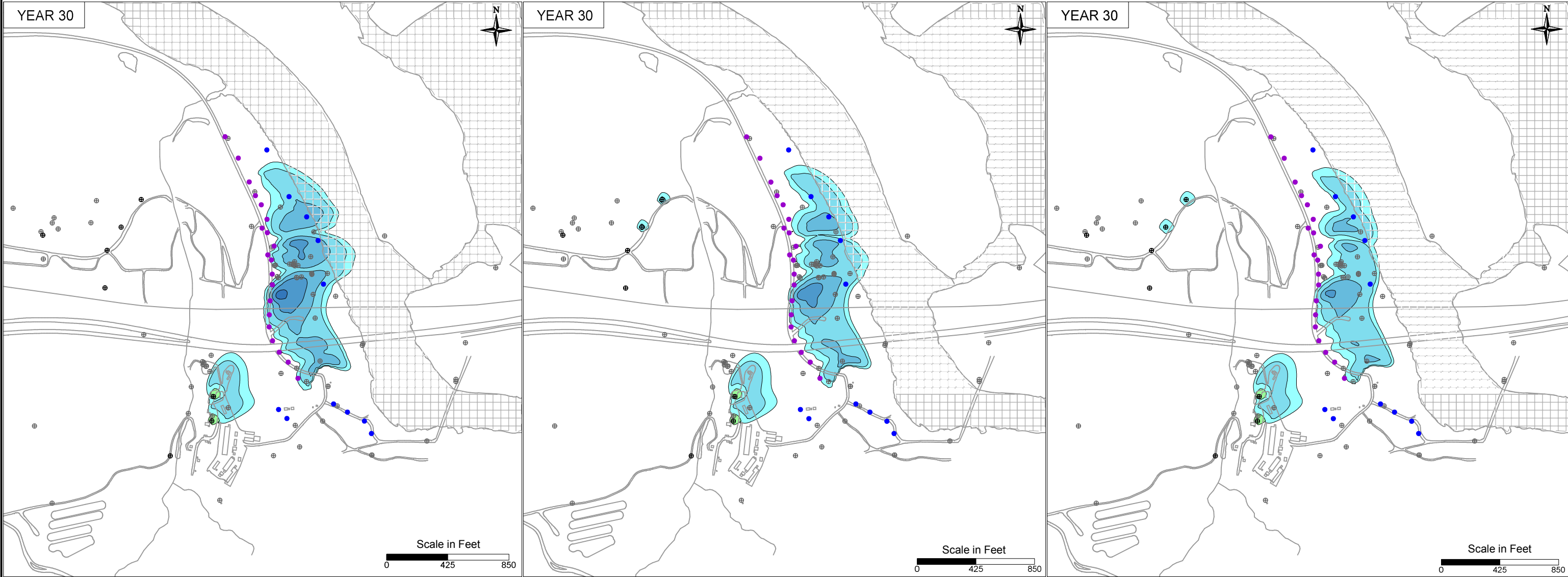
**LEGEND**

- IRZ WELLS
- ⊕ UPGRADIENT INJECTION WELLS
- EXTRACTION WELLS
- ⊕ MONITORING WELLS





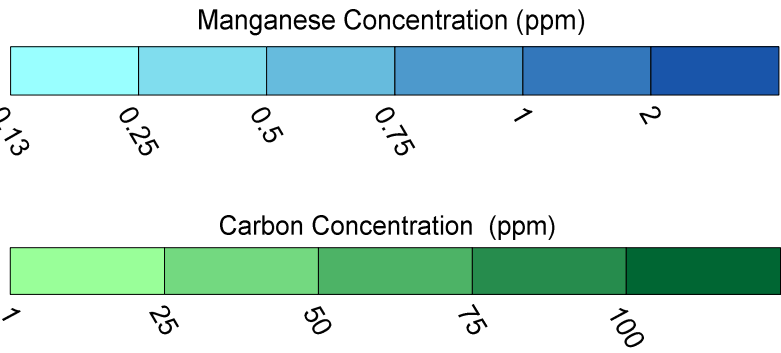




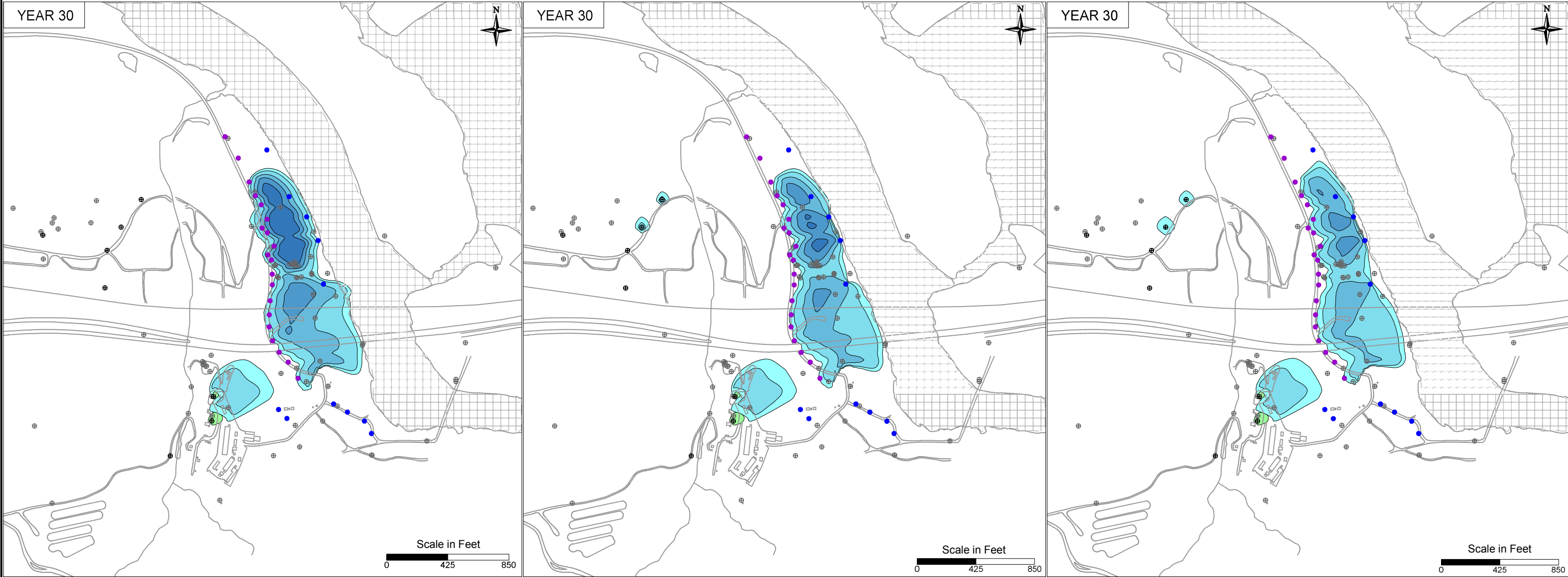
DECREASED RIVERBANK EXTRACTION RATES = 0 GPM

BASE RIVERBANK EXTRACTION RATES = 150 GPM

INCREASED RIVERBANK EXTRACTION RATES = 300 GPM



- LEGEND**
- IRZ WELLS
  - UPGRADIENT INJECTION WELLS
  - EXTRACTION WELLS
  - MONITORING WELLS



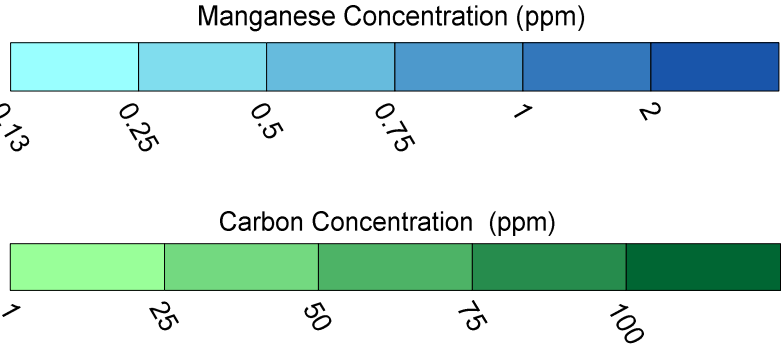
DECREASED RIVERBANK EXTRACTION RATES = 0 GPM

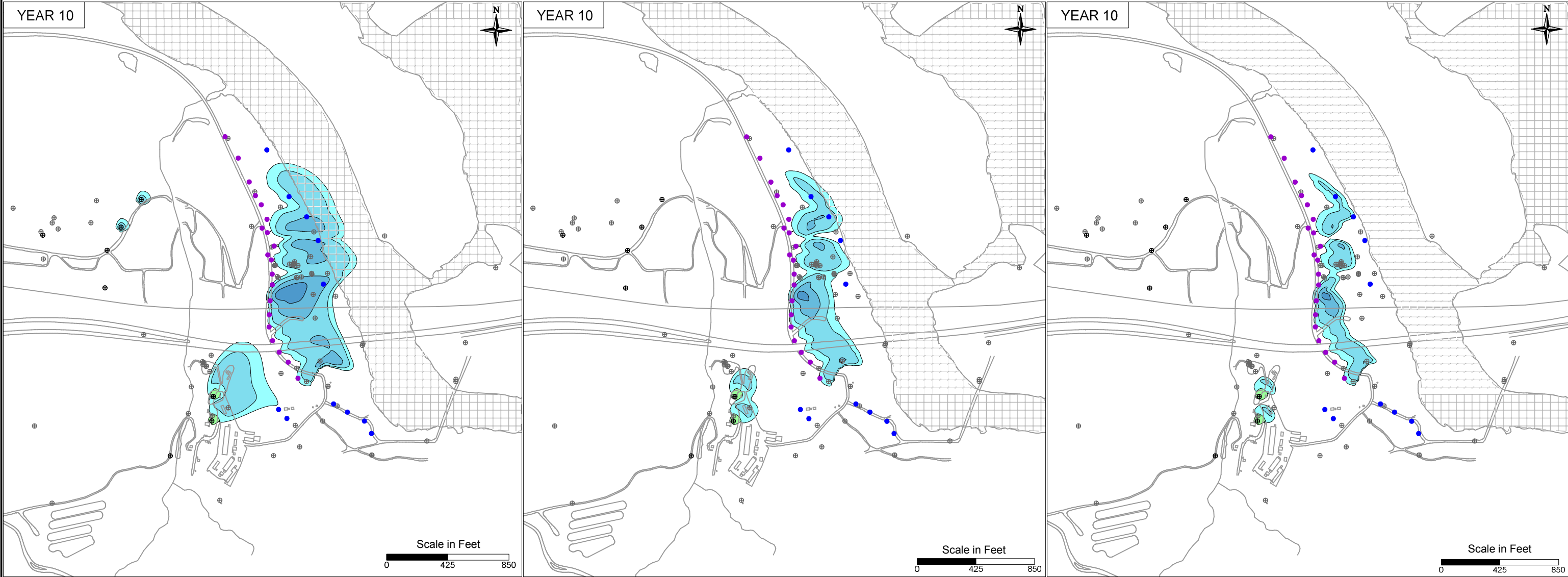
BASE RIVERBANK EXTRACTION RATES = 150 GPM

INCREASED RIVERBANK EXTRACTION RATES = 300 GPM

**LEGEND**

- IRZ WELLS
- UPGRADIENT INJECTION WELLS
- EXTRACTION WELLS
- MONITORING WELLS





DECREASED SORPTION ( $K_f = 0.137$ )

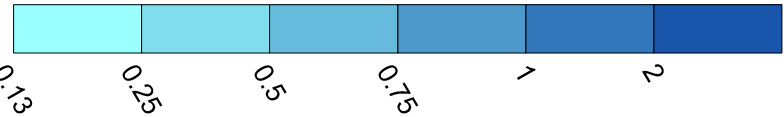
BASE SORPTION ( $K_f = 1.37$ )

INCREASED SORPTION ( $K_f = 6.85$ )

**LEGEND**

- IRZ WELLS
- ⊕ UPGRADIENT INJECTION WELLS
- EXTRACTION WELLS
- ⊕ MONITORING WELLS

Manganese Concentration (ppm)



Carbon Concentration (ppm)

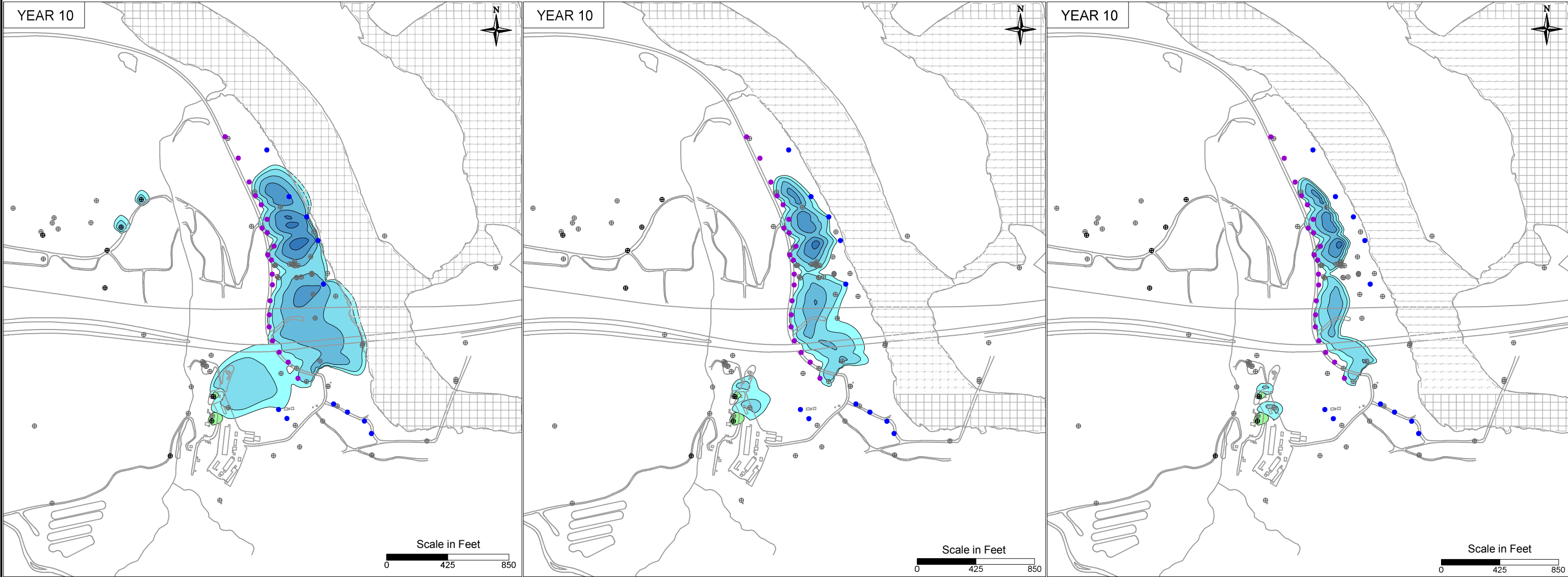


PG&E  
TOPOCK COMPRESSOR STATION  
NEEDLES, CALIFORNIA  
MODELING APPENDIX

MANGANESE SORPTION SENSITIVITY:  
SIMULATED MANGANESE TRANSPORT  
RESULTS FOR YEAR 10 IN MODEL LAYER 2







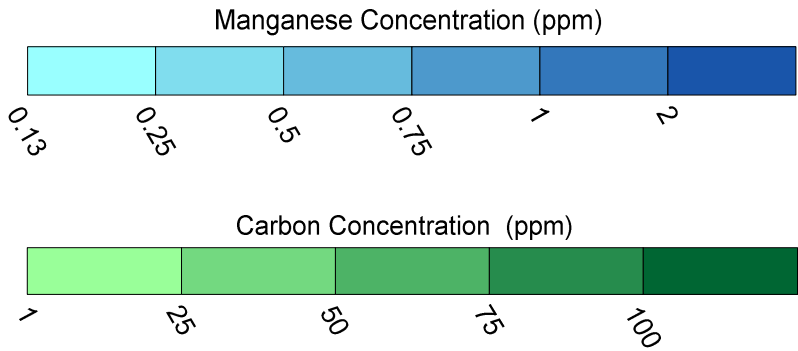
DECREASED SORPTION ( $K_f = 0.137$ )

BASE SORPTION ( $K_f = 1.37$ )

INCREASED SORPTION ( $K_f = 6.85$ )

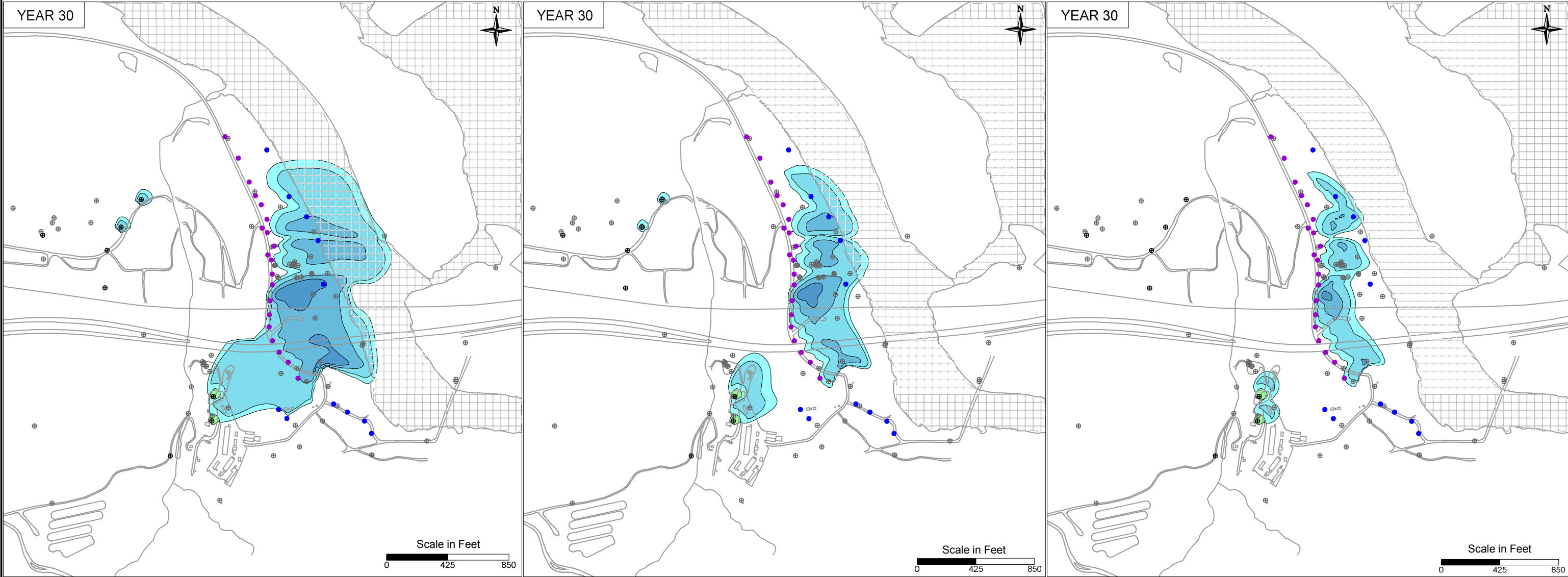
**LEGEND**

- IRZ WELLS
- ⊕ UPGRADIENT INJECTION WELLS
- EXTRACTION WELLS
- ⊕ MONITORING WELLS



PG&E TOPOCK COMPRESSOR STATION NEEDLES, CALIFORNIA MODELING APPENDIX	
MANGANESE SORPTION SENSITIVITY: SIMULATED MANGANESE TRANSPORT RESULTS FOR YEAR 10 IN MODEL LAYER 4	
	FIGURE 10.4-2





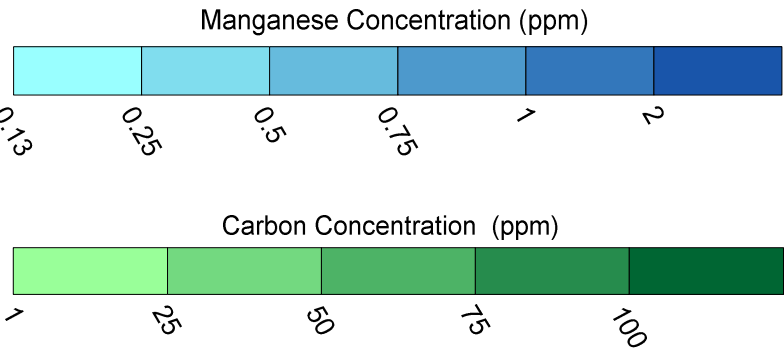
DECREASED SORPTION ( $K_f = 0.137$ )

BASE SORPTION ( $K_f = 1.37$ )

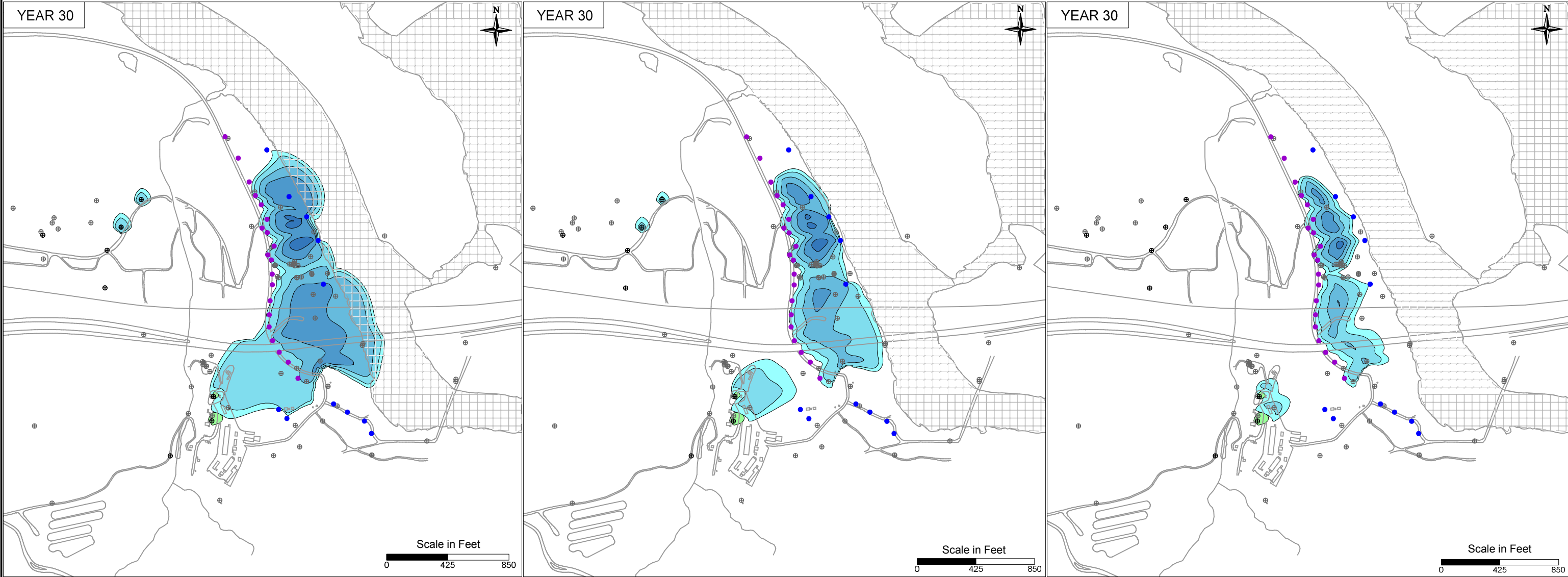
INCREASED SORPTION ( $K_f = 6.85$ )

**LEGEND**

- IRZ WELLS
- ⊕ UPGRADIENT INJECTION WELLS
- EXTRACTION WELLS
- ⊕ MONITORING WELLS



PG&E TOPOCK COMPRESSOR STATION NEEDLES, CALIFORNIA MODELING APPENDIX	
MANGANESE SORPTION SENSITIVITY: SIMULATED MANGANESE TRANSPORT RESULTS FOR YEAR 30 IN MODEL LAYER 2	
	FIGURE 10.4-3



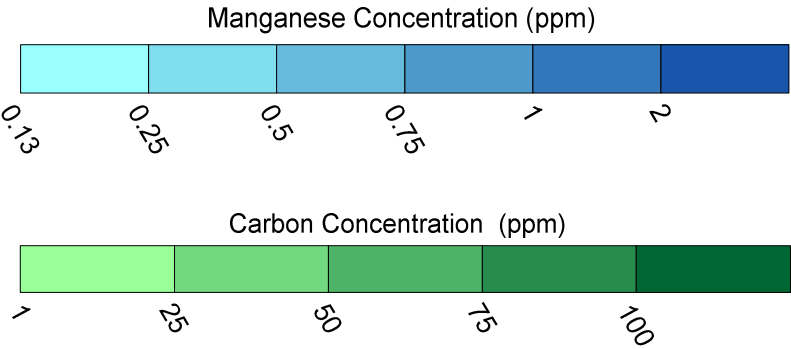
DECREASED SORPTION ( $K_f = 0.137$ )

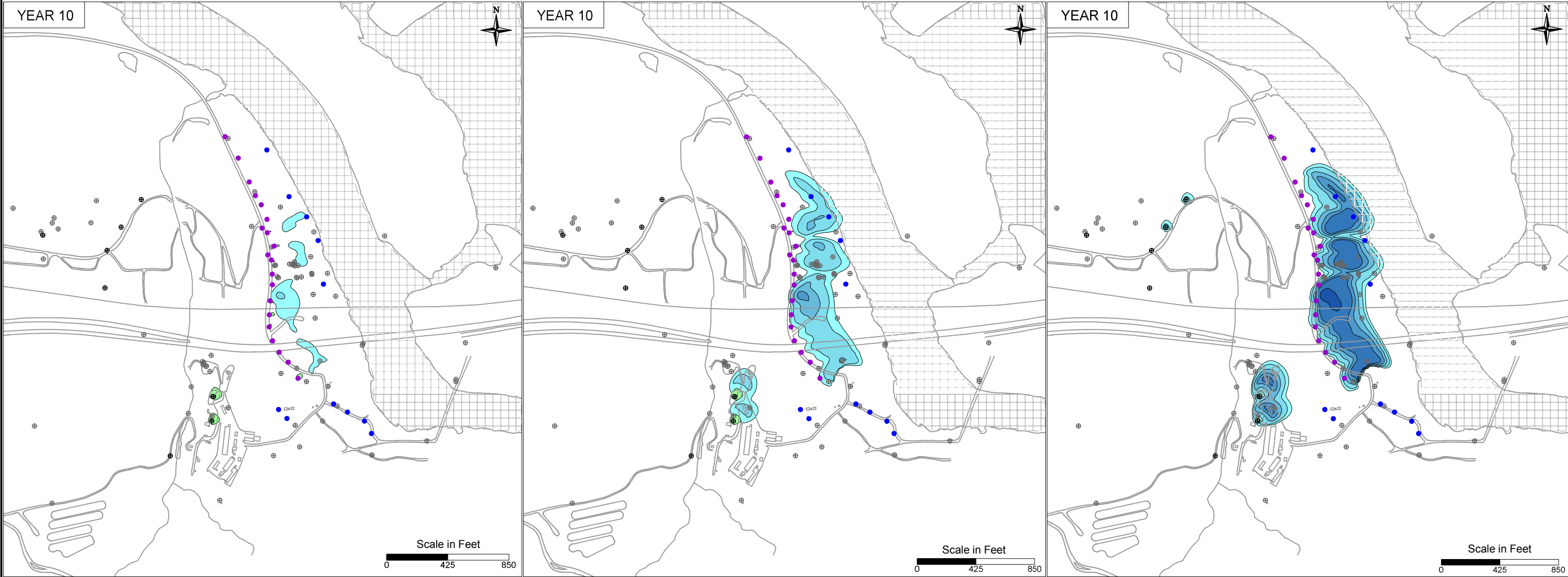
BASE SORPTION ( $K_f = 1.37$ )

INCREASED SORPTION ( $K_f = 6.85$ )

**LEGEND**

- IRZ WELLS
- ⊕ UPGRADIENT INJECTION WELLS
- EXTRACTION WELLS
- ⊕ MONITORING WELLS





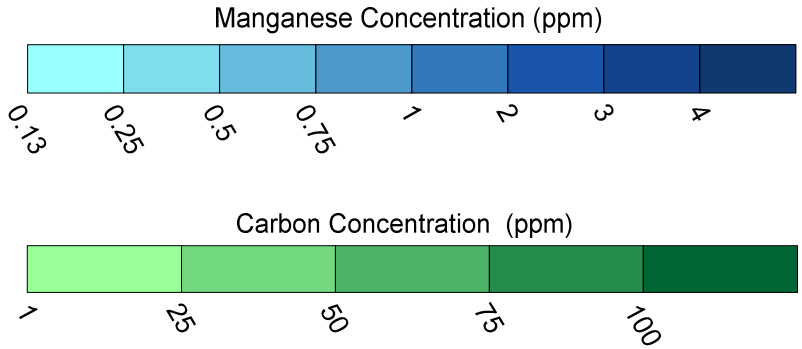
**DECREASED STOICHIOMETRIC RATIO  
FOR GENERATION = 0.005**

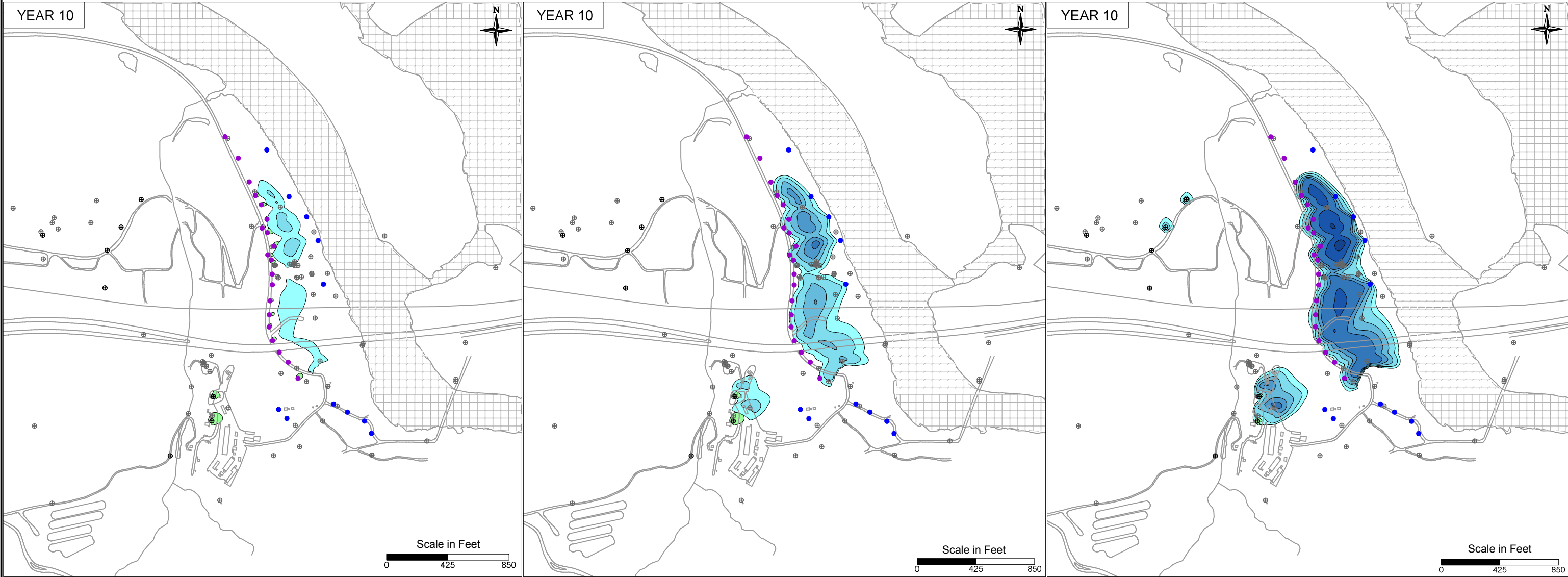
**BASE STOICHIOMETRIC RATIO  
FOR GENERATION = 0.016**

**INCREASED STOICHIOMETRIC RATIO  
FOR GENERATION = 0.05**

**LEGEND**

- IRZ WELLS
- ⊕ UPGRADIENT INJECTION WELLS
- EXTRACTION WELLS
- ⊕ MONITORING WELLS





**DECREASED STOICHIOMETRIC RATIO  
FOR GENERATION = 0.005**

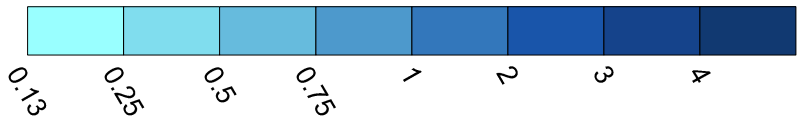
**BASE STOICHIOMETRIC RATIO  
FOR GENERATION = 0.016**

**INCREASED STOICHIOMETRIC RATIO  
FOR GENERATION = 0.05**

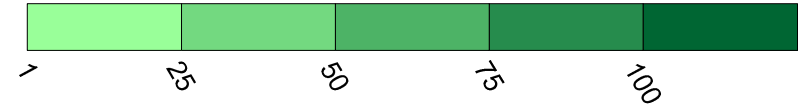
**LEGEND**

- IRZ WELLS
- ⊕ UPGRADIENT INJECTION WELLS
- EXTRACTION WELLS
- ⊕ MONITORING WELLS

Manganese Concentration (ppm)



Carbon Concentration (ppm)



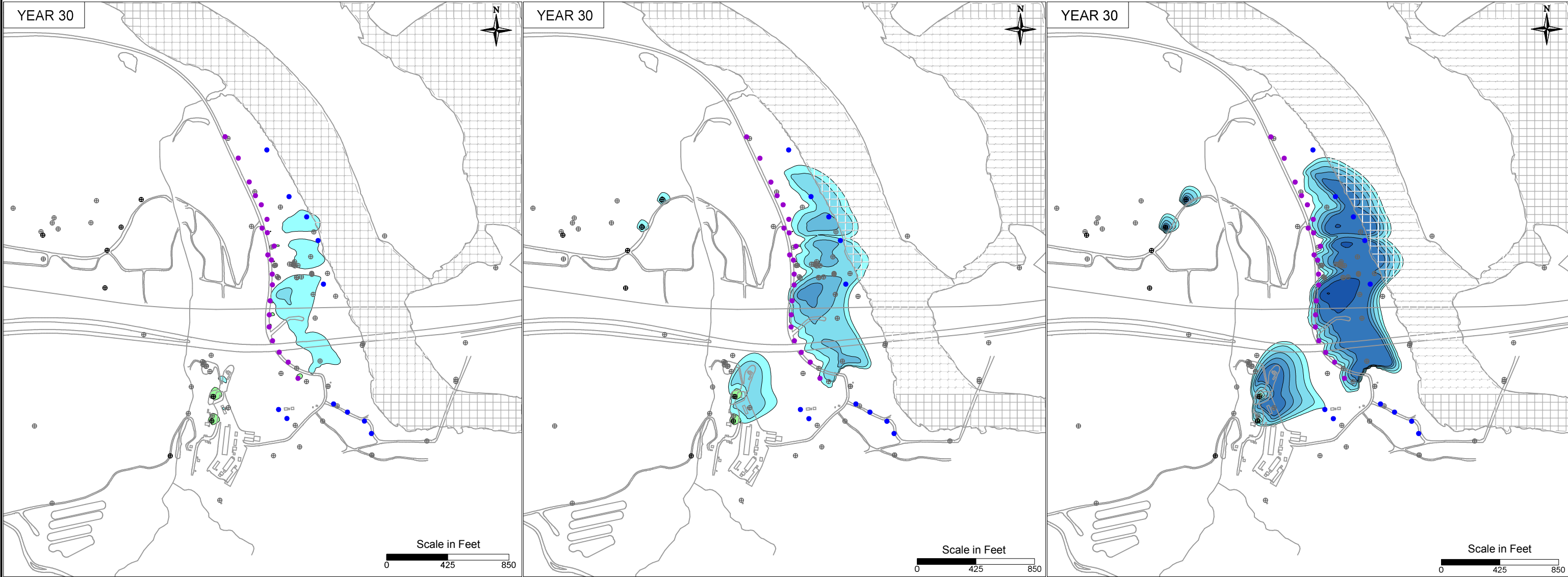
PG&E  
TOPOCK COMPRESSOR STATION  
NEEDLES, CALIFORNIA  
MODELING APPENDIX

**MANGANESE GENERATION SENSITIVITY:  
SIMULATED MANGANESE TRANSPORT  
RESULTS FOR YEAR 10 IN MODEL LAYER 4**



FIGURE  
**10.4-6**





**DECREASED STOICHIOMETRIC RATIO  
FOR GENERATION = 0.005**

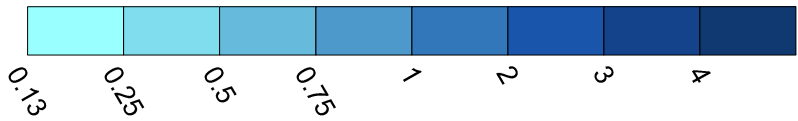
**BASE STOICHIOMETRIC RATIO  
FOR GENERATION = 0.016**

**INCREASED STOICHIOMETRIC RATIO  
FOR GENERATION = 0.05**

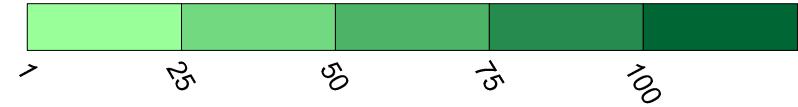
**LEGEND**

- IRZ WELLS
- ⊕ UPGRADIENT INJECTION WELLS
- EXTRACTION WELLS
- ⊕ MONITORING WELLS

Manganese Concentration (ppm)



Carbon Concentration (ppm)



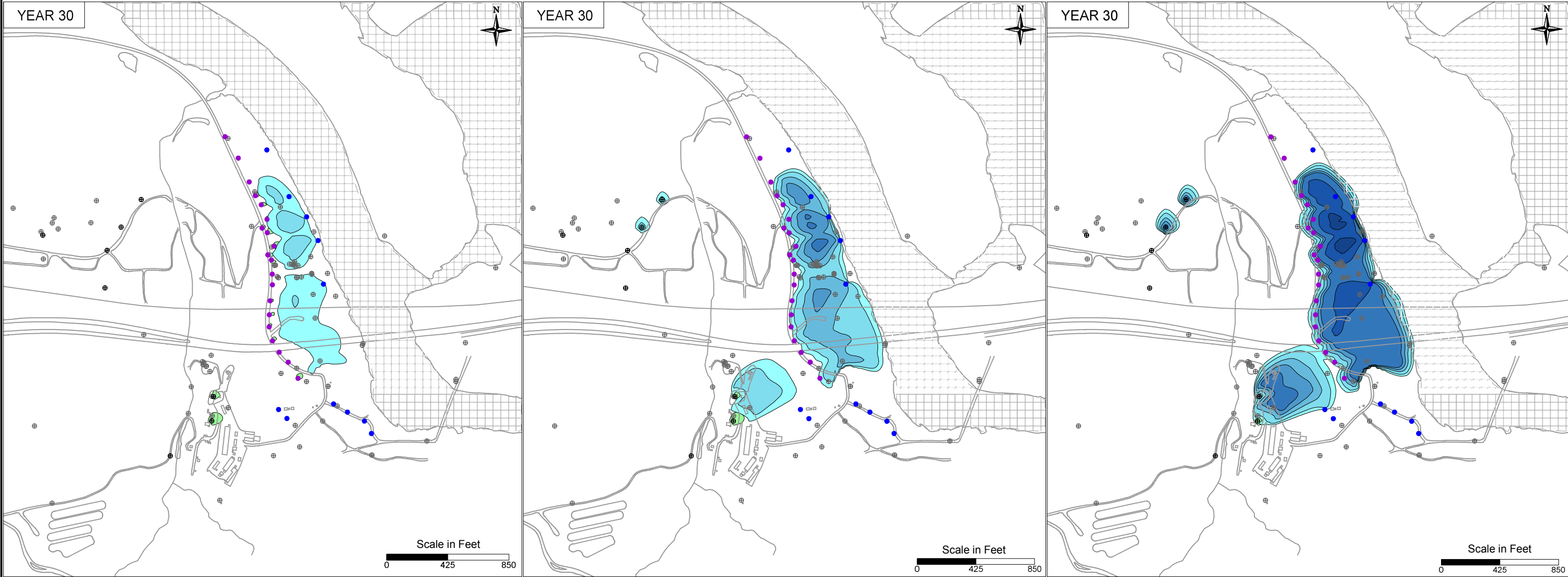
PG&E  
TOPOCK COMPRESSOR STATION  
NEEDLES, CALIFORNIA  
MODELING APPENDIX

**MANGANESE GENERATION SENSITIVITY:  
SIMULATED MANGANESE TRANSPORT  
RESULTS FOR YEAR 30 IN MODEL LAYER 2**



FIGURE  
**10.4-7**





**DECREASED STOICHIOMETRIC RATIO  
FOR GENERATION = 0.005**

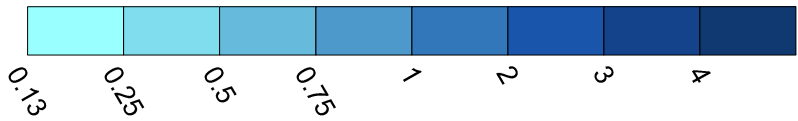
**BASE STOICHIOMETRIC RATIO  
FOR GENERATION = 0.016**

**INCREASED STOICHIOMETRIC RATIO  
FOR GENERATION = 0.05**

**LEGEND**

- IRZ WELLS
- ⊕ UPGRADIENT INJECTION WELLS
- EXTRACTION WELLS
- ⊕ MONITORING WELLS

Manganese Concentration (ppm)



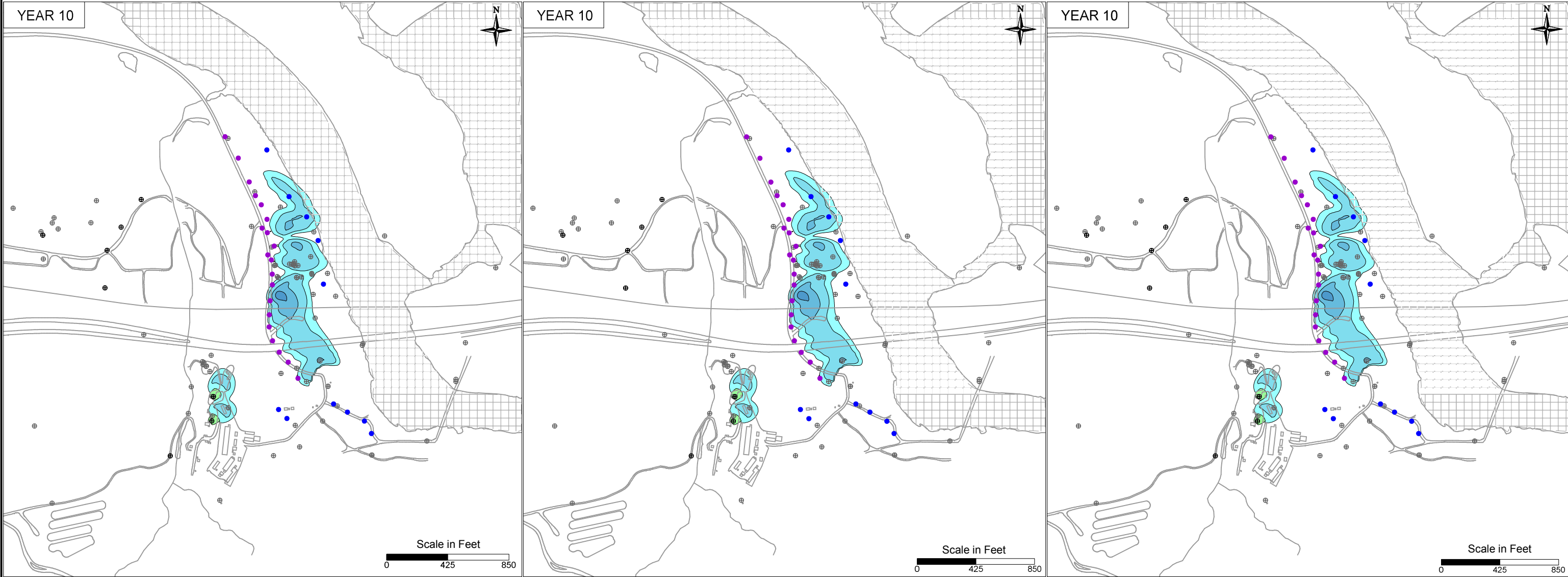
Carbon Concentration (ppm)



PG&E  
TOPOCK COMPRESSOR STATION  
NEEDLES, CALIFORNIA  
MODELING APPENDIX

**MANGANESE GENERATION SENSITIVITY:  
SIMULATED MANGANESE TRANSPORT  
RESULTS FOR YEAR 30 IN MODEL LAYER 4**





DECREASED OXIDATION HALF-LIFE = 15 DAY

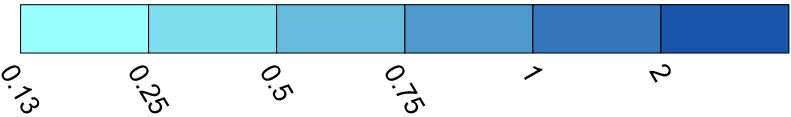
BASE OXIDATION HALF-LIFE = 30 DAY

INCREASED OXIDATION HALF-LIFE = 60 DAY

**LEGEND**

- IRZ WELLS
- ⊕ UPGRADIENT INJECTION WELLS
- EXTRACTION WELLS
- ⊕ MONITORING WELLS

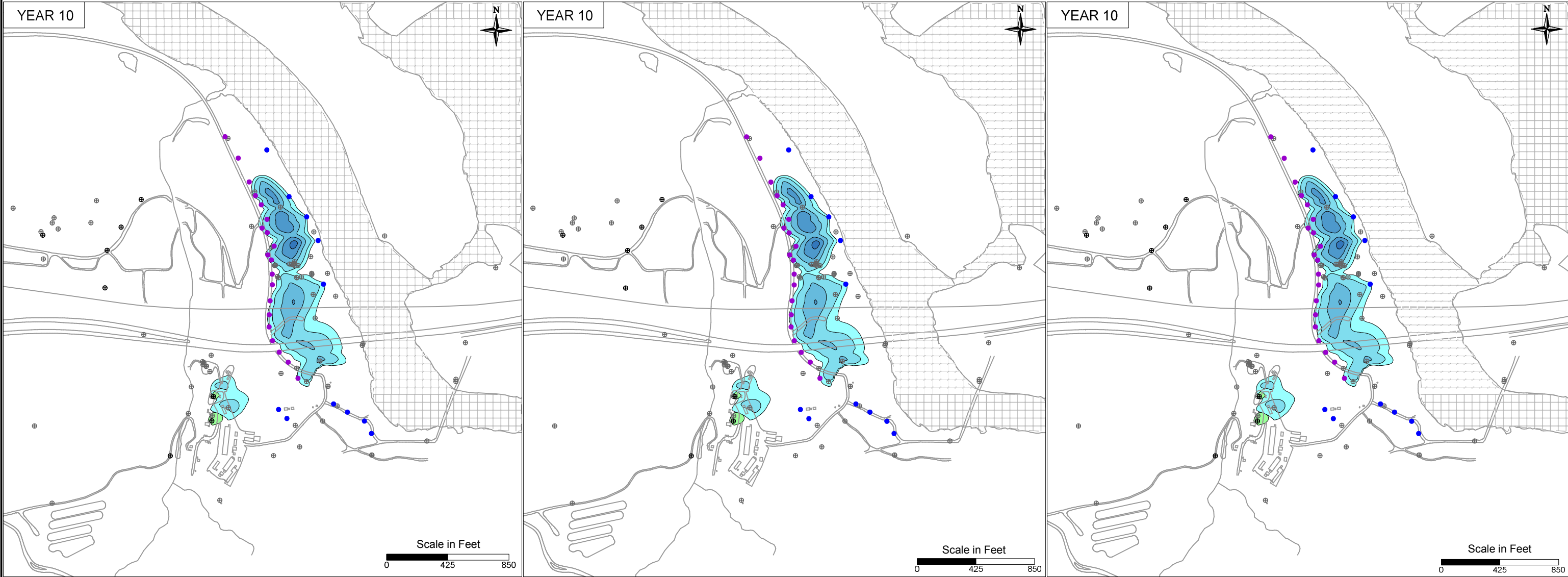
Manganese Concentration (ppm)



Carbon Concentration (ppm)



PG&E TOPOCK COMPRESSOR STATION NEEDLES, CALIFORNIA MODELING APPENDIX	
MANGANESE OXIDATION SENSITIVITY: SIMULATED MANGANESE TRANSPORT RESULTS FOR YEAR 10 IN MODEL LAYER 2	
	FIGURE 10.4-9



DECREASED OXIDATION HALF-LIFE = 15 DAY

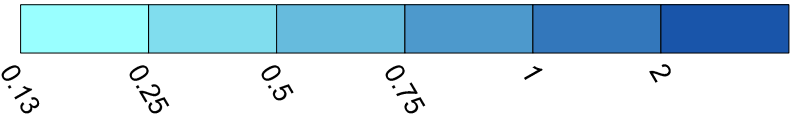
BASE OXIDATION HALF-LIFE = 30 DAY

INCREASED OXIDATION HALF-LIFE = 60 DAY

**LEGEND**

- IRZ WELLS
- ⊕ UPGRADIENT INJECTION WELLS
- EXTRACTION WELLS
- ⊕ MONITORING WELLS

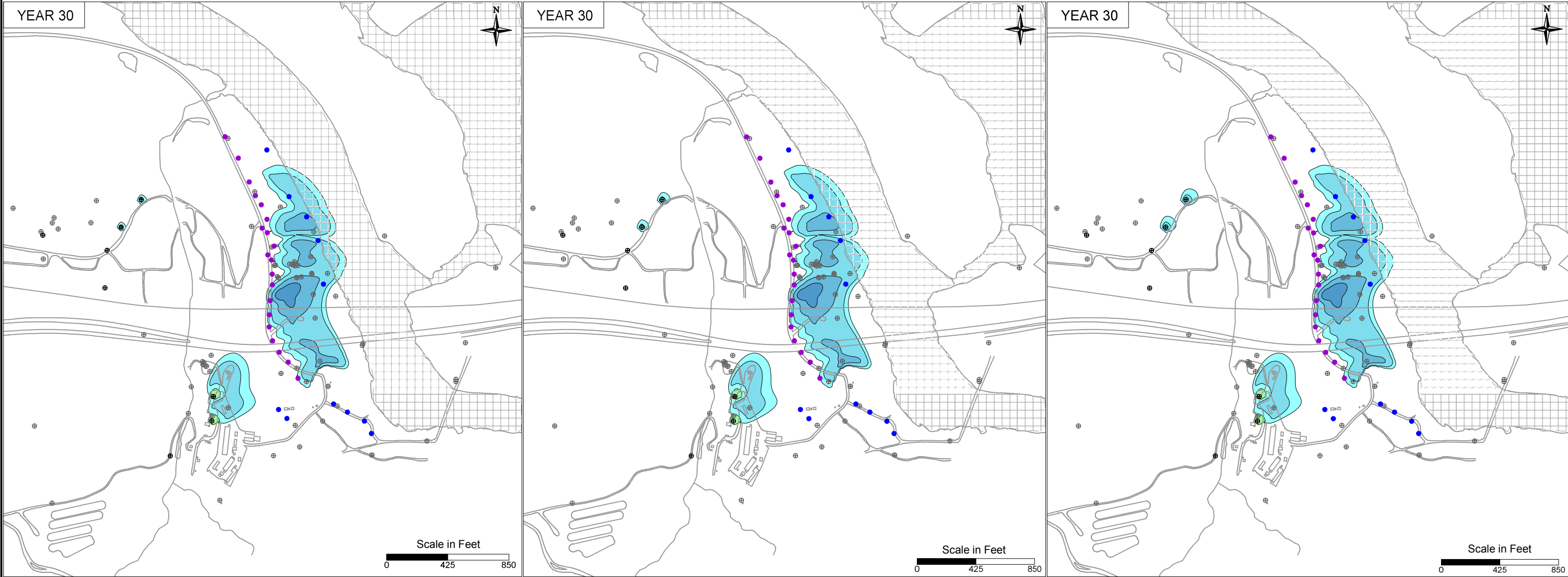
Manganese Concentration (ppm)



Carbon Concentration (ppm)



PG&E TOPOCK COMPRESSOR STATION NEEDLES, CALIFORNIA MODELING APPENDIX	
MANGANESE OXIDATION SENSITIVITY: SIMULATED MANGANESE TRANSPORT RESULTS FOR YEAR 10 IN MODEL LAYER 4	
	FIGURE 10.4-10



DECREASED OXIDATION HALF-LIFE = 15 DAY

BASE OXIDATION HALF-LIFE = 30 DAY

INCREASED OXIDATION HALF-LIFE = 60 DAY

**LEGEND**

- IRZ WELLS
- ⊕ UPGRADIENT INJECTION WELLS
- EXTRACTION WELLS
- ⊕ MONITORING WELLS

Manganese Concentration (ppm)

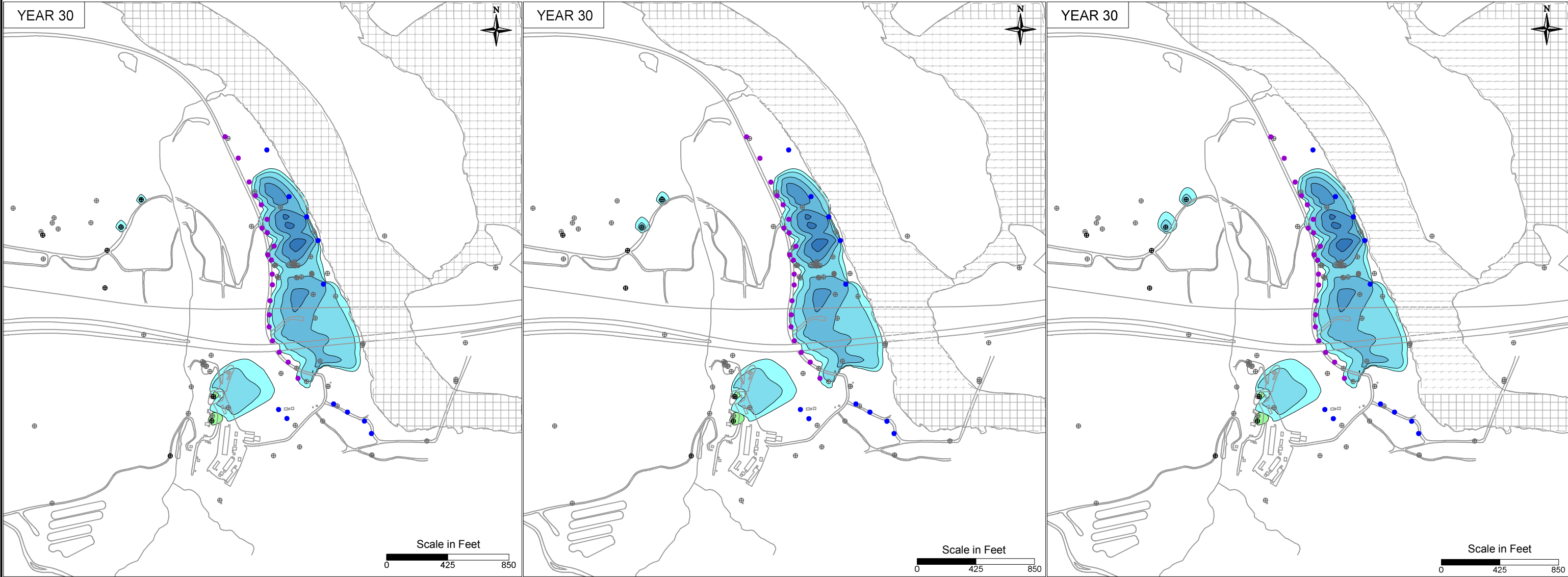


Carbon Concentration (ppm)



PG&E TOPOCK COMPRESSOR STATION NEEDLES, CALIFORNIA MODELING APPENDIX	
MANGANESE OXIDATION SENSITIVITY: SIMULATED MANGANESE TRANSPORT RESULTS FOR YEAR 30 IN MODEL LAYER 2	
	FIGURE 10.4-11





DECREASED OXIDATION HALF-LIFE = 15 DAY

BASE OXIDATION HALF-LIFE = 30 DAY

INCREASED OXIDATION HALF-LIFE = 60 DAY

**LEGEND**

- IRZ WELLS
- ⊕ UPGRADIENT INJECTION WELLS
- EXTRACTION WELLS
- ⊕ MONITORING WELLS

Manganese Concentration (ppm)

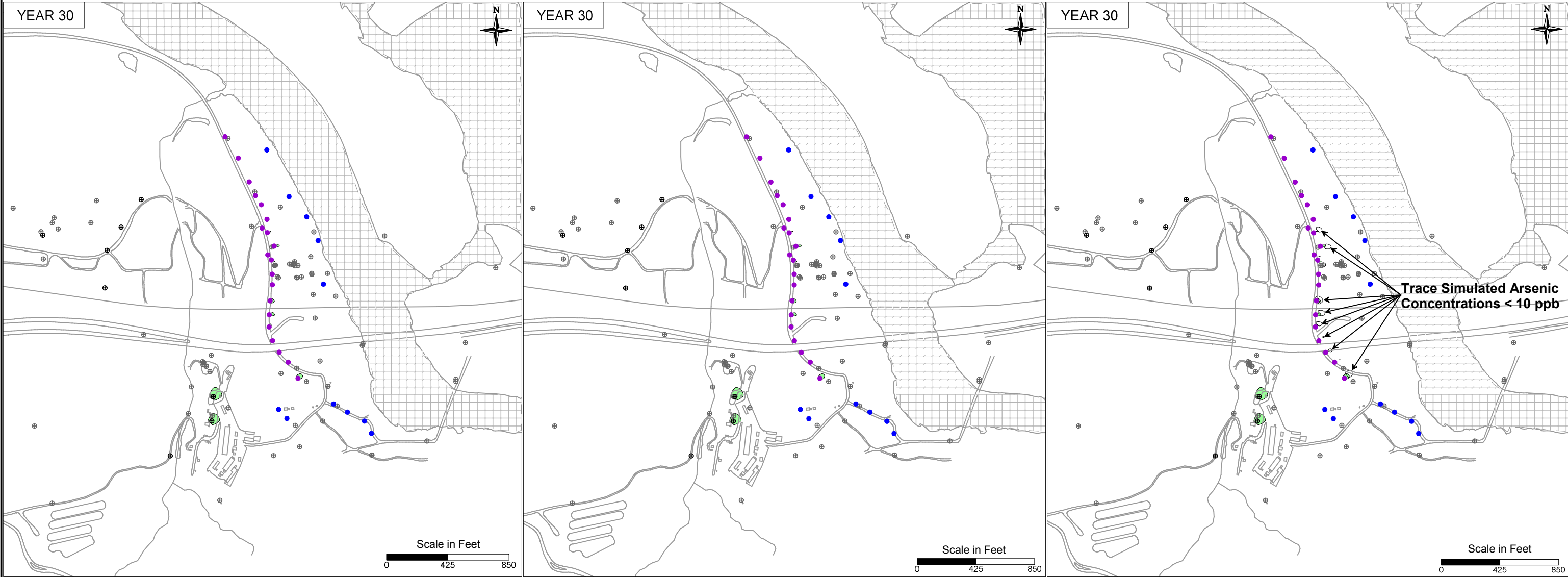


Carbon Concentration (ppm)



PG&E TOPOCK COMPRESSOR STATION NEEDLES, CALIFORNIA MODELING APPENDIX	
MANGANESE OXIDATION SENSITIVITY: SIMULATED MANGANESE TRANSPORT RESULTS FOR YEAR 30 IN MODEL LAYER 4	
	FIGURE 10.4-12





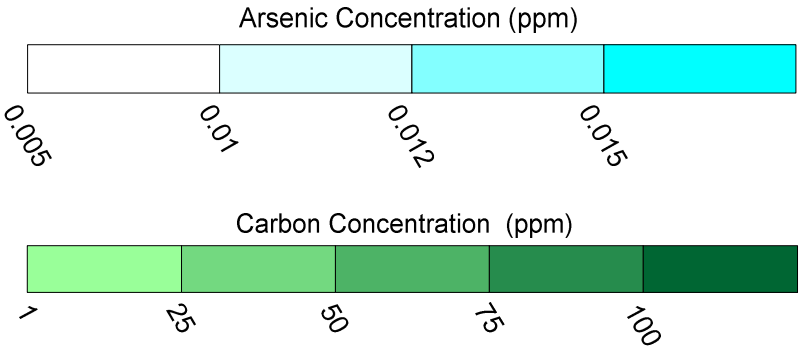
DECREASED STOICHIOMETRIC RATIO  
FOR GENERATION = 0.00005

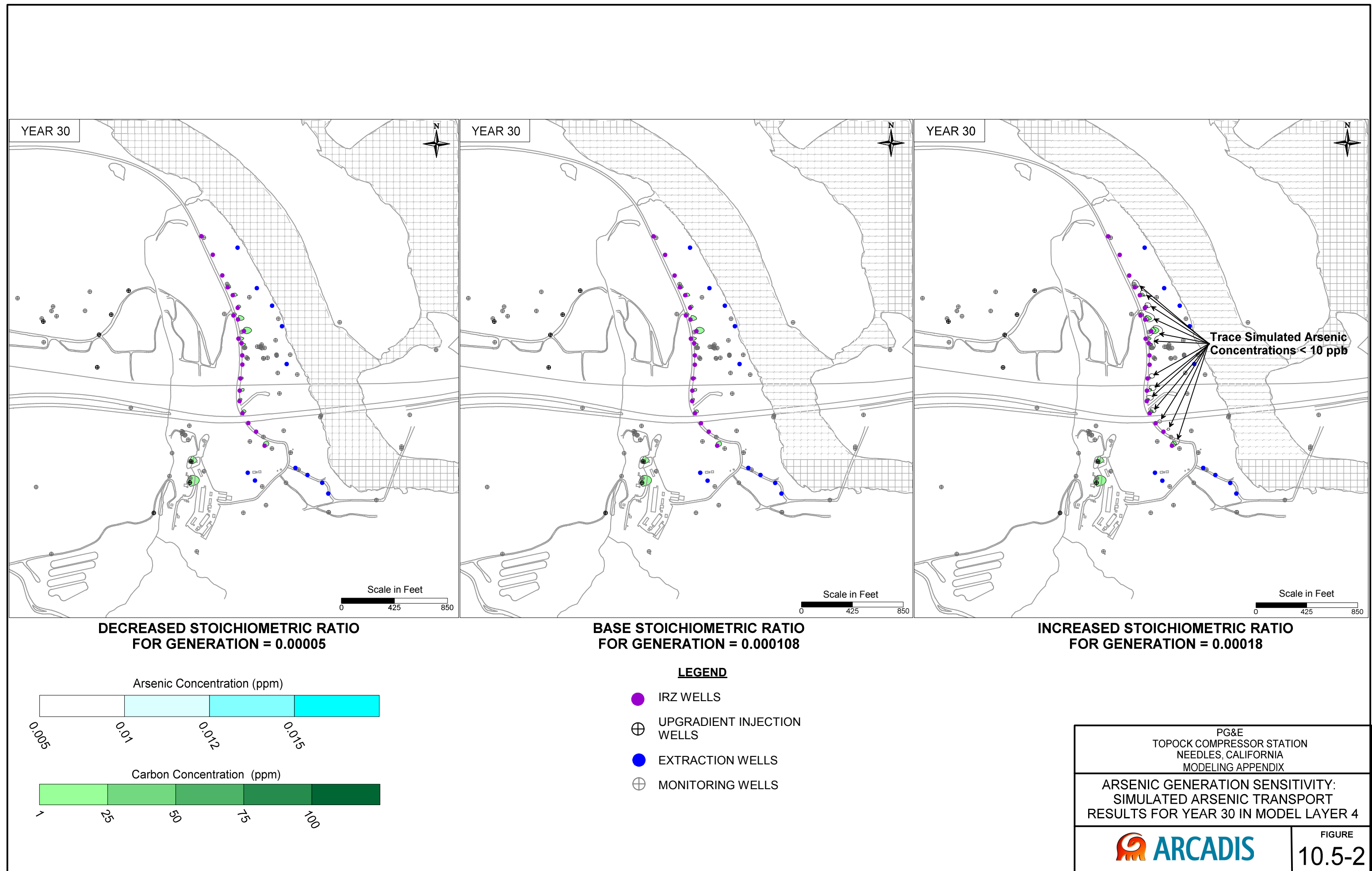
BASE STOICHIOMETRIC RATIO  
FOR GENERATION = 0.000108

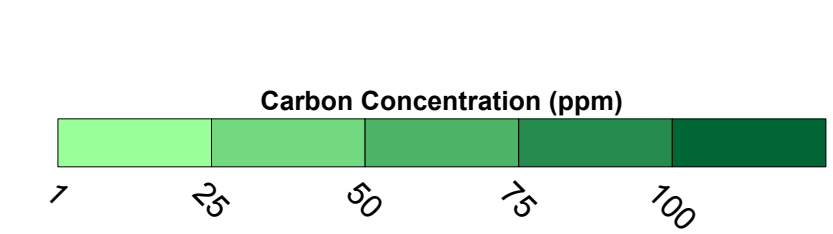
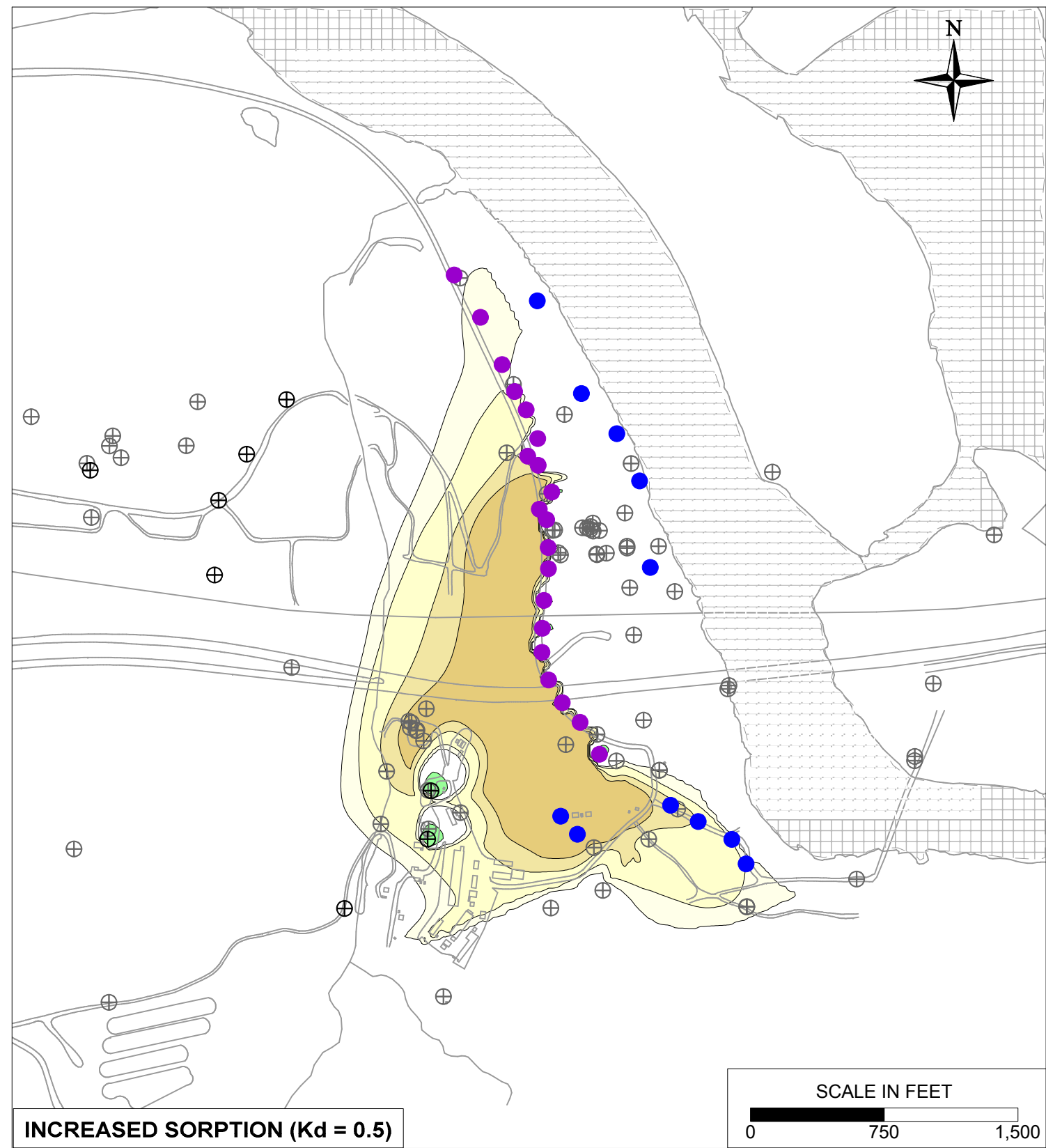
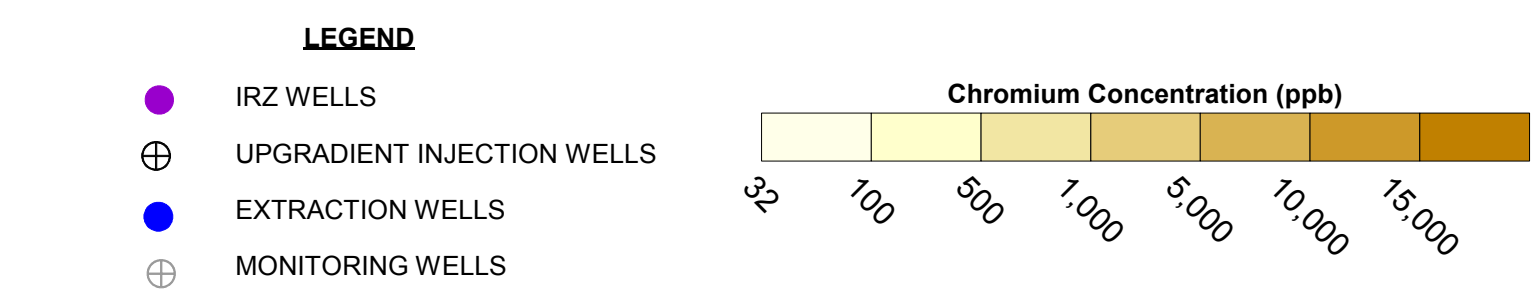
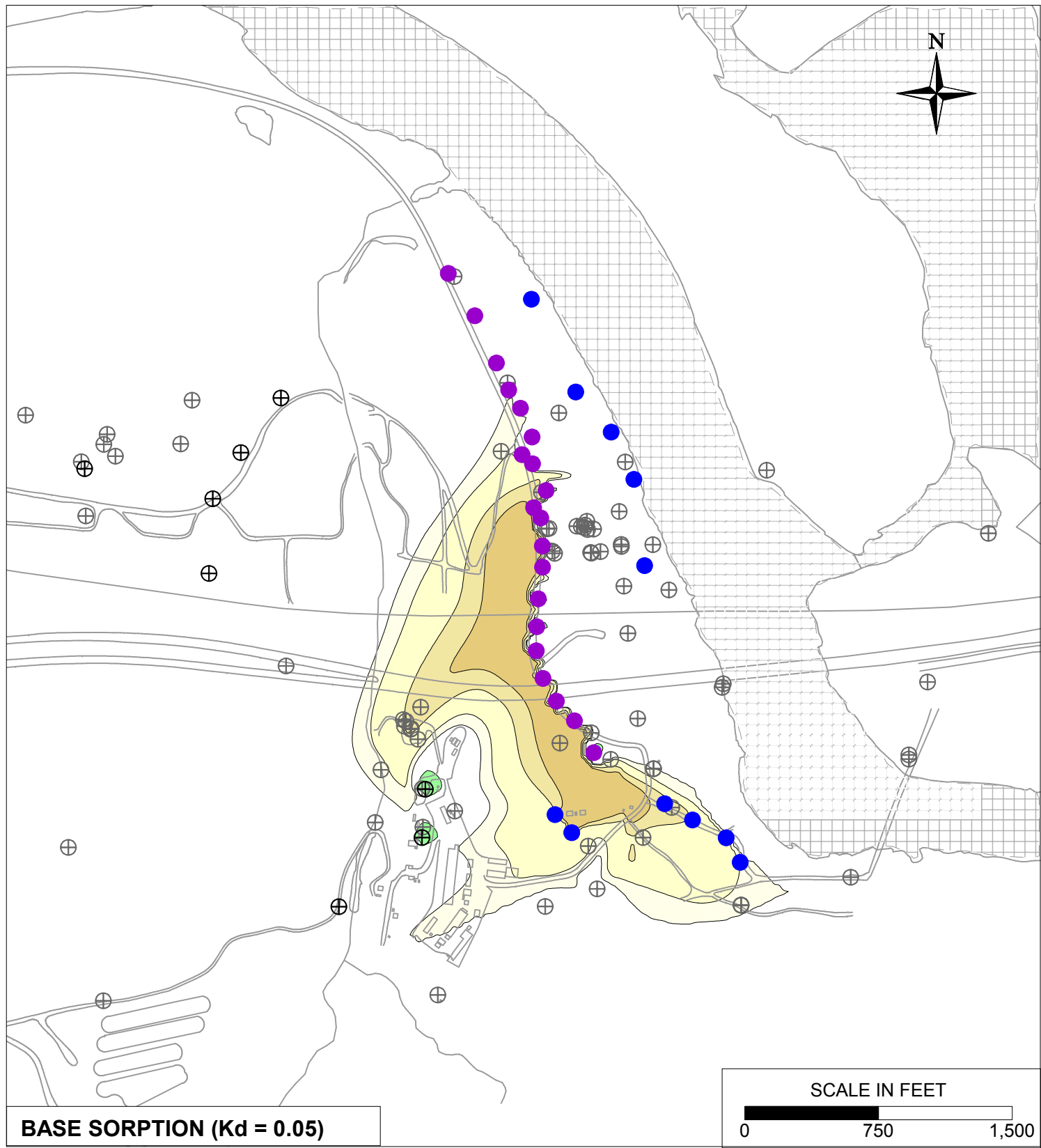
INCREASED STOICHIOMETRIC RATIO  
FOR GENERATION = 0.00018

**LEGEND**

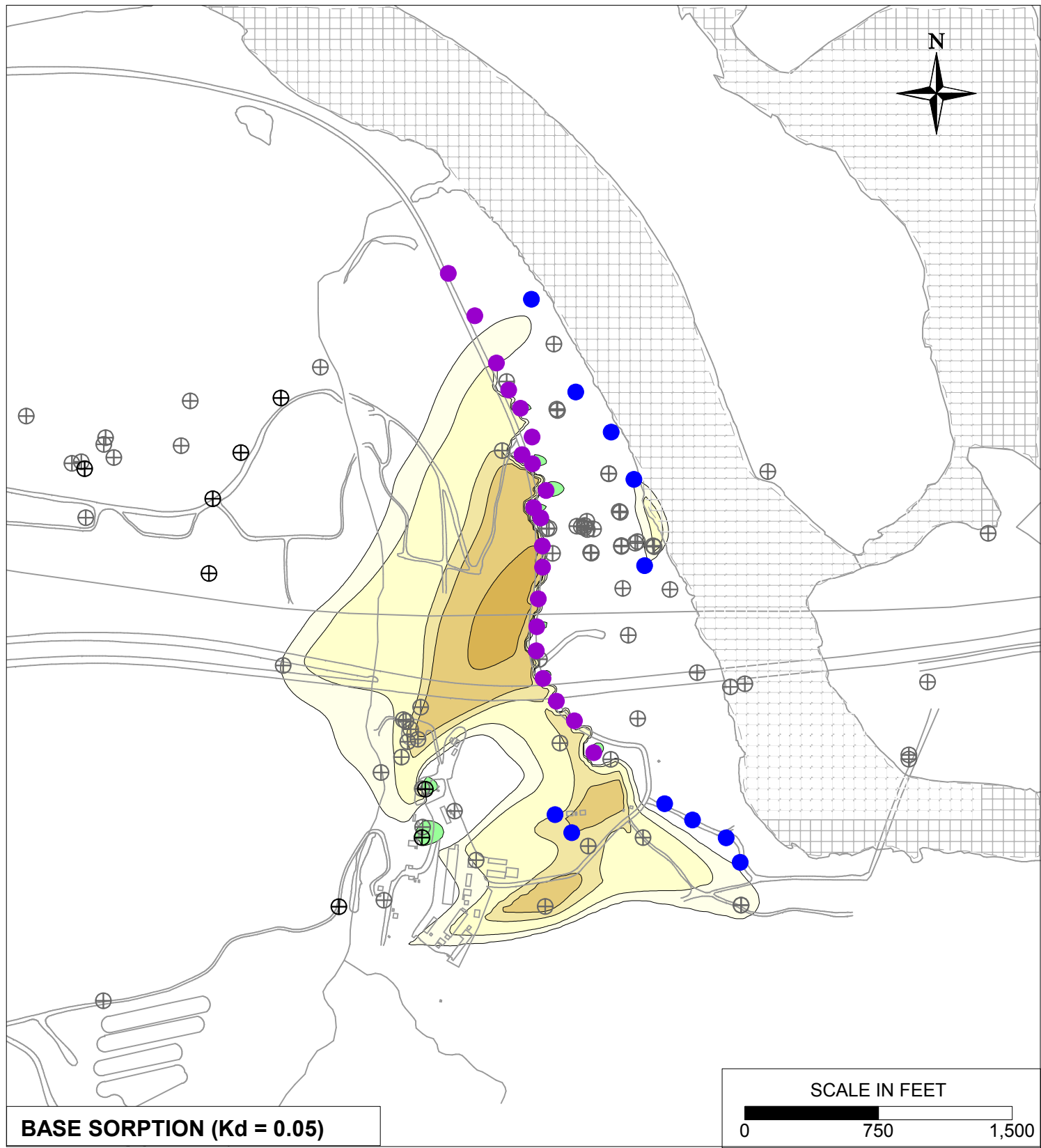
- IRZ WELLS
- UPGRADIENT INJECTION WELLS
- EXTRACTION WELLS
- MONITORING WELLS



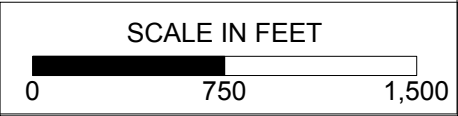






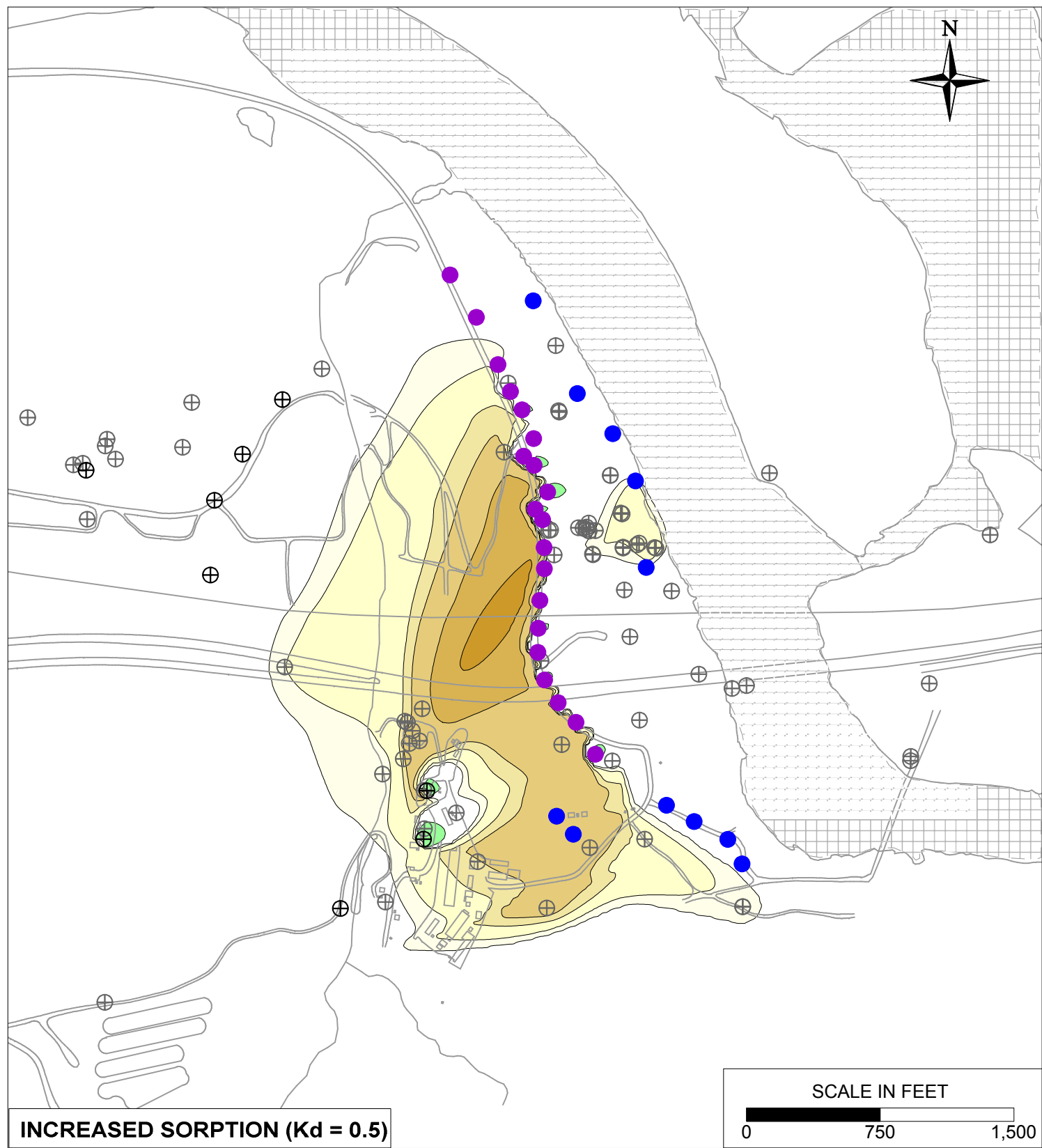
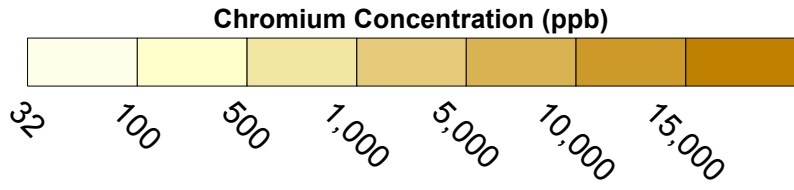


BASE SORPTION ( $K_d = 0.05$ )

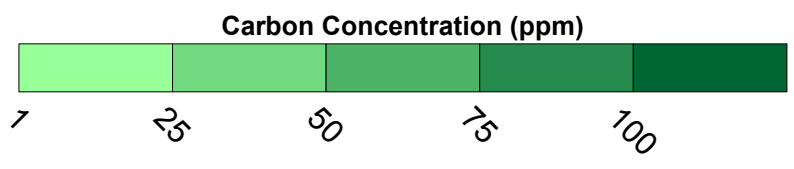
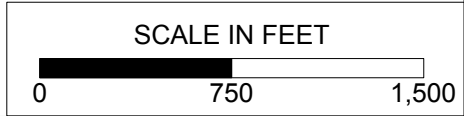


**LEGEND**

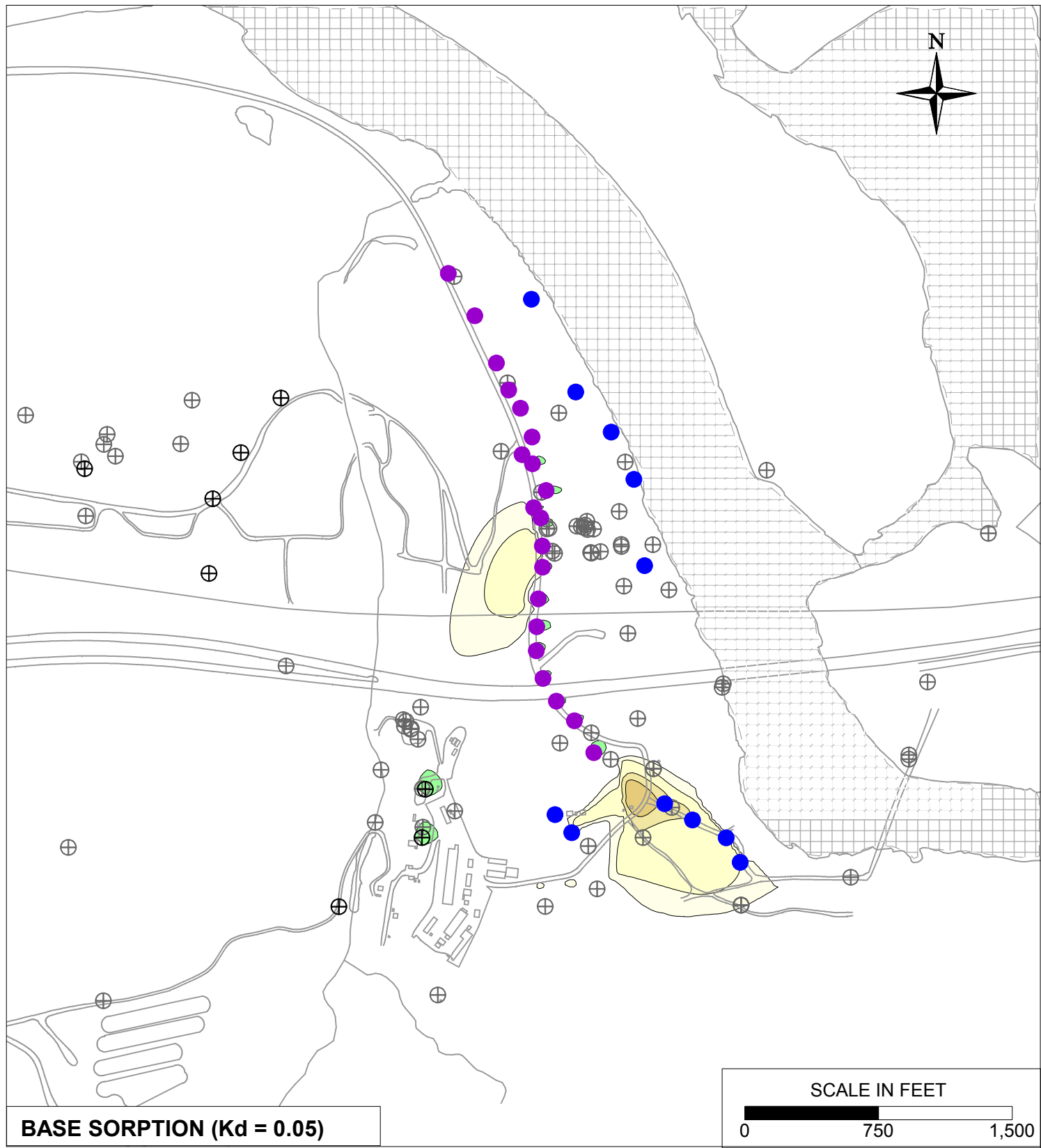
- IRZ WELLS
- ⊕ UPGRAIDENT INJECTION WELLS
- EXTRACTION WELLS
- ⊕ MONITORING WELLS



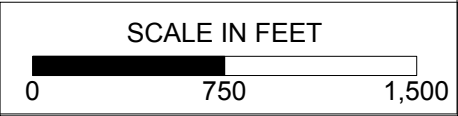
INCREASED SORPTION ( $K_d = 0.5$ )



PG&E TOPOCK COMPRESSOR STATION NEEDLES, CALIFORNIA MODELING APPENDIX	
HEXAVALENT CHROMIUM SORPTION SENSITIVITY: SIMULATED HEXAVALENT CHROMIUM TRANSPORT RESULTS FOR YEAR 10 IN MODEL LAYER 4	
	FIGURE 10.6-2

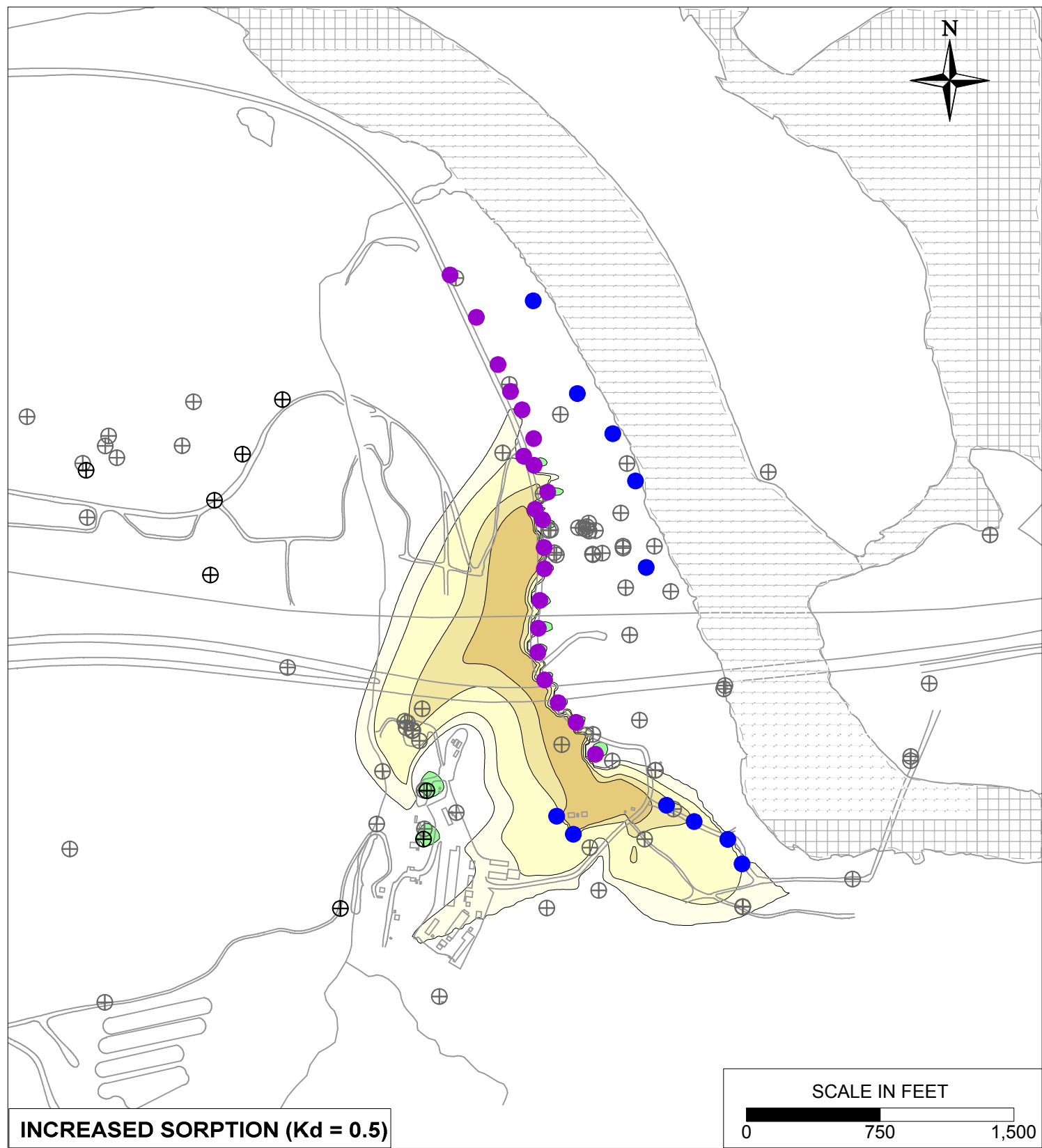
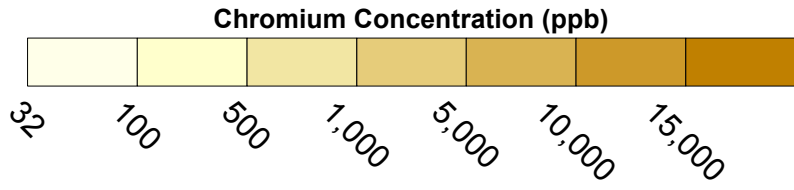


BASE SORPTION ( $K_d = 0.05$ )

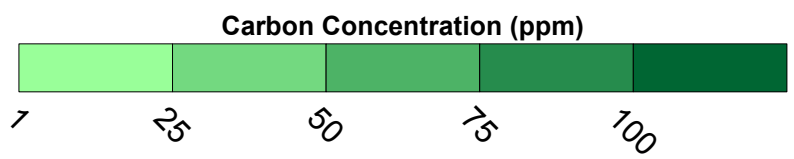
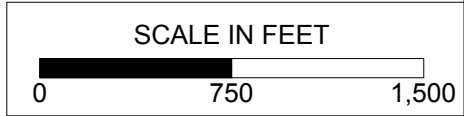


**LEGEND**

- IRZ WELLS
- UPGRADIENT INJECTION WELLS
- EXTRACTION WELLS
- MONITORING WELLS



INCREASED SORPTION ( $K_d = 0.5$ )

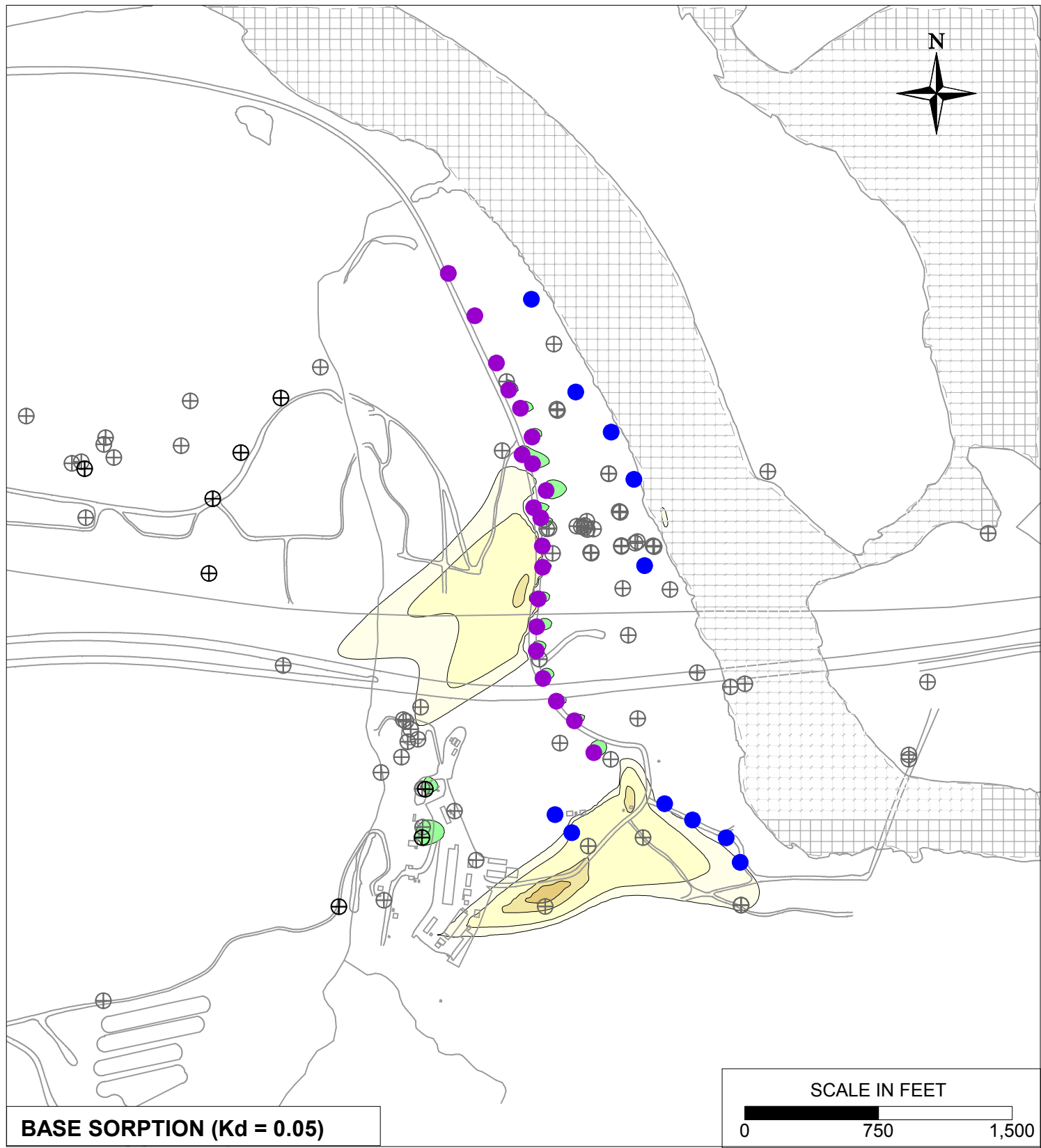


PG&E  
TOPOCK COMPRESSOR STATION  
NEEDLES, CALIFORNIA  
MODELING APPENDIX

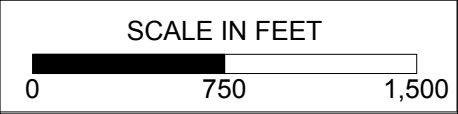
HEXAVALENT CHROMIUM SORPTION SENSITIVITY:  
SIMULATED HEXAVALENT CHROMIUM TRANSPORT  
RESULTS FOR YEAR 30 IN MODEL LAYER 2

FIGURE  
10.6-3



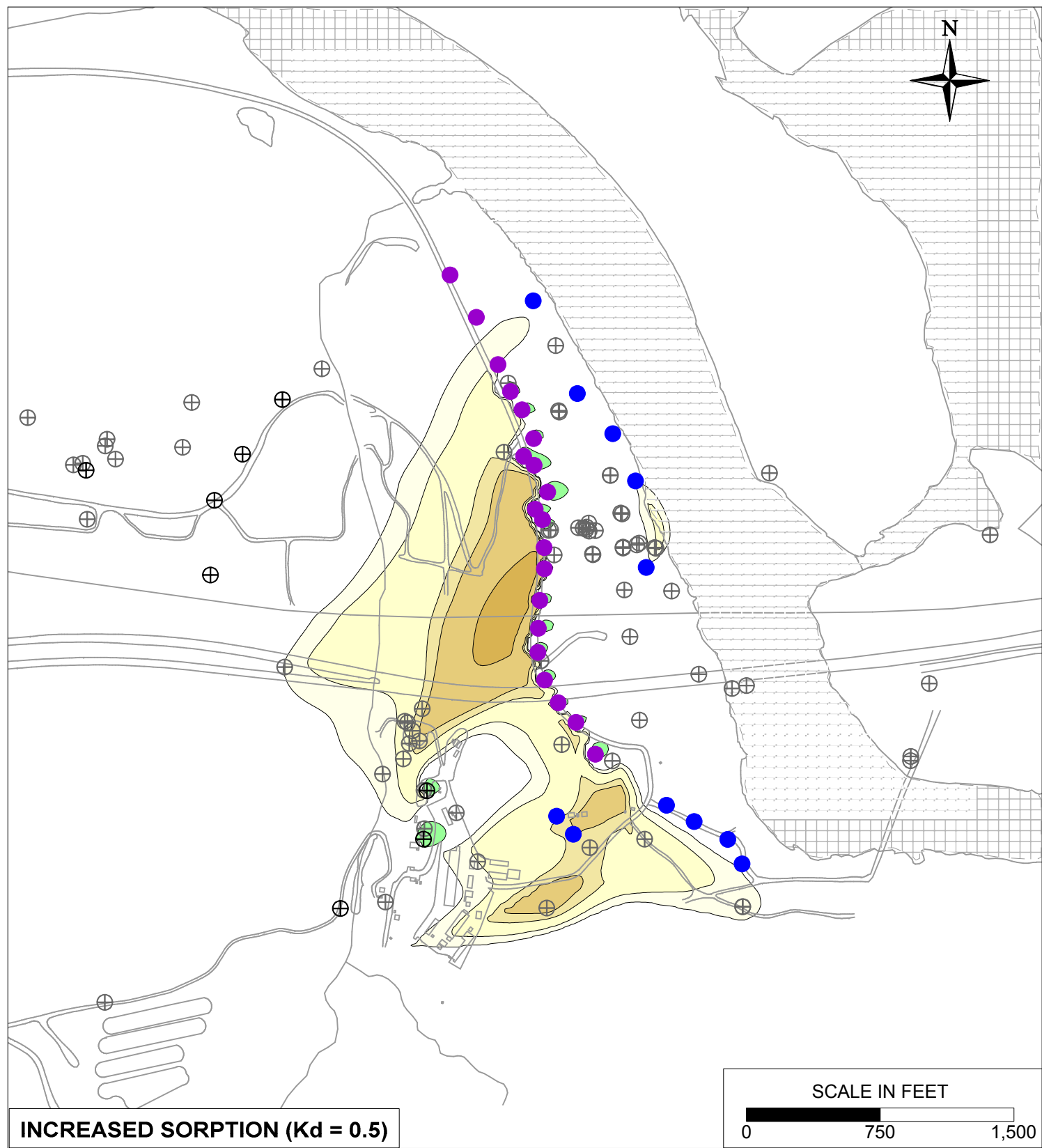
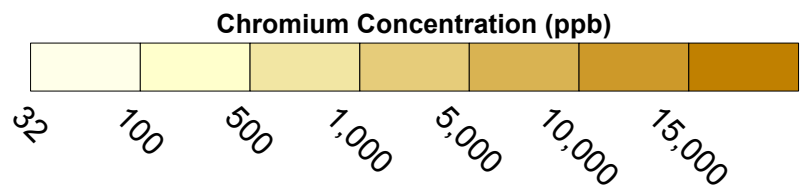


BASE SORPTION ( $K_d = 0.05$ )

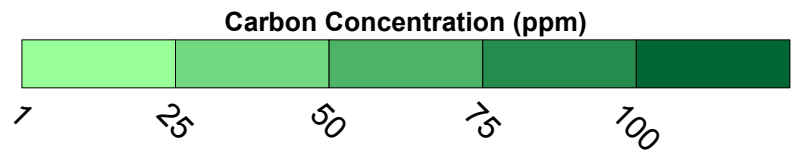
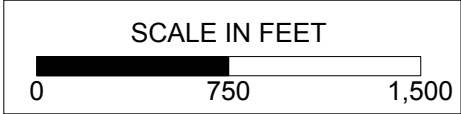


**LEGEND**

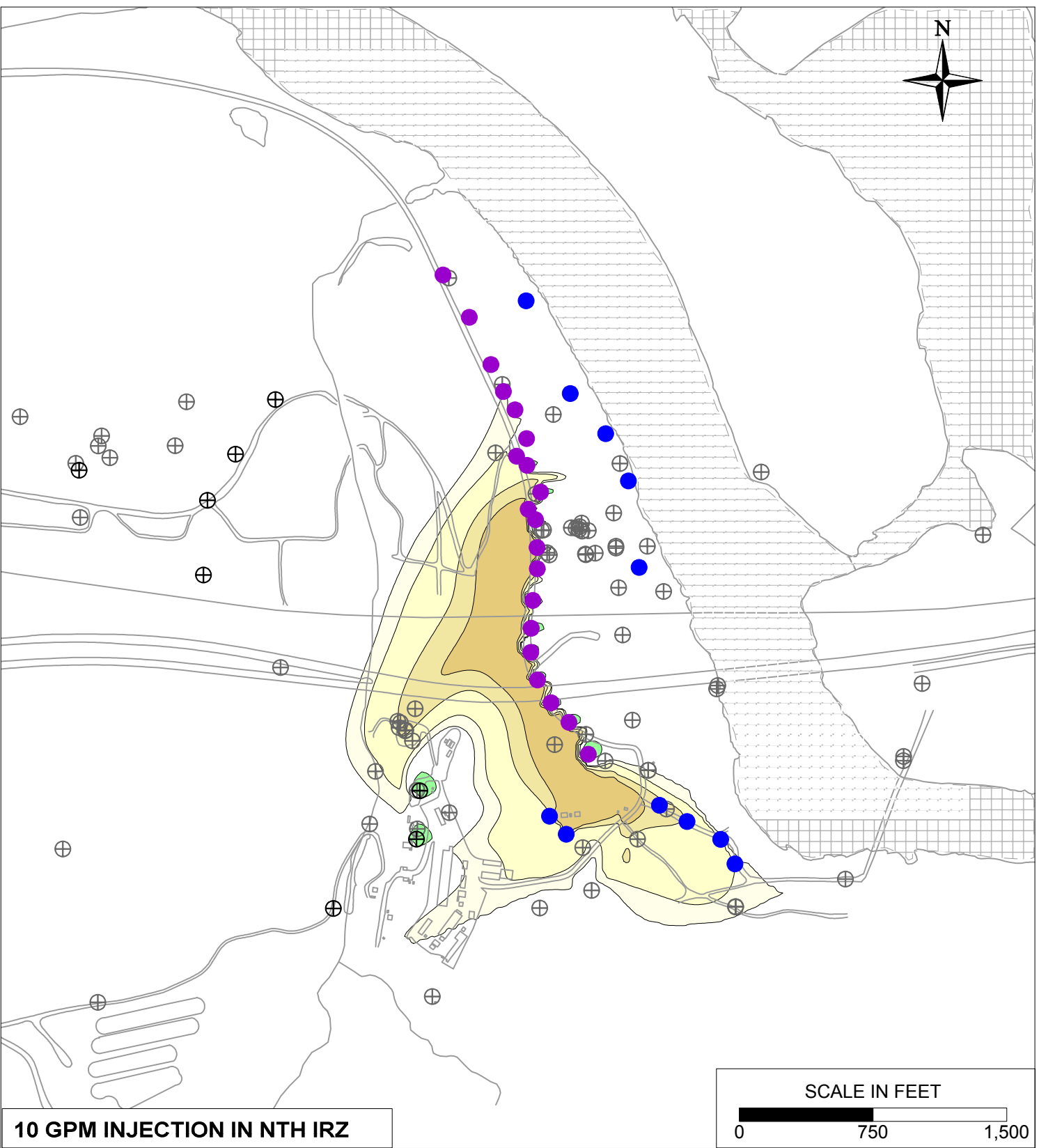
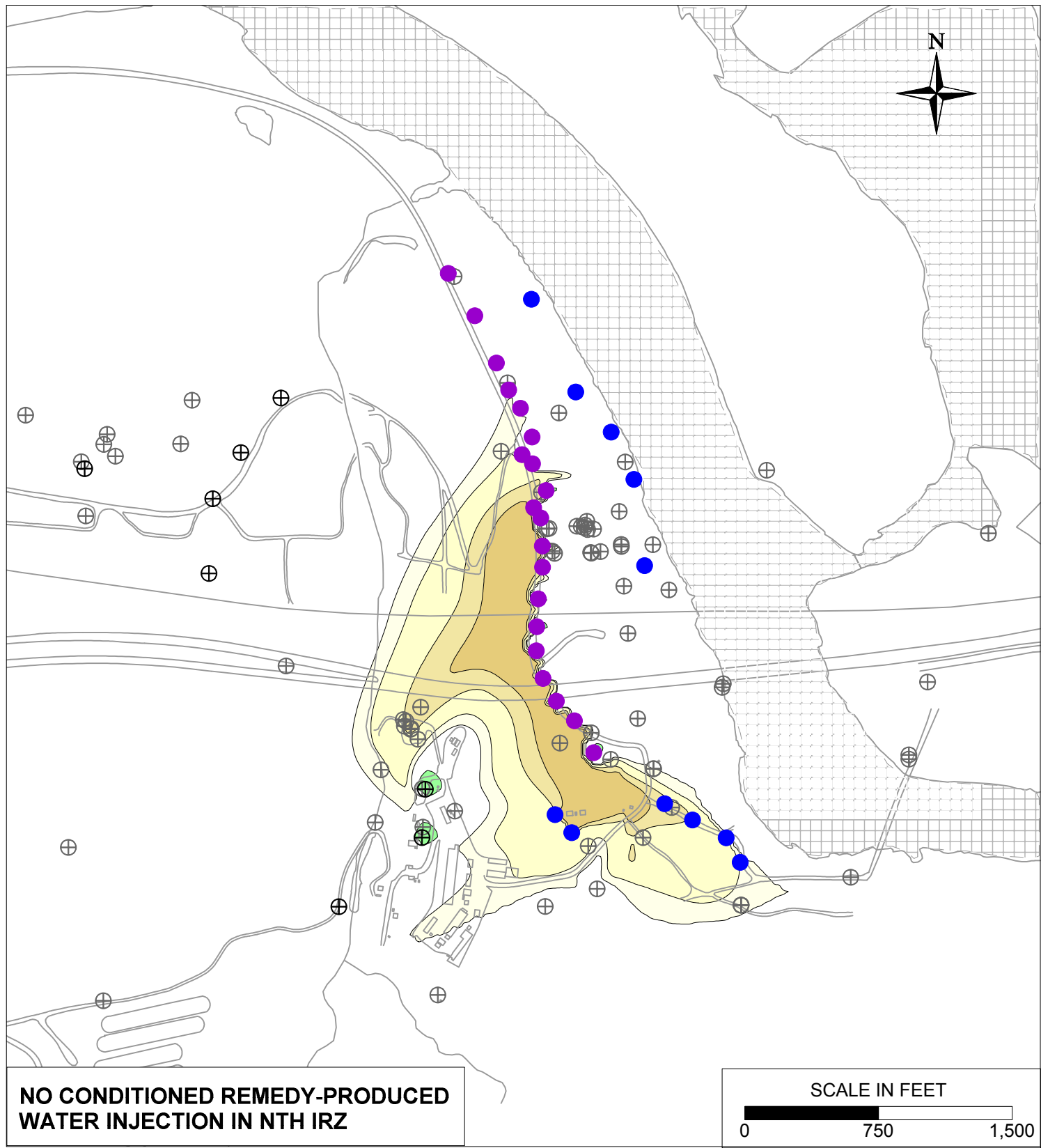
- IRZ WELLS
- ⊕ UPGRADIENT INJECTION WELLS
- EXTRACTION WELLS
- ⊕ MONITORING WELLS



INCREASED SORPTION ( $K_d = 0.5$ )

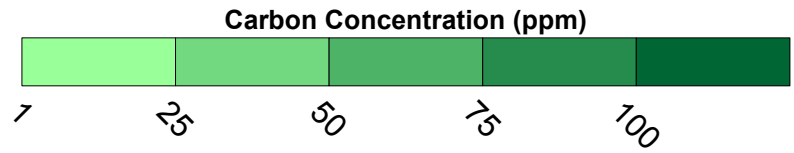
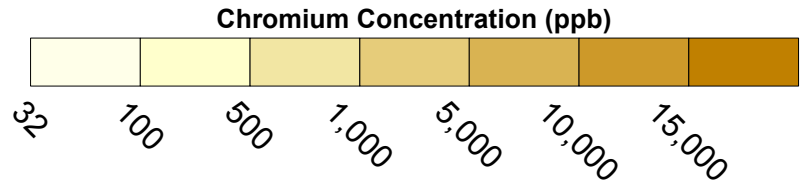


PG&E TOPOCK COMPRESSOR STATION NEEDLES, CALIFORNIA MODELING APPENDIX	
HEXAVALENT CHROMIUM SORPTION SENSITIVITY: SIMULATED HEXAVALENT CHROMIUM TRANSPORT RESULTS FOR YEAR 30 IN MODEL LAYER 4	
	FIGURE 10.6-4



**LEGEND**

- IRZ WELLS
- ⊕ UPGRADIENT INJECTION WELLS
- EXTRACTION WELLS
- ⊕ MONITORING WELLS



PG&E  
TOPOCK COMPRESSOR STATION  
NEEDLES, CALIFORNIA  
MODELING APPENDIX

ADDITION OF CONDITIONED REMEDY-PRODUCED WATER TO NTH IRZ SENSITIVITY: SIMULATED HEXAVALENT CHROMIUM TRANSPORT RESULTS FOR YEAR10 IN MODEL LAYER 2


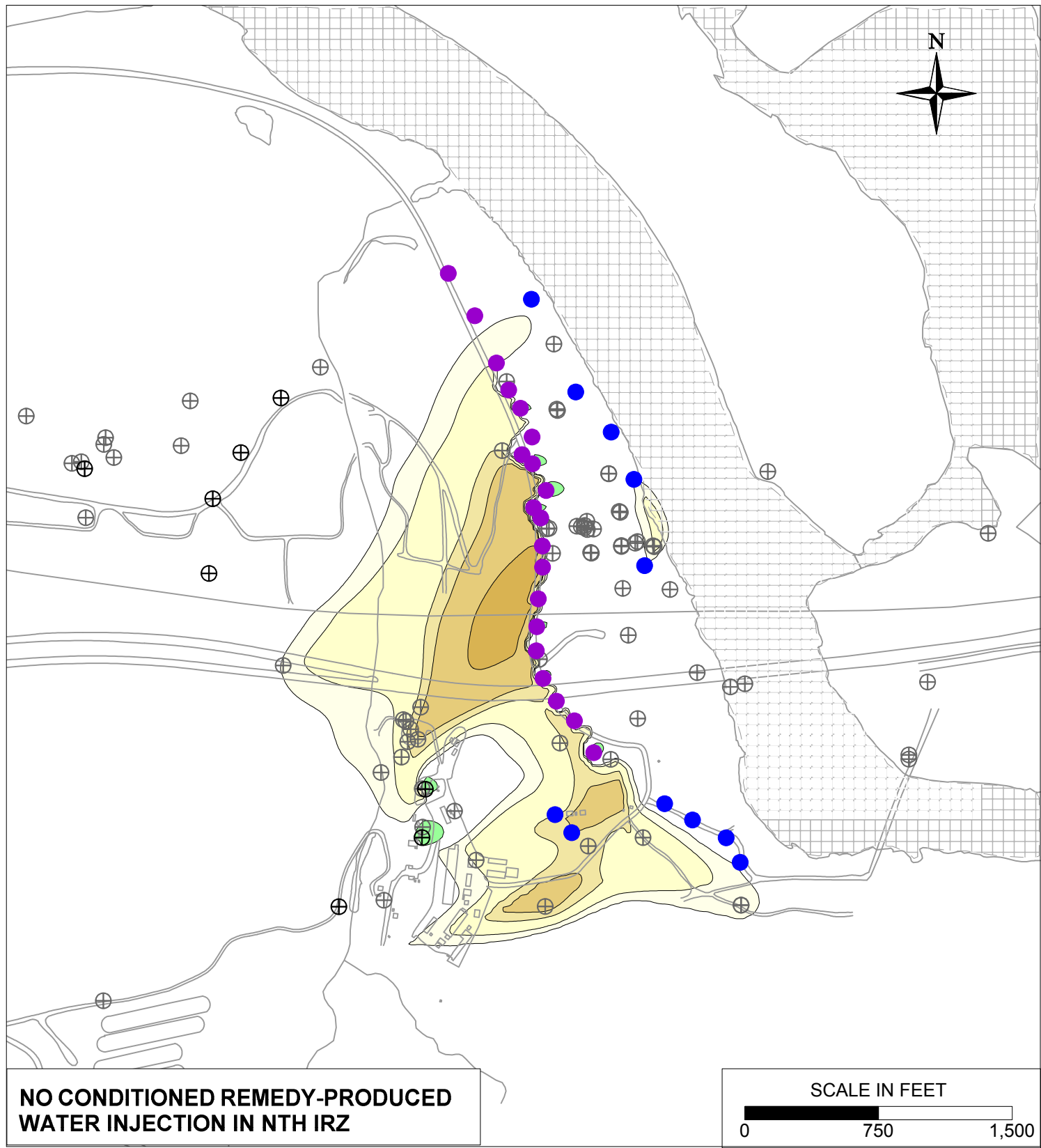
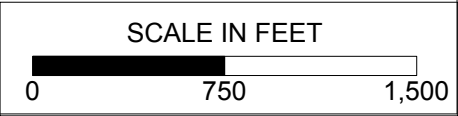
 **ARCADIS**

FIGURE  
**10.7-1**

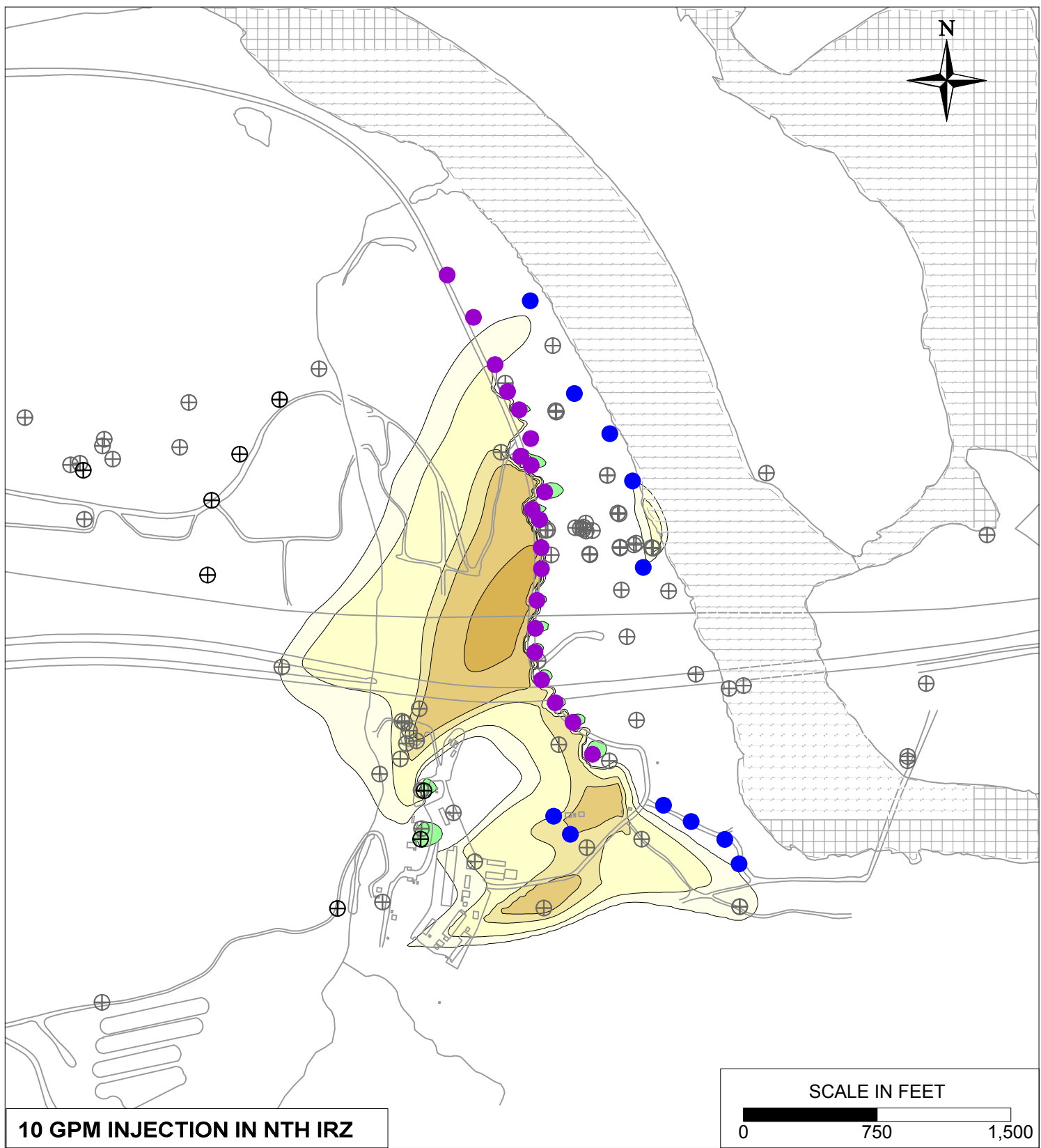
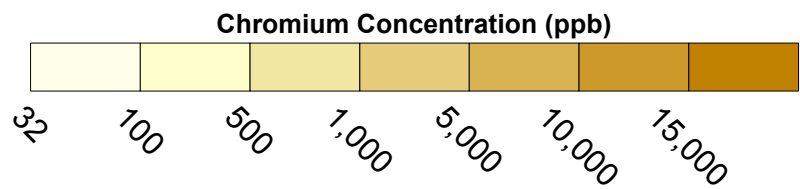


**NO CONDITIONED REMEDY-PRODUCED  
WATER INJECTION IN NTH IRZ**

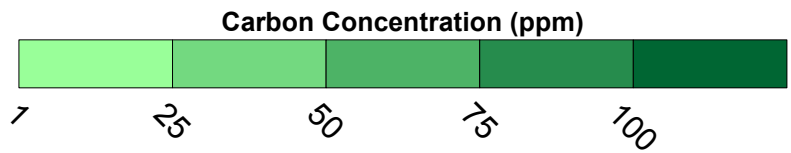
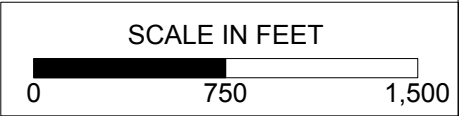


**LEGEND**

- IRZ WELLS
- ⊕ UPGRADIENT INJECTION WELLS
- EXTRACTION WELLS
- ⊕ MONITORING WELLS

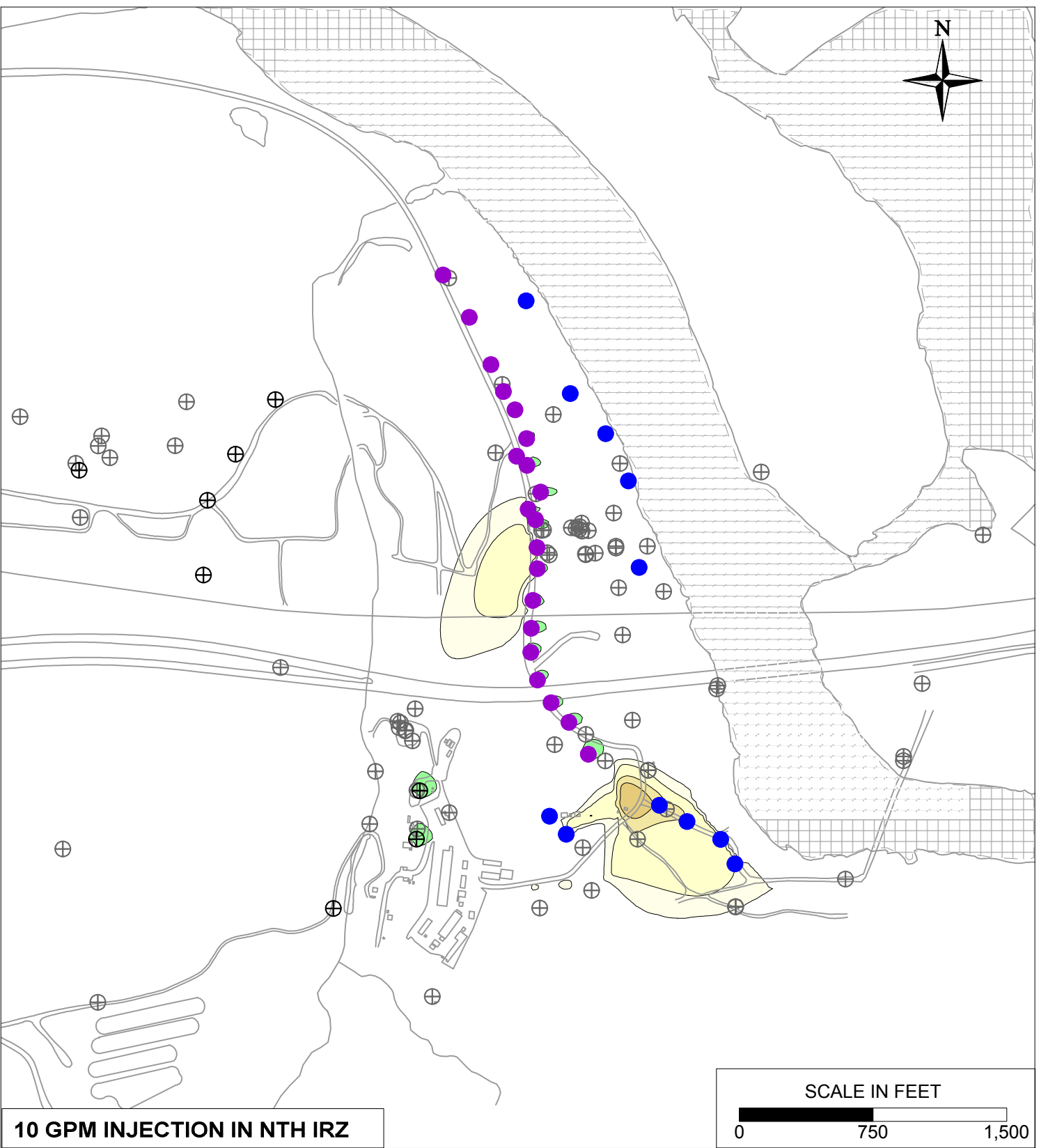
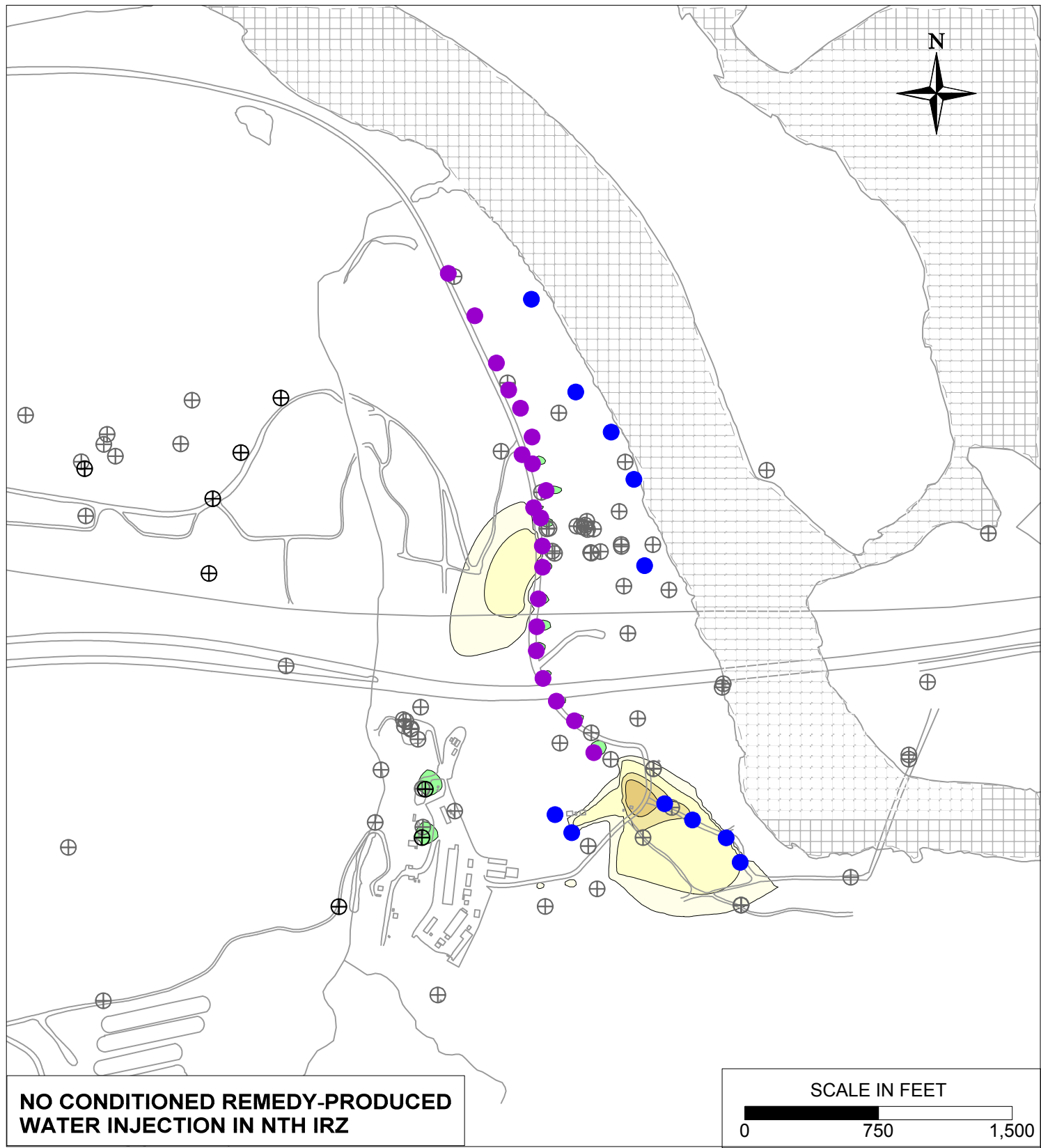


**10 GPM INJECTION IN NTH IRZ**



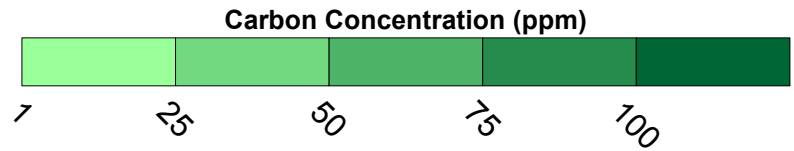
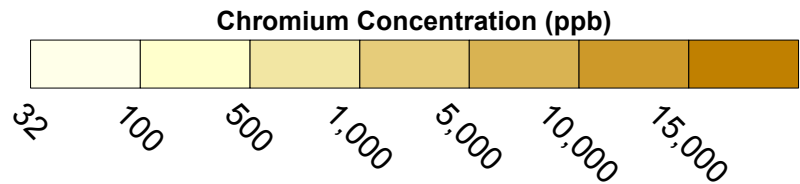
PG&E TOPOCK COMPRESSOR STATION NEEDLES, CALIFORNIA MODELING APPENDIX	
ADDITION OF CONDITIONED REMEDY-PRODUCED WATER TO NTH IRZ SENSITIVITY: SIMULATED HEXAVALENT CHROMIUM TRANSPORT RESULTS FOR YEAR 10 IN MODEL LAYER 4	
	FIGURE <b>10.7-2</b>





**LEGEND**

- IRZ WELLS
- UPGRADIENT INJECTION WELLS
- EXTRACTION WELLS
- MONITORING WELLS

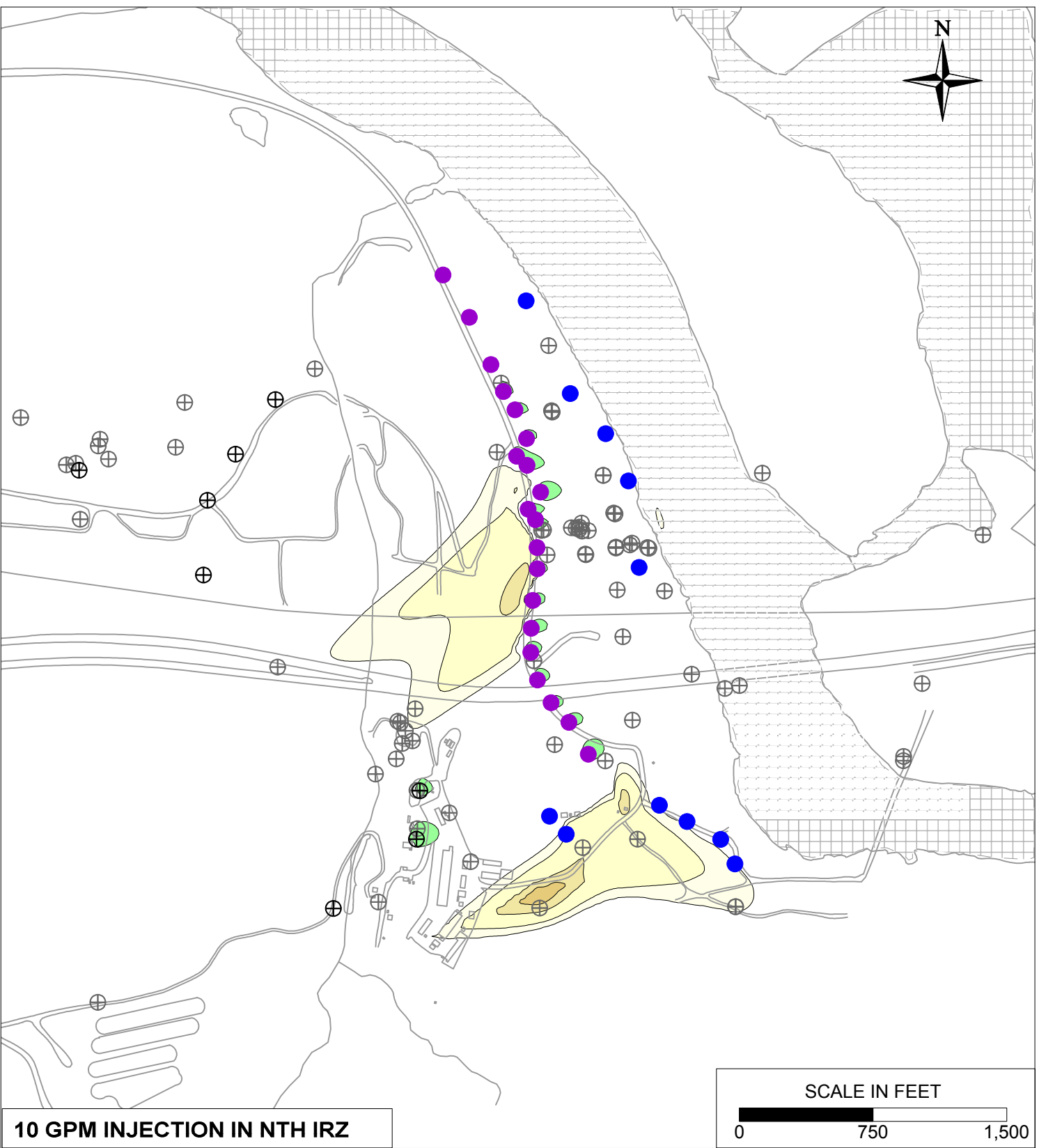
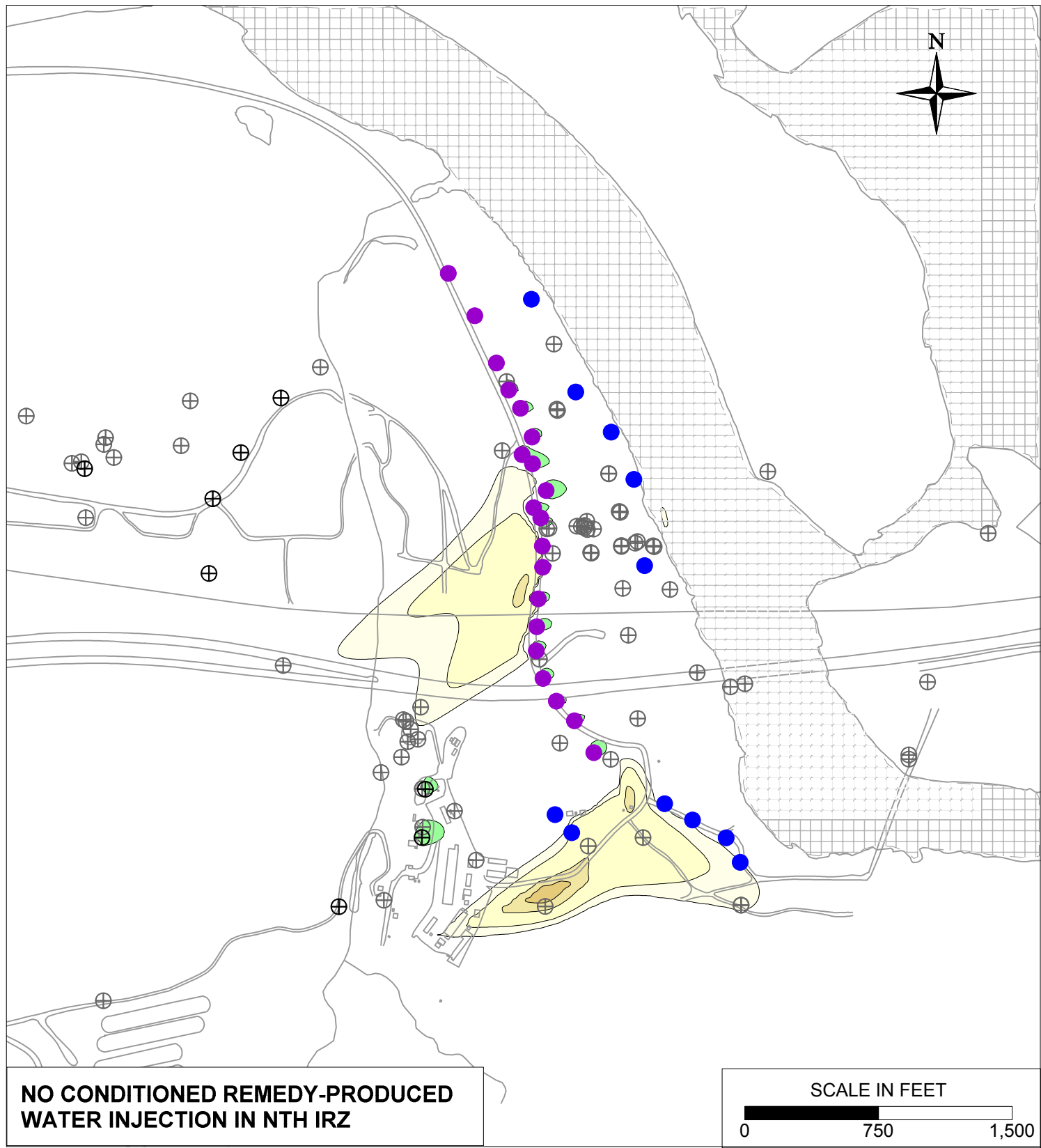


PG&E  
TOPOCK COMPRESSOR STATION  
NEEDLES, CALIFORNIA  
MODELING APPENDIX

ADDITION OF CONDITIONED REMEDY-PRODUCED WATER TO NTH IRZ SENSITIVITY: SIMULATED HEXAVALENT CHROMIUM TRANSPORT RESULTS FOR YEAR 30 IN MODEL LAYER 2

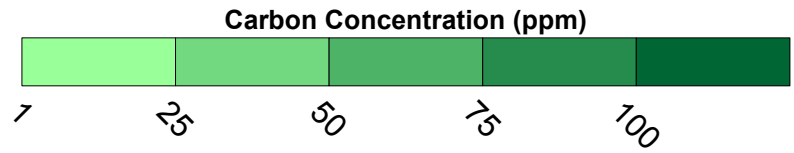
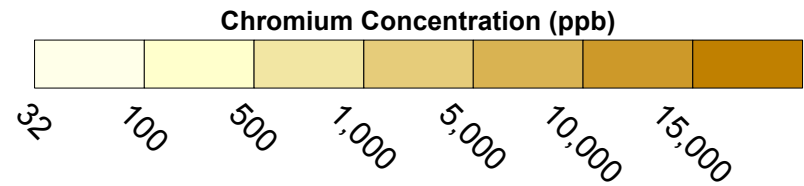
**ARCADIS**

FIGURE  
**10.7-3**



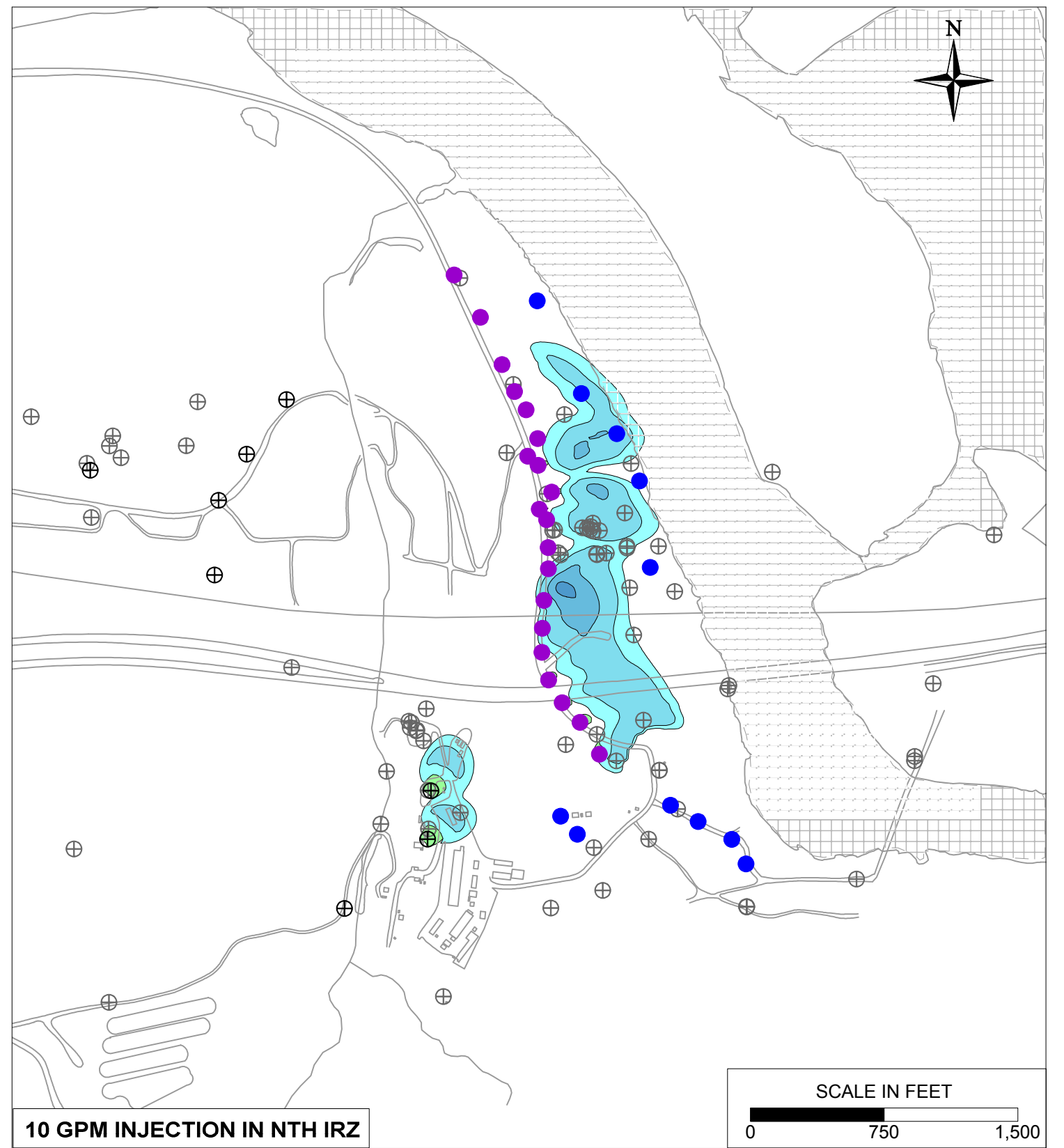
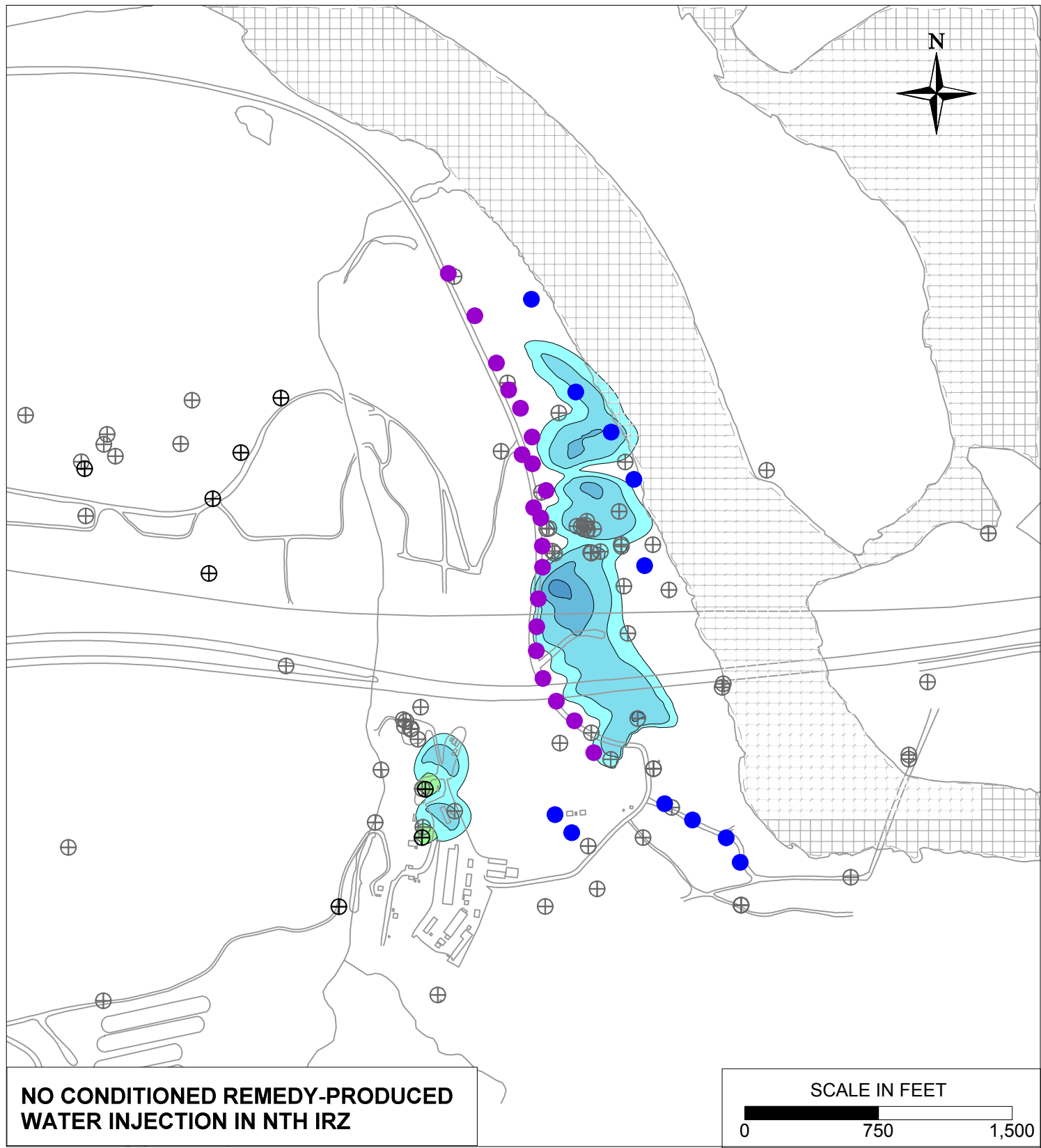
**LEGEND**

- IRZ WELLS
- ⊕ UPGRADIENT INJECTION WELLS
- EXTRACTION WELLS
- ⊕ MONITORING WELLS



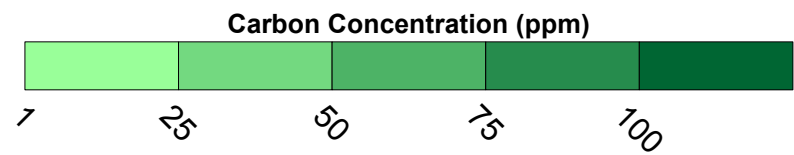
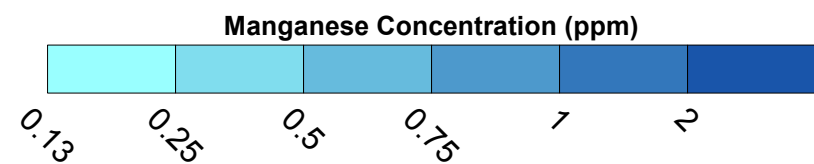
PG&E TOPOCK COMPRESSOR STATION NEEDLES, CALIFORNIA MODELING APPENDIX	
ADDITION OF CONDITIONED REMEDY-PRODUCED WATER TO NTH IRZ SENSITIVITY: SIMULATED HEXAVALENT CHROMIUM TRANSPORT RESULTS FOR YEAR 30 IN MODEL LAYER 4	
	FIGURE <b>10.7-4</b>

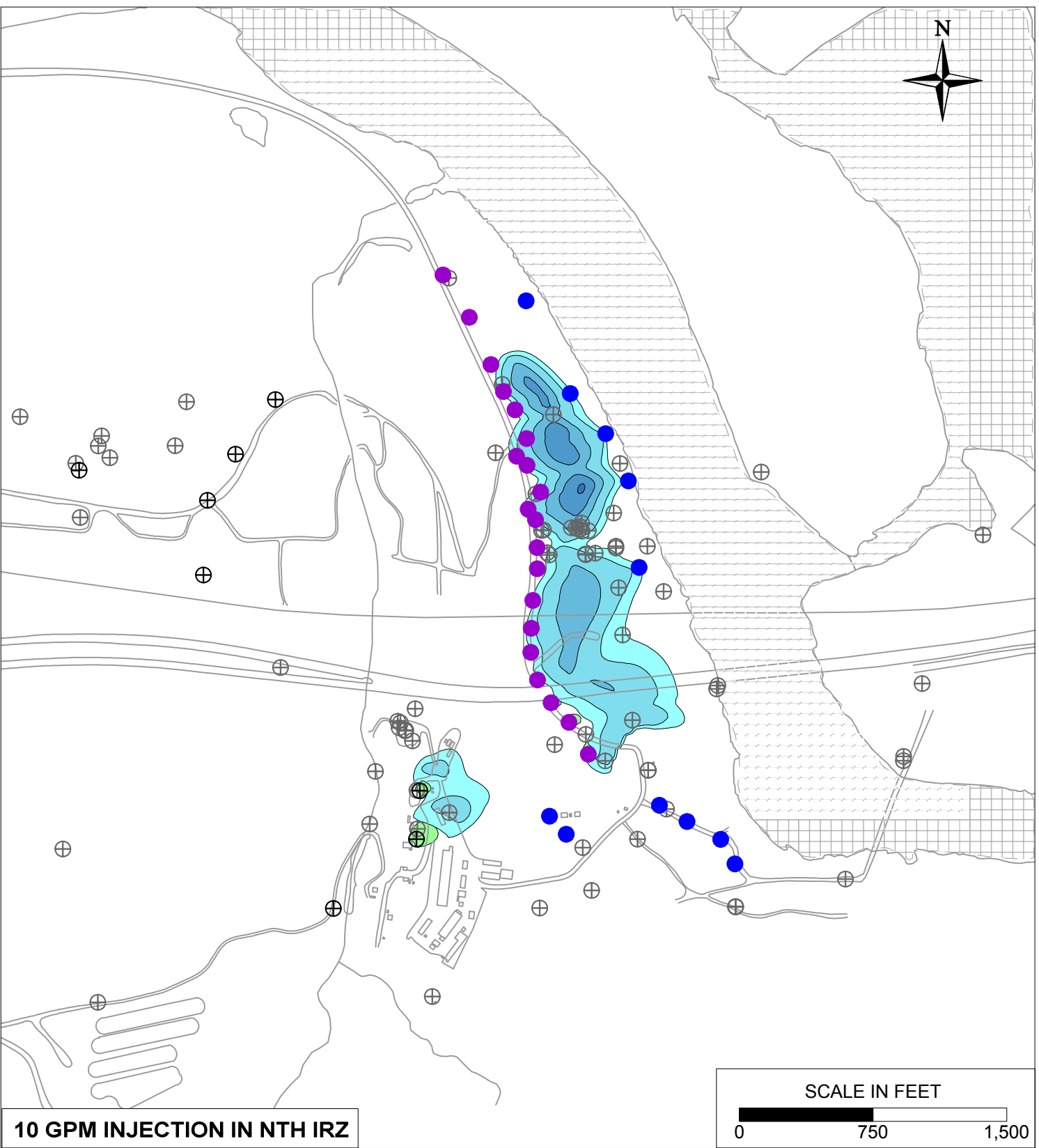
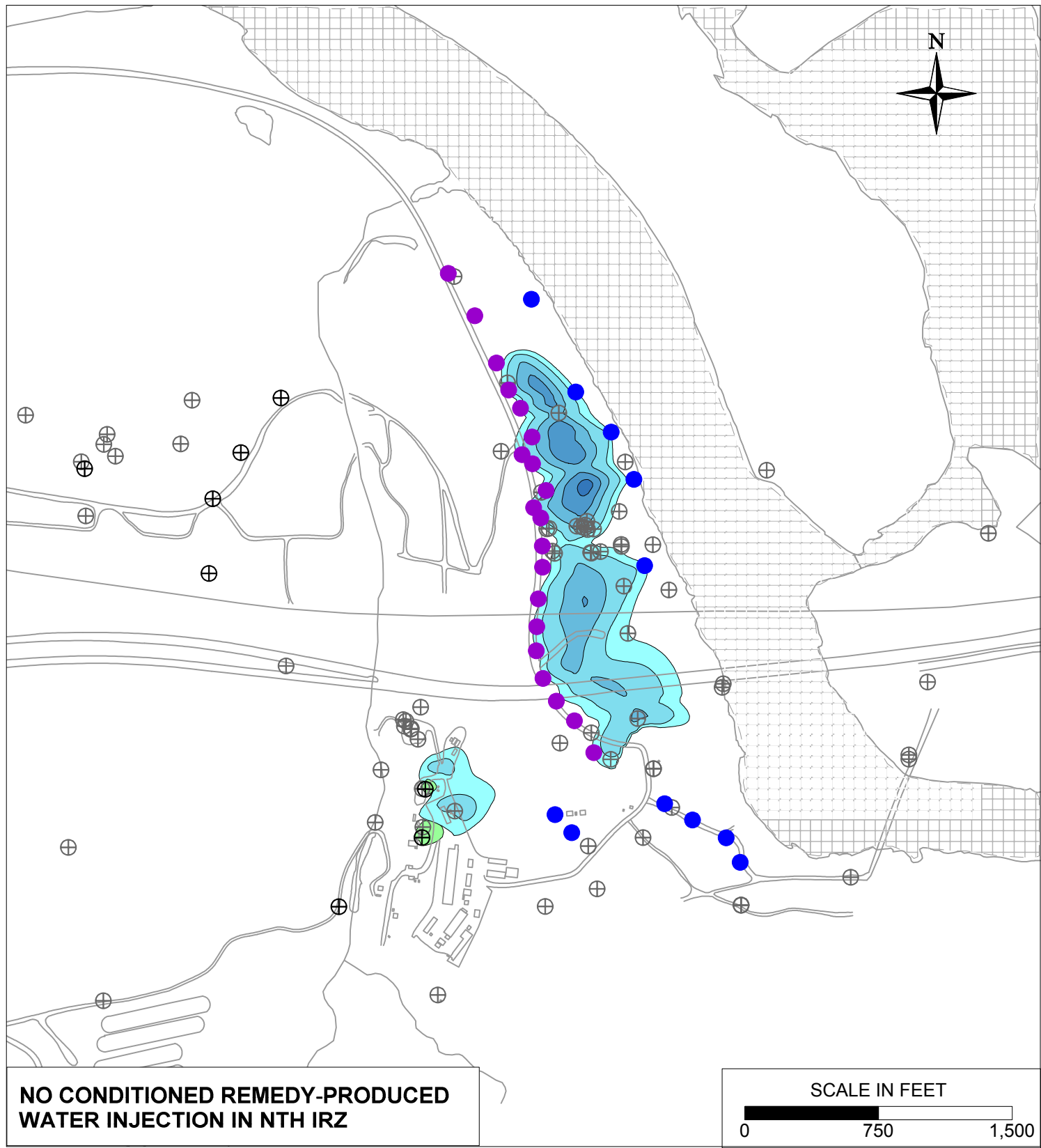




**LEGEND**

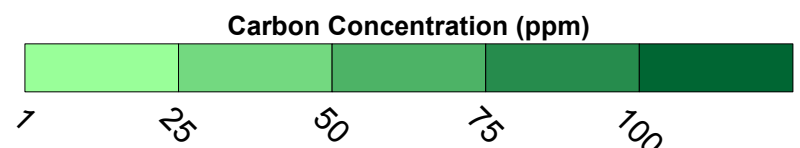
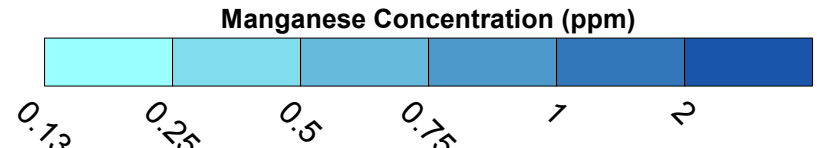
- IRZ WELLS
- ⊕ UPGRADIENT INJECTION WELLS
- EXTRACTION WELLS
- ⊕ MONITORING WELLS



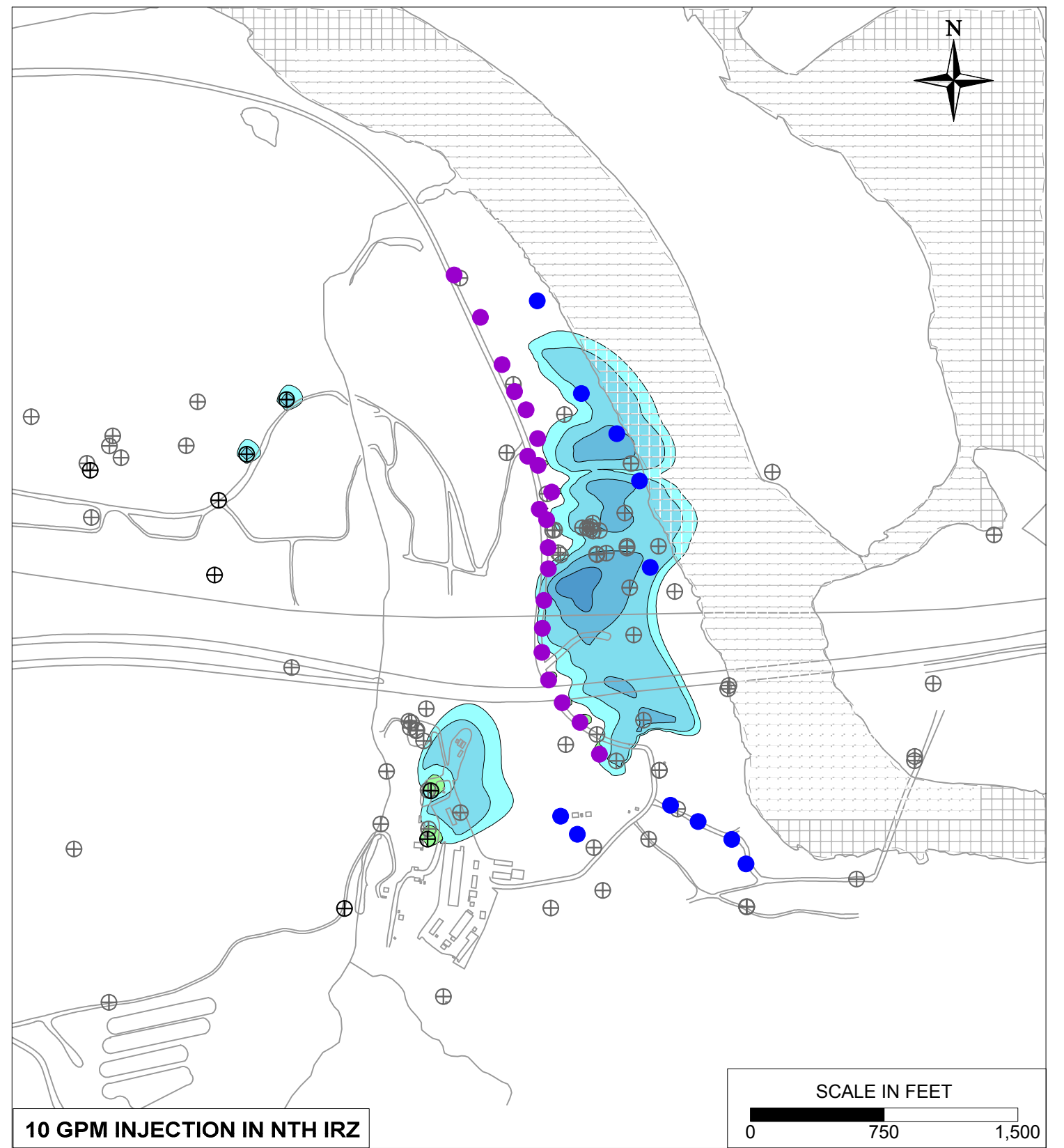
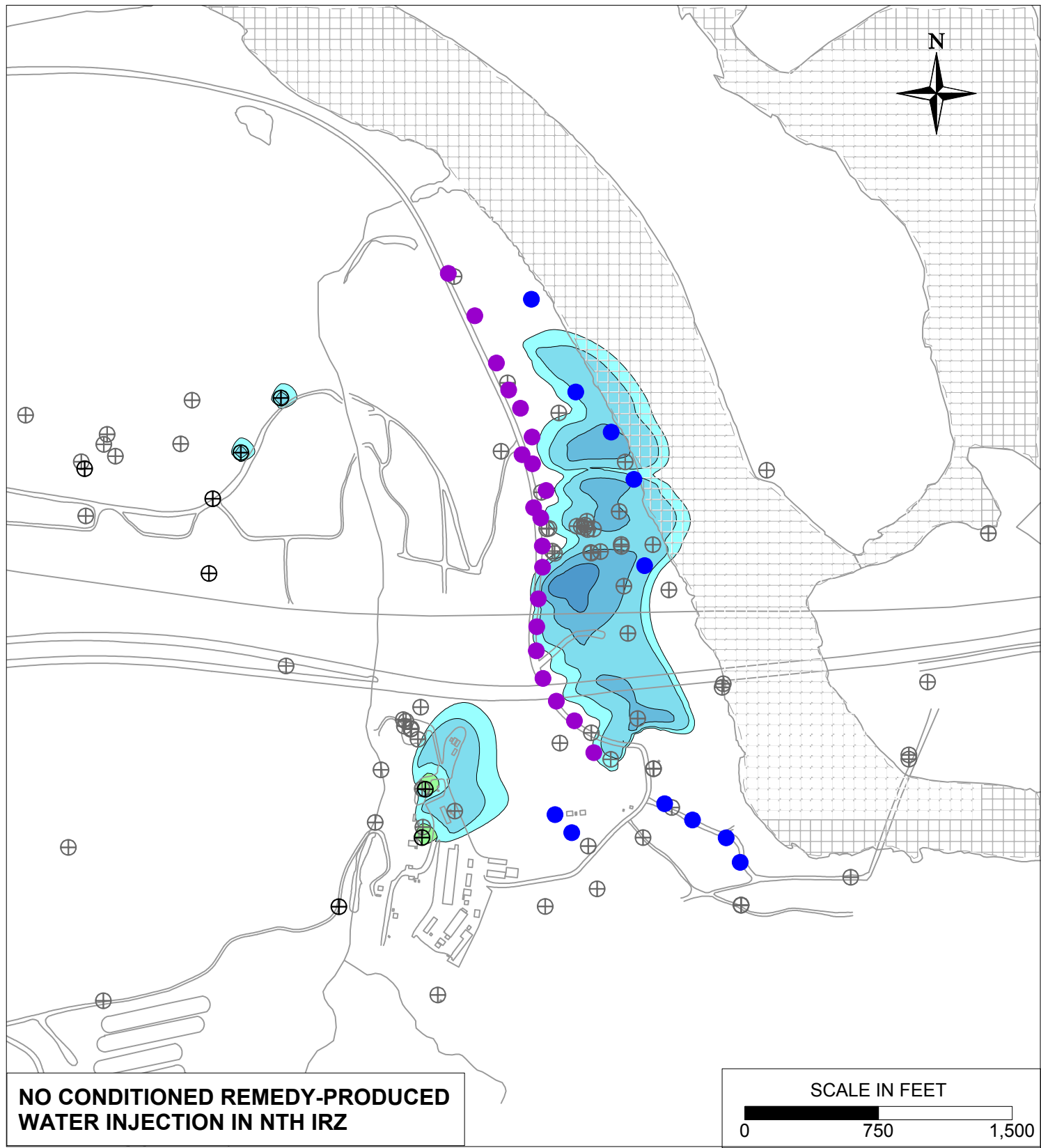


**LEGEND**

- IRZ WELLS
- ⊕ UPGRADIENT INJECTION WELLS
- EXTRACTION WELLS
- ⊕ MONITORING WELLS

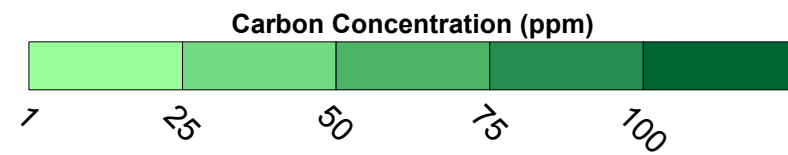
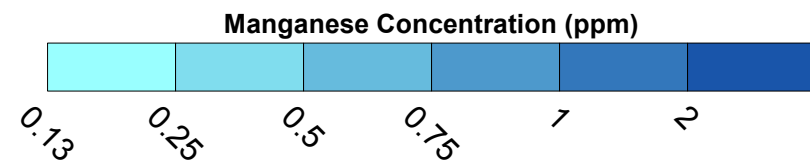


PG&E TOPOCK COMPRESSOR STATION NEEDLES, CALIFORNIA MODELING APPENDIX	
ADDITION OF CONDITIONED REMEDY-PRODUCED WATER TO NTH IRZ SENSITIVITY: SIMULATED MANGANESE TRANSPORT RESULTS FOR YEAR 10 IN MODEL LAYER 4	
	FIGURE <b>10.7-6</b>

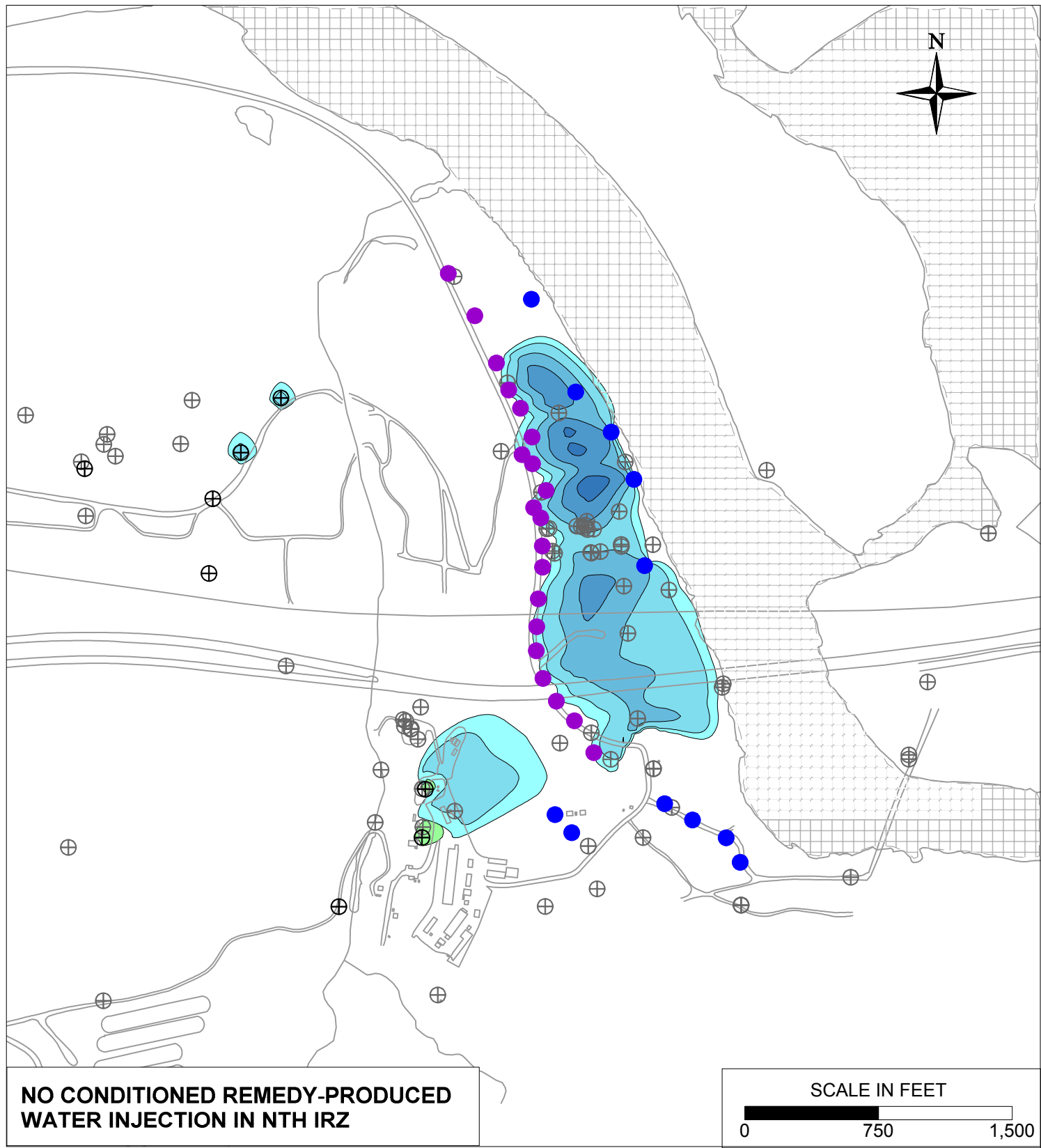


**LEGEND**

- IRZ WELLS
- ⊕ UPGRADE INJECTION WELLS
- EXTRACTION WELLS
- ⊕ MONITORING WELLS

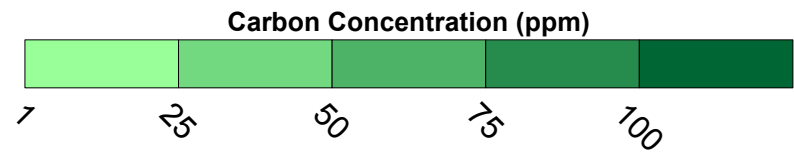
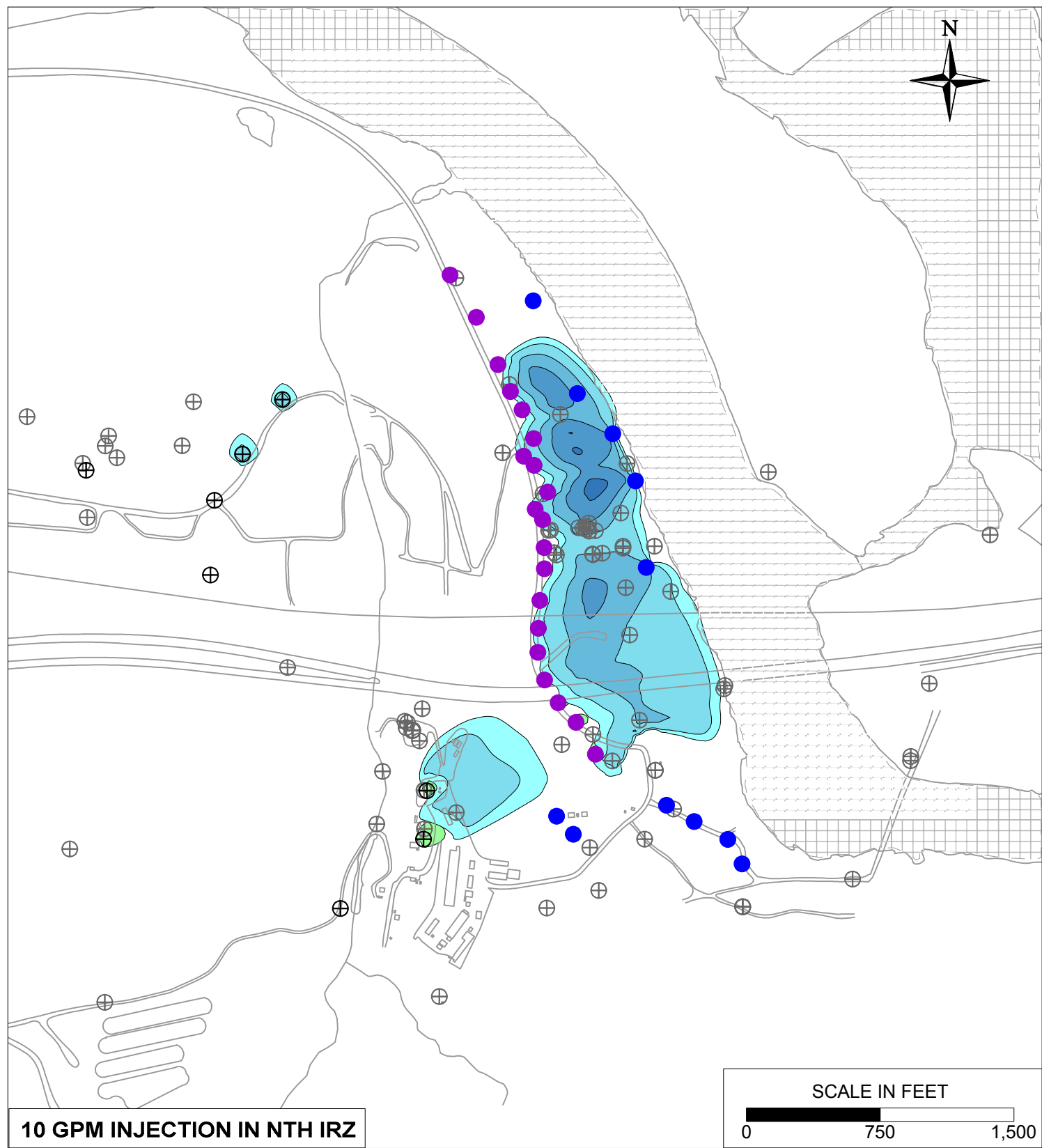
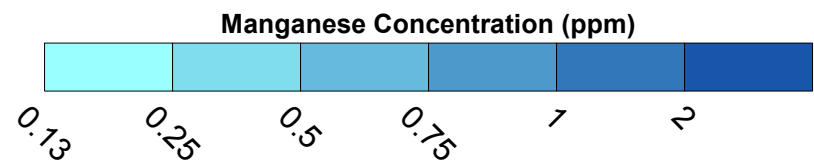




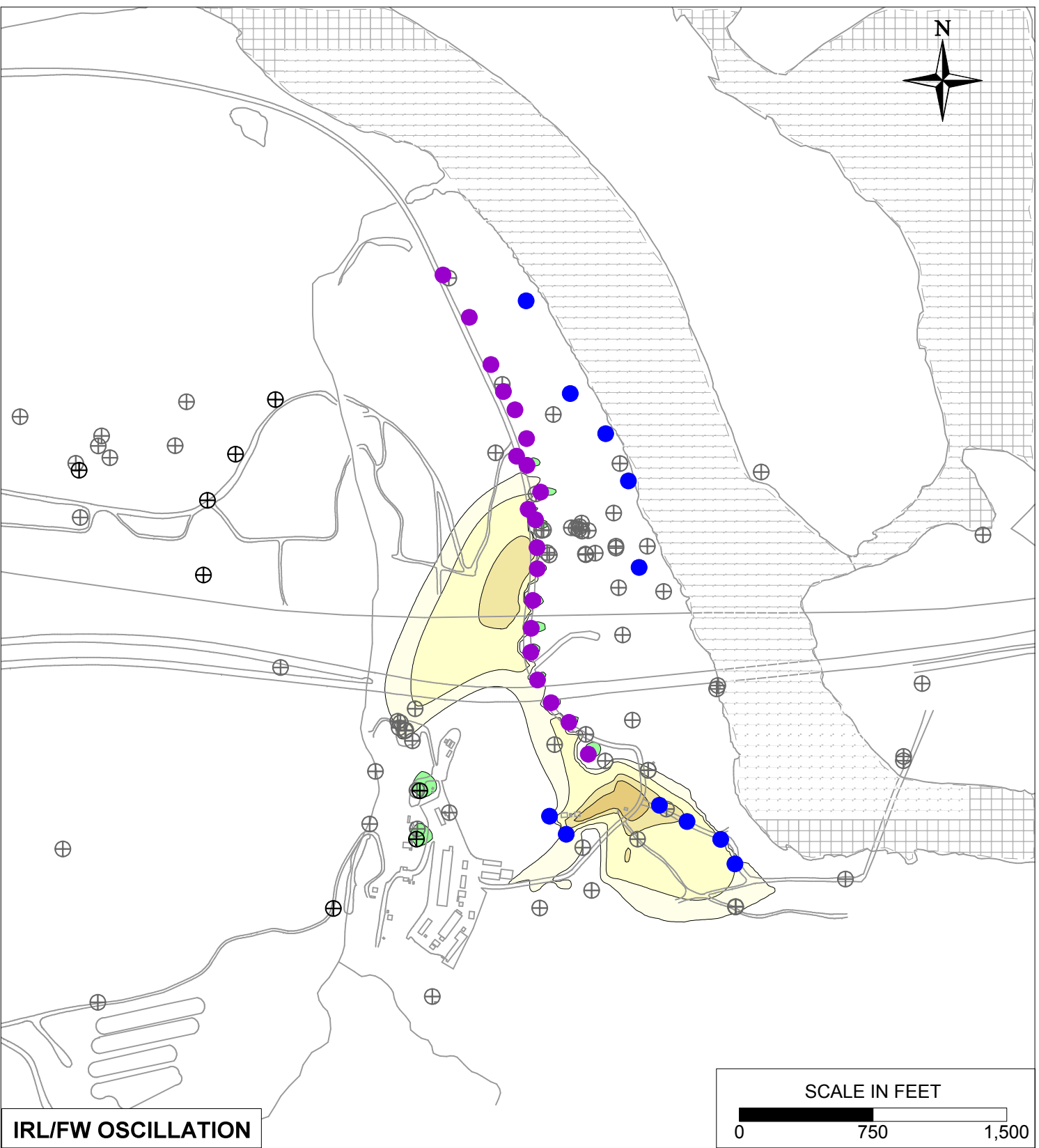
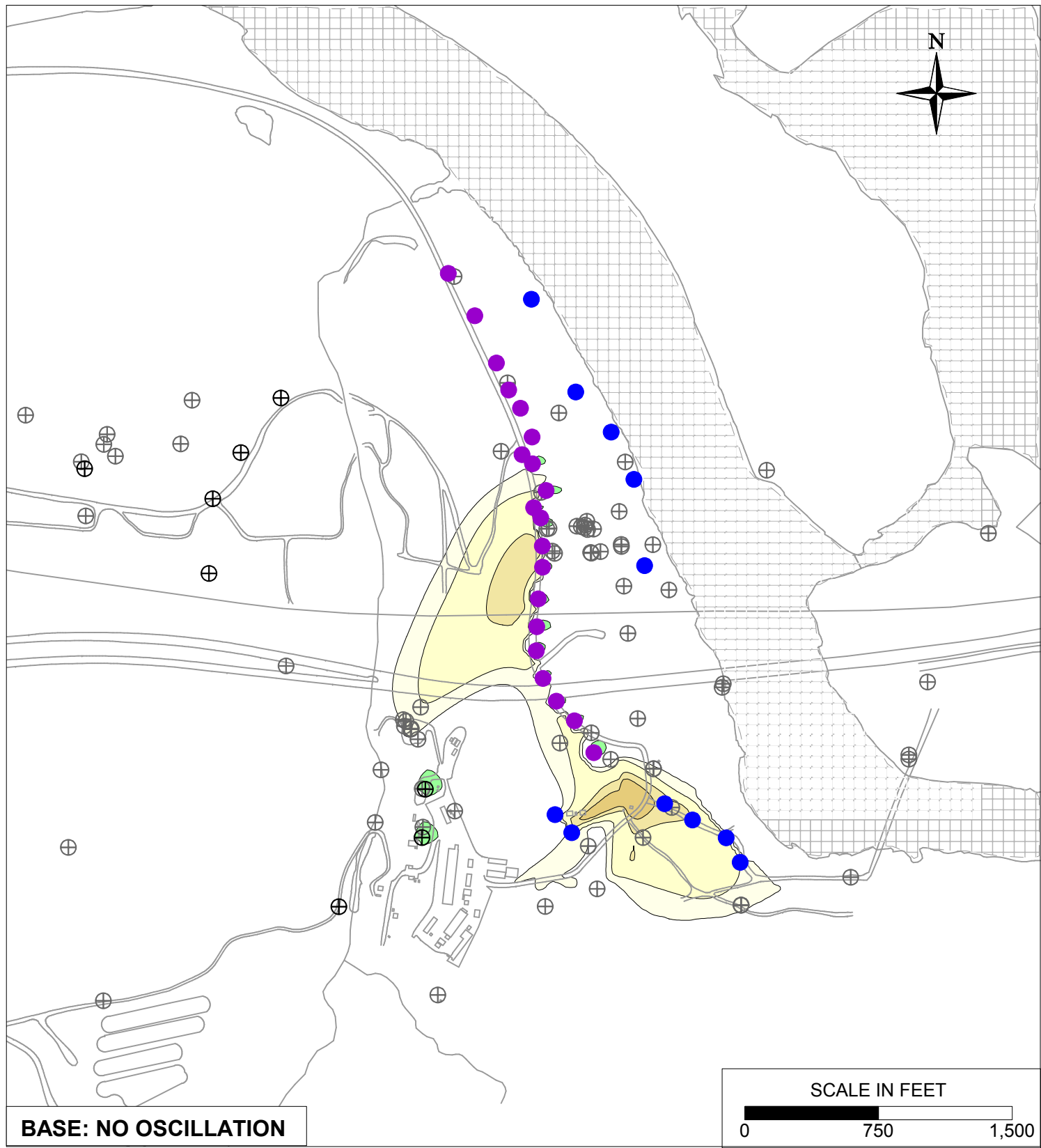


**LEGEND**

- IRZ WELLS
- ⊕ UPGRADIENT INJECTION WELLS
- EXTRACTION WELLS
- ⊕ MONITORING WELLS

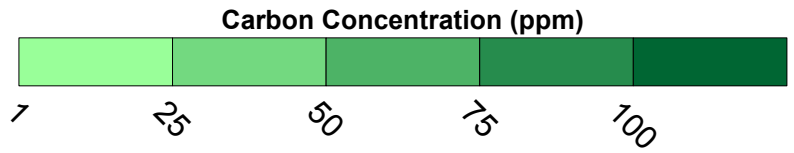
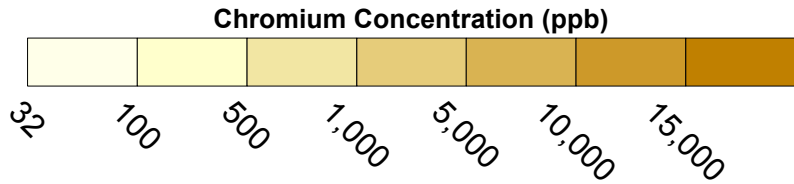


PG&E TOPOCK COMPRESSOR STATION NEEDLES, CALIFORNIA MODELING APPENDIX	
ADDITION OF CONDITIONED REMEDY-PRODUCED WATER TO NTH IRZ SENSITIVITY: SIMULATED MANGANESE TRANSPORT RESULTS FOR YEAR 30 IN MODEL LAYER 4	
	FIGURE <b>10.7-8</b>



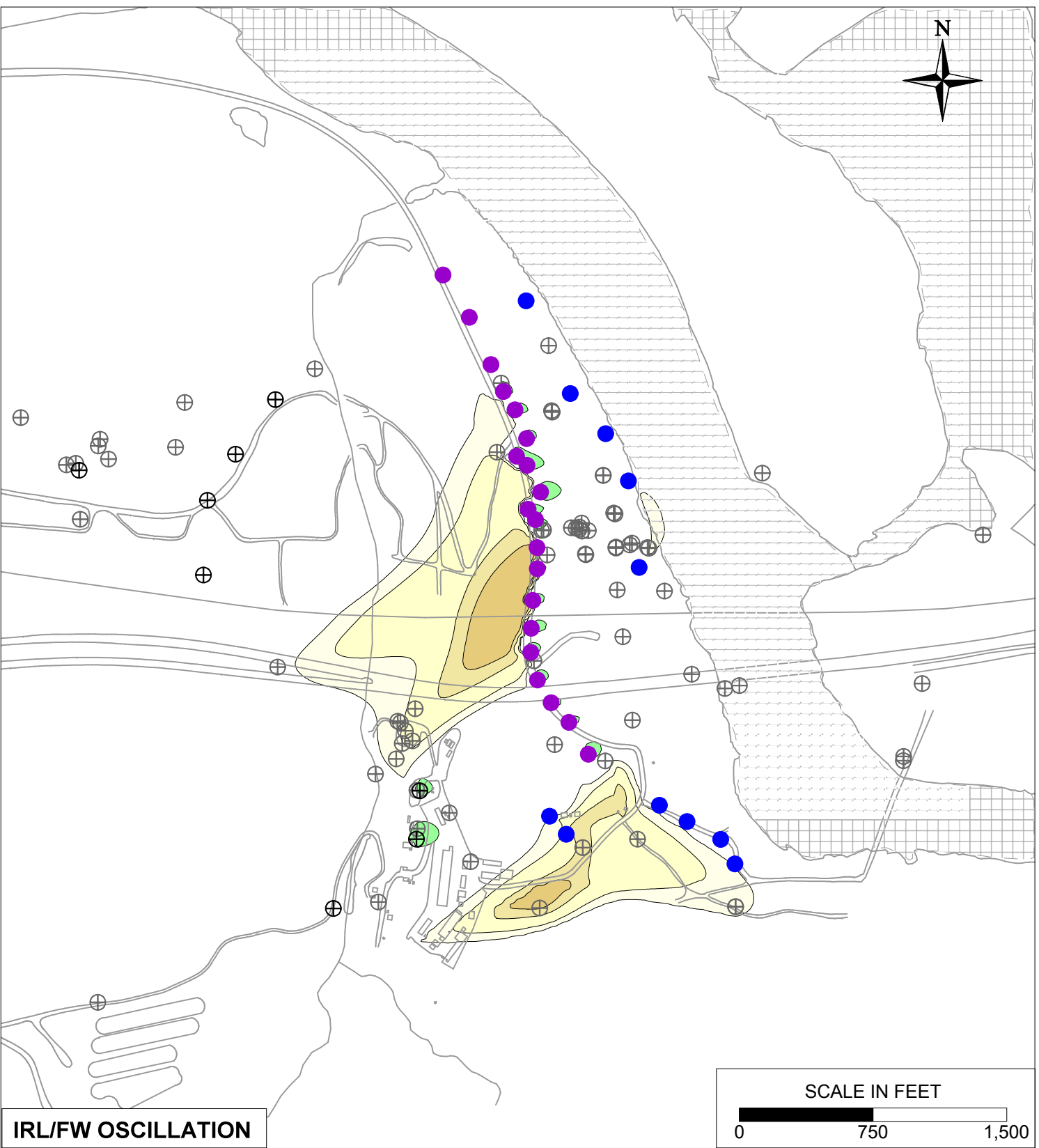
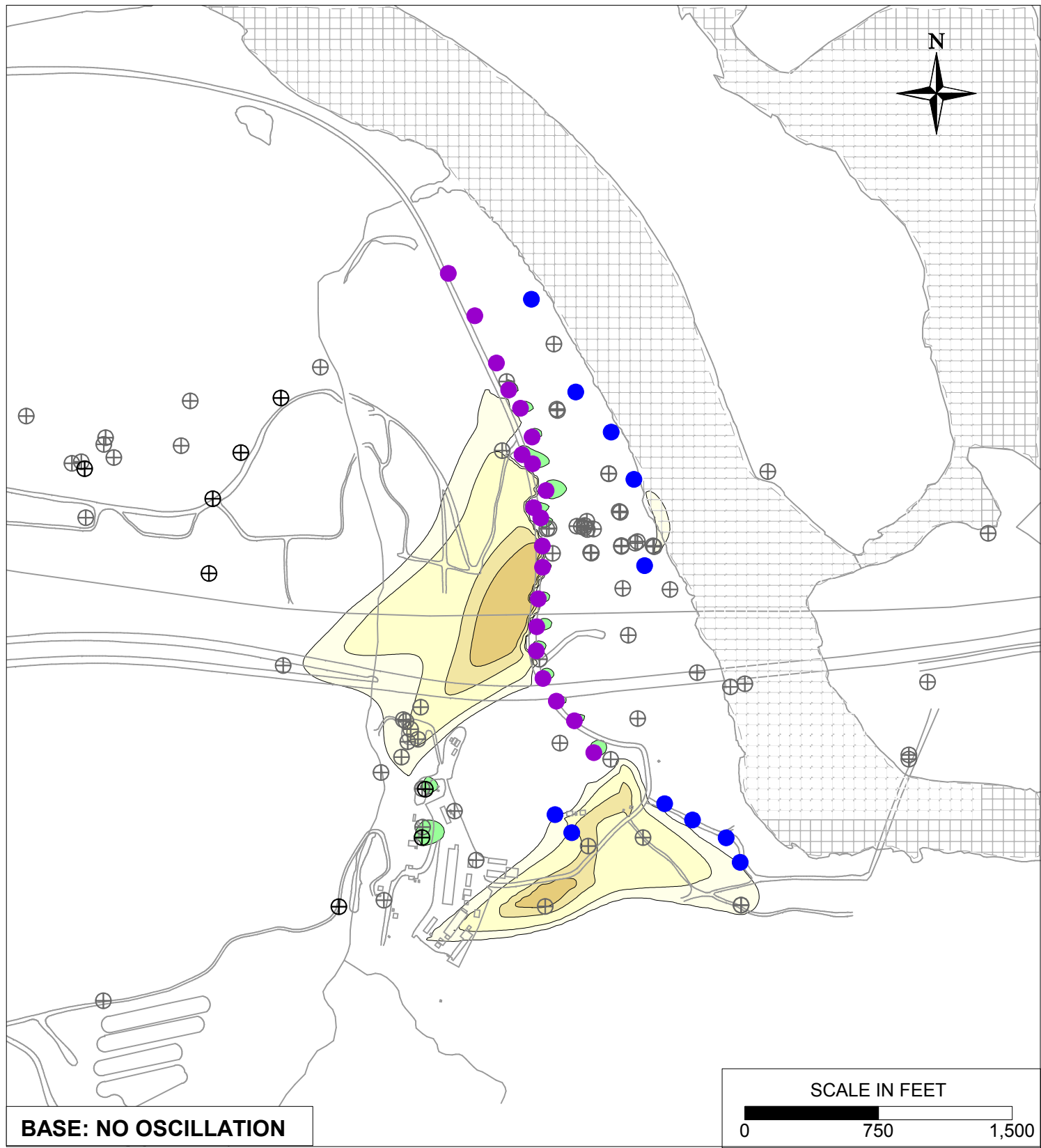
**LEGEND**

- IRZ WELLS
- ⊕ UPGRADIENT INJECTION WELLS
- EXTRACTION WELLS
- ⊕ MONITORING WELLS



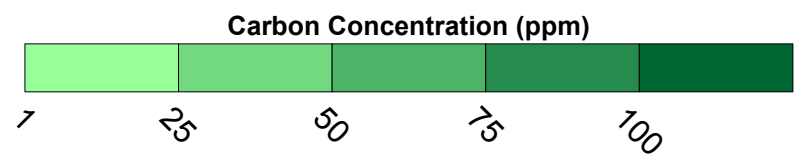
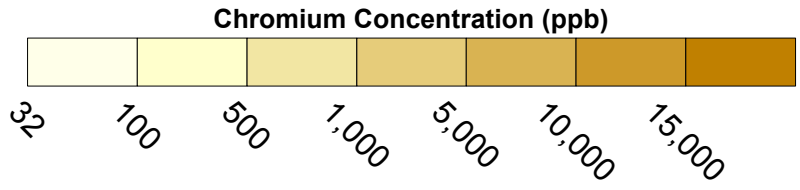
PG&E TOPOCK COMPRESSOR STATION NEEDLES, CALIFORNIA MODELING APPENDIX	
IRL/FW OSCILLATION SENSITIVITY: HEXAVALENT CHROMIUM TRANSPORT RESULTS FOR YEAR 20 IN MODEL LAYER 2	
	FIGURE <b>10.8-1</b>



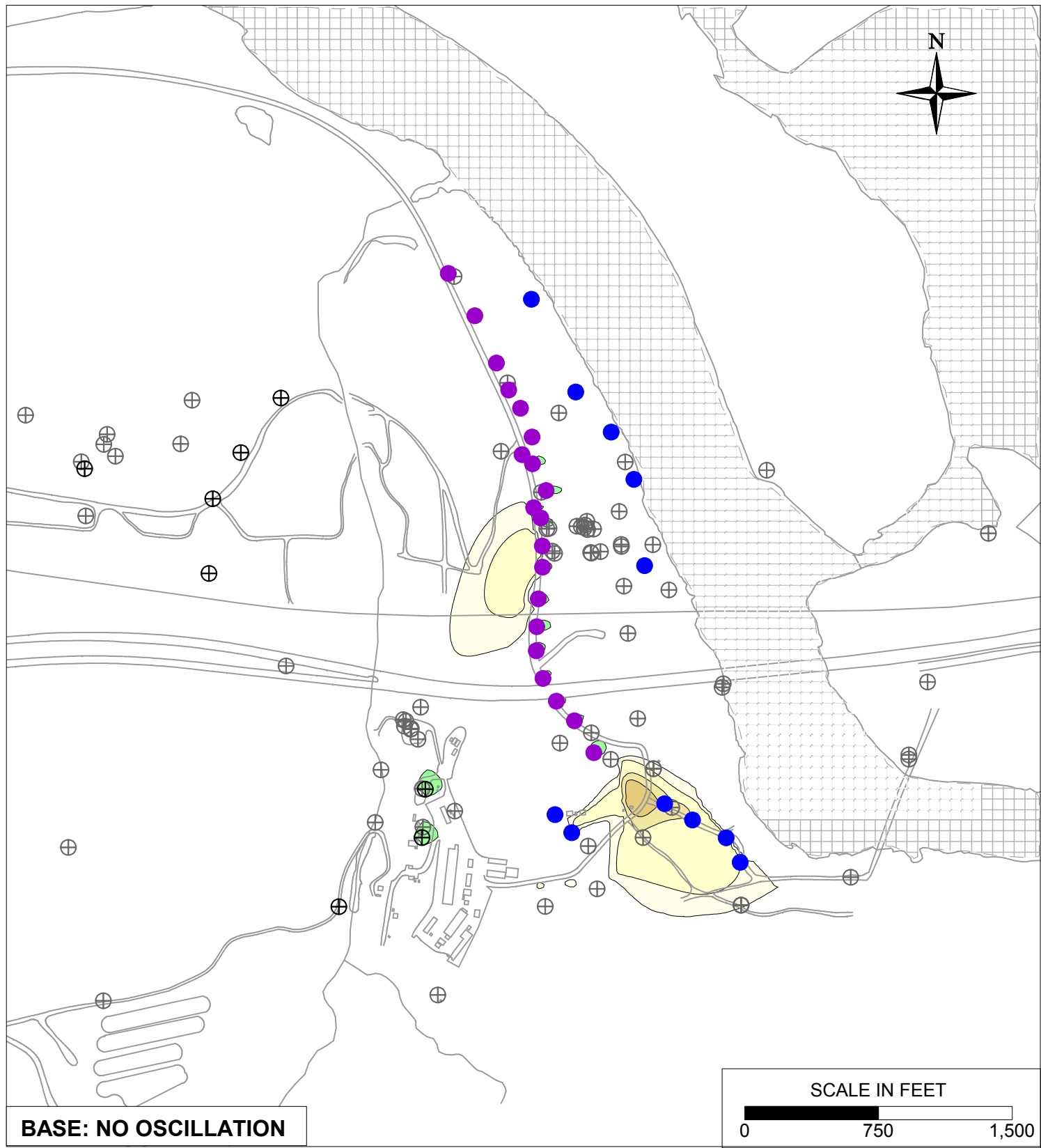


**LEGEND**

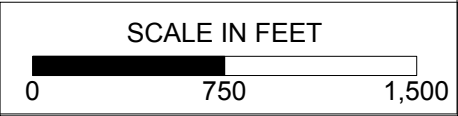
- IRZ WELLS
- ⊕ UPGRADIENT INJECTION WELLS
- EXTRACTION WELLS
- ⊕ MONITORING WELLS



PG&E TOPOCK COMPRESSOR STATION NEEDLES, CALIFORNIA MODELING APPENDIX	
IRL/FW OSCILLATION SENSITIVITY: HEXAVALENT CHROMIUM TRANSPORT RESULTS FOR YEAR 20 IN MODEL LAYER 4	
	FIGURE 10.8-2

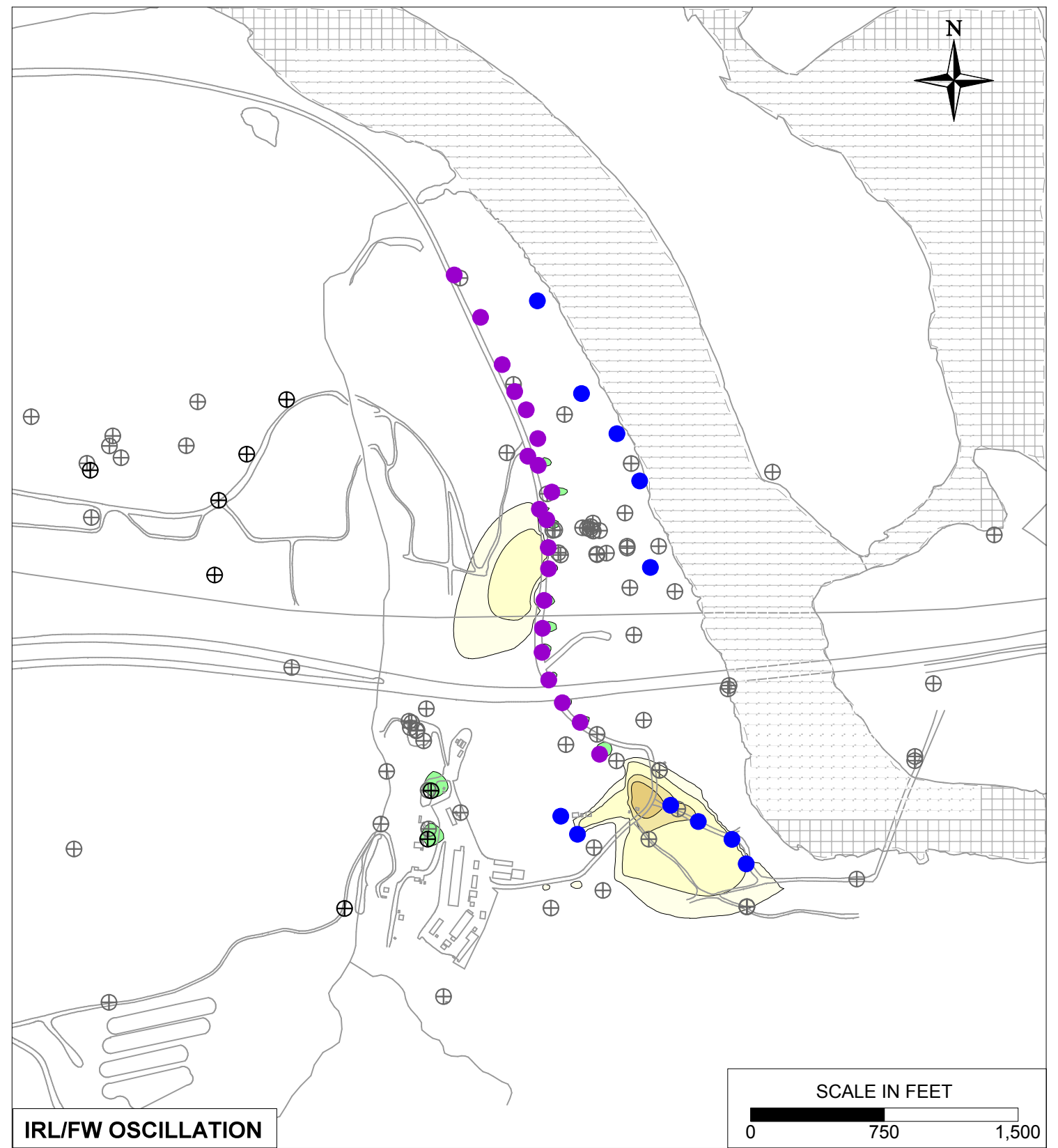
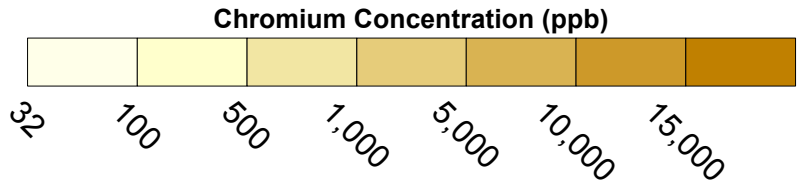


**BASE: NO OSCILLATION**

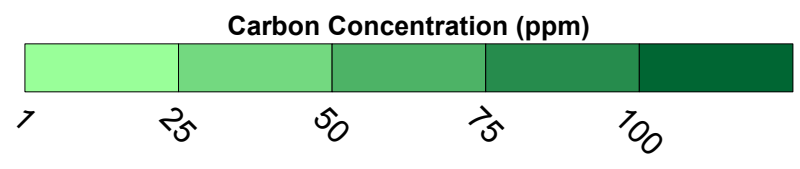
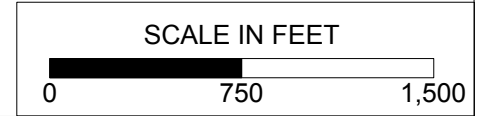


**LEGEND**

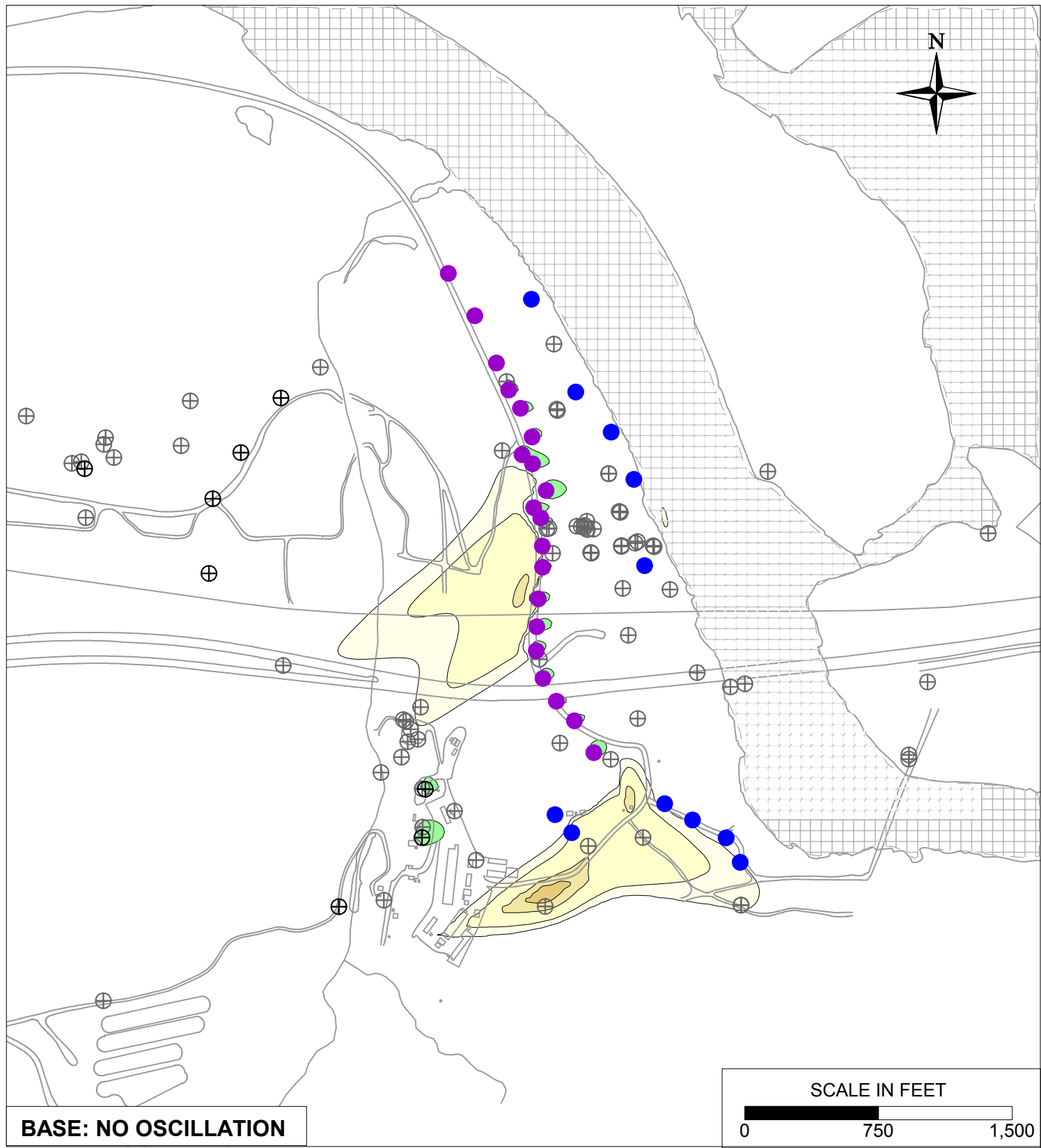
- IRZ WELLS
- ⊕ UPGRADE INJECTION WELLS
- EXTRACTION WELLS
- ⊕ MONITORING WELLS



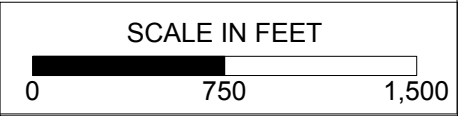
**IRL/FW OSCILLATION**



PG&E TOPOCK COMPRESSOR STATION NEEDLES, CALIFORNIA MODELING APPENDIX	
IRL/FW OSCILLATION SENSITIVITY: HEXAVALENT CHROMIUM TRANSPORT RESULTS FOR YEAR 30 IN MODEL LAYER 2	
	FIGURE 10.8-3

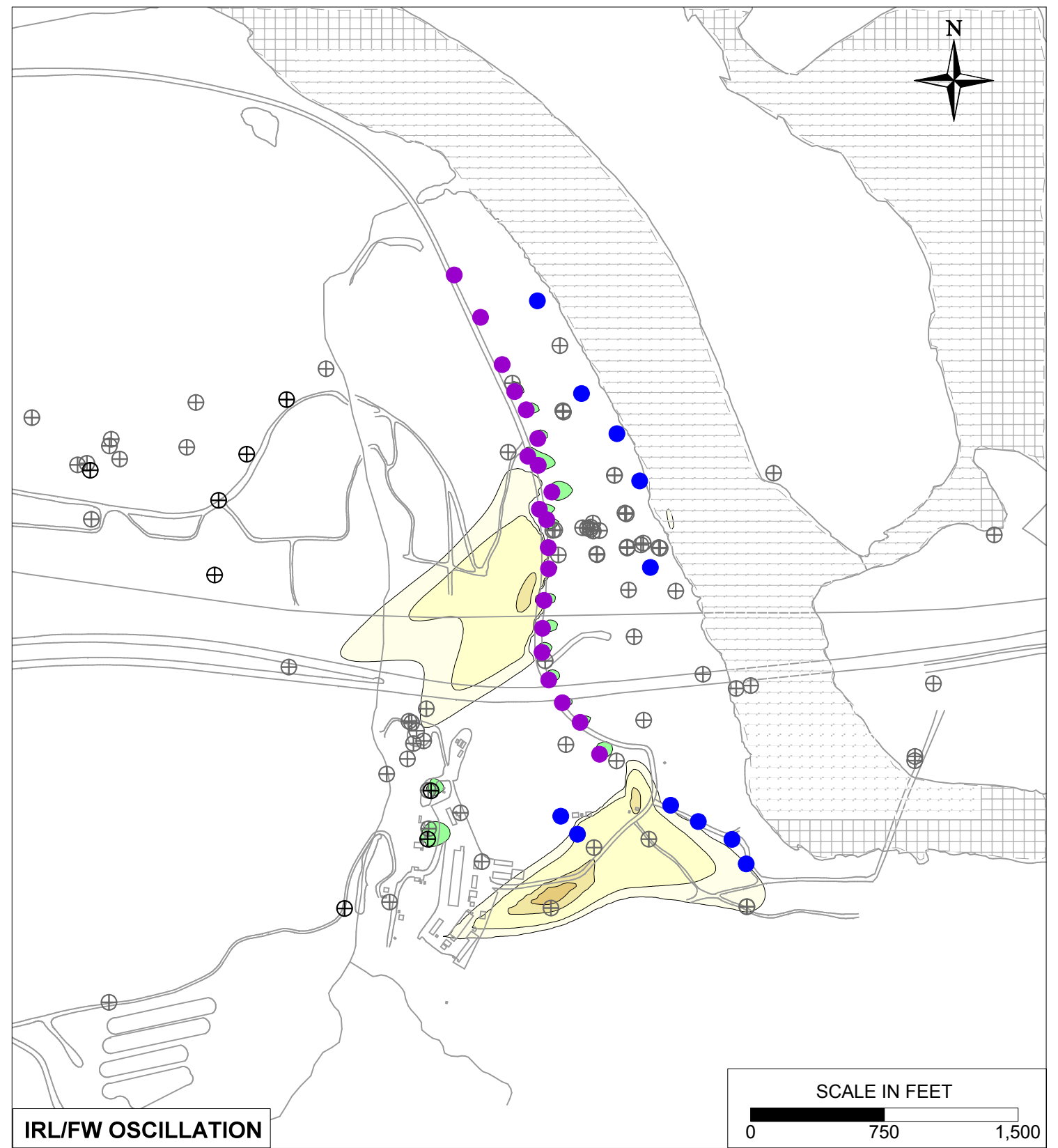
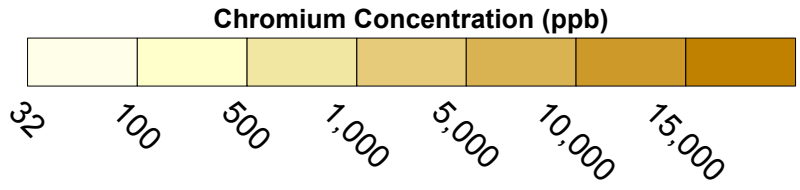


BASE: NO OSCILLATION

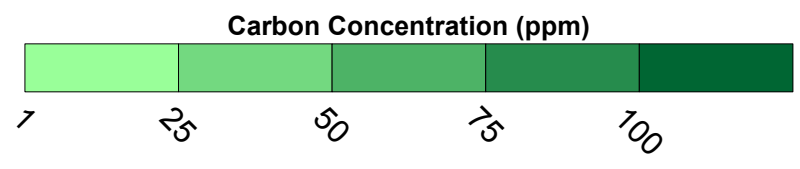
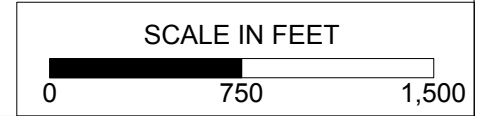


**LEGEND**

- IRZ WELLS
- ⊕ UPGRADIENT INJECTION WELLS
- EXTRACTION WELLS
- ⊕ MONITORING WELLS

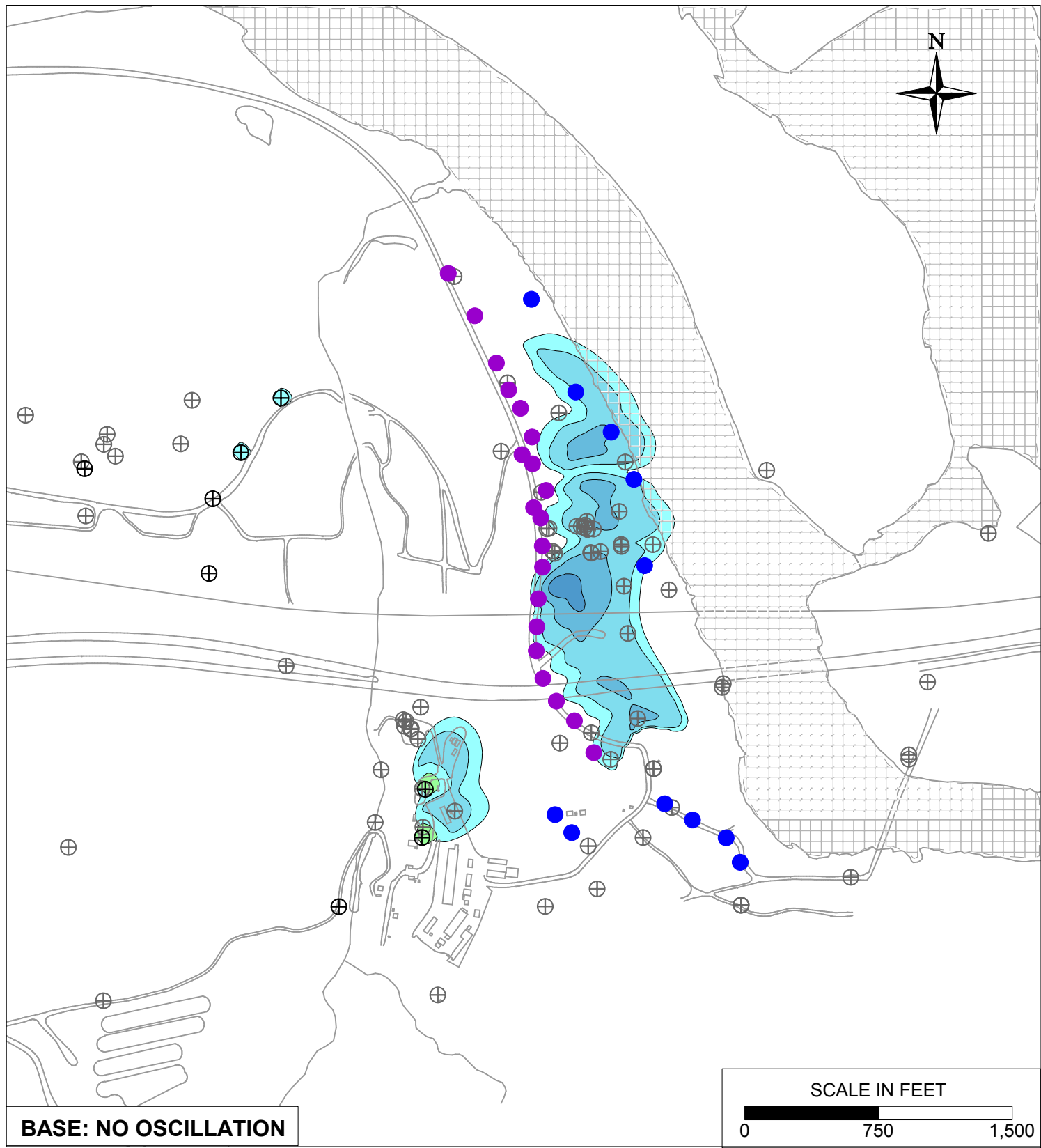


IRL/FW OSCILLATION

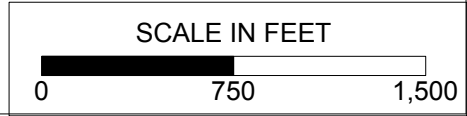


PG&E TOPOCK COMPRESSOR STATION NEEDLES, CALIFORNIA MODELING APPENDIX	
IRL/FW OSCILLATION SENSITIVITY: HEXAVALENT CHROMIUM TRANSPORT RESULTS FOR YEAR 30 IN MODEL LAYER 4	
	FIGURE 10.8-4



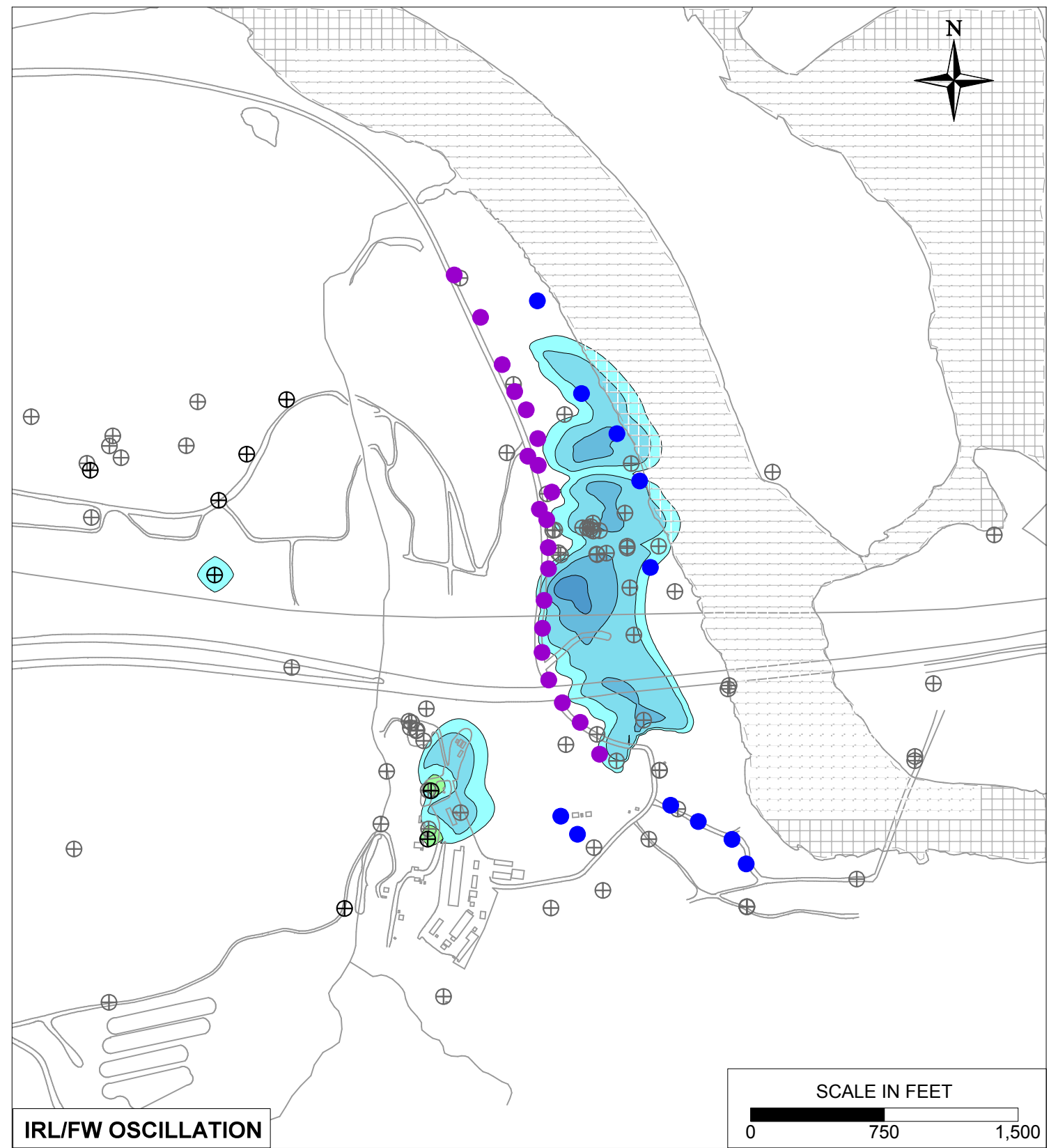
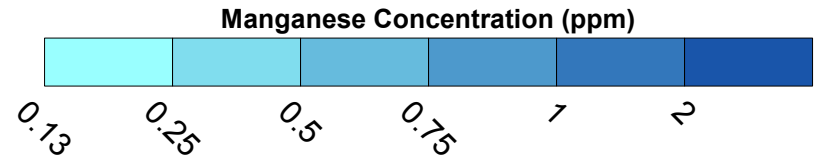


**BASE: NO OSCILLATION**

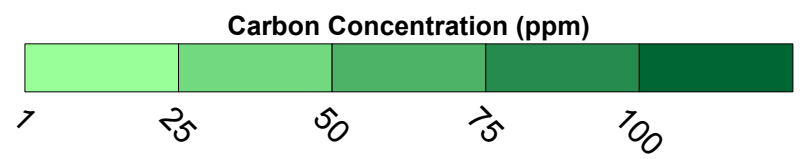
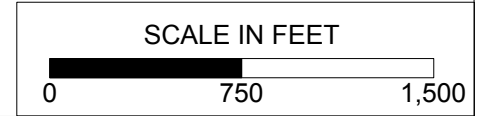


**LEGEND**

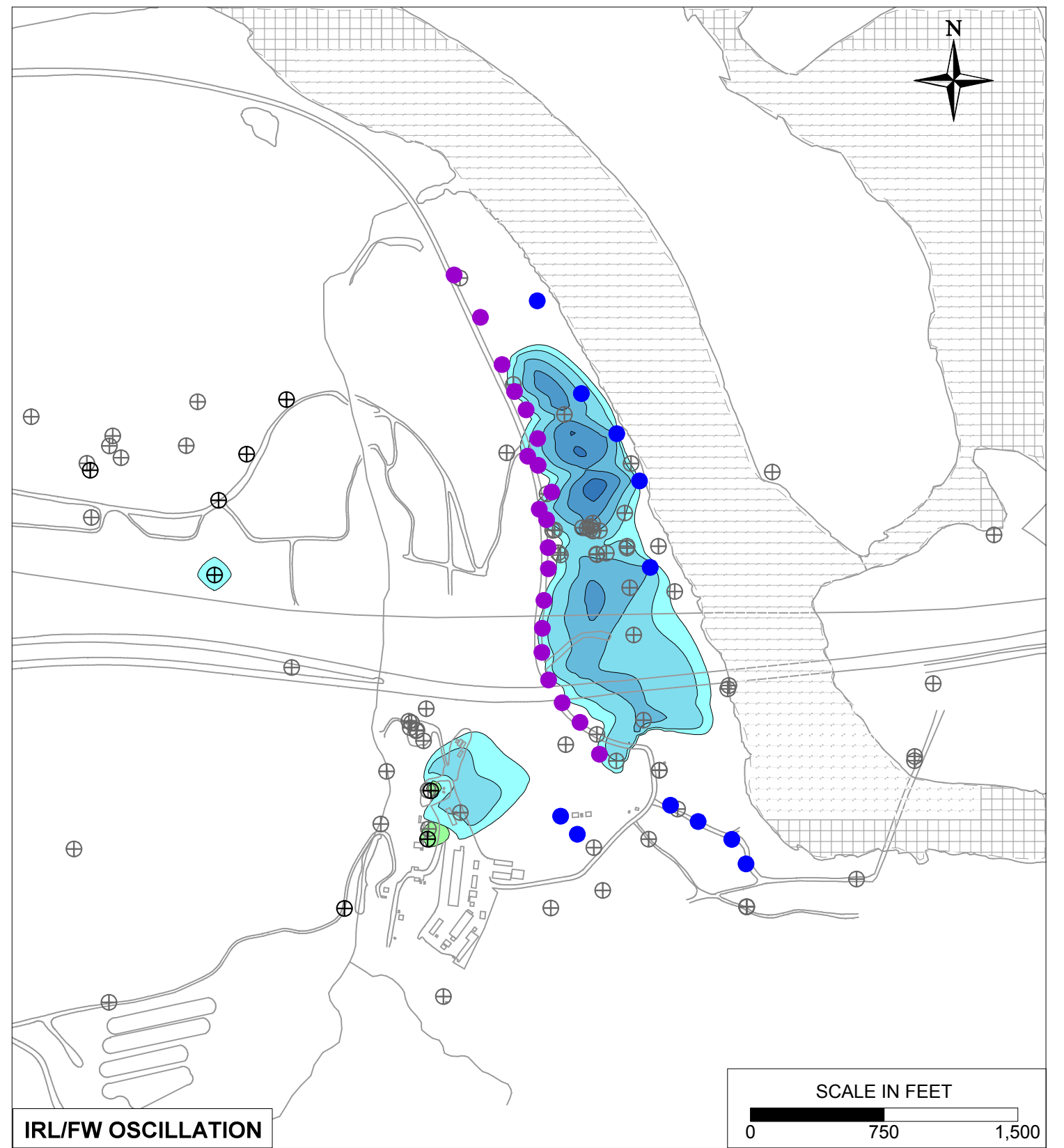
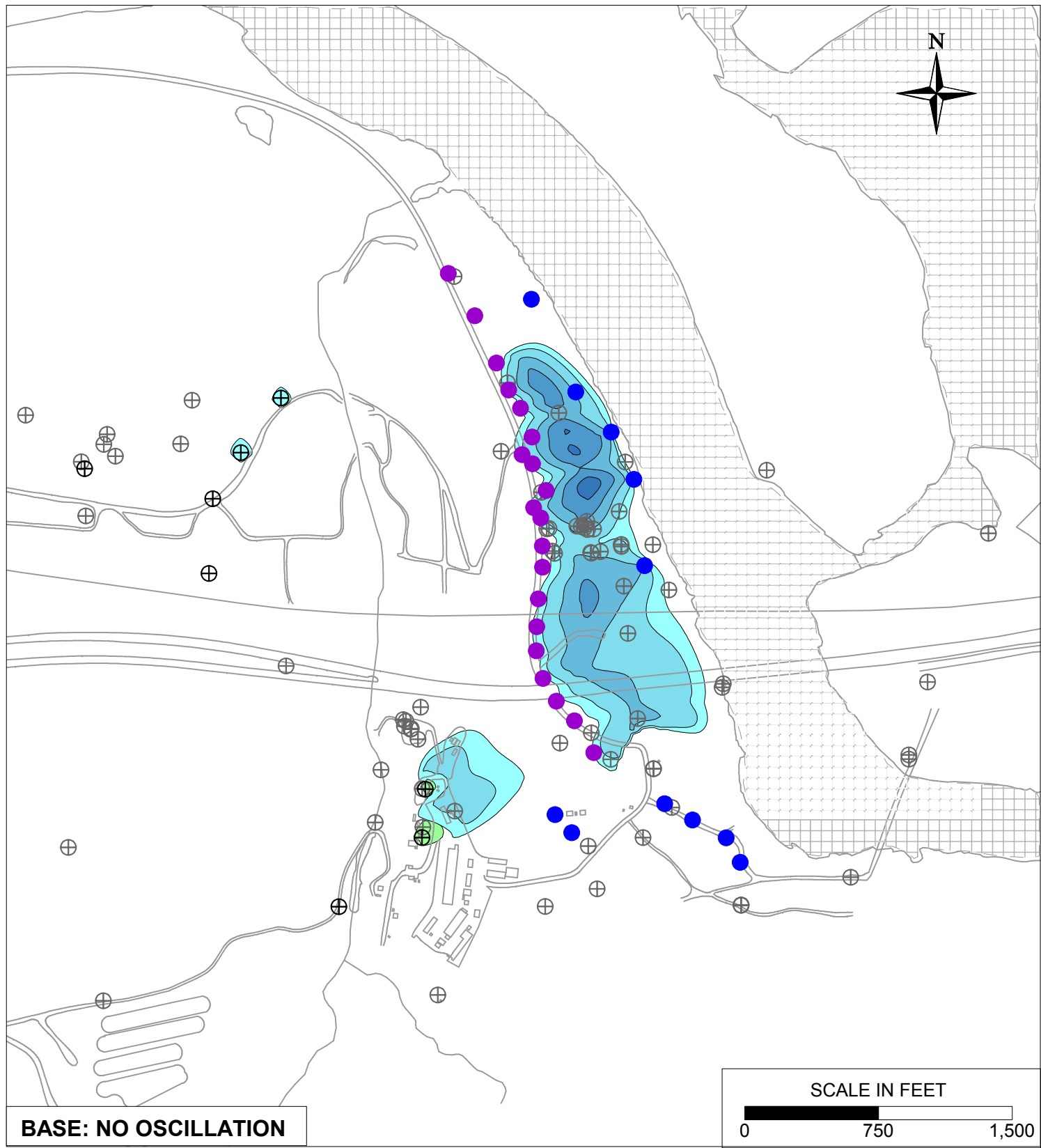
- IRZ WELLS
- ⊕ UPGRADIENT INJECTION WELLS
- EXTRACTION WELLS
- ⊕ MONITORING WELLS



**IRL/FW OSCILLATION**

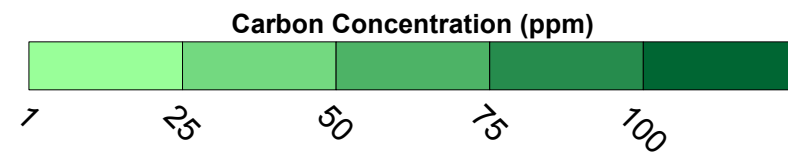
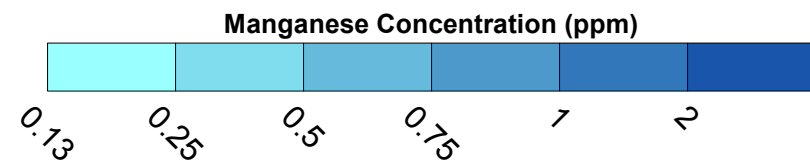


PG&E TOPOCK COMPRESSOR STATION NEEDLES, CALIFORNIA MODELING APPENDIX	
IRL/FW OSCILLATION SENSITIVITY: SIMULATED MANGANESE TRANSPORT RESULTS FOR YEAR 20 IN MODEL LAYER 2	
	FIGURE 10.8-5



**LEGEND**

- IRZ WELLS
- ⊕ UPGRADIENT INJECTION WELLS
- EXTRACTION WELLS
- ⊕ MONITORING WELLS



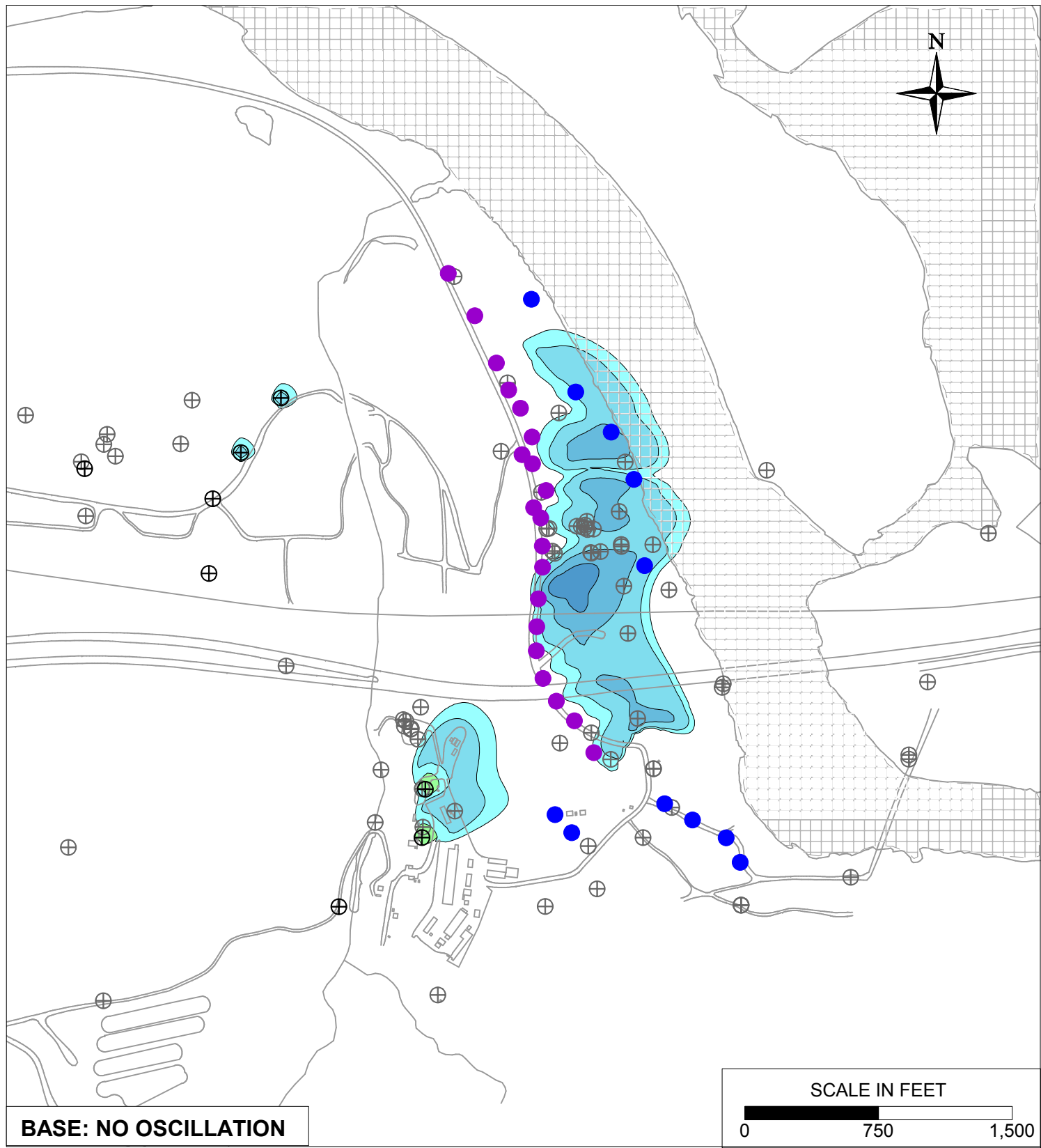
PG&E  
TOPOCK COMPRESSOR STATION  
NEEDLES, CALIFORNIA  
MODELING APPENDIX

IRL/FW OSCILLATION SENSITIVITY:  
SIMULATED MANGANESE TRANSPORT RESULTS  
FOR YEAR 20 IN MODEL LAYER 4

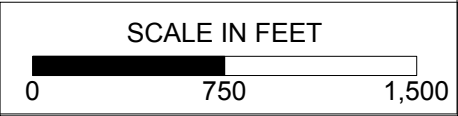


FIGURE  
10.8-6



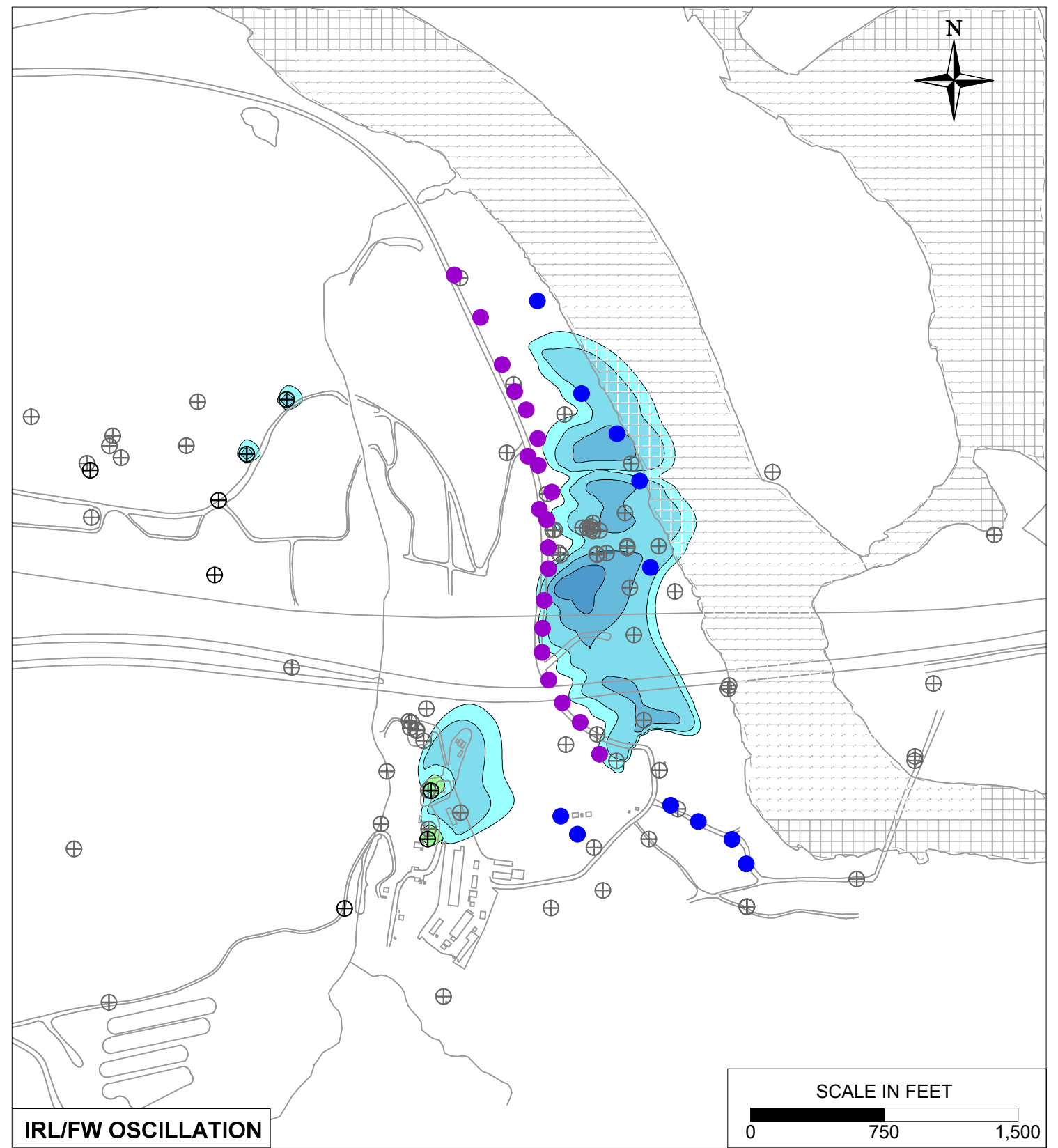
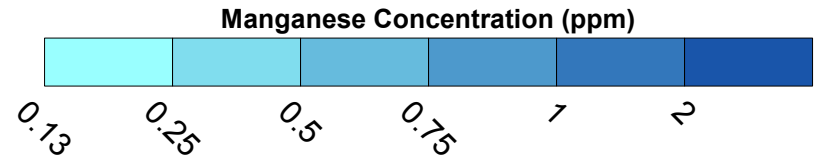


BASE: NO OSCILLATION

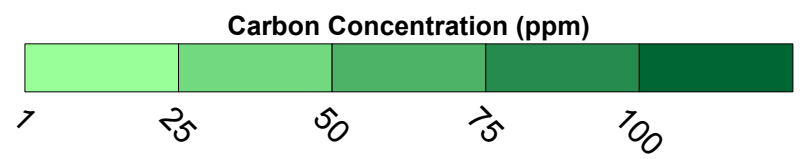
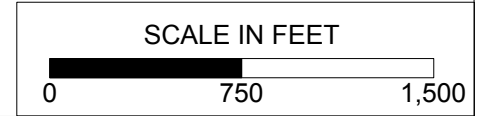


**LEGEND**

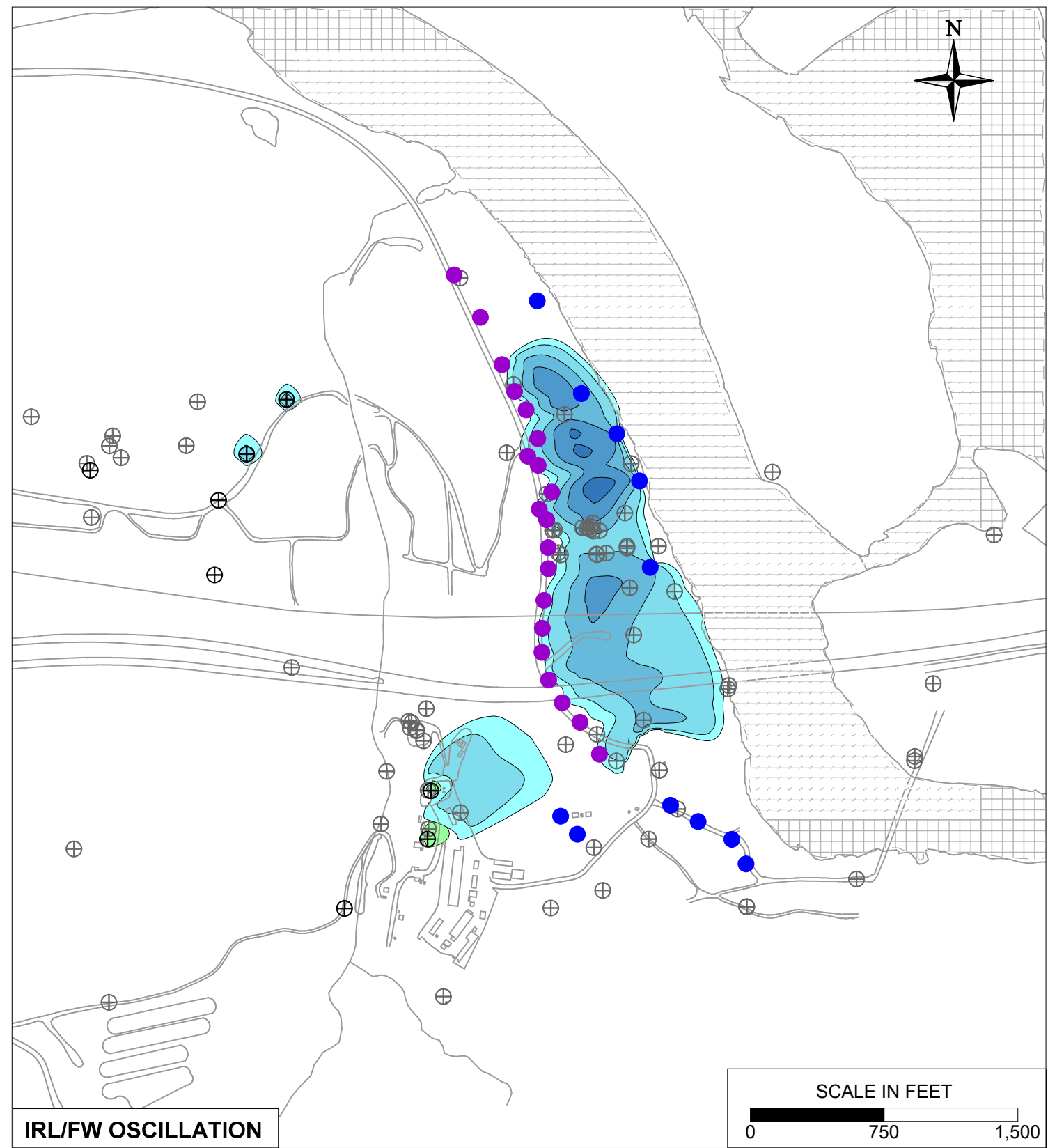
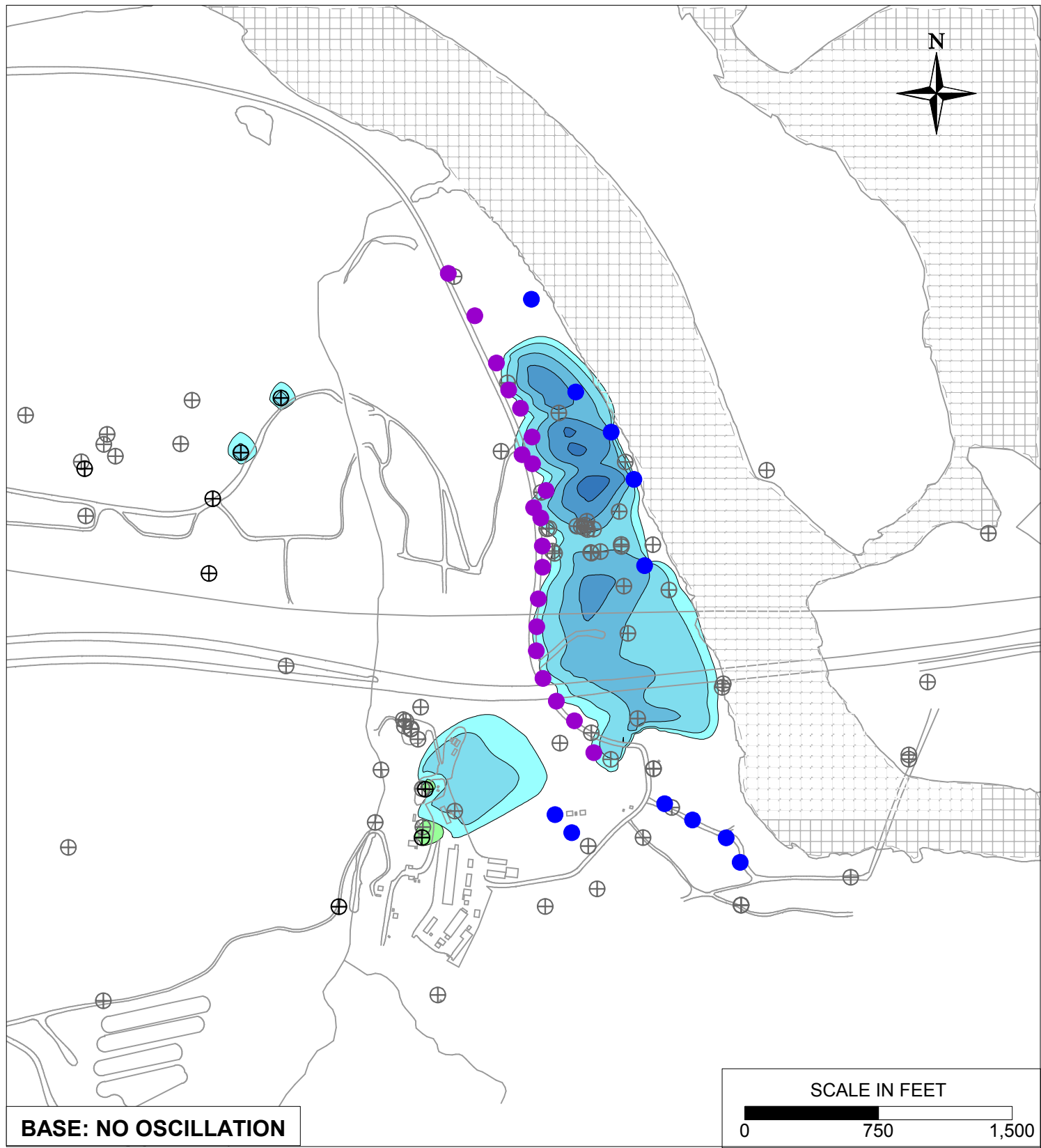
- IRZ WELLS
- ⊕ UPGRADE INJECTION WELLS
- EXTRACTION WELLS
- ⊕ MONITORING WELLS



IRL/FW OSCILLATION

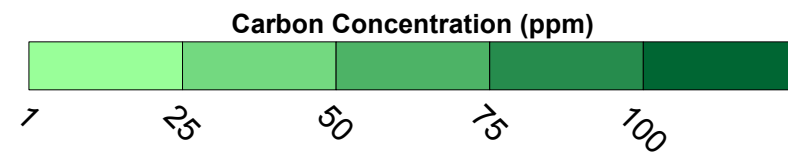
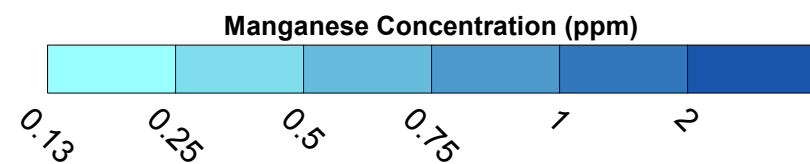


PG&E TOPOCK COMPRESSOR STATION NEEDLES, CALIFORNIA MODELING APPENDIX	
IRL/FW OSCILLATION SENSITIVITY: SIMULATED MANGANESE TRANSPORT RESULTS FOR YEAR 30 IN MODEL LAYER 2	
	FIGURE 10.8-7



**LEGEND**

- IRZ WELLS
- ⊕ UPGRADIENT INJECTION WELLS
- EXTRACTION WELLS
- ⊕ MONITORING WELLS

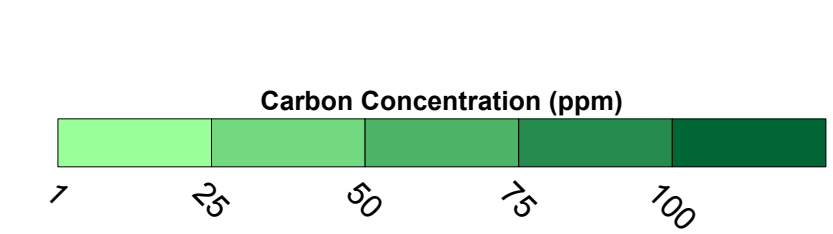
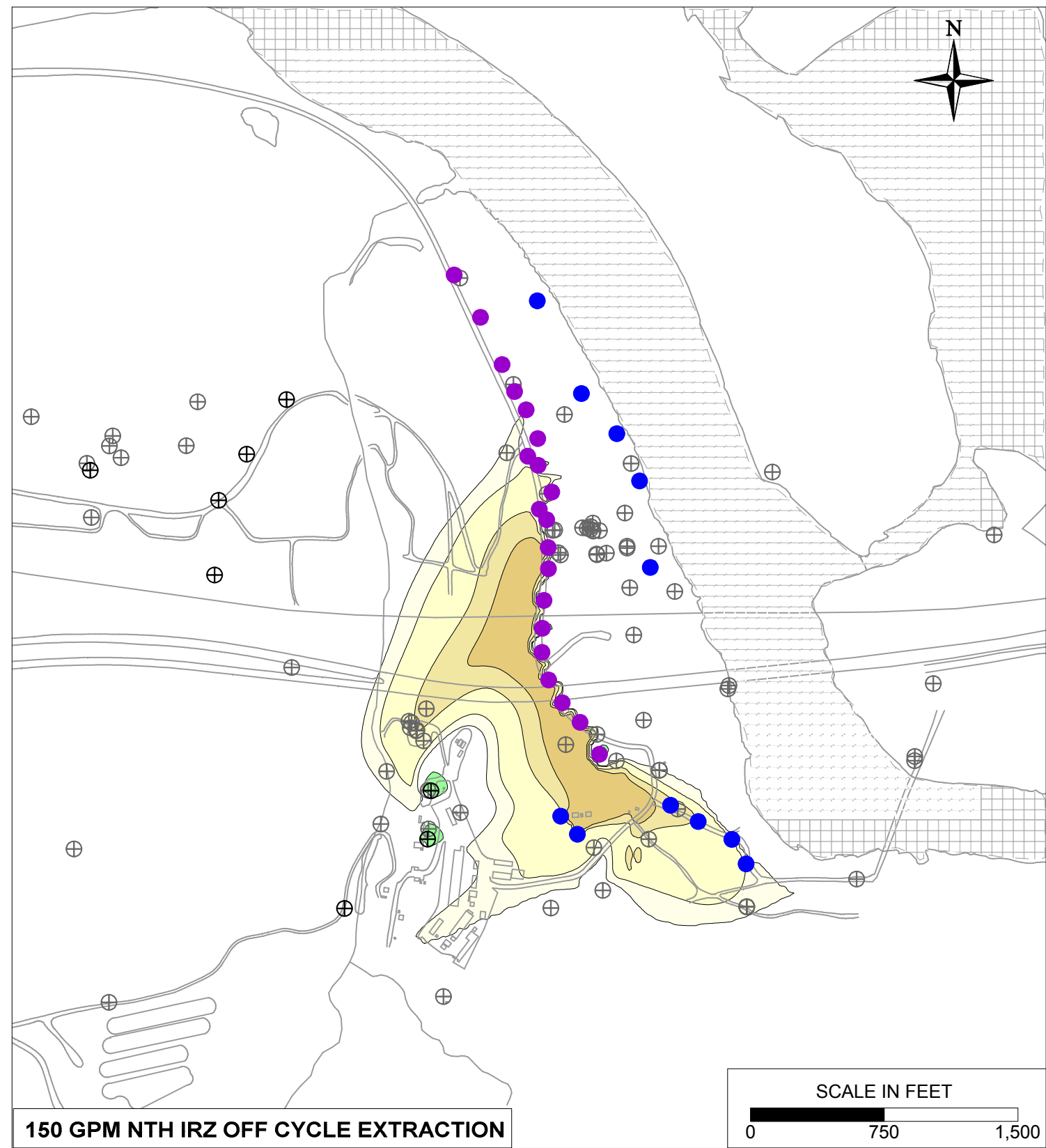
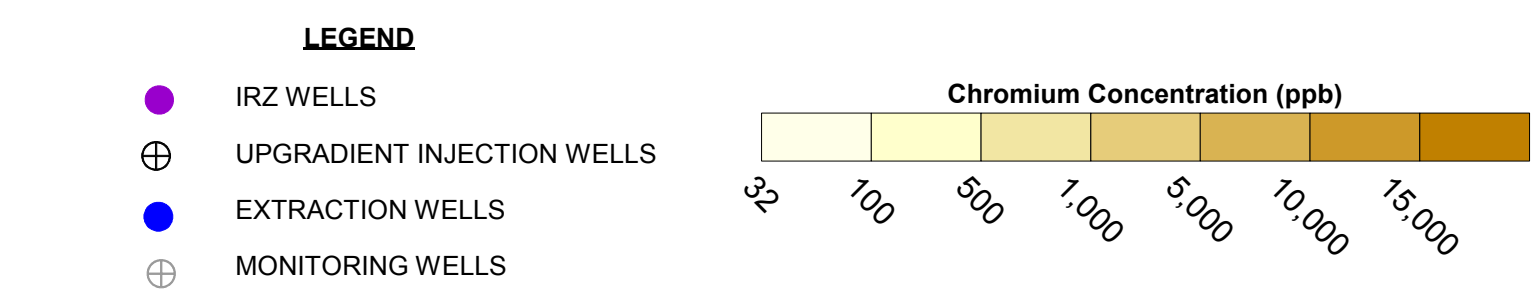
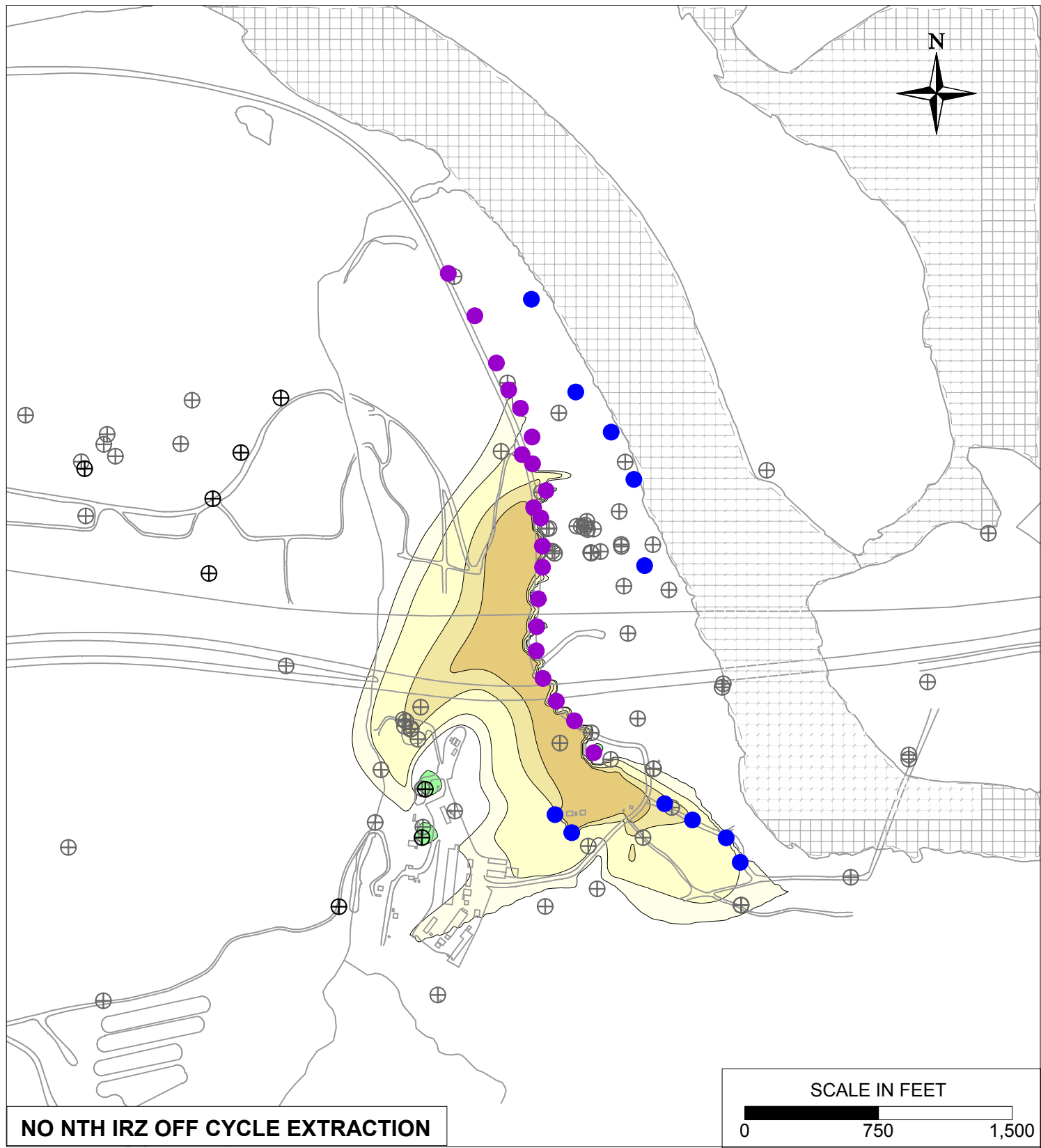


PG&E  
TOPOCK COMPRESSOR STATION  
NEEDLES, CALIFORNIA  
MODELING APPENDIX

IRL/FW OSCILLATION SENSITIVITY:  
SIMULATED MANGANESE TRANSPORT RESULTS  
FOR YEAR 30 IN MODEL LAYER 4



FIGURE  
10.8-8



PG&E  
TOPOCK COMPRESSOR STATION  
NEEDLES, CALIFORNIA  
MODELING APPENDIX

NTH IRZ OFF CYCLE EXTRACTION SENSITIVITY:  
SIMULATED HEXAVALENT CHROMIUM TRANSPORT  
RESULTS FOR YEAR 10 IN MODEL LAYER 2


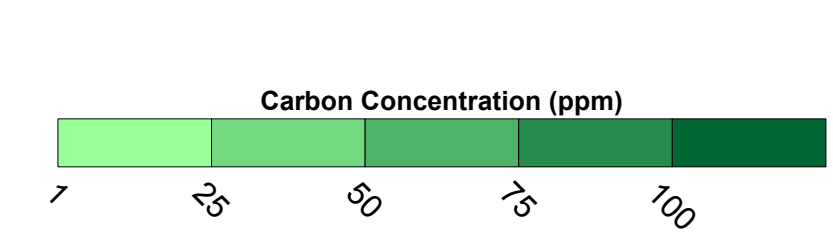
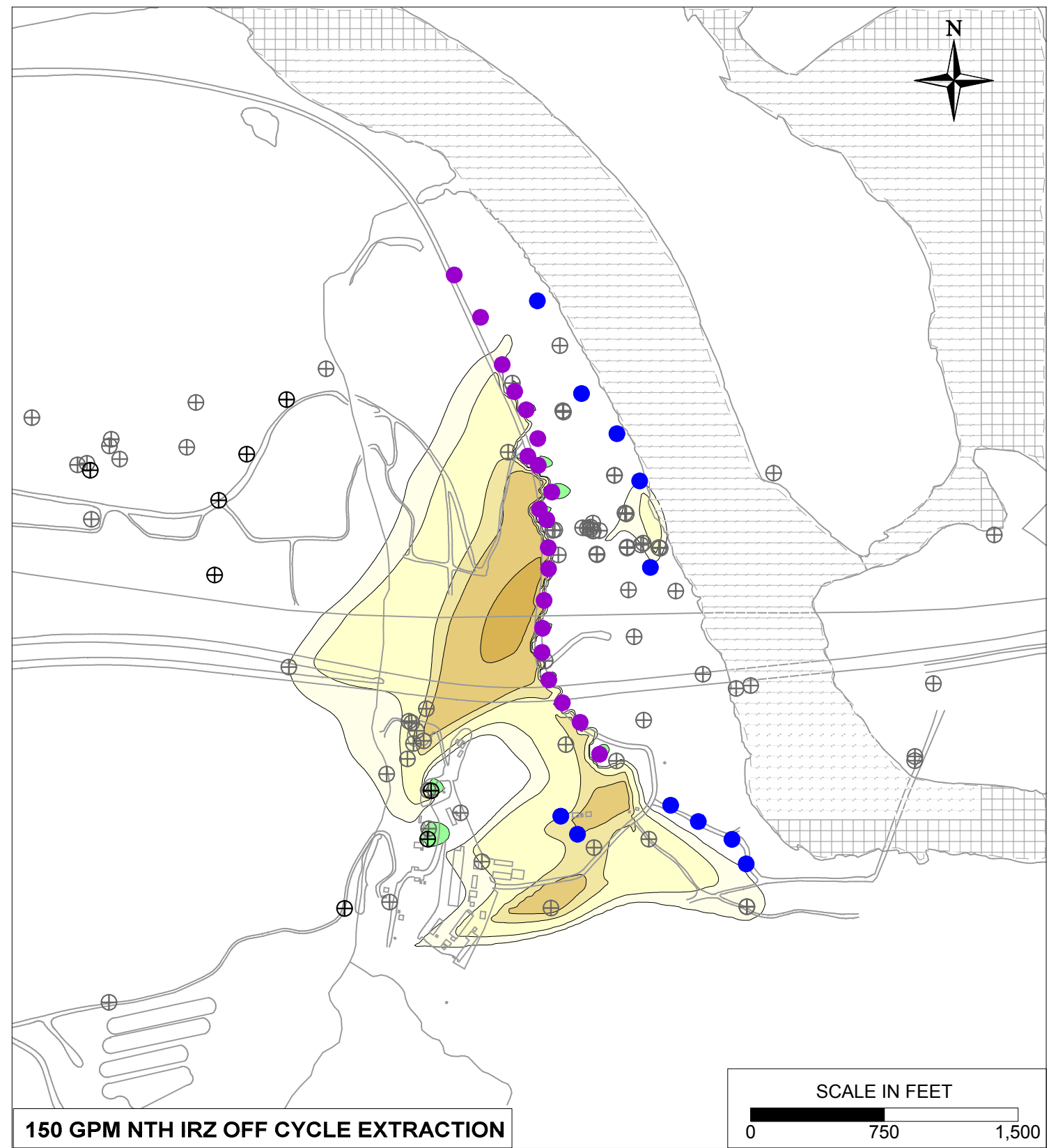
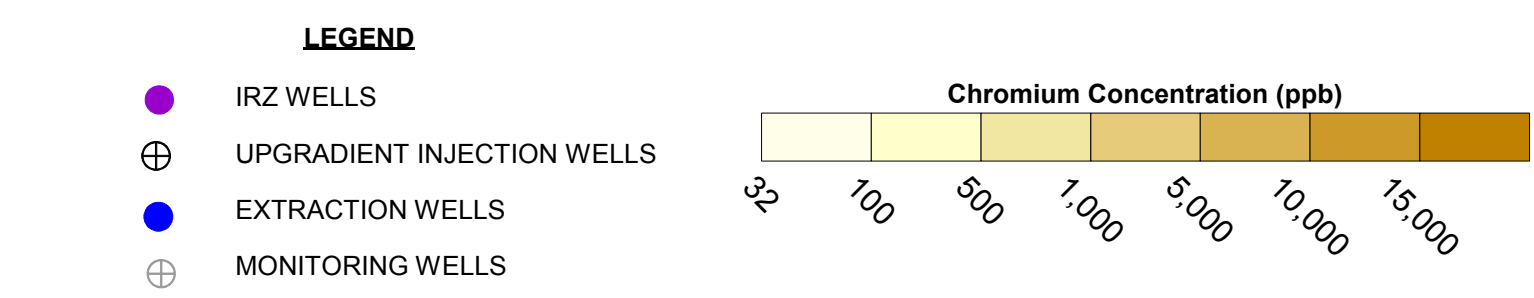
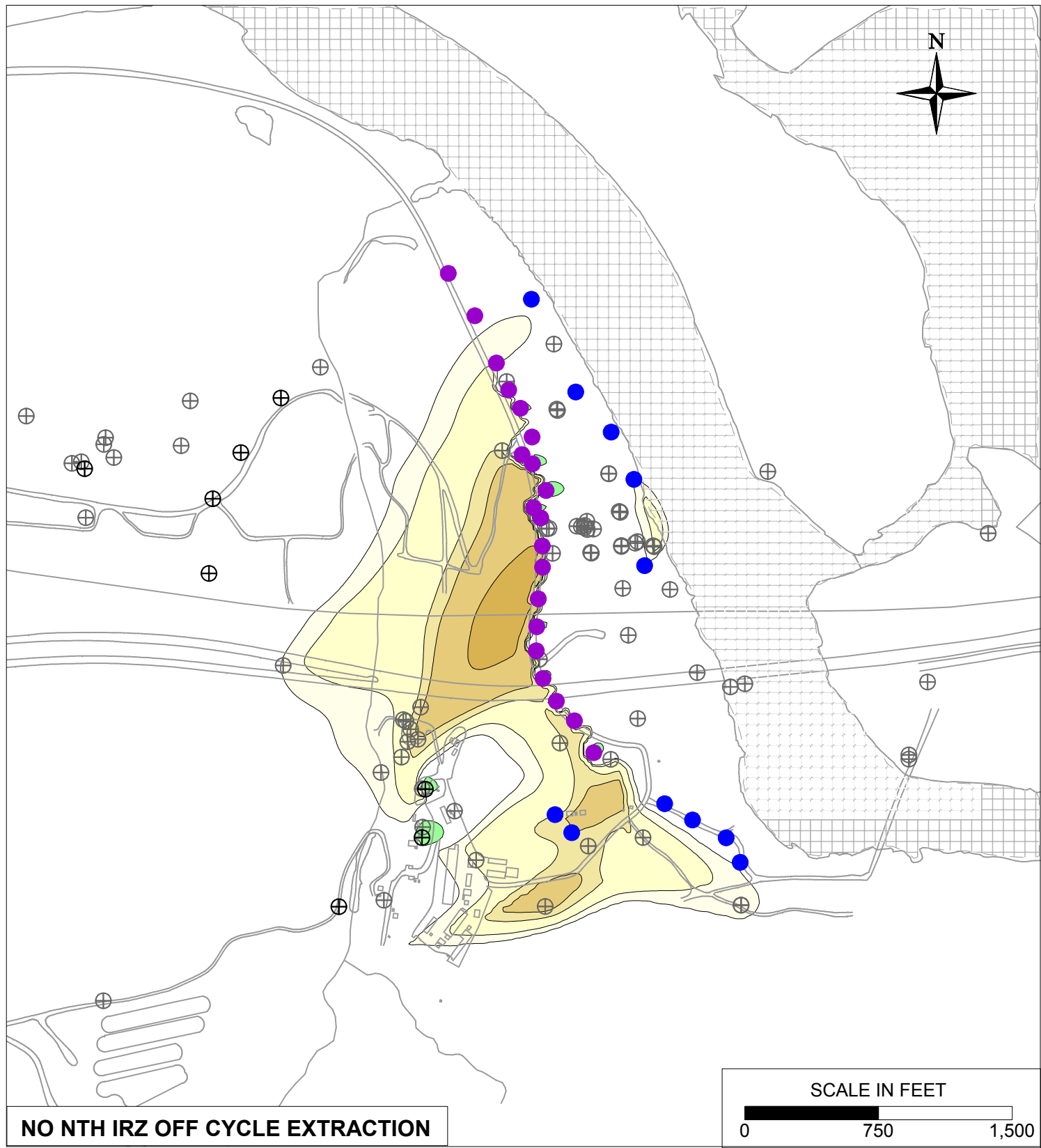
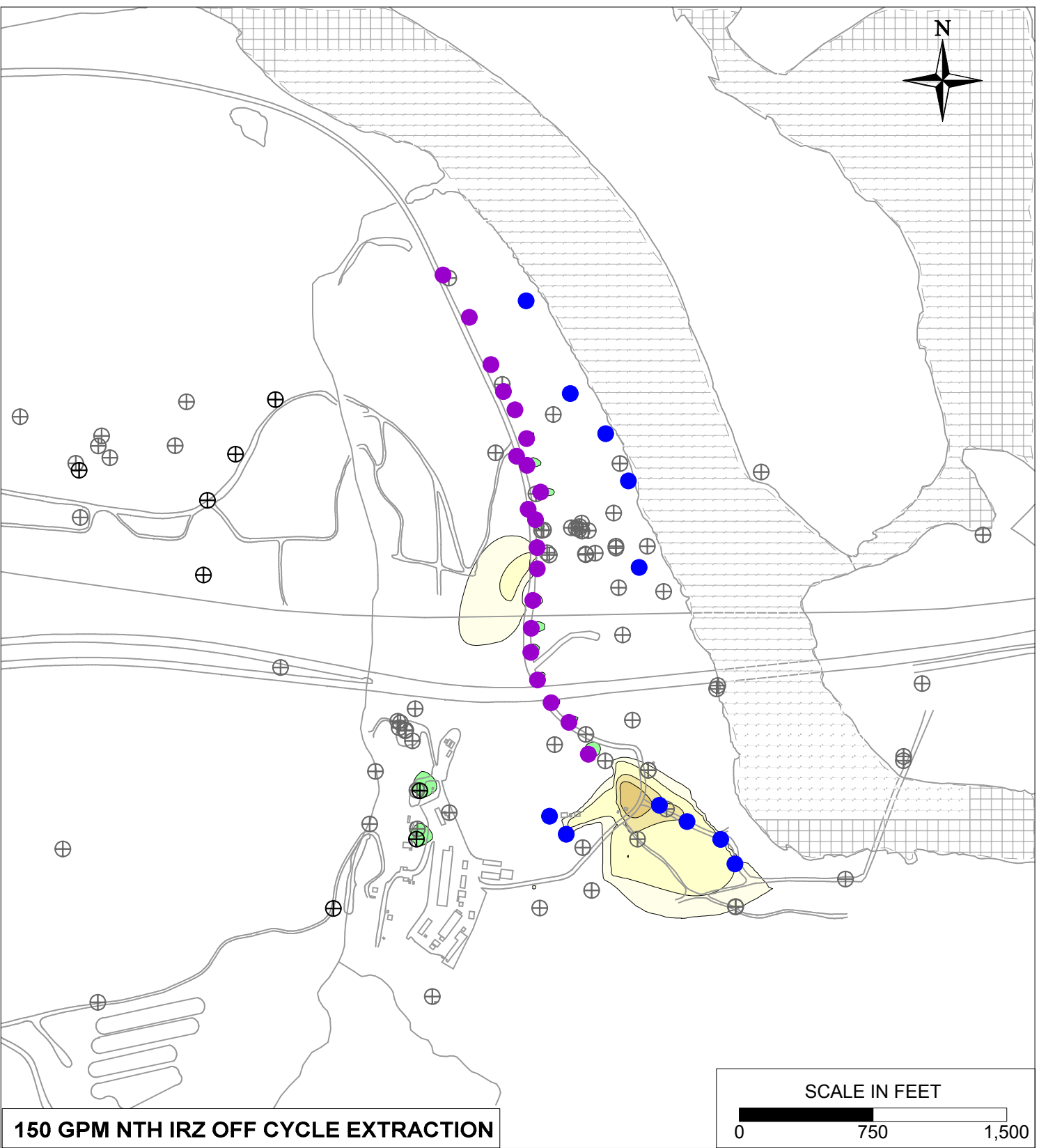
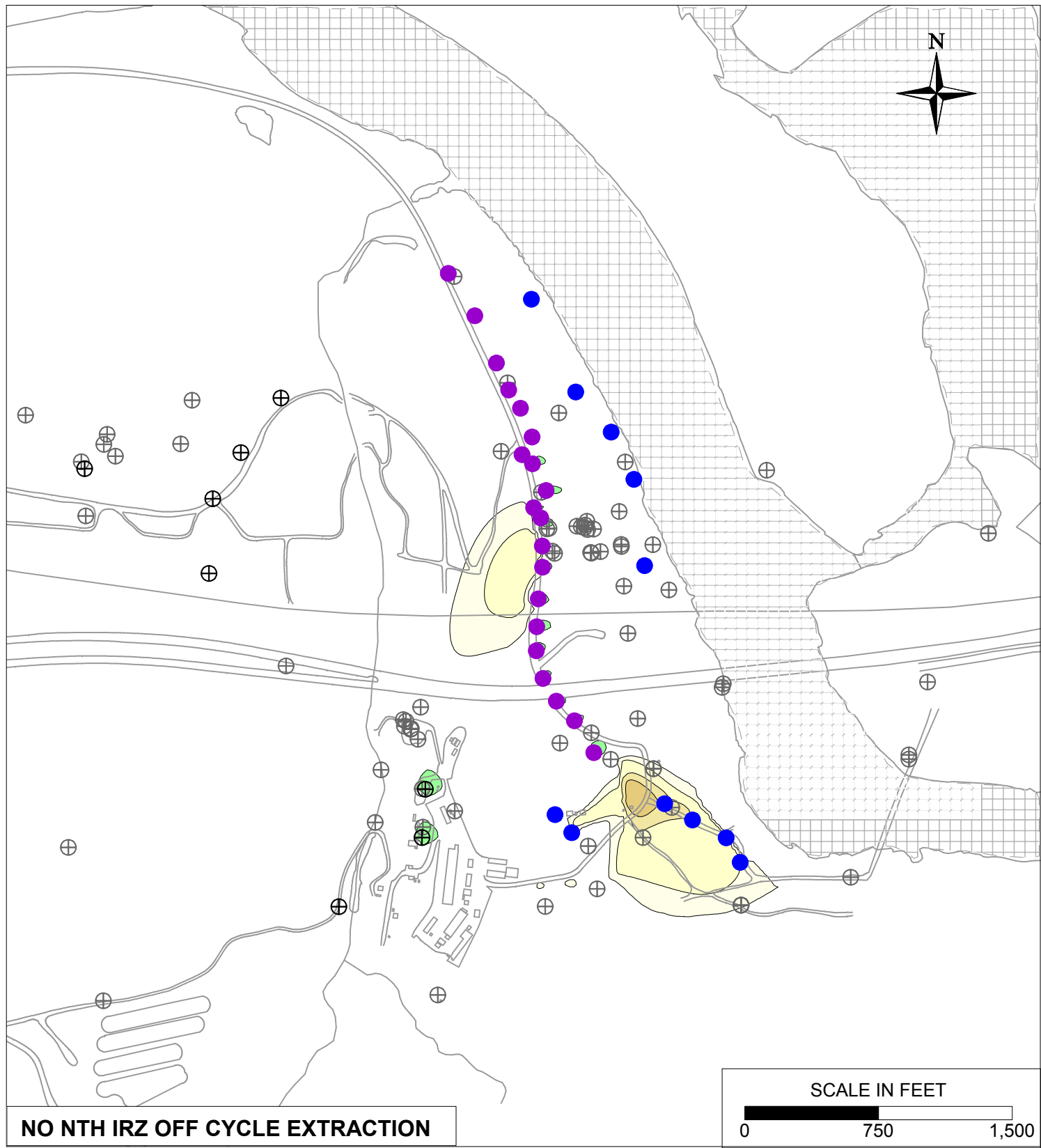
 **ARCADIS**

FIGURE  
10.9-1



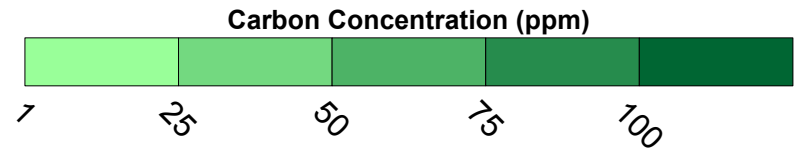
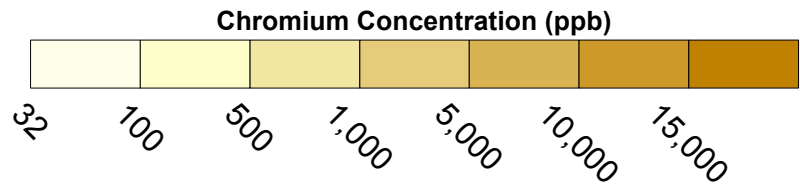


PG&E TOPOCK COMPRESSOR STATION NEEDLES, CALIFORNIA MODELING APPENDIX	
NTH IRZ OFF CYCLE EXTRACTION SENSITIVITY: SIMULATED HEXAVALENT CHROMIUM TRANSPORT RESULTS FOR YEAR 10 IN MODEL LAYER 4	
	FIGURE <b>10.9-2</b>



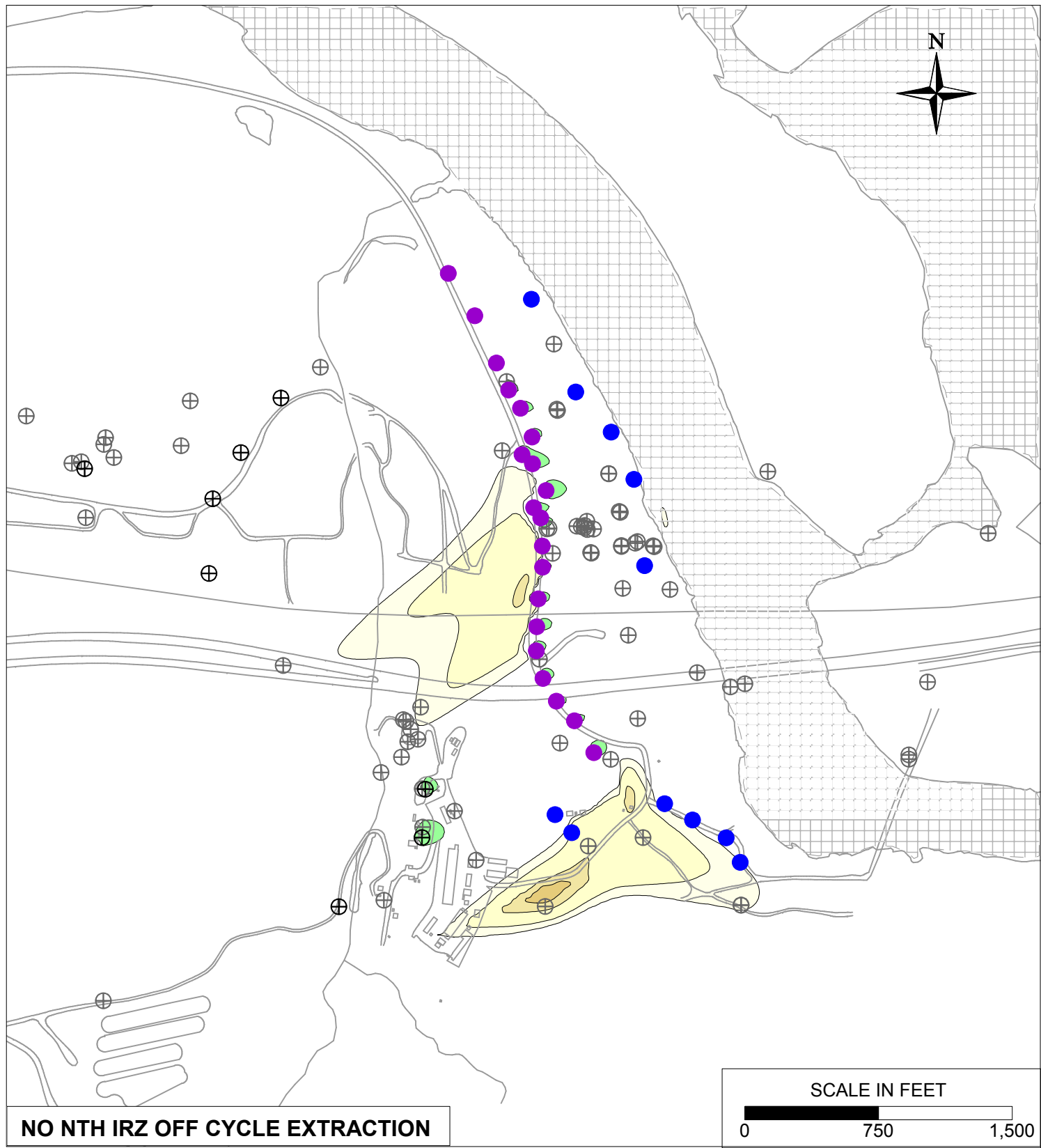
**LEGEND**

- IRZ WELLS
- UPGRADIENT INJECTION WELLS
- EXTRACTION WELLS
- MONITORING WELLS

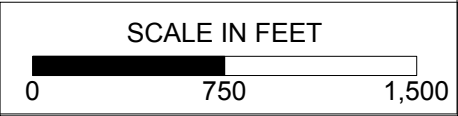


PG&E TOPOCK COMPRESSOR STATION NEEDLES, CALIFORNIA MODELING APPENDIX	
NTH IRZ OFF CYCLE EXTRACTION SENSITIVITY: SIMULATED HEXAVALENT CHROMIUM TRANSPORT RESULTS FOR YEAR 30 IN MODEL LAYER 2	
	FIGURE 10.9-3



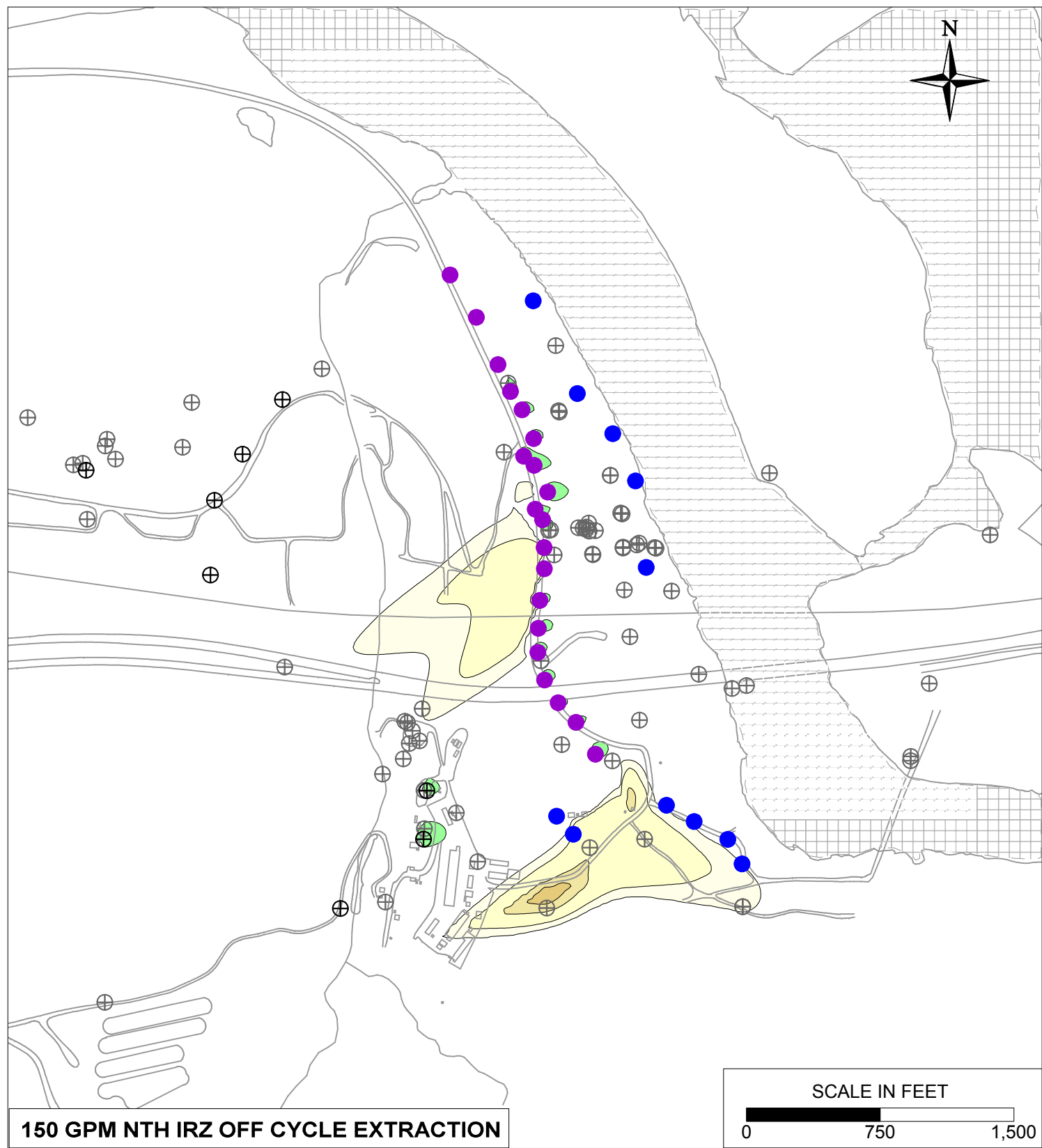
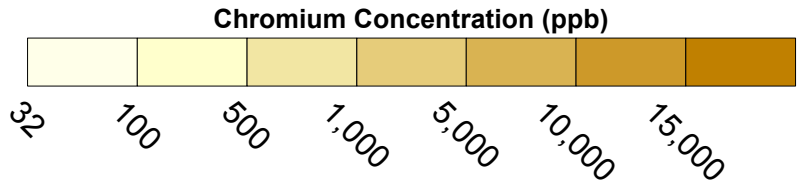


**NO NTH IRZ OFF CYCLE EXTRACTION**

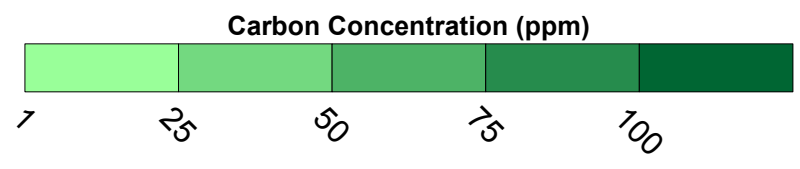
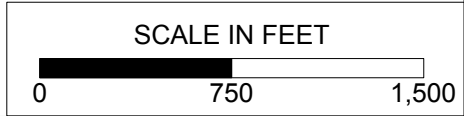


**LEGEND**

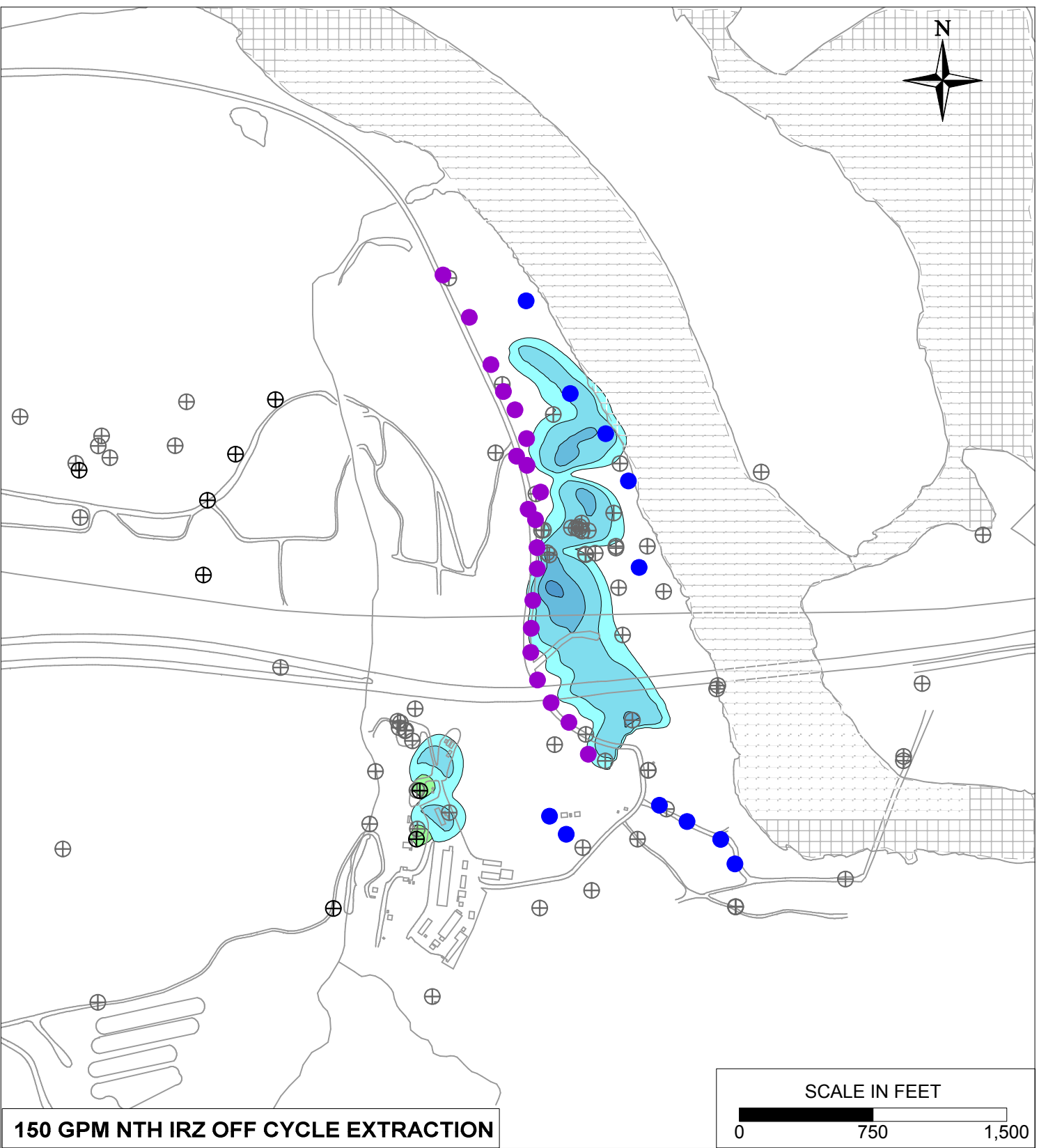
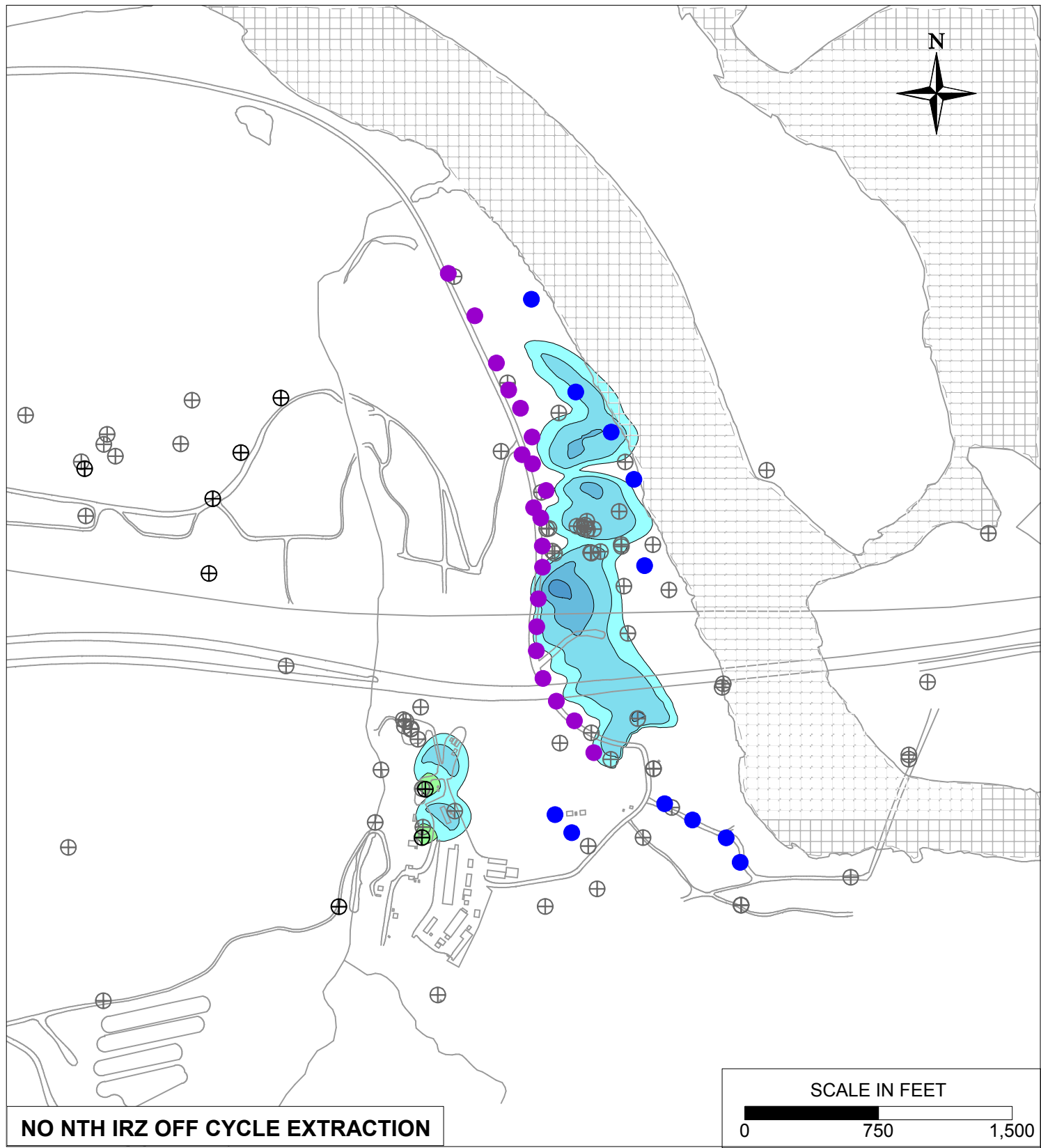
- IRZ WELLS
- ⊕ UPGRADIENT INJECTION WELLS
- EXTRACTION WELLS
- ⊕ MONITORING WELLS



**150 GPM NTH IRZ OFF CYCLE EXTRACTION**

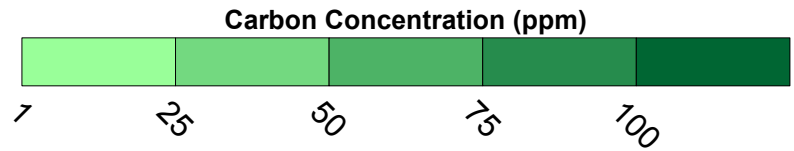
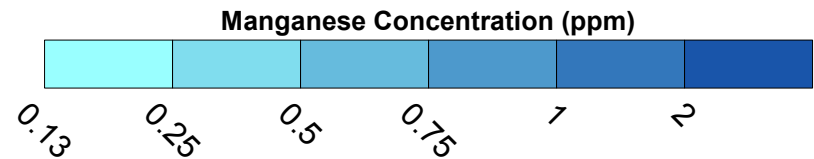


PG&E TOPOCK COMPRESSOR STATION NEEDLES, CALIFORNIA MODELING APPENDIX	
NTH IRZ OFF CYCLE EXTRACTION SENSITIVITY: SIMULATED HEXAVALENT CHROMIUM TRANSPORT RESULTS FOR YEAR 30 IN MODEL LAYER 4	
	FIGURE 10.9-4



**LEGEND**

- IRZ WELLS
- ⊕ UPGRADIENT INJECTION WELLS
- EXTRACTION WELLS
- ⊕ MONITORING WELLS



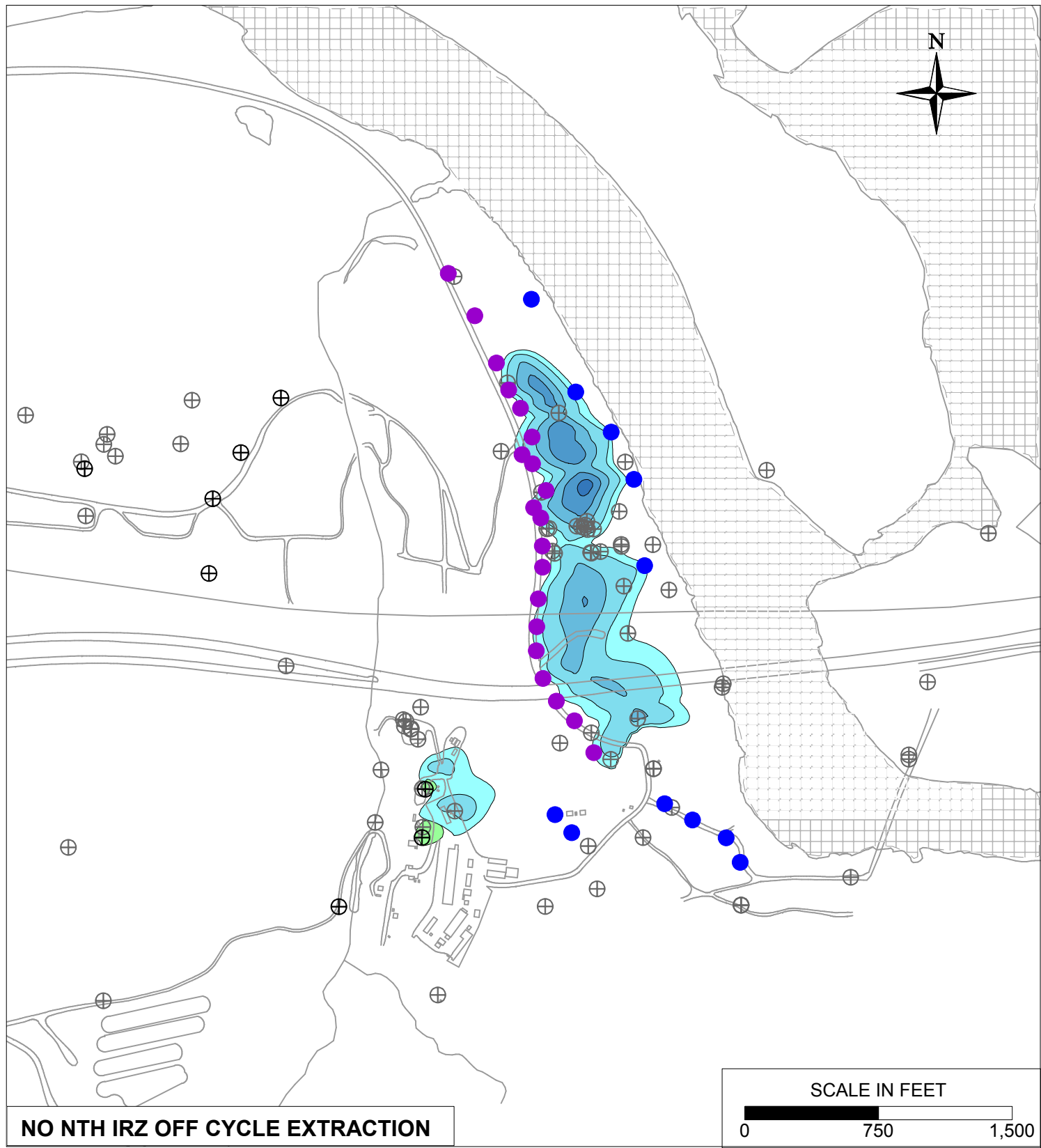
PG&E  
TOPOCK COMPRESSOR STATION  
NEEDLES, CALIFORNIA  
MODELING APPENDIX

NTH IRZ OFF CYCLE EXTRACTION SENSITIVITY:  
SIMULATED MANGANESE TRANSPORT RESULTS  
FOR YEAR 10 IN MODEL LAYER 2

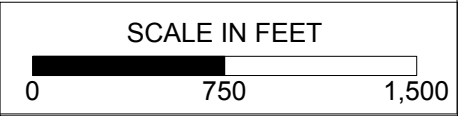


FIGURE

10.9-5

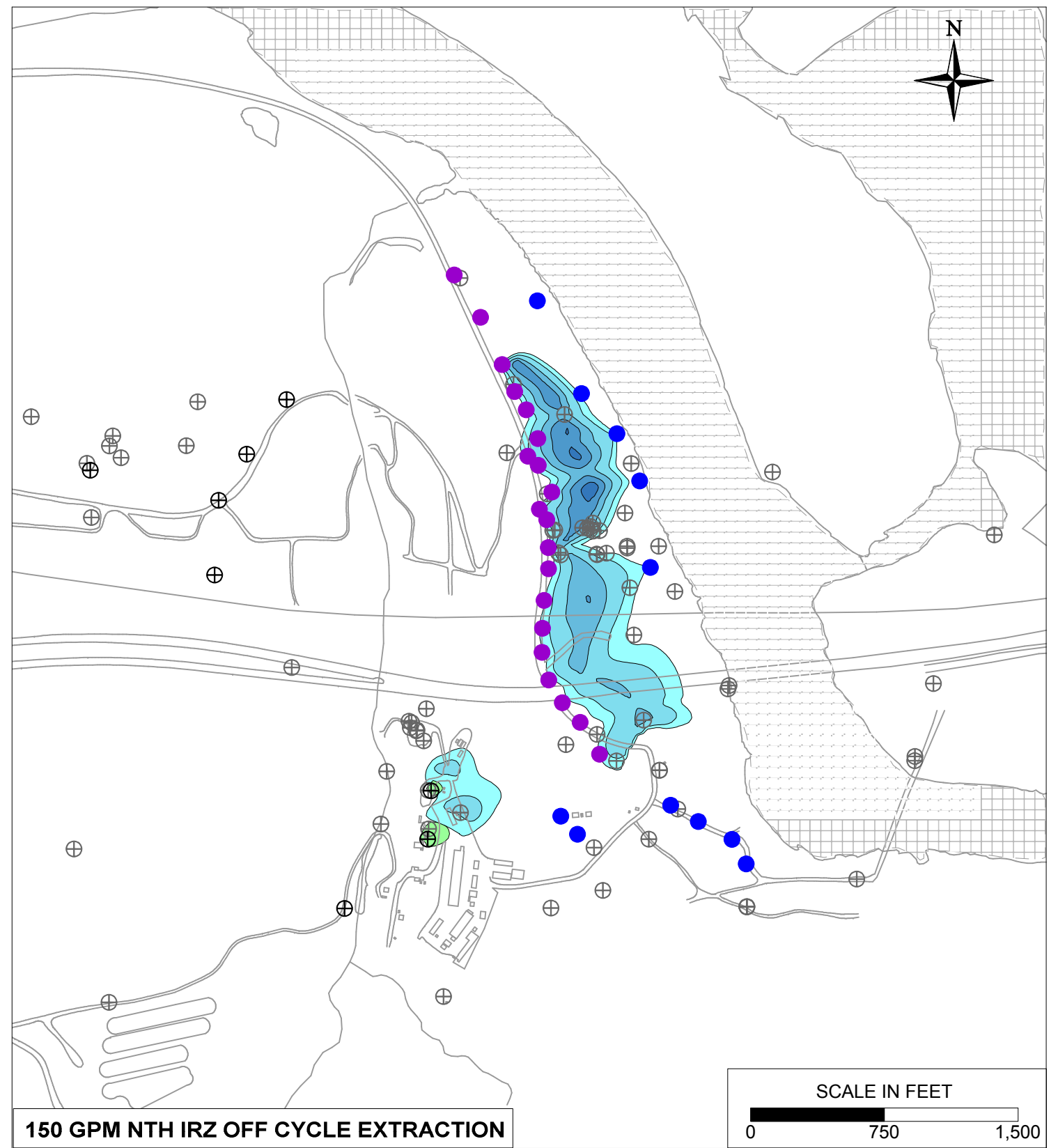
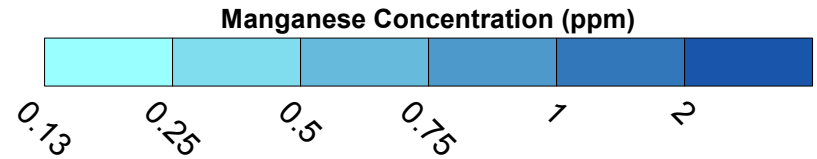


**NO NTH IRZ OFF CYCLE EXTRACTION**

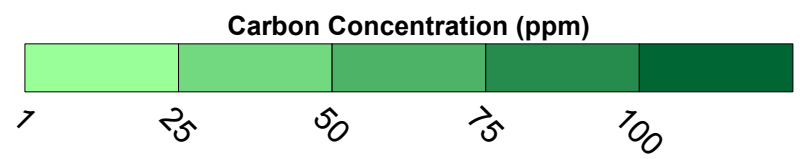
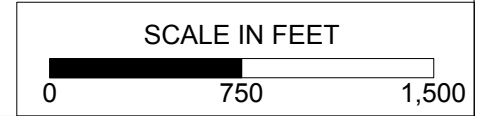


**LEGEND**

- IRZ WELLS
- ⊕ UPGRADIENT INJECTION WELLS
- EXTRACTION WELLS
- ⊕ MONITORING WELLS

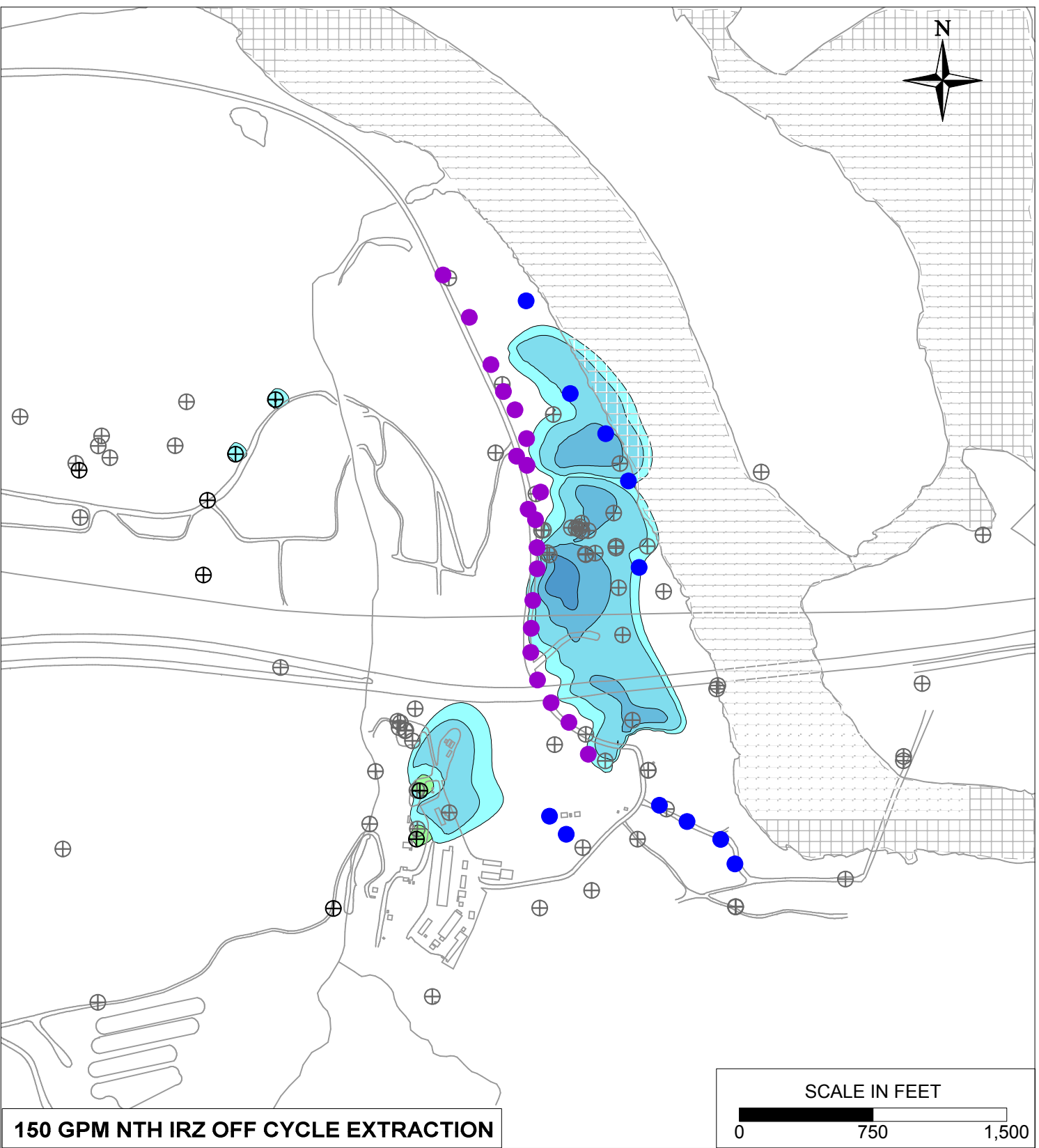
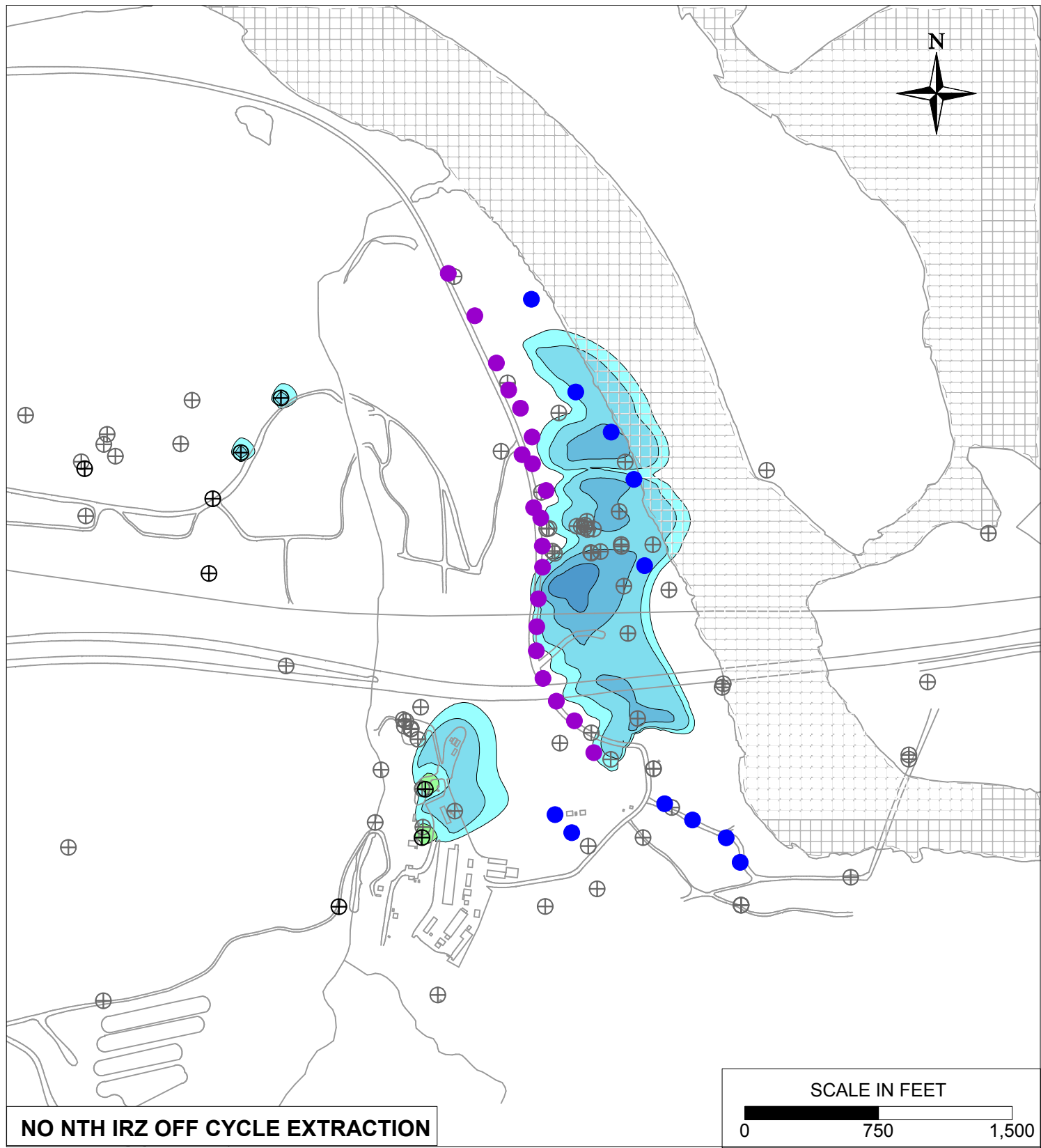


**150 GPM NTH IRZ OFF CYCLE EXTRACTION**



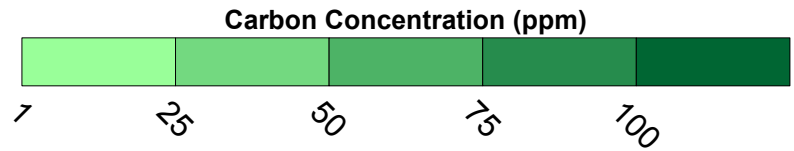
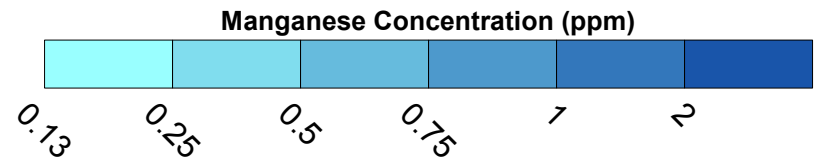
PG&E TOPOCK COMPRESSOR STATION NEEDLES, CALIFORNIA MODELING APPENDIX	
NTH IRZ OFF CYCLE EXTRACTION SENSITIVITY: SIMULATED MANGANESE TRANSPORT RESULTS FOR YEAR 10 IN MODEL LAYER 4	
	FIGURE <b>10.9-6</b>





**LEGEND**

- IRZ WELLS
- ⊕ UPGRADIENT INJECTION WELLS
- EXTRACTION WELLS
- ⊕ MONITORING WELLS

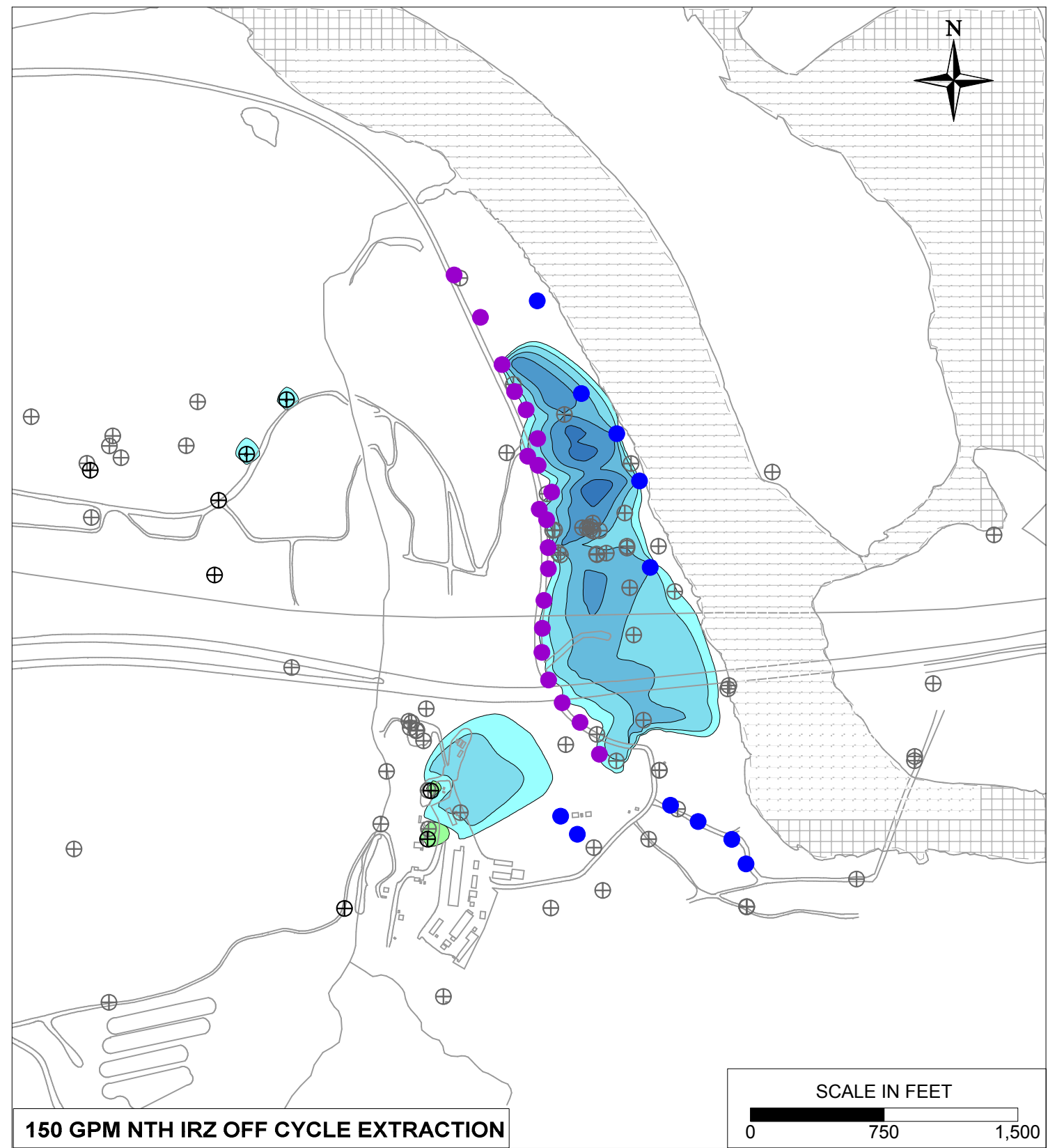
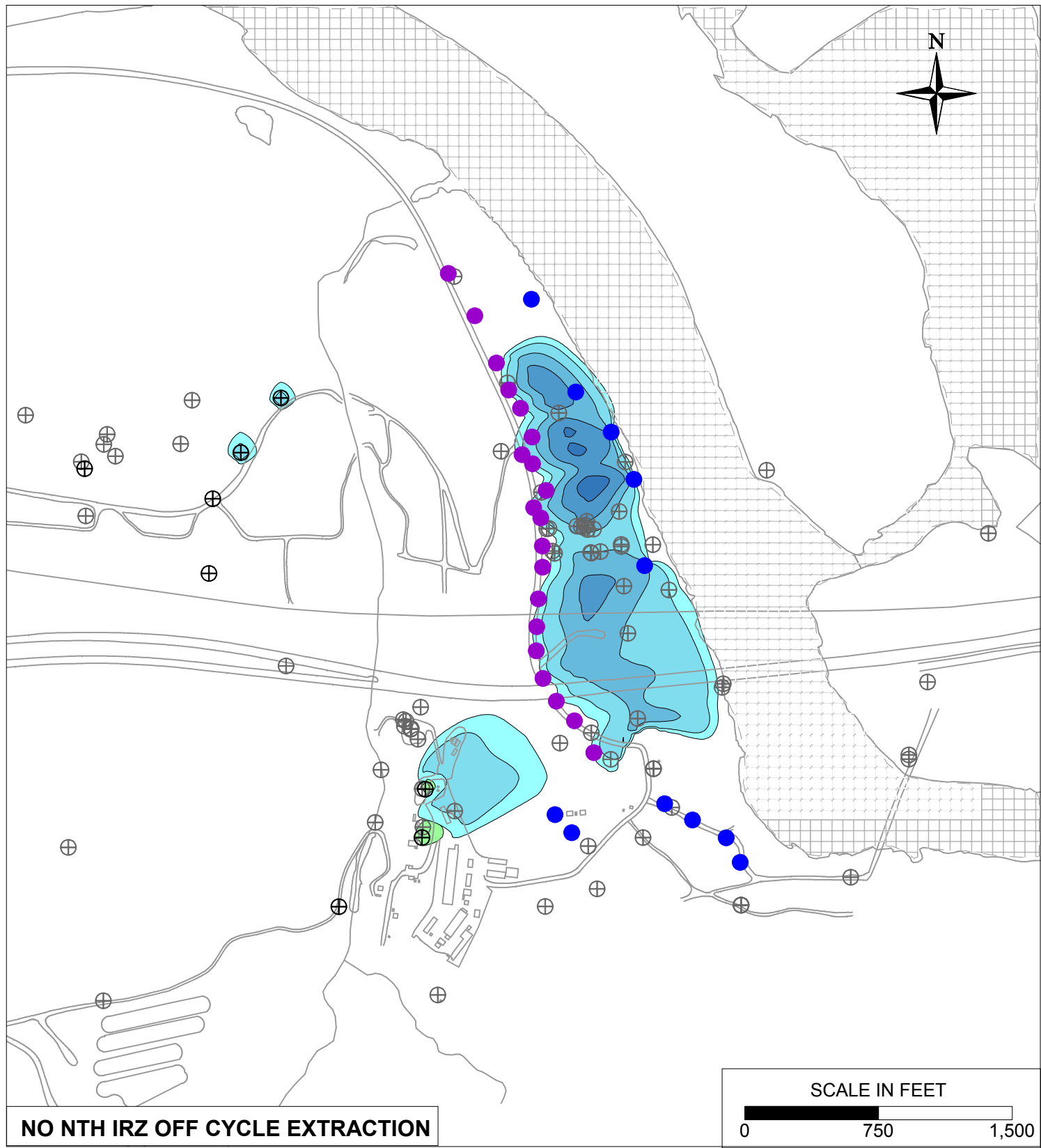


PG&E  
TOPOCK COMPRESSOR STATION  
NEEDLES, CALIFORNIA  
MODELING APPENDIX

NTH IRZ OFF CYCLE EXTRACTION SENSITIVITY:  
SIMULATED MANGANESE TRANSPORT RESULTS  
FOR YEAR 30 IN MODEL LAYER 2

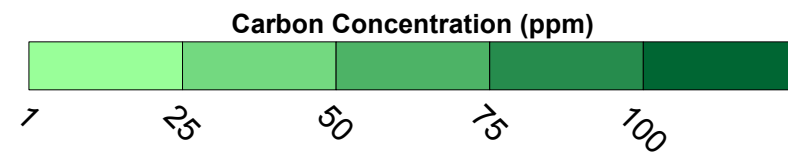
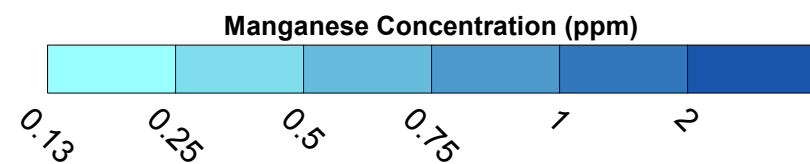


FIGURE  
10.9-7



**LEGEND**

- IRZ WELLS
- ⊕ UPGRADIENT INJECTION WELLS
- EXTRACTION WELLS
- ⊕ MONITORING WELLS



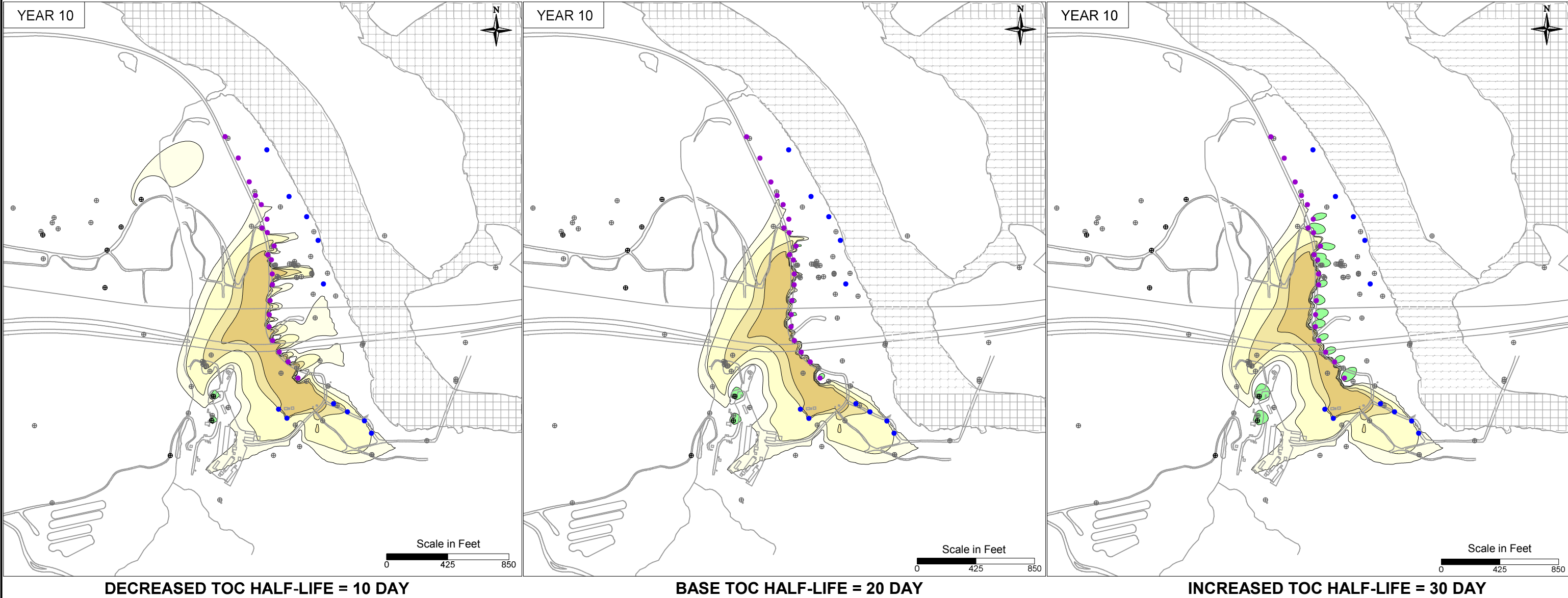
PG&E  
TOPOCK COMPRESSOR STATION  
NEEDLES, CALIFORNIA  
MODELING APPENDIX

NTH IRZ OFF CYCLE EXTRACTION SENSITIVITY:  
SIMULATED MANGANESE TRANSPORT RESULTS  
FOR YEAR 30 IN MODEL LAYER 4



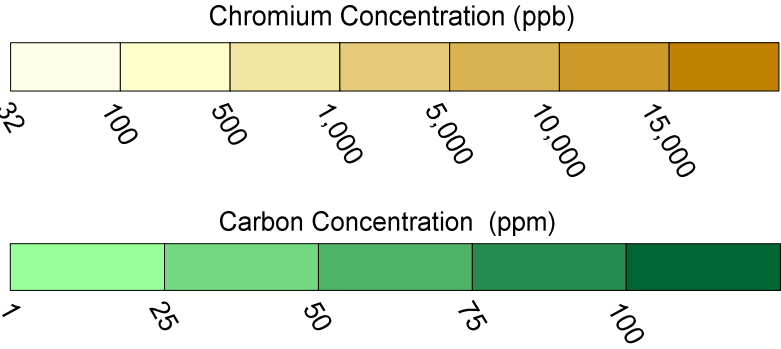
FIGURE  
10.9-8

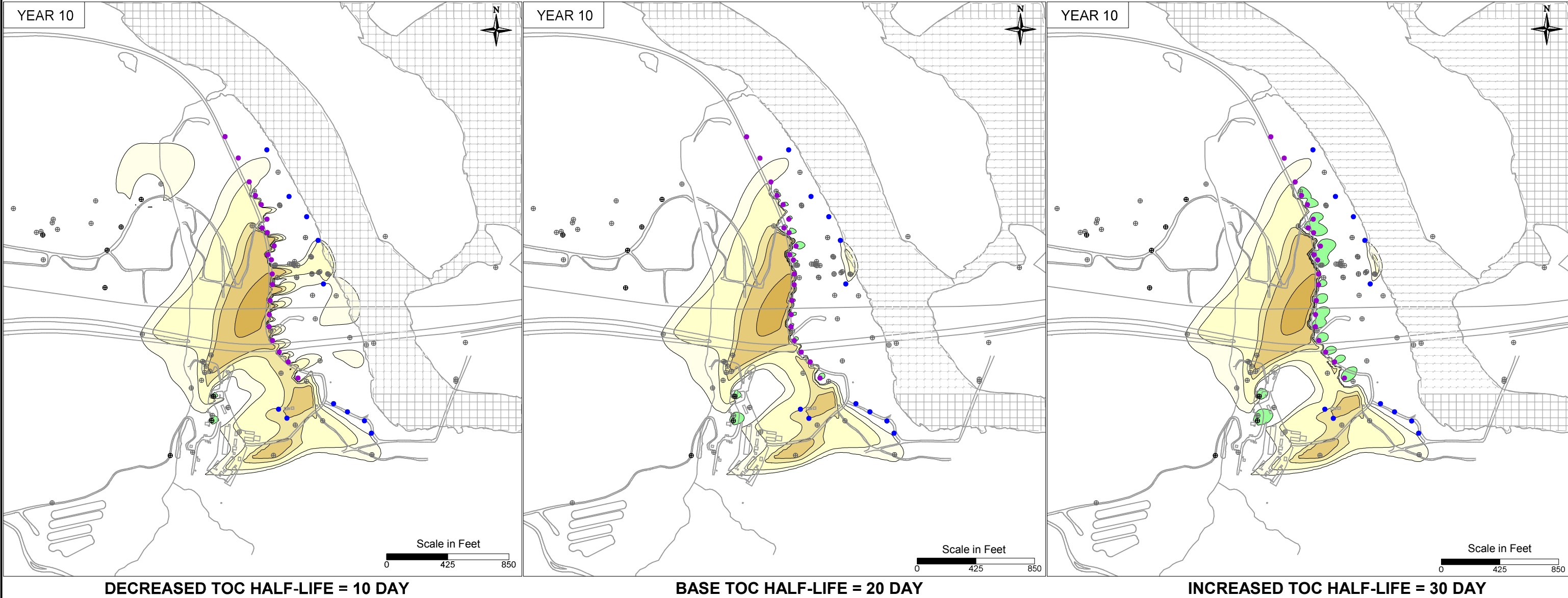




**LEGEND**

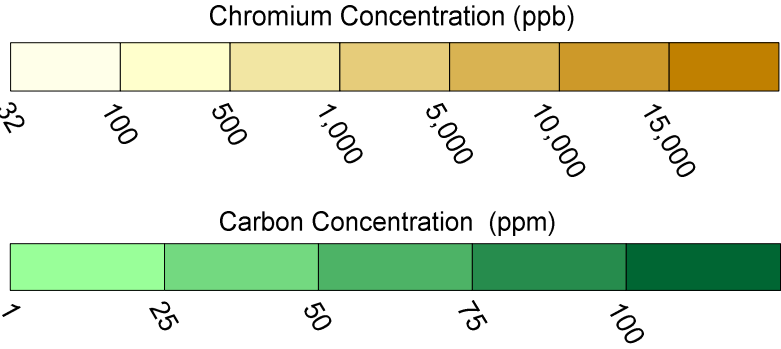
- IRZ WELLS
- UPGRADIENT INJECTION WELLS
- EXTRACTION WELLS
- MONITORING WELLS

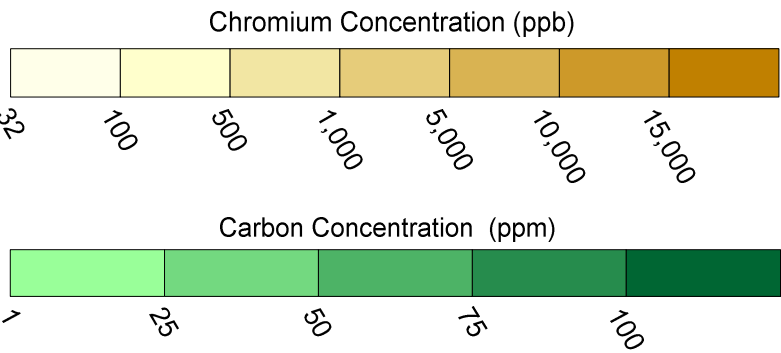
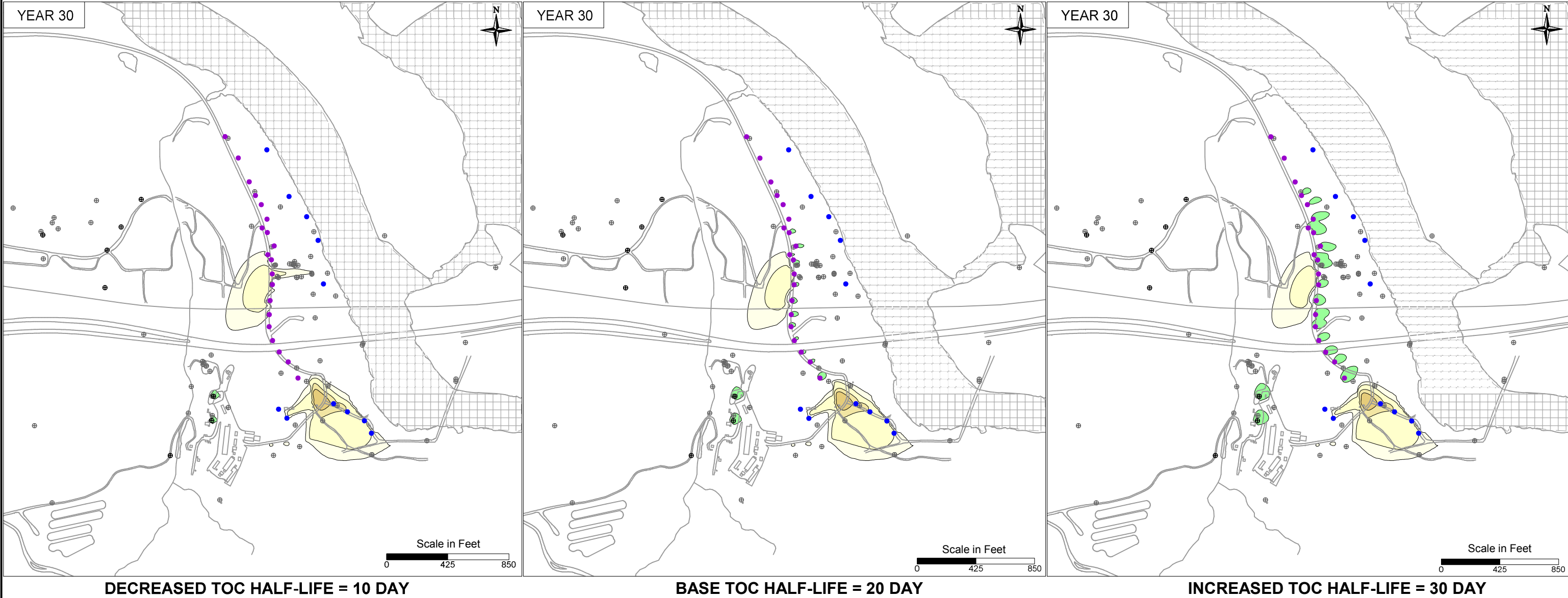




**LEGEND**

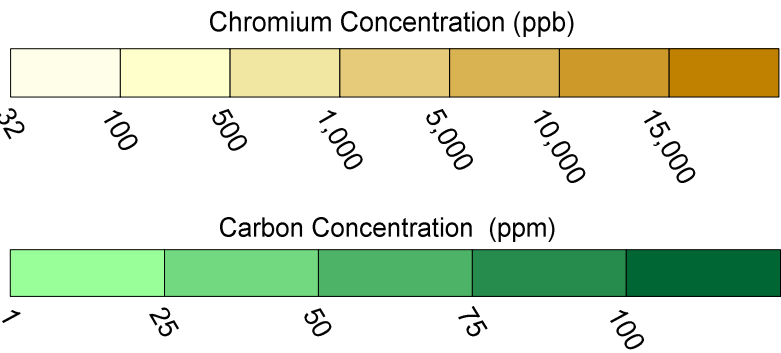
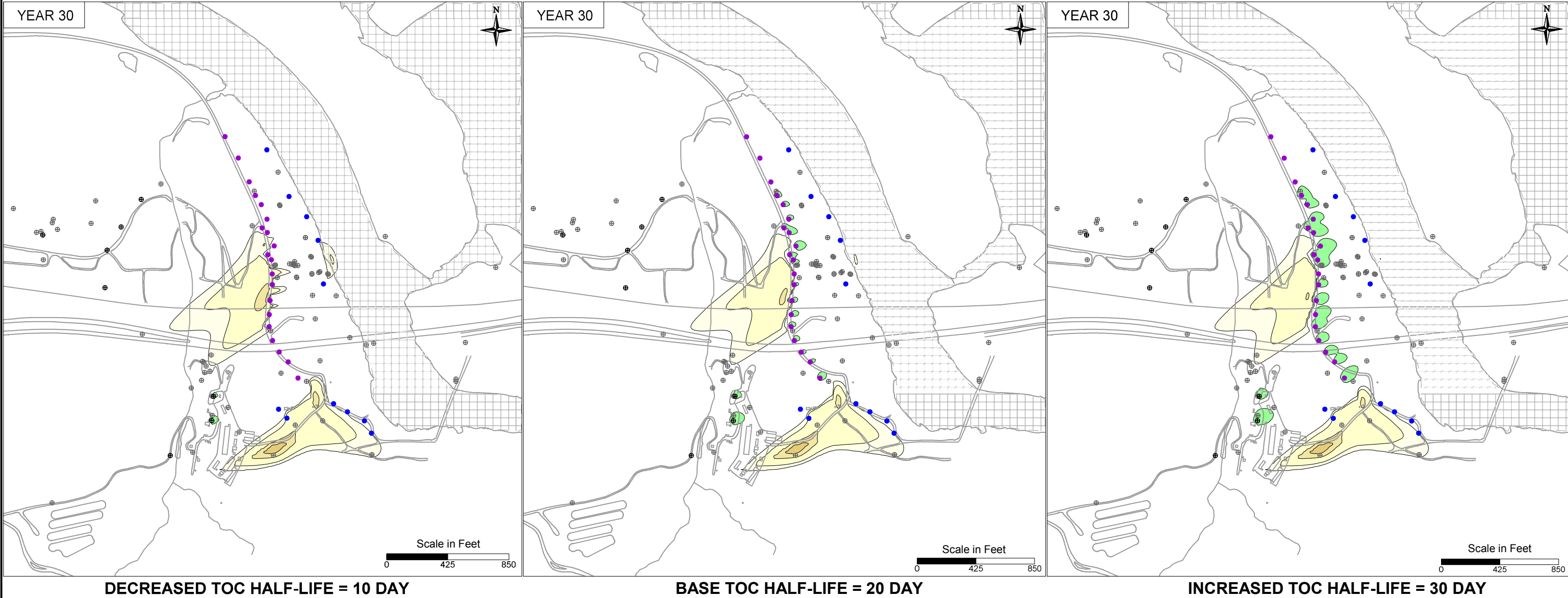
- IRZ WELLS
- ⊕ UPGRADIENT INJECTION WELLS
- EXTRACTION WELLS
- ⊕ MONITORING WELLS





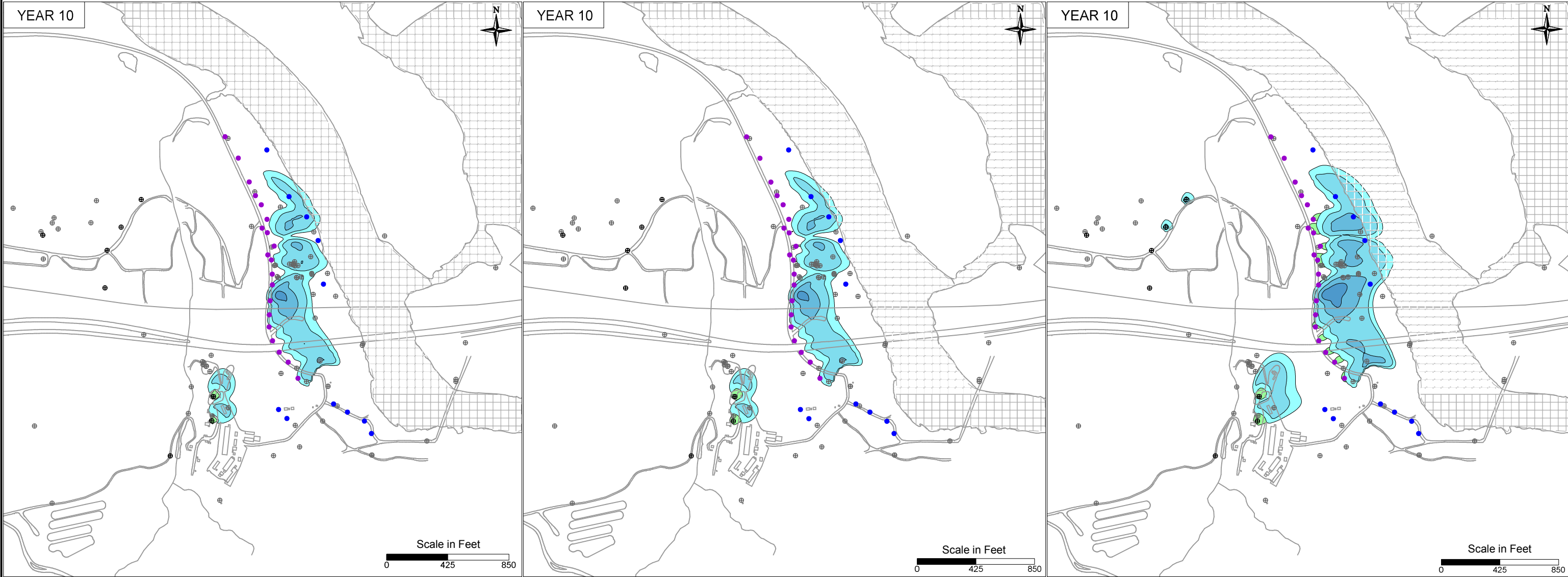
- LEGEND**
- IRZ WELLS
  - ⊕ UPGRADIENT INJECTION WELLS
  - EXTRACTION WELLS
  - ⊕ MONITORING WELLS





- LEGEND**
- IRZ WELLS
  - ⊕ UPGRADIENT INJECTION WELLS
  - EXTRACTION WELLS
  - ⊕ MONITORING WELLS





DECREASED TOC HALF-LIFE = 10 DAY

BASE TOC HALF-LIFE = 20 DAY

INCREASED TOC HALF-LIFE = 30 DAY

**LEGEND**

- IRZ WELLS
- ⊕ UPGRADIENT INJECTION WELLS
- EXTRACTION WELLS
- ⊕ MONITORING WELLS

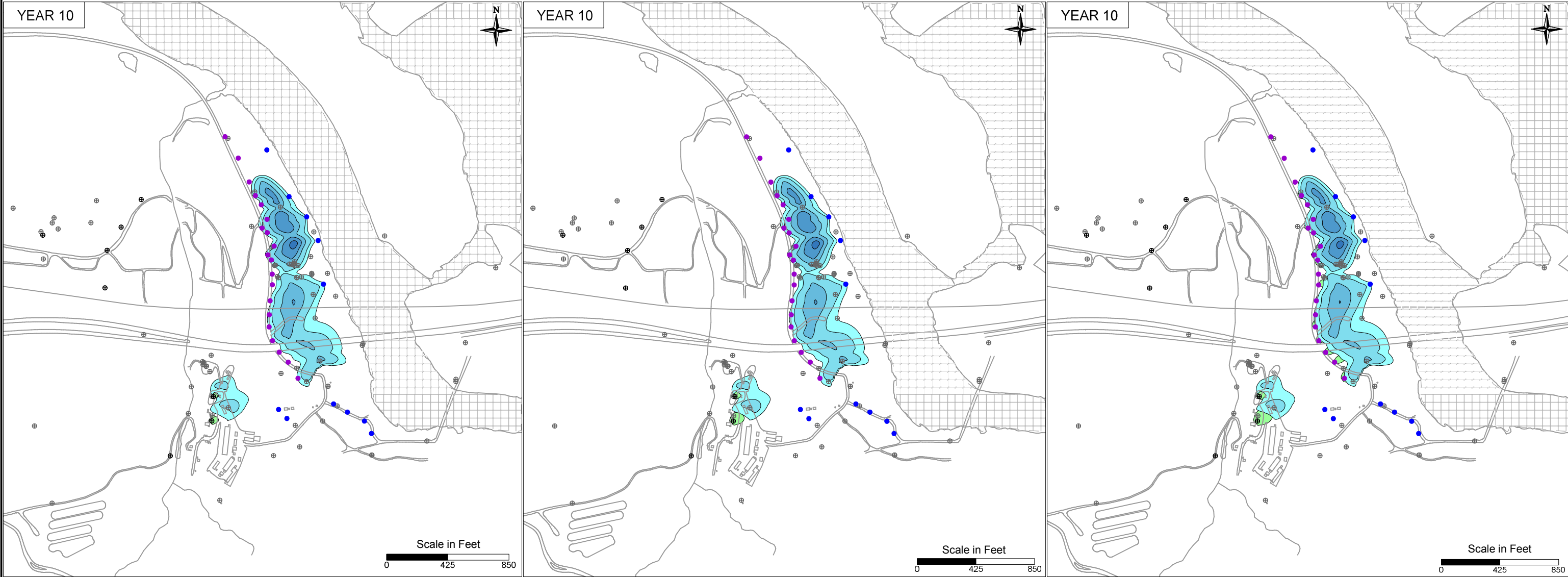
Manganese Concentration (ppm)



Carbon Concentration (ppm)



PG&E TOPOCK COMPRESSOR STATION NEEDLES, CALIFORNIA MODELING APPENDIX	
TOC HALF-LIFE SENSITIVITY: SIMULATED MANGANESE TRANSPORT RESULTS FOR YEAR 10 IN MODEL LAYER 2	
	FIGURE <b>10.10-5</b>



DECREASED TOC HALF-LIFE = 10 DAY

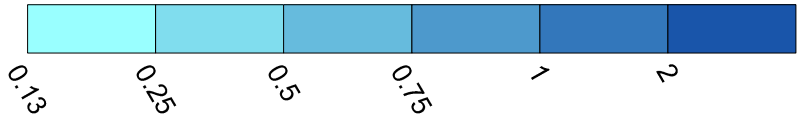
BASE TOC HALF-LIFE = 20 DAY

INCREASED TOC HALF-LIFE = 30 DAY

**LEGEND**

- IRZ WELLS
- ⊕ UPGRADIENT INJECTION WELLS
- EXTRACTION WELLS
- ⊕ MONITORING WELLS

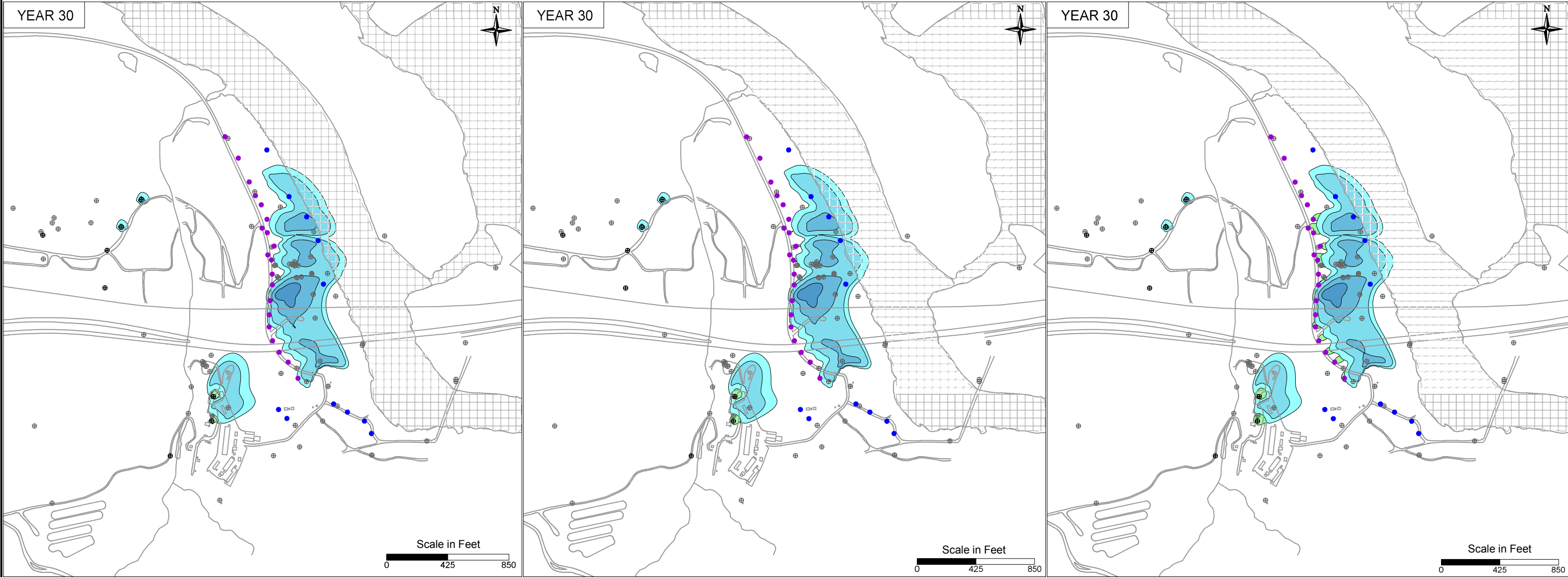
Manganese Concentration (ppm)



Carbon Concentration (ppm)



PG&E TOPOCK COMPRESSOR STATION NEEDLES, CALIFORNIA MODELING APPENDIX	
TOC HALF-LIFE SENSITIVITY: SIMULATED MANGANESE TRANSPORT RESULTS FOR YEAR 10 IN MODEL LAYER 4	
	FIGURE 10.10-6



DECREASED TOC HALF-LIFE = 10 DAY

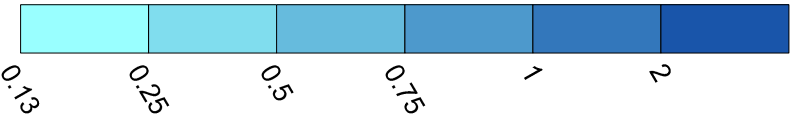
BASE TOC HALF-LIFE = 20 DAY

INCREASED TOC HALF-LIFE = 30 DAY

**LEGEND**

- IRZ WELLS
- ⊕ UPGRADIENT INJECTION WELLS
- EXTRACTION WELLS
- ⊕ MONITORING WELLS

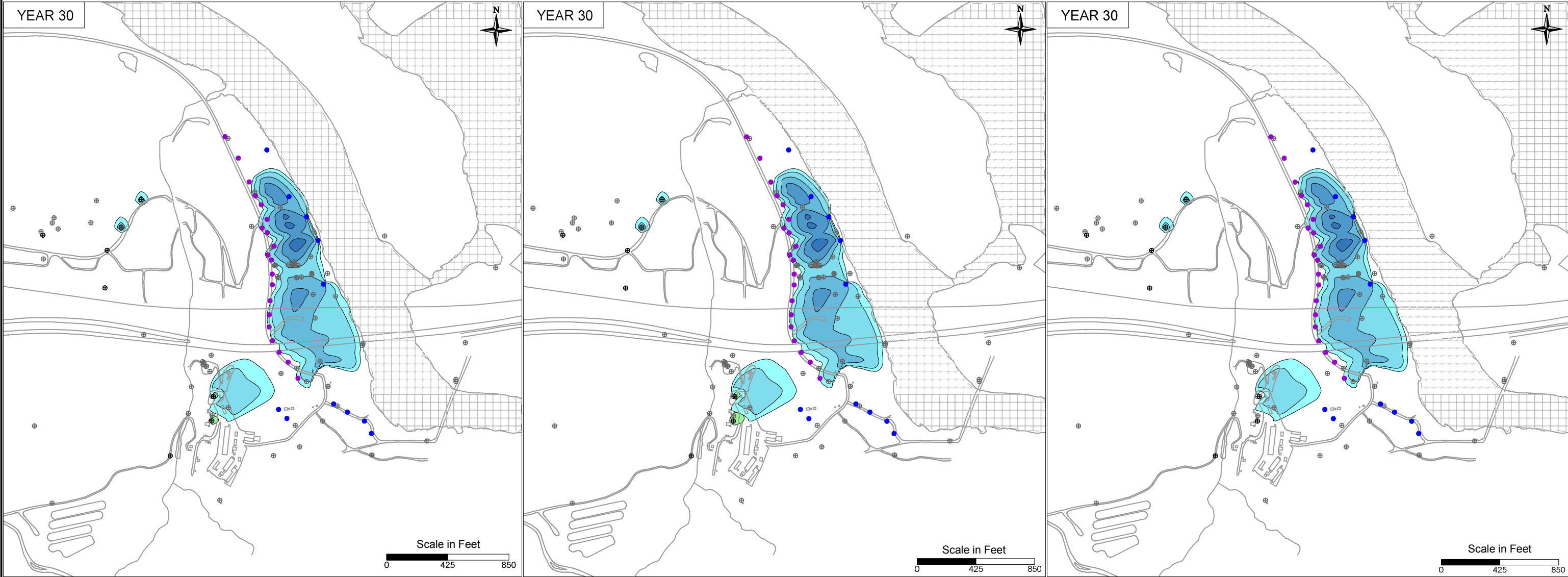
Manganese Concentration (ppm)



Carbon Concentration (ppm)



PG&E TOPOCK COMPRESSOR STATION NEEDLES, CALIFORNIA MODELING APPENDIX	
TOC HALF-LIFE SENSITIVITY: SIMULATED MANGANESE TRANSPORT RESULTS FOR YEAR 30 IN MODEL LAYER 2	
	FIGURE 10.10-7



DECREASED TOC HALF-LIFE = 10 DAY

BASE TOC HALF-LIFE = 20 DAY

INCREASED TOC HALF-LIFE = 30 DAY

**LEGEND**

- IRZ WELLS
- ⊕ UPGRADIENT INJECTION WELLS
- EXTRACTION WELLS
- ⊕ MONITORING WELLS

Manganese Concentration (ppm)

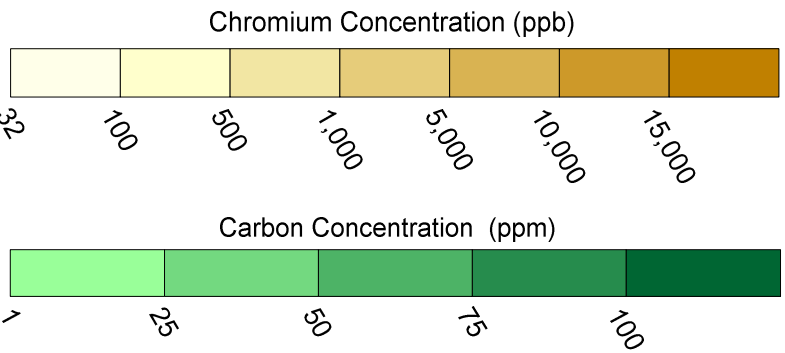
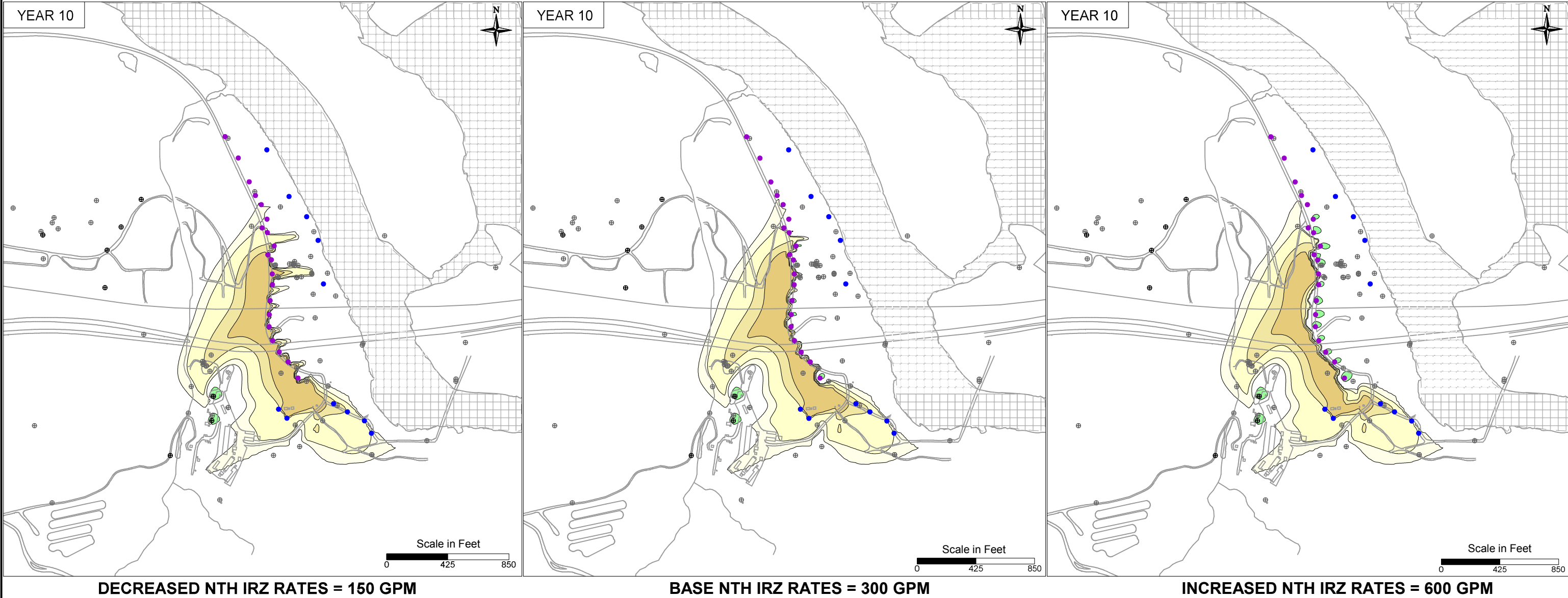


Carbon Concentration (ppm)

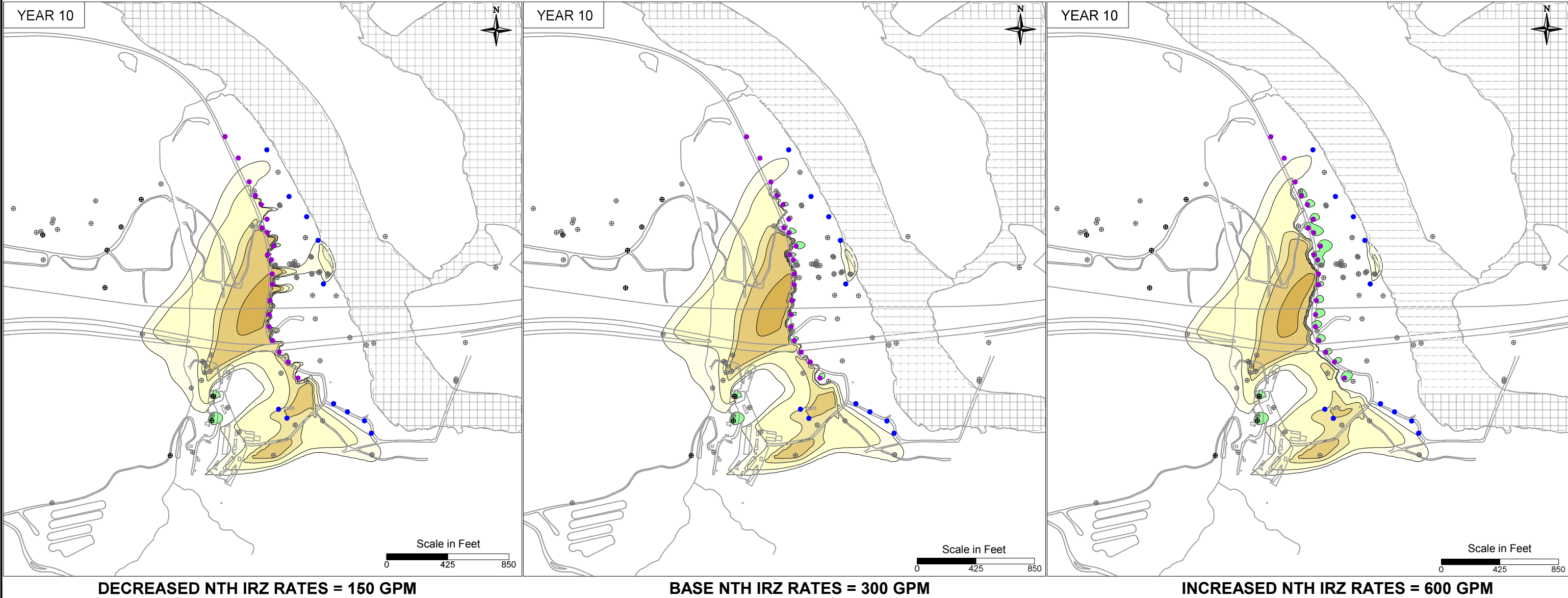


PG&E TOPOCK COMPRESSOR STATION NEEDLES, CALIFORNIA MODELING APPENDIX	
TOC HALF-LIFE SENSITIVITY: SIMULATED MANGANESE TRANSPORT RESULTS FOR YEAR 30 IN MODEL LAYER 4	
	FIGURE 10.10-8



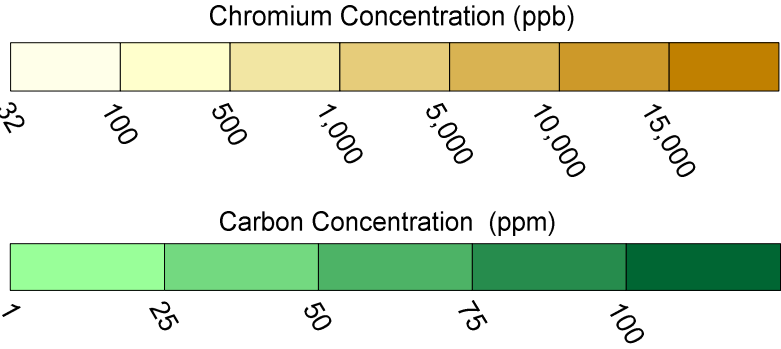


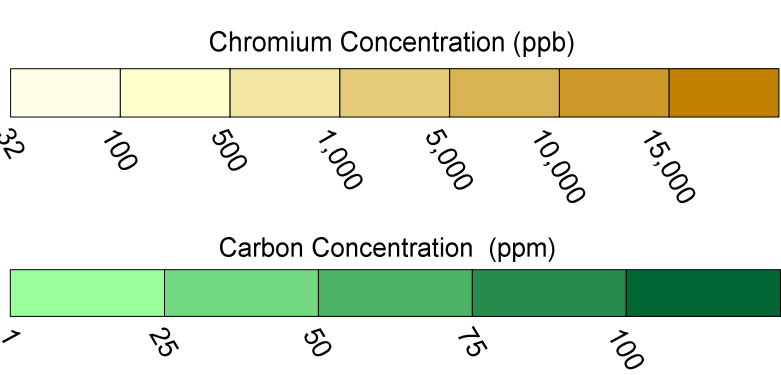
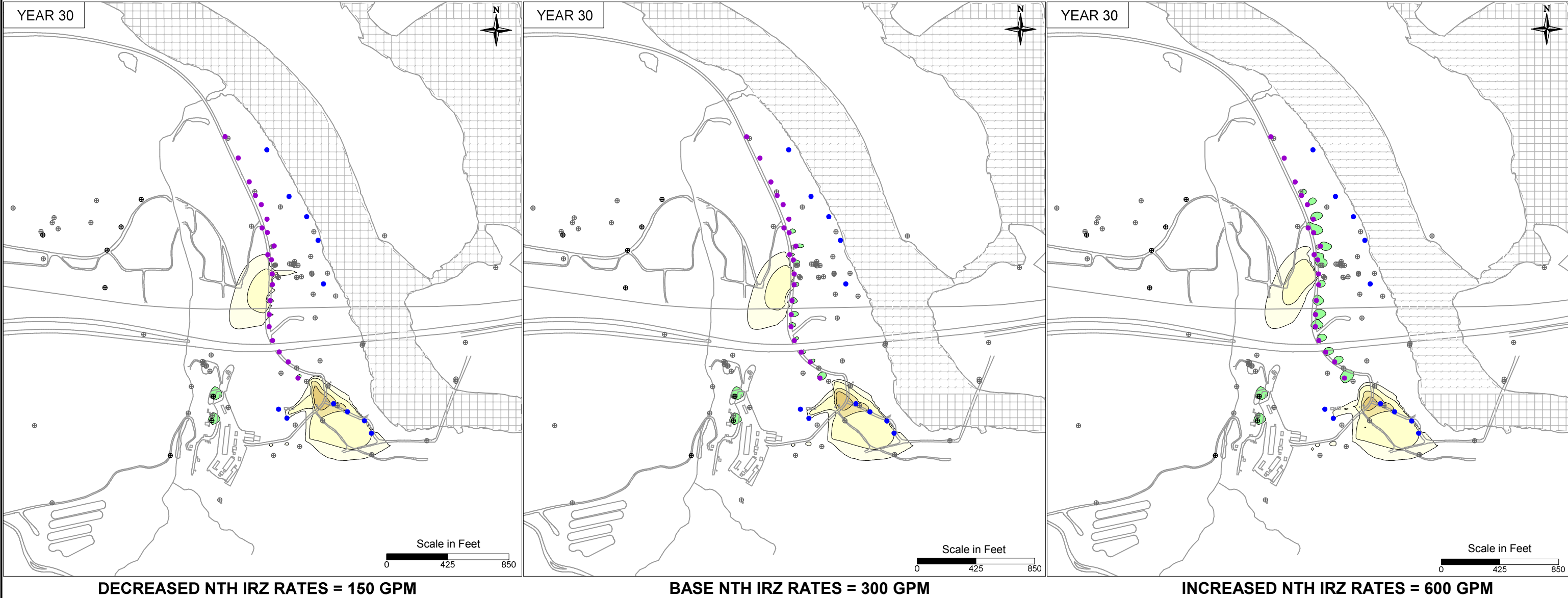
- LEGEND**
- IRZ WELLS
  - UPGRADIENT INJECTION WELLS
  - EXTRACTION WELLS
  - MONITORING WELLS



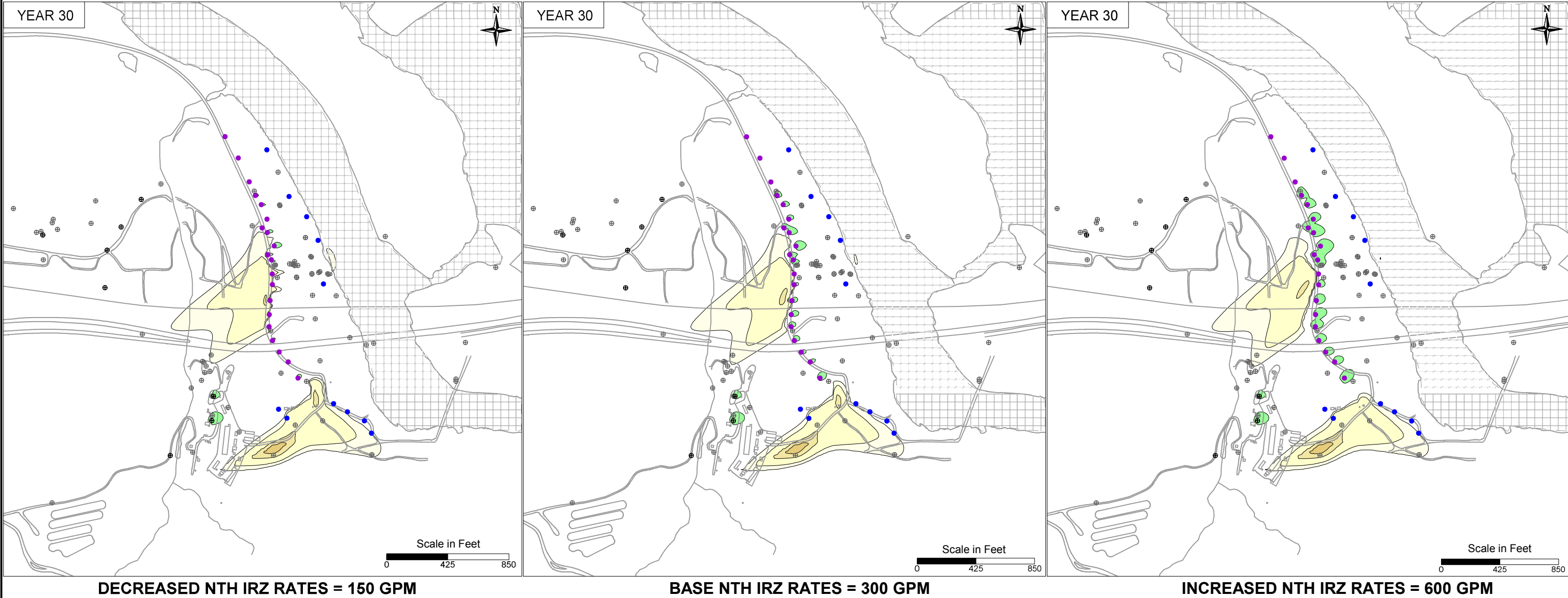
**LEGEND**

- IRZ WELLS
- UPGRADIENT INJECTION WELLS
- EXTRACTION WELLS
- MONITORING WELLS



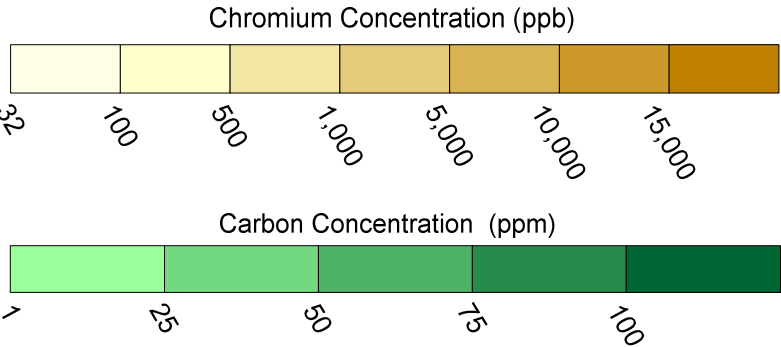


- LEGEND**
- IRZ WELLS
  - ⊕ UPGRADIENT INJECTION WELLS
  - EXTRACTION WELLS
  - ⊕ MONITORING WELLS

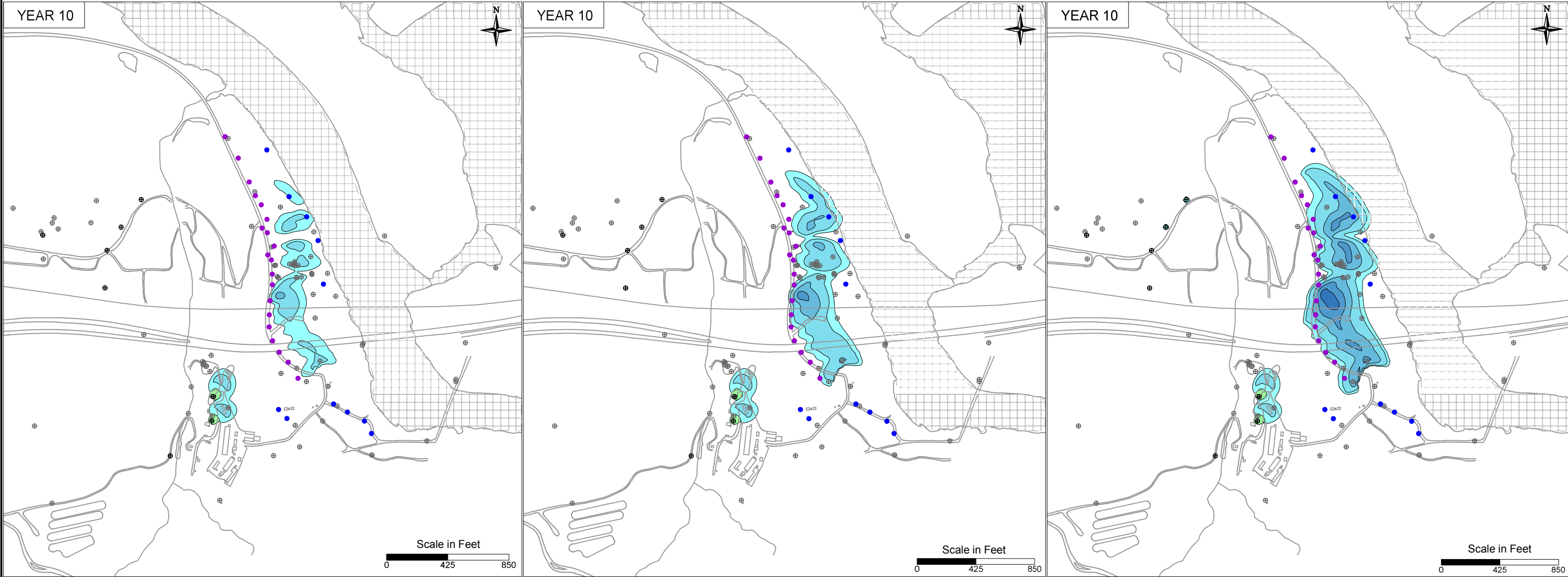


**LEGEND**

- IRZ WELLS
- UPGRADIENT INJECTION WELLS
- EXTRACTION WELLS
- MONITORING WELLS







DECREASED NTH IRZ RATES = 150 GPM

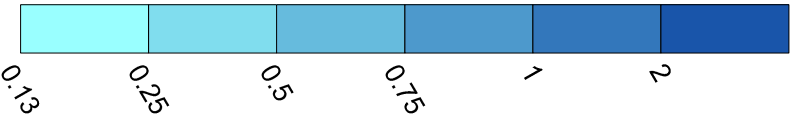
BASE NTH IRZ RATES = 300 GPM

INCREASED NTH IRZ RATES = 600 GPM

**LEGEND**

- IRZ WELLS
- ⊕ UPGRADIENT INJECTION WELLS
- EXTRACTION WELLS
- ⊕ MONITORING WELLS

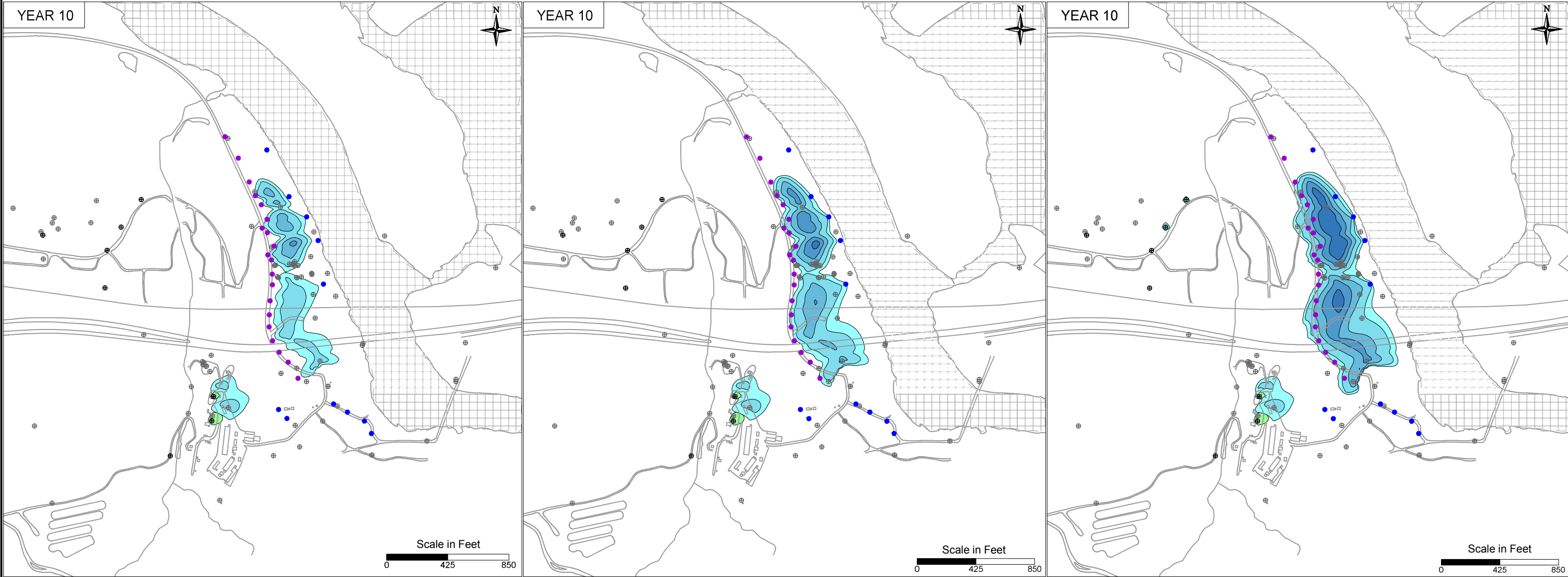
Manganese Concentration (ppm)



Carbon Concentration (ppm)



PG&E TOPOCK COMPRESSOR STATION NEEDLES, CALIFORNIA MODELING APPENDIX	
NTH IRZ RATE SENSITIVITY: SIMULATED MANGANESE TRANSPORT RESULTS FOR YEAR 10 IN MODEL LAYER 2	
	FIGURE 10.11-5



DECREASED NTH IRZ RATES = 150 GPM

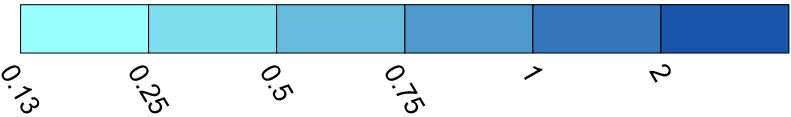
BASE NTH IRZ RATES = 300 GPM

INCREASED NTH IRZ RATES = 600 GPM

**LEGEND**

- IRZ WELLS
- ⊕ UPGRADIENT INJECTION WELLS
- EXTRACTION WELLS
- ⊕ MONITORING WELLS

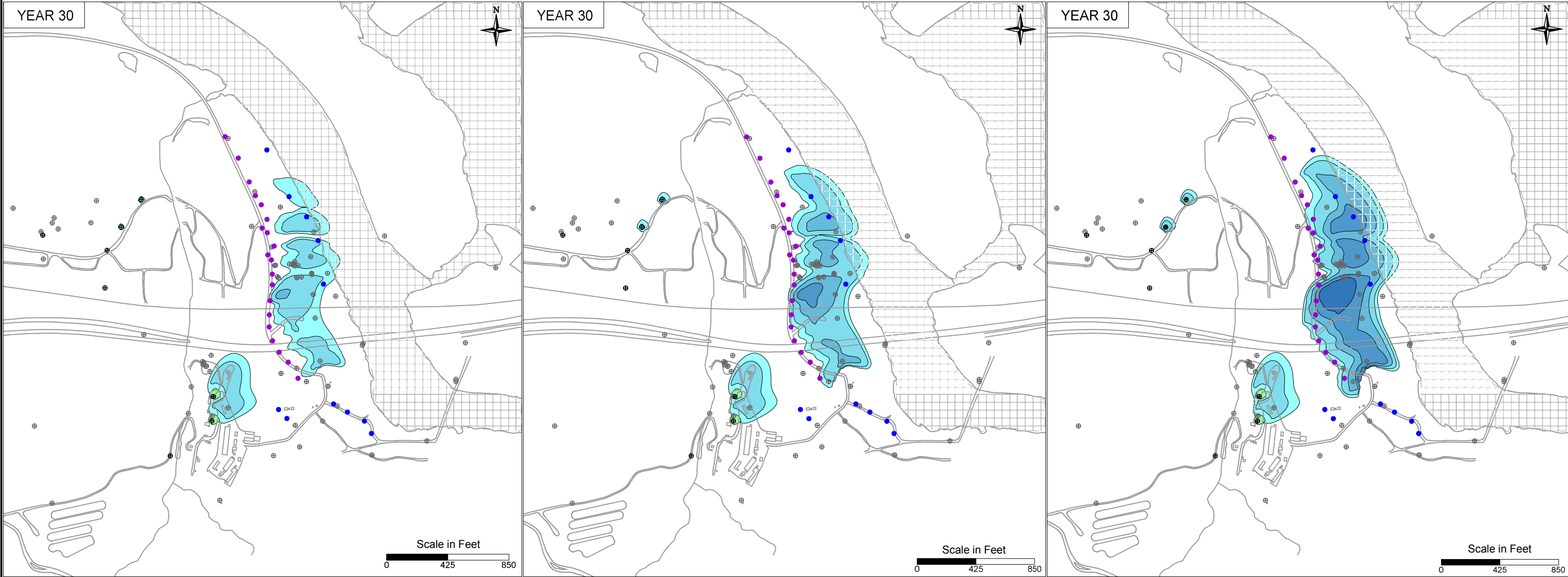
Manganese Concentration (ppm)



Carbon Concentration (ppm)



PG&E TOPOCK COMPRESSOR STATION NEEDLES, CALIFORNIA MODELING APPENDIX	
NTH IRZ RATE SENSITIVITY: SIMULATED MANGANESE TRANSPORT RESULTS FOR YEAR 10 IN MODEL LAYER 4	
	FIGURE <b>10.11-6</b>



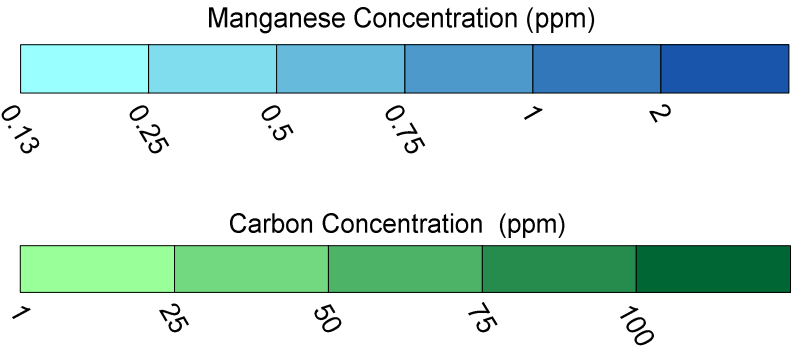
DECREASED NTH IRZ RATES = 150 GPM

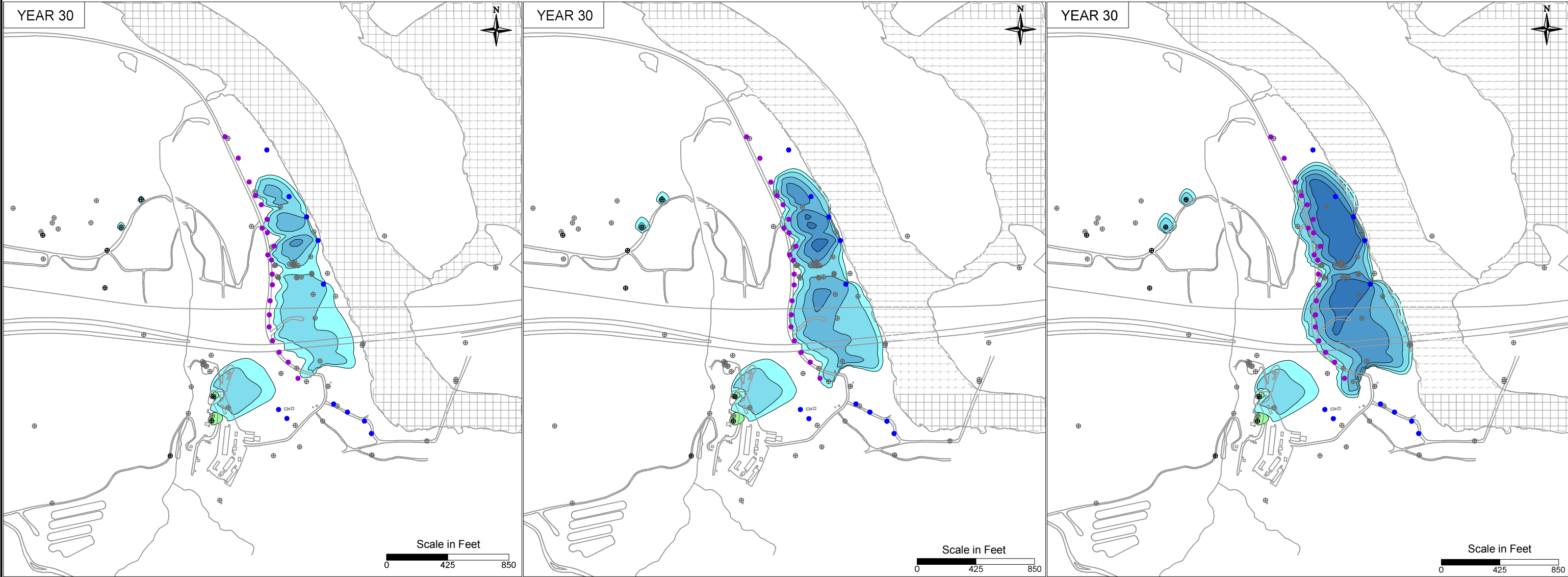
BASE NTH IRZ RATES = 300 GPM

INCREASED NTH IRZ RATES = 600 GPM

**LEGEND**

- IRZ WELLS
- ⊕ UPGRADIENT INJECTION WELLS
- EXTRACTION WELLS
- ⊕ MONITORING WELLS





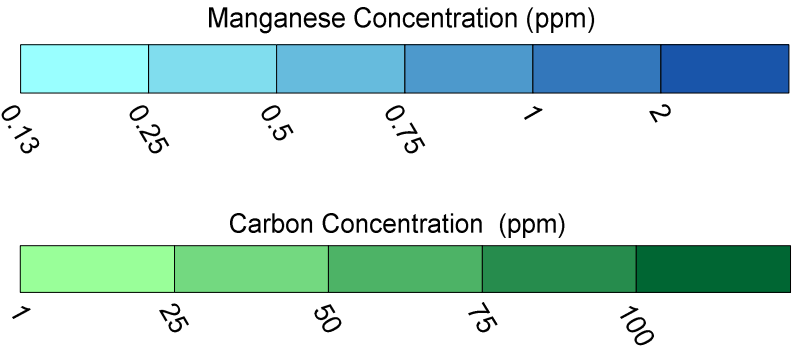
DECREASED NTH IRZ RATES = 150 GPM

BASE NTH IRZ RATES = 300 GPM

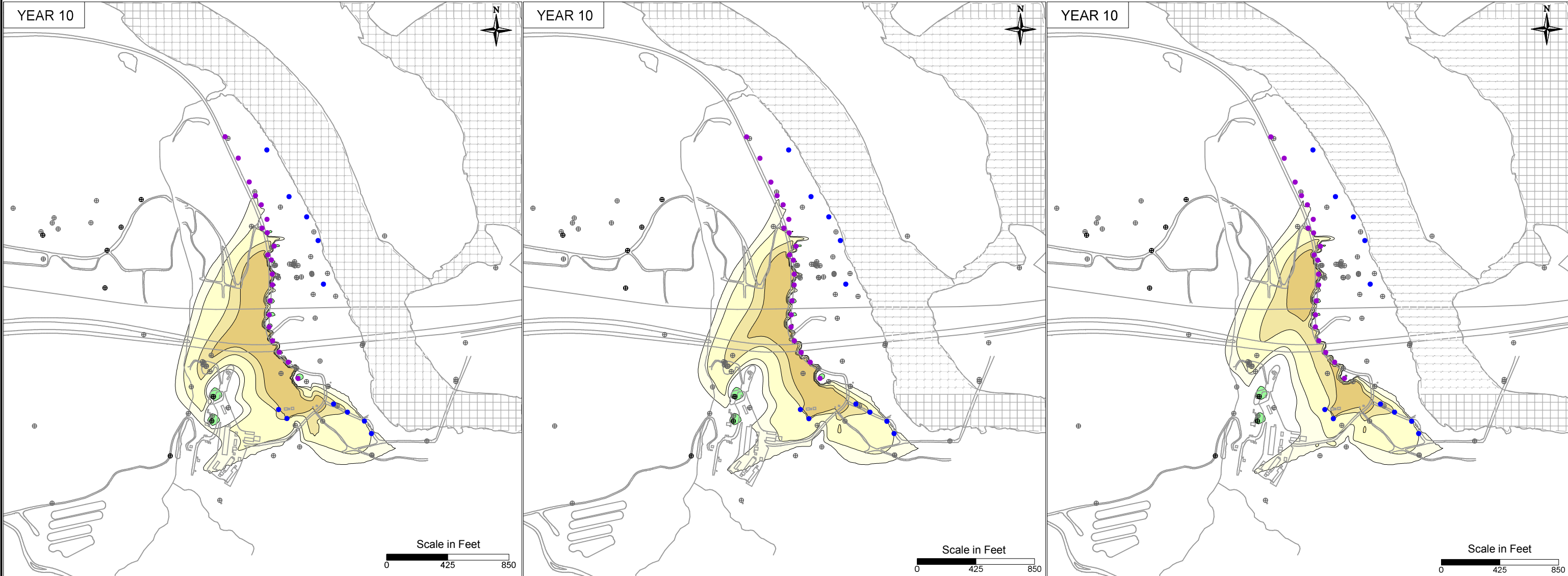
INCREASED NTH IRZ RATES = 600 GPM

**LEGEND**

- IRZ WELLS
- ⊕ UPGRADIENT INJECTION WELLS
- EXTRACTION WELLS
- ⊕ MONITORING WELLS



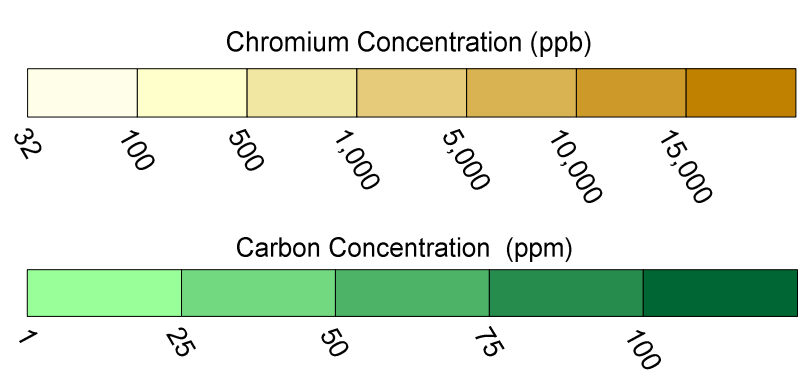




DECREASED FRESHWATER INJECTION RATES = 225 GPM

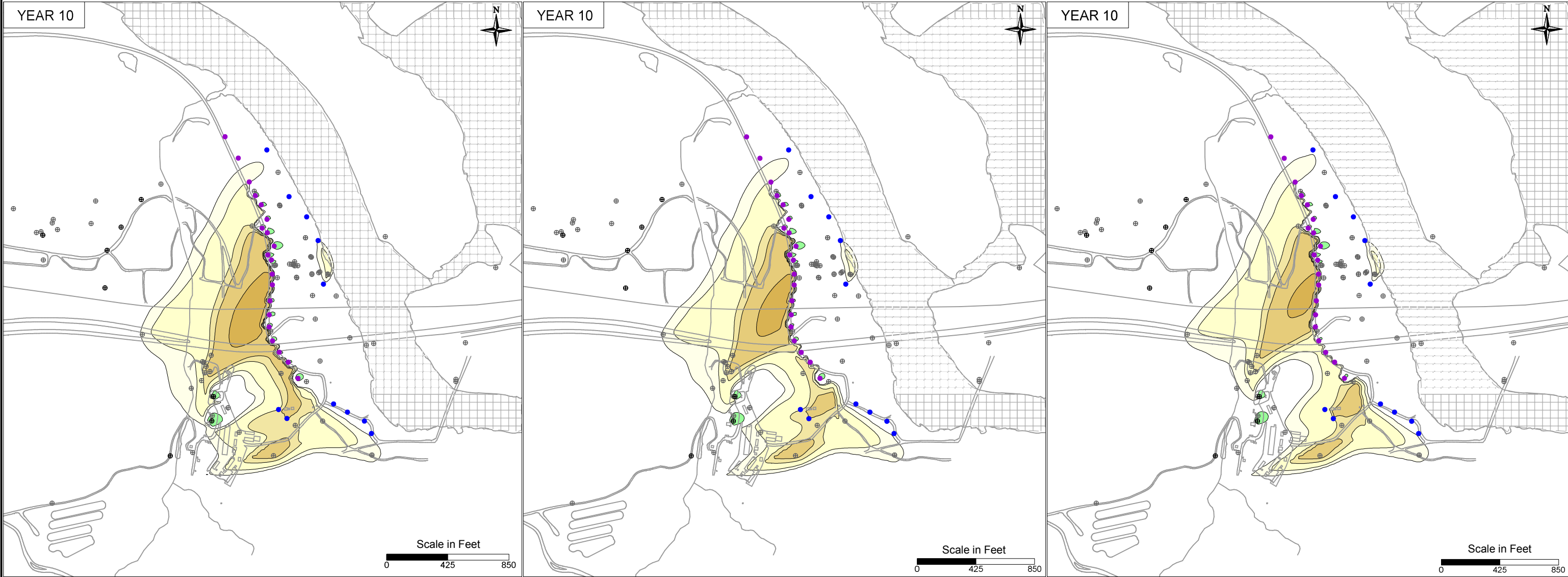
BASE FRESHWATER INJECTION RATES = 450 GPM

INCREASED FRESHWATER INJECTION RATES = 650 GPM



- LEGEND**
- IRZ WELLS
  - ⊕ UPGRADIENT INJECTION WELLS
  - EXTRACTION WELLS
  - ⊕ MONITORING WELLS

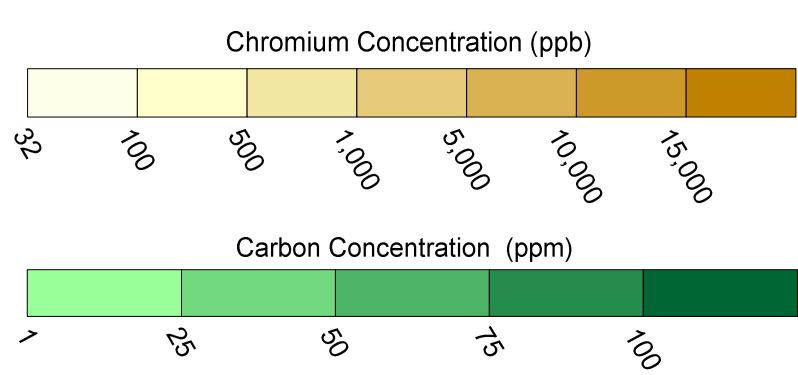
PG&E TOPOCK COMPRESSOR STATION NEEDLES, CALIFORNIA MODELING APPENDIX	
FRESHWATER INJECTION RATE SENSITIVITY: SIMULATED HEXAVALENT CHROMIUM TRANSPORT RESULTS FOR YEAR 10 IN MODEL LAYER 2	
	FIGURE 10.12-1



DECREASED FRESHWATER INJECTION RATES = 225 GPM

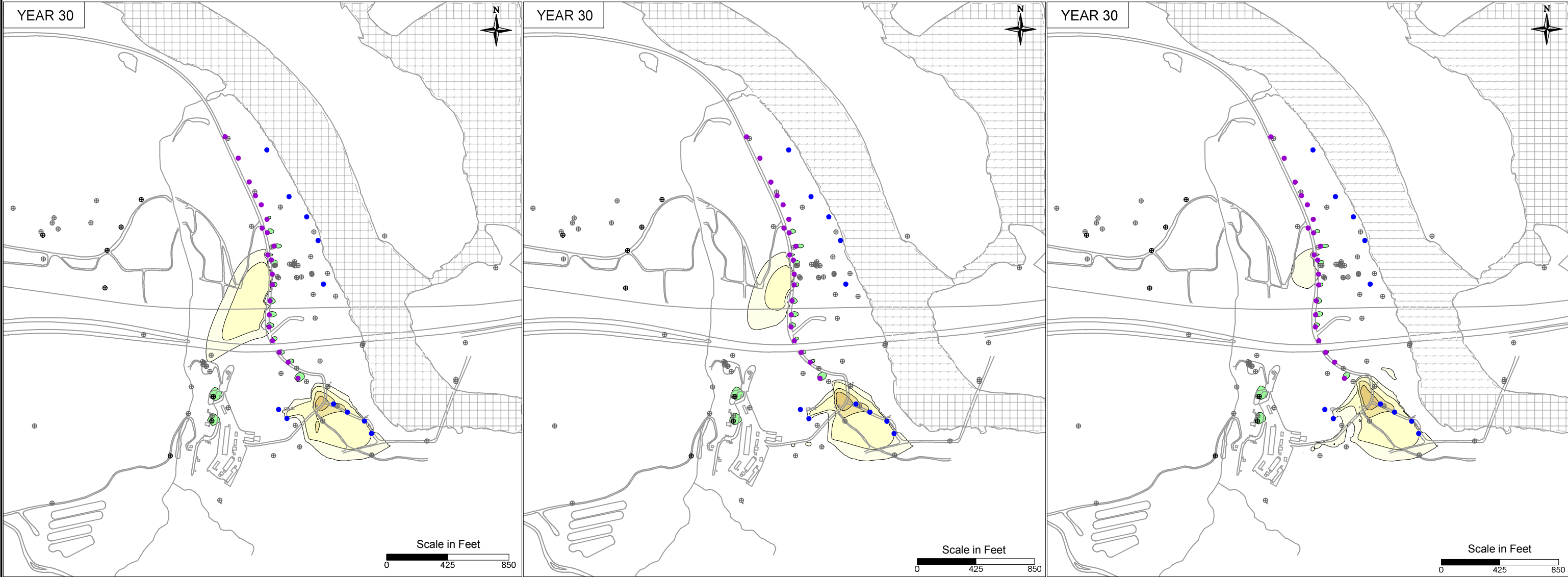
BASE FRESHWATER INJECTION RATES = 450 GPM

INCREASED FRESHWATER INJECTION RATES = 650 GPM



**LEGEND**

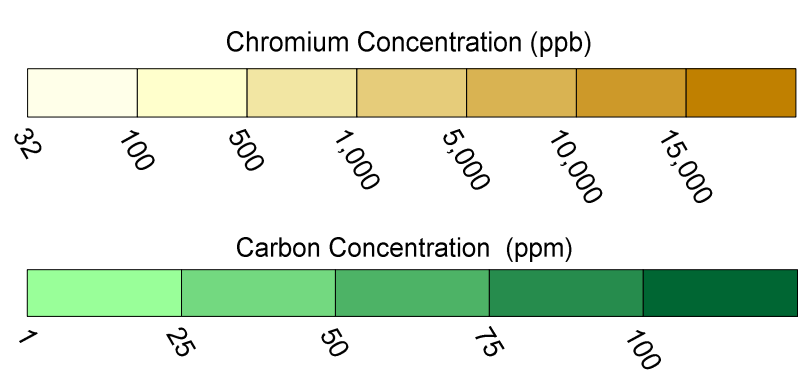
- IRZ WELLS
- UPGRADIENT INJECTION WELLS
- EXTRACTION WELLS
- MONITORING WELLS



DECREASED FRESHWATER INJECTION RATES = 225 GPM

BASE FRESHWATER INJECTION RATES = 450 GPM

INCREASED FRESHWATER INJECTION RATES = 650 GPM



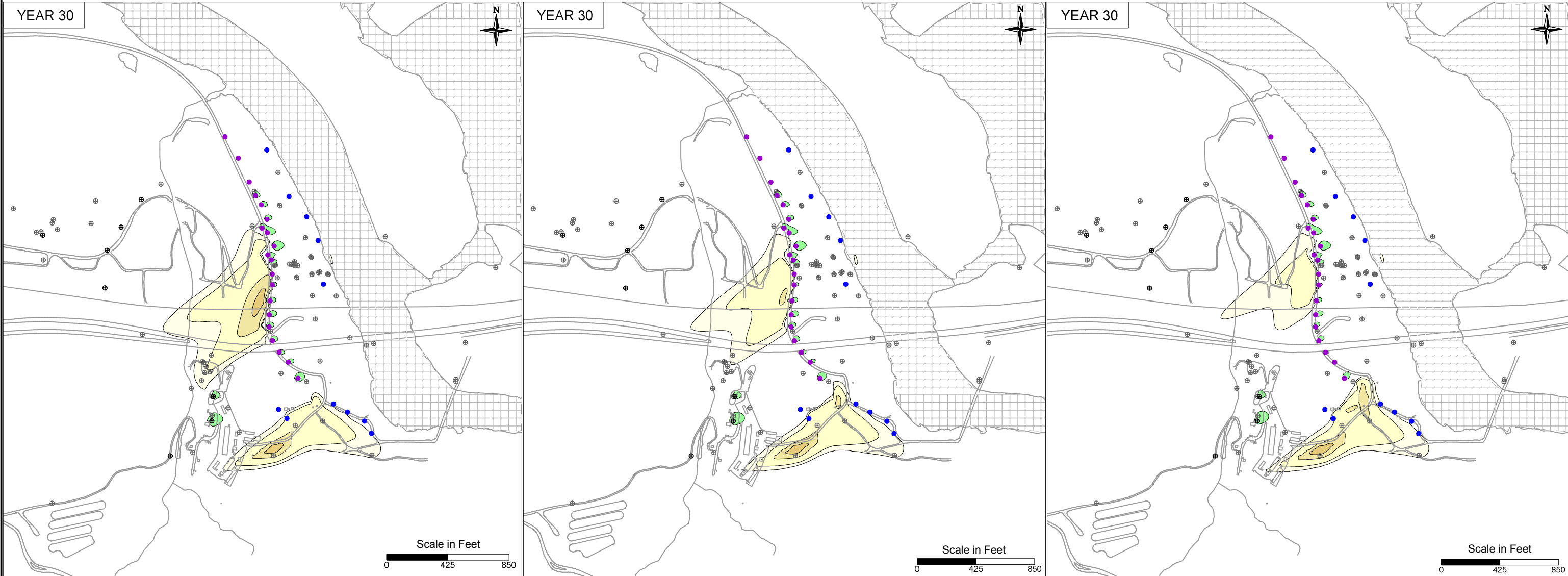
- LEGEND**
- IRZ WELLS
  - UPGRADIENT INJECTION WELLS
  - EXTRACTION WELLS
  - MONITORING WELLS

PG&E  
TOPOCK COMPRESSOR STATION  
NEEDLES, CALIFORNIA  
MODELING APPENDIX

FRESHWATER INJECTION RATE SENSITIVITY:  
SIMULATED HEXAVALENT CHROMIUM TRANSPORT  
RESULTS FOR YEAR 30 IN MODEL LAYER 2

FIGURE  
10.12-3

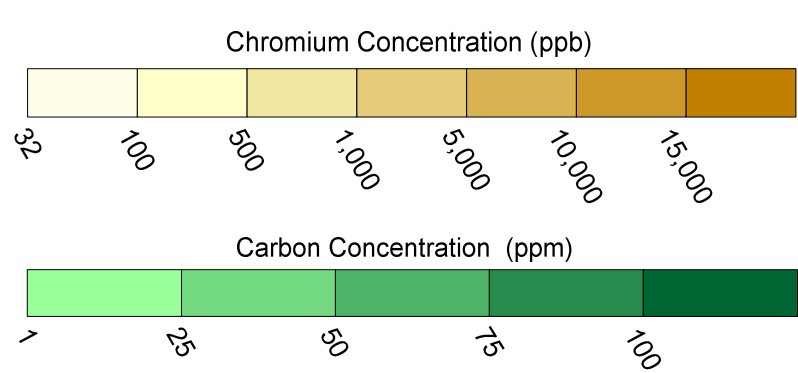




DECREASED FRESHWATER INJECTION RATES = 225 GPM

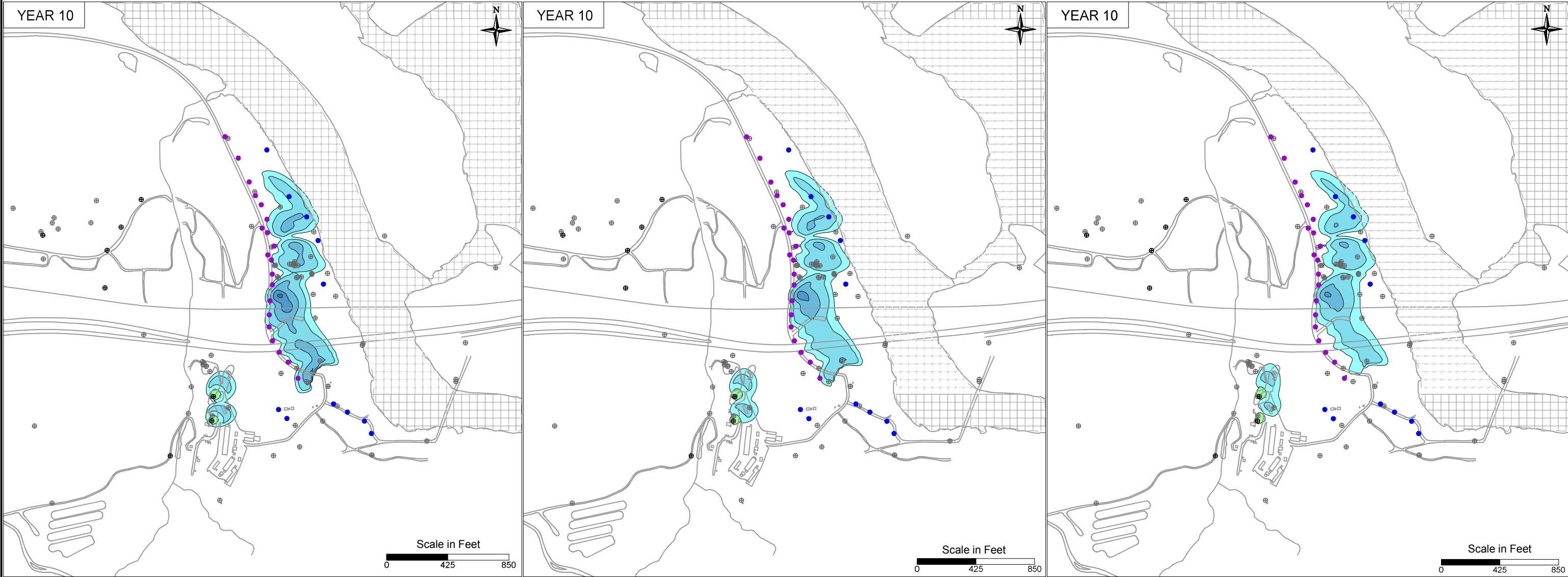
BASE FRESHWATER INJECTION RATES = 450 GPM

INCREASED FRESHWATER INJECTION RATES = 650 GPM



- LEGEND**
- IRZ WELLS
  - ⊕ UPGRADIENT INJECTION WELLS
  - EXTRACTION WELLS
  - ⊕ MONITORING WELLS

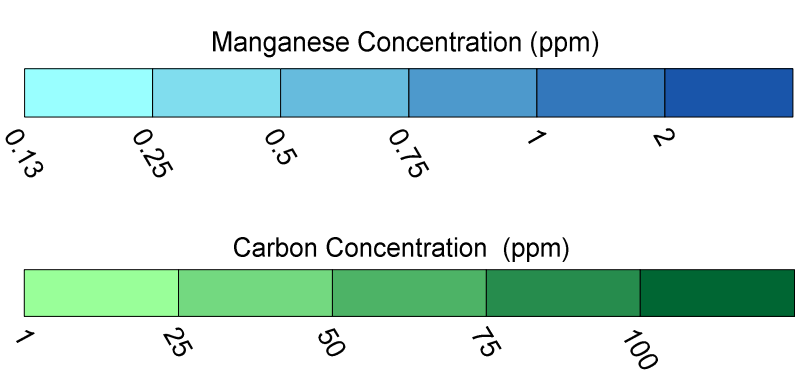




DECREASED FRESHWATER INJECTION RATES = 225 GPM

BASE FRESHWATER INJECTION RATES = 450 GPM

INCREASED FRESHWATER INJECTION RATES = 650 GPM

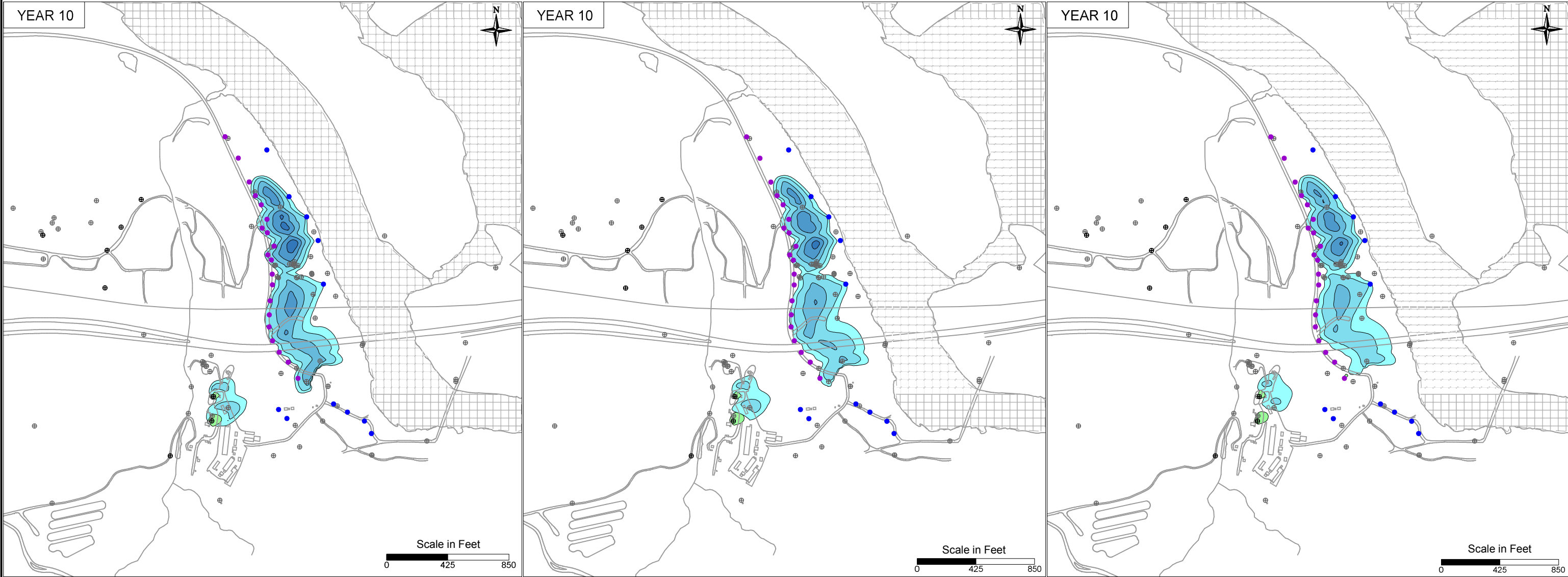


- LEGEND**
- IRZ WELLS
  - ⊕ UPGRADIENT INJECTION WELLS
  - EXTRACTION WELLS
  - ⊕ MONITORING WELLS

PG&E  
TOPOCK COMPRESSOR STATION  
NEEDLES, CALIFORNIA  
MODELING APPENDIX

FRESHWATER INJECTION RATE SENSITIVITY:  
SIMULATED MANGANESE TRANSPORT  
RESULTS FOR YEAR 10 IN MODEL LAYER 2

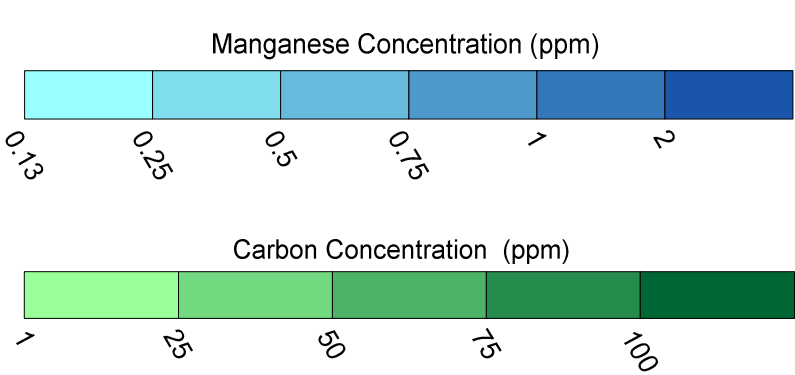
FIGURE  
10.12-5



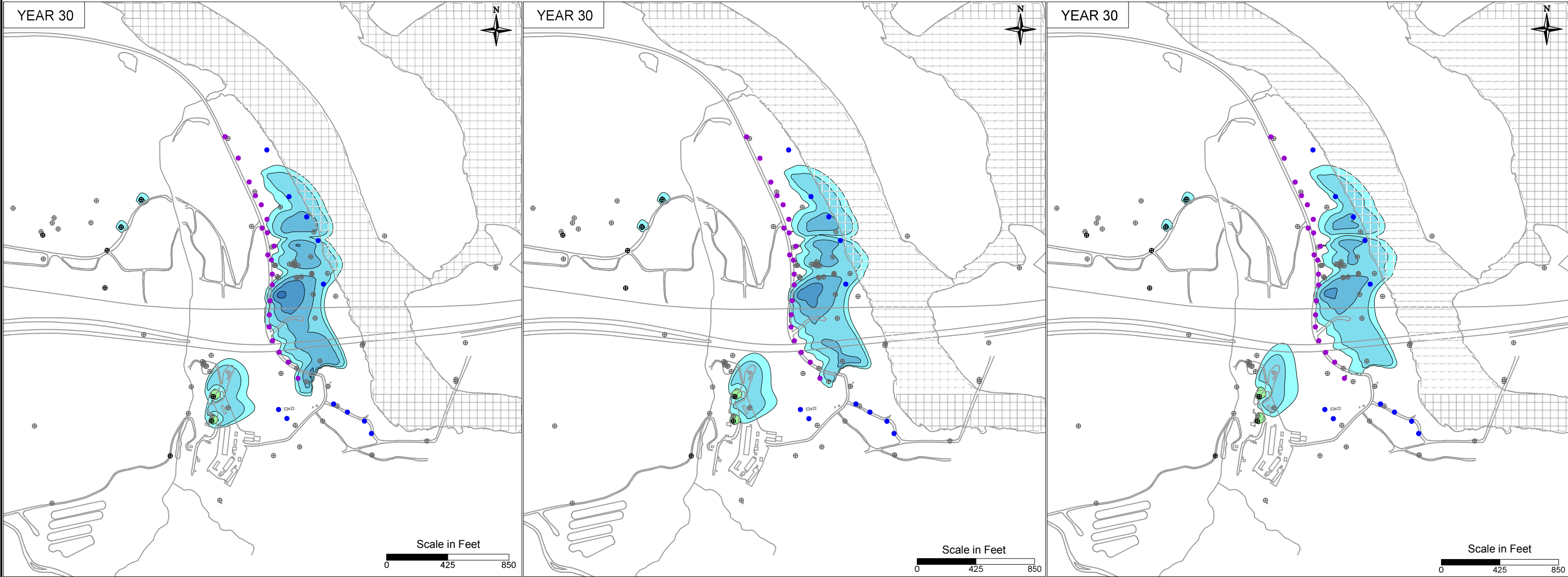
DECREASED FRESHWATER INJECTION RATES = 225 GPM

BASE FRESHWATER INJECTION RATES = 450 GPM

INCREASED FRESHWATER INJECTION RATES = 650 GPM



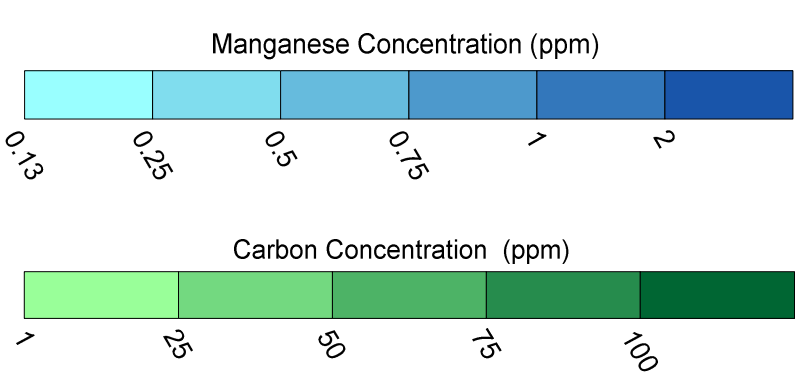
- LEGEND**
- IRZ WELLS
  - ⊕ UPGRADIENT INJECTION WELLS
  - EXTRACTION WELLS
  - ⊕ MONITORING WELLS



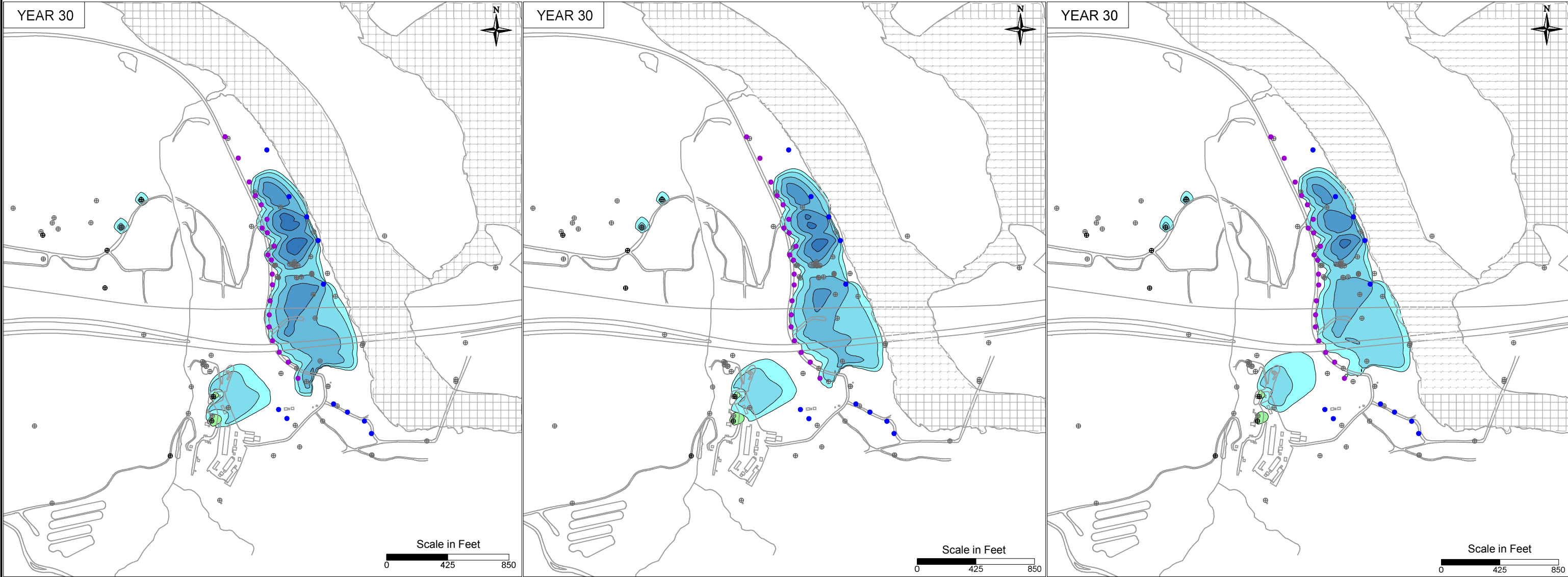
DECREASED FRESHWATER INJECTION RATES = 225 GPM

BASE FRESHWATER INJECTION RATES = 450 GPM

INCREASED FRESHWATER INJECTION RATES = 650 GPM



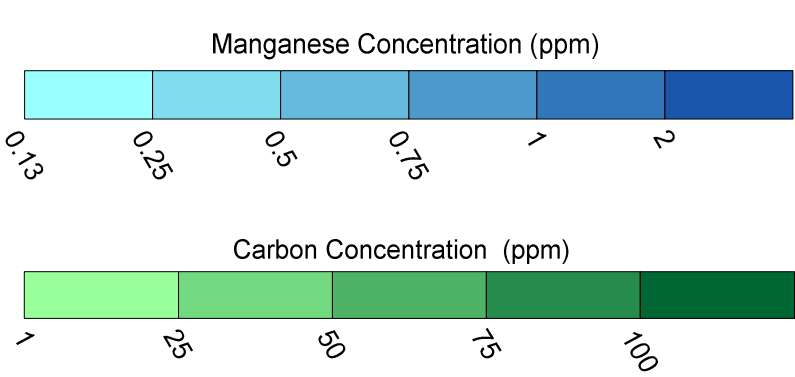
- LEGEND**
- IRZ WELLS
  - UPGRADIENT INJECTION WELLS
  - EXTRACTION WELLS
  - MONITORING WELLS



DECREASED FRESHWATER INJECTION RATES = 225 GPM

BASE FRESHWATER INJECTION RATES = 450 GPM

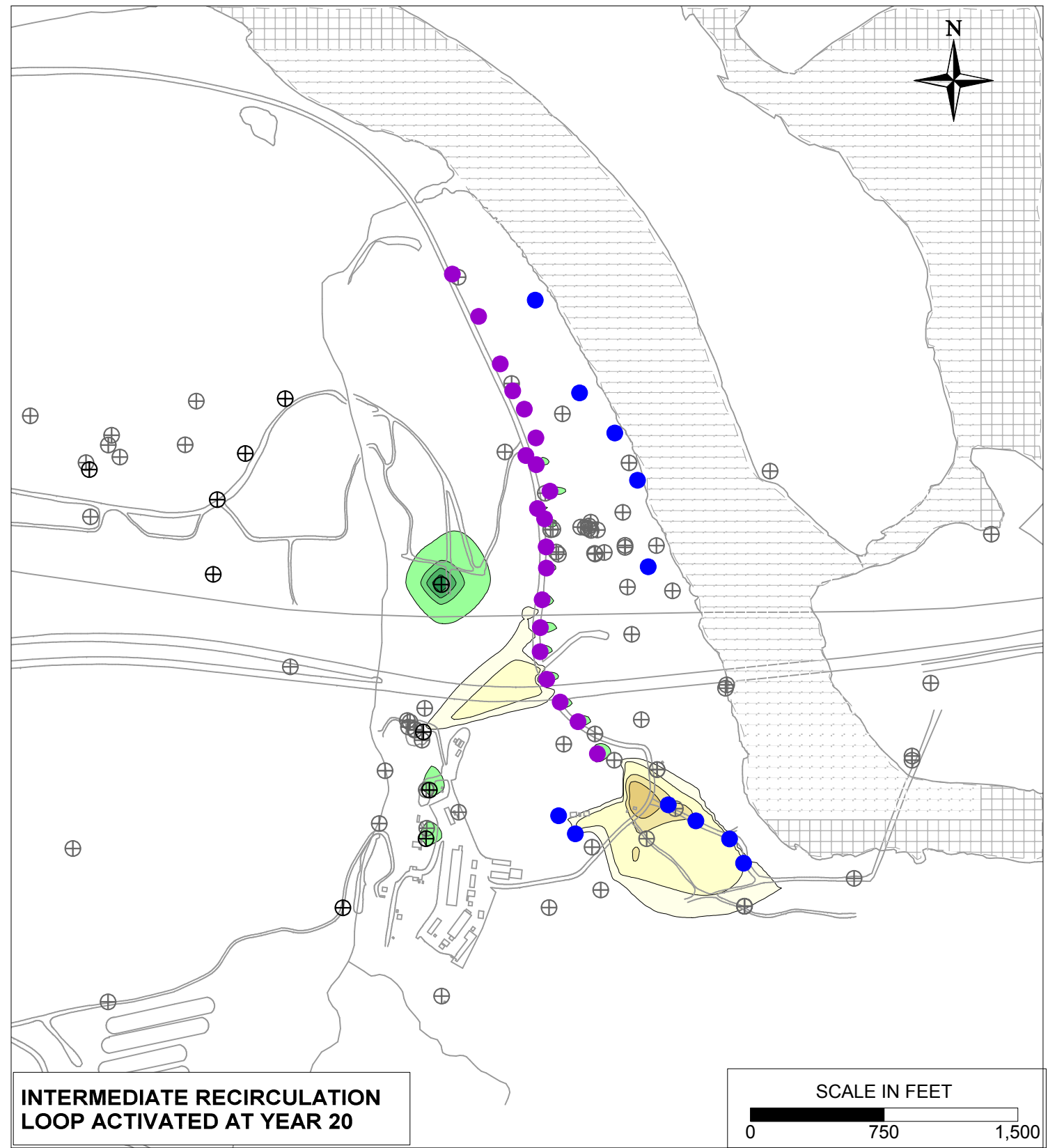
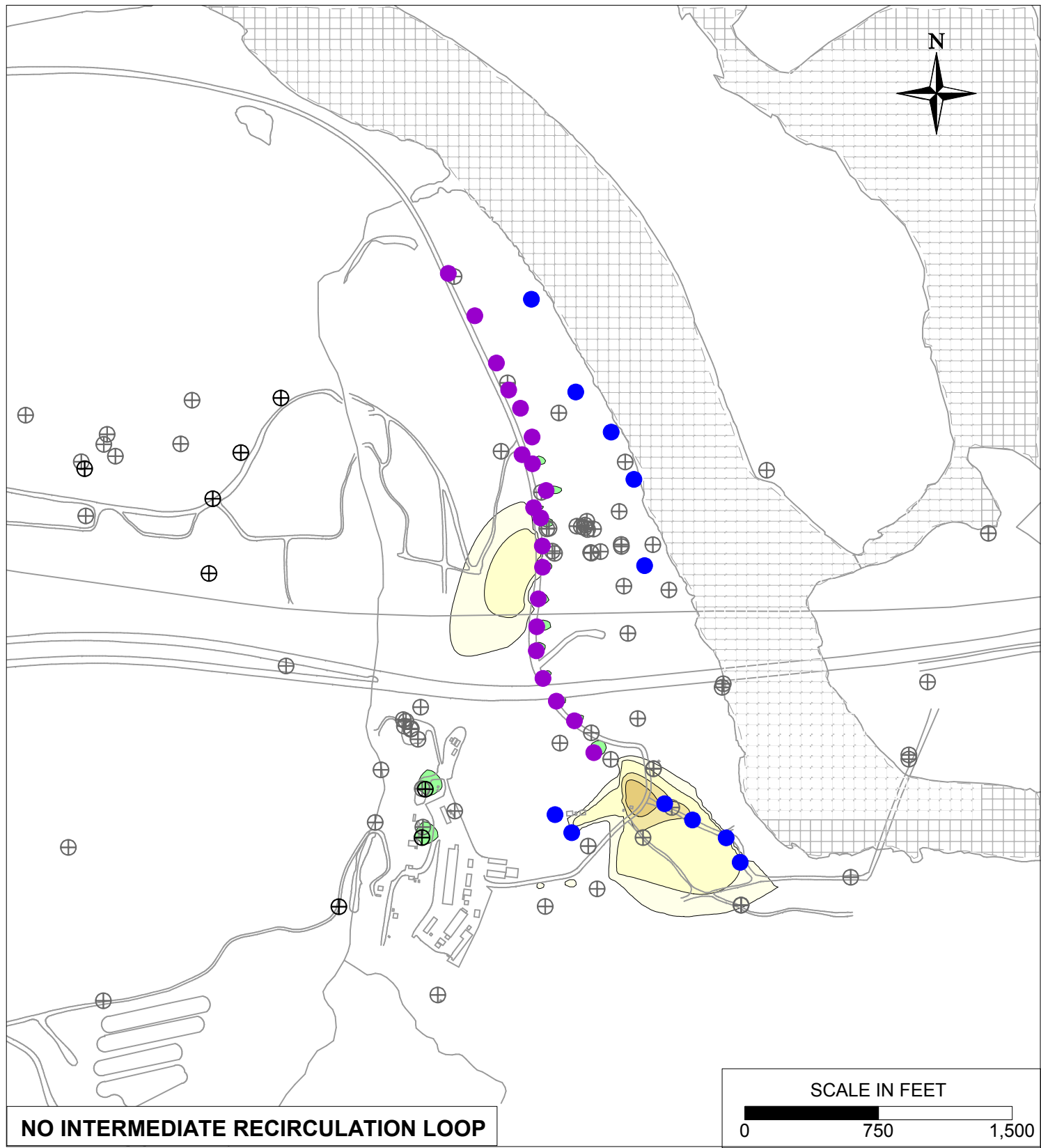
INCREASED FRESHWATER INJECTION RATES = 650 GPM



- LEGEND**
- IRZ WELLS
  - ⊕ UPGRADIENT INJECTION WELLS
  - EXTRACTION WELLS
  - ⊕ MONITORING WELLS

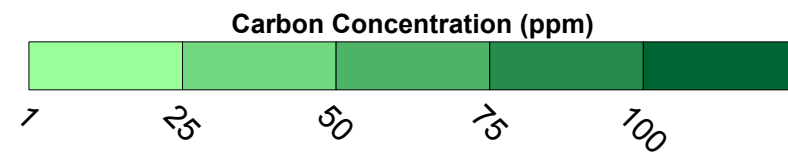
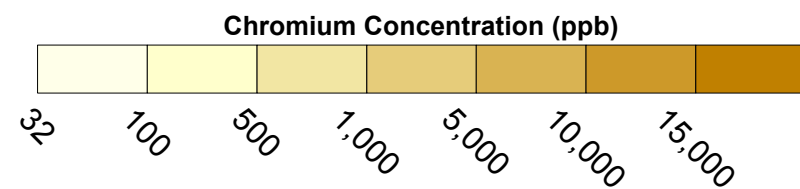
PG&E TOPOCK COMPRESSOR STATION NEEDLES, CALIFORNIA MODELING APPENDIX	
FRESHWATER INJECTION RATE SENSITIVITY: SIMULATED MANGANESE TRANSPORT RESULTS FOR YEAR 30 IN MODEL LAYER 4	
	FIGURE <b>10.12-8</b>





**LEGEND**

- IRZ WELLS
- ⊕ UPGRADIENT INJECTION WELLS
- EXTRACTION WELLS
- ⊕ MONITORING WELLS

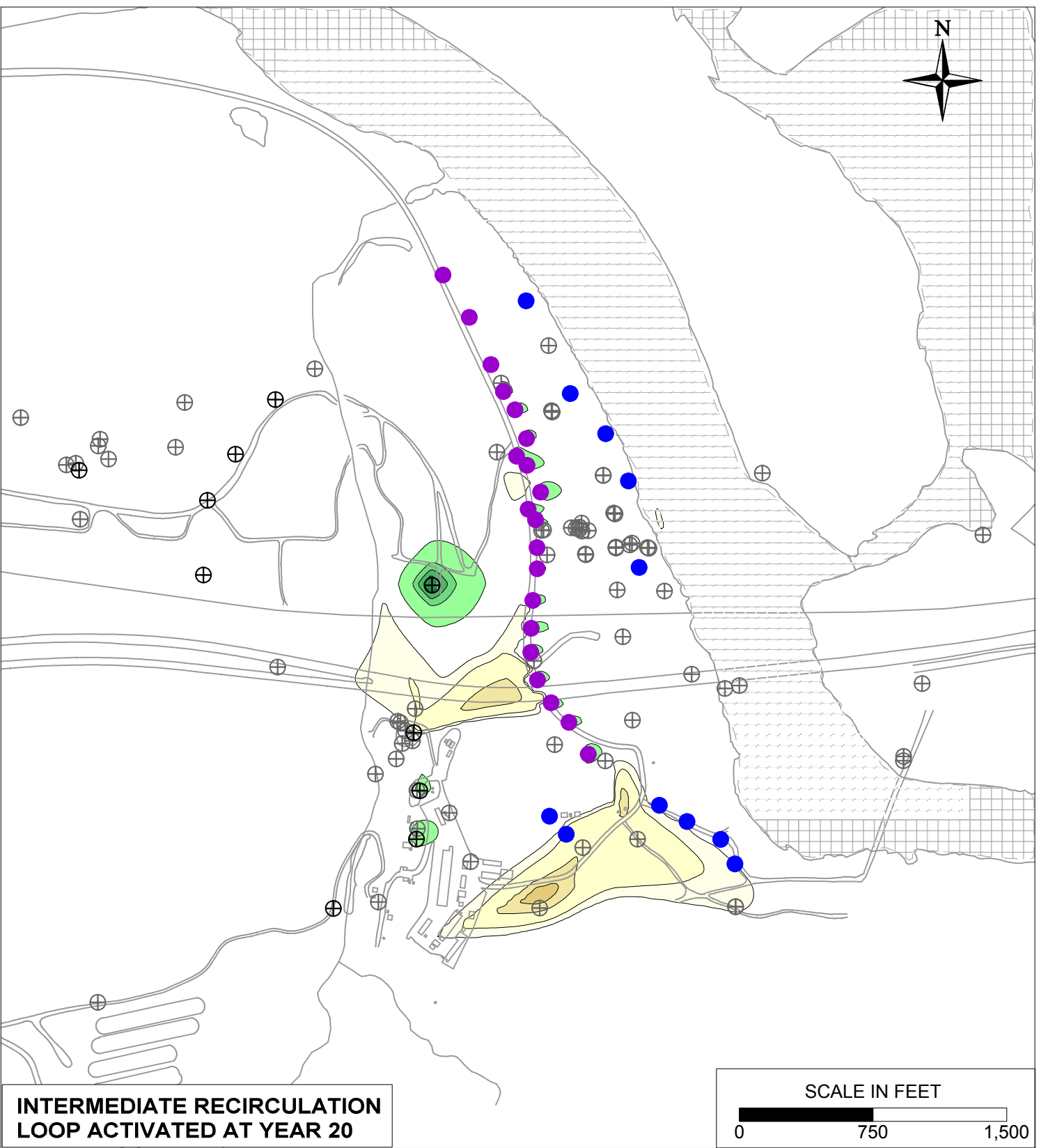
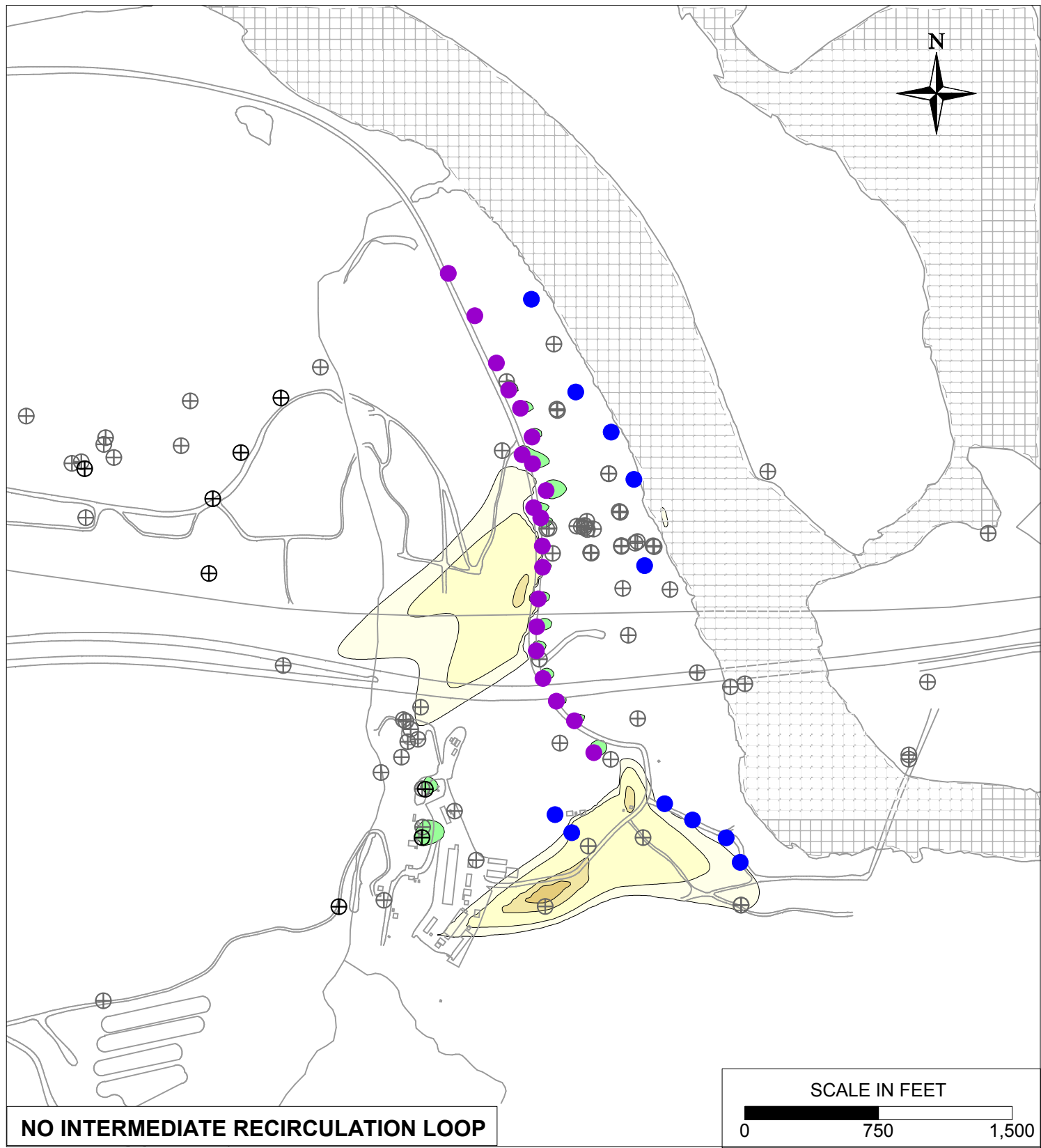


PG&E  
TOPOCK COMPRESSOR STATION  
NEEDLES, CALIFORNIA  
MODELING APPENDIX

INTERMEDIATE RECIRCULATION LOOP  
SENSITIVITY: SIMULATED HEXAVALENT  
CHROMIUM TRANSPORT RESULTS  
FOR YEAR 30 IN MODEL LAYER 2

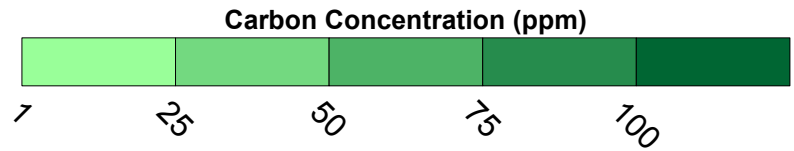
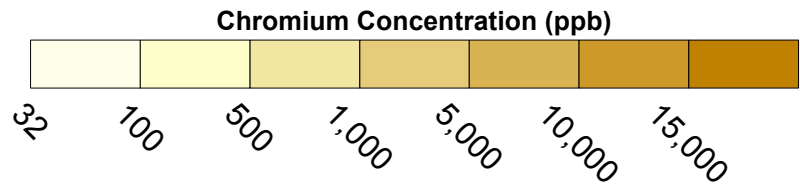


FIGURE  
10.13-1



**LEGEND**

- IRZ WELLS
- ⊕ UPGRADIENT INJECTION WELLS
- EXTRACTION WELLS
- ⊕ MONITORING WELLS

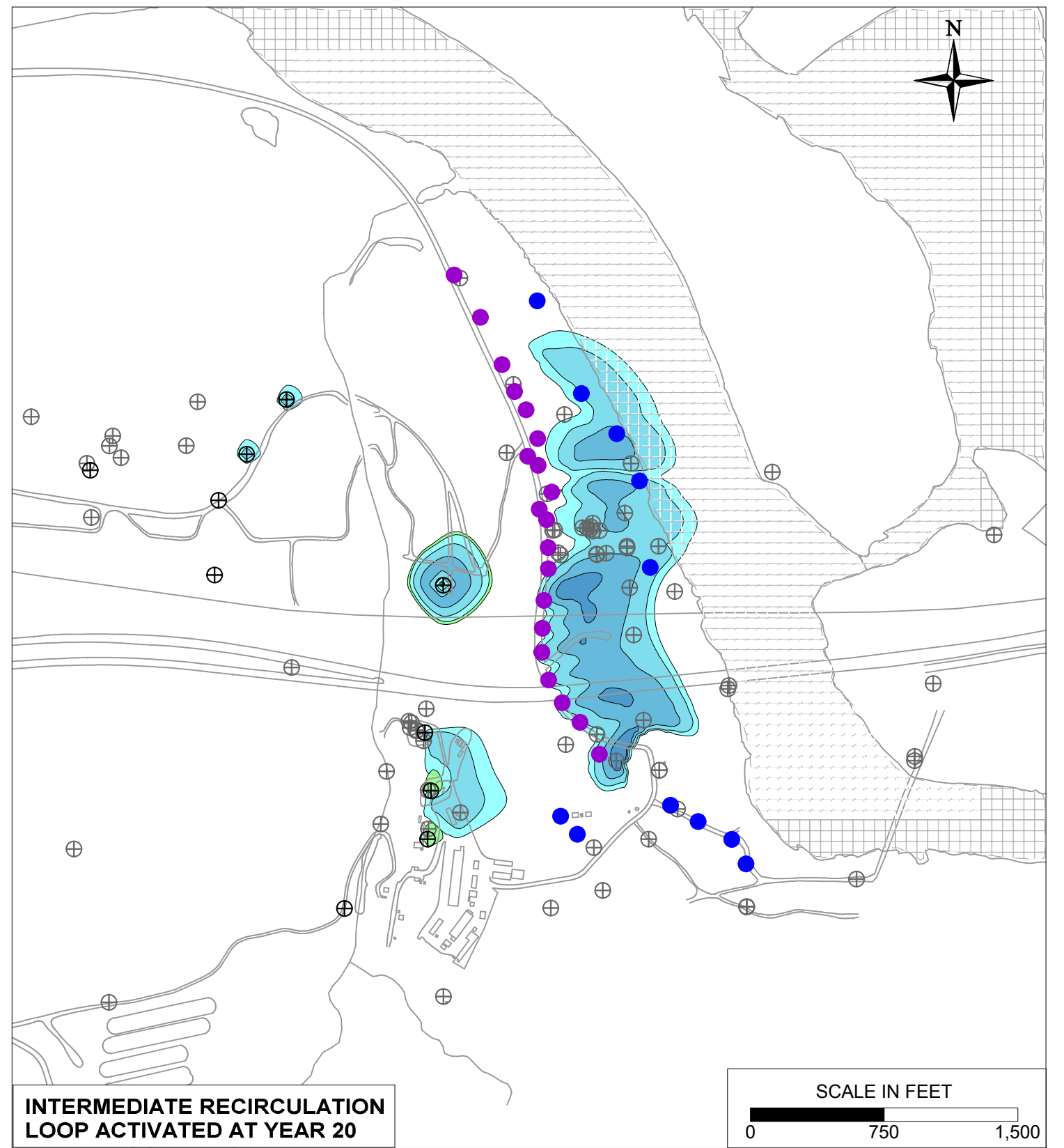
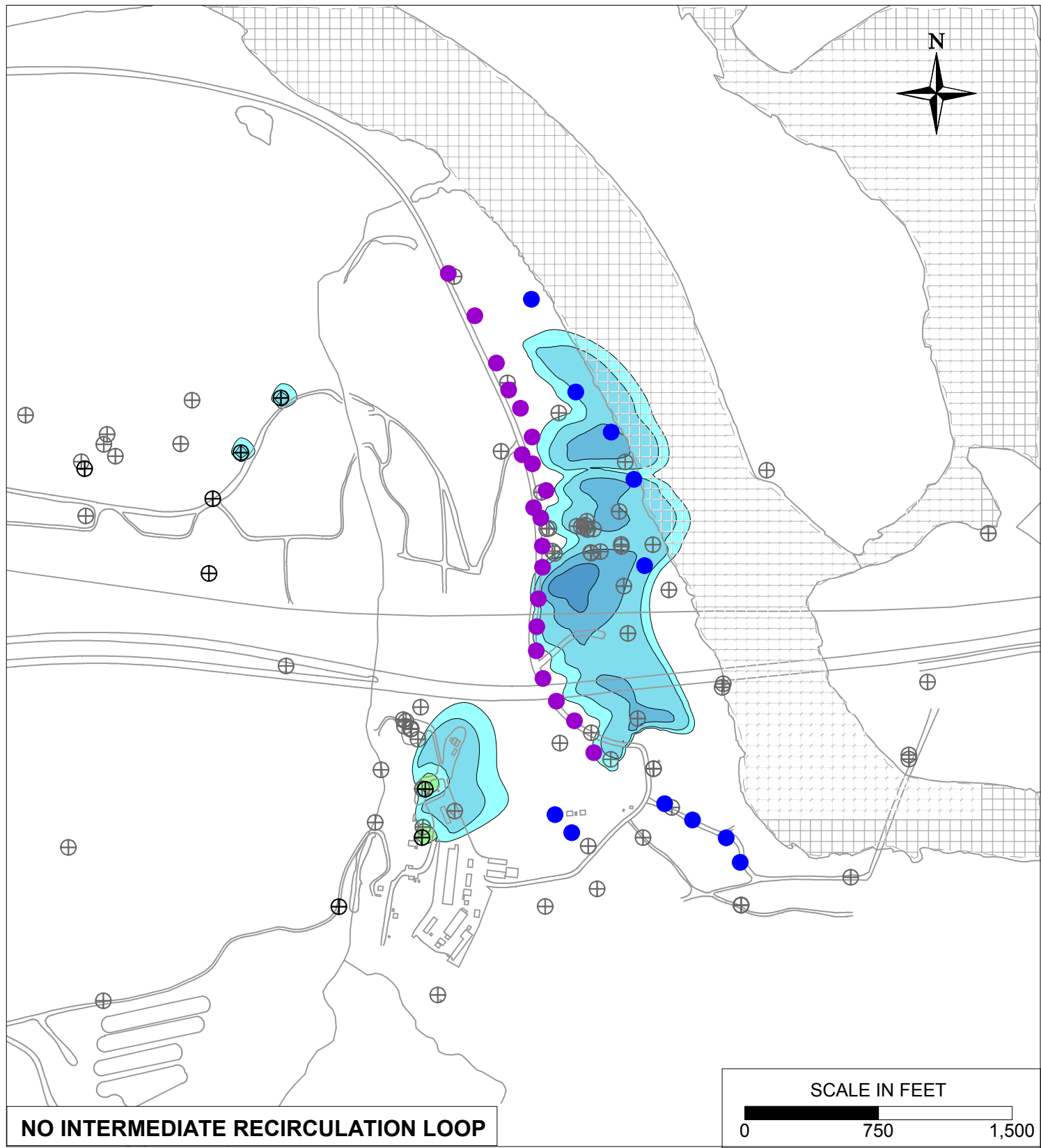


PG&E  
TOPOCK COMPRESSOR STATION  
NEEDLES, CALIFORNIA  
MODELING APPENDIX

INTERMEDIATE RECIRCULATION LOOP  
SENSITIVITY: SIMULATED HEXAVALENT  
CHROMIUM TRANSPORT RESULTS  
FOR YEAR 30 IN MODEL LAYER 4

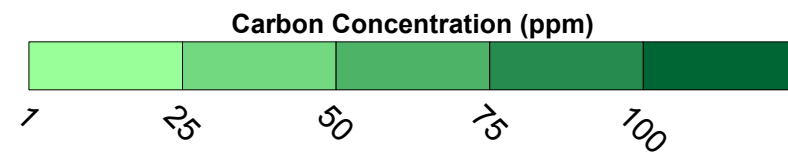
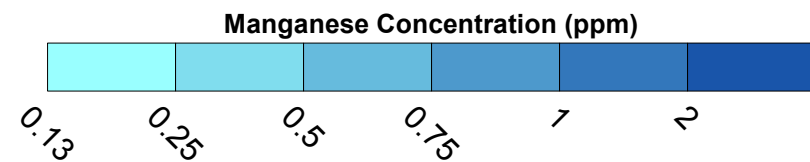


FIGURE  
10.13-2



**LEGEND**

- IRZ WELLS
- ⊕ UPGRADE INJECTION WELLS
- EXTRACTION WELLS
- ⊕ MONITORING WELLS



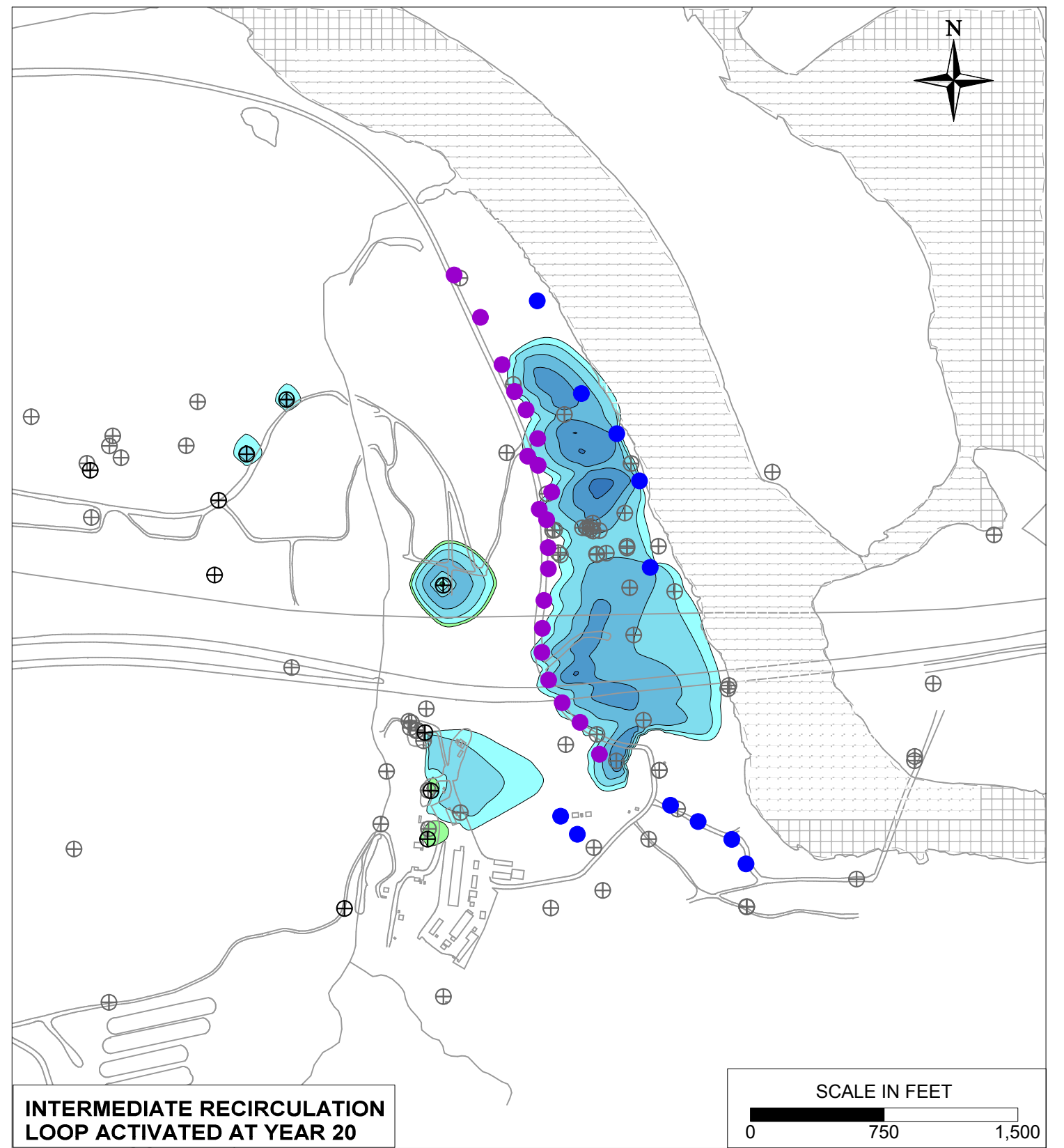
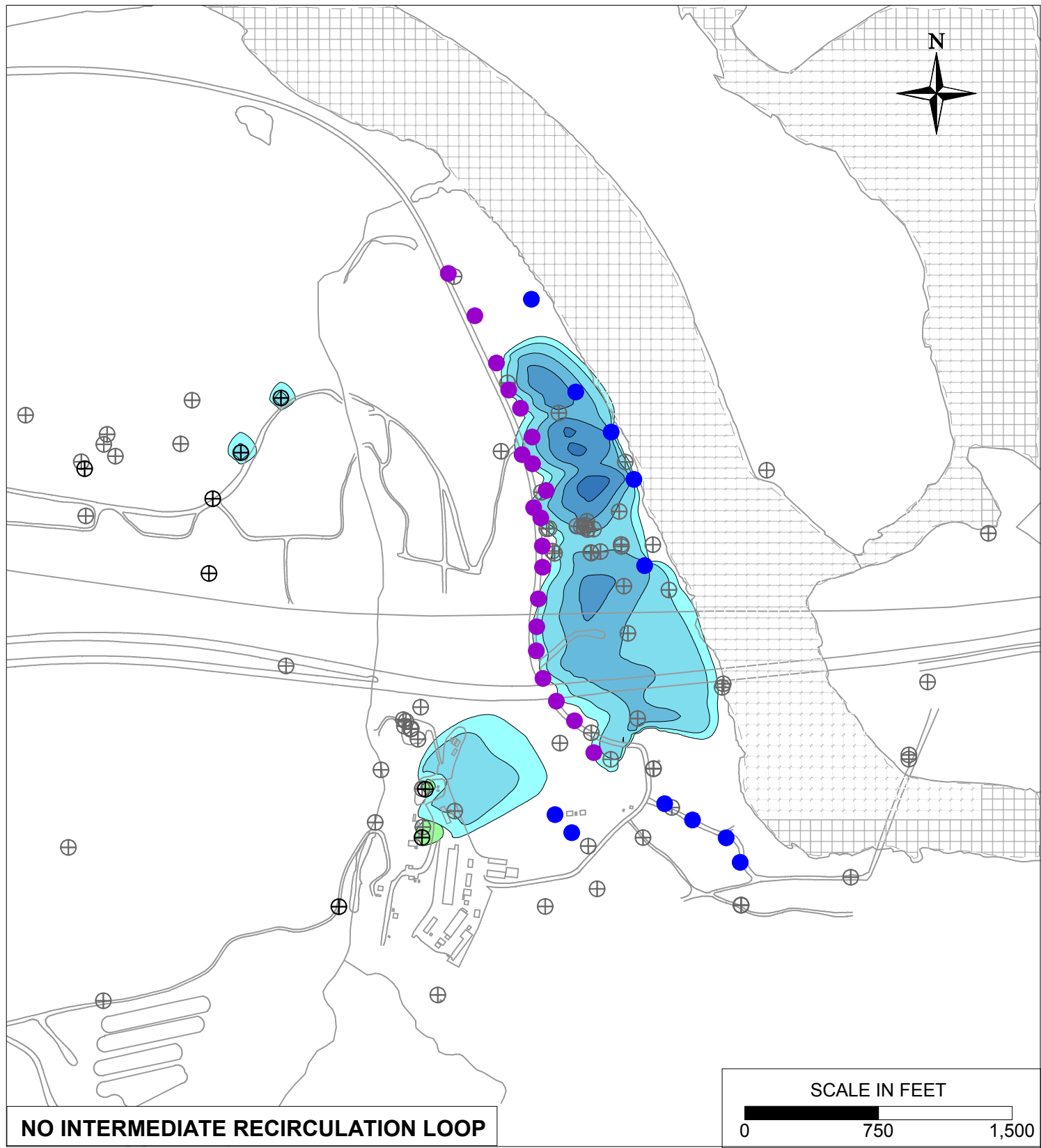
PG&E  
TOPOCK COMPRESSOR STATION  
NEEDLES, CALIFORNIA  
MODELING APPENDIX

INTERMEDIATE RECIRCULATION LOOP  
SENSITIVITY: SIMULATED MANGANESE  
TRANSPORT RESULTS FOR YEAR 30  
IN MODEL LAYER 2



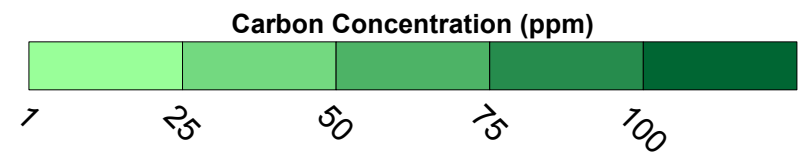
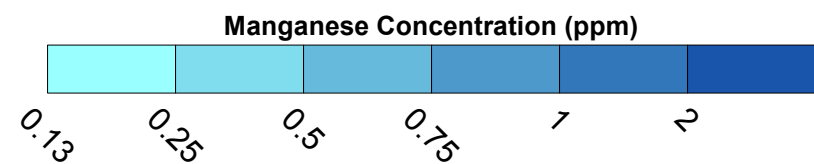
FIGURE  
10.13-3



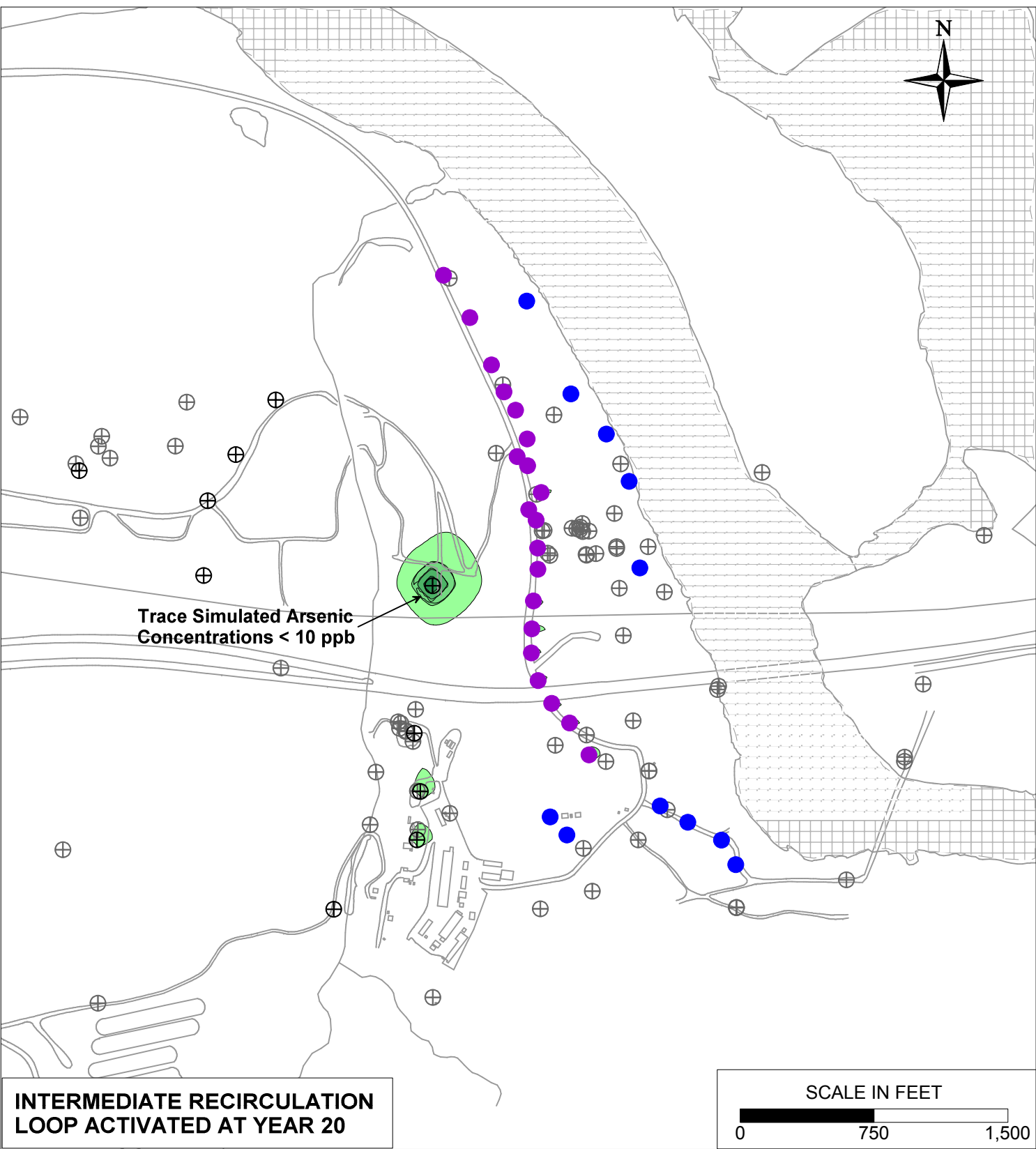
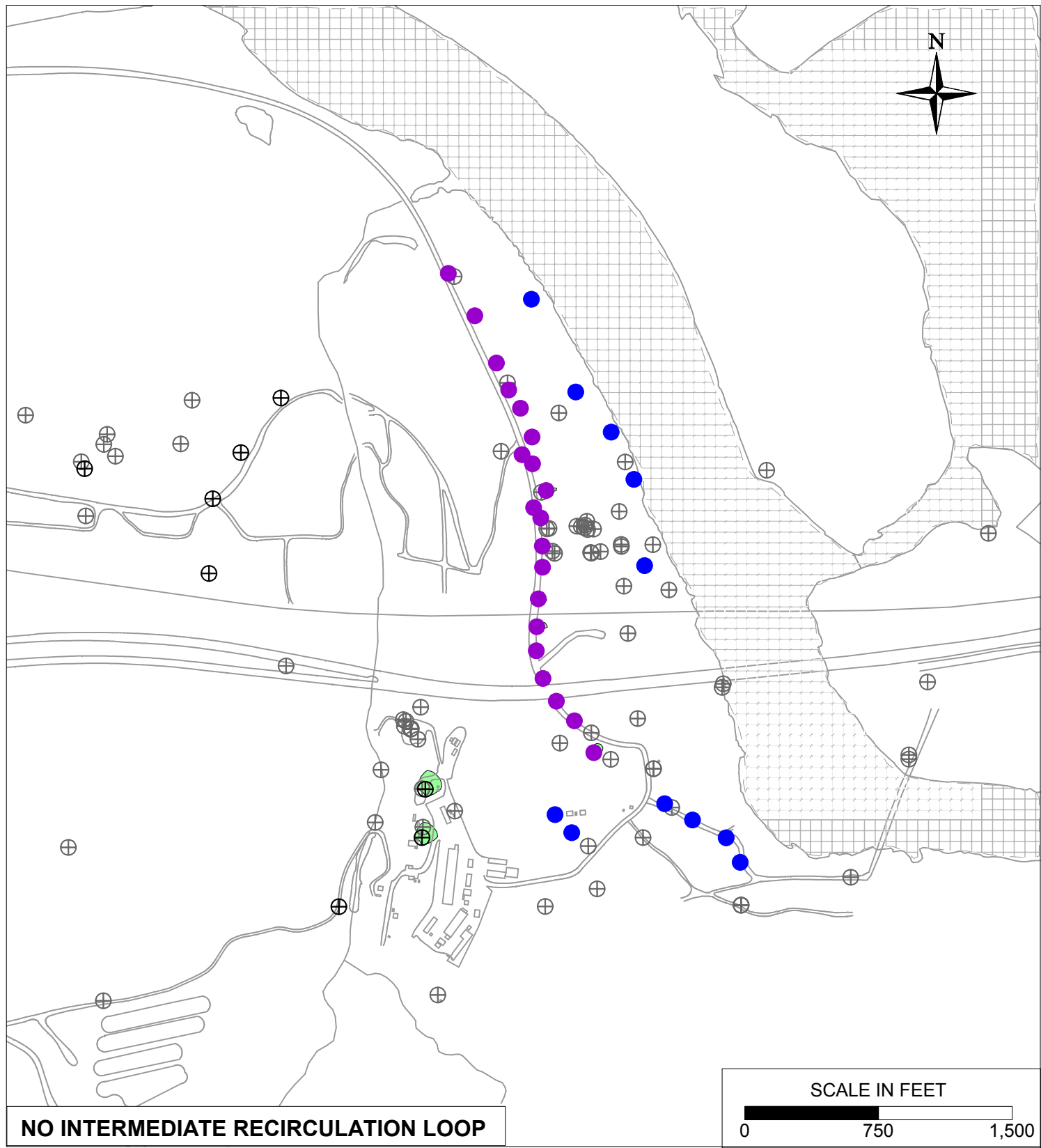


**LEGEND**

- IRZ WELLS
- ⊕ UPGRADE INJECTION WELLS
- EXTRACTION WELLS
- ⊕ MONITORING WELLS

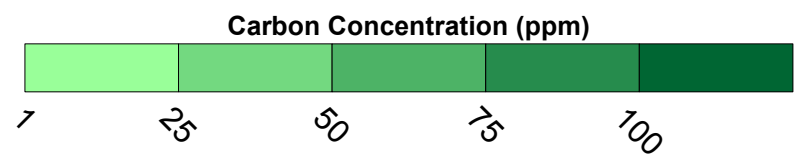
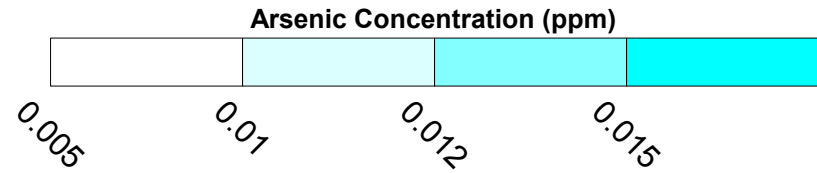






**LEGEND**

- IRZ WELLS
- ⊕ UPGRADIENT INJECTION WELLS
- EXTRACTION WELLS
- ⊕ MONITORING WELLS

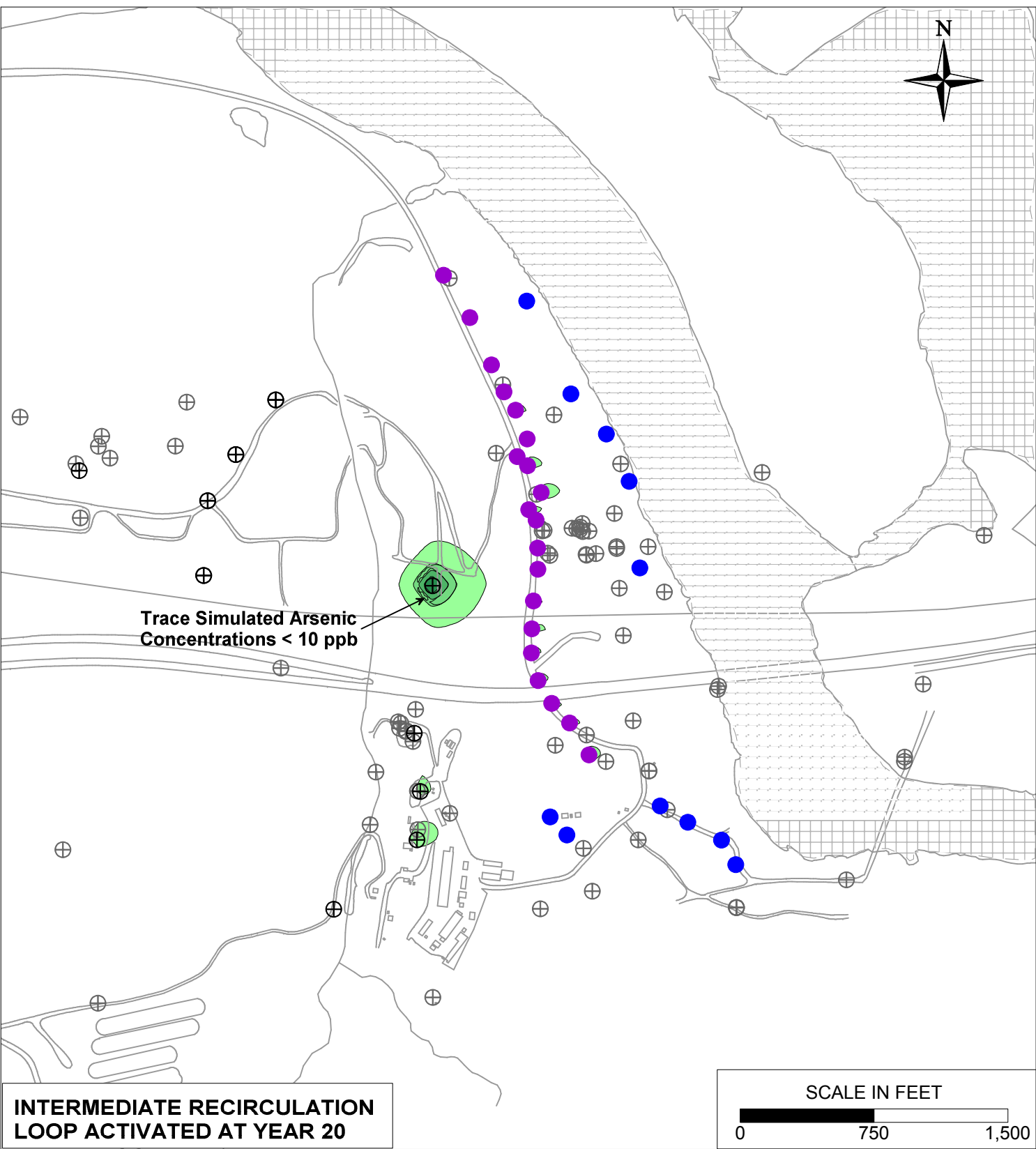
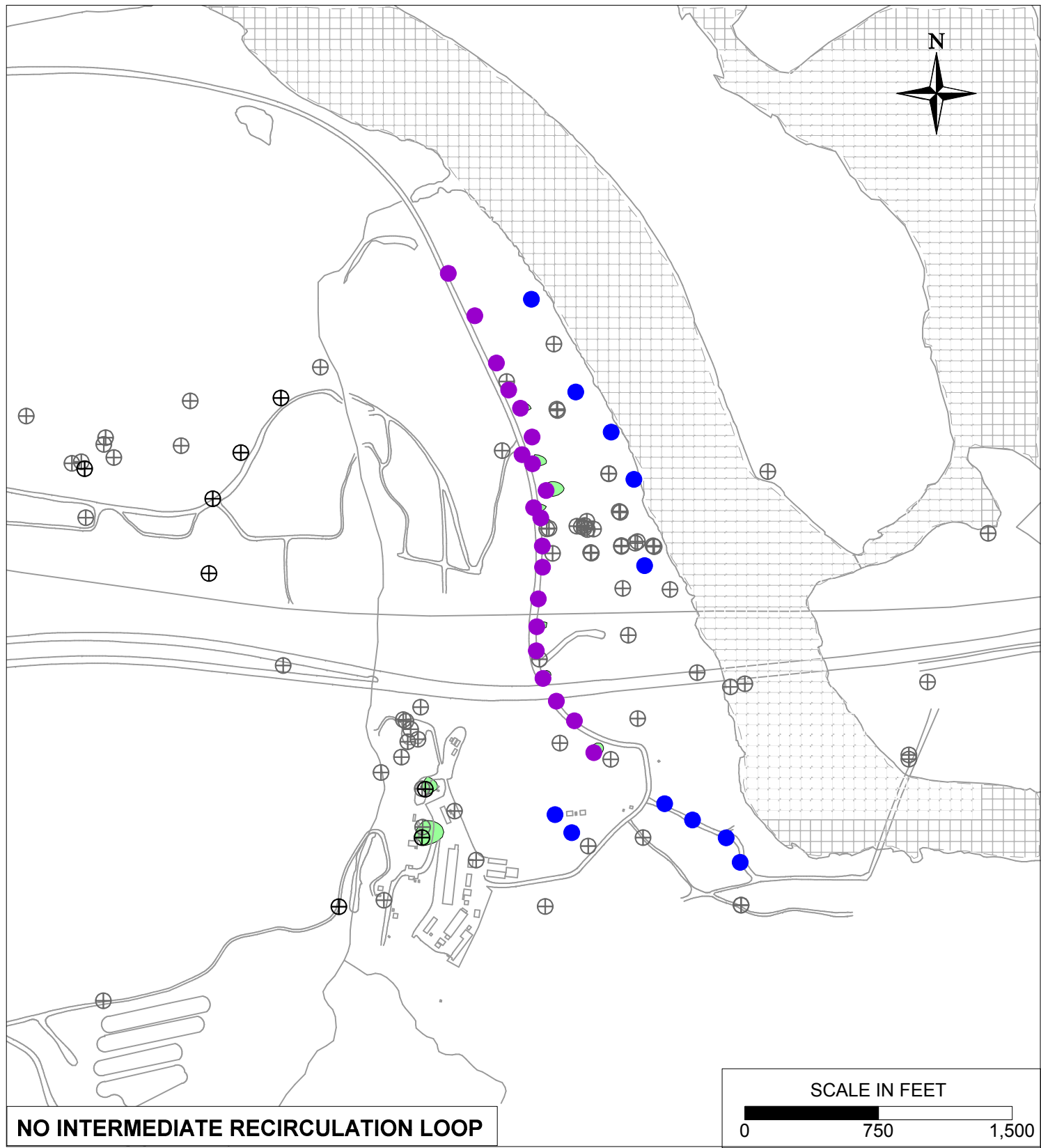


PG&E  
TOPOCK COMPRESSOR STATION  
NEEDLES, CALIFORNIA  
MODELING APPENDIX

INTERMEDIATE RECIRCULATION LOOP  
SENSITIVITY: SIMULATED ARSENIC TRANSPORT  
RESULTS FOR YEAR 30 IN MODEL LAYER 2

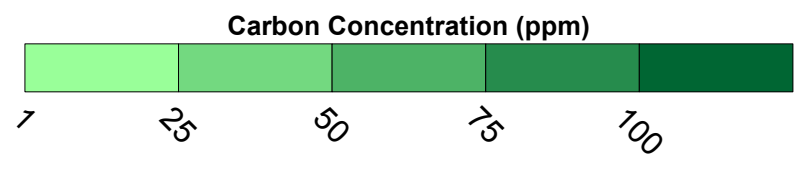
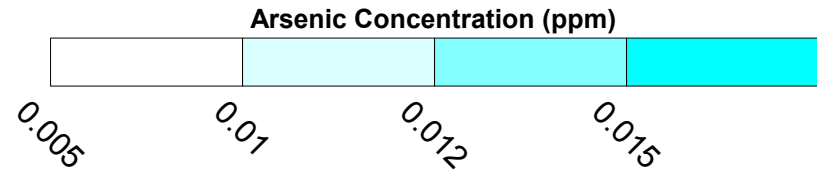


FIGURE  
10.13-5



**LEGEND**

- IRZ WELLS
- ⊕ UPGRADIENT INJECTION WELLS
- EXTRACTION WELLS
- ⊕ MONITORING WELLS

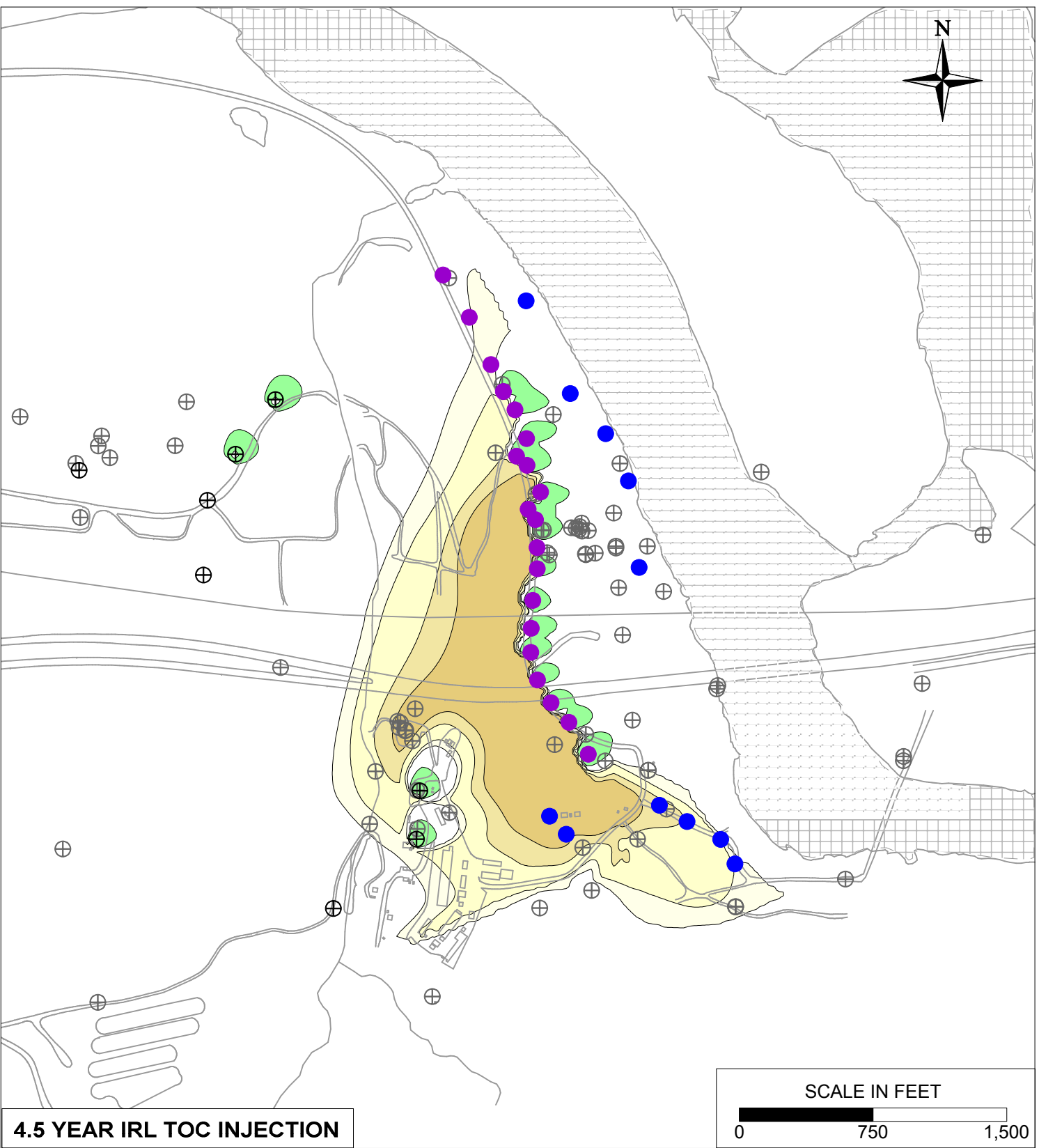
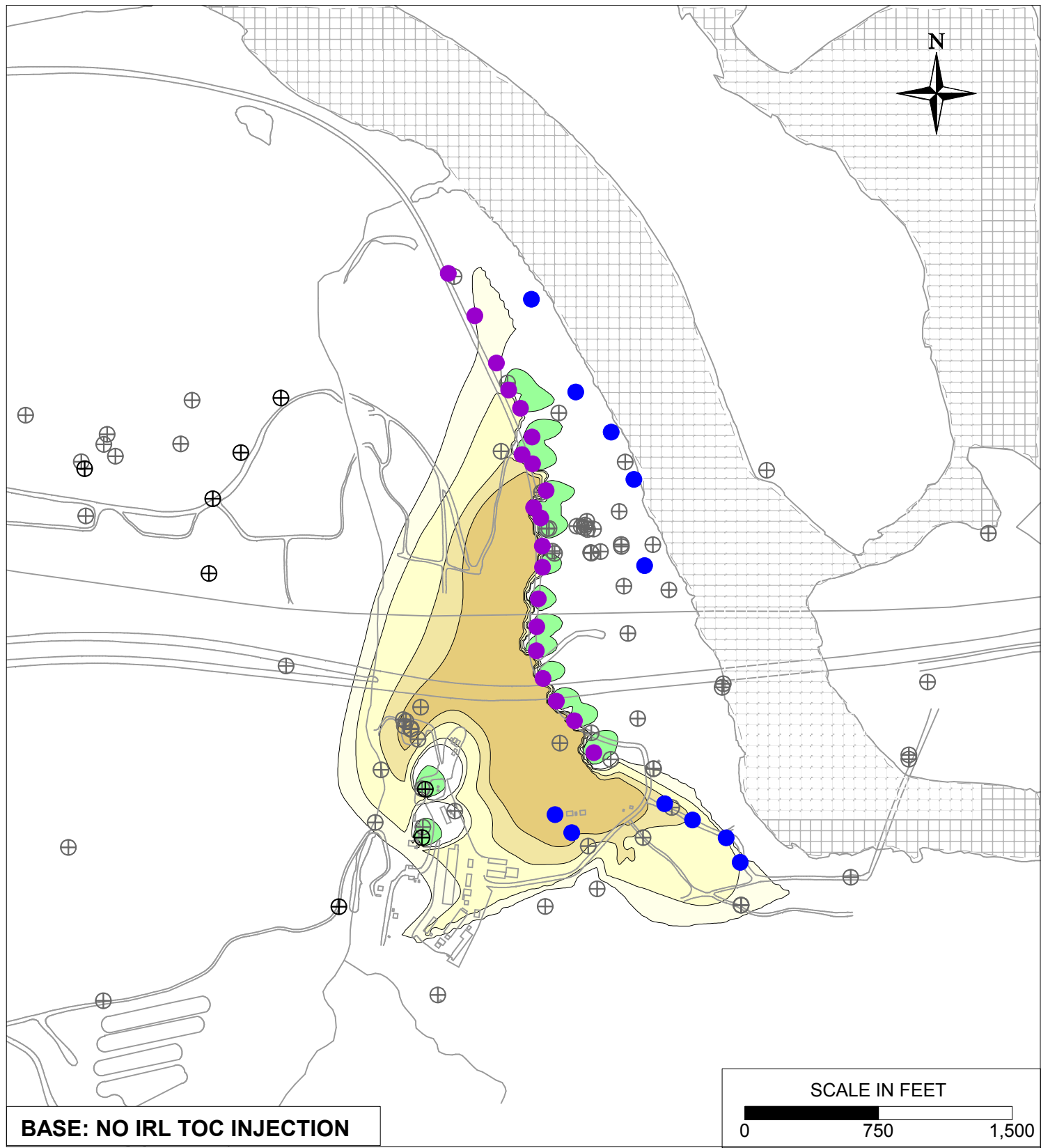


PG&E  
TOPOCK COMPRESSOR STATION  
NEEDLES, CALIFORNIA  
MODELING APPENDIX

INTERMEDIATE RECIRCULATION LOOP  
SENSITIVITY: SIMULATED ARSENIC TRANSPORT  
RESULTS FOR YEAR 30 IN MODEL LAYER 4

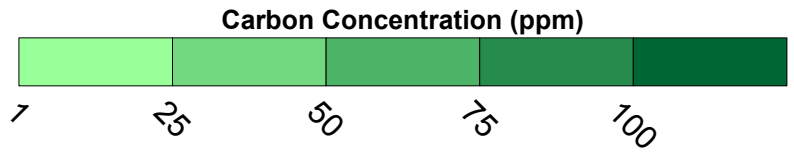
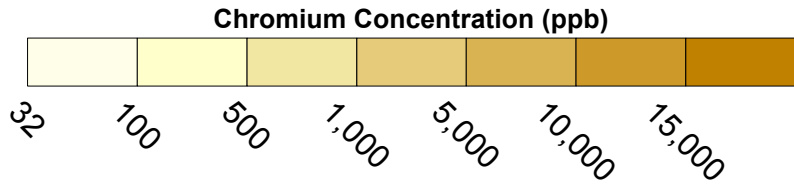


FIGURE  
10.13-6



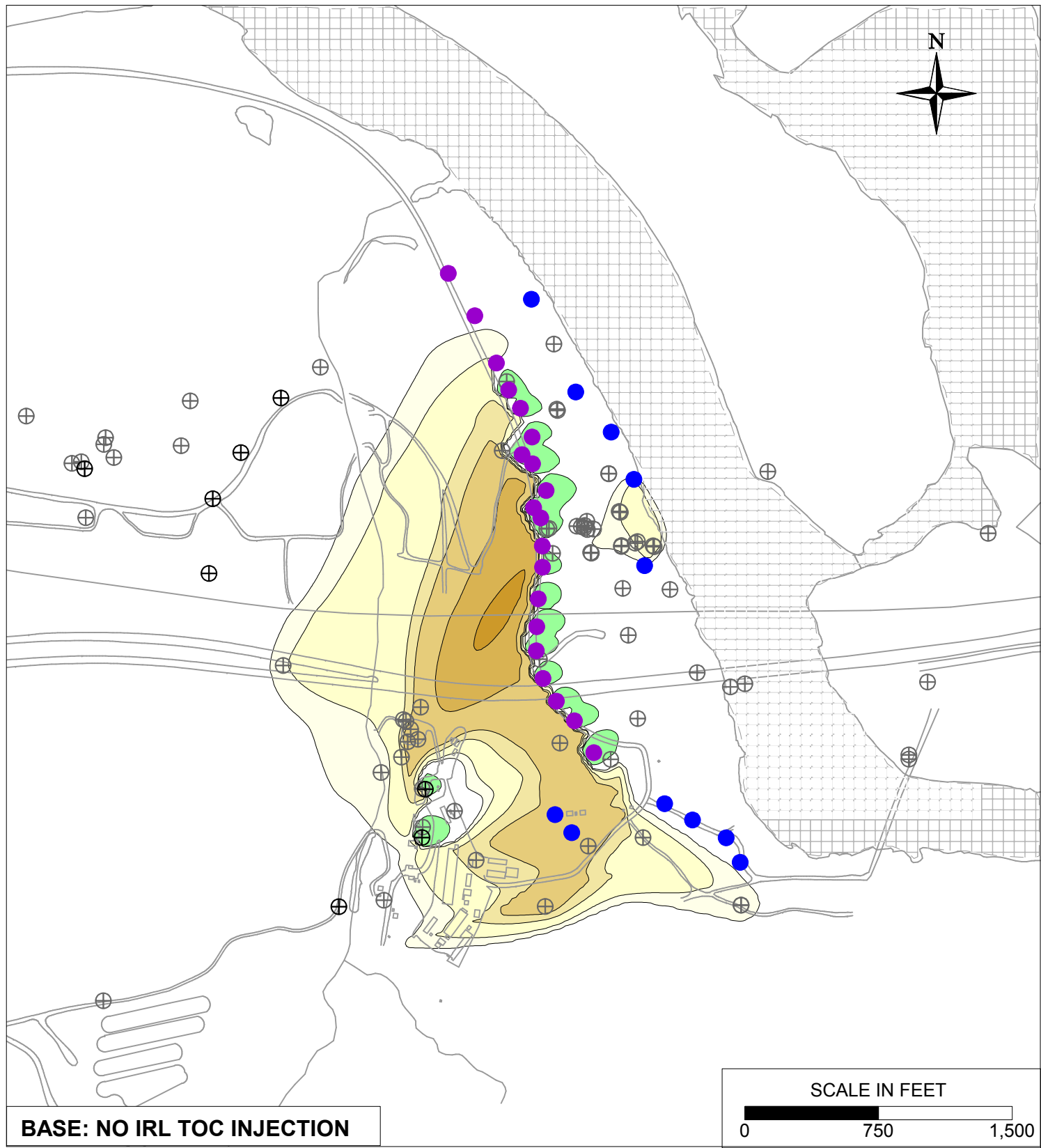
**LEGEND**

- IRZ WELLS
- ⊕ UPGRADIENT INJECTION WELLS
- EXTRACTION WELLS
- ⊕ MONITORING WELLS



PG&E TOPOCK COMPRESSOR STATION NEEDLES, CALIFORNIA MODELING APPENDIX	
4.5 YEAR IRL TOC INJECTION SENSITIVITY: SIMULATED HEXAVALENT CHROMIUM TRANSPORT RESULTS FOR YEAR 5 IN MODEL LAYER 2	
	FIGURE <b>10.14-1</b>

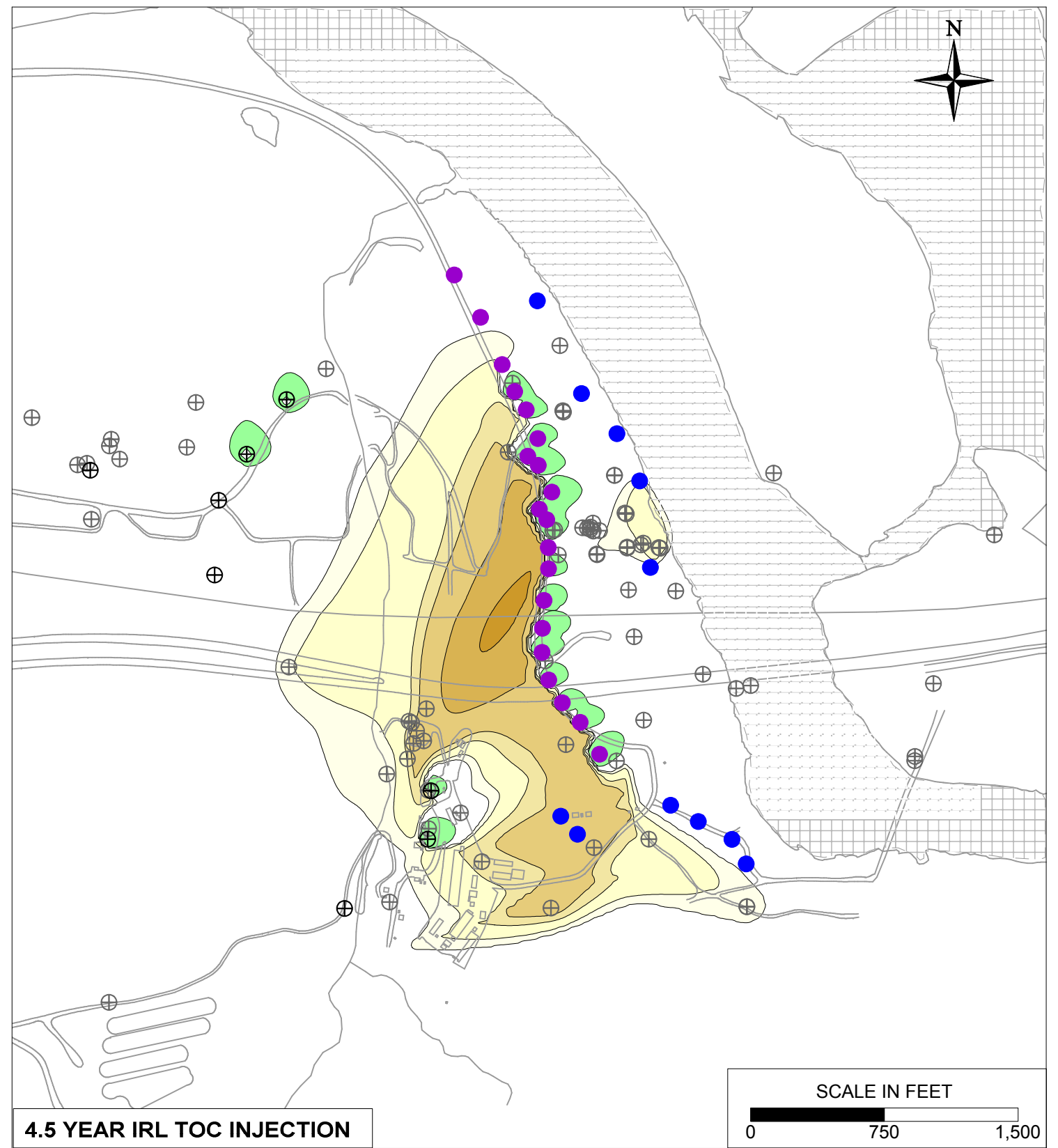
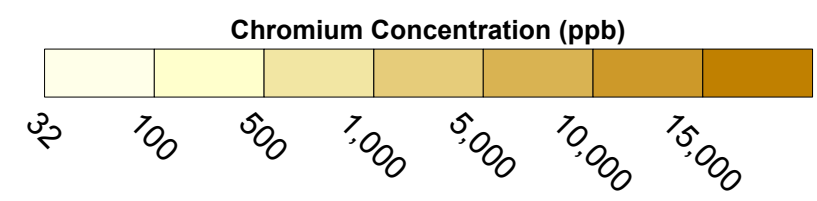




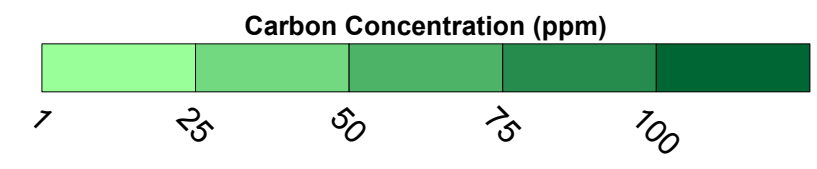
BASE: NO IRL TOC INJECTION

**LEGEND**

- IRZ WELLS
- ⊕ UPGRADIENT INJECTION WELLS
- EXTRACTION WELLS
- ⊕ MONITORING WELLS

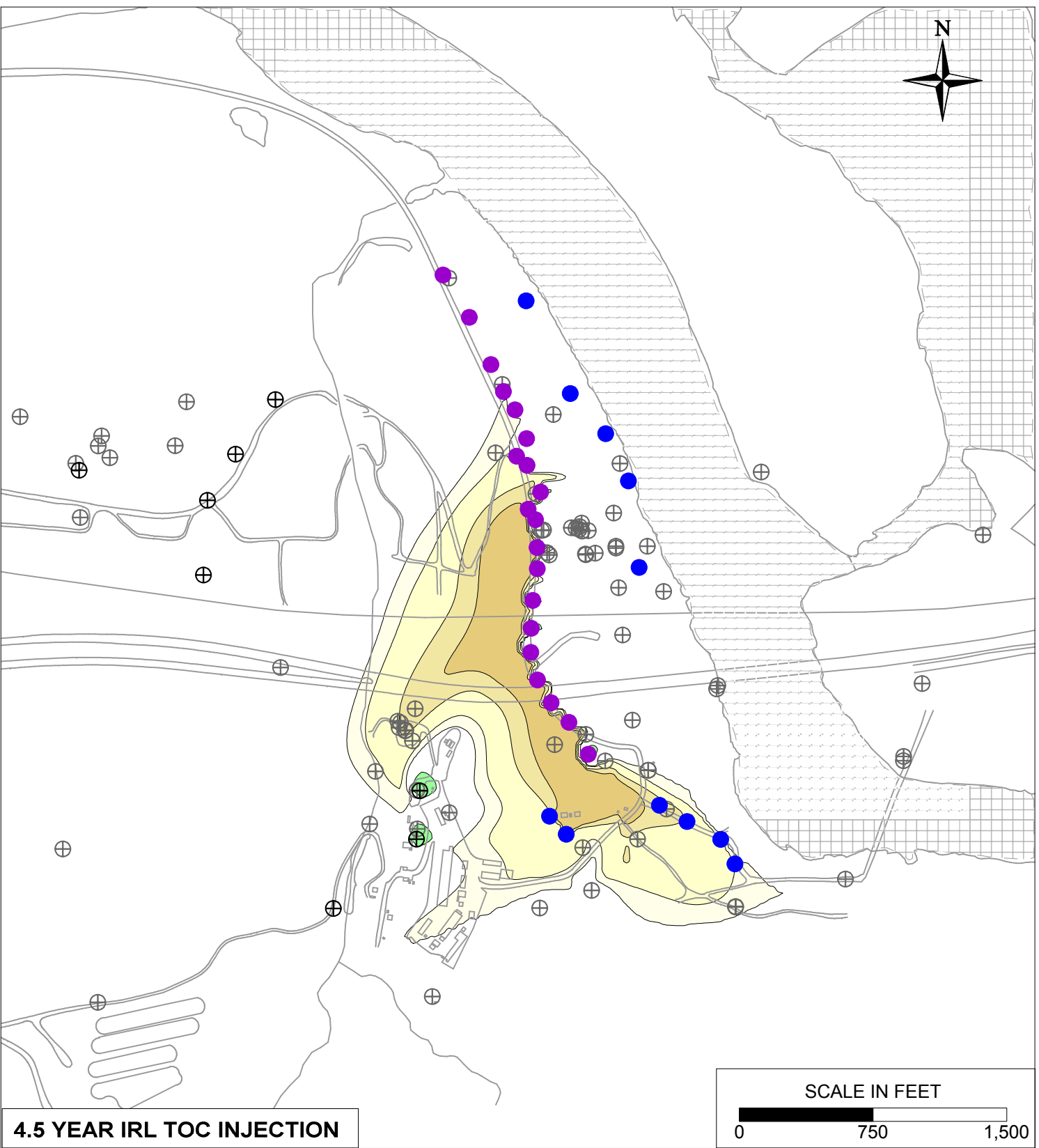
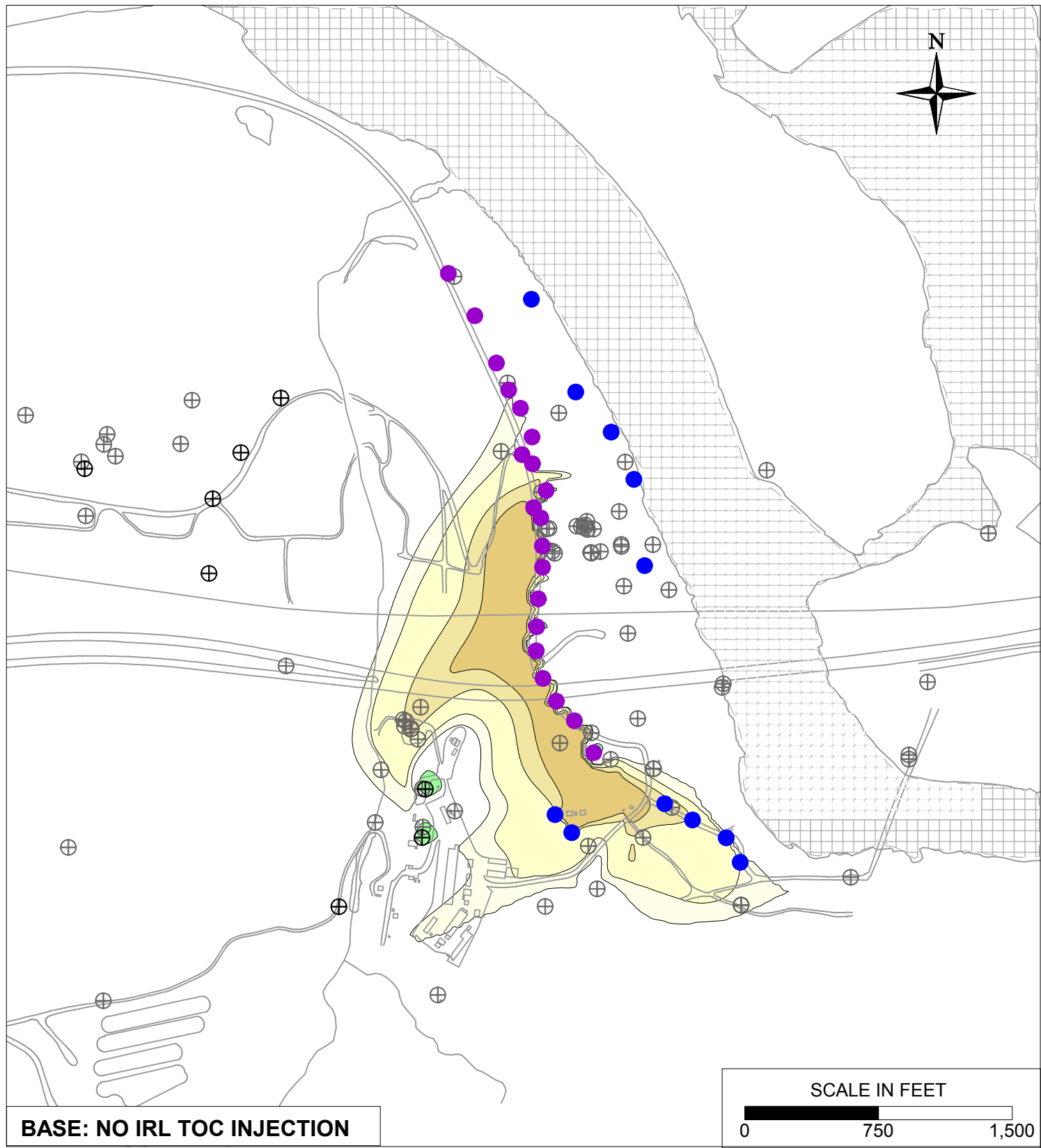


4.5 YEAR IRL TOC INJECTION



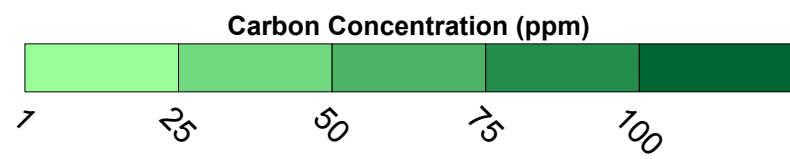
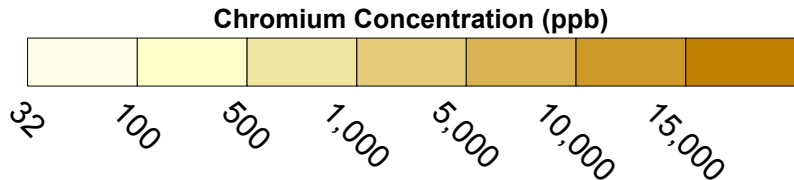
PG&E TOPOCK COMPRESSOR STATION NEEDLES, CALIFORNIA MODELING APPENDIX	
4.5 YEAR IRL TOC INJECTION SENSITIVITY: SIMULATED HEXAVALENT CHROMIUM TRANSPORT RESULTS FOR YEAR 5 IN MODEL LAYER 4	
	FIGURE 10.14-2



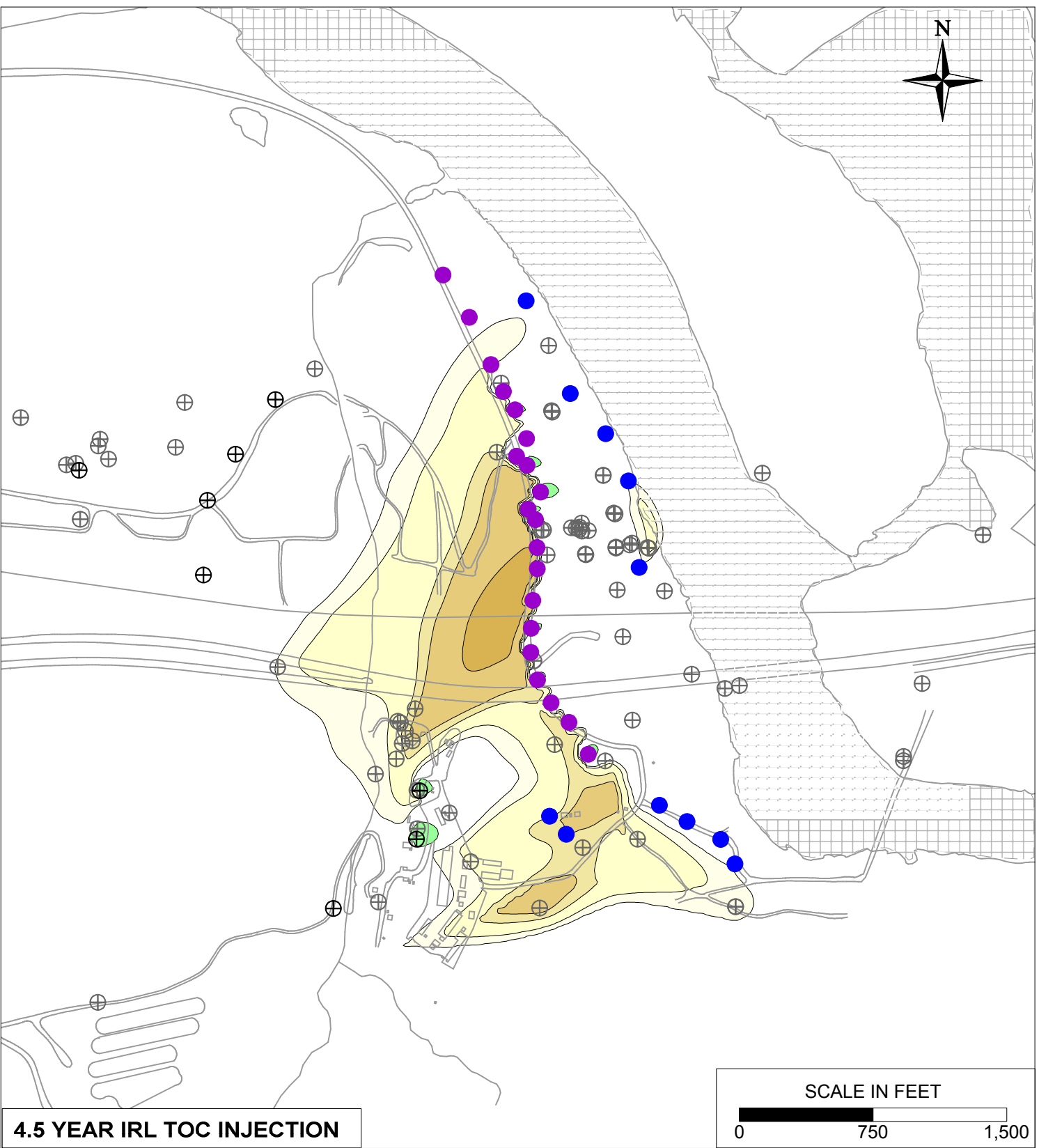
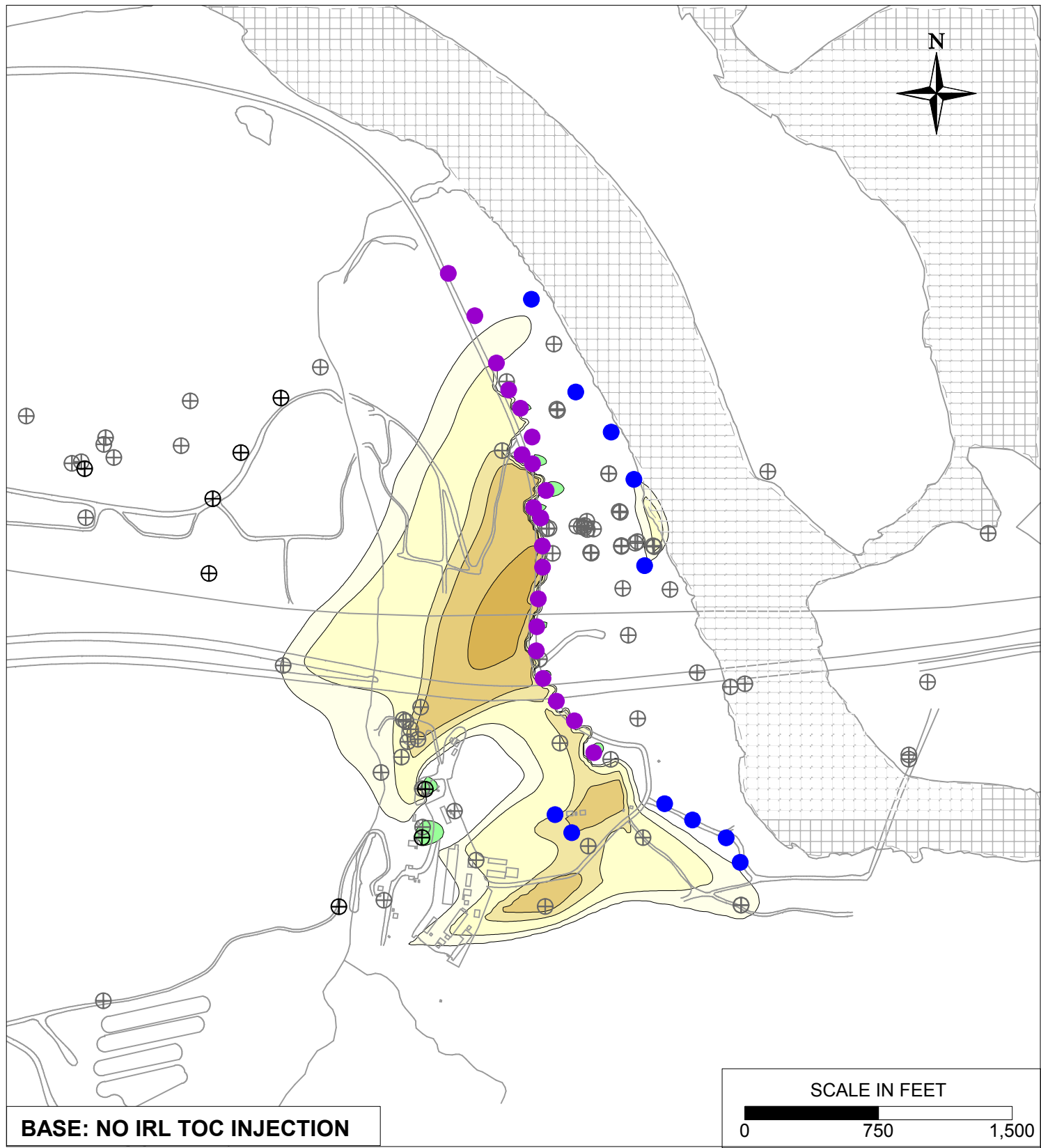


**LEGEND**

- IRZ WELLS
- ⊕ UPGRADIENT INJECTION WELLS
- EXTRACTION WELLS
- ⊕ MONITORING WELLS

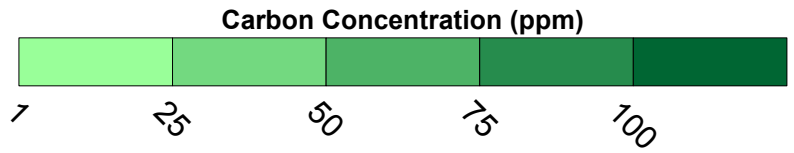
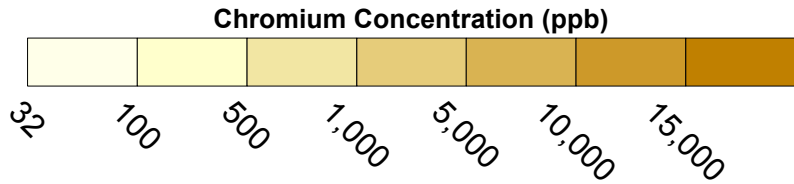


PG&E TOPOCK COMPRESSOR STATION NEEDLES, CALIFORNIA MODELING APPENDIX	
4.5 YEAR IRL TOC INJECTION SENSITIVITY: SIMULATED HEXAVALENT CHROMIUM TRANSPORT RESULTS FOR YEAR 10 IN MODEL LAYER 2	
	FIGURE 10.14-3

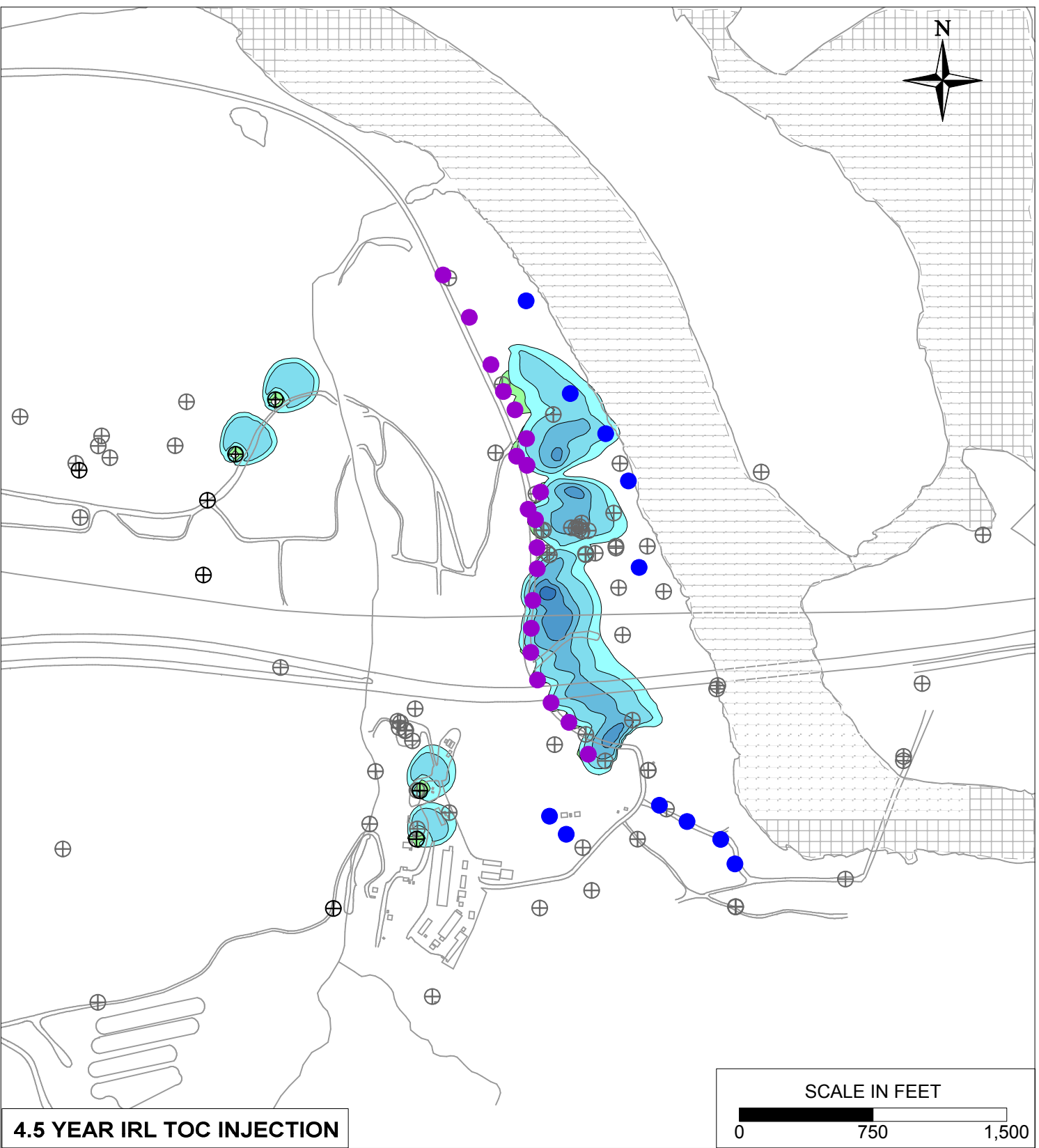
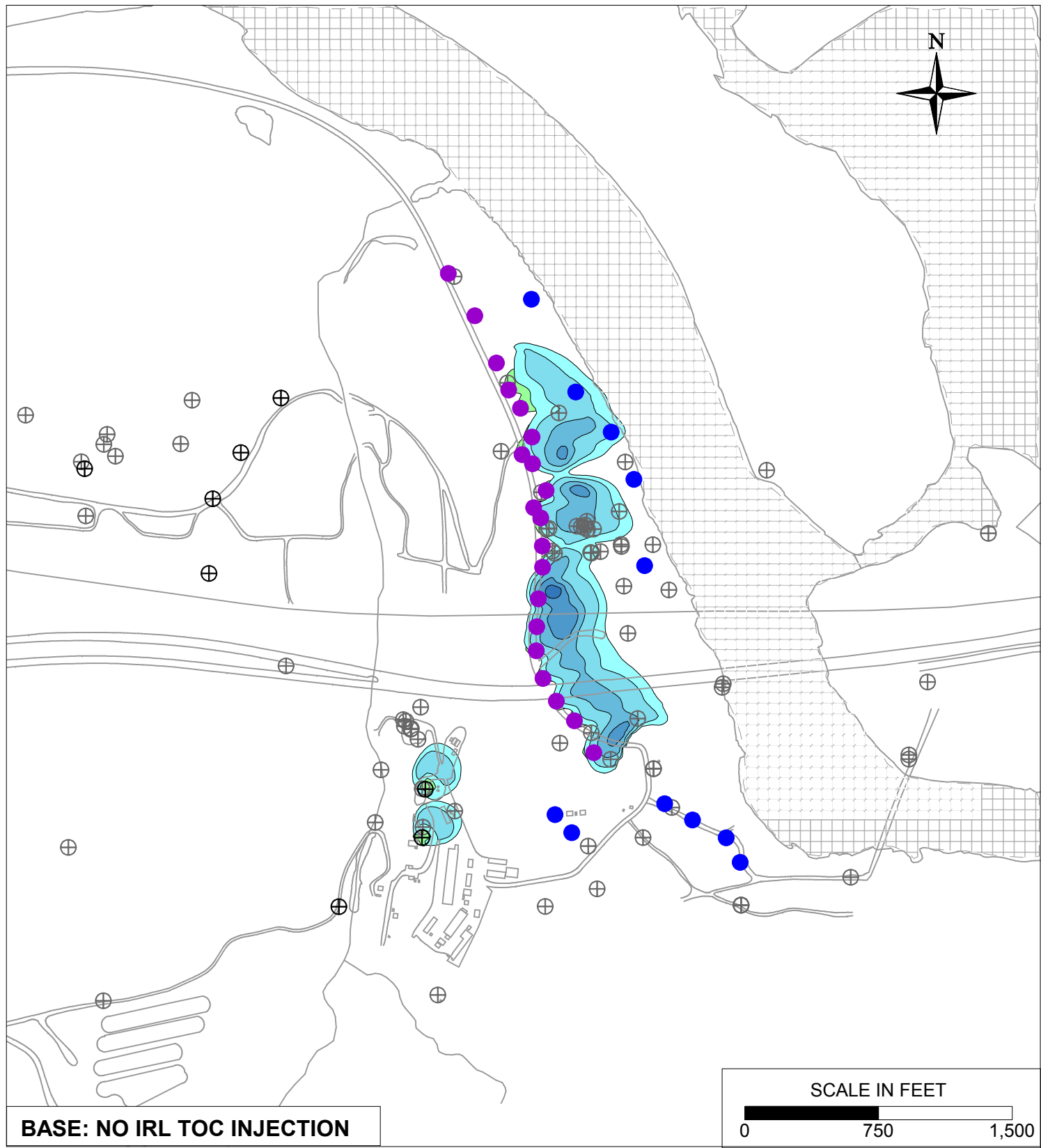


**LEGEND**

- IRZ WELLS
- ⊕ UPGRADIENT INJECTION WELLS
- EXTRACTION WELLS
- ⊕ MONITORING WELLS

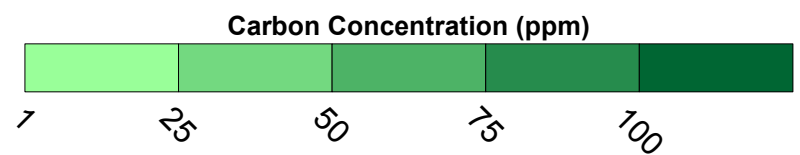
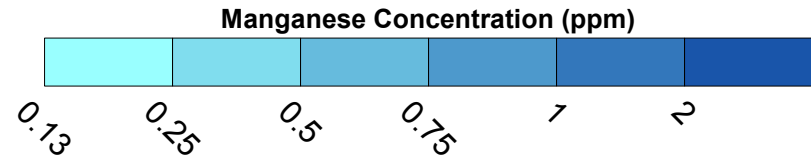


PG&E TOPOCK COMPRESSOR STATION NEEDLES, CALIFORNIA MODELING APPENDIX	
4.5 YEAR IRL TOC INJECTION SENSITIVITY: SIMULATED HEXAVALENT CHROMIUM TRANSPORT RESULTS FOR YEAR 10 IN MODEL LAYER 4	
	FIGURE <b>10.14-4</b>



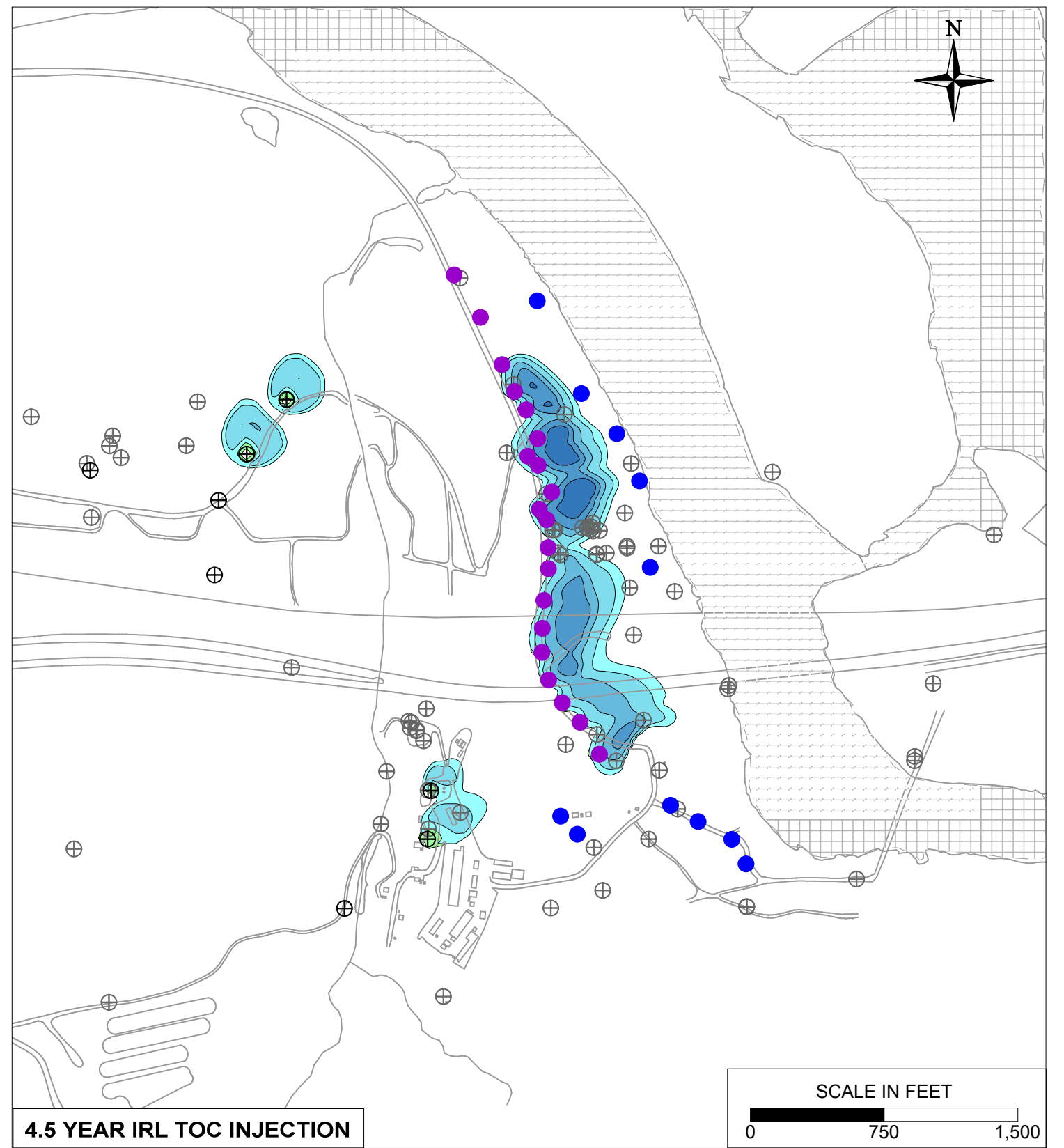
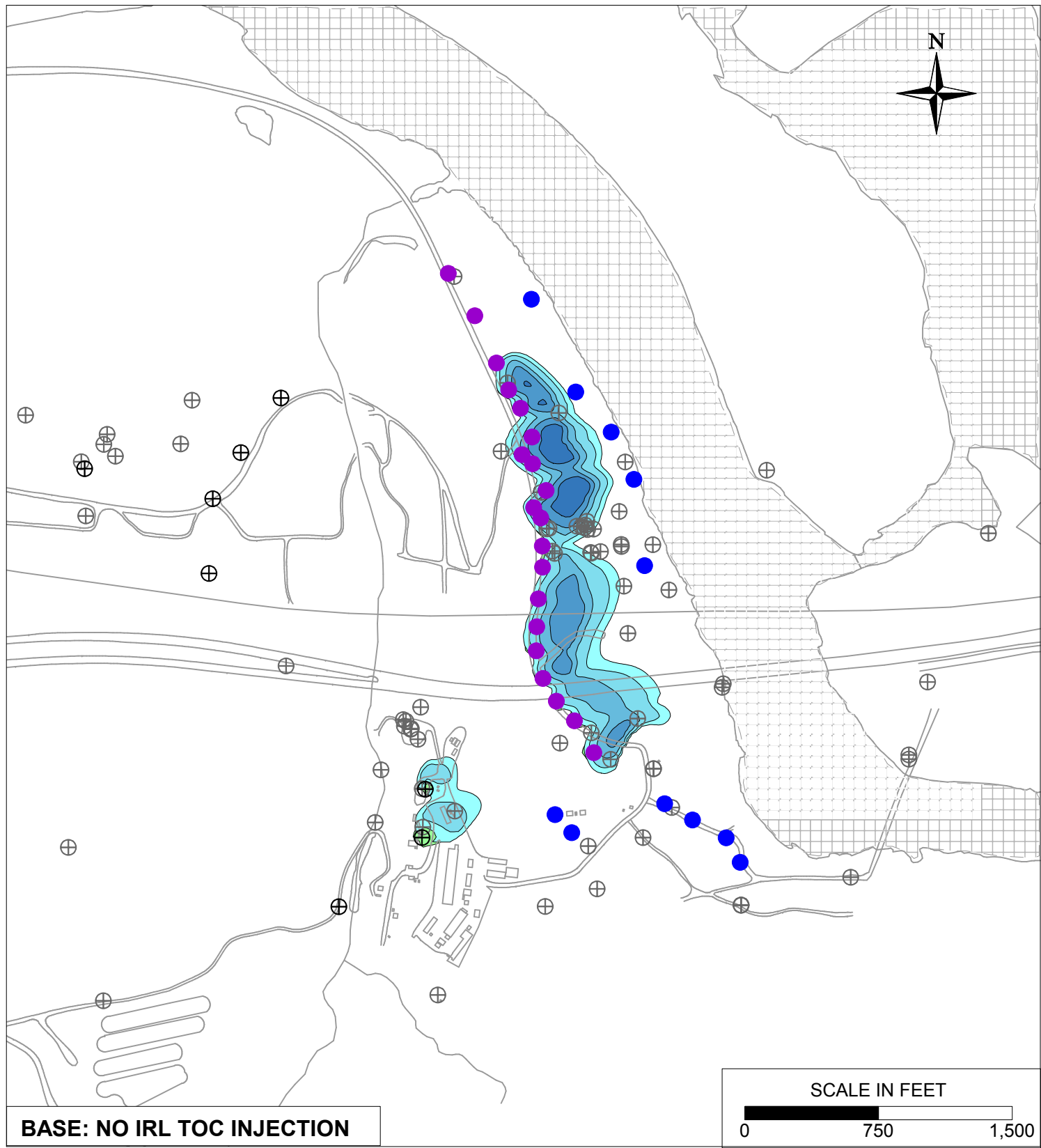
**LEGEND**

- IRZ WELLS
- ⊕ UPGRADIENT INJECTION WELLS
- EXTRACTION WELLS
- ⊕ MONITORING WELLS



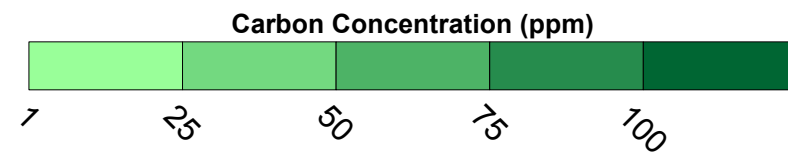
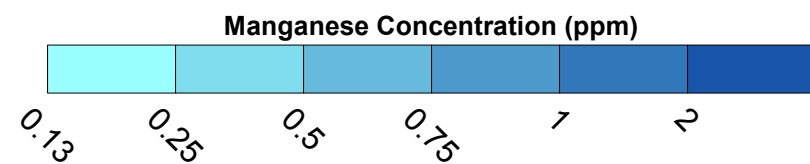
PG&E TOPOCK COMPRESSOR STATION NEEDLES, CALIFORNIA MODELING APPENDIX	
4.5 YEAR IRL TOC INJECTION SENSITIVITY: SIMULATED MANGANESE TRANSPORT RESULTS FOR YEAR 5 IN MODEL LAYER 2	
	FIGURE <b>10.14-5</b>





**LEGEND**

- IRZ WELLS
- ⊕ UPGRADIENT INJECTION WELLS
- EXTRACTION WELLS
- ⊕ MONITORING WELLS



PG&E  
TOPOCK COMPRESSOR STATION  
NEEDLES, CALIFORNIA  
MODELING APPENDIX

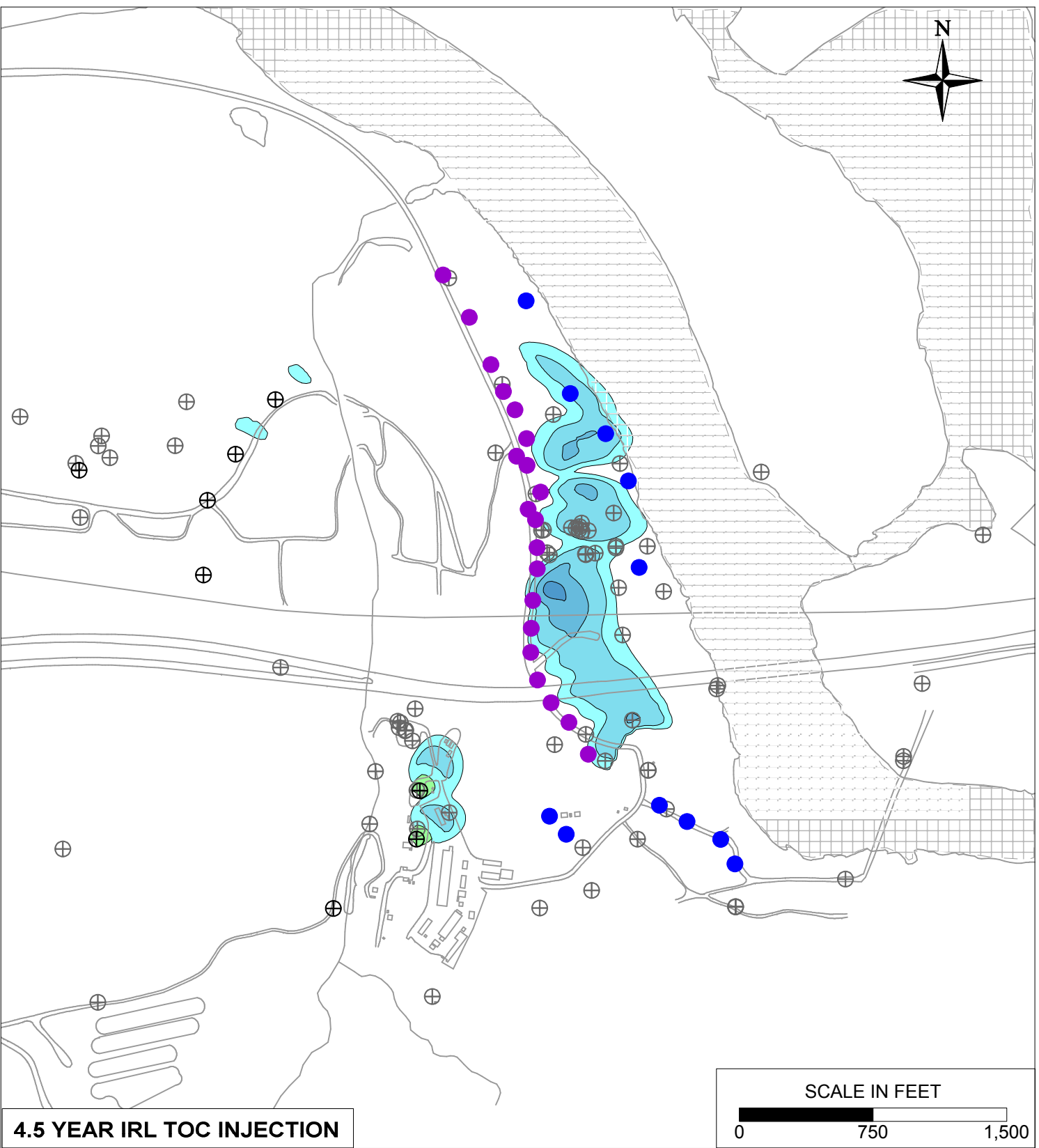
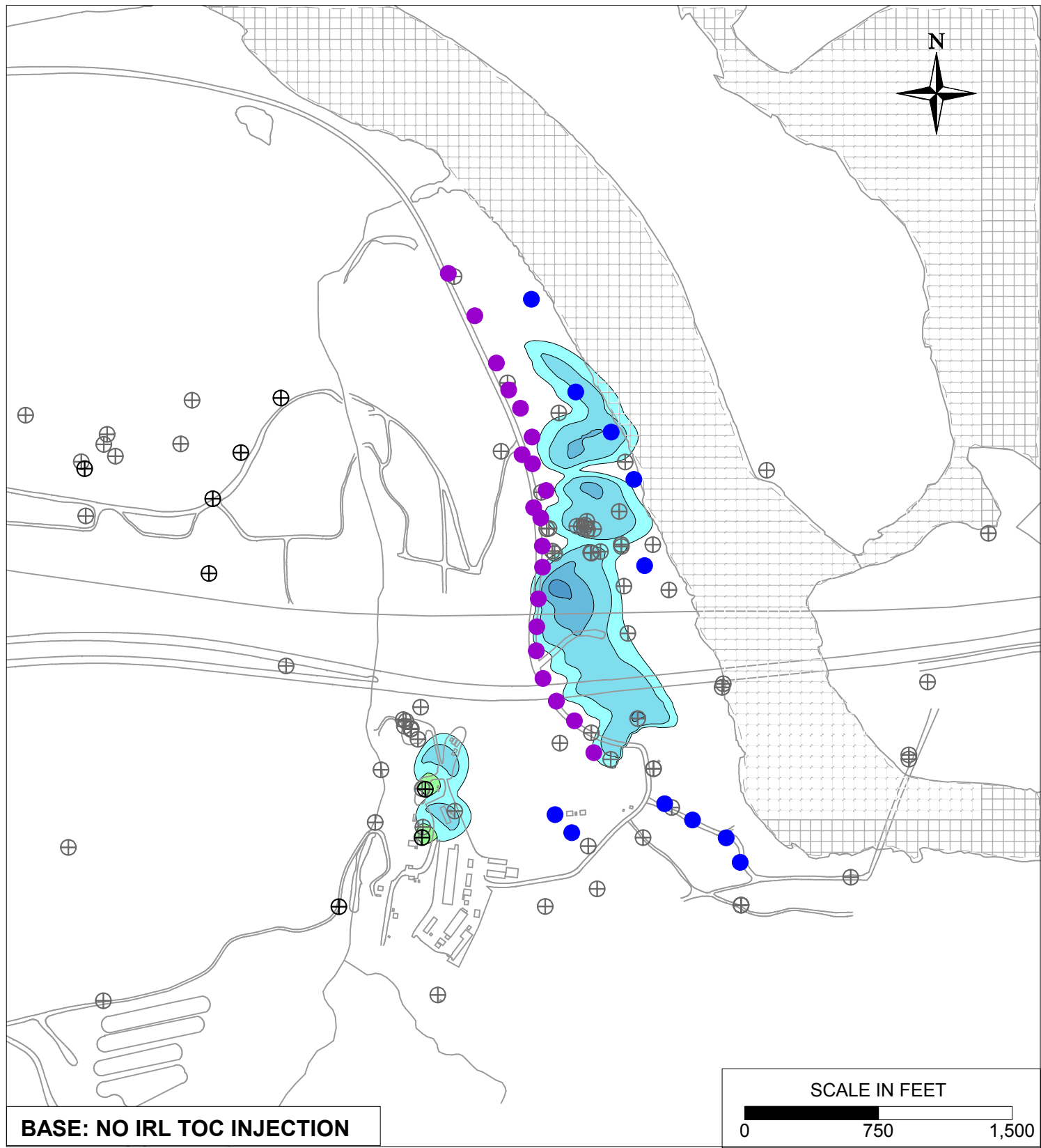
4.5 YEAR IRL TOC INJECTION SENSITIVITY:  
SIMULATED MANGANESE TRANSPORT  
RESULTS FOR YEAR 5 IN MODEL LAYER 4



FIGURE

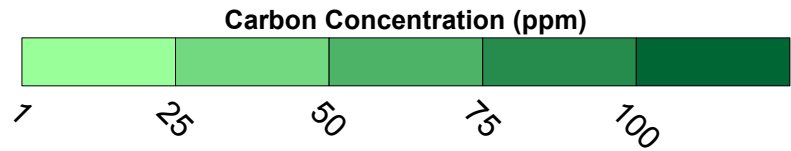
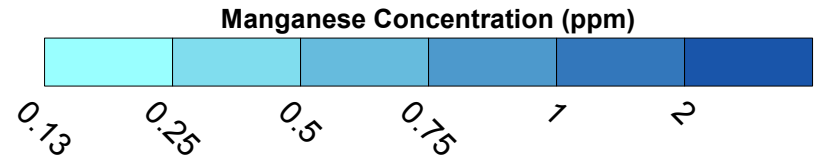
10.14-6





**LEGEND**

- IRZ WELLS
- ⊕ UPGRADIENT INJECTION WELLS
- EXTRACTION WELLS
- ⊕ MONITORING WELLS

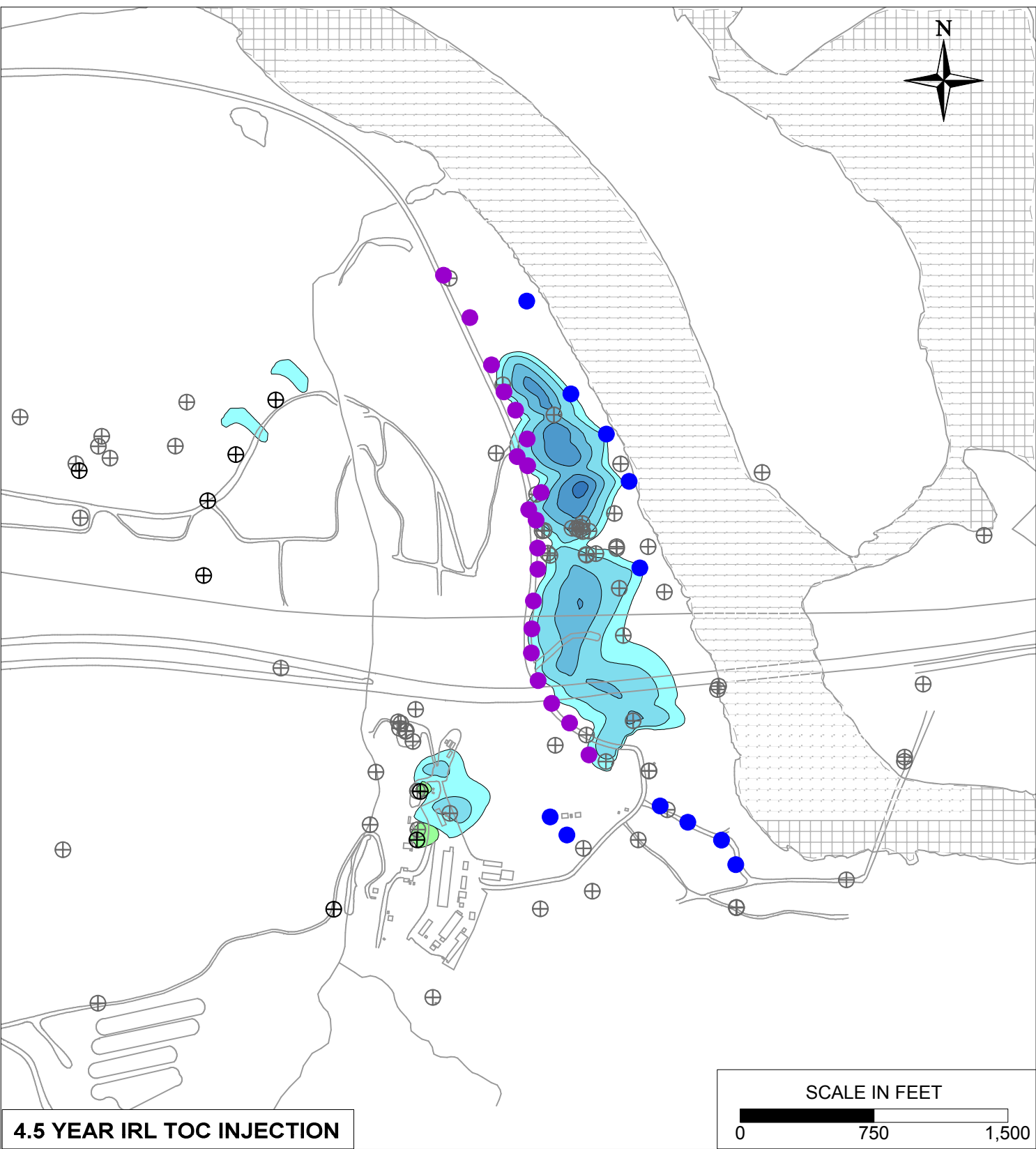
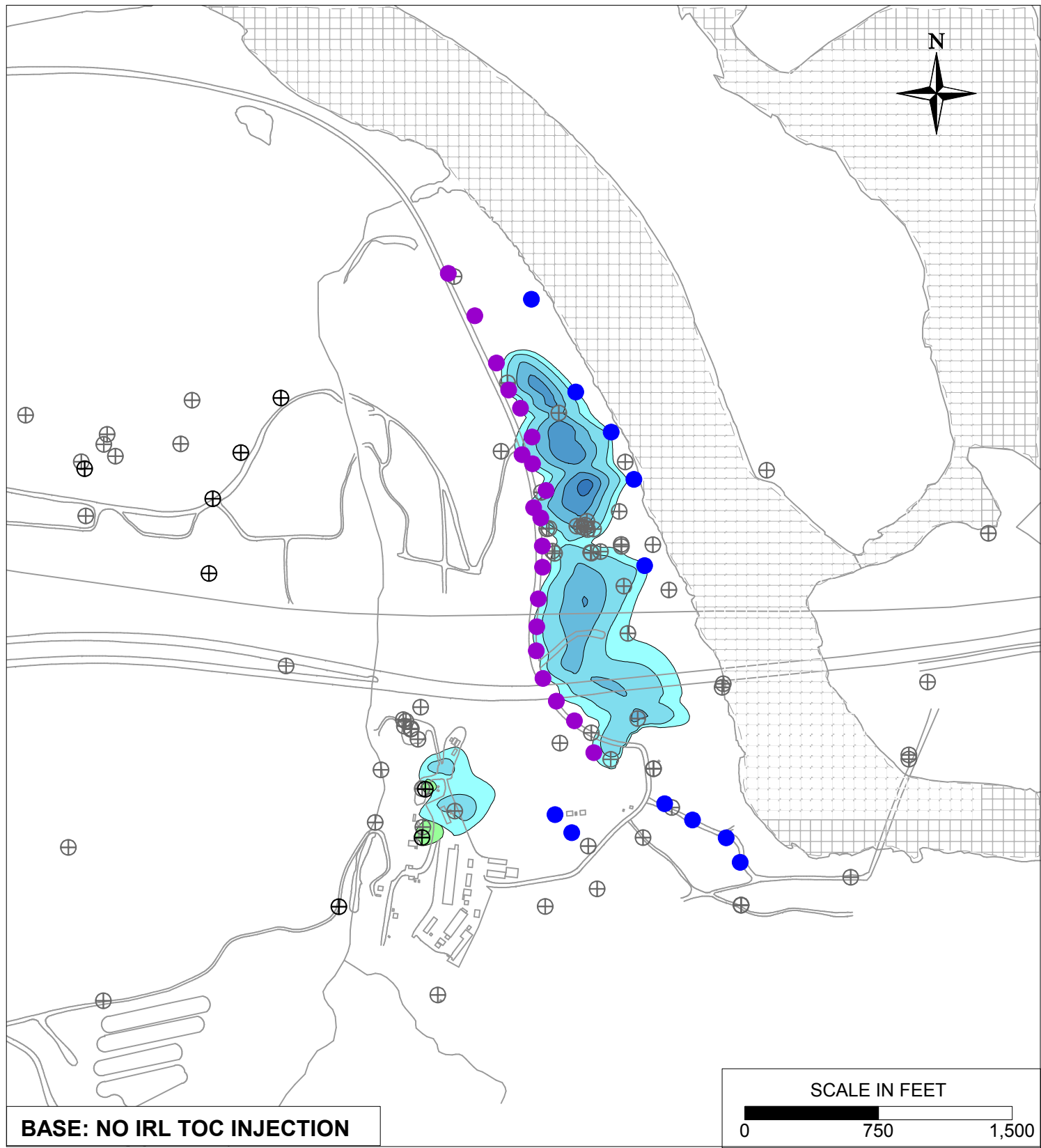


PG&E  
TOPOCK COMPRESSOR STATION  
NEEDLES, CALIFORNIA  
MODELING APPENDIX

4.5 YEAR IRL TOC INJECTION SENSITIVITY:  
SIMULATED MANGANESE TRANSPORT  
RESULTS FOR YEAR 10 IN MODEL LAYER 2

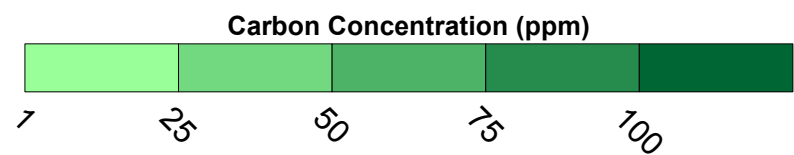
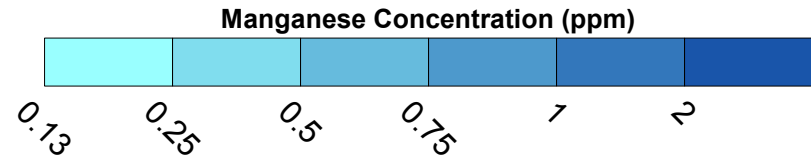


FIGURE  
10.14-7



**LEGEND**

- IRZ WELLS
- ⊕ UPGRADIENT INJECTION WELLS
- EXTRACTION WELLS
- ⊕ MONITORING WELLS

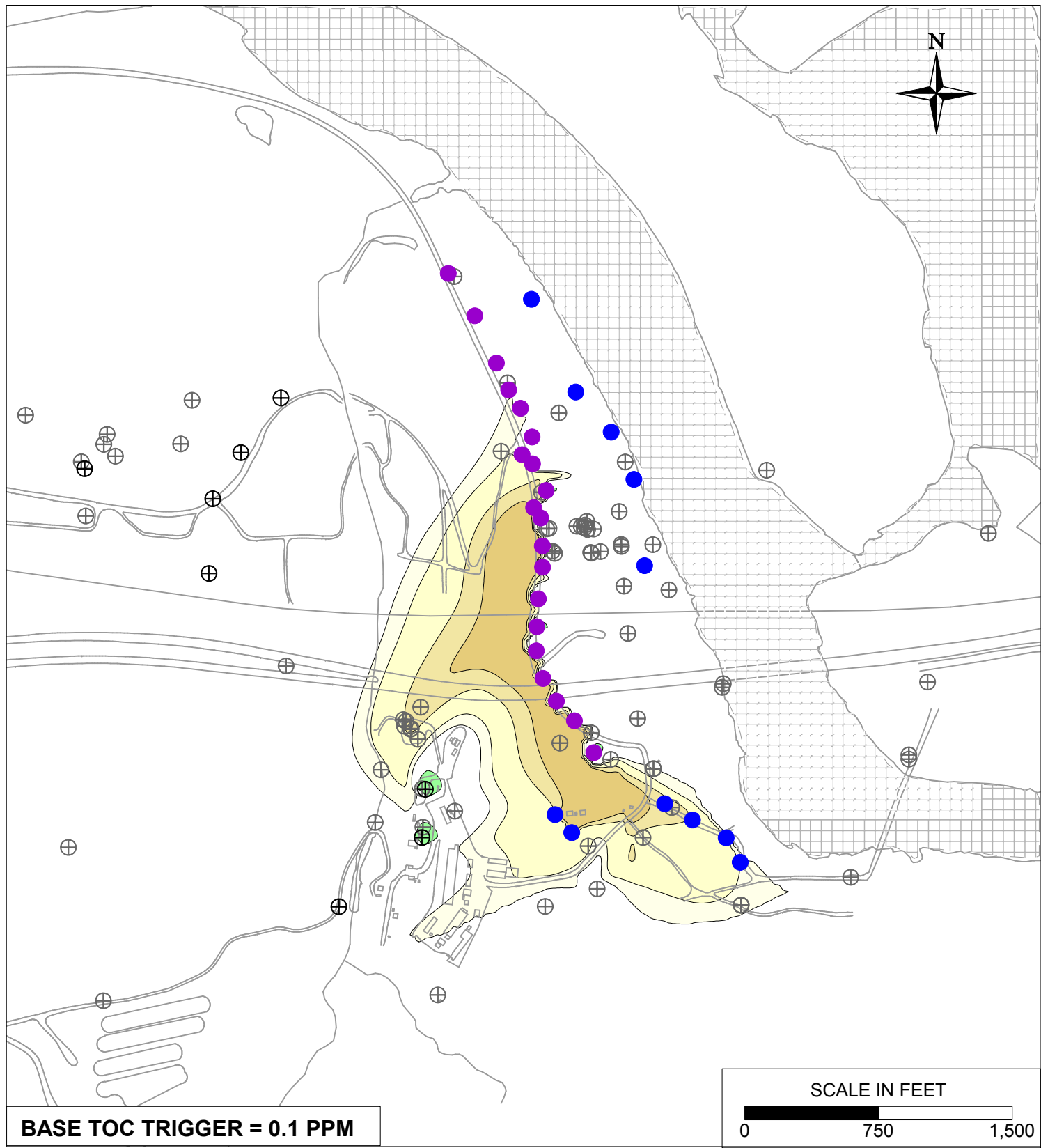


PG&E  
TOPOCK COMPRESSOR STATION  
NEEDLES, CALIFORNIA  
MODELING APPENDIX

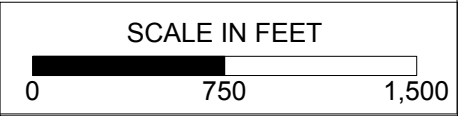
4.5 YEAR IRL TOC INJECTION SENSITIVITY:  
SIMULATED MANGANESE TRANSPORT  
RESULTS FOR YEAR 10 IN MODEL LAYER 4



FIGURE  
10.14-8

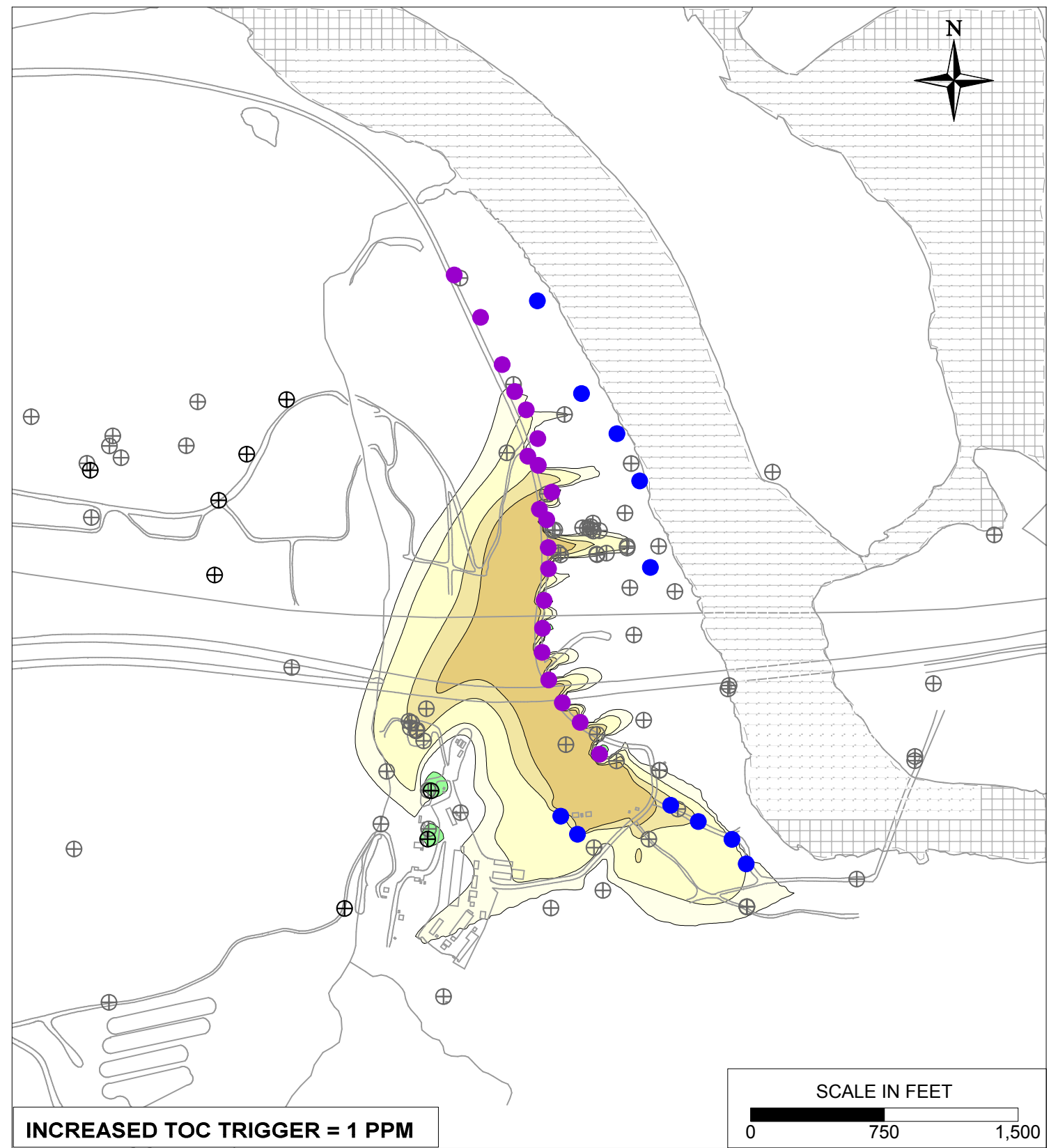
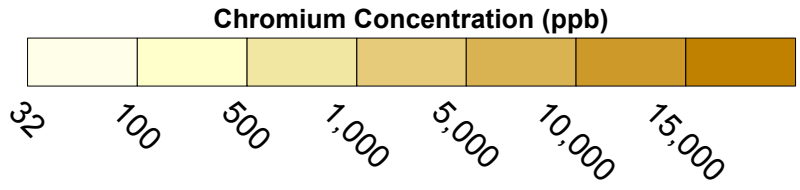


BASE TOC TRIGGER = 0.1 PPM

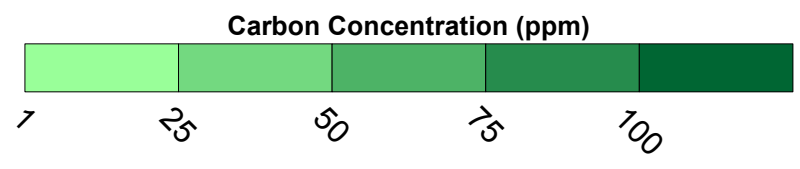
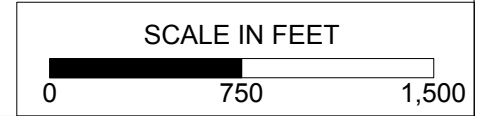


**LEGEND**

- IRZ WELLS
- UPGRADIENT INJECTION WELLS
- EXTRACTION WELLS
- MONITORING WELLS



INCREASED TOC TRIGGER = 1 PPM

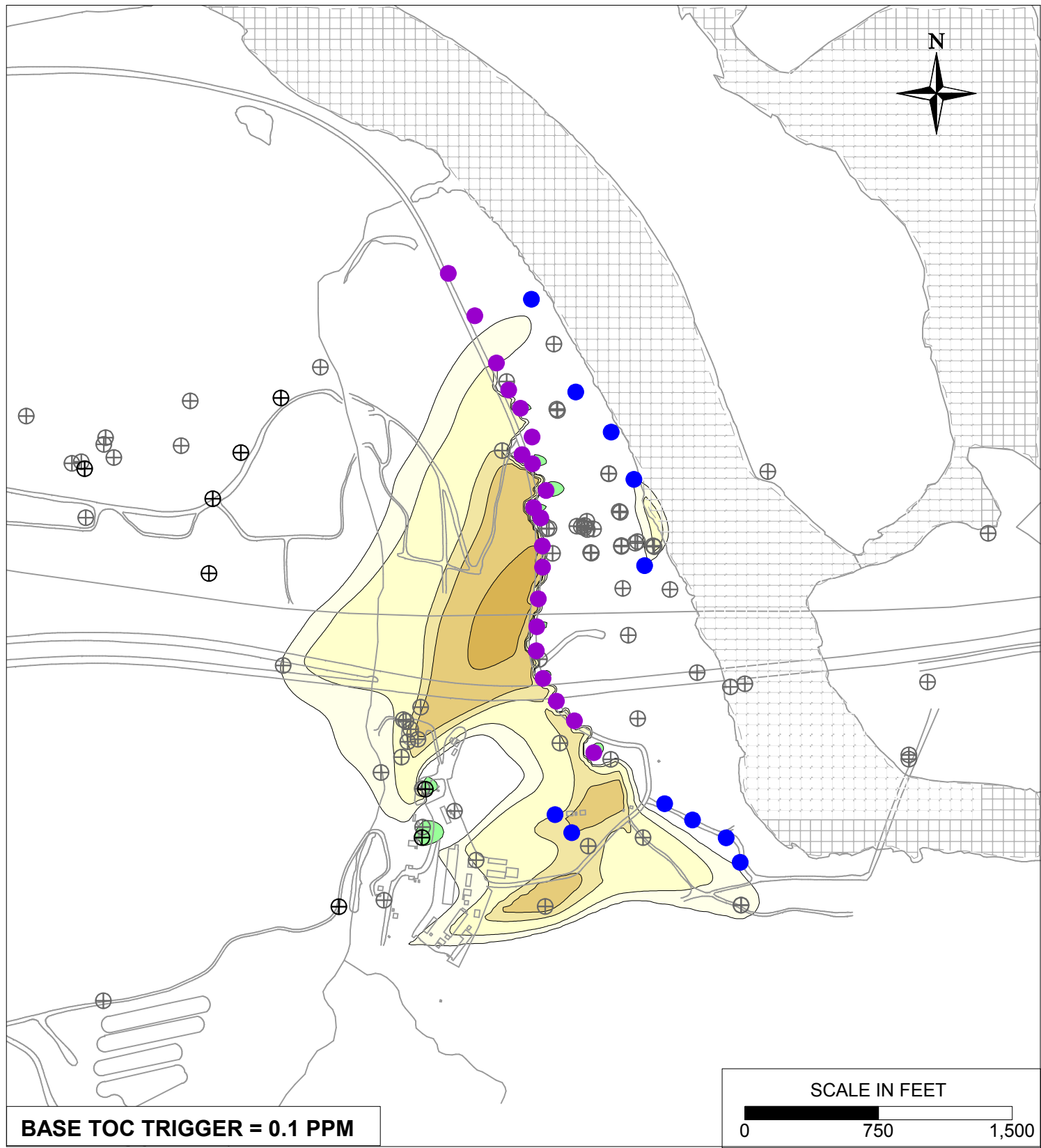


PG&E  
TOPOCK COMPRESSOR STATION  
NEEDLES, CALIFORNIA  
MODELING APPENDIX

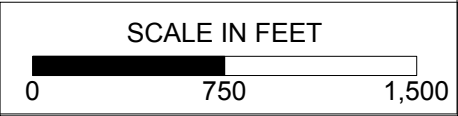
TOC/HEXAVALENT CHROMIUM TRIGGER  
SENSITIVITY: SIMULATED HEXAVALENT  
CHROMIUM TRANSPORT RESULTS FOR  
YEAR 10 IN MODEL LAYER 2

FIGURE  
10.15-1



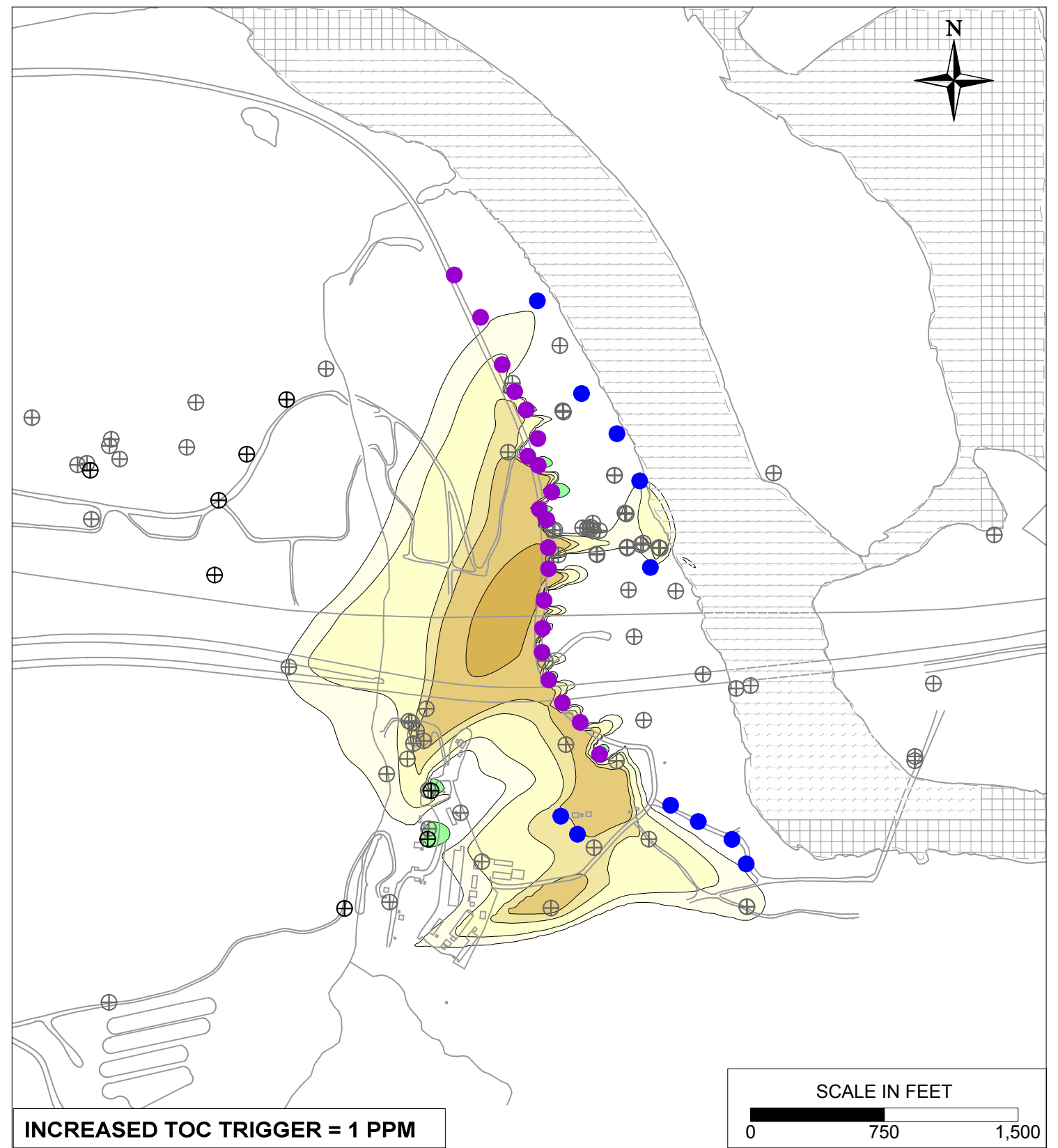
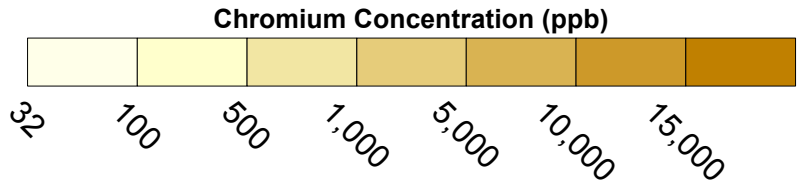


BASE TOC TRIGGER = 0.1 PPM

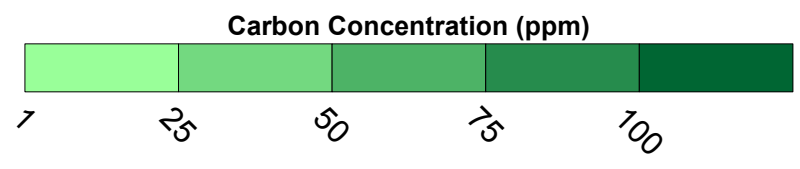
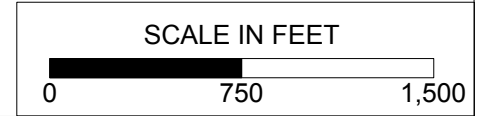


**LEGEND**

- IRZ WELLS
- UPGRADIENT INJECTION WELLS
- EXTRACTION WELLS
- MONITORING WELLS



INCREASED TOC TRIGGER = 1 PPM

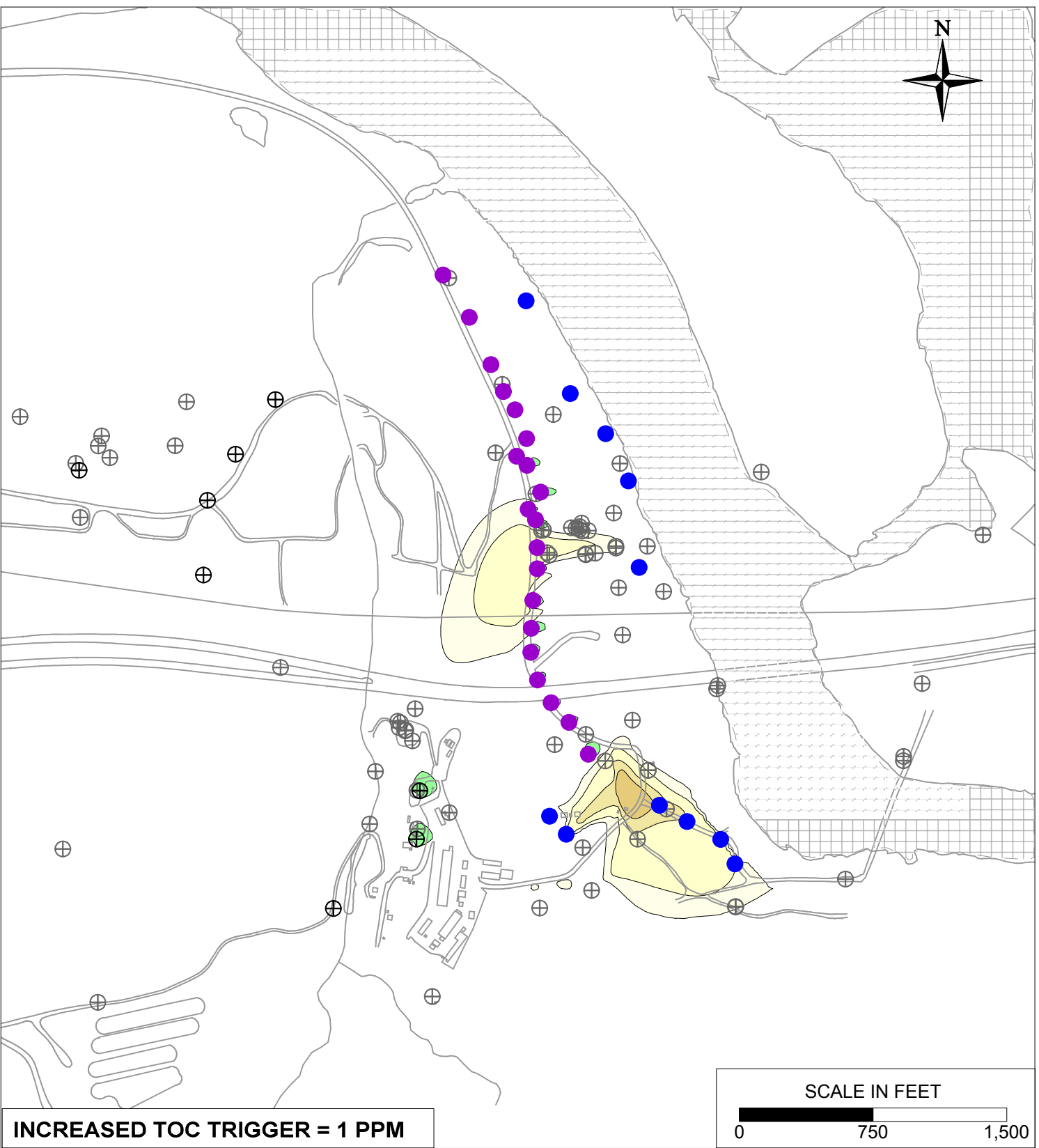
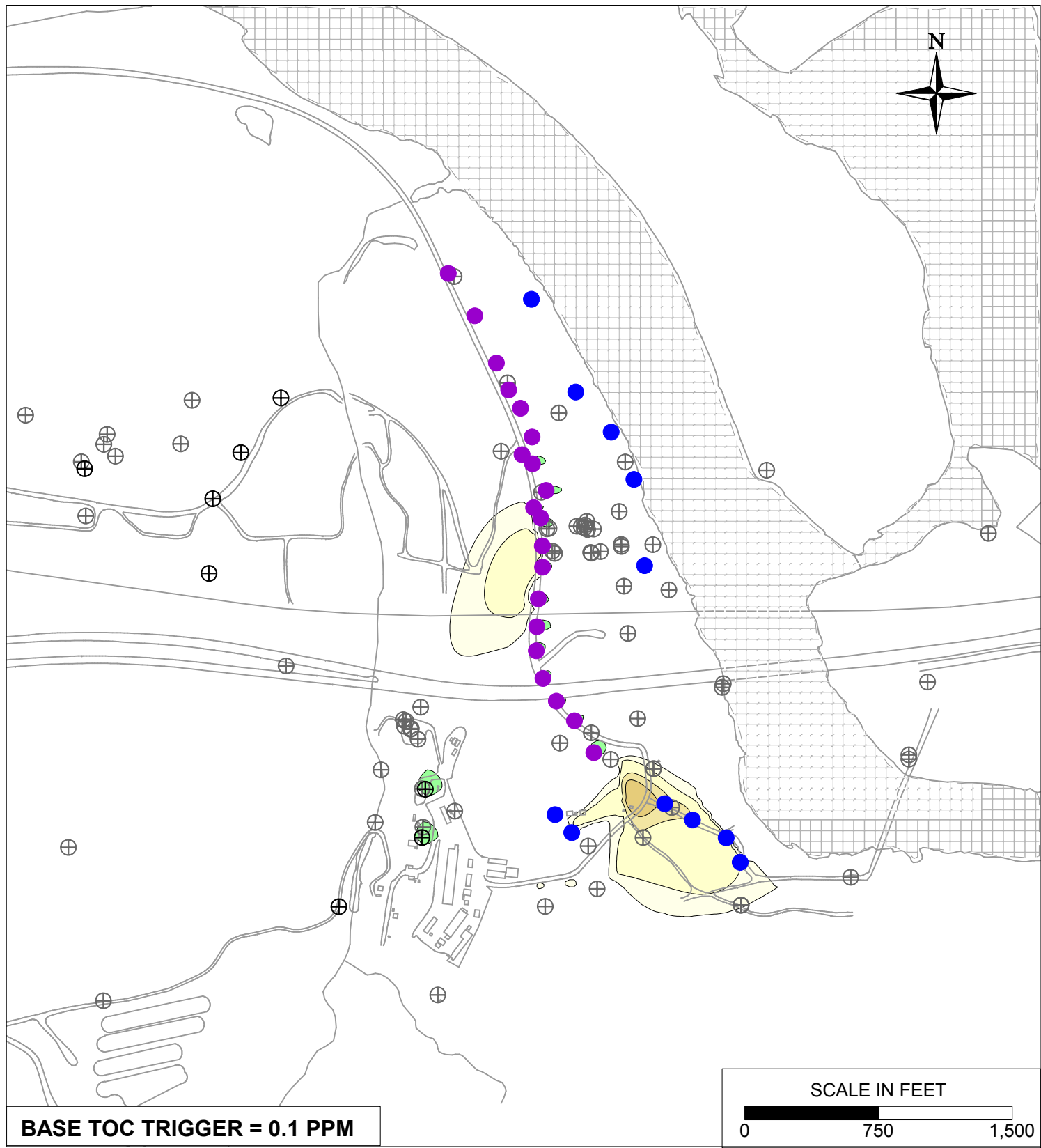


PG&E  
TOPOCK COMPRESSOR STATION  
NEEDLES, CALIFORNIA  
MODELING APPENDIX

TOC/HEXAVALENT CHROMIUM TRIGGER  
SENSITIVITY: SIMULATED HEXAVALENT  
CHROMIUM TRANSPORT RESULTS FOR  
YEAR 10 IN MODEL LAYER 4

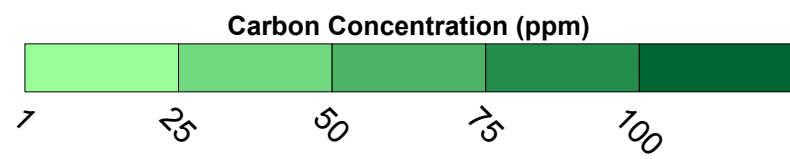
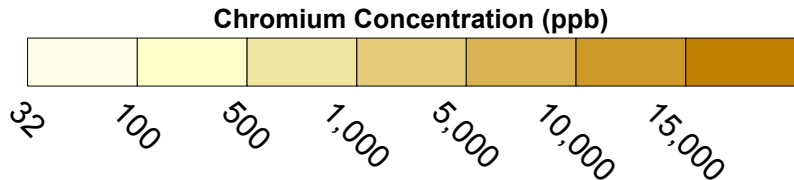
FIGURE  
10.15-2



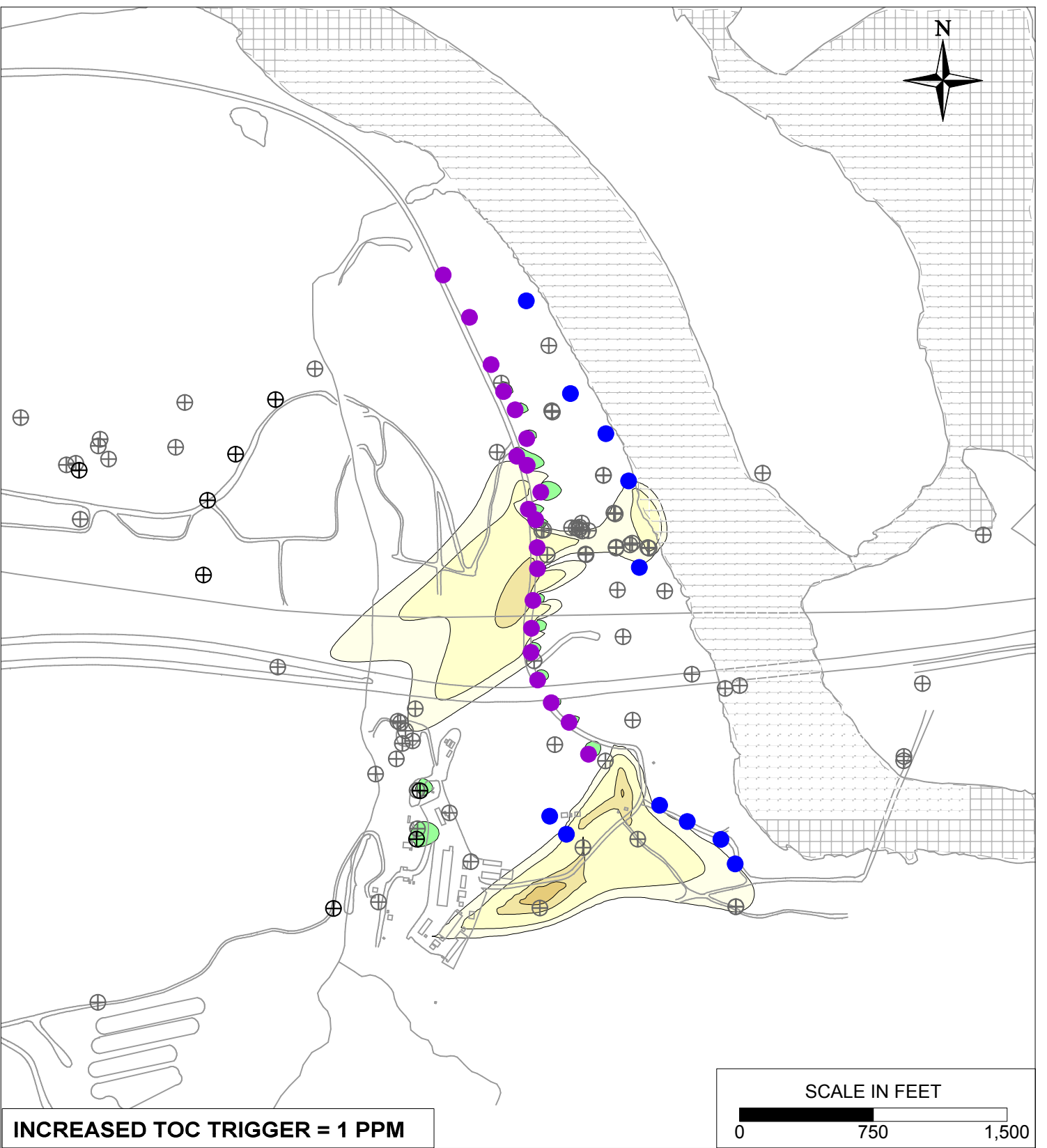
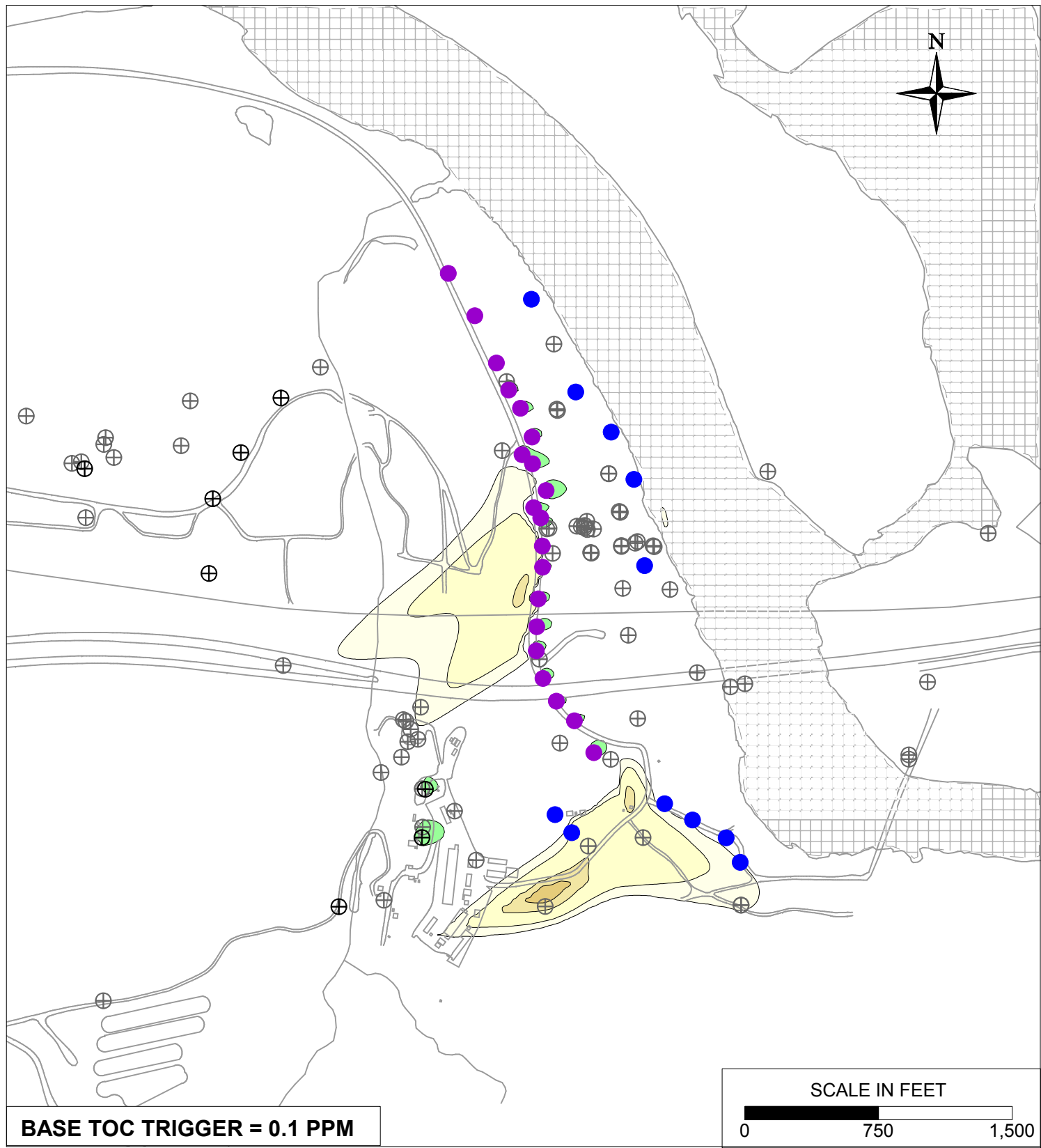


**LEGEND**

- IRZ WELLS
- ⊕ UPGRADIENT INJECTION WELLS
- EXTRACTION WELLS
- ⊕ MONITORING WELLS

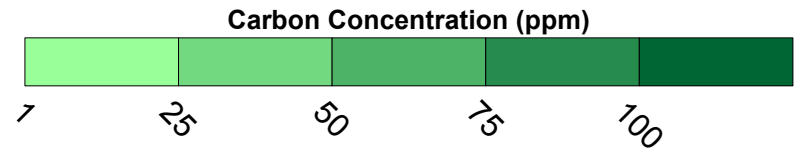
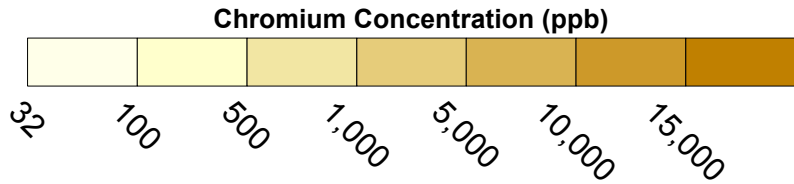


PG&E TOPOCK COMPRESSOR STATION NEEDLES, CALIFORNIA MODELING APPENDIX	
TOC/HEXAVALENT CHROMIUM TRIGGER SENSITIVITY: SIMULATED HEXAVALENT CHROMIUM TRANSPORT RESULTS FOR YEAR 30 IN MODEL LAYER 2	
	FIGURE <b>10.15-3</b>



**LEGEND**

- IRZ WELLS
- ⊕ UPGRADIENT INJECTION WELLS
- EXTRACTION WELLS
- ⊕ MONITORING WELLS



PG&E TOPOCK COMPRESSOR STATION NEEDLES, CALIFORNIA MODELING APPENDIX	
TOC/HEXAVALENT CHROMIUM TRIGGER SENSITIVITY: SIMULATED HEXAVALENT CHROMIUM TRANSPORT RESULTS FOR YEAR 30 IN MODEL LAYER 4	
	FIGURE <span style="font-size: 24pt; font-weight: bold;">10.15-4</span>